

MaNEP

Materials with Novel Electronic Properties

Activity Report 2005 – 2008

MaNEP

Materials with Novel Electronic Properties

Activity Report

2005 – 2008

Contents

1	Summary	3
2	Members and institutions in MaNEP and contacts	5
3	Research	7
	Project 1	7
	Project 2	57
	Project 3	87
	Project 4	102
	Project 5	121
	Project 6	135
4	Three years of MaNEP's life	157
5	Three years of publications	161

Cover: Electron micrograph of a single photon detector (from A. Schilling, UniZH, p. 132)
Rubrene organic crystals (from G. Margaritondo, EPFL, p. 97)
Photoemission spectrum from an underdoped $\text{Bi}_2\text{Sr}_2\text{CuO}_{6+\delta}$ film (from M. Grioni, EPFL, p. 79)
Crystal structure of $\text{Sr}_3\text{Os}_4\text{O}_{14}$ along [001] direction (from J. Karpinski, ETHZ, p. 113)
Calculated electronic charge density in the metal-organic system $\text{Cu}_4\text{OCl}_6\text{daca}_4$ (from J. Mesot, PSI, p. 10)
Collection of microcantilevers on a silicon wafer (from J.-M. Triscone, UniGE, p. 153)

1 Summary

Strong correlations between electrons and their collective behavior combined with enhanced quantum fluctuations, particularly in materials with a low-dimensional crystal structure, are responsible for the most intriguing new states of matter and an immensely rich variety of unusual phenomena. Our search for novel materials and our study of their electronic properties and phases is motivated by fundamental questions as well as by the desire to find materials with new functionalities for future applications.

MaNEP – *Materials with Novel Electronic Properties* – is a **National Centre of Competence in Research**¹ (NCCR) based at the University of Geneva (home institution). Its activities comprise research in most active areas of condensed matter physics with internationally recognized groups in experiment and theory. Studied materials range from quantum spin systems, metallic systems with extraordinary superconducting, magnetic, spectral and transport properties, as well as artificial heterostructures of correlated electron materials to cold atoms in optical lattices and nano-carbon systems incorporating mesoscopic physics.

This report covers the period July 1, 2005 – March 31, 2008, thus nearly the three first years of the second phase of MaNEP. Since its establishment in 2001 MaNEP has grown and unites the main groups in Switzerland in its field with 30 senior members and about 260 researchers in total. At the beginning of the second phase the research structure was changed to six collaborative projects. During the three years of the second phase MaNEP has implemented this new research structure, effectively integrating the efforts between the different MaNEP laboratories. In January/February of each year we organize six one-day meetings, each dedicated to one of the six projects. At these meetings the results obtained so far are discussed in detail among the members of the projects. This report contains an overview of these results for each project.

¹The NCCR depend on and are supervised by the Swiss National Science Foundation.

Research

Project one focuses on the study of some of the key questions in condensed matter physics: the understanding of materials with strong spin and charge interactions. A wide range of phenomena has been studied in strongly interacting electron materials and low-dimensional and quantum fluctuation dominated systems. Examples are the observation of Bose-Einstein condensation and Luttinger liquid properties in quantum spin systems with spin multimer subunits, novel ground state properties in frustrated spin systems, unusual magnetic and metallic behavior in systems like Europium borides and transition metal silicides, charge density wave instabilities with the possible realization of an excitonic insulator, and novel properties of surfaces and interfaces, to mention a few. The report reflects the richness of

this field and covers the advances of experimental investigations and new theoretical concepts.

Project two focuses on the fascinating field of superconductivity. The quest for a microscopic understanding of high temperature superconductivity (HTS) in the cuprates remains a key question, and we report a number of striking results. Theoretical evidence was found that the ground state of a moderately hole-doped Hubbard insulator is a *d*-wave superconductor. This result implies an increase of the kinetic energy in the superconducting phase as other MaNEP researchers have observed in infrared spectroscopy measurements. Signatures of boson coupling to the conduction band has been obtained with several techniques and STS investigations have given a robust evidence that the dip-hump feature in the density of states is due to coupling to a collective mode like

the (π, π) spin wave resonance. Evidence for coupling to a continuum of bosonic excitations comes from infrared measurements and from the waterfall dispersion recently observed in ARPES. Our investigations also show a wealth of novel properties in other superconductors. Examples are noncentrosymmetric superconductors, heavy fermion d -wave superconductors, Chevrel phases, and organic superconductors.

Project three reflects a special attempt to stimulate crystal growth within MaNEP, coordinating the work of four laboratories at ETHZ, PSI, EPFL and UniGE. Indeed, the most intrinsic, and the most reliable information about a novel material is obtained from its single crystalline form, where the influence of defects, dislocations, impurities, and grain boundaries is minimized. During the three last years we report new crystal growth results on a large number of oxides, chalcogenides, silicides and other materials. Over 140 materials in single crystalline form are available for internal and external collaborations. The MaNEP *Single Crystal Catalog* is joined to the description of Project 3. With **Project four**, MaNEP started a particular effort to create synergies and collaborations between solid state chemists and solid state physicists, to arouse a search for new materials with strongly correlated behavior and in particular new superconductors. Several different routes towards new materials are reported including high pressure synthesis, a combinatorial approach, thin film methods, as well as nano structuring, and morphology control. In the first 2 1/2 years of this effort a number of new materials have been found and first investigations of their properties carried out.

Project five focuses on the use of thin epitaxial films and multilayers for basic and applied studies. Numerous important results have been obtained opening up the road towards future engineering of artificial materials exploring the unusual properties of oxide interfaces. A striking result is the observation of superconductivity at the interface between two insulators. Other results in this project cover thin film ferroelectrics, with the study of size effects and screening lengths; polaronic transport in

manganite thin films and the search for polaronic behavior of thin strontium titanate films; as well as the use of thin superconducting films for single photon detectors.

Project six develops applications resulting from MaNEP know-how. Following this idea we have established collaborations with 6 companies on specific questions of interest to these companies. This concerns applications of superconductivity with research on improved wires for high field applications, thin film superconducting fault current limiters and a contribution to the development of a self screened high field magnet for neutron scattering studies; sensors, with the search for a material for high precision ESR determination of weak magnetic fields and the development of novel gas sensors; thin film preparation and applications including the development of superlattices for neutron supermirrors in neutron guides and the preparation and study of ferroelectric thin films for novel devices.

Education, communication and technology transfer

MaNEP is also active in other domains than research. A doctoral school has been installed at the University of Geneva, summer and winterschools are regularly organized, as well as conferences in the field of MaNEP. The Physiscope in Geneva proposes a new and original approach to motivate high school students to get involved in science. The summer internship for women students has become a yearly event at nearly all Swiss universities and federal institutes of technologies.

A special attention is given to communication and knowledge and technology transfer. MaNEP contributes to several outreach events, with the idea of "making the most" out of every public relation opportunity. MaNEP research activities have a strong potential for applications. Collaborations with industrial corporations, such as ABB, Bruker BioSpin, Swiss Neutronics, Metrolab, Phasis and Mecsens are developed.

These activities are described in more details in the chapter *Three years of MaNEP's life*.

2 Members and institutions in MaNEP and contacts

This section provides an up-to-date summary of the organization of MaNEP, the Swiss National Centre of Competence in Research (NCCR) on Materials with Novel Electronic Properties. It comprises a network involving academic institutions and industrial partners. MaNEP started its activities on July 1, 2001.

Research groups (MaNEP Forum)

From academic institutions:

- Philipp Aebi, UniNE
- Dionys Baeriswyl, UniFR
- Christian Bernhard, UniFR
- Gianni Blatter, ETHZ
- Markus Büttiker, UniGE
- Leonardo Degiorgi, ETHZ
- Øystein Fischer, UniGE
- René Flükiger, UniGE
- László Forró, EPFL
- Thierry Giamarchi, UniGE
- Marco Grioni, EPFL
- Martin Hasler, EPFL
- Jürg Hulliger, UniBE
- Januz Karpinski, ETHZ
- Hugo Keller, PSI and UniZH
- Giorgio Margaritondo, EPFL
- Dirk van der Marel, UniGE
- Joël Mesot, PSI
- Frédéric Mila, EPFL
- Elvezio Morenzoni, PSI
- Alberto Morpurgo, UniGE
- Reinhard Nesper, ETHZ
- Hans-Rudolf Ott, ETHZ
- Patrycja Paruch, UniGE
- Christoph Renner, UniGE
- T. Maurice Rice, ETHZ
- Andreas Schilling, UniZH
- Louis Schlapbach, EMPA
- Manfred Sgrist, ETHZ

- Jean-Marc Triscone, UniGE
- Matthias Troyer, ETHZ
- Klaus Yvon, UniGE

From industrial partners:

- M. Abplanalp, ABB
- D. Eckert, Bruker BioSpin

Academic institutions members of MaNEP

- University of Geneva (UniGE), home institution
- University of Neuchâtel (UniNE)
- University of Fribourg (UniFR)
- University of Berne (UniBE)
- University of Zurich (UniZH)
- Federal Institute of Technology, Lausanne (EPFL)
- Federal Institute of Technology, Zurich (ETHZ)
- Paul Scherrer Institute (PSI)
- Materials Science and Technology Research Institute (Empa)

Industrial Partners

- ABB, Baden
- Bruker Biospin, Fällanden
- MecSens, Geneva
- Metrolab, Lausanne
- Phasis, Geneva
- SwissNeutronics, Villigen

Scientific Committee

- Øystein Fischer, UniGE, director
- László Forró, EPFL
- Jürg Hulliger, UniBE
- Christoph Renner, UniGe, deputy director
- Manfred Sigrist, ETHZ
- Jean-Marc Triscone, UniGE
- Dirk van der Marel, UniGE, deputy director

- Lidia Favre-Quattropani, scientific manager
- Sophie Griessen, management assistant
- Matthias Kuhn, knowledge and technology transfer
- Ivan Maggio-Aprile, computer and internet resources
- Gregory Manfrini, technical organization
- Anne Rougemont, communication, until April 2009

Management (UniGE)

- Øystein Fischer, director
- Dirk van der Marel, deputy director
- Christoph Renner, deputy director
- Marie Bagnoud, administrative manager, from December 2008
- Christophe Berthod, education and training
- Adriana Bonito Aleman, communication, from July 2009
- Isabelle Bretton, administrative manager, until September 2008
- Renald Cartoni, technical organization, until March 2009
- Pascal Cugni, accountant
- Michel Decroux, scientific manager, education and training, advancement of women

Advisory Board

- Dave Blank, University of Twente, Enschede, Netherlands
- Robert J. Cava, Princeton University, USA
- Antoine Georges, Ecole Polytechnique, Palaiseau, France
- Denis Jérôme, Université Paris-Sud, Orsay, France
- Piero Martinoli, Università della Svizzera Italiana, Lugano, Switzerland
- Andrew Millis, Columbia University, New York, USA
- George Sawatzky, University of British Columbia, Vancouver, Canada

Contacts

MaNEP
 Department of Condensed Matter Physics
 University of Geneva
 24, quai Ernest-Ansermet
 CH-1211 Geneva 4
 Switzerland

Phone: +41 22 379 30 13
 Fax: +41 22 379 35 89
 Homepage: www.manep.ch
 Email: manep@unige.ch

Prof. Ø. Fischer, director
 Phone: +41 22 379 62 70
 Email: oystein.fischer@unige.ch

Prof. D. van der Marel, deputy director
 Phone: +41 22 379 62 34
 Email: dirk.vandermarel@unige.ch

Prof. C. Renner, deputy director
 Phone: +41 22 379 35 44
 Email: christoph.renner@unige.ch

Marie Bagnoud, administrative manager
 Phone: +41 22 379 62 18
 Email: marie.bagnoud@unige.ch

3 Research

This section reports on the research performed in the six MaNEP projects for the period from July 1st 2005 to March 31st 2008.

The most important publications are outlined in the reference lists by a red mark.

Project 1 **Strongly interacting electrons, low-dimensional and quantum fluctuation dominated systems**

Project leader: M. Sigrist (ETHZ)

Participating members: D. Baeriswyl (UniFR), G. Blatter (ETHZ), M. Büttiker (UniGE), L. Degiorgi (ETHZ), L. Forró (EPFL), T. Giamarchi (UniGE), M. Gioni (EPFL), D. van der Marel (UniGE), J. Mesot (PSI), F. Mila (EPFL), H.R. Ott (ETHZ), T.M. Rice (ETHZ), L. Schlapbach (Empa), M. Sigrist (ETHZ), M. Troyer (ETHZ). Contribution from Ph. Aebi (UniNE) and Ø. Fischer (UniGE).

Introduction: Project 1 of MaNEP covers a wide range of materials and phenomena within the field of strongly correlated electron systems reaching also out to related subjects such as cold atoms in optical lattices and mesoscopic physics. The research effort is driven by materials showing novel phases and phenomena as well as by the development of new experimental techniques which provide access to parameter ranges unreachable so far. While applications of discovered phenomena and material properties are envisioned in the long-term, this project has its main focus on challenging problems in fundamental research of modern condensed matter physics.

Summary and highlights

During the whole period of MaNEP, magnetism has been one of the major subjects, including the localized electronic degrees of freedom of quantum spin systems as well as the subtle magnetic properties of various metallic systems, such as the heavy Fermion compounds, transition metal oxides, transition metal silicides etc. The studies on quantum spin systems lead through an arena of most unusual phases and dynamical properties. The lattice topology plays a decisive role here, e.g. when spin multimer subunits allow for the observation of Bose-Einstein condensation (TlCuCl_3), Luttinger liquid properties ($(\text{Hpip})_2\text{CuBr}_4$) and the remarkable coexistence of both classical and strongly quantum fluctuation dominated features. Frustration opens another door to striking ground state properties such as spin nematic order or spontaneous trimerization.

Various heavy Fermion systems have been in-

vestigated for their magnetic properties using spectroscopic methods such as NMR/NQR as well as newly developed photoemission and X-ray scattering methods which allow to probe aspects of the Kondo and mixed-valence physics of such materials. Unusual magnetic and metallic properties were also found in the giant magnetoresistance system $(\text{Eu,Ca})\text{B}_6$ and the class of transition metal silicides and their variants.

Cold atoms in optical lattices provide a highly flexible laboratory for various different correlated many body systems which have been investigated theoretically leading to interesting conceptual progress in the understanding of dynamical aspects in the context of Mott-insulator superfluid transitions, of correlation features of low-dimensional systems and the related dimensional crossover. Furthermore novel probing techniques suitable for the cold-atom setups are proposed.

An expanding area within Project 1 is the research on metals showing charge density wave

instabilities, which aims at exploring mechanisms alternative to the traditional Peierls instability. Exciting in this context is the possible realization of an excitonic insulator phase and the appearance of superconductivity associated with the CDW quantum phase transition in dichalcogenides.

The electronic properties at surfaces and interfaces are a further new subject (closely related to Project 5) which addresses the electronic reconstruction at interfaces between band and Mott-insulators due to correlation effect and spin splitting effects resulting from Rashba spin-orbit coupling at surfaces. A wide range of unusual phases is also targeted by numerous theoretical studies concentrating on non-magnetic ordered and quantum liquid phases, aspects of Mott-localization, the characterization of quantum phase transitions and phases exhibiting topological order. Moreover a theoretical analysis of so-called supersolid phases sheds new light on their realization in ^4He and antiferromagnetic systems. The experimental studies of the quasi-one-dimensional compounds BaVS_3 and BaVSe_3 at ambient and high pressure show unusual magnetic properties and non-Fermi-liquid behavior in connection with their metal-insulator transition.

1 Magnetism in quantum spin systems

Magnetism is one of the dominant topics within this project. In particular, quantum spin systems have been a very active area including field- and pressure-induced order in spin gap systems and the associated quantum critical behavior as well as the physics of spin systems containing spin multimer subunits which give rise to unusual interplay of “classical” order and features dominated by quantum fluctuation. Moreover, spin systems are also well suited to host novel exotic ordered phases. These subjects have been studied in a strong collaboration between experimental and theoretical groups, including the Laboratory for Neutron Scattering (LNS) around Mesot and Rønnow, Ott’s group and the theory groups of Mila and Troyer.

1.1 Field-induced quantum phase transitions

a) *Quantum statistics and quantum phase transitions in TlCuCl_3* The compound TlCuCl_3 represents a model system of dimerized quantum spins with strong interdimer interactions. After the discovery of a field-induced quantum phase transition and the related Bose-Einstein Condensate (BEC) of magnons, Mesot

and coworkers extended their activities to two other parameters, temperature and pressure, which both trigger interesting quantum behavior. The singlet-triplet dispersion was investigated as a function of temperature by inelastic neutron scattering (INS) experiments on single crystals (Fig. 1). By comparison with a number of theoretical approaches an appropriate quantum statistical model for dimer spin systems at finite temperatures was established, where many-body correlations become particularly important [1]. As a function of pressure, the amount of spin-singlet fluctuations in the materials can be controlled systematically through the pressure-dependence of the exchange interactions and a quantum critical point with tunable magnetic moment was demonstrated earlier [2]. High-resolution inelastic neutron scattering studies revealed the existence of novel elementary excitations, which are not present in a classical description of ordered magnets [2]. The results of systematic experimental and theoretical studies of quantum phase transitions in dimerized materials with main contributions by MaNEP were summarized in a comprehensive review article [3].

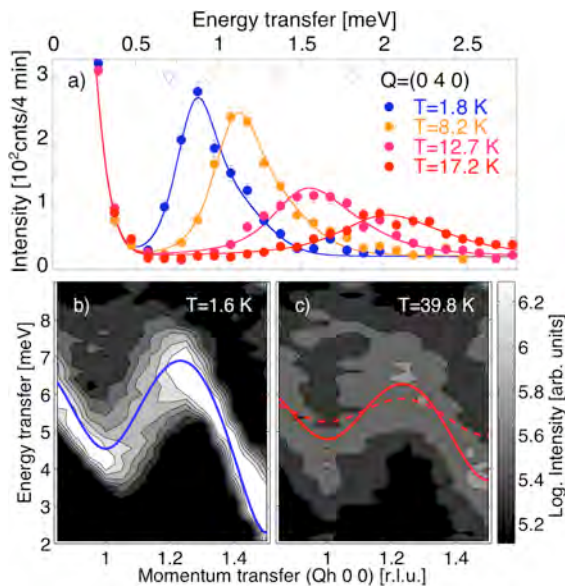


Figure 1: Temperature renormalization of the triplet excitations in TICuCl_3 (a) INS spectra. (b) and (c) INS intensity contour plots measured at 1.6 K and 39.8 K, compared with Bose-mean-field (dashed line) and Troyer-Tsunetsugu-Würtz-mean-field (solid line) theories.

b) *Fractionalized spin excitations in the spin-ladder $(\text{Hpip})_2\text{CuBr}_4$* The compound $(\text{Hpip})_2\text{CuBr}_4$ is the best representation to date of a $S=1/2$ spin ladder antiferromagnet with an energy scale ideally suited for a study of the complete phase diagram of such a spin system. In a series of neutron scattering experiments, the group of Mesot determined the spin Hamiltonian by measuring its excitations in the spin-liquid and the saturated phase. They collected striking evidence for the existence of fractionalized spin excitations in the Luttinger liquid phase of the ladder. The strong-coupling theory was shown to provide an excellent description of the continuous excitation spectrum in this phase. Pushing the experiments to the limits, the phase boundary of the 3D ordering transition below $T = 100$ mK could be determined. Its shape is unexpected and allows for a deeper insight into the limitations of the strong coupling theory.

c) *Transverse and random fields in the Ising ferromagnet $\text{LiHo}_x\text{Y}_{1-x}\text{F}_4$* The Ising ferromagnet LiHoF_4 in a transverse magnetic field undergoes a quantum phase transition, which should be accompanied by the softening to zero energy of the excitations. Using INS, Rønnow and coworkers discovered that the simple electronic mode softening is stalled by hyperfine coupling to the Ho nuclear spins, shifting the critical fluctuations to much lower-energy

mixed electronic-nuclear dynamics [4, 5]. This result feeds current theoretical efforts to assess the region over which a system can be considered quantum critical. Rønnow and collaborators made the counterintuitive prediction that the electronic subsystem actually comes closest to quantum criticality at an elevated temperature where the nuclear spins are thermally smeared, and proved this experimentally. During 2007, they performed a series of experiments on the dilution series $\text{LiHo}_x\text{Y}_{1-x}\text{F}_4$, which due to the dipole coupling becomes a realization of the random field Ising model [119]. The neutron measurements have provided the temperature-field-doping phase diagram, and discovered the ability to switch from ferromagnet to spin glass using respectively classical and quantum annealing protocols. In addition, LiErF_4 was established as a realization of dipole-coupled XY antiferromagnet with a quantum phase transition at 0.4 T and much stronger fluctuations than in LiHoF_4 [6].

d) *Dzyaloshinskii-Moriya (DM) interactions in frustrated magnets* In collaboration with the experimental group of Claude Berthier (Grenoble, France), Mila and coworkers have investigated the properties of the gapped spin-1/2 compound $\text{Cu}_2(\text{C}_5\text{H}_{12}\text{N}_2\text{D}_2)_2\text{Cl}_4$. NMR measurements have revealed the presence of a magnetic field-induced transverse staggered magnetization (TSM) which persists well below and above the field-induced 3D long-range magnetically ordered (FIMO) phase. The symmetry of this TSM is different from that of the TSM induced by the order parameter of the FIMO phase. An extensive Density Matrix Renormalization Group investigation of a spin ladder with intra-dimer Dzyaloshinskii-Moriya interactions was performed, and it was shown that the origin, field dependence, and symmetry of the TSM can be accounted for by this simple model.[7, 8]

This study shows that DM interactions can substantially modify the phase diagram of spin-1/2 Heisenberg ladders in a magnetic field provided they compete with exchange. For non-frustrated ladders, they induce a local magnetization along the DM vector that turns the gapless intermediate phase into an Ising phase with broken translational symmetry, while for frustrated ladders, they extend the Ising order of the half-integer plateau to the surrounding gapless phases of the purely Heisenberg case. Implications for experimental ladder and dimer systems have been discussed.[9]

1.2 Spin multimer systems

a) *Pressure tuned quantum phases in $\text{SrCu}_2(\text{BO}_3)_2$* The compound $\text{SrCu}_2(\text{BO}_3)_2$ is a realization of the Shastry-Sutherland model, which is of particular interest in the context of frustrated quantum magnetism, and has been proposed as physical realization of the theoretically conjectured possibility of a so-called super-solid quantum state. In a series of INS experiments, a reduction of the spin gap as a function of hydrostatic pressure was discovered. To overcome existing limitations in high pressure INS above ≈ 12 kbar, a new high pressure cell was developed and tested successfully up to 16 kbar at 1.5 K. The results indicate a possible quantum phase transition between two gapped phases. The existence of such a phase has been highly debated among theorist [120]. High pressure neutron diffraction data, resolved a new monoclinic structural phase above 50 kbar. Complementary high pressure μSR , ESR, specific heat and exact diagonalization is being pursued with MaNEP collaborators and samples were grown within MaNEP. As a side benefit, state-of-the-art high pressure expertise for neutron spectroscopy and diffraction is now available within MaNEP.

b) *Structure and magnetic excitations of the spin trimer system $\text{Ca}_3\text{Cu}_{3-x}\text{Ni}_x(\text{PO}_4)_4$* Attempting to observe the Bose-Einstein condensation in a quantum spin-trimer system the LNS group at PSI studied the linear trimer $\text{Ca}_3\text{Cu}_{3-x}\text{Ni}_x(\text{PO}_4)_4$ ($x = 0, 1, 2$) system (Cu-Cu-Cu or Cu-Cu-Ni or Ni-Cu-Ni). Determination of the crystal and magnetic structures by neutron powder diffraction [10] revealed that for $x = 1$ the middle position is occupied by Cu^{2+} , whereas the end positions are equally populated by Cu^{2+} and Ni^{2+} . For $x = 2$ the trimers are always of the type Ni-Cu-Ni. While the $x = 0$ and $x = 1$ compounds do not exhibit long-range magnetic ordering down to 1 K, the $x = 2$ compound shows antiferromagnetic ordering below $T_N = 20$ K with the propagation vector star $\mathbf{k} = \{(1/2, 1/2, 0), (-1/2, 1/2, 0)\}$ and magnetic moments of $1.89(1) \mu_B/\text{Ni}^{2+}$ and $0.62(2) \mu_B/\text{Cu}^{2+}$. The relevant trimer interactions are parametrized by means of INS [11] in terms of antiferromagnetic Heisenberg-type nearest-neighbor exchange ($J_{\text{Cu-Cu}} \approx -4.8$ meV for $x = 0, 1$ and $J_{\text{Cu-Ni}} = -0.85(10)$ meV for $x = 1, 2$) and axial anisotropy ($D_{\text{Ni}} = -0.7(1)$ meV for $x = 1, 2$), whereas next-nearest-neighbor exchange was found to be negligibly small.

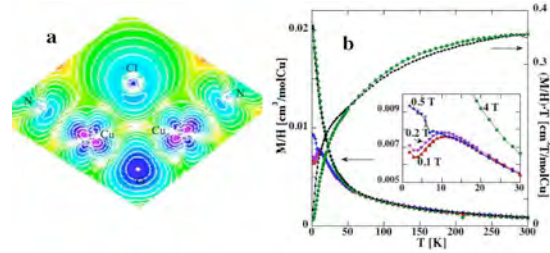


Figure 2: (a) Charge density distribution in $\text{Cu}_4\text{OCl}_6\text{daca}_4$ at $T = 80$ K. (b) Temperature dependence of dc-magnetization (M/H) of the single crystal (points) and powder (black line), and $(M/H) \cdot T$ measured at 0.1 T (right scale). Inset: zoomed 1.8 K–30 K temperature interval of M/H of the crystal.

c) *Magnetic exchange versus molecular vibrations in $\text{Cu}_4\text{OCl}_6\text{daca}_4$ tetrahedra* An isolated tetrahedral cluster of four Cu^{2+} ions is one of the simplest geometrically frustrated quantum spin units. Although being a spin singlet the residual degrees of freedom can lead to complex behavior in a lattice of these spin units. Mesot and collaborators studied a metal-organic $\text{Cu}_4\text{OCl}_6\text{daca}_4$ (daca=diallylcyanamide) system, where tetrahedral clusters are almost ideal and isolated. Extensive experimental characterization and *ab initio* density functional theory calculations of the electronic structure (Fig. 2) as well as *ab initio* molecular dynamics reveal a complex interplay between magnetic exchange, molecular vibrations and plasticity of the Cu^{2+} coordination sphere while cooling [12]. DFT calculations performed in this study show that the unpaired electron is only partially localized in the Cu *d*-states. It is transferred to the oxygen atom and is further delocalized around atomic cores within the molecule. The spin-vibrational Hamiltonian with the antiferromagnetic exchange $J = -1.8$ meV is the most appropriate model to describe the ideal $\text{Cu}_4\text{OCl}_6\text{daca}_4$ system. Studies of this and other cluster systems should promote convergence of theoretical methods for quantum chemistry, electron structure and magnetic models.

d) *Co-existence of order, classical and quantum excitations in the coupled spin tetrahedra of $\text{Cu}_2\text{Te}_2\text{O}_5\text{X}_2$* The materials $\text{Cu}_2\text{Te}_2\text{O}_5\text{X}_2$ ($\text{X}=\text{Cl}, \text{Br}$) are built of moderately coupled tetrahedral units. They represent a challenging example of a system where both, individual intra-tetrahedral cluster properties and collective inter-tetrahedral properties, could be tracked. The complex ground state has been determined by polarized and unpolarized neutron diffraction [13, 14] and the excitation spectrum has been studied by single crystal INS.

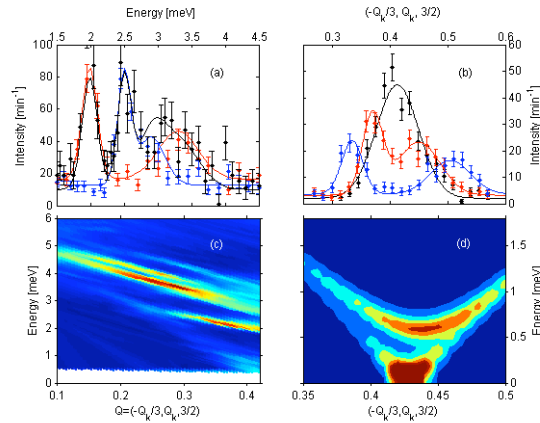


Figure 3: Summary of results on $\text{Cu}_2\text{Te}_2\text{O}_5\text{Cl}_2$. (a) A typical energy scan, showing existence of four gapped modes. (b) A very weak Goldstone mode revealed with the enhanced resolution of IN14, ILL. Experimental (c) and calculated (d) dispersion maps near the incommensurate reciprocal point $(-Q_x/3, Q_y, 3/2)$.

Despite magnetic order, only a fraction of the spectral weight of the excitation spectrum represent spin-waves, while the dominant part remains a gapped reminiscence of the tetrahedron quantum states (Fig. 3). This behavior is to our knowledge unique. Present theoretical discussions provide qualitative agreement but cannot reconcile the presence of order with a dominant gapped mode. A new theoretical framework is necessary to treat classical order and quantum fluctuations on equal footing.

e) $S = 1/2$ spin tubes The structural configuration of the compound $\text{Na}_2\text{V}_3\text{O}_7$ allows for the formation of spin tubes with 9 $S = 1/2$ degrees of freedom on rings which are coupled to form the spin tubes. The compound orders magnetically below 0.1 K. With a model calculation, Ott and collaborators attempted to reproduce the temperature and magnetic field dependencies of the specific heat at low temperatures (Fig. 4). A surprisingly good agreement was obtained by assuming the formation of spin dimers with a broad distribution of antiferromagnetic and, to a much lesser extent, ferromagnetic exchange couplings. The same model is also adequate to reproduce the temperature dependence of the magnetic susceptibility below room temperature. The data were interpreted as an indication that the system is close to a quantum critical point, particularly in low magnetic fields, which may be due to the rather complex exchange pattern among the sites carrying a spin.

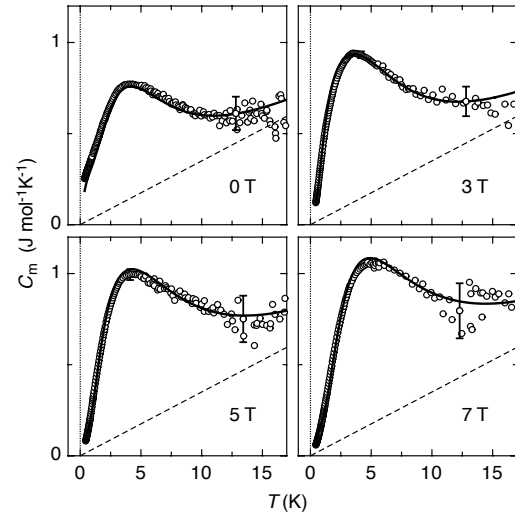


Figure 4: C_m as a function of T for $\text{Na}_2\text{V}_3\text{O}_7$ measured in different external magnetic fields. The solid lines represent the model calculation, including a contribution that is indicated by the broken lines.

1.3 Exotic order in quantum spin systems

a) *The Resonating Valence Bond phase of Quantum Dimer Models* Mila and collaborators have carried on a systematic and exhaustive investigation of the Quantum Dimer Model (QDM) on the triangular lattice. In order to understand the transition between the Resonating Valence Bond (RVB) phase and the so-called plaquette phase, they have developed a Green's function Quantum Monte Carlo approach to study the dynamical properties of the model [15, 16]. In particular, it was shown that soft modes develop upon reducing the dimer-dimer repulsion, indicating the presence of a second-order phase transition into an ordered phase with broken translational symmetry. Mila and coworkers have also shown that these soft modes are non-local, vortex like excitations ('visons') which condense at the transition. They have further investigated the nature of this ordered phase, for which a 12-site unit cell has been previously proposed, with the surprising result that significant Bragg peaks are only present at two of the three high-symmetry points consistent with this unit cell. The absence of a detectable peak was attributed to its small magnitude due to the nearly uniform internal structure of the 12-site crystal cell, which is interpreted as a local RVB structure. In parallel with the numerical simulations, a semi-classical approach to the problem was developed based on a Z_2 -gauge theory representation of the model, and on its dual Ising model, which reproduces all fea-

tures observed numerically and gives a simple and transparent picture of the underlying physics [17].

b) *Quadrupolar order in spin-1 Mott insulators*
 When the SU(2) symmetry is broken in the low-temperature phase of Mott insulators, it is usually due to the development of some kind of magnetic long-range order. This is not the only possibility however. If the order parameter is a higher order tensor, breaking the SU(2) symmetry will not lead to magnetic order. One of the simplest possibilities is quadrupolar order, which can be realized in $S > 1/2$ quantum magnets if the spins are locally in a state with a zero expectation value of the spin operators, as for instance the $S_z = 0$ state of a spin-1. Motivated by recent experiments on NiGa₂S₄ [121], Mila and coworkers have investigated the bilinear-biquadratic spin-1 model on the triangular lattice. Using mean-field theory, exact diagonalization, and SU(3) flavor theory, they have precisely mapped out the phase diagram of that model in a magnetic field [18], with emphasis on the quadrupolar phases and their excitations (Fig. 5). In particular, it was shown that ferroquadrupolar order can coexist with short-range helical magnetic order, and that the antiferroquadrupolar phase is characterized by a remarkable 2/3 magnetization plateau, in which one site per triangle retains quadrupolar order while the other two are polarized along the field. This leads to the conclusion that, in addition to the antiferroquadrupolar phase suggested previously, ferroquadrupolar order is a viable candidate to explain the properties of NiGa₂S₄.

c) *Spontaneous trimerization in frustrated spin chains*
 Simulations of highly frustrated magnets were also performed in a collaboration of Troyer's group with groups at UCSB. A spin nematic phase in two-dimensional frustrated

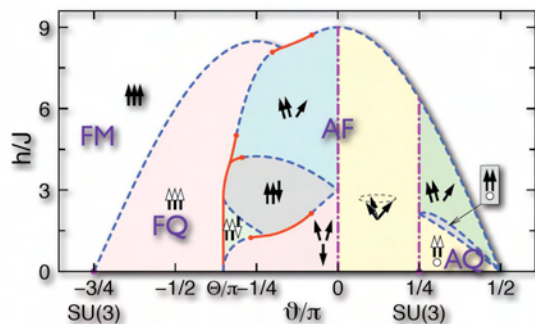


Figure 5: Phase diagram of the bilinear-biquadratic spin-1 Heisenberg model on the triangular lattice in a magnetic field.

magnets, partially breaking SU(2) symmetry was found in [19]. A spontaneous trimerization was found in a DMRG calculations of a spin-1 zig-zag chain with next nearest neighbor coupling [20], and the ordering of a spiral spin liquid in an order-by-disorder phenomenon on a frustrated diamond lattice antiferromagnets was investigated [21].

d) *S = 1 spin chains*
 Compounds with the chemical composition AVX₂O₆ with A= Li or Na, X = Si or Ge, contain structural subunits which may be regarded as spatially well separated chains of V ions. As a consequence of their ionic configuration, the latter carry a spin $S = 1$. The overall structural configuration implies that these spin chains are only weakly coupled and hence the system may be expected to exhibit a ground state with a well developed gap in the spin excitation spectrum, as predicted by Haldane. However, each of the four possible compounds orders antiferromagnetically at temperatures of the order of 20 K, as revealed by results of measurements of the magnetic susceptibility $\chi(T)$ and NMR probing either ⁷Li or ²³Na nuclei between 4 and 300 K. The analysis of the situation of weakly interacting $S = 1$ chains involved a modified random phase approximation which takes into account the results of quantum Monte Carlo (QMC) calculations. In this way, the ratio J_p/J as a function of T_N/T_{max} , where T_{max} denotes the temperature of the susceptibility maximum, was obtained from theory. The calculation implies that the Haldane-type ground state is adopted only if $J_p/J \leq 0.02$. For all the investigated compounds, J_p/J , as determined by the experimental values of T_N and T_{max} , turned out to exceed the critical value men-

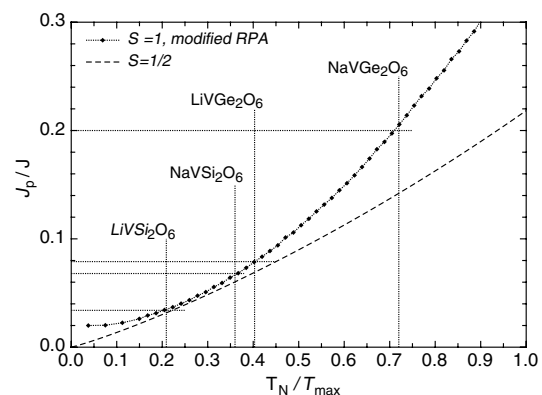


Figure 6: J_p/J as a function of T_N/T_{max} , resulting from the modified RPA approximation. The value of T_N/T_{max} for the AVX₂O₆ compounds are indicated. The dashed line represents $J_p/J(T_N/T_{max})$ for weakly interacting spin $S = 1/2$ chains.

tioned above (Fig. 6). A comparison of $\chi(T)$ as calculated with QMC techniques with experimental data indicated that a more realistic treatment of the situation would require the inclusion of an additional term in the Hamiltonian which describes the single-ion magnetic anisotropy. This would also be a natural choice for explaining the formation of a gap in the excitation spectrum of the ordered phase (not to be confused with the Haldane gap) that is revealed by the temperature dependencies of the NMR spin-lattice relaxation rates below T_N obtained in Ott's group [22, 23, 24] and [122].

e) *Optical properties of $KCuF_3$* The perovskite $KCuF_3$ is presumably one of the best realizations of an ideal 1D antiferromagnetic Heisenberg chain. This effective magnetic dimensionality is a direct consequence of the orbital ordering in this compound, which leads to strong antiferromagnetic exchange $J = 190$ K within the chain (along the c -axis) and a weak ferromagnetic coupling $J' = 0.01 \cdot J$ between the chains, which is responsible for the 3D-antiferromagnetic ordering at the Néel temperature $T_N = 39$ K.

Recent results of resonant X-ray scattering studies had shown a considerable change in the orbital ordering parameter at a temperature of 43 K, close to but well distinguishable from the antiferromagnetic ordering at the Néel temperature $T_N = 39$ K. Using optical spectroscopy van der Marel's group could identify the local orbital excitations which become observable due to their coupling to lattice vibrations, thus forming a vibronic state that allows for the appearance of electric dipole transitions. These local $d-d$ transitions represent a sensitive means to probe change in the local symmetry and, hence, should reflect

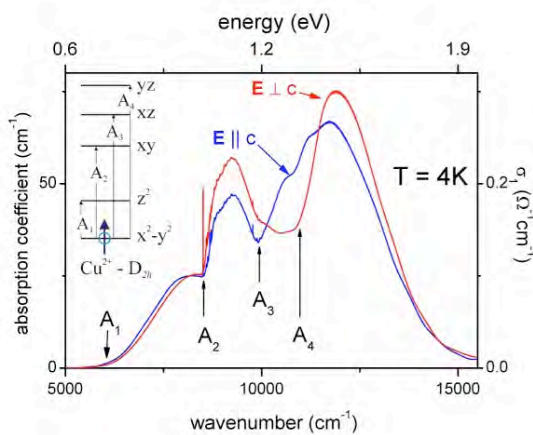


Figure 7: Optical spectra of $KCuF_3$.

the reported changes in orbital ordering. Indeed, upon cooling below 43 K the emergence of very sharp optical absorption features related to these local orbital excitations was observed (Fig. 7). The appearance of these transitions evidences a symmetry breaking at $T = 43$ K, which makes these excitation optically allowed. This structural change can be seen as a precursor for the antiferromagnetic ordering that locks in at 39 K and might be a generic feature of orbitally ordered antiferromagnetic systems, as indicated by similar changes in the orbital order parameter in manganite system like $LaMnO_3$ or $La_{0.5}Sr_{1.5}MnO_4$.

f) *Entanglement and quantum spin dynamics on the square lattice of $Cu(DCOO)_2 \cdot 4D_2O$* An intriguing example of coexistence of magnetic order and excitations of a purely quantum nature was found in $Cu(DCOO)_2 \cdot 4D_2O$ (CFTD), which is an excellent realization of one of the central quantum many-body Hamiltonians, namely the $S = 1/2$ Heisenberg antiferromagnet on a square lattice. In addition to fundamental theoretical interest, this model describes the undoped parent compounds of the high temperature superconductors. The polarized and unpolarized neutron studies by Rønnow and collaborators [25] of the transverse (one-magnon) and longitudinal (two-magnon) spin dynamics show that long-wavelength excited states are well-described by classical spin-wave theory. However, at short wavelengths, a dramatic quantum effect was discovered, centered on the $(\pi, 0)$ point (Fig. 8). Comparisons with numerical stud-

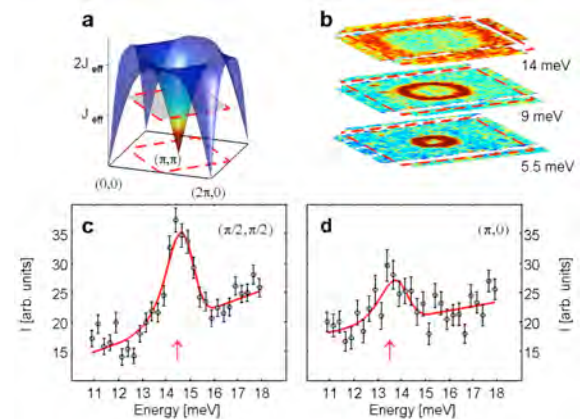


Figure 8: (a) Classically expected spin-wave dispersion surface of the 2D Heisenberg antiferromagnet. (b) Constant energy slices (shaded plane in (a)) through the measured excitation spectrum. (c)-(d) Energy cuts at the high-symmetry positions on the Brillouin zone boundary, revealing a 50% reduction of spectral weight at the special $(\pi, 0)$ point.

ies, which fit the short-wavelength anomalies, and analytical theories, which are in qualitative agreement, indicate that although the system displays classical order, singlet correlations play a key role in the short wavelength physics. This would imply an experimental observation of the resonating valence bonds that a group of leading theorist argue responsible for high-temperature superconductivity.

2 Spectroscopy of heavy Fermion and mixed-valence $4f$ -electron systems

The present understanding of heavy Fermion systems, inter-metallic compounds containing ions with partially filled f -shells, is based on the lattice version of the Kondo or Anderson model. The complexity incorporated in these apparently simple models is reflected in the large body of different low-energy physics encountered in the numerous known compounds. Within MaNEP this area has mainly been tackled by spectroscopic methods, such as NMR and NQR in Ott's group to explore unusual cooperative magnetic properties. A deeper understanding of the Kondo physics in such materials can be obtained from the newly developed hard-X-ray photoemission spectroscopy (HAXPES) and from high-resolution X-ray absorption spectroscopy pursued by Griener and collaborators. Moreover, we report here also on developments with resonant inelastic X-ray scattering (RIXS) on the charge transfer insulator NiO as it is in method and aim related. Several of the reported studies have only become possible due to the extensive development of measurement techniques at high-pressure and low-temperature within the MaNEP activity.

2.1 Low-temperature magnetic properties of PrCu_2

The Van Vleck paramagnet PrCu_2 is characterized by a cooperative Jahn-Teller transition at 7.6 K, induced by the interaction between the Pr^{3+} quadrupole moments [123]. The energies of the $4f$ -electrons singlets split by the crystal electric field are shifted at the transition and the structure changes from orthorhombic to monoclinic [124]. Consistent with the persisting Van Vleck-type paramagnetism, no anomaly is observed in the magnetic susceptibility down to 2 K [125, 126].

An antiferromagnetic order of the Pr magnetic moments was claimed to be indicated by a recent muon-spin-resonance (μSR) experiment [127]. Since this result is quite unexpected, Ott

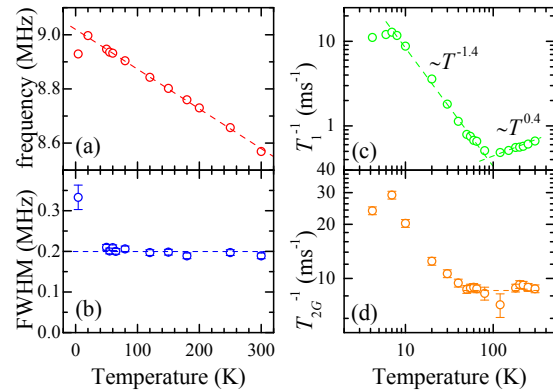


Figure 9: Left: ^{63}Cu NQR frequency (a) and line-width (b), as extracted from the NQR spectra and spin. Right: spin lattice (c) and spin-spin (d) ^{63}Cu NQR relaxation rates.

and collaborators decided to check it by means of NMR/NQR measurements [26].

The measured powder Cu-NMR spectra obtained between 300 K and 10 K show no anomaly around 65 K, contrary to expectations triggered by the μSR result. Because of the complexity of the NMR spectra, it was not possible to extract all the microscopic parameters characterizing the electric field gradient and the hyperfine coupling. Therefore NQR measurements were carried out in the range between 4 and 300 K. Also these data show no signature of a magnetic order at 65 K. Neither the NQR frequency (Fig. 9a) nor the NQR line-width (Fig. 9b) show any feature at 65 K. It is expected that the onset of an internal magnetic field would induce a shift of the line position or at least cause a broadening. Magnetic order is also expected to result in a freezing of the nuclear spin dynamics, contrary to what is observed in the spin-lattice (Fig. 9c) and spin-spin (Fig. 9d) relaxation rates, which are strongly enhanced below 80–60 K.

On the basis of the obtained data and of an *ab initio* calculation of the electronic structure of PrCu_2 [26], Ott and coworkers suggest an explanation of the observed discrepancy between NMR/NQR and μSR . The interpretation is that slow electronic spin fluctuations on the time-scale of $1 \mu\text{s}$ are present in PrCu_2 and are averaged to zero in NMR/NQR experiments, whereas they are strongly enhanced by the implanted muon and detected as a static internal field in μSR .

2.2 Pressure induced variation of the ground state of CeAl_3

Since 1975, CeAl_3 is known as the prototype compound of a heavy electron system with

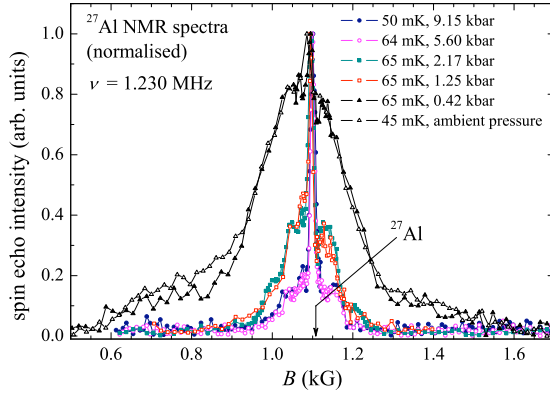


Figure 10: ^{27}Al -NMR spectra at various pressures recorded at low temperatures.

a strongly enhanced effective charge carrier mass [128]. Although the material has been investigated with many techniques, measurements probing microscopic properties under pressure have not been made so far. Previous microscopic investigations were done at ambient pressure and suggested an inhomogeneous ground state made up of two different phases [129, 130]; one of them exhibiting quasi static magnetic correlations, leading to a distribution of local magnetic fields at the Al sites, and a second, paramagnetic phase. The recent ^{27}Al -NMR study under pressure done in Ott's group and at very low temperatures, done under very demanding experimental conditions, provided evidence that CeAl_3 is driven away from a magnetic instability by the application of pressure [27, 28].

In Fig. 10, ^{27}Al -NMR spectra at various pressures recorded at low temperatures are shown. At ambient pressure, these results confirm the quoted earlier measurements, where a broad background signal was observed in the NMR spectrum, reflecting the magnetically correlated phase. The superimposed narrower line was interpreted to originate from nuclei in the paramagnetic phase. From the raw data recorded under pressure it is evident that dramatic changes are induced already by modest pressures of approximately 1 kbar. The NMR spectrum narrows considerably and can be reproduced by simulations of ^{27}Al -NMR spectra showing that the ground state is homogenous for pressures exceeding 1.25 kbar.

In addition, the spin lattice relaxation rate (SLRR) was measured for pressures exceeding 1.25 kbar. Most obvious is the significant reduction of $(T_1 T)^{-1}(T)$ with increasing pressure by almost 2 orders of magnitude in the covered pressure range. This signals a diminishing density of electronic states at the Fermi energy and is in qualitative agreement with the

pressure induced reduction of the Knight shift components that results from the analysis of the ^{27}Al -NMR spectra. Below 1 K, the temperature variation of $(T_1 T)^{-1}(T)$ is weak for non zero pressures. Considering the spectra in Fig. 10 and the $T_1^{-1}(T)$ data, it may be concluded that the pressure-induced single phase does not order magnetically above 50 mK.

In CeAl_3 , the inhomogeneous ground state is quenched by the application of moderate pressures. The so-called correlated phase, reflected in the broad part of the low-pressure Al-NMR spectra, vanishes upon increasing external pressure between 0.42 and 1.25 kbar. The remaining phase is modified in the sense that, with increasing pressure, $D(E_F)$ is considerably reduced, as reflected in the SLRR and in the Knight shift. This is consistent with the pressure dependence of macroscopic quantities such as the specific heat or the electrical resistivity. The observations imply that the inhomogeneous ground state at ambient pressure is indeed an intrinsic property of CeAl_3 and that the broad line, previously attributed to a magnetically correlated phase, is not simply an artifact.

2.3 Tuning the antiferromagnetic transition in CePd_2In

The heavy electron system CePd_2In is known to order antiferromagnetically below 1.23 K [131, 132]. In magnetically ordering heavy electron compounds, this transition is usually the result of a competition between Kondo screening and RKKY coupling including both the localized Ce^{3+} 4f electrons and the conduction electrons. Changing the lattice parameters is expected to change also the balance between those two interactions and therefore influence the antiferromagnetic transition. In Fig. 11, NQR spectra recorded at $p = 7.5$ kbar are shown. From the splitting of the resonance line below T_N and also from the analysis of SLRR, it is evident that the transition temperature is enhanced by the application of external pressure [29]. It is concluded that the antiferromagnetically ordered ground state is not quenched by the application of pressure, at least not in the available pressure range of $0 < p < 14.6$ kbar. While the Doniach Kondo necklace model would predict a reduction of T_N with increasing pressure, CePd_2In is not the only compound with an opposite behavior. The increase of the Néel temperature T_N with increasing pressure signals a gain of strength of the RKKY interaction (which favors the antiferromagnetic order) with respect to the Kondo

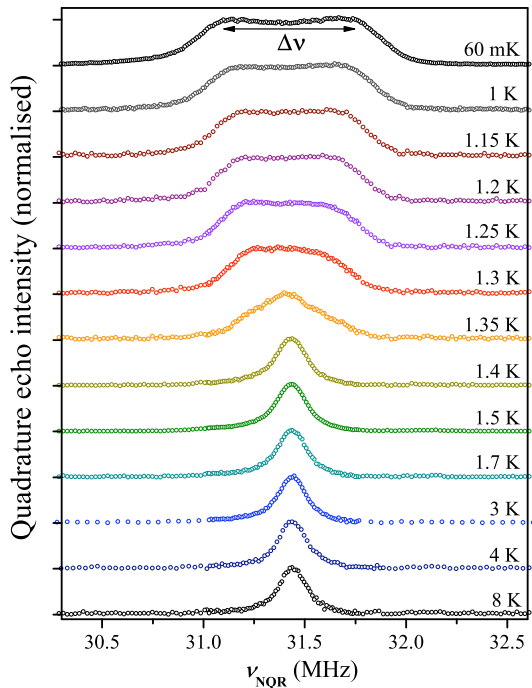


Figure 11: ^{115}In NQR spectra recorded at $p = 7.5$ kbar for various temperatures.

screening in this pressure range. Inspecting the NQR spectra and the spin lattice relaxation rate, Ott and collaborators concluded that the arrangement of the moments in the magnetically ordered phase is not affected by these pressures.

2.4 HAXPES and RIXS of strongly correlated electron systems

a) *Hard X-ray photoemission* Conventional photoemission (PES) and ARPES in the UV or soft X-ray range are intrinsically surface-sensitive probes, due to the short photoelectron escape depth (2-10 Å). While this is a valuable feature in surface science studies, problems may arise when comparing photoemission and bulk-sensitive transport or thermodynamic probes, especially in strongly correlated materials. This limitation can be partially overcome by increasing the excitation energy, since the escape depth of the photoelectrons increases with their kinetic energy. Probing depths of 50–100 Å for valence band states can be achieved with photons of 6–10 keV, but extremely bright X-ray sources are required to compensate the dramatic reduction of the photoemission cross section compared to the UV experiments. Grioni's group has performed hard X-ray photoemission (HAXPES) measurements of metallic Yb-based intermediate valence compounds, with the dedicated VolPE

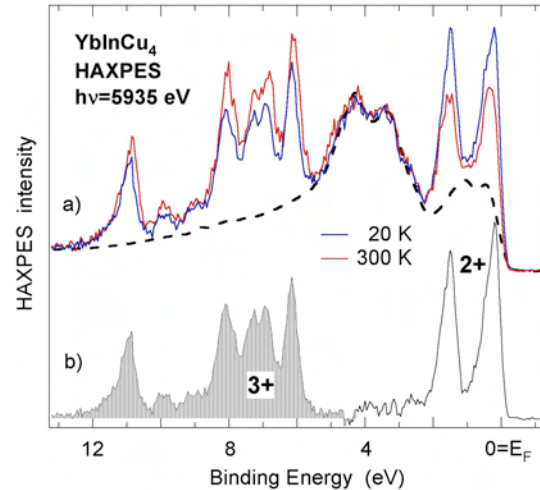


Figure 12: a) HAXPES spectra of the Kondo system YbInCu_4 at two temperatures. The dashed line is the spectrum of LuInCu_4 after removal of an atomic-like $4f$ doublet. The Yb $4f$ spectral function at 20 K, obtained by subtracting the LuInCu_4 signal is shown in b).

spectrometer at beamline ID16 of the ESRF (Grenoble). An interpretation of UV photoemission data in these strongly correlated materials is notoriously problematic because the strength of the interactions is heavily renormalized at the surface. The HAXPES data, which are not contaminated by an overlapping surface signal, yield a direct view of the $4f$ states in these systems, and enable a more reliable determination of the relative weight of the Yb^{3+} and Yb^{2+} configurations in the mixed ground state (Fig. 12) [30]. The spectra clearly reveal the characteristic many-body Kondo resonance and its spin-orbit satellite near the Fermi level. Moreover, a comparison of the sister Lu-substituted compounds, with a core-like filled $4f$ shell, yields an accurate determination of the bulk Yb $4f$ spectral function. These results are important because they unambiguously demonstrate that spectral weight is progressively transferred with increasing temperature from the Kondo resonance to the Yb^{3+} manifold. This provides a clear spectroscopic confirmation of the thermal depopulation of the singlet ground state occurring over the Kondo temperature scale, predicted by the Anderson impurity model [133].

b) *High-resolution XAS under pressure* Truly bulk-sensitive spectroscopic information can be obtained in photon in – photon out measurements, namely by X-ray absorption (XAS) in the fluorescence detection mode, and resonant X-ray scattering (RIXS). Due to their resonant character, these spectroscopical techniques

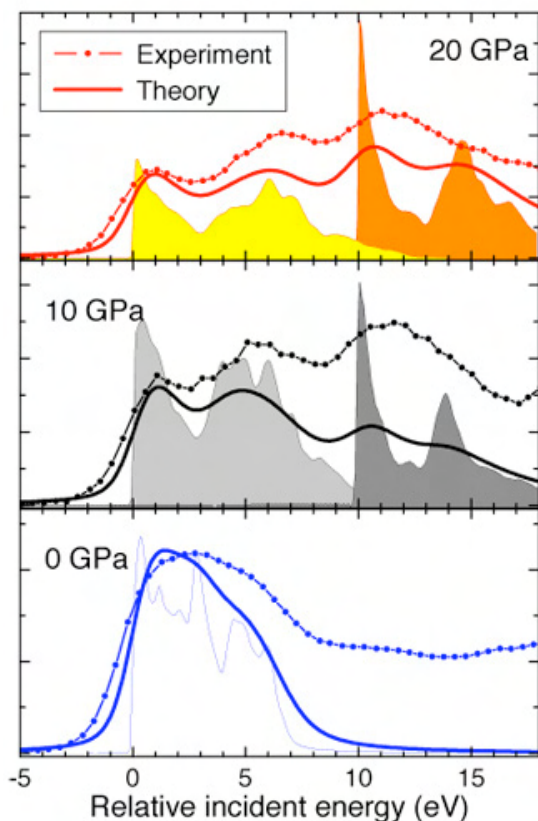


Figure 13: Experimental (dots) and calculated (solid lines) PFY-XAS spectra of metallic Yb at various pressures. The shaded areas under the 10 GPa and 20 GPa curves are the calculated Yb(2+) and Yb(3+) contributions.

provide both chemically and orbitally selective information. The large (1000–10000 Å) penetration depth of the hard X-ray photons is compatible with experiments under pressure in specially designed diamond cells. Grioni's group has utilized Yb L_3 ($2p \rightarrow 5d$) absorption spectroscopy to determine the pressure dependence of the Yb valence in metallic Yb [31]. Yb is divalent ($4f^{14}$) at ambient conditions, but pressure is known to favor the smaller Yb^{3+} ($4f^{13}$) ion. This partial delocalization of the $4f$ states is reflected in changes of the unoccupied conduction band, which is probed by XAS. In the experiment, the large spectral broadening (several eV's) of conventional XAS, a consequence of the short lifetime of the deep Yb $2p$ core hole, was effectively removed by selecting a well-defined radiative channel (the $3d \rightarrow 2p$ $L\alpha$ emission) in the high-resolution partial fluorescence yield (PFY) mode. The dramatic change of the measured XAS line shape, which evolves with pressure towards that of an intermediate valence compound, illustrates the progressive increase of the Yb valence with pressure, from 2 to 2.55 at 20 Gpa (Fig. 13). These

changes can be reproduced by a theory based on pressure-dependent first-principle supercell calculations of the density of states within the Falicov-Kimball model, including a complete solution of the dynamical screening of the Yb core hole.

c) *Resonant inelastic X-ray scattering* Resonant inelastic X-ray scattering (RIXS), also known as resonant X-ray Raman spectroscopy, is a second-order optical process where the resonant excitation of a core state is followed by a radiative decay. RIXS has the typical chemical selectivity of a core spectroscopy, with two distinct advantages: i) its energy resolution is not intrinsically limited by lifetime broadening effects, and ii) the final states are not restricted to those accessible via dipole transitions as in XAS. RIXS is therefore a powerful probe of neutral single-particle and collective excitations in solids. Grioni's group, in collaboration with a group from Milano, has performed a benchmark high-resolution RIXS experiment on NiO, a prototypical strongly correlated material [32]. The measurements were performed through the Ni $M_{2,3}$ ($3p \rightarrow 3d$; $h\nu = 67$ eV) absorption edge, at beam line SIS of the Swiss Light Source (SLS). With an experimental resolution $\Delta E = 130$ meV several low-energy losses could be identified in the RIXS spectra. They are assigned to the excited states of the Ni d^8 configuration in an octahedral environment, for a crystal field parameter $10 Dq = 1$ eV, in agreement with independent estimates. A closer analysis shows that these spectral features are actually split by the interatomic exchange in antiferromagnetic NiO. A line shape analysis allows the exchange energy to be estimated at 125 ± 15 meV, in agreement with measurements of the spin wave dispersion by neutrons. The shallowest excitations, at that energy scale, are masked by the prominent elastic peak in the $M_{2,3}$ edge data, but not in high-resolution Ni $L_{2,3}$ ($3p \rightarrow 3d$) spectra, measured more recently by Grioni and collaborators at the dedicated soft X-ray RIXS spectrometer ADDRESS of the SLS (Fig. 14). The new data give the first direct evidence by RIXS of the dispersion of the magnon losses. These results confirm that RIXS in the soft X-ray domain yields momentum-dependent bulk-sensitive information on the electronic structure of strongly correlated materials, including insulators, complementary to ARPES, optics, and neutrons.

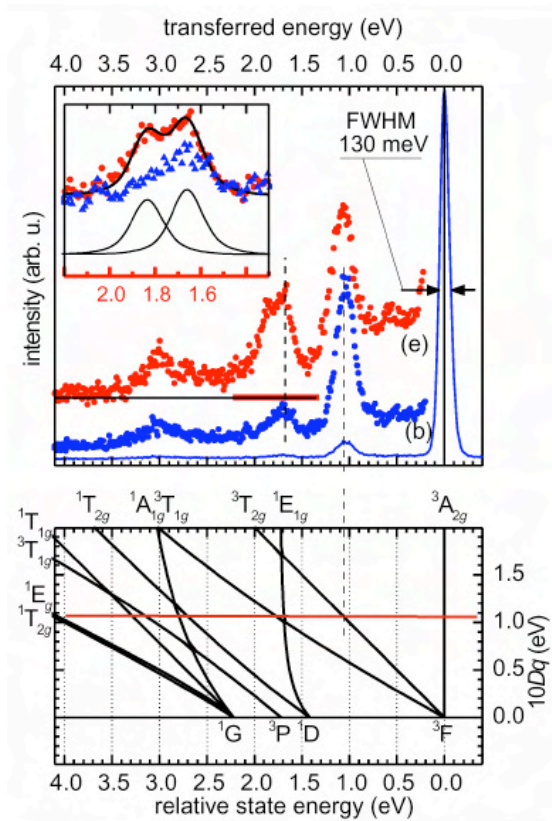


Figure 14: (Top) High-resolution RIXS spectra at two excitation energies through the Ni $M_{2,3}$ absorption edge. The energy splitting of the ${}^3T_{2g}$ state induced by the exchange field is highlighted in the inset. The crystal field excited states can be easily assigned by comparison with the Tanabe-Sugano diagram (bottom).

3 Magnetic metals and metamagnetic transitions

In this subproject, several spectroscopic and theoretical studies on the magnetic behavior and the influence of magnetism on transport properties in metals have been performed. Materials of special interest here include systems showing giant magnetoresistance effects such as $(\text{Eu,Ca})\text{B}_6$ studied in Degiorgi's and Ott's teams and compounds like FeSi or FeSb₂ and their relatives investigated by van der Marel and coworkers, which as narrow-gap semiconductors may be close to magnetic instabilities leading to metal-insulator transition. Moreover the nature of the low-temperature phases associated with metamagnetic transitions, as observed in the ruthenate bilayer compound $\text{Sr}_3\text{Ru}_2\text{O}_7$, are studied theoretically by Rice, Sigrist and collaborators. A motivation for some of these studies lies naturally in the possible applications of magnetoresistance effects as well as the close connection with spintronics.

3.1 Magneto-optical investigations of giant magneto-resistive materials

Because of the potential technological applications, materials exhibiting colossal magnetoresistive (CMR) effects are of high current interest in solid state physics. Europium hexaboride (EuB_6) and the well known manganites (discussed in the section on transition metal oxides), for which the onset of ferromagnetism is accompanied by a dramatic reduction of the electrical resistivity, are primary examples, that have intensively been studied.

a) $\text{Eu}_{1-x}\text{Ca}_x\text{B}_6$ The team of Degiorgi and Ott has first concentrated on the series of cubic $\text{Eu}_{1-x}\text{Ca}_x\text{B}_6$, which displays interesting correlations between magnetic, transport and optical properties. The high temperature electronic transport of EuB_6 , a ferromagnet (FM) below $T_C \sim 12$ K, relies on a small effective electron density. The magnetic properties are dominated by the half-filled $4f$ shell of divalent Eu, which accounts for the measured magnetic moment of $7\mu_B$ per formula-unit. The strong coupling of transport properties to the magnetization was revealed by measurements of the magneto-optical properties, which unveiled a substantial blue shift of the plasma edge in the optical reflectivity with decreasing temperature and increasing magnetic field. These remarkable results correlate with the precipitous drop in the dc resistivity just below T_C , and the large negative magnetoresistance observed near T_C . The intimate relation between magnetization and electronic conductivity also emerged from experiments on the $\text{Eu}_{1-x}\text{Ca}_x\text{B}_6$ series. The Ca-substitution leads to significant changes of the magnetic and electronic properties. The FM transition temperature decreases with increasing Ca content and stoichiometric CaB_6 exhibits no magnetic order.

A theoretical approach to explain the behavior of EuB_6 , as well as offering specific predictions for the electronic properties of the $\text{Eu}_{1-x}\text{Ca}_x\text{B}_6$ series, is based on a double-exchange scenario. This scenario may be regarded as an effective theory for the Kondo lattice problem in the limit of a very small number of carriers. The reduced itinerant carrier concentration places the Fermi level near a magnetization dependent mobility edge, which emerges in the spectral density because of the disordered spin background and/or Ca-doping. A FM metal to insulator crossover is expected as a function of the position of the Fermi level with respect to the mobility edge, which can be tuned by the Ca-content [33].

The goal of this work was to present and ana-

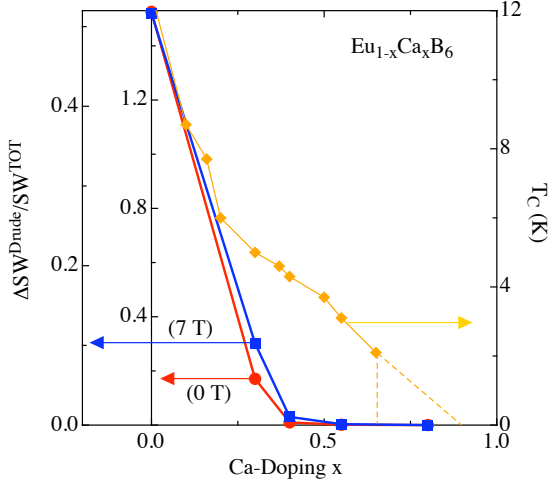


Figure 15: Dependence of the Curie temperature, T_C , on Ca-doping, compared to $\Delta SW^{Drude}/SW^{TOT}$, the change of the spectral weight in the Drude component, normalized by the total spectral weight (at 0 or 7 T) encountered in $\sigma_1(\omega)$ up to about 1 eV. The dashed lines for $T_C(x)$ above $x \sim 0.7$ schematically define the interval of T and Ca-content, where a cluster spin glass phase was established.

lyze the measured magneto-optical data of the $\text{Eu}_{1-x}\text{Ca}_x\text{B}_6$ series. Replacing Eu by Ca has direct consequences on the electrodynamic response. It influences the distribution of the spectral weight between the metallic (Drude) component and excitations at non-zero energy in the absorption spectrum for different Ca-contents at different temperatures and magnetic fields. Fig. 15 displays the variation of the normalized Drude spectral weight (i.e. $\Delta SW^{Drude}/SW^{TOT}$) as a function of x , in comparison with the variation of T_C for the $\text{Eu}_{1-x}\text{Ca}_x\text{B}_6$ series. The ranges on the vertical axes were chosen such that $T_C(x = 0)$ coincides with the renormalized changes of the Drude spectral weight, inserting SW^{TOT} for either 0 or 7 T. For both values of SW^{TOT} , Degiorgi and collaborators obtain the same type of variation with x . ΔSW^{Drude} decreases sharply between $x = 0$ and 0.3, reaching zero at approximately 50% Ca-content. The x -dependence of ΔSW^{Drude} reveals the reduction of the maximum of itinerant charge carriers with increasing x in $\text{Eu}_{1-x}\text{Ca}_x\text{B}_6$, previously indicated by results of resistivity Hall effect and optical response measurements. The behavior of $\Delta SW^{Drude}/SW^{TOT}(x)$ mimics indeed the crossover from a metallic ferromagnet (for $x < 0.4$) to a ferromagnetic Anderson insulator for higher Ca concentration. These magneto-optical investigations on the $\text{Eu}_{1-x}\text{Ca}_x\text{B}_6$ series provide therefore support for the phase diagram that emerges from the double-exchange

model predictions.

b) EuIn_2P_2 Degiorgi's and Ott's groups have extended their study to the compound EuIn_2P_2 , which belongs to the broad class of materials known as Zintl compounds. The Zintl concept for the formation of compensated-valence inter-metallic compounds is based on a complete charge transfer from an alkali or alkaline-earth element to a post-transition element of the groups 13 (IIIA) or 15 (VA) in the periodic table. The concept was later extended to synthesize more complicated inter-metallic compounds with new types of structures and a variety of physical properties, such as magnetic order and superconductivity. Concerning magnetism, Zintl-phase compounds with rare-earth elements as one of the regular constituents were investigated. For EuIn_2P_2 , the magnetic order involves the local moments of the partially occupied Eu 4*f*-electron orbitals and is thought to be induced by common exchange interactions. In the latter case, the onset of magnetic order is accompanied by a considerable reduction of the electrical resistance in the ordered state and related magnetoresistance effects upon the application of external magnetic fields. In view of similar observations in previous studies of materials, such as the perovskites LVO_3 ($L = \text{La, Lu}$ and Y), EuO and EuB_6 , and the discovery of giant magneto-optical effects, at least in EuB_6 (see above), it seemed of interest to probe the optical properties of EuIn_2P_2 in a wide spectral range and, in addition, their variation with temperature and external magnetic field [34]. Fig. 16 displays the measured reflectivity $R(\omega)$ as a function of temperature (panel (a)), and as a function of magnetic field at 10 and 30 K (panels (b) and (c)), respectively. The main panels of Fig. 16 emphasize the far-infrared (FIR) range, where the temperature and magnetic field dependences are significant. Above 50 K, the magnetic field dependence is negligible. The inset of Fig. 16a displays $R(\omega)$ across the entire measured spectral range at room temperature. It exhibits a metallic component with a plasma edge at very low frequencies ($\omega \leq 250 \text{ cm}^{-1}$), a strong infrared active phonon mode, peaking at 270 cm^{-1} with a shoulder on its high frequency tail, a broad excitation centered at 600 cm^{-1} and several absorptions above 1000 cm^{-1} . The strong absorption centered at 600 cm^{-1} bears a striking similarity with what has been often observed in heavy-electron or Kondo materials and was ascribed to excitations across the hybridization gap (HG). For each combination

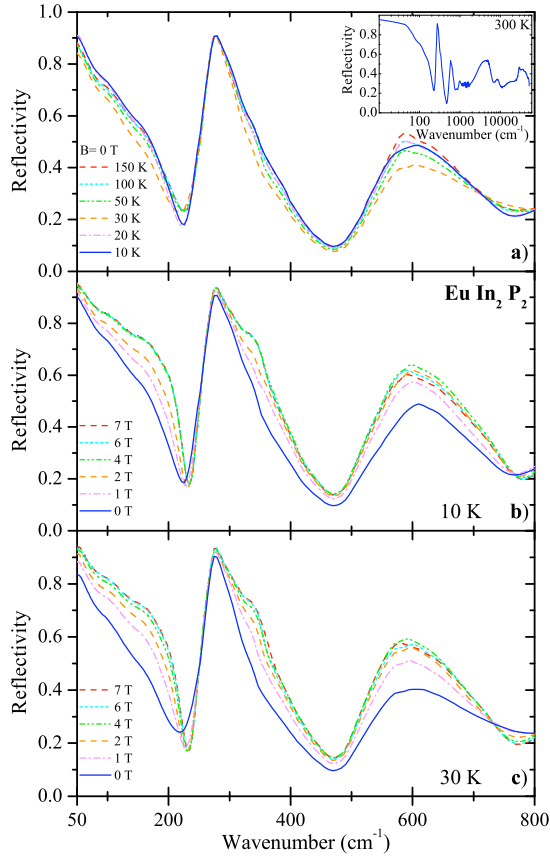


Figure 16: Reflectivity spectra $R(\omega)$ of EuIn_2P_2 in the infrared spectral range as a function of temperature at $B = 0$ T (a). Panels (b) and (c) show $R(\omega)$ at 10 and 30 K, and in magnetic fields between 0 T and 7 T, respectively. The inset in panel (a) displays $R(\omega)$ at 300 K in the whole measured spectral range (logarithmic energy scale).

of temperature and magnetic field the high-frequency parts of all spectra merge. Remarkable is the extremely low plasma edge which suggests that EuIn_2P_2 is a system with a low itinerant charge-carrier density. The reflectivity is significantly influenced by magnetic field (Fig. 16b and 16c), much less, however, by temperature (Fig. 16a).

The decomposition of the optical properties into their characteristic components (i.e. metallic component, HG, phonon and interband transitions) also provides the basis for discussing the distribution of the spectral weight (S) in the absorption spectrum. The spectra were described within the phenomenological Lorentz-Drude approach, ascribing the Drude term to the metallic component and a selection of Lorentz harmonic oscillators (HO) to the finite frequency excitations. Fig. 17 shows the spectral weight distribution for some of these components as a function of magnetic field at selected temperatures. Included are the effective

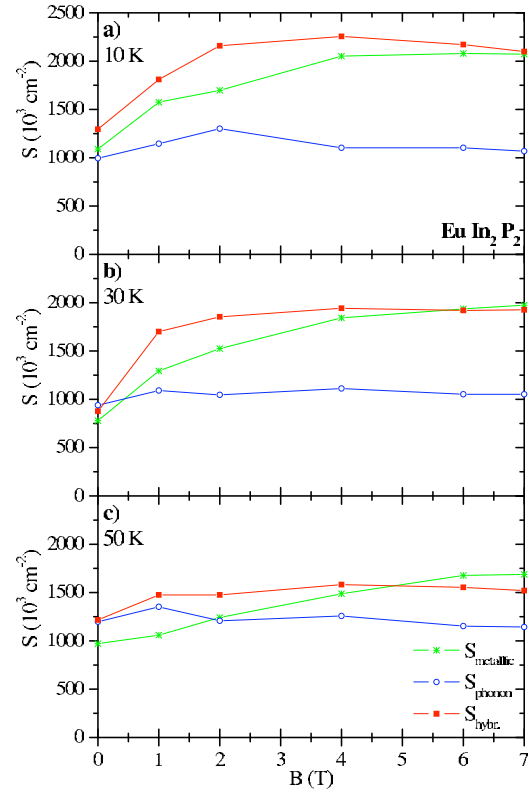


Figure 17: Magnetic field dependence of the spectral weight distribution S at (a) 10, (b) 30 and (c) 50 K in the effective metallic component ($S_{\text{metallic}} = \omega_p^2(\text{Drude}) + \omega_p^2(150 \text{ cm}^{-1})$), the lattice phonon mode ($S_{\text{phonon}} = \omega_p^2(270 \text{ cm}^{-1}) + \omega_p^2(310 \text{ cm}^{-1})$) and the hybridization gap feature ($S_{\text{hybr.}} = \omega_p^2(600 \text{ cm}^{-1}) + \omega_p^2(590 \text{ cm}^{-1})$). ω_p^2 is the squared plasma frequency and mode strength for the Drude term and HO at the resonance frequency given in the brackets, respectively.

metallic component, i.e. the Drude term plus its high frequency tail described by the HO at 150 cm^{-1} , the phonon signal at 270 cm^{-1} together with its high frequency shoulder at 310 cm^{-1} and the broad absorption peaking at 600 cm^{-1} . The most significant result of the spectral weight analysis presented in Fig. 17 is the remarkable gain of spectral weight of the effective metallic component (i.e. for frequencies $\omega \leq 200 \text{ cm}^{-1}$) and the HG feature centered at about 600 cm^{-1} . It is particularly pronounced at 30 K and even more so at 10 K (Fig. 17a and 17b). The renormalized density of states is significantly enhanced both at low temperatures and in high magnetic fields and is due to the increasing hybridization between the localized $4f$ states and the itinerant states of the d bands. This immediately leads to an enhancement of the transition probability, across the HG, i.e. a gain of the mode strength. The enhancements of the metallic component and

HG excitation tend to saturate in high magnetic fields at all temperatures. This saturation is actually expected because of the fully ordered magnetic state in high fields. The spectral weight for all components of $\sigma_1(\omega)$ remains almost constant at any fields above 50 K (Fig. 17c), confirming the direct experimental observation that at these temperatures, there is nearly no magnetic field dependence in the $R(\omega)$ spectra. In order to satisfy the optical sum rule, the gain of spectral weight of the low energy excitations of EuIn_2P_2 below 30 K is accounted for by an equivalent loss of signal at high energies, possibly above 1 eV. The transfer of weight from energies even higher than the experimentally covered spectral range seems to be a common feature of highly correlated systems.

The non-negligible enhancement of spectral weight in $\sigma_1(\omega)$ into the low-energy metallic component with increasing magnetic field implies a release of additional charge carriers upon spin polarizing the material. Therefore, EuIn_2P_2 shares common features with other CMR compounds. In interpreting the data on EuIn_2P_2 , similarly to the $\text{Eu}_{1-x}\text{Ca}_x\text{B}_6$ series (see above), again the recently developed concepts based on the double-exchange scenario is favored, which, although by no means unique, catches some of the experimental findings.

3.2 Condon domains at metamagnetic transition

Recently the metamagnetism in correlated metallic systems, especially the example of the bilayer $\text{Sr}_3\text{Ru}_2\text{O}_7$, have been studied mainly in the context of unusual quantum phase transition and quantum critical behavior [134]. It has been noticed that the metamagnetic transition can be associated with a quantum critical end point. Interestingly, a novel low-temperature phase has been observed in high-quality samples, whose nature has not been identified yet [135]. Motivated by this finding, Binz, Braun, Rice and Sigrist discuss the possible occurrence of Condon domains around the metamagnetic transition as possible explanation for this new phase [35]. The conditions for Condon domains could be realized at very low temperatures, if the metamagnetic transition constitutes a discontinuous, first-order, transition. Demagnetization effects due to the long-ranged dipole forces would then favor the formation of magnetic domains, so-called Condon domains. There are various structures of these domains, most simple the lattice of bubbles and stripes whose stability depends on the applied field strength. Such domain struc-

tures would have an influence on the transport properties as observed in the experiments [35]. The experimental relevance of this proposal is still under debate. Experimentally the unusual low-temperature phase at the metamagnetic transition is insensitive to the sample geometry so that the Condon domain scenario is most likely not a consistent explanation. On the other hand, Condon domains are inevitable for samples with strong demagnetization effects and should be observable. This is the first theoretical study of this effect for a metamagnetic transition.

3.3 Optical study of FeSi, MnSi, FeGe and $\text{Fe}_{1-x}\text{Co}_x\text{Si}$

Future technologies based on the idea that the spin of a charge carrier can be controlled are commonly referred to as spintronics. Efforts to produce materials for spintronics have mostly focused on thin film III-V semiconductors alloyed with manganese. Another route to magnetic semiconductors relies on carrier doping into narrow band, strongly correlated insulators. Transition metal monosilicides display in interesting and potentially useful combination of magnetism and semiconducting properties. Bulk single crystals can be grown by standard techniques. FeSi is a paramagnetic semiconductor, which owes its strong paramagnetism to electron-correlation effects. The isostructural and iso-electronic compounds FeGe is metallic at all temperatures and becomes helimagnetic below room temperature. It has been argued by Anisimov *et al.*, that the difference in electronic structure between FeSi and FeGe consists of a relative shift of the majority and minority spin bands for the latter material, result confirmed by *ab initio* cluster calculations. Also the alloy $\text{Fe}_{1-x}\text{Co}_x\text{Si}$ and the pure compound MnSi order helimagnetically at temperatures of typically 50 K or below.

The group of van der Marel has observed the evolution of a low-energy (0.22 eV) interband transition in FeGe, and a clear signature of a Drude-like free carrier with a strongly temperature dependent scattering rate, like in MnSi (Fig. 18). However a large finite conductivity remains below the interband transition which appears to be the high-energy tail of the free carrier response, due to the coupling to bosonic degrees of freedom, which are most likely spin fluctuations in the present case. The frequency dependent effective mass and scattering rate derived from the optical data indicate the formation of dressed quasiparticles with a mass renormalization factor of 5. Similar to FeSi, the

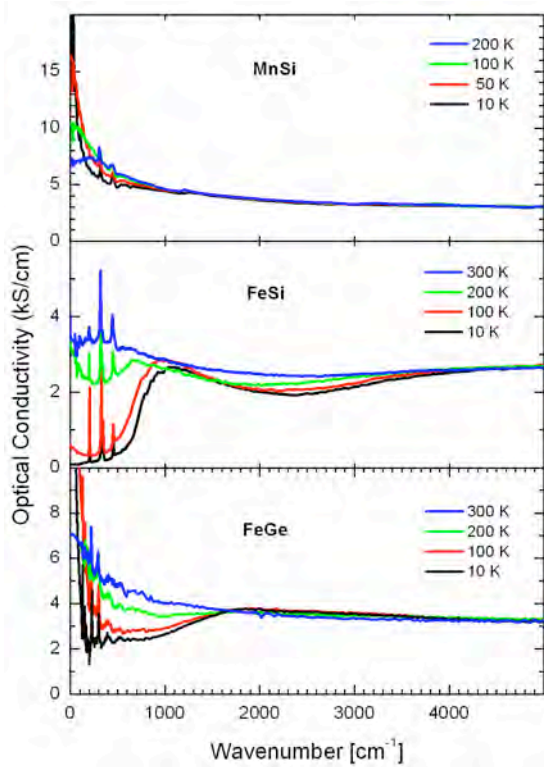


Figure 18: Optical conductivity of MnSi, FeSi and FeGe. When the temperature is lowered, spectral weight is removed below 1000 cm^{-1} in FeSi and FeGe. This graph shows that this spectral weight is not recovered up to at least 0.5 eV .

spectral weight in FeGe is not recovered over a broad frequency range, an effect usually attributed to the influence of the on-site Coulomb interaction.

Partial Co substitution for Fe produces a spin-polarized doped semiconductor. The spin-polarization causes suppression of the metallic reflectivity and increased scattering of charge carriers, in contrast to what happens in other magnetic semiconductors, where magnetic order reduces the scattering. The loss of metallicity continues progressively even into the fully polarized state, and entails as much as a 25% reduction in average mean-free path. The observed effect can be attributed to a deepening of the potential wells presented by the randomly distributed Co atoms to the majority spin carriers. This mechanism inverts the sequence of steps for dealing with disorder and interactions from that in the classic Al'tshuler Aronov approach — where disorder amplifies the Coulomb interaction between carriers — in that here, the Coulomb interaction leads to spin polarization which in turn amplifies the disorder-induced scattering.

In a further step, van der Marel and collaborators have measured core-level absorption spec-

tra at the $2p - 3d$ edge of MnSi, FeSi and CoSi. From a comparison with theoretical calculations taking into account the local $3d$ calculations (multiplet theory) and standard LDA calculations, one learns that the valence fluctuations are suppressed by a factor of 2.5 due to the intra-atomic Coulomb repulsion between electrons occupying the $3d$ states of the transition metal atoms. The electron-electron interactions therefore appear to influence the electronic structure of this material quite strongly, but not strongly enough to suppress completely the valence fluctuations of the ground state. This implies that the magnetism in this material is intermediate between the two extremes of itinerant bands and local moments.

3.4 Field-induced transition in narrow-gap semiconductors

In a study by Rice and Sigrist with Anisimov's group, the magnetic properties of FeSb₂ have been analyzed based on band structure calculations (LDA), which show that this compound is a narrow-gap semiconductor and, thus, completely loses magnetism at low temperatures, analogous to FeSi. The calculations using augmented local density approximation (LDA+U) reveal, however, that for large enough onsite repulsion U ($> 2.6 \text{ eV}$) this material could become a ferromagnetic metal with a moment of $1\mu_B$ per Fe [36]. Since experimentally the system is non-magnetic, such a transition could, in principle, be induced by an external magnetic field through a level crossing transition between the non-magnetic semiconducting and the ferromagnetic metallic state. Such a field-induced transition would obviously constitute a strong magnetoresistance effect. These properties are similar to the earlier findings on FeSi – FeGe with the former being a narrow-gap semiconductor and the latter a ferromagnetic metal.

4 Cold atoms in optical lattices

Cooling atoms to the nanoKelvin regime allows for the realization and study of new phase transitions and their associated phases, with an interesting synergy emerging between the fields of quantum atom optics and condensed matter physics. Topics of current interest are the study of the superfluid to Mott-insulator quantum phase transition appearing in cold bosonic systems subject to an optical lattice, the striving for the realization of a BCS-type condensate in a fermionic system and its crossover to a BEC condensation of bosonic molecules, the investigation of effects due to

disorder and reduced dimensionality (dimensional crossover) and the proposal and implementation of novel quantum phases belonging to new universality classes and associated transitions. As these systems are more difficult to probe, also novel measurement techniques have to be invented. Within MaNEP so far this is exclusively a theoretical activity by the groups of Blatter, Giamarchi and Troyer.

4.1 Superfluid-Mott insulator transition

In the past, Blatter and collaborators have studied the instability towards the Mott insulator appearing in one-dimensional confined Bose gases [37], the appearance of a supersolid phase in two-dimensional fermion-boson mixtures [38], the instability towards phase separation [39], and the implementation of a ring-exchange term with quantum optical means leading to a lattice gauge theory [40]. In their most recent work, they study the bosonic Mott-insulator to superfluid quantum phase transition in an optical lattice [41, 42].

a) *Excitations in the Bose-Hubbard model*
Bosonic atoms subject to an optical lattice are accurately described by the Bose-Hubbard

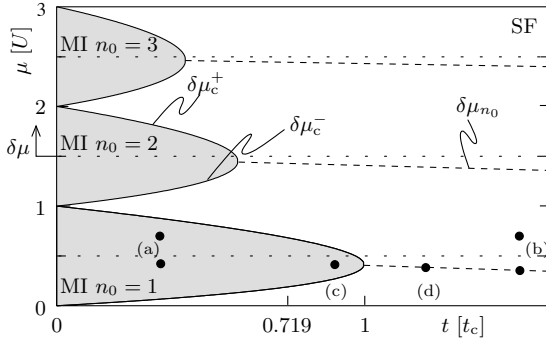


Figure 19: Mean-field phase diagram of the Bose-Hubbard model with disconnected incompressible Mott-insulating phases (grey shaded areas at small hopping t ; density is pinned at integer values n_0), and a connected superfluid phase. The lines $\delta\mu_c^\pm$ mark the second-order quantum phase transition separating these phases. The commensurate filling in the Mott lobes is exported into the superfluid along the lines $\delta\mu_{n_0}$ (bent downward) where particle-hole symmetry is preserved. A truncation scheme is used in order to discuss one lobe at a time. Black dots mark the positions where the spectra of Fig. 20 have been evaluated. The chemical potential difference $\delta\mu$ is measured away from the lobe midpoint at $t = 0$.

Hamiltonian [136]

$$H_{\text{BH}} = -t \sum_{\langle i,j \rangle} a_i^\dagger a_j + \frac{U}{2} \sum_i \delta n_i^2 - \delta\mu \sum_i n_i \quad (3.1)$$

with a_i^\dagger the bosonic creation operator for a Wannier state at site i , $n_i = a_i^\dagger a_i$ the number operator, and $\delta n_i = n_i - n_0$ the deviations of the particle number from a mean filling n_0 . Depending on the value of the nearest neighbor hopping amplitude t , the on-site interaction U , and the chemical potential $\delta\mu$, the Bose-Hubbard model exhibits a superfluid or an insulating (with $n_0 \in \mathbb{N}$ particles per site) ground state, separated by a quantum phase transition (Fig. 19). The phase diagram has been investigated on a mean-field level, using perturbation theory, and via numerical quantum Monte Carlo methods.

The present study concentrates on dynamical properties of the Bose-Hubbard model in

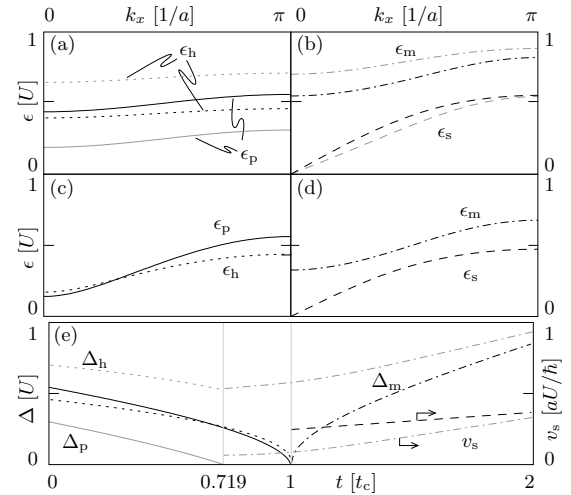


Figure 20: Panels (a)-(d) show spectra for different points in the $n_0 = 1$ lobe of the phase diagram 19 (energies measured in units of U). Results refer to 2D with dispersion along k_x . Panels (a) and (c) refer to the Mott phase, with the full line corresponding to the particle branch and the dashed line to the hole branch. (a) $t = t_c/3$; black lines display dispersions on the line $\delta\mu_{n_0}$, gray lines correspond to $\delta\mu = 0.2U$; change in chemical potential produces a shift in the spectra. (c) $t = 0.9t_c$ and $\delta\mu = \delta\mu_{n_0}$; note the reduction in the gaps $\Delta_{p(h)}$ as compared to (a). Panels (b) and (d) refer to the superfluid phase with sound- and massive modes given by dashed and dash-dotted lines, respectively. (b) $t = 1.5t_c$; black and gray lines refer to the chemical potentials $\delta\mu = \delta\mu_{n_0}$ and $\delta\mu = 0.2U$. (d) $t = 1.2t_c$ closer to the transition and with $\delta\mu = \delta\mu_{n_0}$. Panel (e) gives the gap values $\Delta_p, \Delta_h, \Delta_m$ and the sound velocity v_s for $t \in [0, 2t_c]$ and $\delta\mu = \delta\mu_{n_0}$ and $\delta\mu = 0.2U$. The value $t \approx 0.719t_c$ corresponds to the phase boundary for $\delta\mu = 0.2U$.

the limit of strong interactions. In particular, the interest lies in finding the spectra and eigenstates in the Mott-insulating as well as in the superfluid phase close by. Weakly interacting theories such as the Gross-Pitaevskii equation or the Bogoliubov theory cannot capture the physics close to localization. On the other hand, strong coupling perturbation approaches are often incapable to correctly describe the broken U(1)-symmetry phase. A Hilbert-space truncation-technique due to Altman *et al.* [137] was used to derive an effective Hamiltonian H_{eff} for the excitations. The results of such a calculation are shown in Fig. 20: the Mott-insulator phase is characterized by two gapped modes (Fig. 20(a) and (c)), while the strongly correlated superfluid nearby exhibits one gapped (Higgs) and one sound (Goldstone) mode (Fig. 20(b) and (d)). Fig. 20(e) traces the evolution of the gaps and the sound velocity with increasing value of the hopping parameter t .

b) *Low energy field theories* The Bose-Hubbard model generates two *effective* low-energy field theories for the complex order-parameter field ψ (Fig. 21) For weak interaction $U\bar{n} \ll t$, the length scale is set by the healing length $\xi_{\text{GP}} = a\sqrt{t/U\bar{n}} \gg a$, and one arrives at the Galilean-invariant Gross-Pitaevskii theory (non-linear Schrödinger equation; \bar{n} is the mean filling per site) $\mathcal{L}_{\text{GP}}(\psi) = \psi^* \hbar \partial_\tau \psi + U\bar{n} \xi_{\text{GP}}^2 |\nabla \psi|^2 + U|\psi|^4/2$. The effective Galilean invariance *ensures* that at zero temperature there is only one sound (Goldstone) mode, but no amplitude mode independent of first sound.

Quite remarkably, close to the superfluid-insulator transition at $U \sim t\bar{n}$, the combined action of the lattice and the interaction leads to a Lorentz-invariant critical theory (non-linear Klein-Gordon equation) [138]. The diverging

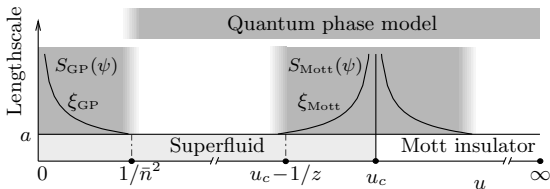


Figure 21: Schematic overview of models describing the superfluid phase of lattice bosons. For small (dimensionless) interactions $u = U/2t\bar{n}z < 1/\bar{n}^2$, the Bose-Hubbard model is well approximated by the continuum Gross-Pitaevskii action $S_{\text{GP}}(\psi)$. Close to the critical interaction $u \approx u_c = 2$, the dynamics is described by the Klein-Gordon type theory $S_{\text{Mott}}(\psi)$. For $u > 1/\bar{n}^2$, the Bose-Hubbard model is equivalent to the quantum phase model.

correlation length $\xi_{\text{Mott}} \propto 1/\sqrt{z(u_c - u)}$ near the (commensurate) superfluid–Mott-insulator transition at $u = U/2t\bar{n}z = 2$ allows for a description in terms of a continuum Lorentz-invariant critical theory $\mathcal{L}_{\text{Mott}}(\psi) = |\hbar \partial_\tau \psi|^2/tz + tz(u_c - u)[\xi_{\text{Mott}}^2 |\nabla \psi|^2 - |\psi|^2] + U|\psi|^4/2$, with $z = 2d$ the coordination number and $J = 2t\bar{n}$. As a consequence, this theory admits the possibility of independent amplitude (Higgs) and phase (Goldstone) modes. The emergent (Higgs) mode involves a collective oscillation of the amplitude $|\psi|$ of the order parameter with a frequency that vanishes at the transition. Such oscillation of the order parameter is accompanied by a local change in the non-condensed fraction, leaving the local density unchanged. Furthermore, this mode is independent of the usual sound mode; this can be understood from the fact that the order parameter vanishes towards the transition while the density remains constant.

c) *Quantum phase model* The question of how the Higgs mode emerges upon increasing the interaction U should be addressed within a *microscopic* theory that explicitly accounts for the interplay between interactions and the lattice, as is done by the quantum phase model

$$\hat{H}_{\text{QPM}} = -J \sum_{\langle i,j \rangle} \cos(\hat{\phi}_i - \hat{\phi}_j) + \frac{U}{2} \sum_i \delta \hat{n}_i^2 \quad (3.2)$$

with the Josephson coupling $J = 2t\bar{n}$, a suitable approximation of the Bose-Hubbard model for large filling \bar{n} . Here, the conjugate operators $\hat{\phi}_i$ and $\delta \hat{n}_i$, $[\hat{\phi}_i, \delta \hat{n}_j] = i\hbar \delta_{ij}$, describe the local phase and deviation from mean filling, respectively.

For analysis of the quantum phase model a dynamical variational approach [139] was applied, which accounts for both phase and amplitude degrees of freedom and allows to capture the low-energy physics of a depleted condensate near the Mott-insulator transition. Blatter and coworkers have derived the static properties in a mean-field approach and have identified the insulator-superfluid transition. The extension of the formalism to include dynamical features within a Gaussian approximation provides the excitations [42]. These then have been used to determine the kinetic response function amenable to experimental tests [140].

d) *Comparison with experiments* While cold atoms in optical lattices excel in their tuneability, they do suffer from a limited number of tools available for their characterization. In fact, so far only two experimental techniques

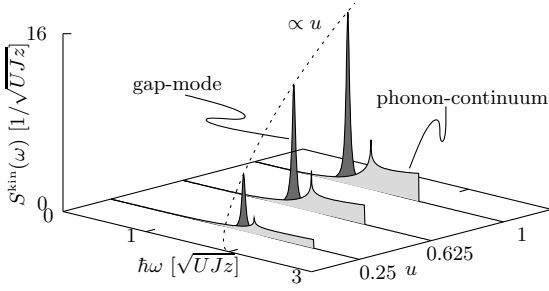


Figure 22: The response function to the lattice modulation $S^{\text{kin}}(\omega)$ within the quadratic theory for different values of the interaction strength u in two dimensions. The dark gray peak relates to the absorption of a single amplitude mode at $\hbar\omega = \Delta_\sigma$ (for illustrational purposes the delta-peak a finite width is given). The area in faint gray corresponds to the two-phonon continuum excited at energies below twice the phonon bandwidth $\hbar\omega \leq 2W_\phi$ (the logarithmic divergence is a density-of-states effect peculiar to two dimensions). Both absorption probabilities scale as u at small u .

are being used to determine the dynamical properties of cold atoms in an optical lattice, Bragg spectroscopy described by the dynamic structure factor

$$S(\mathbf{q}, \omega) = \sum_n |\langle n | \delta\rho_{-\mathbf{q}} | 0 \rangle|^2 \delta(\omega - \omega_{n0}) \quad (3.3)$$

with $\delta\rho_{\mathbf{q}}$ the density-fluctuation operator (the sum runs over all eigenstates $|n\rangle$), and lattice modulation [140] involving the kinetic response function

$$S_{(x)}^{\text{kin}}(\omega) = \sum_n \left| \langle n | T_{(x)} | 0 \rangle \right|^2 \delta(\omega - \omega_{n0}) \quad (3.4)$$

with $T_{(x)} = \sum_{\langle i,j \rangle_{(x)}} a_i^\dagger a_j$ the hopping operator along the direction (x) . In their work, Huber *et al.* [41] have determined both response functions using the truncation technique, where interesting interference effects in the lattice modulation experiments were found. The result for the kinetic response function calculated within the quantum rotor model is shown in Fig. 22. It was found that both amplitude and sound modes contribute to the response. While experiments have provided evidence for the presence of such a mode [141], their spectral resolution does not yet allow for its detailed analysis.

4.2 Low-dimensional systems and dimensional crossover

a) *Low dimensional structures and Luttinger liquids* Cold atomic gases allow to realize one-dimensional structures for bosons or fermions and, thus, to probe the associated physics of

Luttinger liquids. Several experiments have already addressed these properties for single-component bosonic systems. Giamarchi and coworkers have investigated what happens for two component bosonic systems, which mimic separate excitations for the “charge” and “spin” leading to the physics of spin-charge separation in one dimension. Since for bosons the preferred exchange is ferromagnetic, regimes that would not be available for fermionic systems can be explored here. In addition, on a practical side, bosons are well controlled in current experiments allowing for a good test of the computed properties.

First the interaction between the two species of bosons is tuned to provide dominant antiferromagnetic exchanges. Then the two-component system of bosons lead to a “standard” Luttinger liquid with “spin” and “charge” excitations. Simulations using a time-dependent density matrix renormalization group (DRMG) procedure showed that with realistic parameters this system would offer an excellent probe for the property of spin-charge separation [43, 44]. This is specially appealing since spin-charge separation is extremely hard to probe in condensed matter systems [142]. Moreover, the spectral function was computed finding very good agreement between the numerics and analytical calculations [45].

The case when the interactions provide dominant ferromagnetic exchange (such as isotropic interactions) leads to a radically new physics. The one-dimensional system is not a Luttinger liquid anymore [46], but belongs to a new universality class, which is a remarkable fact in one dimension, analogous to finding non-Fermi-liquid behavior in higher dimensions. Giamarchi and coworkers computed the correlation functions of such a system and show in Fig. 23 the spin-spin correlation function. Spin excitations are much more localized than in a Luttinger liquid and possess at short time a sub-diffusive behavior where the spin excitation diffuses in space x as $x^2 \sim \log(t)$, thus very slowly with time t . This phase is also related to several other situations such as the case of an impurity in a Luttinger liquid or Caldeira-Leggett models. This study is only at the beginning and will be continued.

Finally, up to very recently in cold atomic gases, phases with non-local interactions could not be explored. However the experimental progress in the realization of quantum degenerate atomic and molecular gases with dominating dipole-dipole interactions have shown the potential to bridge that gap. The possible quantum phases of a dipolar bosonic gas

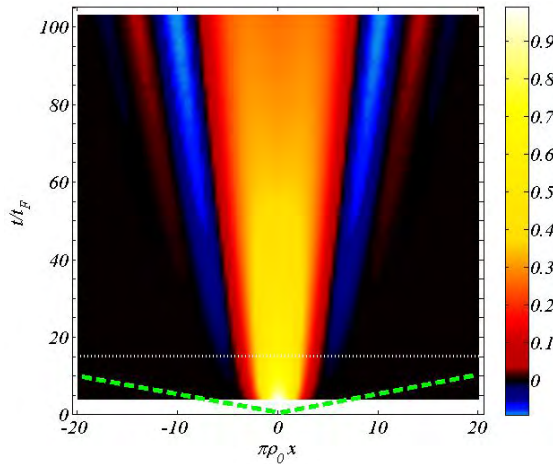


Figure 23: Spin correlation function for a ferromagnetic two component Bose gas. The system is in a new universality class compared to a Luttinger liquid. In particular the spin excitations are strongly localized while they would propagate with a constant velocity in a Luttinger liquid.

in a planar array of one-dimensional homogeneous tubes was investigated using bosonization methods [47]. An external field is applied to align the dipoles. The different tubes are coupled by the presence of the dipolar interaction. A ‘sliding Luttinger liquid phase’ (SLL) was found, a phase that was proposed in the context of high- T_c systems in condensed matter. This phase is novel in a bosonic system. The surprising feature of the SLL is that even though the system is two dimensional, the main characteristic of one-dimensional systems, as algebraically decaying correlations, survive. Furthermore a charge density ordered phase occurs, which can be either a stripe phase or a checkerboard ordering depending on the dipole direction. Giamarchi and collaborators proposed how these phases can be measured in quantum gases.

b) *Coupled low dimensional structures and deconfinement transition* A system made of weakly coupled one dimensional bosonic tubes realized in the Esslinger group [143] allows to study a dimensional crossover between the one-dimensional (Luttinger liquid) and the three-dimensional physics. This dimensional crossover — or when the chains are in a Mott state, deconfinement transition — is relevant to systems in condensed matter such as the organic conductors [48].

Motivated by these experiments, Giamarchi and collaborators studied coupled one-dimensional tubes both for bosons [49] and fermions [50, 51]. For bosons, the phase diagram was determined, as shown in Fig. 24. The

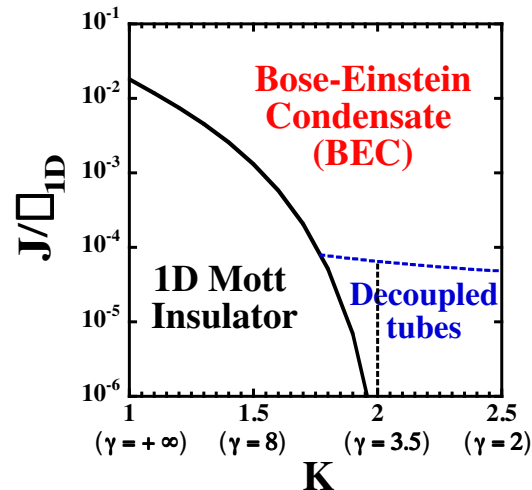


Figure 24: Phase diagram of coupled bosonic tubes as a function of the repulsion γ between the bosons and of the inter-tube hopping J . K is the Luttinger parameter inside each tube. There is a deconfinement transition between a 1D Mott insulating phase and an anisotropic 3D superfluid.

phase boundary depends crucially on the Luttinger properties of the individual tubes. This description, which correctly incorporates the interactions, goes beyond the Gross-Pitaevskii description of an anisotropic superfluid, valid only for weak interactions. In particular it was found that, as a consequence of the interactions, a massive amplitude mode exists in the 3D superfluid in addition to the standard massless Goldstone mode characteristics of phase fluctuations [49].

Cazalilla, Ho and Giamarchi and collaborators have analyzed the phase diagram of coupled chains of fermions, both for standard Hubbard chains and for chains where the two species of fermions (two spins or isospins) have different hoppings. This system presents different phases than the standard Hubbard model. In particular the second case leads to the opening of a spin gap [50] and single-particle hopping between the tubes is suppressed, when the tubes are weakly coupled, leading to a spin-triplet superconducting ground state, for purely repulsive local interactions [51].

Finally, Cazalilla *et al.* investigated the case of two dimensional pancakes of bosons, coupled by Josephson hopping [52]. Experimentally a system of two parallel harmonically trapped 2D (pancakes) cold gases of Rb was realized in the ENS group to probe the physics of the Berezinsky-Kosterlitz-Thouless (BKT) transition for decoupled pancakes and the even richer phenomena beyond the BKT physics when the Josephson coupling was turned on.

This allows to control the competition between the phase coherence among the pancakes and the thermally excited vortices in each plane, leading to the so-called deconfinement transition. The effect of coupling is observable, for example, in a change of the universal exponents at the transition, and the superfluid fraction experiences a jump in the crossover. The techniques developed in this study had a direct application also for the layered superconductors described in Project 2.

4.3 Probes for cold atomic gases

Despite the high degree of tuneability and control offered by cold quantum gases, they are difficult to probe. This makes the identification of exotic quantum phases extremely involved and generates the demand for new detection techniques. Giamarchi and coworkers have thus focused on two aspects of this question in this year's project: (1) they analyzed in depth one of the technique (shaking technique) that was used by the Zurich group to probe the transition between a superfluid and a Mott insulator; (2) they proposed a new technique, analogous to the STM in condensed matter, to be able to make local probing in cold atomic systems.

An experimental technique to probe the excitation spectrum in a gas of bosonic atoms relies on the driving of the system by periodic modulations of the optical lattice potential. There was considerable debate on what is exactly probed by this technique. A linear response analysis of the response to such a modulation has been performed [53]. To go beyond such a linear response analysis (the experiment uses a very large modulation) and to include additional effects such as the parabolic confinement potential, Kollath *et al.* used a novel DMRG technique dealing also with non-equilibrium effects. Treating in this way the full time evolution of the excited atomic gas leads to the interpretation of the experimental observations [54]. It was shown, in particular, that the presence of a peak at an energy $2U$ in the absorption spectrum (U local interaction) is a direct measure of the degree of incommensurability in the system.

Giamarchi's group has applied the same analysis for the shaking of a fermionic system [55]. Here it was shown that the absorption peaks give a remarkably accurate measure of the interaction U , which is difficult to obtain otherwise. Moreover an excellent correlation between the absorption peak weight and the degree of antiferromagnetic correlation was

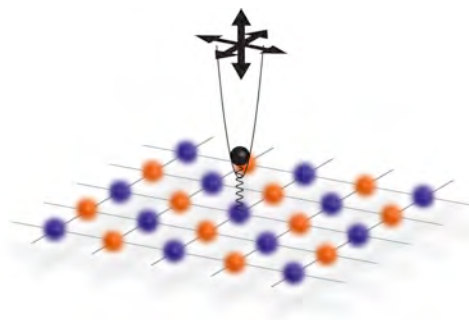


Figure 25: Cold Atom Tunneling microscope (CAT), using an ion in a magnetic trap to probe for local properties in an optical lattice.

found, which is useful in analyzing the connection with the Hubbard model.

The probe discussed above, as all the existing ones, are essentially probing homogeneously the atomic gas. Because trapped cold atomic systems are inherently inhomogeneous, involving spatially separated phases, a local probe would be highly desirable. Giamarchi and coworkers [56] proposed a novel experimental setup, similar to the scanning tunneling microscope (STM) in condensed matter, to locally probe cold atomic gases. This probe relies on the coherent coupling of a single particle to the atomic system, as depicted in Fig. 25. Depending on the measurement sequence, either the local density, with a resolution on the nanometer scale, or the single particle correlation function in real time can be observed. The realization of such a probe will open the possibilities to investigate locally the properties of exotic quantum phases. In this work, Giamarchi and collaborators showed how the various possible phases for a two-dimensional Hubbard system of fermions in an optical lattice could be identified.

4.4 Coupled double well superlattices

The generation of states with long-distance entanglement is crucial for many applications in quantum communication. A method is proposed for a robust and well-controlled generation of such states through the dynamics of cold bosonic atoms loaded on a double well superlattice. Such systems have already been realized by the group of Immanuel Bloch in Mainz. The scheme by Giamarchi and coworkers iteratively swaps the entanglement between pairs of atoms by controlling the tunneling between the double wells. In the limit of deep wells and large on-site repulsion one can describe the system by a Heisenberg chain with (ferromagnetic) time-dependent exchange con-

starts $J_1(t)$, $J_2(t)$. For a well-chosen time dependence (a periodic interchange of the two coupling constants) long-range entanglement can be dynamically generated starting with an initial product state of nearest-neighbor spin triplets (or singlets) [144].

In the case of homogeneous couplings ($J_1 = J_2 = \text{constant}$), the many-body dynamics can lead to the formation of states of mixed correlations, in which antiferromagnetic short-distance correlations are mixed with ferromagnetic correlations at longer distances [144]. This state is also characterized by a high degree of multi-particle entanglement.

4.5 Numerical simulations of cold atomic gases

The goal of the computational approach to cold atoms is to provide access to quantities which can often not be measured directly in experiment and to develop computational approaches on the *ab initio* level.

a) *Fermions* Troyer and coworkers have introduced the notion of adiabatic quantum simulation and shown that it is technologically feasible to check whether the ground state of the two-dimensional Hubbard model is a d -wave resonating valence bond (RVB) state [57]. This approach solves the problem posed by the very hot temperatures of about $T/E_F \approx 0.3$ in current experiments, which were determined using a thermometry method proposed by Troyer and collaborators [58]. The behavior of fermions trapped in a three-dimensional optical lattice was calculated, when they are swept across the Feshbach resonance. By solving the fermion problem on lattices of similar size to the experiments, a quantitative explanation of the experiments could be given [145] also by using this to measure the temperature of fermionic gases.

b) *Bosons* In bosonic models, Troyer's group can do full *ab initio* simulations of systems of sizes comparable to experiments. In a one-dimensional simulation, they investigated the occurrence of a quasi-condensate at finite temperatures in a trap and showed that it survives up to the strong interaction limit [59]. In two dimensions, they have studied the effect of the trap shape (quadratic or quartic) on the sharpness of the crossover from a superfluid to a Mott insulator in optical lattice experiments with bosons [60]. By calculating the entropy in a trapped Bose gas, they can calculate the temperature change when they adiabatically change the repulsion between bosons in optical lattices. These results show that there

is minimal heating across the Mott transition, and substantial heating only sets in deep inside the Mott phase [61].

c) *Bose-Fermi mixtures* Troyer and coworkers also focused their research efforts on the phase diagram of Boson-Fermion mixtures on optical lattices. This model is a prototypical bridge between condensed matter physics and quantum optics, since it shows how cold atomic gases can be used to realize variants of standard condensed matter models. In quantum Monte Carlo simulations they have determined the rich ground state phase diagram of the one-dimensional version of the model. They have determined the phase diagram at double half filling [62] and studied effects of the confining trap on the formation of superfluid and Mott regions [63, 64].

d) *Universal behavior of resonant fermions* The connection between the BCS theory of superconductivity with pairing in momentum space and the Bose-Einstein condensation (BEC) of bosonic "molecules" consisting of two fermions tightly bound in real space is a long-standing problem. While this BEC-BCS crossover is not a phase transition, there is a universal behavior at the resonance point at which the energy of a bound pair of two fermions is in resonance with the bottom of the band of unbound fermions. In the dilute limit, all properties at this point are universal in units of the reduced temperature T/E_F where E_F is the Fermi energy. Using large-scale quantum Monte Carlo simulations, Troyer and collaborators could determine the value of the universal properties including the universal critical temperature at this point [65, 66].

5 Charge density wave systems

Charge density wave (CDW) systems have recently attracted renewed interest, since in many cases the mechanism leading to this ordered phase is not clear. The Peierls mechanism relying on Fermi surface nesting is indeed often not compatible with the electronic structure found in the studied materials. Thus the question arises whether in some systems alternative mechanisms are at work, such as the realization of an excitonic insulator state mediating lattice distortions, as suggested below for 1T-TiSe₂. A further intriguing aspect lies in the discovery of superconductivity near the quantum critical point of the CDW state under pressure or through intercalation in systems such as 1T-TiSe₂ and 1T-TiS₂. These studies were performed in the groups of Aebi, Degiorgi and

Forró. Optical measurements were carried out by van der Marel and coworkers on another class of CDW systems with complex phase diagrams, the $R_5\text{Ir}_4\text{Si}_{10}$.

5.1 Infrared study of the charge-density-wave rare-earth polychalcogenides $R\text{Te}_n$

Following Peierls' idea, Fermi surface nesting is a most favorable condition to realize a CDW instability which leads to the opening of an energy gap at the Fermi level, i.e. quasi-1D metals are among the best candidates. Several families of materials, including the transition-metal di- and trichalcogenides, the molybdenum and tungsten oxides, such as the blue and purple bronzes, and the organic charge transfer salts, have been studied intensively over several decades.

In recent years the rare-earth polychalcogenide $R\text{Te}_n$ (R stands for rare earth, and $n=2, 2.5$ and 3) systems have attracted a great deal of interest, due to their intrinsic low dimensionality. These materials are also characterized by a layered structure, consisting of corrugated rare-earth-chalcogen slabs alternated with planar chalcogen square lattices (i.e. single layer for di- and double layer for tri-tellurides). The interest in these systems has recently also been promoted by the astonishing discovery of a pressure induced superconducting state in CeTe_2 below 2.7 K which is competing with the CDW phase (T_{CDW} well above 300 K) and with magnetic order ($T_N \sim 4.3$ K).

Degiori and coworkers have investigated the $R\text{Te}_3$ and $R\text{Te}_2$ series by optical means. Optical spectroscopic methods have been generally proven to be a powerful experimental tool in order to address the relevant absorption features associated with the CDW ground state. Their first optical reflectivity data on $R\text{Te}_3$ (R=La, Ce, Nd, Sm, Gd, Tb and Dy), collected over an extremely broad spectral range, provide information on both the Drude component and the single-particle peak, ascribed to the contributions due to the free charge carriers and to the excitation across the CDW gap, respectively. They have then measured the pressure dependence of the optical reflectivity on CeTe_3 at 300 K (i.e. in the CDW state). Upon increasing the externally applied pressure, the excitation due to the CDW gap decreases, analogous to the observation when the lattice was compressed by substituting rare earth ions with a large ionic radius by ones with small one. Furthermore, the metallic (Drude) weight was found to be moderately enhanced with chemical pressure (i.e. along

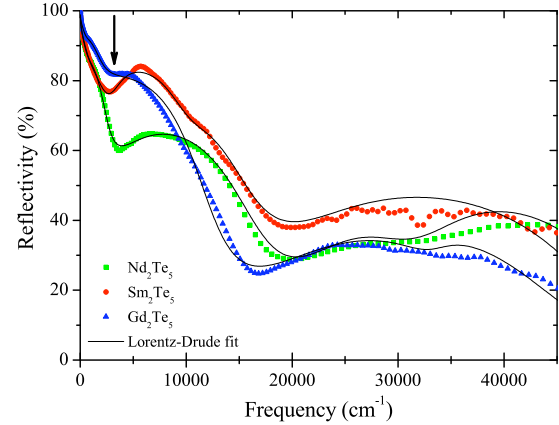


Figure 26: Optical reflectivity $R(\omega)$ of $R_2\text{Te}_5$ with $R= \text{Nd}, \text{Sm}$ and Gd at 300 K. Thin lines are the Lorentz-Drude fit. The arrow points out the depletion at about 4000 cm^{-1} .

the rare earth series). Similar behaviors were discovered in the $R\text{Te}_2$ series, as well. These results demonstrate that chemical and applied pressure similarly affect the electronic properties and equivalently govern the onset of the CDW state in $R\text{Te}_2$ and $R\text{Te}_3$. The reduction of the effect that the CDW condensate has on the states at the Fermi surface through the shrinking lattice constant is most likely a consequence of a quenching of the nesting conditions, driven by the modification of the electronic structure because of the lattice compression.

In comparison to $R\text{Te}_2$ and $R\text{Te}_3$, little is known about the $R_2\text{Te}_5$ family of compounds. Their orthorhombic crystal structure is intermediate between that of $R\text{Te}_2$ and $R\text{Te}_3$, comprising alternating single and double Te planes sandwiched between RTe corrugated block layers. The existence of this class of compounds raises the question of whether separate modulation wave vectors might exist on the single and double Te planes, respectively, and, if so, how these wave vectors might interact or compete with each other.

Fig. 26 displays the optical reflectivity $R(\omega)$ spectra for the $R_2\text{Te}_5$ (R= Nd, Sm and Gd) compounds at 300 K. The spectra turn out to be temperature independent between 10 and 300 K. Two features are clearly evident: the overall metallic behavior with a plasma edge onset at about $1.7 \times 10^4 \text{ cm}^{-1}$, and a broad absorption, overlapped to the plasma edge and peaked around 5000 cm^{-1} . This latter absorption leads to a more or less pronounced depletion in $R(\omega)$ (arrow in Fig. 26), bearing striking similarities with previous data on $R\text{Te}_3$ and $R\text{Te}_2$. By applying the phenomenological Lorentz-Drude approach Degiori and collabo-

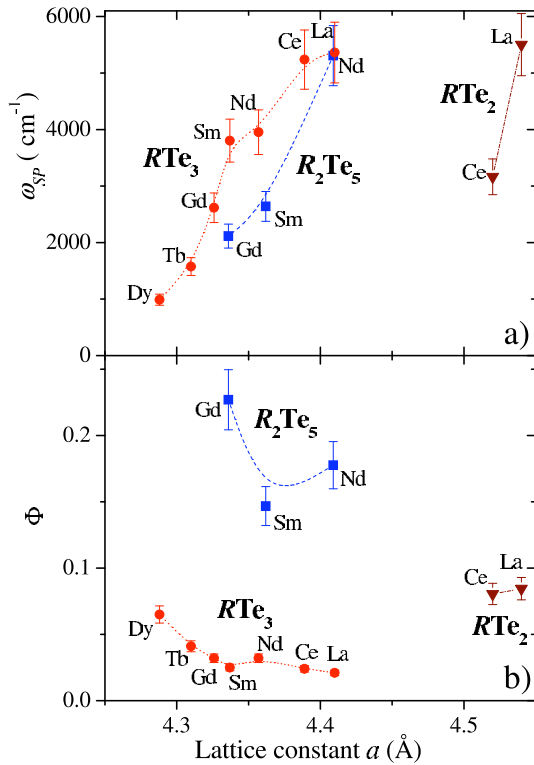


Figure 27: a) The single particle peak frequency ω_{SP} (i.e. the CDW gap excitation) and b) the ratio Φ for the fraction of the ungapped Fermi surface are shown as a function of the in-plane lattice constant a for the R_2Te_5 , RTe_3 and RTe_2 series.

rators extract from the absorption spectrum of the rare-earth polychalcogenide R_2Te_5 ($R=Nd, Sm$ and Gd) compounds the excitation energy of the CDW gap and estimate the fraction Φ of the Fermi surface which remains ungapped by the formation of the CDW condensate (Fig. 27). In analogy to previous findings on the related RTe_n ($n=2$ and 3) families, they establish the progressive closing of the CDW gap (Fig. 27a) and the moderate enhancement of the metallic component upon chemically compressing the lattice. The decrease of the CDW gap upon compressing the lattice thus generalizes the concepts already developed for the RTe_2 and RTe_3 series. Such a suppression of the CDW gap signals indeed a reduction in the quality of nesting upon applying pressure, therefore inducing a lesser impact of the CDW condensate on the electronic properties, and leads to a release of additional charge carriers, manifested by the shift of weight from the gap feature into the metallic component of the optical response. Therefore, the fraction Φ of the ungapped Fermi surface (Fig. 27b) is enhanced by reducing the lattice constant.

5.2 Transition metal dichalcogenides

From a vast class of transition metal dichalcogenide (TMC) compounds, $1T-TaS_2$ and $1T-TiSe_2$ — which share a $1T$ polytype stacking between the adjacent layers, and therefore have the smallest unit cell compared to the $2H$ or the $4H$ polytype systems — have been chosen for investigation. Despite their structural simplicity both compounds show a rich abundance of phases.

a) $1T-TaS_2$ Even at ambient external conditions the quasi-two-dimensional material $1T-TaS_2$ features a highly complex phase diagram, with a commensurate CDW phase, accompanied simultaneously by a Mott localization at low temperatures to an incommensurate CDW phase and eventually a metallic phase at high temperatures. The Mott localization melts through a nearly commensurate CDW phase at intermediate temperatures and displays an intriguing thermal hysteresis, which hints at an additional hidden nearly commensurate CDW phase. Forró and coworkers have applied pressure and traced the evolution of the commensurate charge density wave phase through a vast range of pressures 0–25 GPa. The commensurate CDW phase and consequently the Mott localization collapse at a pressure of about 1 GPa, followed by the establishment of a mixed nearly commensurate CDW phase consisting of CDW domains and metallic stripe-like features. Amazingly, a superconducting state emerges at low temperatures, with a maximum superconducting transition temperature of 6 K, as soon as at the CDW phase is suppressed. Even more perplexing is the fact that the superconductivity persists through the entire pressure range 1–25 GPa with apparently little variation in the transition temperature. Forró and collaborators suggest that the superconductivity arises in the nearly commensurate phase and that the Cooper pairing mechanism may be related to the proximity of the metallic stripe-like modulations to the CDW domains in that phase. The phase diagram was constructed from resistivity measurements under pressure (Fig. 28) and is summarized in Fig. 29. High temperature and high pressure studies are essential to determine the nature and the dominant scattering mechanism in this system once it becomes metallic above 8 GPa.

In a collaboration of the groups of Aebi and Forró, the temperature dependence of the electronic structure of $1T-TaS_2$ has also been analyzed by ARPES. Density functional theory was used to calculate and com-

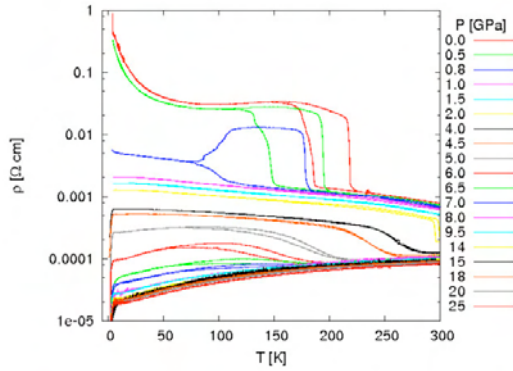


Figure 28: The resistivity in the pressure range 0–25 GPa and temperature range 1.3–300 K.

pare the imaginary part of the static electronic susceptibility characterizing the nesting strength. While nesting appears to play a role in the high-temperature phase, the ARPES line shapes reveal peculiar spectral properties which are not consistent with the standard two-dimensional Peierls scenario for the formation of a CDW. The temperature depen-

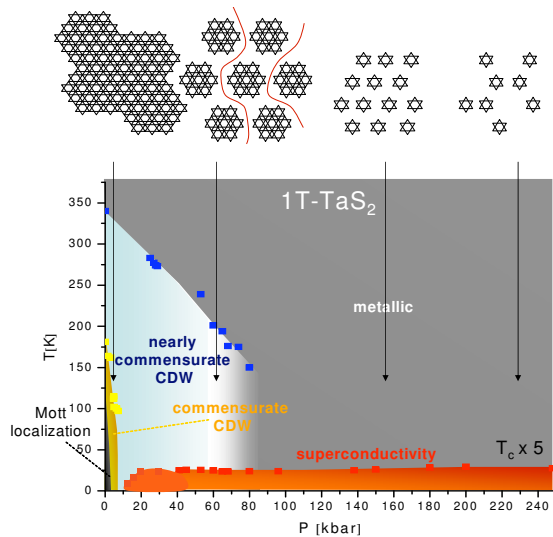


Figure 29: Pressure temperature phase diagram of $1T\text{-TaS}_2$: the Mott localization and the commensurate CDW phase melt at 0.8 GPa, the lattice structure for these both phases is composed of interlocking David star-like deformations. The nearly commensurate CDW phase extends over the pressure range 1–7 GPa and may be visualized as roughly hexagonal domains suspended in an inter-domain phase, where the inter-domain phase forms stripes. The pressure shrinks the domains. From the nearly commensurate CDW state the first signatures of superconductivity appear and remain roughly at 5 K throughout the entire pressure range 3–25 GPa. In the pressure range 8–25 GPa the system may be described as a fluid of mobile David stars interspersed in a metallic matrix.

dence of these anomalous spectral features suggests a lattice-distortion enhanced electron-phonon interaction [67].

b) *Evidence for an excitonic insulator phase in $1T\text{-TiSe}_2$* TiSe_2 has intrigued scientists for a long time due to the mystery around the origin of a CDW at low temperature. Now strong evidence has been found for the realization of an exotic ground state, the excitonic insulator phase [146]. TiSe_2 has an electronic structure near the Fermi energy comparable to that of a semimetal, as its valence and conduction bands are slightly overlapping through an indirect gap. In the case of the excitonic insulator phase, the Coulomb interaction, weakly screened due to the low free carrier density, is strong enough to bind together an electron in the conduction band and a hole in the valence band, forming excitons (Fig. 30). Once temperature decreases, a scenario similar to BCS superconductivity starts to work, as illustrated schematically in Fig. 30. Since the valence and the conduction bands are indirectly overlapping, the energy to create excitons is negative. Thus they will form spontaneously and then condense into a macroscopic state. Due to the mixed nature of excitons, this state induces a new periodicity in the system characterized naturally by the distance between the valence and the conduction bands. In other words, exciton condensation leads the system towards a CDW phase with a purely electronic origin.

High-resolution angle-resolved photoemission experiments on $1T\text{-TiSe}_2$ by Aebi and collabo-

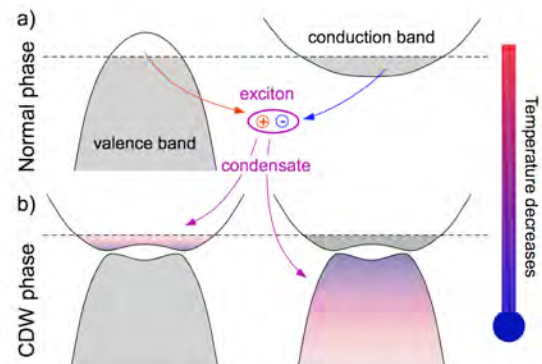


Figure 30: Schematic picture of the CDW phase transition in the excitonic insulator phase model. At high temperature (a), the electronic structure of TiSe_2 near the Fermi energy consists of a valence and a conduction bands which overlap slightly and indirectly. At low temperature (b), excitons, consisting of holes in the valence band and electrons in the conduction band, condensate in a macroscopic quantum state, leading to the CDW phase.

rators in both its normal phase at room temperature and its low-temperature CDW phase have been carried out [68]. At low temperature the photoemission spectra are strongly modified, with large band renormalizations at high-symmetry points of the Brillouin zone and a very large transfer of spectral weight to backfolded bands. A calculation of the spectral function for an excitonic insulator phase reproduces the experimental features with very good agreement. This gives strong evidence in favor of the excitonic insulator scenario as a driving force for the CDW transition in 1T-TiSe₂ (Fig. 31).

The possibility of encountering here an exotic mechanism for the CDW instability, the realization of an excitonic insulator, puts 1T-TiSe₂ on a special stage. This material shows a commensurate 2 × 2 × 2 structural distortion accompanying the CDW. Pressure suppresses this CDW, possibly by depleting the excitonic condensate in the system. At a critical pressure of 2 GPa, when the CDW phase is completely suppressed, Forró and coworkers observe a narrow dome of superconductivity bracketed by a pressure range of 1.5–3.5 GPa. The maximum superconducting transition temperature is 1.8 K. Preliminary measurements in a magnetic field indicate a very low critical field of the order of a few hun-

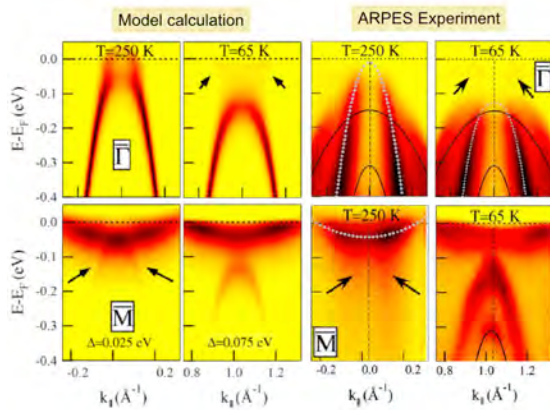


Figure 31: (Right) ARPES data taken at the X09LA beamline of the SLS on 1T-TiSe₂ samples. At 250 K, the system is in the normal phase, above the transition. At 65 K, it is in the CDW phase where one clearly sees at the border of the Brillouin zone (the so-called M point) replica of the bands originally situated in the center of the Brillouin zone (the Γ point). (Left) Simulated intensity maps derived from the excitonic insulator model, above and below the CDW transition. Arrows mark the presence of weak spectral weight. Note that the simulation only treats the topmost of the three bands present at Γ in the experiment.

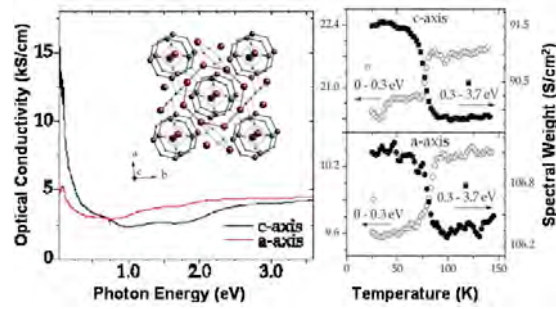


Figure 32: Optical conductivity of Lu₅Ir₄Si₁₀ (left panel). Right panel: Temperature dependence of the integrated optical conductivity below the charge density wave gap (from 0 to 0.3 eV, open circles), and above the gap (0.3 to 3.7 eV, closed circles).

dred Gauss, which is in strong contrast with the superconducting phase reached through Cu intercalation (Cu_xTiSe₂) [147]. Magnetization measurements under pressure to study the nature of the critical magnetic field are in progress.

5.3 Optical properties of the R₅Ir₄Si₁₀ – family

At ambient pressure Lu₅Ir₄Si₁₀ exhibits an interesting interplay of a CDW occurring at 83 K with the superconducting state at 3.9 K. Er₅Ir₄Si₁₀ has two CDW transitions ($T_1 = 150$ K and $T_2 = 55$ K) and a phase transition at 2.8 K from a paramagnetic to an antiferromagnetic phase. The group of van der Marel studied the optical conductivity of a single crystal of Lu₅Ir₄Si₁₀ along the two main crystal orientations. The anisotropy of the electronic bands in the optical conductivity shown in Fig. 32 is weak, indicating that this material has a 3-dimensional Fermi surface. Below the transition temperature, a weak suppression of the optical conductivity indicates the opening of a gap on part of the Fermi surface, with a maximum value of 90 meV. The ratio $2\Delta/k_B T_C = 12$ for the gap maximum is much larger than the prediction from weak coupling theory, which points toward strong coupling. This interpretation is further supported by the fact that spectral weight from below the gap region is found to be recovered in the broad energy range up to about 0.5 eV, i.e. far above the maximum gap value.

6 Surface and interface properties

Interfaces between different materials can give rise to interesting new phases through the reconstruction of electronic states and correlation effects. Theoretical studies of the electronic and transport properties at interfaces between

a band- and a Mott insulator have been carried out in Sigrist's group. A further aspect of interfaces and surfaces is the fact that inversion symmetry is broken. The induced spin-orbit coupling effect has Rashba-like structure and leads to a spin splitting in the electronic band structure as has been observed by means of ARPES in the groups of Aebi and Grioni for BiAg₂ and Mg-W-interfaces.

6.1 Electronic reconstruction and transport in artificially structured materials

Interfaces between materials with different properties are of great interest in condensed matter physics and applications, because they provide the environment for novel electronic phases not available in the bulk and have a high potential for novel devices. This subject has gained new momentum with the tremendous progress in the fabrication of high-quality heterostructures in recent years, especially using certain types of transition metal oxides, e.g. LaTiO₃ – SrTiO₃ or LaAlO₃ – SrTiO₃ heterostructures [148, 149]. In this sense this discussion is also strongly connected with the Project 5. Since it contains important fundamental aspects of electron correlation it will be reported here.

Rüegg, Pilgram and Sigrist have studied aspects of strong electron correlations for a model of a BI/MI/BI sandwich heterostructure where BI is a band insulator and MI can be tuned from the simple metallic to the Mott insulating regime by varying the on-site repulsion within an extended Hubbard model [69]. The theoretical treatment of this continuous modification of electronic properties poses a considerable challenge. Among the first to tackle this problem were Okamoto and Millis who have used dynamical mean field theory (DMFT) to deal with the correlation effects [150]. As an alternative approach Ruegg *et al.* extended the Kotliar-Ruckenstein slave-boson mean-field scheme to the case of inhomogeneous systems. This allows a rather efficient analysis of the electronic properties over a wide range of on-site interaction strengths and geometrical parameters of the sandwich structure. Correlation effects manifest themselves in the marked separation between the weakly (Hartree) and strongly correlated (Mott) regimes, visible most spectacularly in the behavior of the charge rearrangement and the optical conductivity, indicating a correlation induced change in the charge fluctuation behavior. In the limit of strong interactions the coherent quasiparticles are confined to the interface region and are

responsible for the metallic behavior. Overall the strong renormalization effects of this quasi-two-dimensional multi-band system can be very well observed in this method, as long as long range order (magnetism, superconductivity, ...) is ignored. The aspect of order is the topic of future studies.

The complex and strongly renormalized band structure of these heterostructures involves both strongly dispersing and nearly localized bands, a situation which may provide favorable conditions to enhance thermopower effects. Ruegg *et al.* analyze the low-temperature electric and thermal transport properties in the same type of heterostructure as above based on the slave-boson approach. The transport quantities are derived from the Boltzmann transport equation in the relaxation time approximation. It can be shown that the strong electron interactions have a significant influence both on the Drude weight (free carrier response) and on the low-temperature thermoelectricity. The width of the Mott-insulating material is identified as the most important parameter, in particular, this parameter allows to optimize the thermoelectric powerfactor at low temperatures. This study is still in progress.

6.2 Spin-split states at BiAg₂-surfaces

The degeneracy of the spin states in a solid is the result of the combined time-reversal and inversion symmetries. When the former is broken in a magnetic field, states of opposite spin are separated in energy, a situation typically encountered in ferromagnets. However, the spin degeneracy may also be lifted by the spin-orbit interaction in a non-magnetic material when inversion symmetry is broken either in the bulk or at the surface (Rashba effect) [151]. The energy and momentum splittings are proportional to the atomic spin-orbit interaction, and to the electric field at the surface layer [152]. This effect has been experimentally verified by ARPES for the nearly-free-electron Shockley surface state at the Au(111) surface [153], with a small characteristic energy splitting $\Delta E = 2$ meV. The group of Grioni has now demonstrated a much larger separation of the spin-orbit split bands in ordered surface alloys formed by large-Z elements at the Ag(111) surface. For a one-layer BiAg₂ alloy a *giant* $\Delta E = 200$ meV splitting was observed, with a correspondingly large momentum offset $\Delta k = \pm 0.13 \text{ \AA}^{-1}$ of the two sub-bands (Fig. 33) [70]. The enhanced band separation has led to the first observation by scanning tunneling spectroscopy (STS) of a 1D-like divergence at

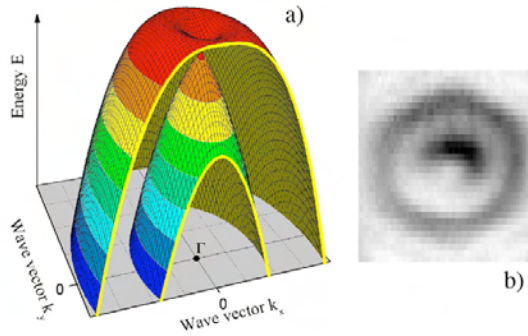


Figure 33: a) Calculated energy dispersion for the nearly-free-electron spin-orbit split bands. b) Constant energy contours ($E = -180$ meV) of the two sub-bands measured in the BiAg_2 alloy by ARPES.

the band edge in the electron density of states [71]. The band separation and band filling are reduced in the isostructural PbAg_2 alloy, which is consistent with the lower valence of Pb, and with the smaller atomic spin-orbit parameter. The experimental data are well reproduced by fully relativistic band structure calculations, which underline the importance of an in-plane component of the electric field as a source of the large splitting (Fig. 33a). As an extension of this work, spin-orbit split states have now been realized on a Si(111) substrate, by growing the BiAg_2 surface alloy on a silver buffer layer. These results open the way to a manipulation of the spin states by tuning the surface chemical composition.

6.3 Rashba spin-splitting at the Mg-W-interface

Quantum well states are a consequence of confinement in a quantum cavity. In this study Aebi and collaborators investigate with photoemission the influence of the interface electronic structure on the quantum well state energy dispersion in ultra-thin Mg(0001) films on W(110). Coupling between the sp -derived quantum well states and the substrate across the interface becomes manifest in deviations from the free-electron-like dispersion behavior. Most importantly, a marked level splitting was observed, which is interpreted as due to the Rashba effect at the interface. Such an interfacial electron beam splitting on materials with strong spin-orbit coupling is an essential ingredient for novel spintronic devices. The combination of a quantum cavity with a heavy, electron reflecting substrate reveals spin-splitting effects in ultra-thin films without conventional magnetism being involved. [72]

7 Theory of exotic many body states and quantum phase transitions

Strongly correlated many body systems provide an immense reservoir for unusual phases and physical properties whose theoretical description represents a challenge on the analytical and the computational level. Here we report on a series of theoretical studies of the groups of Baeriswyl, Mila, Sigrist and Troyer. They are devoted to the treatment of models, such as the Hubbard- and the t - J model near the Mott-insulating state, and the discussion of intriguing phases such as the supersolids, valence bond solids and phases displaying topological order. Moreover this section also considers the discussion of quantum phase transitions between different ground states. These studies are in parts motivated by the physics encountered in real materials such as the cuprates and cobaltates. However, also model related aspects are addressed as well as issues being potentially relevant in the context of quantum computation.

7.1 Competition between magnetism and superconductivity on the triangular lattice

Mila and collaborators have investigated the phase diagram of the t - J model on a triangular lattice using a variational Monte Carlo approach [73]. They have used an extended set of Gutzwiller projected fermionic trial wave functions allowing for simultaneous magnetic and superconducting order parameters. Upon electron doping (with a hopping integral $t < 0$), this phase is surprisingly stable variationally up to $n = 1.4$, while the $d_{x^2-y^2} + id_{xy}$ order parameter is rather weak and disappears at $n = 1.1$. For hole doping, however, the coplanar magnetic state is almost immediately destroyed and $d_{x^2-y^2} + id_{xy}$ superconductivity survives down to $n = 0.8$. For lower n , between 0.2 and 0.8, saturated ferromagnetism occurs. Moreover, there is evidence for a narrow spin density wave phase around $n = 0.8$. Commensurate flux phases were also considered, but these turned out not to be competitive at finite doping. These results show that the single-band t - J model is not sufficient to explain the occurrence of superconductivity in hydrated cobaltates.

7.2 Aspects of Mott-localization

The Hubbard model undergoes a (Mott) metal-insulator transition as a function of the onsite repulsion U at $T = 0$ and for $n = 1$ (half filling). In cases where this transition is not pre-

ceded by the onset of antiferromagnetic long-range order, for instance for the honeycomb lattice [154, 155], the critical value U_c separates the regimes of delocalized and localized many-electron states. This is explicitly confirmed by variational studies in the group of Baeriswyl using two types of wave functions, a (delocalized) Gutzwiller ansatz for $U < U_c$ and its dual wave function, a localized state for $U > U_c$ [156].

Away from half filling, the Mott transition is replaced by a crossover. An important physical quantity signaling this crossover is the Drude weight D , which is expected to be proportional to the number of electrons in the delocalized (Fermi liquid) regime, but to the number of holes (of the doped Mott insulator) in the localized regime. This picture agrees with exact (Bethe ansatz) calculations for the one-dimensional Hubbard model, yielding a crossover from a $D \sim n$ behavior for small U to a $D \sim 1 - n$ behavior at large U . Starting from $U_c = 0$ for $n = 1$ Baeriswyl and collaborators find that the crossover value $U_c(n)$ increases as n decreases. Thus doping the Hubbard model at a fixed value of U can lead from an initial localized state at half filling to a delocalized metallic state away from half filling. A similar behavior is found for 1D spinless fermions coupled by a nearest-neighbor repulsion. Baeriswyl, Eichenberger and Gut have earlier suggested that such a crossover occurs in layered cuprates, namely from a localized underdoped phase to a delocalized overdoped phase [74].

An alternative approach for describing this crossover is, in terms of a dual pair of variational wave functions, one linked to the filled Fermi sea, the other to the fully localized limit for $U \rightarrow \infty$, in analogy to the approach used for the Mott transition at half filling. Unfortunately, this procedure is very challenging, especially in two dimensions, where the ground state for $U \rightarrow \infty$ is known only for very special lattices, such as those with ‘‘cage symmetry’’.

7.3 Ground states of the t - t' Hubbard chain

The t - t' Hubbard chain, defined by the Hamiltonian

$$\begin{aligned}
 H = & - t \sum_{i,\sigma} \left(c_{i,\sigma}^\dagger c_{i+1,\sigma} + c_{i+1,\sigma}^\dagger c_{i,\sigma} \right) \\
 & + t' \sum_{i,\sigma} \left(c_{i,\sigma}^\dagger c_{i+2,\sigma} + c_{i+2,\sigma}^\dagger c_{i,\sigma} \right) \\
 & + U \sum_i n_{i,\uparrow} n_{i,\downarrow} \quad (3.5)
 \end{aligned}$$

($t > 0$, $t' > 0$), represents a highly non-trivial extension of the simple Hubbard model ($t' = 0$). This is due to the Fermi ‘‘surface’’, which changes from 2 Fermi points for $t' < 0.5t$ to 4 Fermi points for $t' > 0.5t$, or from one-chain to two-chain behavior. The group of Baeriswyl investigated the phase diagram for $n = 1$ (half filling) in the U - t' plane. For a fixed value of U there are two transitions as t' varies, a first transition from a region with a charge gap, but no spin gap (the case of the simple Hubbard chain) to a region with finite charge and spin gaps, and a second transition from the region with two gaps to one with a finite spin, but no charge gap. This second transition is an insulator-to-metal transition which had been previously described as a dielectric catastrophe [75]. In a more recent work Baeriswyl and coworkers have used both analytical (bosonization) and numerical (DMRG) techniques for describing the two transitions and for characterizing the various phases [76]. The gross features of the phase diagram are well described by the standard theory of commensurate-incommensurate transitions. For the transition line $t'_c(U)$ separating the metallic phase from the spin-gapped insulator they have derived an explicit analytical expression.

Using DMRG calculations a detailed numerical analysis of the excitation spectrum was performed and the charge and spin density distributions in various sectors of the phase diagram were calculated. In particular, the evolution of the charge and spin gap with increasing next-nearest-neighbor hopping amplitude t' was studied. Evidence for a spin gap was found in the parameter range $0.5t < t' < t'_c$, in agreement with previous studies. It has been shown here that the change in the topology of Fermi surface at the insulator-metal transition is reflected in the appearance of incommensurate modulations of the charge density. Incommensurate spin-density distributions in the triplet sector are always present in the metallic phase, but can also appear independently in the spin-gapped insulator due to frustration.

For $t' \gg t$, Baeriswyl and collaborators have argued that the insulator-metal transition can be best understood starting from the limit of two uncoupled chains. At small U , turning on the zigzag coupling between the chains destroys the commensurability present for a single chain, and leads to a metallic phase. At large U , the system is insulating and behaves as two weakly coupled Heisenberg chains. The obtained estimate shows that the insulator-

metal transition in this regime occurs when the shift in the Fermi energy is comparable to the size of the charge gap in the isolated Hubbard chain.

7.4 Valence-bond order in bisimplex lattices

Frustrated lattices show a large variety of ground states, ordered and disordered. In an extensive study, Indergand and collaborators (Sigrist'group) have investigated ordered phases which can occur in the Hubbard and t - J -model as special fractional fillings on various bisimplex lattices, such as the kagome, the pyrochlore and the checkerboard lattice [77, 78]. It has been shown that a metal-insulator transition can occur together with a peculiar valence bond order which breaks inversion symmetry. In order to provide evidence for this type of ordered phase various theoretical methods (plaquette perturbation theory, Gutzwiller renormalization mean field theory, exact diagonalization, DMRG and CORE, N-patch weak-coupling renormalization group theory for the kagome chain) have been applied yielding a consistent support for valence bond ordered phases if the electron concentration corresponds to two electrons per unit cell. For example on the kagome lattice the valence-bond ordered state has stronger correlations on one set of triangles (e.g. up tri-

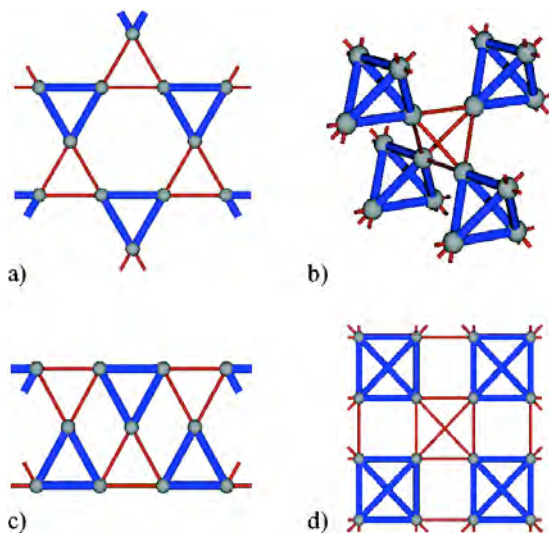


Figure 34: Four different bisimplex-lattices. The kagome lattice (a) and the pyrochlore lattice (b) together with their lower dimensional analogues, the kagome strip (c) and the checkerboard lattice (d). The two types of corner sharing units (“up” vs “down”) are distinguished by the line width. They correspond to the bond order wave symmetry breaking pattern occurring at a filling of two electrons per unit cell.

angles) and weaker ones on the others (down triangles), while analogous patterns are found for the other bisimplex lattices (Fig. 34). This class of systems are a representative case for a bond order purely based on electronic interaction without invoking electron-phonon interaction.

7.5 Supersolids

The supersolid phase combines two properties which seem mutually exclusive: liquid and solid. Thus it would represent an exotic quantum state if it were realized in nature. Here we report on numerical simulation for ^4He in Troyer’s group and an alternative realization in a quantum antiferromagnet by Mila’s group.

a) *Supersolid helium* Following experimental evidence for the possible existence of a supersolid in ^4He [157, 158], Troyer and coworkers have performed *ab initio* quantum Monte Carlo simulations of solid helium and found that a perfect helium crystal is insulating and not a supersolid. They found that the Andreev-Lifshitz-Chester vacancy mechanism for a supersolid is unstable in helium since vacancies attract and phase-separate instead of Bose-condensing [79]. This attraction between vacancies and interstitials is also observed in classical Lennard-Jones crystals [80] and solid helium is thus still a quite classical solid. Since a perfect single crystal of solid ^4He is insulating, the phenomenon observed by Kim and Chan is most likely due to crystal defects. Troyer and collaborators show, using quantum Monte Carlo simulations, that superflow can occur along grain boundaries [81] and screw dislocations [82].

While the supersolid phase of matter is thus excluded in perfect helium crystals there is evidence for the existence of lattice supersolids: lattice supersolids can be realized using gases of ultra-cold polar molecules in triangular optical lattices [83].

b) *Supersolid phases of quantum antiferromagnets* From a theoretical point of view, the existence of a supersolid phase is now well documented for a number of lattice bosonic models [83][159, 160, 161]. Bosonic models can also be realized in quantum antiferromagnets, a rather clean way being to consider weakly coupled dimers in a magnetic field. Around the critical field where one of the triplets crosses the singlet, a hard-core boson description is very natural. In this mapping, an empty site represents a singlet, an occupied site a triplet, and the chemical potential describes

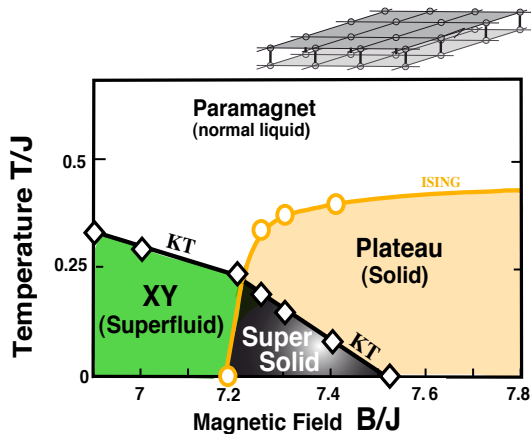


Figure 35: Magnetic-field-temperature phase diagram of the bilayer system depicted on the top. The supersolid region (dark gray) is displayed together with its neighboring phases: superfluid, solid, paramagnet.

the magnetic field. Regarding the possible low-temperature phases, an insulating solid phase signals a magnetization plateau, a Bose-Einstein condensation represents magnetic ordering of the transverse spin components, and a supersolid phase corresponds to the coexistence of both orders. In the first part of this study, Mila's group has investigated the signatures of such a supersolid phase in a quantum antiferromagnet, namely a spin-1/2 bilayer, with emphasis on a precise characterization of the quantum and thermal phase transitions out of the supersolid state [84]. The resulting magnetic-field-temperature phase diagram is depicted in Fig. 35. They have shown that both $T = 0$ quantum phase transitions (superfluid-supersolid and supersolid-solid) as well as the thermal transition (supersolid-paramagnet) display special features of direct experimental relevance. In particular, the melting of the supersolid is a two-step process in contrast to standard transitions usually observed in quantum antiferromagnets.

In the second part of this study, Mila and collaborators have investigated more realistic bosonic models of frustrated quantum magnets, in which the kinetic energy of the bosons is suppressed due to frustration and not to anisotropic exchange couplings [85]. In this situation, the kinetic energy is dominated by correlated hopping processes, and these processes induce a very strong tendency towards supersolid phases, even in cases where no plateau can be stabilized.

7.6 Exotic quantum phase transitions

Recently a theory of deconfined quantum criticality [162] has been proposed for an unconventional quantum phase transition between two phases with different broken symmetries. According to Landau theory such a phase transition should be of first order, but it has been conjectured that in quantum systems a second order quantum phase transition with deconfined fractionalized excitations could exist in bosonic or magnetic systems. By simulating the effective action of the proposed deconfined critical point, Troyer and collaborators could show that in the $U(1) \times U(1)$ -symmetric case the transition is weakly first order, in contrast to the proposed theory [86], but they have preliminary evidence in spin-1 quantum magnets that in a $SU(2)$ -symmetric model such an unusual second order quantum critical point may exist [87].

7.7 Topological phases and anyonic models

Strongly correlated quantum systems can exhibit unusual quantum liquid phases with topological order. Such a phase, if realized in an experiment, would pave the way towards stable, robust and decoherence-free quantum bits: since the information is encoded in a non-local topological property no local source of noise can destroy the phase. Troyer and collaborators have shown by quantum Monte Carlo simulations that an abelian topological phase would be stable under imperfect realization with large corrections or noise terms, and is also stable under local dissipation [88]. While the stability against noise was theoretically expected Troyer and coworkers could quantitatively analyze the breakdown of the phase at a second order quantum phase transition in the Ising universality class and clarify the previously unclear stability against dissipation. Since no material exhibits topological quantum liquid phases without edge states, a promising route to realize these phases is in artificial devices emulating quantum lattice models with topological phases. The first such proposal was to realize a quantum dimer model on a triangular lattice, built from an array Josephson junctions [89]. Troyer and collaborators have recently performed simulations to quantitatively determine the microscopic operating parameters of such a device [90]. The results show that while such a device will indeed exhibit topological order, however the operating temperatures are far too low for current technology. Even more interesting is a non-abelian topological phase with deconfined non-abelian any-

onic excitations, since their braiding would allow universal quantum computation. To investigate the interactions between such anyons, Troyer and collaborators have developed an anyonic version of a quantum spin model, which could be realized e.g. by trapping anyonic quasiparticles on quantum dots in non-abelian fractional quantum Hall states. They have solved the anyonic chain with nearest neighbor interactions and have solved the one-dimensional chain of anyons, realizing a mapping of anyonic quantum chains to minimal models of conformal field theories [91]. As an extension they studied models with longer-range interactions, generalizing the Majumdar-Ghosh spin chain to anyonic matter, and found a plethora of phases stabilized by topological symmetries, and a number of special phase transitions [92]. It turns out that these anyonic chains exactly map to many exactly solvable statistical mechanics models that so far were just toy models now have microscopic realizations.

8 Phase diagram of BaVS₃ and BaVSe₃

Due to an interplay between charge, spin and orbital degrees of freedom, quasi-one-dimensional BaVS₃ has for a long time attracted both experimental and theoretical interest. A series of phase transitions which the compound undergoes, as well as its rich phase diagram, have yet to be completely understood. At ambient pressure, a structural transition occurs at $T_s \sim 240$ K, followed by a metal-insulator transition which takes place at $T_{MI} \sim 70$ K, and finally a magnetic ordering appears at $T_X \sim 30$ K.

The recent studies in Forró's group have focused mainly on understanding the high-pressure phase, marked by a sharp suppression of the metal-insulator transition above $p \gtrsim 1.7$ GPa and an appearance of a non-Fermi liquid behavior for $p \gtrsim 2.0$ GPa. Ott's group addresses the magnetic properties in a detailed NMR study.

8.1 The collapse of the metal-insulator transition in BaVS₃

One of the important questions pertaining to the physics of BaVS₃ is what happens to the magnetic transition when pressure is applied. In order to trace the phase diagram of this compound, electrical resistivity as a function of temperature, pressure, and magnetic field was measured in high purity single crystals. The metal-insulator (MI) transition collapses to $T = 0$ at the critical pressure value, $p_{cr} \approx 2$ GPa

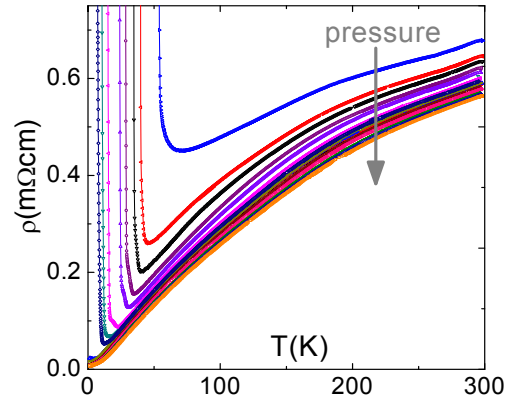


Figure 36: The temperature dependence of resistivity of a BaVS₃ sample is shown for different pressures.

(Figs. 36 and 37). In the 1.8–2.0 GPa pressure range, where the MI transition appears below 20 K, one can observe a sudden collapse of the MI phase boundary upon increasing pressure. Indeed, the MI phase boundary collapses to zero within the narrow pressure range of 0.3 GPa around the critical pressure, p_{cr} . This indicates that the transition is more complex than a smooth pressure-induced three-dimensionalization of the system, common in quasi-one dimensional materials. Furthermore, at a fixed pressure a magnetic field may induce insulator to metal transition. In high quality samples, a hysteresis appears in all measured physical quantities in the 1.8–2.0 GPa region, both in function of temperature and of magnetic field. Since the appearance of hysteresis is the usual sign of a first order phase transition, it can be concluded that in the pressure region where the $T_{MI} < T_X$ the order of MI transition is changed: from the ambient

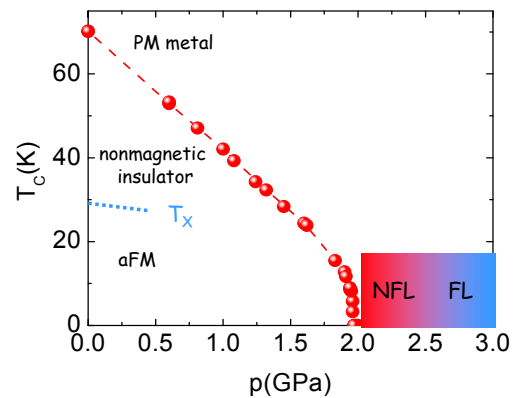


Figure 37: Phase diagram of BaVS₃, encompassing numerous phases: from a low-pressure insulating ground state, to a high-pressure non-Fermi liquid phase.

pressure second order, it now becomes a first order transition. All these observations point to the fact that there is a crossing of the MI and the magnetic phase boundaries upon increasing pressure, at $T \sim 20$ K, implying that the magnetic transition has only a weak pressure dependence, in contrast to the MI transition.

8.2 The high-pressure non-Fermi liquid state

Understanding the high-pressure non-Fermi liquid (NFL) state of BaVS_3 is another major challenge. At high temperatures, the compound is a metal with its vanadium d^1 -electron shared between the broad quasi-one dimensional d_{z^2} band and the narrow, but more isotropic e_g band. At a critical pressure $p_{cr} \sim 2$ GPa, where MI transition is suppressed, a NFL behavior with a power-law dependence of the resistivity ($\rho = \rho_0 + AT^n$) sets in. In order to clarify the microscopic origin of this NFL and understand the role of the d_{z^2} and e_g electrons in this state, Forró and coworkers applied pressure, $p > p_{cr}$, and magnetic field to tune the interaction within and in-between these bands. With pressure, one can tune the power-law exponent from the value of $n \approx 1.5$ at p_{cr} , to $n \sim 1.9$ at $p \sim 2.8$ GPa. Similarly, the parameters A and ρ_0 show a strong pressure dependence. These results indicate that close to the phase boundary, below ~ 15 K, substantial charge density wave fluctuations still exist in BaVS_3 above p_{cr} . They give the NFL character of the resistivity. Since these fluctuations disappear with pressure, the NFL behavior is replaced by a standard Fermi liquid behavior.

8.3 NMR study of BaVS_3

From earlier experiments, a sequence of phase transitions with decreasing temperature has been identified for BaVS_3 . New measurements in Ott's group probing the magnetic susceptibility $\chi(T)$ and the NMR response of the ^{51}V nuclei of single crystalline samples at low temperatures were made, covering temperatures from 0.1 to 300 K. In $\chi(T)$ the previously established metal-insulator transition at 69 K is reflected in a distinct cusp. No evidence for the previously reported magnetic transition at 30 K in powder samples is found in $\chi(T)$ but the loss of the NMR signal close to that temperature indicates very rapid magnetic fluctuations in a narrow temperature window. A discontinuous change of the resonance shift at 30 K and an order of magnitude enhancement of the NMR line width from above to below 30 K confirm the occurrence of some type of transition (Fig. 38). At very low temperatures,

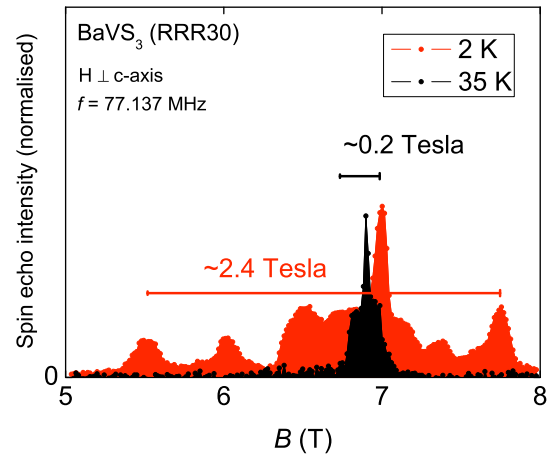


Figure 38: ^{51}V NMR field sweep spectra of BaVS_3 above and below $T_X = 30$ K.

$\chi(T)$ reveals field dependent broad maxima and hysteresis effects, without any clear evidence for another phase transition, however. The magnetic response probed by NMR is very complicated below 30 K. The line-width of the NMR signal increases considerably with decreasing temperature and the position of the signal depends very strongly on the relative orientation between the crystal lattice and the external magnetic field. Progress in establishing the magnetic behavior of this compound at very low temperatures may be expected only if larger high-quality single crystals become available.

8.4 BaVSe_3

A valuable insight into the high pressure behavior in BaVS_3 may be acquired from the study of its sister compound, BaVSe_3 . It is only with the synthesis of high-quality single crystals of BaVSe_3 by H. Berger that it has become possible to perform reliable high-pressure studies of this compound. The larger selenium atom replaces the sulphur atom, producing the quasi-one dimensional structure almost identical to the one of BaVS_3 , but with an increase in the orbital overlaps between the chains. As a result, the physical properties of BaVSe_3 are very similar to those of BaVS_3 under high pressure. Namely, this compound is metallic in the whole temperature range. It undergoes a ferromagnetic transition at $T_c \approx 42$ K, resembling the magnetic transition in BaVS_3 at $T_X \approx 30$ K. Furthermore, the resistivity at low temperatures shows a powerlaw dependence with an exponent $n \approx 2$, which is a characteristic of Fermi liquid behavior.

9 Two-dimensional transition metal oxides

Layered transition metal oxides are known for their large variety of unusual properties, low-temperature phase and puzzling phase transitions. The most prominent CuO_2 -systems leading to high-temperature superconductors are part of Project 2 related to the superconductivity. In this project Na_xCoO_2 has been studied mainly in Ott's group at $x = 0.5$ with the enigmatic magnetic and metal-insulator transitions and at $x \approx 0.7$ with the puzzling magnetic behavior of the metallic system showing also signatures of local Co moments. Moreover manganese films have been investigated by scanning tunneling spectroscopy in Fischer's group in order to gain insight in the interplay of spin, orbital, charge and lattice degrees of freedom and also to probe whether phase separation plays a role in the electronic properties of these materials.

9.1 Na_xCoO_2 - Spin and charge configurations

The compound series Na_xCoO_2 ($0 < x < 1$) provides a system where both spin and charge degrees of freedom are confined to Co planes which, together with an oxygen network and intercalated planes of different arrangements of Na atoms, form the crystal lattice. It turns out that the Na subsystem does not participate in electronic and magnetic responses of the compounds directly, but the concentration x has, nevertheless, a strong influence on the physical properties of the individual compounds. A special case is $x = 0.5$. These measurements of the magnetic susceptibility $\chi(T)$ and the NMR response of the ^{23}Na nuclei identified the magnetic nature of a phase transition with an onset at 88 K (Fig. 39) [93]. This is quite puzzling because the preceding paramagnetic phase is characterized by a weak Pauli-type susceptibility, i.e. there is no evidence for the presence of localized moments on the Co sites. The temperature dependence of both $\chi(T)$ and the NMR spin-lattice relaxation rate $T_1^{-1}(T)$ indicate a loss of magnetic degrees of freedom with decreasing temperature above the transition. Below the transition, the internal staggered fields lead to two magnetically inequivalent Na sites with a constant ratio of the corresponding hyperfine fields with decreasing temperature. With respect to electronic transport, it is noted that the conductivity σ is very low and decreases with decreasing temperature below 300 K. The phase transition at 88 K is clearly not reflected in $\sigma(T)$. At 53 K, a discontinuous change of the negative slope $\partial\sigma/\partial T$ to a much enhanced negative

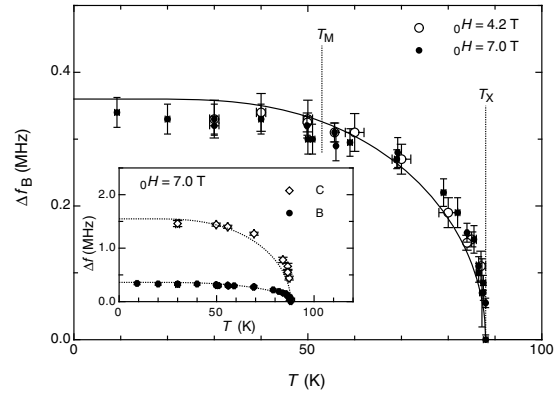


Figure 39: Width Δf_B of the rectangle-shaped NMR signal B as a function of temperature T . Δf_B is extracted from the ^{23}Na NMR spectra measured in magnetic fields $\mu_0H = 4.2$ T and $\mu_0H = 7.0$ T. Inset: Δf of the signals B and C .

value is observed. At very low temperatures, $\sigma(T)$ tends to saturate to a low but still non zero value. The NMR responses indicate that no significant charge rearrangement occurs at either of the two transitions. Although the NMR response indicates some magnetic component for the transition at 53 K, the temperature dependence of the hyperfine fields does not reveal a significant change of these values at and below this transition.

For $x > 0.5$, the compounds are metallic. The

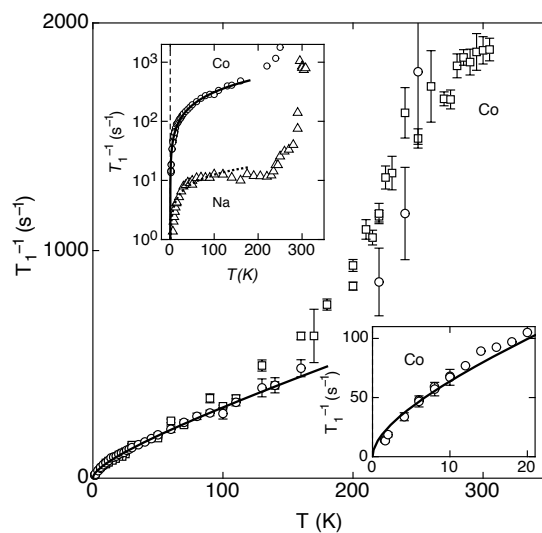


Figure 40: Temperature dependence of the ^{59}Co spin-lattice relaxation rate $^{59}T_1^{-1}$ measured in two different external magnetic fields and temperatures between 1.5 and 300 K. Lower inset: Details of $^{59}T_1^{-1}(T)$ at low temperatures. Upper inset: comparison of the $^{59}T_1^{-1}(T)$ and $^{23}T_1^{-1}(T)$ data (^{59}Co and ^{23}Na). The solid and dotted lines represent fits to the data.

NMR data for the compound $\text{Na}_{0.7}\text{CoO}_2$ is anomalous across the entire temperature range below 300 K, however (Fig. 40) [94]. Below room temperature, Ott and collaborators observed considerable reductions of the spin lattice relaxation rates for both ^{23}Na and ^{59}Co nuclei by one to two orders of magnitude, without a clear indication for the reasons of this reduction [94]. In particular, no clear evidence for any charge redistribution within the system has been found. The temperature dependence of the magnetic susceptibility $\chi(T)$ reflects a Curie-Weiss type behavior above 100 K. Below a transition region, yet another Curie-Weiss type feature with much reduced values for the effective moment and the paramagnetic Curie temperature is obtained at $T < 20$ K. The spin-lattice relaxation rates for both types of nuclei at very low temperatures indicate the absence of magnetic order above 0.1 K and confirm the confinement of itinerant charge carriers to the Co planes. Although the $\chi(T)$ features mentioned above indicate the presence of local moments on Co sites, the NMR data, especially the rather unusual behavior of the temperature variations of the Knight shift and the spin-lattice relaxation rates, are interpreted as revealing the itinerant nature of the Co derived d electrons

For both these compounds, the magnetic and electronic properties are anomalous in many ways. No convincing models have yet been found to explain these observations.

9.2 Local electronic properties of manganite thin films

In manganite compounds such as $\text{La}_{0.67}\text{Ca}_{0.33}\text{MnO}_3$ (LCMO), the resistivity ρ can be switched from insulating ($d\rho/dT < 0$) to metallic ($d\rho/dT > 0$) by cooling across the ferromagnetic Curie temperature or through the application of a magnetic field. The transport properties of the high-temperature phase have been attributed to the presence of polarons [163, 164, 165], electrons trapped in a local lattice distortion, but there is currently no consensus on the fate of these polarons at the transition. While some authors claim that the onset of magnetic order delocalizes the trapped electrons [163, 164], others observe a remaining polaronic signature at low temperatures [166, 167]. In addition, intrinsic phase separation has been proposed to play a major role at the transition, with the huge decrease of resistivity stemming from the percolation of metallic domains growing in an insulating matrix [168]. Scanning tunneling

spectroscopy (STS) is an ideal technique to probe electronic properties and their spatial dependence, but its capabilities have not yet been fully exploited in manganite studies since most works either report the thermal behavior of single spectra [169, 170] or conductance maps at a single energy [170, 171]. Furthermore, results on films of the same nominal composition are often conflicting (for example, Ref. [171] observes strong inhomogeneities in conductance maps while Ref. [170] fails to do so). The contribution of Fischer's group to the understanding of these problems relies, firstly, on the growth and careful characterization of the samples, and secondly, on the study of the spatial dependence of electronic properties not only at zero bias, but also at energies of the order of the polaronic binding energy.

These studies show that substrate-induced strain modifies macroscopic transport properties of manganite films but also that an inhomogeneous structural relaxation process takes place on increasing thickness when mismatch with the substrate is large (see Project 5). This coexistence of regions with different degrees of strain within a film implies the presence of regions with different (local) transport properties, a situation to be avoided if one expects to gain insight into the intrinsic properties of these materials.

Fischer and collaborators have therefore studied two kinds of structurally homogeneous LCMO samples: ultra-thin and homogeneously highly-strained films grown on SrTiO_3 (STO) and homogeneously weakly-strained films grown on NdGaO_3 (NGO). In this study, the high strain film is 28 nm thin and has a metallic-insulating transition of about 150 K, while the low-strain film is 42 nm thick and has a transition temperature of about 220 K. STS measurements were performed in a setup constructed as a part of this project, that allows temperature stabilization in the range 4.2 to ~ 320 K. For both types of films, the topography exhibits plateaus separated with steps of unit-cell-multiple height and no substantial difference in the spectroscopic features was observed between different plateaus [95]. All the conductance measurements were calculated from $I(V)$ and normalized as $(dI/dV)/(I/V)$ in order to remove the tunnel barrier dependence [96].

Tunneling spectra measured on manganite thin films reveal a gap at low bias, seen as a kink, a conductance depletion, and a weak zero-bias conductance. This kink occurs at approximately 0.2–0.3 eV, roughly twice the polaron binding energy obtained from resistivity. Pre-

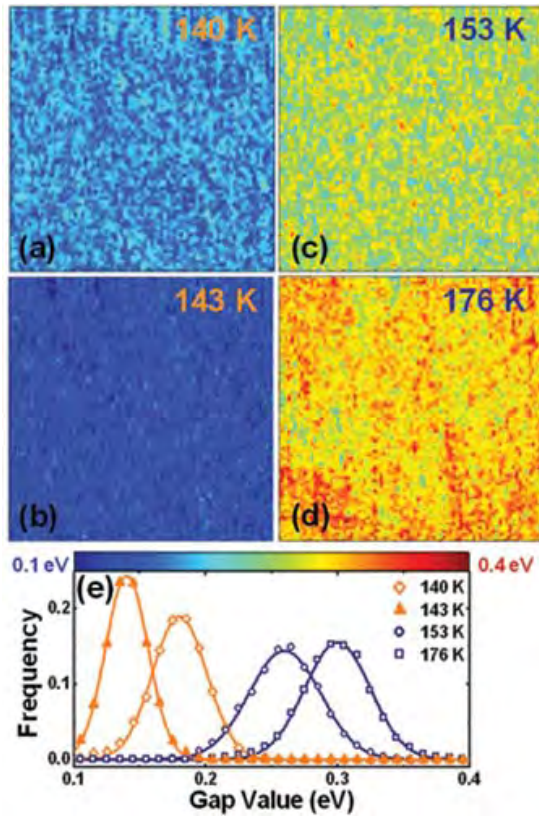


Figure 41: Mapping of local gap values at (a) 140, (b) 143, (c) 153 and (d) 176K. All maps correspond to $60 \times 60 \text{ nm}^2$ areas with a resolution of $0.75 \text{ nm}/\text{pixel}$. (e) Distributions of gap values (symbols) obtained from the maps fitted with a Gaussian law (lines).

vious measurements have shown that the spectra are gapped at all temperatures, not only in the high temperature ‘insulating’ phase, but more strikingly also in the low-temperature ‘metallic’ phase [96]. At room temperature, the gap tends to vanish, indicating a change in the nature of the polarons. Films have proven to be ideal systems to investigate electronic phase separation in the absence of chemical and crystalline inhomogeneities. Fig. 41 shows maps of local gap values for a highly-strained film, at temperatures close to the metal-insulator transition, where phase separation would be most likely. Within the experimental resolution, a single gap is detected everywhere, reflecting the film homogeneity and indicating that a phase separation between ‘metallic’ and ‘insulating’ domains does not occur at length scales greater than 1 nm . Similar conclusions are found when considering the spectroscopic properties at energies close to the Fermi level. The behavior of local spectroscopic properties for the weakly and highly strained samples is shown in Fig. 42. At high temperatures, both types of films present roughly the same spectral characteristics. They exhibit roughly the

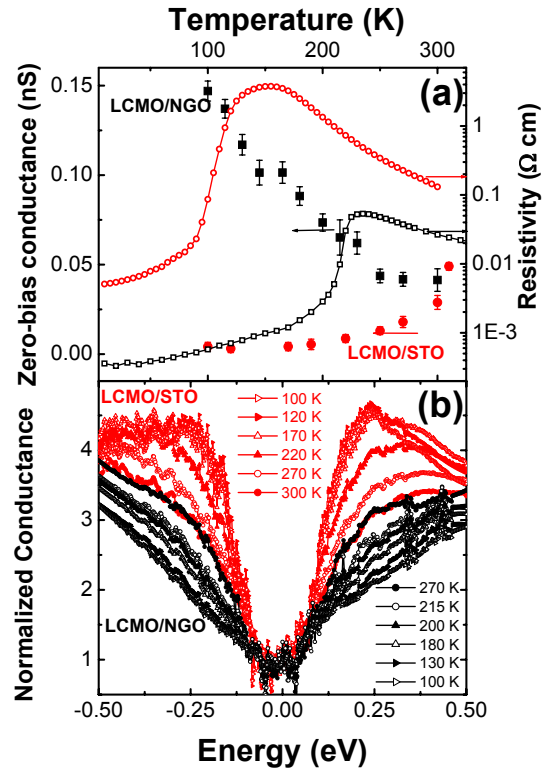


Figure 42: (a) Resistivity and zero-bias conductance as a function of temperature for a 42 nm thick film on NGO (black) and a 28 nm thick film on STO (red). (b) Normalized conductance curves for different temperatures.

same zero-bias conductance values (Fig. 42a) and the spectral shape of both films is similar (Fig. 42b).

There is a sharp contrast between the two kinds of films when the temperature is reduced. In the case of weak strain, zero-bias conductance is low and roughly constant at high temperatures but increases upon cooling through the transition. Highly strained films exhibit zero-bias conductance values similar to those of the weakly strained film at high temperatures, which rapidly decrease on cooling. On decreasing temperature, the spectral shape also evolves differently for both kinds of samples. Films on STO become increasingly insulating upon cooling, the kink becomes more marked and the depletion sharper, and eventually peak-like features develop on the edges of the depletion [96]. The peaks are more developed on the positive bias side, which corresponds to the unoccupied states in the sample. On the other hand, in weakly strained films the kink becomes less marked on cooling and no peak-like features develop down to 100 K . For both samples, the characteristic energy of the kink decreases on decreasing temperature. This intriguing behavior appears to be related

to the strain state. However, since STM is a surface-sensitive technique, further studies have to be undertaken to discern if the observed behavior represents that of the bulk of the film or it stems from a different phase induced at the surface. Cation segregation and changes in the Mn valence have been reported to occur at the surface of manganite films [172, 173] and the formation of a charge-ordered surface state induced by the truncated symmetry has been proposed [174]. On the other hand, strain modifies the balance of the different interactions taking place in manganites, and it could give rise to a phase with a different nature altogether.

However, the zero-bias conductance temperature dependence is consistent with the evolution of the gap-edge peaks for both films. For the highly strained film, the zero bias conductance decreases while the peaks develop possibly indicating a transfer of spectral weight from the Fermi level to the gap-edge energies. For the weakly strained film, the zero bias conductance peak increases together with a vanishing of the peaks. More measurements have to be done to check whether the trend of the spectral characteristics of the highly-strained films proceeds at temperatures much lower than the transition temperature.

10 Spectroscopy and transport properties in bismuth and carbon-based systems

Graphite and bismuth, as important examples of elemental semi-metals, represent a material class with outstanding electronic properties [175, 176]. While most basic aspects of these apparently simple materials are well established, still many experimental effects are not understood. Much enthusiasm drives this field again since the recent discovery of the production of single-layer graphene flakes [177, 178]. In this section we report on investigations of the optical properties of bismuth in van der Marel's group showing the presence of plasmon excitations. The same group also studied the issue of the universal optical conductance of graphite. Sigrist and collaborators discuss the problem of Anderson localization in graphene ribbons showing that under certain circumstances one perfectly conducting channel is surviving in this type of quantum wire. The Empa team around Groening investigates the defects on graphite and carbon nanotubes and the possible application to design in this way devices behaving like quantum dots.

10.1 Infrared plasmarons in elemental bismuth

The optical and infrared properties of bismuth provide a fascinating picture of an elemental semi-metal. In their study van der Marel and collaborators have focussed on the frequency and temperature dependence of the optical properties of single-crystal bismuth by means of FT spectroscopy in the IR and visible spectral range. The optical data show an absorption anomaly in an energy range which is incompatible with any of the direct interband transitions. In the experiment a tiny prepeak structure precedes a pronounced absorption peak in the mid-infrared region. As displayed in Fig. 43, this anomaly has a temperature dependence following the gradual reduction of the screened plasma frequency ω_p^* with decreasing T . The onset of the prepeak absorption always appears above ω_p^* which demonstrates a close relation between the two effects. An extended Drude analysis reveals that the position of the absorption feature corresponds to an abrupt increase of the scattering rate. This corresponds very much to the ex-

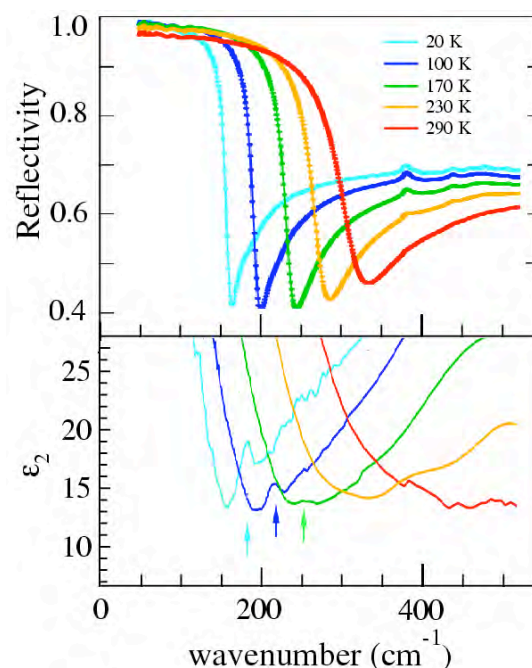


Figure 43: (a) Infrared reflectivity of pure bismuth for 6 different temperatures. The deep minimum corresponds to the screened plasma frequency for each temperature. (b) According to conventional wisdom the plasma peak can not be observed in the imaginary part of the dielectric function: electromagnetic waves have transverse polarization, whereas plasmons are longitudinal. However, ϵ_2 exhibits a weak but distinct absorption peak at the screened plasma frequency. This is a possible consequence of charge-carrier plasmon interactions.

pectations in the case of electron-boson interaction. The electron-energy-loss-boson function obtained from experiment together with the expected plasmon peak lead to a second feature centered at the same frequency as the prepeak. This provides an unambiguous proof for a coupling between the electron system and a longitudinal bosonic collective mode, an interaction known as a *plasmaron*. To the best of our knowledge this represents the first optical observation of such interaction.

10.2 Universal optical conductance of graphite

One of the most remarkable macroscopic manifestations of quantum mechanics is the appearance of a universal conductance e^2/h , where e is the elementary charge and h is the Planck constant, in various physical phenomena. This value appears in the quantum Hall effect [179, 180], in the superconductor-insulator transition in two dimensions [181, 182] and in 1D ballistic transport [183, 184, 185]. Notably, all these observations were restricted so far to the DC transport. Monolayer graphene [186, 178] represents an interesting example, where the optical, or AC, conductance due to optical interband transitions is expected to be frequency independent and solely determined by the same universal value [187, 188, 189] in a broad range of photon energies:

$$G_1(\omega) = G_0 \equiv \frac{e^2}{4h} \approx 6.08 \cdot 10^{-5} \Omega^{-1} \quad (3.6)$$

(index '1' refers to the real part). Quite remarkably, $G_1(\omega)$ does not depend on microscopic parameters that normally determine optical properties of materials. This is a consequence of the unusual low-energy electronic structure that resembles the dispersion of relativistic particles [178]. At energies considerably smaller than the bandwidth (~ 2 eV), the dispersion of monolayer graphene features massless electron and hole conical bands $\epsilon_{e,h}(\mathbf{k}) = \pm \hbar v_F |\mathbf{k} - \mathbf{k}_D|$ formed by the p_z orbitals (as shown in the inset of Fig. 44c), where \mathbf{k}_D is the momentum of the Dirac point (there are two of them at the points K and K' of the Brillouin zone) and $v_F \approx 10^6$ m/s is the Fermi velocity. This type of dispersion is qualitatively different from more common quadratic massive bands, as has been most convincingly demonstrated by a $E_n(B) \propto \text{sign}(n) \sqrt{|n|B}$ field dependence of Landau levels [177, 190, 191, 192].

The absolute value of the optical conductance in graphene, the determination of which is an experimentally challenging task, has not yet been reported. However, it is legiti-

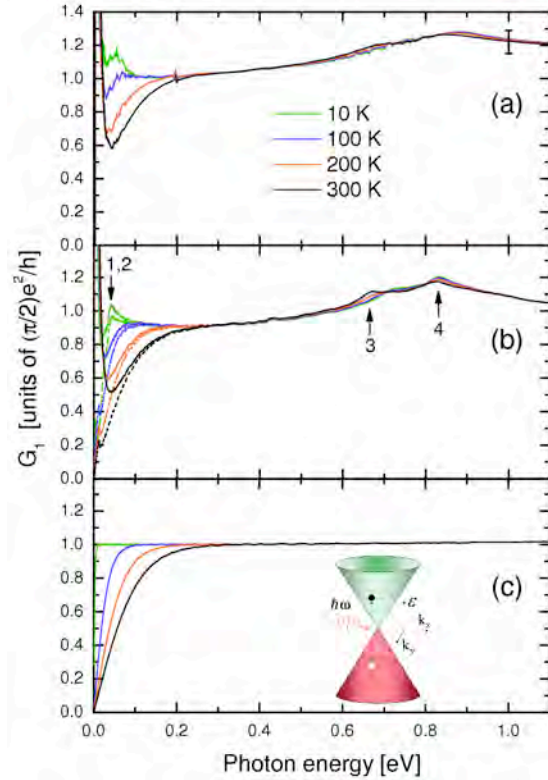


Figure 44: The real part of the optical sheet conductance of graphite per layer (a - experiment, b - calculation) as well as the calculated conductance of isolated undoped graphene (c). In panel (b) the dashed lines indicate the interband conductance only, while the solid line represent the total conductance with a Drude peak added (the scattering rate is 5 meV). In panel (c) the thermally activated Drude peak is not shown.

mate to ask whether the predicted universality can already be observed in the conventional bulk graphite. The experimental results of van der Marel's group show that the answer is affirmative, and it can be shown that this result is expected based on the classical Slonczewski-Weiss-McClure (SWMcC) band model of graphite [193, 194].

10.3 Localization behavior in disordered graphene ribbons

The recent controlled fabrication of graphene (single-layer graphite sheets) has opened an intense theoretical and experimental research activity on the properties of electrons with relativistic energy dispersion. Interesting are also the boundaries of this system where unusual edge states can appear. In narrow graphene ribbons (quantum wires) such edge states play a crucial role for the transport properties. Most impressively this can be seen in graphene ribbons with zigzag edges, where edge states

entirely dominate the low-energy transport [195]. The two inequivalent Dirac points in the graphene band structure appear as two valleys in the graphene zigzag ribbon, which are well separated in momentum space. In their recent study on disordered ribbons Wakabayashi, Takane and Sigrist show that in each valley the propagating modes include one chiral mode originating from a partially flat band due edge states [97]. This feature is the origin of a conducting channel remaining delocalized even in the disordered system, if the impurity scattering does not connect the two valleys, i.e. for long-range impurity potentials. In contrast, ribbons with short-range impurity potentials exhibit ordinary localization behavior as inter-valley scattering is not suppressed. The two regimes belong to different universality classes: unitary for long-range and orthogonal for short-range impurity potentials. This finding may be relevant for devices made of graphene as it was shown that natural disorder (e.g. warping of graphene sheets) corresponds to long length scale disorder, such that a single perfectly conducting channel could survive in quantum wires.

10.4 Defects in carbon nanostructures

Groening and collaborators at Empa have investigated the role of local defects on the atomic scale on influencing the local electronic properties of graphitic carbon systems which have attracted much attention also for their potential for novel devices.

The exposure of graphite surfaces to a hydrogen electron cyclotron resonance (ECR) plasma is very effective in creating single defects of C-H chemisorption and C-vacancy type [98][196], where both kind of defects act as electron scatterers. Due to the point-like Fermi surface (at the k points of the first Brillouin zone) of graphite the electron scattering leads to a characteristic superstructure in the vicinity of the defects [196]. Next the influence of H-ECR plasma induced defects for single walled carbon nanotubes (SWNT) was investigated. Characteristic signatures of the local density of states (LDOS) of vacancy-H complexes have been identified and compared to DFT calculations. This investigation could explain the appearance of very characteristic mid-gap symmetric electronic states, which can be attributed to a pair of interacting chemisorbed H-atoms on semiconducting SWNT. As in the case of graphite, electron scattering at the defects on the SWNT could be observed by the characteristic $(\sqrt{3} \times \sqrt{3})R30^\circ$ superstructure.

However the scattering proved to be not strong enough to lead to the formation of quasi bound states between two closely (approx. 10 nm) spaced defects. Eventually, to increase the probability of vacancy formation (which are strongly scattering defects) Groening and collaborators have used medium energy (200-1500 eV) Ar ion bombardment to induce the desired defects yielding quasi bound states (QBS) on metallic tubes due to the electron confinement between two defects. Such a defect induced electron resonator on a SWNT is highly interesting because it can be regarded as a “quantum dot with leads”.

a) *Defects on Graphite* Groening’s group has succeeded in identifying the electron scattering mechanism of H-plasma induced defects on graphite as large momentum scattering with a wave vector of k_F in the first Brillouin zone. They successfully compared the standing wave interference patterns of the scattered electron waves between several defects to tight-binding calculations [98]. It was observed that the interference pattern as measured by STM at low bias (50 mV) exhibited a characteristic $(\sqrt{3} \times \sqrt{3})R30^\circ$ where a multitude of different patterns could be seen.

From the experiment and the comparison to the simulation it could be concluded that the interference patterns originate from a large momentum scattering of the electron waves at the defects similar to a Friedel-type oscillation, where the scattering vector of $2 \cdot k_F$ is reduced to k_F by an Umklapp-process.

b) *Defects on SWNT* In analogy to the investigation of ECR-plasma induced defects on graphite, Groening and coworkers investigate the same type of defects on SWNT. Three main questions have been addressed in this regard:

- 1) What is the influence of the defects on the local band structure and can the defects be used for a local band gap engineering, e.g. can the band gap of semiconducting SWNT be modified locally?
- 2) Can quantum dots states be created in a resonator between two defects?
- 3) What is the influence of the 1D character of the SWNT on the electron scattering, e.g. are effects associated to a Luttinger-liquid model for the electrons visible?

By combination of STM with STS the interference pattern formation as a function of semiconducting and metallic tubes has been investigated as shown in Fig. 45. The same superstructure as in graphite appears for metallic SWNT. Due to the 1D character of the SWNT

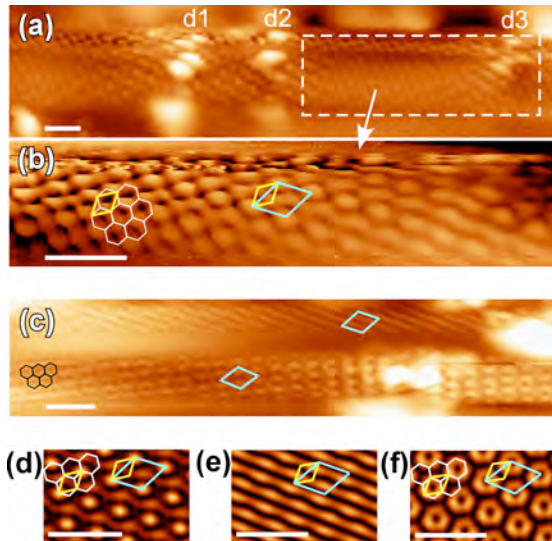


Figure 45: (a) STM topography image of a semiconducting tube in a bundle ($U_s = 1.6$ V, $I_s = 0.35$ nA, $\Delta z = 2.4$ Å, the image is flattened for higher contrast). Three defect sites are indicated by the labels d1–d3. (b) Detail STM image of (a) showing the region between d2 and d3 as indicated by the dashed rectangle in (a). Close to d3 the reconstruction of the charge density can be well observed. The 1×1 and unit-cells are indicated. On the left hand side the unperturbed honeycomb lattice is evidenced. (c) STM topography image of two metallic SWNT showing two different reconstruction patterns near defect sites ($U_s = 1$ V, $I_s = 0.1$ nA, $\Delta z = 1.63$ Å). (d) – (f) Calculated spatial maps of the LDOS (see [99]).

the superstructure extends to quite large distances of up to 6–10 nm from the defect. A similar superstructure is also observed on semiconducting tubes (Fig. 45a and 45b) with a smaller range and amplitude compared to the metallic ones [99].

The appearance of sharp, spatially localized peaks in the LDOS is also characteristic for the hydrogen ECR-plasma induced defects on semiconducting SWNT. Single peaks can be observed at the Fermi energy as for the metallic ones, but also at other energetic positions in the conduction or valence band [100]. More often however than single peaks, for semiconducting tubes sharp double peaks were observed in the LDOS symmetric around the mid-gap energy (see dI/dV line scan map at 5 K in Fig. 46 with double peaks P4–P5, P6–P7 and P8–P9). Using DFT calculations these double peaks could be attributed to orbital bonding-antibonding splitting of pairs of nearby H-atoms. An effective attractive lattice mediated interaction favors the proximity of adsorbed H-atoms [100]. This is different for nitrogen ECR-plasma induced defects which show also sharp peaks in the STS spectra. However, double peak struc-

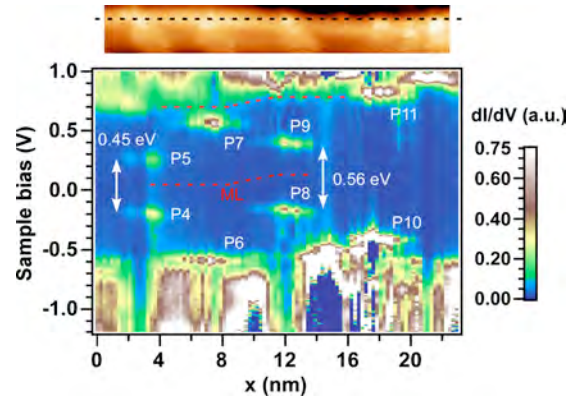


Figure 46: Upper panel: STM topography image of a (6,2) semiconducting SWNT with a series of hydrogen plasma induced defects. Lower panel: Scanning tunneling spectroscopy mapping of the along the line indicated in the topography image showing different mid-gap symmetric states at the defect positions.

tures are absent indicating that adsorbed N-atoms tend to avoid each other.

c) *Quasi bound states* Although electron scattering could be observed in the case of hydrogen and nitrogen ion bombardment of the tubes as evidenced by the reconstruction of the STM atomic lattice of the SWNT, a clear quantized electron states (quasi bound electron states) between two defects was not visible. These quasi bound states (QBS) would originate from a sufficiently strong confinement of the electronic states between two defects separated by 10–20 nm. The use of medium energy (200–1500 eV) Ar ion bombardment created sufficiently strong scattering defects, that the appearance of QBS could be observed. Fig. 47 shows a section of a metallic SWNT irradiated by 200 eV Ar ions resulting in a series of defects on the tube with a stochastic separation around 10 nm. The STS spectroscopy map shown in the lower part, shows the appearance of QBS in different defect bounded sections of the tubes. The QBS can be identified by the standing electron wave between the defects which varying wave length as a function of the energy (sample bias). As the band crossing in metallic SWNT is close to the Fermi energy at 0 V, similar QBS can be observed in the occupied and unoccupied density of states. In accordance with the band dispersion the level spacing is of the order of 100–200 meV for defect separations around 10 nm. This level spacing is considerably higher than kT at room temperature (25 meV) and therefore should be relevant for electron transport even at room temperature. These experiments clearly show that electron

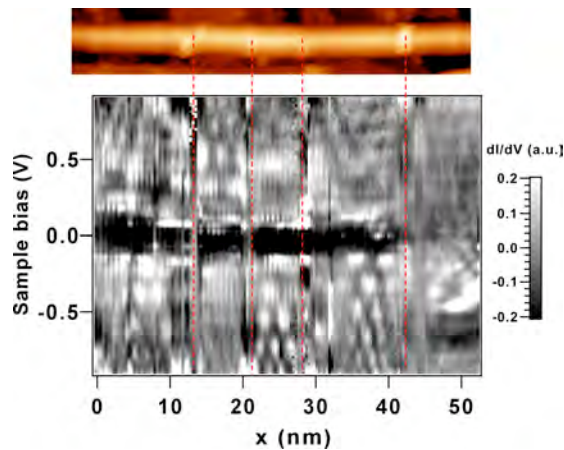


Figure 47: Upper panel: STM topography image of a metallic SWNT with a series of 200 eV Ar-ion induced defects. Lower panel: Line STS mapping of the local density of states around the Fermi energy. In the defect bounded sections between 20-30 nm and 30-40 nm the appearance of QBS is clearly observable, by the standing wave patterns with decreasing wave length as the energy (sample bias) decreases.

confinement using artificial defects on SWNT can be used to create Quantum Dots (QD), where in the case of metallic SWNT these QD would already have electrical leads.

11 Mesoscopics: quantum coherent electron transport

Carbon based nano-systems can display properties, which lead to the field of mesoscopic physics. Within this project also various questions in the context of mesoscopic physics are addressed by Büttiker's group who also extends the discussion to areas concerned with basic aspects of quantum measurements which are relevant for problems appearing in the context of quantum computation devices.

11.1 Two-particle Aharonov-Bohm effect

The standard Aharonov-Bohm (AB) effect can be considered as the interference of a particle with itself. Astonishingly, two particles emitted by two completely independent metallic contacts enclosing an AB flux would yield an effect visible in the shot noise of the conductor even without a single particle AB effect [197]. A suitable geometry could be realized in a two-dimensional quantum Hall sample as proposed by Samuelsson, Sukhorukov and Büttiker [101] where no single-particle interference occurs. In such an interferometer a cross-correlation between currents would be sensitive to the AB flux, as a consequence of

the fact that the correlation probes two-particle processes [101].

Following the suggestion of Ref. [101] four experimental teams have realized samples with an intent to measure a two-particle AB effect in a shot noise correlation. Thus far only Neder *et al.* [198] from the group of M. Heiblum at the Weizmann Institute of Science have succeeded convincingly demonstrating the two-particle interference effect.

The significance of the two-particle AB-effect lies in the fact that it should be possible to violate a Bell inequality since the resulting states are orbitally entangled. A violation of a Bell inequality requires sixteen correlation measurements on this structure. In recent work Büttiker and collaborators examined a quantum state tomographic method [102] which requires the same number of correlation measurements as the violation of the Bell inequality but since the reduced two particle density matrix is obtained it determines a number for the degree of entanglement and not only a yes or no answer as the Bell inequality. A brief review of this subject is given in Ref. [103].

11.2 Dynamics of a quantum coherent capacitor

Interest in quantum coherent electron transport in the AC regime has been revived recently thanks to progress made in controlling and manipulating small high mobility mesoscopic structures driven by high frequency periodic voltages at ultra low temperatures. The state-of-the-art includes the realization of high frequency single electron sources, which might be important for metrology. In Ref. [199] this was achieved by applying large amplitude periodic voltage pulses of a few hundred MHz on the gate of a mesoscopic capacitor. The accuracy of this single electron emitter was analyzed theoretically in Ref. [104]. The frequencies of interest here are in the GHz range. A quantization occurs only if the period of the pulse is long compared to the RC-time of the capacitor. Thus the dynamics of charge relaxation is of central importance for these experiments.

Of particular interest is the work of Gabelli *et al.* [200], who succeeded in measuring both the in and out of phase parts of the linear AC conductance $G(\omega) = I(\omega)/V(\omega)$ of a mesoscopic capacitor at the driving frequency $\omega \approx 1$ GHz. The capacitor consists of a sub-micrometer Quantum Dot (QD) connected to an electron reservoir via a tunable Quantum Point Contact (QPC) and capacitively coupled to a metallic back or top gate (Fig. 48).

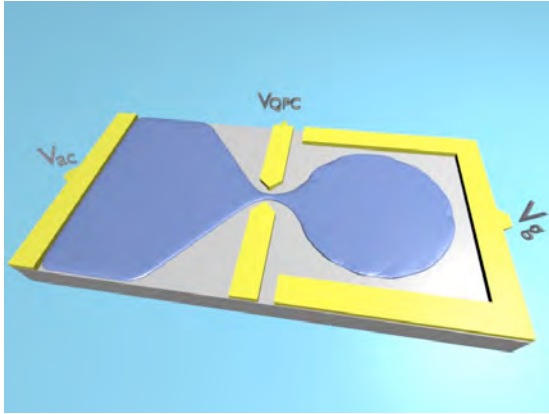


Figure 48: Mesoscopic capacitor: a cavity is connected via one lead to an electron reservoir at voltage V_{ac} and capacitively coupled to a gate with voltage V_g . Only one contact formed by a quantum point contact permits carrier exchange. The voltage V_{qpc} controls the transmission through the quantum point contact.

The question “What is the RC-time of a quantum coherent capacitor?” has been theoretically addressed by Büttiker, Thomas and Prêtre [201]. In the low-frequency regime $\omega \ll 1/\tau_{RC}$, where τ_{RC} is the RC-time of the system, the response is determined by an electrochemical capacitance C_μ and a charge relaxation resistance R_q . Together these determine the RC-time in complete analogy to the classical case: $\tau_{RC} = R_q C_\mu$. The quantum RC-time obtained from their product is sensitive to the quantum coherence of the system and consequently displays typical mesoscopic fluctuations [105][202, 203]. Surprisingly, for a coherent capacitor with a single channel, only the capacitance fluctuates and the resistance is found to be constant and given by half a resistance quantum [201]

$$R_q = \frac{h}{2e^2}. \quad (3.7)$$

This quantization has indeed been observed experimentally [200] thus establishing a novel manifestation of quantum coherence in the AC regime.

The interesting question is the length scale on which coherence is necessary for the AC effect [106]. Unlike in the quantization of conductance where coherence over the width of point contact is sufficient, the quantization of the charge relaxation resistance requires coherence over the entire capacitance plate (the quantum dot). Thus the quantized charge relaxation resistance in Eq. (3.7) is indeed very sensitive to dephasing.

A further surprising aspect is the fact that the quantization of the charge relaxation resistance

$R_q = h/(2e^2)$ is not depending on the transmission probability. For a coherent capacitor connected via a single spin polarized channel to a reservoir the quantization of R_q is truly universal and holds even in the Coulomb blockade regime [107].

Of course, no matter how pure the samples are, a spurious interaction with environmental degrees of freedom, is unavoidable, and introduces dephasing into the system. It is thus of interest to ask how dephasing affects the quantization of the single channel charge relaxation resistance and to investigate the crossover from the coherent to the incoherent regime. It is furthermore important to be able to distinguish on a theoretical level between finite temperature effects and effects due to pure dephasing and to understand the interplay between these two fundamental mechanisms. Intuitively, one would expect that in the presence of strong enough dephasing, the QD starts behaving like an electron reservoir. Nigg and Büttiker find that for the QD to become a true electron reservoir it is necessary that many channels participate in the inelastic relaxation process which a true reservoir must provide [106]. They employ a description of dephasing provided by the voltage and dephasing probe models [108, 109], where one attaches a fictitious probe to the system which can absorb and reemit electrons from or into the conductor. If the probe supports only one channel, the charge relaxation resistance of the *fully incoherent* mesoscopic capacitor is given by [106]

$$R_q = \frac{h}{2e^2} + \frac{h}{e^2} \frac{1-T}{T}, \quad (3.8)$$

with T as the transmission probability. Hence, the charge relaxation resistance is the sum of the resistance as found from the (original) Landauer formula $h/e^2(1-T)/T$ and *one* interface resistance $h/(2e^2)$ [204, 205]. Remarkably, this is also the value of R_q obtained in the high temperature limit for the coherent system, illustrating an interesting relation between single channel dephasing and temperature induced phase averaging [106].

As remarked above, the quantized resistance given by Eq. (3.7) has been measured. The experiment sees similarly a strong increase of the charge relaxation resistance as the QPC is closed (presumably when the electron dwell time in the dot becomes long compared to the dephasing length). However, the difference between Eq. (3.7) and Eq. (3.8) is possibly too small to be experimentally observed.

11.3 Quantumness of two level systems

Can an experimental physicist prove that the system he is observing is truly a quantum system? The best known example of such a test is Bell's inequality (BI), originally devised to demonstrate quantum non-locality. The seminal work by Leggett and Garg [206] provides another inequality involving only one quantum variable together with a set of projective measurements. While the lesson of BI is that quantum correlations are non-local, the lesson of the Leggett-Garg inequality (LGI) is that quantum measurement is fundamentally an *invasive* procedure. An interesting parallel between the two inequalities is that the role of hidden variables in the BI is played by trajectories in the LGI. The belief that the quantum system really takes a definite classical trajectory between two points (chosen from an arbitrary probability distribution) may be disproved with the LGI.

Büttiker and coworkers propose a generalization of the LGI using quantum non-demolition (QND) measurements weakly measuring the quantum state by pumping current [110]. Weak measurements, in contrast to projective measurements, obtain partial information about the state from an inherently noisy output, so wavefunction collapse happens continuously. In the solid state, the typically weak coupling between system and detector implies that weak measurements are the norm. A generic problem that arises in making a projective measurement out of many weak measurements is that the quantum system has its own Hamiltonian dynamics that effectively rotates the continuous measurement basis, destroying the state. The way around this problem is with QND measurements.

The studied system is schematically shown in Fig. 49. Two coupled dots represent a charge qubit. The tunnel coupling of the dots permits an electron to be in the upper or lower dot or in a superposition of these two states. The electron position is measured with the help of a quantum point contact. This is a narrow orifice for electrons with a conductance that depends on nearby charges. A sequence of voltage kicks of duration smaller than the oscillation period of the qubit is applied to the QPC, alternating in sign every half oscillation period. For this detector the different positions of the electron in the double dot give rise to different currents measured in response to the voltage pulse. Note that if the qubits were for certain on the red path current would flow to the right, and if the qubits were for certain on the blue path current would flow to the left.

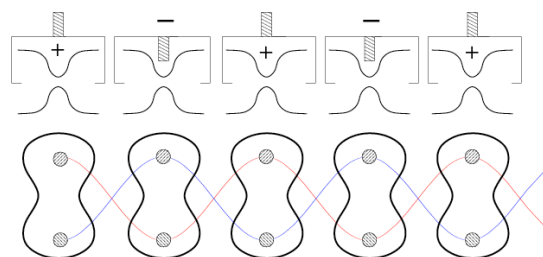


Figure 49: Visualization of the kicked QND measurement. A voltage pulse is applied to the QPC, followed by a quiet period of zero voltage bias, lasting for a Rabi oscillation period, followed by another pulse, and so on. The up/down variation is depicted, where the kicks come every half period, and the sign of the voltage pulse alternates with every kick. Read-out of the coherent superposition of trajectories (red or blue) occurs by measuring the sign of the current, and corresponds to an elementary quantum pump.

Thus under the combined action of the voltage pulses and the oscillations of the qubit, the system acts as a pump. Büttiker and collaborators analyze in detail how with the help of such a kicked quantum non-demolition pump a Leggett-Garg type inequality can be violated and the quantumness of the qubit be demonstrated.

12 New algorithms and new instruments

Developments of new algorithms to simulate quantum systems are a key component of the contribution from Troyer's group with the expansion of ALPS (Algorithms and Libraries for Physics Simulations). A simulation package is provided by Ott and collaborators for NMR spectra analysis.

12.1 Impurity solvers for dynamical mean field theory.

Troyer's group has developed a new quantum Monte Carlo solver [111] for dynamical mean field theory (DMFT) and the fermionic impurity problem [207]. The new solver is based on diagrammatic expansion in the non-local hybridization of DMFT, combined with an exact summation over all permutations of the fermion lines. The latter trick removes the fermionic negative sign problem for a single-site impurity problem. Benchmarks show [112] that for the prototypical infinite-dimensional case the new algorithm performs many orders of magnitudes better times better than the standard Hirsch-Fye algorithm [208] and allows to reach about 50-100 times lower temperatures, which is very important in studying the low

temperature regime important for the Kondo effect and other impurity problems. This new QMC solver substantially speeds up all kinds of DMFT simulations, including cluster variants.

12.2 Fermionic simulations.

The negative sign incurred upon exchange of fermions leads to the “negative sign problem” of fermionic Monte Carlo simulations, preventing accurate simulations due to an exponential increase in computer time with increasing particle number and inverse temperature. Since the sign-problem is nondeterministic polynomially (NP) hard, there is almost certainly no general solution. Besides developing a new efficient worm algorithm for simulations of attractive Hubbard models [65, 66], a proposal for a sign-problem free algorithm for the repulsive Hubbard model has been examined [113, 114]

12.3 Optimized ensembles

Troyer and collaborators have developed an algorithm to optimize temperature sets for parallel tempering simulations [115], based upon ideas of extended ensemble simulations, reviewed in Ref. [116], and have extended these optimized ensemble simulations to quantum systems [117]. These algorithms give huge speedup at first order phase transitions, and allow the direct computation of the partition function, free energy and entropy which are inaccessible in Monte Carlo simulations in the canonical ensemble.

12.4 The ALPS project.

The ALPS team around Troyer has published release 1.3 of their open source ALPS software [118] for the simulation of quantum systems, making modern algorithms available to non-experts.

12.5 Solid-state NMR spectra simulation package

NMR is a powerful tool in experimental solid-state physics, as it is sensitive to the static and dynamical properties of nuclear spins and can provide useful information on the magnetic state of crystalline solids. Nonetheless, the interpretation of the NMR spectra is, in many cases, rather difficult because of the simultaneous presence of quadrupolar and hyperfine interactions acting at the same level. When this happens the positions and intensities of the

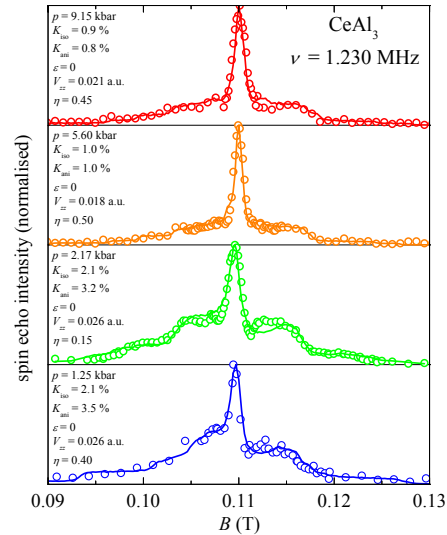


Figure 50: Field sweep ^{27}Al NMR powder-spectra of CeAl_3 at 64 mK and high-pressure. Symbols: experimental data, solid lines: simulations. The essential numerical fit parameters, namely the isotropic (K_{iso}) and anisotropic (K_{ani}) Knight-shift, its axial asymmetry (ϵ), the principal axis electric-field-gradient (V_{zz}), and its in-plane anisotropy (η) are displayed in the panels.

spectral features cannot be connected to the microscopic properties of the system in a simple way.

One possible solution is the employment of numerical routines to simulate the experimental spectra. Although many NMR simulation codes are commercially available, to the best of our knowledge none of them is especially designed for solid-state NMR. For this reason Ott and collaborators developed a simple but efficient *Fortran77* code devoted to this purpose. The program input embodies the microscopic parameters describing the hyperfine as well as the quadrupolar interaction, from which the nuclear-spin Hamiltonian is constructed. A numerical diagonalization provides the eigenenergies and eigenvectors, which eventually allow to establish the transition frequencies and intensities and thus the spectrum. Different isotopes and/or lattice sites can be considered for the simulation. It is also possible to carry out frequency or field sweep spectra calculations for either single crystalline or powder specimens.

Fig. 50 shows the NMR spectra of CeAl_3 at high pressure and low temperature calculated with this program and compared with the experimental data [28]. The good agreement between the simulated and measured spectra provides reasonable values for the microscopic parameters characterizing the electric-field gradient

and the hyperfine coupling at the Al-site.

13 Collaborative efforts

A major component in collaborative efforts is the encouragement to form communities working on similar topics and materials. Within Project 1 this is especially visible in the areas of quantum spins, charge density wave systems, exotic phases (e.g. supersolids and novel order parameters), spin splitting in surface states, metal-insulator transitions in BaVS_3 , LiCu_2O_2 and cold-atoms in optical lattices. For these topics collaboration and providing a common forum to discuss a subject has been very stimulating and generated new synergies which would not be likely found without MaNEP. An important aspect is the discussion between experimental groups and theorists. In parts this occurs within MaNEP through direct collaborations which is mainly seen in the areas of quantum spin systems and charge density wave instabilities. Computational techniques empower within MaNEP not only the theoretical groups, but ALPS and the tutorials provided by Troyer's group make simulations also available to experimental groups for testing models, e.g. for quantum spin systems. An important aspect of the collaboration is also in the sample production which has led to an intensive relation between different labs with different expertise in crystal growth under special conditions. Within all projects MaNEP as network has facilitated taking up new developments through the combination of widely spread competences.

14 Goals for the next year

Project 1 incorporates the work of more than 15 research teams and over 10 basic themes. Thus, it is not easy to cover all the plans and goals in detail and we restrict here on some of the main targets for the final year of the phase II.

a) *Quantum spin systems* The neutron scattering group will continue their studies of the spin excitations in the spin ladder $(\text{Hpip})_2\text{CuBr}_4$ all the way to the fully polarized state. On the theoretical side the magnetization curve of $\text{SrCu}_2(\text{BO}_3)_2$ will be analyzed including magnetization plateaus and to explain the nature of a new phase in this compound reached under pressure, based on the Shastry-Sutherland model.

b) *Charge density wave systems* The investigation of the rare-earth-polytelluride family will be continued using optical tools and doing

measurements at Elettra under pressure. Moreover, Raman and X-ray scattering studies are planned. Further ARPES and transport studies are planned for the dichalcogenide compounds in order to elucidate the nature of the CDW phase and to explore the phase diagram under pressure.

c) *Cold-atoms in optical lattices* In this field the theoretical study of low-dimensional atomic gases will be continued, in particular, with the focus on the effect of controlled disorder (speckle or dichromatic lattices) in the interacting systems, which can be experimentally realized. Interfaces in strongly correlated quantum atomic systems will be investigated, in particular, the transmission and reflection properties of superfluid-Mott-insulator boundaries and its physical implications such as transport of entropy and heat. Furthermore, a study of the effect of fluctuations on the behavior of strongly correlated Josephson junctions is planned.

d) *Magnetism in metals* Magneto-optical and dichroism studies will be pursued for the alloys $\text{Fe}_{1-x}\text{Co}_x\text{Si}$, $\text{Mn}_{1-x}\text{Co}_x\text{Si}$ and $\text{Mn}_{1-x}\text{Ni}_x\text{Si}$ to explore their magnetic and metallic properties. Theoretical studies of the metamagnetism in the bilayer ruthenates will include the effect of spin-orbit coupling in order to explain the peculiar field direction dependence of low-temperature properties.

e) *Properties of semi-metals* Magneto-optical and pressure techniques will be applied to investigate the metal-insulator transition of the $\text{Bi}_{1-x}\text{Sb}_x$ alloys and semi-metallic heavy Fermion compounds.

f) *Carbon systems* For single-walled carbon nanotubes the electron scattering mechanisms leading to resonant bound states in ion-beam treated tubes will be studied, in order to elucidate the difference between armchair and zigzag tubes. Moreover the effect of the adsorption of atomic hydrogen on nanotubes will be further investigated to clarify the nature of the symmetric electronic midgap states previously discovered. Transport and magnetic properties of nano-graphene ribbons will be further investigated theoretically.

g) *RIXS* At the Swiss Light Source resonant X-ray scattering experiments will be performed to study electronic excitations in strongly correlated oxides, most notably NiO and CuO .

h) *Mesoscopics* The research efforts on mesoscopic physics aim at the characterization of high-frequency single-electron sources with respect to the coherence properties of emitted states and the noise. A further target is the discussion of the interaction induced deviations from Onsager symmetries in non-linear transport. In the area of quantum measurements Bell tests in electrical conductors at finite temperature shall be performed.

i) *Interfaces in heterostructures* Magnetic order and transport properties of interfaces in the heterostructures of correlated electron systems will be investigated theoretically. The extension of these studies to multi-orbital systems is intended.

j) *Theory of many-body systems* Theoretical efforts to understand and describe the properties of a lightly doped Mott insulators within the Hubbard and t - J -model will continue. Computational studies on the exotic phases with anyonic excitations remain an important issue for the coming year.

k) *BaVS₃ and BaV₂Se₃* Efforts to explore the phase diagram and non-Fermi liquid properties near the metal-insulator transition under pressure will continue. This activity will, however, depend on the progress of producing better single-crystals of these materials.

MaNEP-related publications

- ▶ [1] C. Rüegg, B. Normand, M. Matsumoto, C. Niedermayer, A. Furrer, K. W. Krämer, H. U. Güdel, P. Bourges, Y. Sidis, and H. Mutka, *Phys. Rev. Lett.* **95**, 267201 (2005).
- ▶ [2] C. Rüegg, B. Normand, M. Matsumoto, A. Furrer, D. McMorrow, K. Krämer, H.-U. Güdel, S. N. Gvasaliya, H. Mutka, and M. Boehm, *Phys. Rev. Lett.* (2008).
- [3] T. Giamarchi, C. Rüegg, and O. Tchernyshyov, *Nature Phys.* **4**, 198 (2008).
- ▶ [4] H. M. Rønnow, R. Parthasarathy, J. Jensen, G. Aeppli, T. F. Rosenbaum, and D. McMorrow, *Science* **308**, 389 (2005).
- [5] H. M. Rønnow, J. Jensen, R. Parthasarathy, G. Aeppli, T. F. Rosenbaum, D. McMorrow, and C. Kraemer, *Phys. Rev. B* **75**, 054426 (2007).
- [6] C. Kraemer, *Magnetische Eigenschaften von LiErF₄ – Eine Untersuchung mittels Neutronenstreuung*, Master's thesis, ETHZ (2006).
- ▶ [7] M. Clémancey, H. Mayaffre, C. Berthier, M. Horvatić, J.-B. Fouet, S. Miyahara, F. Mila, B. Chiari, and O. Piovesana, *Phys. Rev. Lett.* **97**, 167204 (2006).
- [8] S. Miyahara, J.-B. Fouet, S. R. Manmana, R. M. Noack, H. Mayaffre, I. Sheikin, C. Berthier, and F. Mila, *Phys. Rev. B* **75**, 184402 (2007).
- ▶ [9] K. Penc, J.-B. Fouet, S. Miyahara, O. Tchernyshyov, and F. Mila, *Phys. Rev. Lett.* **99**, 117201 (2007).
- [10] V. Y. Pomjakushin, A. Furrer, D. V. Sheptyakov, E. V. Pomjakushina, and K. Conder, *Phys. Rev. B* **76**, 174433 (2007).
- [11] A. Podlesnyak, V. Pomjakushin, E. V. Pomjakushina, K. Conder, and A. Furrer, *Phys. Rev. B* **76**, 064420 (2007).
- [12] O. Zaharko, J. Mesot, L. A. Salguero, R. Valentí, M. Zbiri, M. Johnson, Y. Filinchuk, B. Klemke, K. Kiefer, M. Mys'kiv, T. Strassle, and H. Mutka, *arXiv:0801.1507* (2008).
- [13] O. Zaharko, H. Rønnow, J. Mesot, S. J. Crowe, D. M. Paul, P. J. Brown, A. Daoud-Aladine, A. Meents, A. Wagner, M. Prester, and H. Berger, *Phys. Rev. B* **73**, 064422 (2006).
- [14] O. Zaharko, H. M. Rønnow, A. Daoud-Aladine, S. Streule, F. Juranyi, J. Mesot, H. Berger, and P. Brown, *Low Temp. Phys.* **31**, 814 (2005).
- [15] A. Ralko, M. Ferrero, F. Becca, D. Ivanov, and F. Mila, *Phys. Rev. B* **74**, 134301 (2006).
- [16] A. Ralko, M. Ferrero, F. Becca, D. Ivanov, and F. Mila, *Phys. Rev. B* **76**, 140404 (2007).
- [17] G. Misguich and F. Mila, *Phys. Rev. B* (2008).
- ▶ [18] A. Läuchli, F. Mila, and K. Penc, *Phys. Rev. Lett.* **97**, 087205 (2006).
- ▶ [19] A. Läuchli, J. C. Domenge, C. Lhuillier, P. Sindzingre, and M. Troyer, *Phys. Rev. Lett.* **95**, 137206 (2005).
- [20] P. Corboz, A. M. Läuchli, K. Totsuka, and H. Tsunetsugu, *Phys. Rev. B* **76**, 220404(R) (2007).
- [21] D. Bergman, J. Alicea, E. Gull, S. Trebst, and L. Balents, *Nature Phys.* **3**, 487 (2007).
- [22] B. Pedrini, J. L. Gavilano, D. Rau, H. R. Ott, S. M. Kazakov, J. Karpinski, and S. Wessel, *Phys. Rev. B* **70**, 024421 (2004).
- [23] B. Pedrini, S. Wessel, J. L. Gavilano, H. R. Ott, S. M. Kazakov, and J. Karpinski, *Eur. Phys. J. B* **55**, 219 (2007).
- [24] P. Vonlanthen, K. B. Tanaka, A. Goto, W. G. Clark, P. Millet, J. Y. Henry, J. L. Gavilano, H. R. Ott, F. Mila, C. Berthier, M. Horvatic, Y. Tokunaga, P. Kuhns, A. P. Reyes, and W. G. Moulton, *Phys. Rev. B* **65**, 214413 (2002).
- [25] N. B. Christensen, H. M. Rønnow, D. F. McMorrow, A. Harrison, T. G. Perring, M. Enderle, R. Coldea, L. P. Regnault, and G. Aeppli, *Proc. Nat. Acad. Sci. USA* **104**, 15264 (2007).
- [26] A. Sacchetti, M. Weller, J. L. Gavilano, R. Mudliar, B. Pedrini, K. Magishi, H. R. Ott, R. Monnier, B. Delley, and Y. Ōnuki, *arXiv:0709.3009* (2007).
- [27] M. Weller, J. L. Gavilano, A. Sacchetti, and H. R. Ott, *Physica B* **403**, 834 (2008).
- [28] M. Weller, J. L. Gavilano, A. Sacchetti, and H. R. Ott, *Phys. Rev. B* **77**, 132402 (2008).
- [29] M. Weller, J. Hinderer, J. L. Gavilano, B. Pedrini, D. Rau, I. Sheikin, M. Chiao, and H. R. Ott, *Physica B* **378-380**, 892 (2006).
- [30] L. Moreschini, C. Dallera, J. J. Joyce, J. L. Sarrao, E. D. Bauer, V. Fritsch, S. Bobev, E. Carpena, S. Huotari, G. Vankó, G. Monaco, P. Lacovig, G. Panaccione, A. Fondacaro, G. Paolicelli, P. Torelli, and M. Griioni, *Phys. Rev. B* **75**, 035113 (2007).
- [31] C. Dallera, O. Wessely, M. Colarieti-Tosti, O. Eriksson, R. Ahuja, B. Johansson, M. I. Katsnelson, E. Annesse, J.-P. Rueff, G. Vankó, L. Braicovich, and M. Griioni, *Phys. Rev. B* **74**, 081101(R) (2006).

- ▶ [32] S. G. Chiuzbaian, G. Ghiringhelli, C. Dallera, M. Grioni, P. Amann, X. Wang, L. Braicovich, and L. Patthey, *Phys. Rev. Lett.* **95**, 197402 (2006).
- ▶ [33] G. Caimi, A. Perucchi, L. Degiorgi, H. R. Ott, V. M. Pereira, A. H. Castro Neto, A. D. Bianchi, and Z. Fisk, *Phys. Rev. Lett.* **96**, 016403 (2006).
- ▶ [34] F. Pfuner, L. Degiorgi, H. R. Ott, A. Bianchi, and Z. Fisk, *Phys. Rev. B* **77**, 024417 (2008).
- ▶ [35] B. Binz, H. B. Braun, T. M. Rice, and M. Sgrist, *Phys. Rev. Lett.* **96**, 196406 (2006).
- [36] A. V. Lukoyanov, V. V. Mazurenko, V. I. Anisimov, M. Sgrist, and T. M. Rice, *Eur. Phys. J. B* **53**, 205 (2006).
- [37] H. P. Büchler, G. Blatter, and W. Zwirger, *Phys. Rev. Lett.* **90**, 130401 (2003).
- [38] H. P. Büchler and G. Blatter, *Phys. Rev. Lett.* **91**, 130404 (2003).
- [39] H. P. Büchler and G. Blatter, *Phys. Rev. A* **69**, 063603 (2004).
- ▶ [40] H. P. Büchler, M. Hermele, S. D. Huber, M. P. A. Fisher, and P. Zoller, *Phys. Rev. Lett.* **95**, 040402 (2005).
- ▶ [41] S. D. Huber, E. Altman, H. P. Büchler, and G. Blatter, *Phys. Rev. B* **75**, 085106 (2007).
- ▶ [42] S. D. Huber, B. Theiler, E. Altman, and G. Blatter, *Phys. Rev. Lett.* **100**, 050404 (2008).
- [43] A. Kleine, C. Kollath, I. P. McCulloch, T. Giamarchi, and U. Schollwöck, *Phys. Rev. A* **77**, 013607 (2007).
- [44] A. Kleine, C. Kollath, I. P. McCulloch, T. Giamarchi, and U. Schollwöck, *to be published in New J. Phys.* (2008).
- [45] A. Iucci, G. A. Fiete, and T. Giamarchi, *Phys. Rev. B* **75**, 205116 (2007).
- ▶ [46] M. B. Zvonarev, V. V. Cheianov, and T. Giamarchi, *Phys. Rev. Lett.* **99**, 240404 (2007).
- ▶ [47] C. Kollath, J. S. Meyer, and T. Giamarchi, *to be published in Phys. Rev. Lett.* (2008).
- [48] T. Giamarchi, *Chem. Rev.* **104**, 5037 (2004).
- ▶ [49] M. A. Cazalilla, A. F. Ho, and T. Giamarchi, *New J. Phys.* **8**, 158 (2006).
- ▶ [50] M. A. Cazalilla, A. F. Ho, and T. Giamarchi, *Phys. Rev. Lett.* **95**, 226402 (2005).
- [51] M. A. Cazalilla, A. F. Ho, and T. Giamarchi, in *Series on advances in Quantum Many-Body theories vol. 10, "Recent progress in many body theories"*, S. Hernandez and H. Cataldo, eds. (World Scientific, 2006), preprint cond-mat/0605419.
- [52] M. A. Cazalilla, A. Iucci, and T. Giamarchi, *Phys. Rev. A* **75**, 051603(R) (2007).
- [53] A. Iucci, M. A. Cazalilla, A. F. Ho, and T. Giamarchi, *Phys. Rev. A* **73**, 041608 (2006).
- ▶ [54] C. Kollath, A. Iucci, T. Giamarchi, W. Hofstetter, and U. Schollwöck, *Phys. Rev. Lett.* **97**, 050402 (2006).
- [55] C. Kollath, A. Iucci, I. P. McCulloch, and T. Giamarchi, *Phys. Rev. A* **74**, 041604(R) (2006).
- ▶ [56] C. Kollath, M. Köhl, and T. Giamarchi, *Phys. Rev. A* **76**, 063602 (2007).
- ▶ [57] S. Trebst, U. Schollwöck, M. Troyer, and P. Zoller, *Phys. Rev. Lett.* **96**, 250402 (2006).
- [58] H. G. Katzgraber, A. Esposito, and M. Troyer, *Phys. Rev. A* **74**, 043602 (2006).
- [59] C. Gils, L. Pollet, A. Vernier, F. Hébert, G. G. Batrouni, and M. Troyer, *Phys. Rev. A* **75**, 063631 (2007).
- [60] O. Gygi, H. G. Katzgraber, M. Troyer, S. Wessel, and G. G. Batrouni, *Phys. Rev. A* **73**, 063606 (2006).
- [61] L. Pollet, C. Kollath, K. Van Houcke, and M. Troyer, arXiv:0801.1887 (2008).
- ▶ [62] L. Pollet, M. Troyer, K. Van Houcke, and S. M. A. Rombouts, *Phys. Rev. Lett.* **96**, 190402 (2006).
- [63] L. Pollet, C. Kollath, M. Troyer, and S. Ulrich, *Phys. Rev. A* **77**, 023608 (2006).
- [64] F. Hébert, F. Haudin, L. Pollet, and G. G. Batrouni, *Phys. Rev. A* **76**, 043619 (2007).
- ▶ [65] E. Burovski, N. V. Prokof'ev, B. V. Svistunov, and M. Troyer, *Phys. Rev. Lett.* **96**, 160402 (2006).
- [66] E. Burovski, N. V. Prokof'ev, B. Svistunov, and M. Troyer, *New J. Phys.* **8**, 153 (2006).
- [67] F. Clerc, C. Battaglia, M. Bovet, L. Despont, C. Monney, H. Cercellier, M. Garnier, P. Aebi, H. Berger, and L. Forró, *Phys. Rev. B* **74**, 155114 (2006).
- ▶ [68] H. Cercellier, C. Monney, F. Clerc, C. Battaglia, L. Despont, M. G. Garnier, H. Beck, P. Aebi, L. Patthey, H. Berger, and L. Forró, *Phys. Rev. Lett.* **99**, 146403 (2007).
- [69] A. Rüegg, S. Pilgram, and M. Sgrist, *Phys. Rev. B* **75**, 195117 (2007).
- ▶ [70] C. R. Ast, J. Henk, A. Ernst, L. Moreschini, M. C. Falub, D. Pacilé, P. Bruno, K. Kern, and M. Grioni, *Phys. Rev. Lett.* **98**, 186807 (2007).
- [71] C. R. Ast, G. Wittich, P. Wahl, R. Vogelgesang, D. Pacilé, M. C. Falub, L. Moreschini, M. Papagno, M. Grioni, and K. Kern, *Phys. Rev. B* **75**, 201401(R) (2007).
- ▶ [72] C. Koitzsch, C. Battaglia, F. Clerc, L. Despont, M. G. Garnier, and P. Aebi, *Phys. Rev. Lett.* **95**, 126401 (2005).
- [73] C. Weber, A. Läuchli, F. Mila, and T. Giamarchi, *Phys. Rev. B* **73**, 014519 (2006).
- [74] D. Baeriswyl, D. Eichenberger, and B. Gut, *Phys. Stat. Sol. (b)* **244**, 2299 (2007).
- [75] C. Aebischer, D. Baeriswyl, and R. M. Noack, *Phys. Rev. Lett.* **86**, 468 (2001).
- ▶ [76] G. I. Japaridze, R. M. Noack, D. Baeriswyl, and L. Tincani, *Phys. Rev. B* **76**, 115118 (2007).
- [77] M. Indergand, A. Läuchli, s. Capponi, and M. Sgrist, *Phys. Rev. B* **74**, 064429 (2006).
- [78] M. Indergand, C. Honerkamp, A. Läuchli, D. Poilblanc, and M. Sgrist, *Phys. Rev. B* **75**, 045105 (2007).
- ▶ [79] M. Boninsegni, A. B. Kuklov, L. Pollet, N. Prokof'ev, B. V. Svistunov, and M. Troyer, *Phys. Rev. Lett.* **97**, 080401 (2006).
- [80] P. N. Ma, L. Pollet, M. Troyer, and F. C. Zhang, arXiv:0710.3940 (2007).
- ▶ [81] L. Pollet, M. Boninsegni, A. B. Kuklov, N. V. Prokof'ev, B. V. Svistunov, and M. Troyer, *Phys. Rev. Lett.* **98**, 135301 (2007).
- ▶ [82] M. Boninsegni, A. Kuklov, L. Pollet, N. Prokof'ev, B. V. Svistunov, and M. Troyer, *Phys. Rev. Lett.* **99**, 035301 (2007).
- ▶ [83] S. Wessel and M. Troyer, *Phys. Rev. Lett.* **95**, 127205 (2005).
- ▶ [84] N. Laflorencie and F. Mila, *Phys. Rev. Lett.* **99**, 027202 (2007).
- ▶ [85] K. P. Schmidt, J. Dorier, A. Laeuchli, and F. Mila, *Phys. Rev. Lett.* **100**, 090401 (2008).
- ▶ [86] A. B. Kuklov, N. V. Prokof'ev, B. V. Svistunov, and M. Troyer, *Ann. Phys.* **321**, 1602 (2006).

- ▶ [87] K. Harada, N. Kawashima, and M. Troyer, *J. Phys. Soc. Jpn.* **76**, 013703 (2007).
- ▶ [88] S. Trebst, P. Werner, M. Troyer, K. Shtengel, and C. Nayak, *Phys. Rev. Lett.* **98**, 070602 (2007).
- [89] L. B. Ioffe, M. V. Feigel'man, A. Iosevich, D. Ivanov, M. Troyer, and G. Blatter, *Nature* **415**, 503 (2002).
- [90] A. F. Albuquerque, H. G. Katzgraber, M. Troyer, and G. Blatter, arXiv:0708.0191 (2007).
- ▶ [91] A. Feiguin, S. Trebst, A. W. W. Ludwig, M. Troyer, A. Kitaev, Z. Wang, and M. H. Freedman, *Phys. Rev. Lett.* **98**, 160409 (2007).
- [92] S. Trebst, E. Ardonne, A. Feiguin, D. A. Huse, A. W. W. Ludwig, and M. Troyer, arXiv:0801.4602 (2008).
- [93] B. Pedrini, J. L. Gavilano, S. Weyeneth, E. Felder, J. Hinderer, M. Weller, H. R. Ott, S. M. Kazakov, and J. Karpinski, *Phys. Rev. B* **72**, 214407 (2005).
- [94] J. L. Gavilano, B. Pedrini, K. Magishi, J. Hinderer, M. Weller, H. R. Ott, S. M. Kazakov, and J. Karpinski, *Phys. Rev. B* **74**, 064410 (2006).
- [95] S. Seiro, Y. Fasano, I. Maggio-Aprile, O. Kuffer, and Ø. Fischer, *J. Mag. Mat.* **310**, e243 (2007).
- ▶ [96] S. Seiro, Y. Fasano, I. Maggio-Aprile, E. Koller, O. Kuffer, and Ø. Fischer, *Phys. Rev. B* **77**, 020407(R) (2008).
- ▶ [97] K. Wakabayashi, Y. Takane, and M. Sigrist, *Phys. Rev. Lett.* **99**, 036601 (2007).
- ▶ [98] P. Ruffieux, M. Melle-Franco, O. Gröning, M. Biemann, F. Zerbetto, and P. Gröning, *Phys. Rev. B* **71**, 153403 (2005).
- ▶ [99] G. Buchs, P. Ruffieux, P. Gröning, and O. Gröning, *Appl. Phys. Lett.* **90**, 013104 (2007).
- ▶ [100] G. Buchs, A. V. Krashennikov, P. Ruffieux, P. Gröning, A. S. Foster, R. M. Nieminen, and O. Gröning, *New J. Phys.* **9**, 275 (2007).
- [101] P. Samuelsson, E. V. Sukhorukov, and M. Büttiker, *Phys. Rev. Lett.* **92**, 026805 (2004).
- ▶ [102] P. Samuelsson and M. Büttiker, *Phys. Rev. B* **73**, 041305 (2006).
- [103] M. Büttiker and P. Samuelsson, *Ann. Phys. (Leipzig)* **16**, 751 (2007).
- ▶ [104] M. Moskalets, P. Samuelsson, and M. Büttiker, *Phys. Rev. Lett.* **100**, 086601 (2008).
- [105] M. Büttiker and S. E. Nigg, *Nanotechnology* **18**, 044029 (2007).
- ▶ [106] S. E. Nigg and M. Büttiker, *Phys. Rev. B* **77**, 085312 (2008).
- ▶ [107] S. E. Nigg, R. López, and M. Büttiker, *Phys. Rev. Lett.* **97**, 206804 (2006).
- ▶ [108] S. Pilgram, P. Samuelsson, H. Förster, and M. Büttiker, *Phys. Rev. Lett.* **97**, 066801 (2006).
- [109] H. Förster, P. Samuelsson, S. Pilgram, and M. Büttiker, *Phys. Rev. B* **75**, 035340 (2007).
- ▶ [110] A. N. Jordan, A. N. Korotkov, and M. Büttiker, *Phys. Rev. Lett.* **97**, 026805 (2006).
- ▶ [111] P. Werner, A. Comanac, L. de Medici, A. J. Millis, and M. Troyer, *Phys. Rev. Lett.* **97**, 076405 (2006).
- [112] E. Gull, P. Werner, A. Millis, and M. Troyer, *Phys. Rev. B* **76**, 235123 (2007).
- [113] F. F. Assaad, P. Werner, P. Corboz, E. Gull, and M. Troyer, *Phys. Rev. B* **72**, 224518 (2005).
- [114] P. Corboz, M. Troyer, A. Kleine, I. P. McCulloch, U. Schollwöck, and F. F. Assaad, *Phys. Rev. B* **77**, 085108 (2008).
- [115] H. G. Katzgraber, S. Trebst, D. Huse, and M. Troyer, *J. Stat. Mech.* p. P03018 (2006).
- [116] S. Trebst, D. A. Huse, E. Gull, H. G. Katzgraber, U. H. E. Hansmann, and M. Troyer, in *Computer Simulation Studies in Condensed Matter Physics XIX*, D. P. Landau, S. P. Lewis, and H.-B. Schüttler, eds. (Springer, 2007), Springer Proceedings in Physics.
- ▶ [117] S. Wessel, N. Stoop, E. Gull, S. Trebst, and M. Troyer, *J. Stat. Mech.* p. P12005 (2007).
- ▶ [118] A. F. Albuquerque, F. Alet, P. Corboz, P. Dayal, A. Feiguin, S. Fuchs, L. Gamper, E. Gull, S. Gürtler, A. Honecker, R. Igarashi, M. Körner, M. Kozhevnikov, A. Läuchli, S. R. Manmana, M. Matsumoto, I. P. McCulloch, F. Michel, R. M. Noack, G. Pawłowski, L. Pollet, T. Pruschke, U. Schollwöck, S. Todo, S. Trebst, M. Troyer, P. Werner, and S. Wessel, *J. Mag. Mat.* **310**, 1187 (2007).

Other references

- [119] D. M. Silevitch, D. Bitko, J. Brooke, S. Ghosh, G. Aeppli, and T. F. Rosenbaum, *Nature* **448**, 567 (2007).
- [120] S. Miyahara and K. Ueda, *J. Phys.: Cond. Mat.* **15**, R327 (2003).
- [121] S. Nakatsuji, Y. Nambu, H. Tonomura, O. Sakai, S. Jonas, C. Broholm, H. Tsunetsugu, Y. Qiu, and Y. Maeno, *Science* **309**, 1697 (2005).
- [122] J. L. Gavilano, S. Mushkolaj, H. R. Ott, P. Millet, and F. Mila, *Phys. Rev. Lett.* **85**, 409 (2000).
- [123] H. R. Ott, K. Andres, P. S. Wang, Y. H. Wong, and B. Lüthi, in *Crystal field effects in metals and alloys*, A. Furrer, ed. (Plenum, New York, 1977), p. 84.
- [124] J. K. Kjems, H. R. Ott, S. M. Shapiro, and K. Andres, *J. Phys. (Paris)* **C6**, 1010 (1978).
- [125] P. Ahmet, M. Abliz, R. Settai, K. Sugiyama, Y. Ōnuki, T. Takeuchi, K. Kindo, and S. Takayanagi, *J. Phys. Soc. Jpn.* **65**, 1077 (1996).
- [126] K. Andres, E. Bucher, J. P. Maita, and A. S. Cooper, *Phys. Rev. Lett.* **28**, 1652 (1972).
- [127] A. Schenck, F. N. Gygax, and Y. Ōnuki, *Phys. Rev. B* **68**, 104422 (2003).
- [128] K. Andres, J. E. Graebner, and H. R. Ott, *Phys. Rev. Lett.* **35**, 1779 (1975).
- [129] S. Barth, H. R. Ott, F. N. Gygax, B. Hitti, E. Lippelt, A. Schenck, and B. C., *Phys. Rev. B* **39**, 11695 (1989).
- [130] J. L. Gavilano, J. Hunziker, and H. R. Ott, *Phys. Rev. B* **52**, R13106 (1995).
- [131] A. D. Bianchi, E. Felder, A. Schilling, M. A. Chernikov, F. Hulliger, and H. R. Ott, *Z. Phys. B* **99**, 69 (1995).
- [132] P. Vonlanthen, J. L. Gavilano, B. Ambrosini, D. Heisenberg, F. Hulliger, and H. R. Ott, *Z. Phys. B* **102**, 347 (1997).
- [133] N. E. Bickers, D. L. Cox, and J. W. Wilkins, *Phys. Rev. B* **36**, 2036 (1987).
- [134] S. A. Grigera, P. Gegenwart, R. A. Borzi, F. Weickert, A. J. Schofield, R. S. Perry, T. Tayama, T. Sakakibara, Y. Maeno, A. G. Green, and A. P. Mackenzie, *Science* **306**, 1154 (2004).
- [135] R. A. Borzi, S. A. Grigera, J. Farrell, R. S. Perry, S. J. S. Lister, S. L. Lee, D. A. Tennant, Y. Maeno, and A. P. Mackenzie, *Science* **315**, 214 (2007).
- [136] D. Jaksch, C. Bruder, J. I. Cirac, C. W. Gardiner, and P. Zoller, *Phys. Rev. Lett.* **81**, 3108 (1998).

- [137] E. Altman and A. Auerbach, *Phys. Rev. Lett.* **89**, 250404 (2002).
- [138] S. Sachdev, *Quantum Phase Transitions* (Cambridge University Press, Cambridge, UK, 1999).
- [139] R. Jackiw and A. Kerman, *Phys. Lett. A* **71**, 158 (1979).
- [140] T. Stöferle, H. Moritz, C. Schori, M. Köhl, and T. Esslinger, *Phys. Rev. Lett.* **92**, 130403 (2004).
- [141] C. Schori, T. Stöferle, H. Moritz, M. Köhl, and T. Esslinger, *Phys. Rev. Lett.* **93**, 240402 (2004).
- [142] O. M. Auslaender, A. Yacoby, R. de Picciotto, K. W. Baldwin, L. N. Pfeiffer, and K. W. West, *Science* **295**, 825 (2002).
- [143] T. Stöferle, H. Moritz, C. Schori, M. Köhl, and T. Esslinger, *Phys. Rev. Lett.* **92**, 130403 (2004).
- [144] P. Barmettler, A. M. Rey, E. Demler, M. Lukin, I. Bloch, and V. Gritsev, *Quantum many-body dynamics of coupled double well superlattices* (2008), unpublished.
- [145] M. Köhl, H. Moritz, T. Stöferle, K. Günter, and T. Esslinger, *Phys. Rev. Lett.* **94**, 080403 (2005).
- [146] D. Jérôme, T. M. Rice, and W. Kohn, *PR* **158**, 462 (1967).
- [147] E. Morosan, H. Zandbergen, B. Dennis, J. Bos, Y. Onose, T. Klimczuk, A. Ramirez, N. Ong, and R. Cava, *Nature Phys.* **2**, 544 (2006).
- [148] A. Ohtomo, D. A. Muller, J. L. Grazul, and H. Y. Hwang, *Nature* **419**, 378 (2002).
- [149] A. Ohtomo and H. Y. Hwang, *Nature* **427**, 423 (2004).
- [150] S. Okamoto and A. J. Millis, *Nature* **428**, 630 (2004).
- [151] Y. A. Bychkov and E. I. Rashba, *Sov. Phys.-JETP* **39**, 78 (1984).
- [152] L. Petersen and P. Hedegard, *Surf. Sci.* **459**, 49 (2000).
- [153] S. LaShell, B. A. McDougall, and E. Jensen, *Phys. Rev. Lett.* **77**, 3419 (1996).
- [154] S. Sorella and E. Tosatti, *Europhys. Lett.* **19**, 699 (1992).
- [155] L. M. Martelo, M. Dzierzawa, L. Siffert, and D. Baeriswyl, *Z. Phys. B* **103**, 335 (1997).
- [156] M. Dzierzawa, D. Baeriswyl, and M. Di Stasio, *Phys. Rev. B* **51**, 1993(R) (1995).
- [157] E. Kim and M. H. W. Chan, *Science* **305**, 1941 (2004).
- [158] E. Kim and M. H. W. Chan, *Nature* **427**, 225 (2004).
- [159] D. Heidarian and K. Damle, *Phys. Rev. Lett.* **95**, 127206 (2005).
- [160] R. G. Melko, A. Paramekanti, A. A. Burkov, A. Vishwanath, D. N. Sheng, and L. Balents, *Phys. Rev. Lett.* **95**, 127207 (2005).
- [161] N. Prokof'ev, *Adv. Phys.* **56**, 381 (2007).
- [162] T. Senthil, A. Vishwanath, L. Balents, S. Sachdev, and M. P. A. Fisher, *Science* **303**, 1490 (2004).
- [163] A. J. Millis, P. B. Littlewood, and B. I. Shraiman, *Phys. Rev. Lett.* **74**, 5144 (1995).
- [164] A. J. Millis, B. I. Shraiman, and R. Mueller, *Phys. Rev. Lett.* **77**, 175 (1996).
- [165] M. Jaime, M. B. Salamon, M. Rubinstein, R. E. Treece, J. S. Horwitz, and D. B. Chrisey, *Phys. Rev. B* **54**, 11914 (1996).
- [166] A. Lanzara, N. L. Saini, M. Brunelli, F. Natali, A. Bianconi, P. G. Radaelli, and S.-W. Cheong, *Phys. Rev. Lett.* **81**, 878 (1997).
- [167] C. Hartinger, F. Mayr, A. Loidl, and T. Kopp, *Phys. Rev. B* **73**, 024408 (2006).
- [168] E. Dagotto, *Nanoscale Phase Separation and Colossal Magnetoresistance* (Springer-Verlag, Berlin, 2003).
- [169] J. Y. T. Wei, N. C. Yeh, and R. P. Vasquez, *Phys. Rev. Lett.* **79**, 5150 (1997).
- [170] J. Mitra, M. Paranjape, A. K. Raychaudhuri, N. D. Mathur, and M. G. Blamire, *Phys. Rev. B* **71**, 094426 (2005).
- [171] M. Fäth, S. Freisem, A. A. Menovsky, Y. Tomioka, J. Aarts, and J. A. Mydosh, *Science* **285**, 1540 (1999).
- [172] J. Choi, J. Zhang, S.-H. Liou, P. A. Dowben, and E. W. Plummer, *Phys. Rev. B* **59**, 13453 (1999).
- [173] S. Valencia, A. Gaupp, W. Gudat, L. Abad, L. Balcells, A. Cavallaro, B. Martínez, and F. J. Palomares, *Phys. Rev. B* **73**, 104402 (2006).
- [174] M. J. Calderón, L. Brey, and F. Guinea, *Phys. Rev. B* **60**, 6698 (1999).
- [175] X. Du, S.-W. Tsai, D. L. Maslov, and A. F. Hebard, *Phys. Rev. Lett.* **94**, 166601 (2005).
- [176] Y. Kopelevich, J. C. M. Pantoja, R. R. da Silva, and S. Moehlecke, *Phys. Rev. B* **73**, 165128 (2006).
- [177] K. S. Novoselov, A. K. Geim, S. V. Morozov, D. Jiang, M. I. Katsnelson, I. V. Grigorieva, S. V. Dubonos, and A. A. Firsov, *Nature* **438**, 197 (2005).
- [178] A. K. Geim and K. S. Novoselov, *Nature Mat.* **6**, 183 (2007).
- [179] K. v. Klitzing, G. Dorda, and M. Pepper, *Phys. Rev. Lett.* **45**, 494 (1980).
- [180] R. B. Laughlin, *Phys. Rev. B* **23**, 5632 (1981).
- [181] H. M. Jaeger, D. B. Haviland, A. M. Goldman, and B. G. Orr, *Phys. Rev. B* **34**, 4920 (1986).
- [182] M. P. A. Fisher, G. Grinstein, and S. M. Girvin, *Phys. Rev. Lett.* **64**, 587 (1990).
- [183] M. Büttiker, Y. Imry, R. Landauer, and S. Pinhas, *Phys. Rev. B* **31**, 6207 (1985).
- [184] B. J. van Wees, H. van Houten, C. W. J. Beenakker, J. G. Williamson, L. P. Kouwenhoven, D. van der Marel, and C. T. Foxon, *Phys. Rev. Lett.* **60**, 848 (1988).
- [185] D. A. Wharam, T. J. Thornton, R. Newbury, M. Pepper, H. Ahmed, J. E. F. Frost, D. G. Hasko, D. C. Peacock, D. A. Ritchie, and G. A. C. Jones, *J. Phys. C* **21**, L209 (1988).
- [186] K. S. Novoselov, A. K. Geim, S. V. Morozov, D. Jiang, Y. Zhang, S. V. Dubonos, L. V. Grigorieva, and A. A. Firsov, *Science* **306**, 666 (2004).
- [187] T. Ando, Y. S. Zheng, and H. Suzuura, *J. Phys. Soc. Jpn.* **71**, 1318 (2002).
- [188] V. P. Gusynin, S. G. Sharapov, and J. P. Carbotte, *Phys. Rev. Lett.* **96**, 256802 (2006).
- [189] L. A. Falkovsky and A. A. Varlamov, *Eur. Phys. J. B* **56**, 281 (2007).
- [190] Y. Zhang, Y.-W. Tan, H. L. Stormer, and P. Kim, *Nature* **438**, 201 (2005).
- [191] M. L. Sadowski, G. Martinez, M. Potemski, C. Berger, and W. A. de Heer, *Phys. Rev. Lett.* **97**, 266405 (2006).
- [192] Z. Jiang, E. A. Henriksen, L. C. Tung, Y.-J. Wang, M. E. Schwartz, M. Y. Han, P. Kim, and H. L. Stormer, *Phys. Rev. Lett.* **98**, 197403 (2007).
- [193] J. W. McClure, *Phys. Rev.* **108**, 612 (1957).

- [194] J. C. Slonczewski and P. R. Weiss, *Phys. Rev.* **109**, 272 (1958).
- [195] K. Wakabayashi and M. Sigrist, *Phys. Rev. Lett.* **84**, 3390 (2000).
- [196] P. Ruffieux, O. Gröning, P. Schwaller, L. Schlapbach, and P. Gröning, *Phys. Rev. Lett.* **84**, 4910 (2000).
- [197] M. Büttiker, *Phys. Rev. Lett.* **68**, 843 (1992).
- [198] I. Neder, N. Ofek, Y. Chung, M. Heiblum, D. Mahalu, and V. Umansky, *Nature* **448**, 333 (2007).
- [199] G. Fève, A. Mahé, J. M. Berroir, T. Kontos, B. Plaçais, D. C. Glattli, A. Cavanna, B. Etienne, and Y. Jin, *Science* **316**, 1169 (2007).
- [200] J. Gabelli, G. Fève, J. M. Berroir, B. Plaçais, A. Cavanna, B. Etienne, Y. Jin, and D. C. Glattli, *Science* **313**, 499 (2006).
- [201] M. Büttiker, H. Thomas, and A. Prêtre, *Phys. Lett. A* **180**, 364 (1993).
- [202] V. A. Gopar, P. A. Mello, and M. Büttiker, *Phys. Rev. Lett.* **77**, 3005 (1996).
- [203] P. W. Brouwer and M. Büttiker, *Europhys. Lett.* **37**, 441 (1997).
- [204] Y. Imry, in *Directions in Condensed Matter Physics. Memorial volume in honor of Sheng-keng Ma*, G. Grinstein and G. Mazenko, eds. (World Scientific, Singapore, 1986), p. 101.
- [205] R. Landauer, *Z. Phys. B* **68**, 217 (1987).
- [206] A. J. Leggett and A. Garg, *Phys. Rev. Lett.* **54**, 857 (1985).
- [207] A. Georges, G. Kotliar, W. Krauth, and M. J. Rozenberg, *Rev. Mod. Phys.* **68**, 13 (1996).
- [208] J. E. Hirsch and R. M. Fye, *Phys. Rev. Lett.* **56**, 2521 (1986).

Project 2

Superconductivity, unconventional mechanisms and novel materials

Project leader: D. van der Marel (UniGE)

Participating members: D. Baeriswyl (UniFR), C. Bernhard (UniFR), G. Blatter (ETHZ), Ø. Fischer (UniGE), T. Giamarchi (UniGE), M. Gioni (EPFL), H. Keller (PSI), D. van der Marel (UniGE), J. Mesot (PSI), E. Morenzoni (PSI), T.M. Rice (ETHZ), M. Sigrist (ETHZ). Contributions from H.R. Ott and J.-M. Triscone (UniGE).

Introduction: The research in this project is on the properties of novel superconducting materials, in particular noncentrosymmetric superconductors such as CePt₃Si, Ce₁₁₅ *d*-wave superconductors, and Chevrel-phase superconductors, organic superconductors, the superconducting interface between LaAlO₃ and SrTiO₃, MgB₂, ZrB₁₂ and inversion asymmetric superconducting pyrochlore osmates. The surface melting of Abrikosov flux-line lattices was studied theoretically, and the competition between superconductivity and magnetism was studied in multi-layers of superconducting and magnetic oxide materials. The microscopic properties of high T_c cuprate materials were subject of theoretical studies and a wide variety of experimental techniques.

Summary and highlights

The recent discovery of noncentrosymmetric superconductor such as CePt₃Si has created opportunities for discovering novel phenomena related to the parity mixing of pairing channels with spin zero and spin one. An example is the prediction by Iniotakis, Fujimoto and Sigrist that the interface between twin domains of opposite spin-orbit coupling provides an environment allowing flux lines with fractional flux quanta to be formed [1]. Their presence could have strong implications on the flux creep behavior in such superconductors.

Almost half a century ago Fulde, Ferrell, Larkin, and Ovchinnikov (FFLO) have predicted that, close to the Pauli-limit, a superconductor may enter a state of matter where the superconducting condensate has a finite momentum and the order parameter develops regularly spaced planar nodes perpendicular to the vortex lines. This state has been elusive for more than four decades, but recently this so-called FFLO state was observed in the layered organic superconductor (BEDT-TTF)₂Cu(NCS)₂ by Lortz *et al.* (UniGe) using calorimetry and magnetic torque measurements upto 28 Tesla [2].

Another candidate for the FFLO state is CeCoIn₅, a *d*-wave heavy-fermion superconductor with a critical temperature $T_c = 2.3$ K. Using neutron-scattering with a magnetic field parallel to the *c*-axis, a collaboration of the group of Mesot (PSI) and researchers from Los Alamos, Brookhaven, and the universities of Indiana, Notre Dame, and Birmingham, observed a rich phase diagram for different mag-

netic fields and temperatures, exhibiting an alternation of rhombic, square and hexagonal symmetries of the vortex lattice [3]. This behavior -far from the standard Abrikosov vortex lattice- may have its origin in the *d*-wave symmetry of the order parameter, and lends support to earlier claims that near the Pauli-limit this material enters an FFLO state.

Interfaces between different materials represent a rapidly growing field, where unique phenomena can occur which can not be realized in bulk materials. LaAlO₃ and SrTiO₃ are both insulators, but at the interface between these two insulators a dense and mobile electron fluid is formed. A collaboration of the groups of Triscone (UniGe) and Mannhart (University of Augsburg, Germany) studied the properties of this fluid at low temperatures, and observed that it becomes even superconducting below 0.2 Kelvin [4], close to the T_c of *n*-doped SrTiO₃. The thickness of this superconducting layer was argued to be less than 10 nanometers, implying that this superconductor is effectively 2-dimensional. Indeed the characteristics of the transition were found to be consistent with those of a 2D electron system undergoing a Berezinskii-Kosterlitz-Thouless (BKT) transition.

In the field of cuprate high T_c superconductivity, the big — still unanswered — challenges emerge from their complex phase diagram. The interplay between superconductivity, magnetism, stripes or stripe-like order, spontaneous time-reversal symmetry breaking and quantum criticality is central in theoretical and experimental approaches. While the

Hubbard model is universally considered as a ‘minimal model’ for the electronic properties of the cuprates, the question whether or not it can explain superconductivity has not received a definite answer yet. An important step in this direction was obtained by the group of Baeriswyl who, using a novel variational wave function which generalizes previously used trial states [5, 6], found that ground state of a hole doped Hubbard insulator with a hole concentration between 5 and 20% is a d -wave superconductor. In their calculation the kinetic of the electrons increases when the system becomes superconducting, a trend which is precisely opposite to the prediction by the BCS theory. This result agrees with trends reported by the group of van der Marel for the temperature dependence of the free carrier optical spectral weight of under- and optimally-

doped Bi-2212 [7, 8, 9], Bi-2223 [10], and Hg-1201 [11].

Signatures of the coupling of bosons to the conduction bands, such as phonons or spin-waves, can be seen in spectroscopic probes of the electrons near the Fermi energy, in particular angle resolved photoemission (ARPES), scanning tunneling spectroscopy (STS) and infrared spectroscopy (IRS). Using STS Fischer’s group has obtained robust evidence that the dip-hump feature in the single particle spectral function of the cuprates is due to a collective bosonic mode like the (π, π) spin-wave resonance [12]. Evidence for coupling to a continuum of bosonic excitations up to 0.3 eV is implied by the strong coupling analysis of infrared spectra [13] and from the ‘waterfall’ dispersion recently observed in ARPES data of $\text{La}_{2-x}\text{Sr}_x\text{CuO}_4$ [14].

1 Novel superconductors

1.1 Surface bound states of CePt_3Si

Until recently superconductivity in metals without inversion center has been a largely unexplored area of superconductivity. With the discovery of the heavy Fermion superconductor CePt_3Si in 2003, the investigation of the unusual properties of this class of superconductors started. Non-centrosymmetry af-

flicts the electronic properties through spin-orbit coupling which leads to a characteristic spin-splitting of the electronic bands. This has a strong effect on Cooper pairing at the Fermi surface resulting in a non-unitary pairing state. It was shown by several groups that this pairing state displays parity mixing involving both spin-singlet and spin-triplet character.

A non-trivial phase structure of the gap function can lead to Andreev bound states at surfaces and interfaces of an unconventional superconductor. In the presence of line nodes the $s \pm p$ -wave state proposed by Frigeri *et al.* [15] for CePt_3Si satisfies the conditions for such quasiparticle states with subgap energies. These bound states could be detected through resonant quasiparticle tunneling and appear as so-called zero-bias anomalies in the I - V -characteristics. The study by Sigrist’s group was motivated by the aim that such spectral tunneling features could provide a mean to probe the presence of nodes as well as the symmetry of the mixed-parity state [16]. In particular, for the $s \pm p$ -wave state it was found that I - V -spectrum depends in a characteristic way on the tunneling direction providing the selection rule: in plane tunneling would show a zero-bias anomaly (Fig. 1), while it should be absent for the c -axis direction.

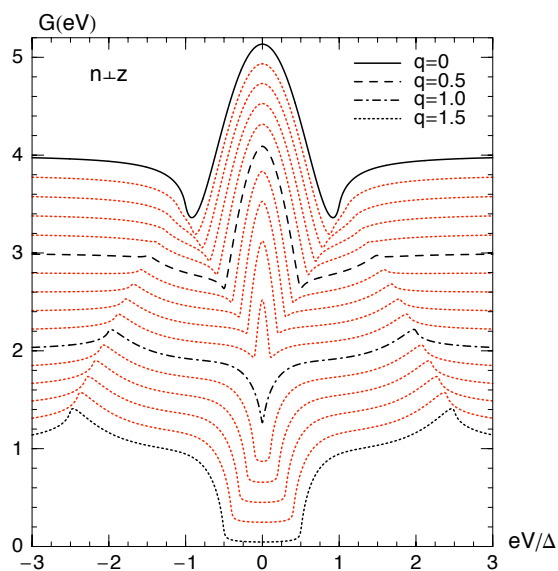


Figure 1: Normalized low-temperature conductance $G(eV)$ for a normal metal/non-centrosymmetric superconductor junction with boundary orientation $\mathbf{n} \perp \mathbf{z}$. The ratio q of the gap amplitudes for s - and p -wave component is varied from 0 to 1.5 in steps of 0.1.

1.2 Fractional flux lines on twin boundaries of CePt_3Si

Intrinsic interfaces separating twin domains of opposite spin-orbit coupling in the crystal can yield intriguing effects. Sigrist’s group has

been analyzing this situation for the case of CePt₃Si for which two distinct twin domains are possible [1]. The mixed parity phase can lead to Andreev bound states at such interfaces, possibly observable by STS measurements, and a locally time reversal symmetry breaking (two-fold degenerate) phase can occur. Line defects separating the two degenerate interface states constitute flux lines enclosing flux which is only a fraction of a flux quantum. The fact that a conventional vortex in the superconductor can decay into two fractional ones which are strongly pinned on the interface, implies that such interface states would provide a strong impediment for the flux creep behavior of such superconductors. This flux creep effect is under experimental investigation now.

1.3 Josephson effect between CePt₃Si and a conventional superconductor

The Josephson effect between a mixed-parity phase in a non-centrosymmetric superconductor such as CePt₃Si and a conventional superconductor involves some aspects of selection rules. Sigrist and collaborators have examined the Josephson coupling along different directions [17]. It is interesting that, for certain directions only, the even-parity part of the pair wave function can couple to the order parameter of the conventional superconductor. For other directions spin-orbit coupling allows to couple both even- and odd-parity. For such junctions the intrinsic Josephson phase may vary between the two values 0 and π depending on the contributions of the two spin-split Fermi surfaces. This would give rise to distorted interference patterns in a magnetic field, similar to those found in 45°-asymmetric grain boundaries of cuprate superconductor films. This property could explain recent experiments by a Japanese group [78].

1.4 Coexistence of superconductivity and antiferromagnetism in CePt₃Si

CePt₃Si has an antiferromagnetic transition at $T_N = 2.2$ K slightly above the onset of superconductivity at $T_c = 0.45$ K. The behavior under pressure suggests that the superconducting phase is associated with a magnetic quantum phase transition, analogous to other Ce-based heavy Fermion superconductors. In previous studies ignoring the antiferromagnetic order, it was shown that the spin susceptibility has a very specific anisotropy in the superconducting state [18], which has been verified experimentally for other similar

non-centrosymmetric superconductors such as CeRhSi₃. However, for CePt₃Si experimental results are in conflict with this theoretical prediction [79]. In a recent study in Sigrist's group, the role of antiferromagnetism in CePt₃Si was analyzed theoretically [19, 20]. The presence of antiferromagnetism was identified as the prime cause for the discrepancy between theory and experiment for the spin susceptibility. In this context, testable predictions have been made for the behavior of the superconducting state as a function of pressure. Moreover, it was shown that the structure of the spin fluctuations in CePt₃Si favoring A-type order would favor an $s \pm p$ -wave pairing state consistent with the superconducting properties found experimentally so far.

1.5 Optical properties and electronic structure of CeMIn₅ (M = Co, Rh, Ir)

Cerium based compounds are well known to exhibit strongly correlated electronic phenomena. Among them, the materials of the CeMIn₅ (M = Co, Rh, Ir) group have recently attracted considerable attention for their unusual superconductivity and, presumably, proximity to a quantum critical point with pressure and magnetic field as tuning parameters. In collaboration with D. Basov at UCSD (San Diego) van der Marel's group has determined the infrared conductivity CeMIn₅ (M = Co, Rh, Ir) in the photon energy range from 2 meV to 4.5 eV using the combination of near normal incidence reflectivity (2 meV–0.8 eV) and ellipsometry (0.8–4.5 eV) [21]. In all compounds signatures of the formation of a coherent state is found. In CeCoIn₅ and CeIrIn₅, which do not order magnetically but become superconducting, the spectral weight is recovered in a frequency range that is considerably larger than the hybridization gap. However, as a result of the competition with anti-ferromagnetism, the energy region where the coherent state occurs is much lower in the CeRhIn₅ compound that orders magnetically.

1.6 Neutron scattering study of the FFLO phase in CeCoIn₅

Many superconducting materials allow the penetration of magnetic fields in a mixed state in which the superfluid is threaded by a regular lattice of Abrikosov vortices, each carrying one quantum of magnetic flux. The phenomenological Ginzburg-Landau theory, based on the concept of characteristic length scales, has generally provided a good description of the

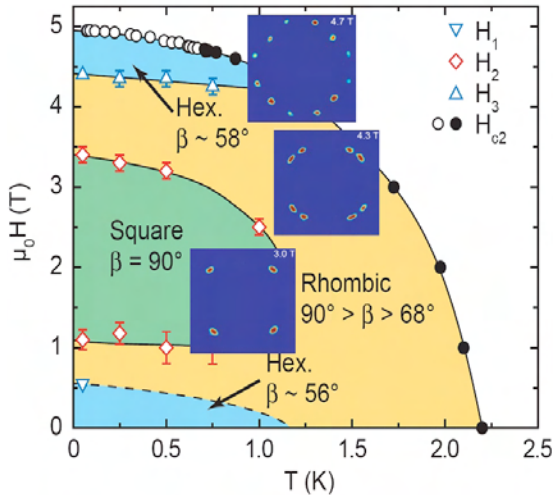


Figure 2: Structural phase diagram for the VL in $CeCoIn_5$ with the magnetic field parallel to the c -axis.

Abrikosov vortex lattice (VL) state. After having established the B vs T phase diagram of the VL (Fig. 2), a collaboration of the group of Mesot with researchers from UCI, University of Notre Dame, University of Birmingham, Los Alamos National Laboratory and Brookhaven National Laboratory conducted neutron-scattering measurements of the vortex lattice form factor in the heavy-fermion superconductor cerium-cobalt-indium ($CeCoIn_5$) and found that this form factor increases with increasing field — opposite to the expectations within the Abrikosov-Ginzburg-Landau paradigm. The anomalous field dependence of the form factor is attributed to Pauli paramagnetic effects around the vortex cores and from the proximity of the superconducting state to a quantum critical point [3].

1.7 High Pressure XAS and RIXS of heavy fermion superconductors

The unusual properties of the cuprates have stimulated a strong interest in non-conventional mechanisms of pairing. In particular, in magnetic heavy fermions compounds like e.g. $CePd_2Si_2$ or $CeIn_3$, spin or valence fluctuations associated with the strongly correlated $4f$ states, could replace the phonons as the glue that binds electrons in Cooper pairs [80]. In these compounds, superconductivity is found in narrow regions around a quantum critical point (QCP), where the system can be driven by hydrostatic pressure from the magnetic to the superconducting phase. High-resolution X-ray absorption in the partial-fluorescence yield mode (PFY-XAS)

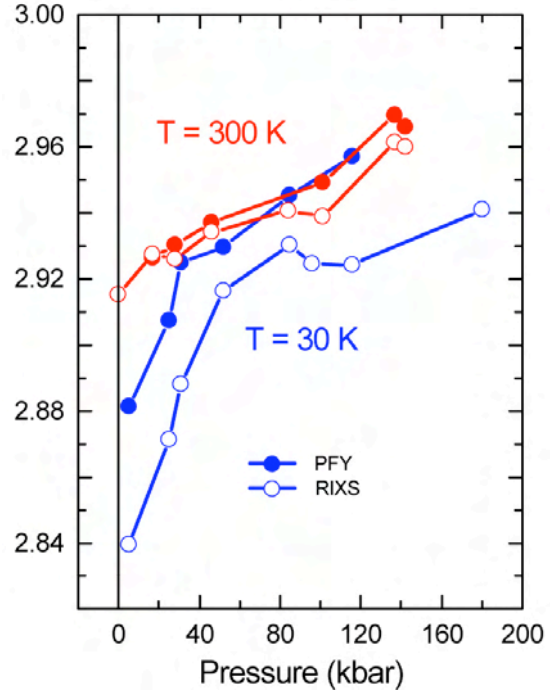


Figure 3: Yb valence in $YbRh_2Si_2$ as a function of pressure and temperature estimated from PFY-XAS and RIXS experiments.

and resonant X-ray scattering experiments (RIXS) can provide a direct microscopic view of the $4f$ occupation in a region of the phase diagram that is strongly influenced by the QCP. Such experiments are very challenging, since they require cryogenic conditions and high hydrostatic pressures, but are now feasible at the $Yb L_3$ ($2p \rightarrow 5d$; $h\nu = 8.9$ keV) absorption edge [22, 23, 24]. In collaboration with scientists from Milano (Dallera), Grenoble (Knebel) and Paris (D’Astuto) the group of Grioni measured at beam line ID 26 of the ESRF the temperature and pressure dependence of the Yb valence in the Yb-based heavy fermion compounds $YbNi_2Ge_2$ and $YbRh_2Si_2$ (Fig. 3). In all cases the valence increases with increasing pressure and temperature, with a clear deviation from the pure Yb^{3+} configuration in the vicinity of the QCP.

1.8 The two colors of MgB_2

Magnesium diboride MgB_2 , which contains graphene-like boron planes, is an interesting example of a non-cuprate ‘high- T_c ’ superconductor ($T_c \approx 40$ K). In addition, it clearly shows a rare phenomenon of a two-gap superconductivity. The anisotropic optical conductivity of MgB_2 between 0.1–3.7 eV on single crystals by the spectroscopic ellipsometry and reflectance measurements [25] was studied by van der

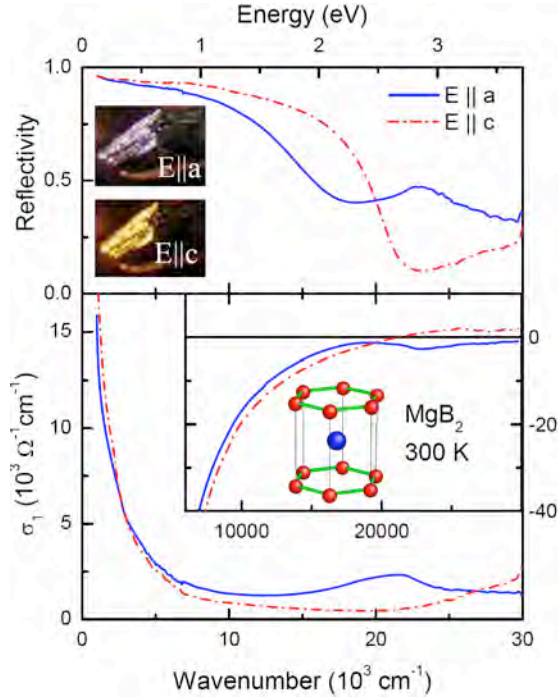


Figure 4: Reflectivity (top panel), optical conductivity and the dielectric constant (bottom panel) of MgB_2 at 300 K for two polarizations. The photographs on the top panel are made on the *ac*-oriented surface in polarized light.

Marel and collaborators (Fig. 4). The bare (unscreened) plasma frequency ω_p was observed to be almost isotropic and equal to 6.3 eV, which contrasts some earlier reports of a very small value of ω_p . The data indicate that the σ -bands are characterized by a stronger electron-phonon coupling λ but smaller impurity scattering γ_{imp} , compared to the π -bands. The optical response along the boron planes is marked by an intense interband transition at 2.6 eV, due to which the reflectivity plasma edges along the *a*- and *c*-axes are shifted with respect to each other. This shift explains a double color appearance of MgB_2 . The optical spectra are in good agreement with the published *ab initio* band structure and electron-phonon coupling calculations.

1.9 Electron scattering by defects in MgB_2

In earlier work [26] investigating the two-band character of the superconductivity of MgB_2 by measurements of the temperature and magnetic-field dependence of the thermal conductivity $\kappa(T, H)$ in the mixed state, Ott and collaborators have identified the relative contributions of the electrons in either the σ - or the π band to the thermal transport below T_c . This work was extended to single crystals of $\text{Mg}_{1-y}\text{Al}_y\text{B}_2$ and $\text{MgB}_{2-x}\text{C}_x$ ($x, y < 0.1$), i.e.

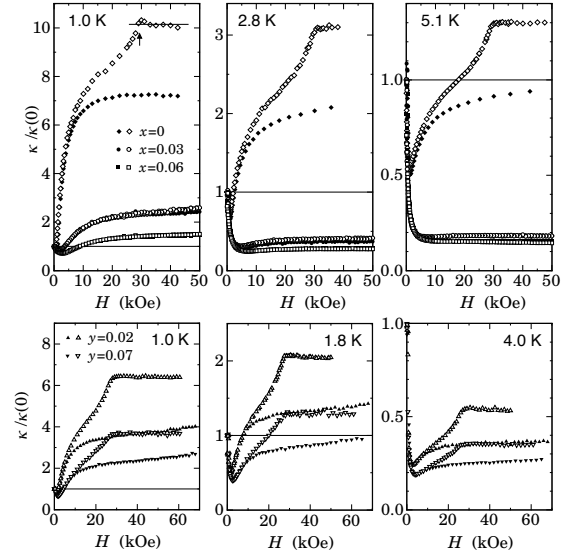


Figure 5: Magnetic field induced variations of the thermal conductivity $\kappa(H)$ in the mixed state of superconducting $\text{Mg}(\text{B}_{1-x}\text{C}_x)_2$ (upper panel) and $\text{Mg}_{1-y}\text{Al}_y\text{B}_2$ (lower panel). The open and closed symbols are data for *H* oriented parallel and perpendicular to the *c*-axis, respectively.

on material with impurities on either the Mg or the B sublattice [27, 28]. In pure MgB_2 the electronic heat transport is divided almost equally between the electrons occupying states in the σ - and the π band. Low concentrations of C on B sites reduce the heat conduction by electrons occupying σ -band states by 2 orders of magnitude, i.e. the heat transport is almost entirely carried by π -band electrons. Replacing small amounts of Mg by Al on the corresponding sublattice enhances the *intra*band scattering of electrons of both bands in approximately the same way. For both types of defects, the data on $\kappa(T, H)$ indicate, however, that the *inter*band scattering is not significantly affected by the introduction of either type of defect (Fig. 5). The gap anisotropy between the σ - and the π band is thus preserved in either case.

1.10 Zirconium dodecaboride: transport and optical properties

In zirconium dodecaboride ($T_c = 6$ K), boron atoms make up a three-dimensional network forming spacious B_{24} cages, which accommodate metal ions. The van der Marel group determined the optical conductivity of ZrB_{12} using ellipsometry in the range 0.8–4.6 eV and IR reflectometry in the range 6 meV–0.8 eV from 300 K down to 20 K [29]. The Drude plasma frequency and interband optical conductivity calculated by the self-consistent, fullpotential linear muffin-tin orbital method agree well with

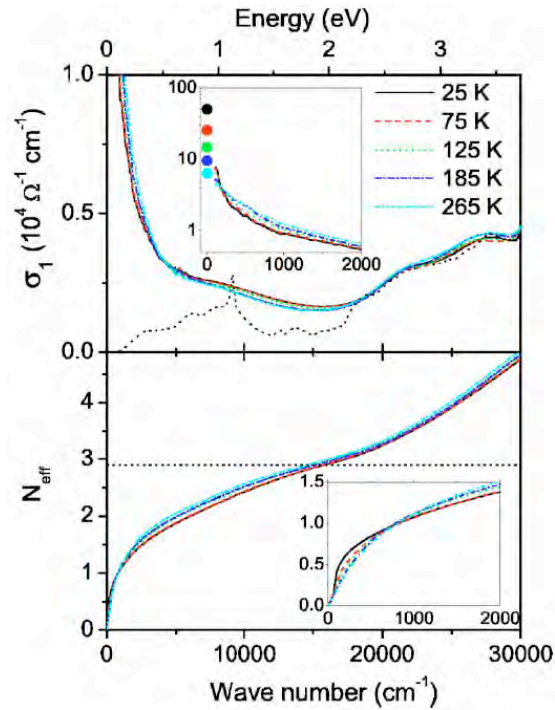


Figure 6: Top panel: optical conductivity of ZrB_{12} at selected temperatures. Inset: low-energy part; symbols represent the DC conductivity. The dotted line shows the interband conductivity from LDA calculation. Bottom panel: effective number of carriers per unit cell. Inset: low-frequency part; the horizontal dotted line corresponds to the calculated plasma frequency of 6.3 eV.

experimental data (Fig. 6). The Eliashberg function $\alpha^2F(\omega)$ extracted from optical spectra features two peaks at about 25 and 80 meV, in agreement with specific heat data. The total coupling constant is $\lambda_{tr} = 1.0 \pm 0.35$. The low-energy peak presumably corresponds to the displacement mode of Zr inside B_{24} cages, while the second one involves largely boron atoms. An unexpected removal of about 10 % of the Drude spectral weight was observed. This effect may be caused by the delocalization of the metal ion from the center of the boron cluster.

1.11 Thermal spectroscopy of the vibrational modes in superconducting materials

When measured with a high accuracy, specific heat, electrical resistivity and thermal expansivity can be regarded as “thermal spectroscopies”. A complete set of these data gives rich information on the interplay between lattice vibrations (specific heat), anharmonicity (thermal expansion) and electronic properties (resistivity). A method to obtain the phonon density of states from specific heat,

the electron-phonon coupling function from resistivity and the mode Gruneisen parameter from thermal expansion was developed, which in some cases can compete with standard determinations as e.g. inelastic neutron or X-ray scattering. Although the energy resolution is limited, a great advantage of the phonon density of states obtained from specific heat is that it provides absolute values and is not bothered by the different scattering cross sections of the atoms forming the structure. Detailed analyses were performed by R. Lortz *et al.* (UniGe) on superconductors with structures based on ions in oversized crystalline cages with very low-lying (‘rattling’) phonon modes: the clathrates Ba_8Si_{46} and $Ba_{24}Si_{100}$, the borides ZrB_{12} , YB_6 and LuB_{12} , the linear Chevrel phases $Tl_2Mo_6Se_6$, $In_2Mo_6Se_6$ and the pyrochlore KOs_2O_6 [30, 31, 32]. From the analysis it was possible to identify the phonon modes responsible for superconductivity. Some of these superconductors revealed themselves as textbook examples, where superconductivity is mediated by a single soft phonon mode.

1.12 KOs_2O_6 and $RbOs_2O_6$

The discovery of superconductivity in the β -pyrochlore osmate compounds AOs_2O_6 ($A = K, Rb, Cs$) [81, 82, 83] has highlighted the question of the origin of superconductivity in classes of materials which possess geometrical frustration [84, 85]. The reported absence of inversion symmetry in the crystal structure of KOs_2O_6 [33] raises the question of its Cooper pair symmetry and the possibility of spin singlet-triplet mixing [34, 35, 36].

Scanning tunneling spectroscopy (STS) measurements on atomically flat regions of the as-grown surface of KOs_2O_6 were performed by the group of Fischer [37]. With 9.6 K, this compound displays the highest- T_c of the β -pyrochlores. Fitting the spectra (dI/dV) and their derivatives (i.e. d^2I/dV^2) at different temperatures revealed that KOs_2O_6 is fully gapped with an anisotropy of around 30% [38]. In addition, the observed spectra are compatible with an $s - p$ -wave spin-triplet mixed state which is allowed if the compound lacks inversion symmetry.

The magnetic properties of the samples were also investigated. Magnetization vs. temperature was measured at different fields, in Field-Cooled (FC) and Zero-Field-Cooled (ZFC) conditions. This measurement gives the critical temperature T_{c2} as well as the temperature of irreversibility T_{irr} , defined as the tem-

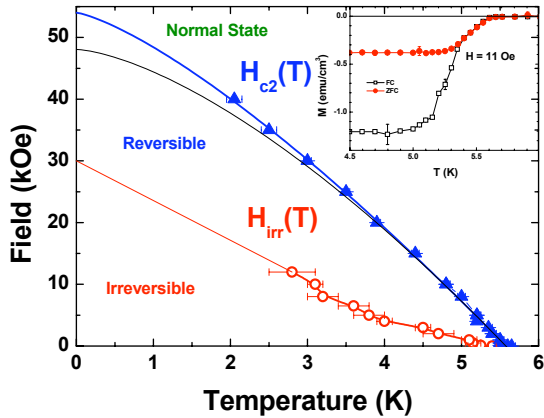


Figure 7: Vortex Phase Diagram of RbOs_2O_6 . Lines are guides to the eye. Inset: magnetization vs. temperature in FC and ZFC at a field of 11 Oe

perature where the FC and ZFC curves split (inset of Fig. 7). The vortex phase diagram was then constructed, shown in Fig. 7. Compared to most superconductors, for example $\text{Bi}_2\text{Sr}_2\text{Ca}_2\text{Cu}_3\text{O}_{10+\delta}$, the reversible zone is very large. This means that the vortex pinning is very low in this compound.

1.13 Transport and specific heat measurements in quasi-1D molybdenum cluster condensates and quasi-3D Chevrel phase compounds

For many years, the scientific community has sought a compound to bridge the gap between conventional BCS type-II superconductors and the high- T_c cuprates. With their extremely short coherence lengths (as low as 23 Å in PbMo_6S_8) [39] and high upper critical fields, Chevrel phase superconductors appear to be an ideal candidate for this role. Although these materials crystallize in a quasi-3D structure comprising weakly-coupled Mo_6X_8 ($X = \text{S}, \text{Se}, \text{Te}$) clusters, it is also possible to condense such clusters into infinite-length chains, thus forming the $\text{M}_2\text{Mo}_6\text{X}_6$ family which includes the most highly one-dimensional superconductors currently known.

Fischer and collaborators have measured the low-temperature characteristics of the quasi-particle DOS of superconducting PbMo_6S_8 for the first time using scanning tunneling spectroscopy. In light of these results, a highly anisotropic gap function is the likely explanation for the low-energy excitations observed in the spectra. In particular, the measurements are well described by 3D d -wave models compatible with the rhombohedral symmetry of PbMo_6S_8 . Interestingly, the spatial dependence of some of the compatible gaps is very reminis-

cent of the peculiar shape of the first Fermi surface sheet. Such d -wave superconductivity in PbMo_6S_8 could result from the very short coherence length which would favor the appearance of a repulsive component in the coupling interaction [39]. The combination of possible d -wave symmetry, a large $2\Delta_0/k_B T_c$ ratio and short coherence length in PbMo_6S_8 is strongly reminiscent of the high T_c superconductors and calls for further investigation.

Quasi-1D $\text{M}_2\text{Mo}_6\text{Se}_6$ ($M = \text{Tl}, \text{In}, \text{Rb}$) were studied using AC susceptibility, electrical transport and specific heat techniques. The low-dimensional nature of these materials is immediately apparent in the superconducting transitions for $M = \text{Tl}, \text{In}$ which are substantially broadened in a magnetic field [40, 41]. This effect is significantly greater in $\text{Tl}_2\text{Mo}_6\text{Se}_6$ due to its reduced coherence volume. The magnitude of the broadening cannot be explained by conventional 3D thermal fluctuations, although a 1D model developed for superconducting nanowires [86] gives more realistic transition widths.

By combining the data for the lattice specific heat with the electrical resistivity, the approximate phonon densities of states (PDOS) and electron-phonon coupling were measured for $M = \text{Tl}, \text{In}$ (Fig. 8) [41]. The PDOS obtained compare well with previous neutron scattering data [87], displaying a strong low-energy (5–7 meV) Einstein-type mode from the M ion vibration, together with a set of intra-chain modes in the 10–30 meV range. Electrons in

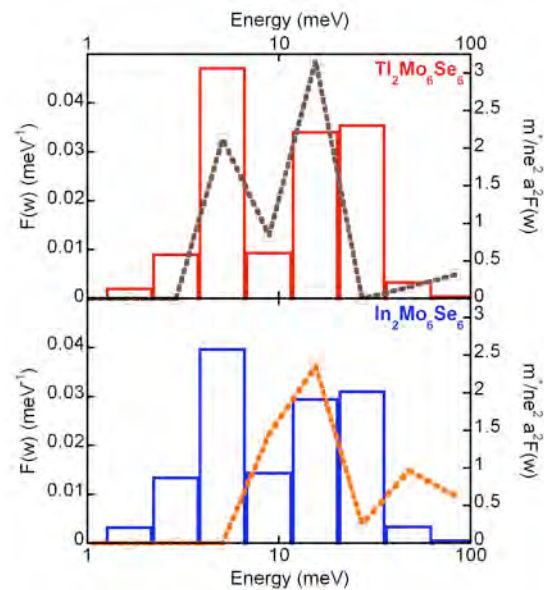


Figure 8: Phonon density of states (histogram) and normalised electron-phonon transport coupling function $\alpha_{tr}^2 F_w$ (line) for $\text{Tl}_2\text{Mo}_6\text{Se}_6$ and $\text{In}_2\text{Mo}_6\text{Se}_6$.

Tl₂Mo₆Se₆ couple strongly to both low and high-energy modes, whereas In₂Mo₆Se₆ only displays a coupling with the high-energy intra-chain modes. From the specific heat data, the BCS coupling ratios $2\Delta/k_B T_c \geq 5$ and 3.5 for M = Tl, In respectively. This implies that although not entirely responsible for superconductivity, the Einstein mode from the Tl atom is able to “boost” superconductivity in Tl₂Mo₆Se₆. In contrast, Rb₂Mo₆Se₆ undergoes a broad metal-insulator transition at $T \sim 170$ K.

1.14 Specific heat study of the FFLO phase in (BEDT-TTF)₂Cu(NCS)₂

The layered organic superconductor (BEDT-TTF)₂Cu(NCS)₂ was studied by R. Lortz (UniGe) in the high-field laboratory in Grenoble in fields up to 28 T with a high-precision micro-relaxation calorimeter [2]. When the field was applied parallel to the superconducting planes, the superconducting transition became of first-order in fields above 21 T (Fig. 9). This is a clear sign that the Pauli limit for superconductivity is reached. Above this field, the upper critical field line exhibits a sharp upturn and a second phase transition appears within the superconducting phase. A comparison with a theoretical model shows that the observed phase is a realization of a Fulde-Ferrel-Larkin-Ovchinnikov state. This phase has been

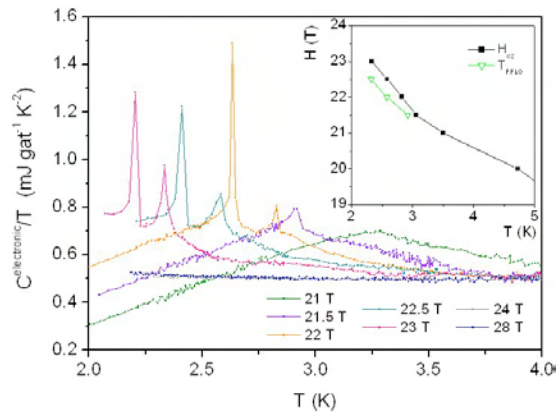


Figure 9: Electronic contribution to the specific heat of the organic superconductor (BEDT-TTF)₂Cu(NCS)₂ in high magnetic fields applied parallel to the superconducting layers. The superconducting transition becomes of first order when the Pauli limit for superconductivity is reached. A second first-order transition within the superconducting phase represents the transition into an inhomogeneous Fulde-Ferrel-Larkin-Ovchinnikov state. Inset: phase diagram showing the sharp upturn of the H_{c2} line due to the presence of an FFLO state (black squares) and the transition into the FFLO state (green triangles).

before only identified in the heavy-fermion superconductor CeCoIn₅. In a following experiment the existence of this phase was confirmed by means of magnetic torque measurements.

1.15 Local ferroelectric field-effect in superconducting Nb-doped SrTiO₃.

The long term goal of this project is to create superconducting nanostructures in thin oxide films using the ferroelectric field effect. The group of Triscone fabricated heterostructures by growing first, using pulsed laser deposition (PLD), high quality epitaxial metallic 1 weight% Nb-doped SrTiO₃ (Nb-STO) thin films on insulating TiO₂-terminated SrTiO₃ (STO) substrates. Then, using RF-magnetron sputtering, a ferroelectric PbZr_{0.2}Ti_{0.8}O₃ (PZT) film was grown onto the metallic Nb-STO film. Switching the polarization of the PZT with an atomic force microscope (AFM) allows to change the carrier concentration of the Nb-STO film at the nanoscale. The reversal of the polarization induces a shift in the superconducting critical temperature [42]. As can be seen in Fig. 10, over a given temperature range, the Nb-STO is in the superconducting or non-

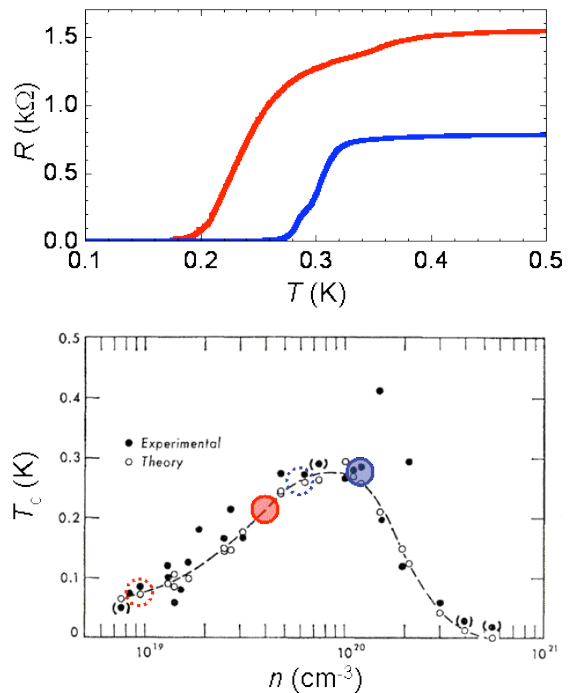


Figure 10: Top: resistance vs temperature of a 150 Å Nb-STO film for the two polarization states of the 500 Å PZT top layer. Bottom: the corresponding points on the phase diagram of doped SrTiO₃ (from [88]) are shown by the red and blue points. The carrier concentration is estimated using the Hall effect at 200 K. The dashed circles show the estimated T_c 's that one would expect for half the initial doping.

mal state, depending on the polarization orientation. Ultimately this technique will be applied to define normal state regions in a superconducting background (or the inverse) to create vortex pinning centres, SQUID's, Josephson junctions or other mesoscopic devices.

Working on the improvement of the Nb-STO and PZT thin film growth, a large PZT ferroelectric polarization of $20 \mu\text{C}/\text{cm}^2$ was obtained using 10 nm thick metallic Nb-STO, allowing an induced change in carrier concentration of up to $8 \cdot 10^{19} \text{ (cm}^{-3}\text{)}$. At room temperature, the carrier concentration and the resistivity are changing by a factor as large as 3.5 and 4.2 upon polarization reversal. The initial doping level of the Nb-STO films is 1 weight-% which is close to the optimal doping for superconductivity. This however explains why the T_c shift is not very important as observed on Fig. 10. Using a 0.5 weight-% doped thin film, and assuming an identical PZT polarization, much larger T_c shifts could be expected (about 200 mK), as illustrated by the dashed circles on Fig. 10 (bottom).

1.16 The $\text{LaAlO}_3/\text{SrTiO}_3$ system

At the interfaces between complex oxides, systems with unusual and novel electronic properties can be generated. The interest in the physics of such interfaces has been largely boosted by the 2004 discovery of Ohtomo and Hwang of metallic conduction at the interface between LaAlO_3 and TiO_2 terminated SrTiO_3 [89]. A possible explanation for this phenomenon is the so-called "polar catastrophe" scenario. This phenomenon is related to the polarity discontinuity at the interface between non-polar (001) SrTiO_3 planes and polar LaAlO_3 atomic planes. When these are stacked on top of each other, an electric potential develops and increases as the film thickness increases. Above a critical thickness, an electronic reconstruction may take place which could lead to a charge transfer at the interface (thus explaining the observed conductivity), creating a quasi two dimensional electron gas.

The group of Jochen Mannhart (University of Augsburg) has been actively working on these interfaces [90]. In collaboration with this group, Triscone's group studied the transport properties at very low temperatures (down to 25 mK) to reveal the ground state of this conducting interface.

The ground state of this electron gas turned out to be a superconducting condensate for samples grown in Augsburg as well as those

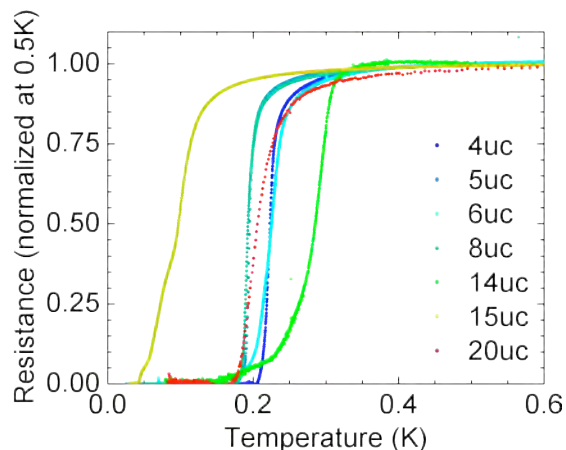


Figure 11: Resistance versus temperature for several $\text{SrTiO}_3/\text{LaAlO}_3$ samples with different LaAlO_3 thicknesses grown in Augsburg and Geneva revealing a transition to a superconducting state.

grown in Geneva. Thus, remarkably, the interface between these two insulating oxides is found to be superconducting! (Fig. 11) The superconducting transition temperature is about 200 mK and the observed characteristic superconducting properties reflect the two dimensional nature of this system. More specifically, the footprint was investigated of a Berezinskii-Kosterlitz-Thouless (BKT) transition expected in a 2D superconductor.

In the ideal BKT framework, one expects that the voltage versus current curves follow a power law behavior $V \sim I^a$, with the exponent a jumping from 1 to 3 at the BKT transition temperature. In a real system with a finite size the transition is smoothed. However, the transition temperature is, as in the infinite size case, defined by the relation $a(T_{BKT}) = 3$. Independently, the resistance versus temperature curve should follow a particular behavior: $R = R_0 \cdot \exp(-b(T/T_{BKT} - 1)^{1/2})$ close to T_{BKT} .

The resistance measurements are consistent with these expressions. Both of these predictions have been checked for an 8uc sample and give remarkably similar T_{BKT} values, close to 200 mK as can be seen on Fig. 12. More details can be found in reference [4]. The deviation from the ideal case has been checked to be due to the finite size of the current path.

2 Quantum matter

2.1 Density functional theory of (surface) melting in layered superconductors

The melting of the vortex lattice is one of the most striking aspects of the phenomenology of high-temperature superconductors. It is now

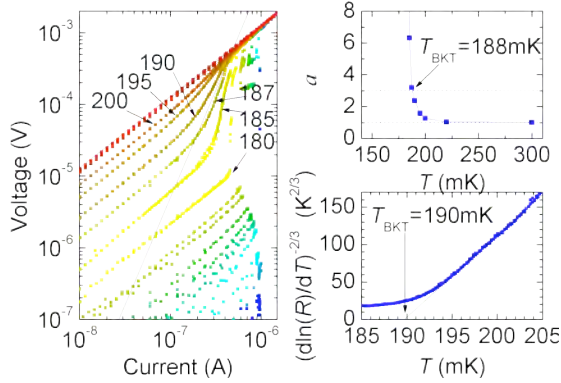


Figure 12: V - I characteristics, a versus T , and $(d \ln R/dT)^{-2/3}$ versus T , signatures of the 2D BKT superconducting transition.

both theoretically and experimentally established that enhanced thermal fluctuations render the Abrikosov flux-line lattice unstable to a vortex liquid over a large part of the B - T phase diagram in these materials [91]. Much interest has been devoted to the melting transition in extremely anisotropic materials such as $\text{Bi}_2\text{Sr}_2\text{CaCu}_2\text{O}_8$. The large value of the anisotropy in these materials motivates their modeling in terms of a one dimensional array of magnetically-coupled two-dimensional superconducting layers with no inter-layer Josephson coupling. Vortex lines are then described by linear arrangements (stacks) of pancake vortices, whose highly anisotropic interactions are mediated only by the magnetic field [92].

Blatter and collaborators [43] combine the methodology of a mean-field substrate model [93] with the classical density functional theory (DFT) of freezing [94]. A free-energy functional was derived in terms of a scalar order-parameter profile and used to derive a simple formula describing the temperature dependence of the melting field, (Fig. 13). The central quantity in the theory, the direct correlation function between pancake vortices, is described in a novel way exploiting the layered structure of the system: the strong and long-range in-plane correlations are obtained from Monte Carlo data, while the weak but long-range out-of-plane interaction is treated perturbatively. The latter then provides the mean-field substrate potential stabilizing the solid phase beyond the two-dimensional situation. The theoretical predictions are in good agreement with simulation data and largely improve on previous results obtained via purely analytical (e.g. hypernetted chain equations) closure schemes. The theoretical framework is thermodynamically consistent (in contrast to previous

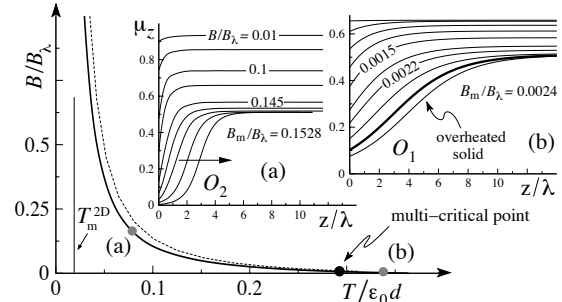


Figure 13: Comparison of the melting line $B_m(T)$ obtained via the DFT-substrate approach (present work, full line) with that of Dodgson et al. (dashed line). Top right: numerical solutions of the order-parameter profile μ_z for different fields B increasing from top to bottom: (a) at $T = 0.08 \epsilon_0 d$ (O_2 transition with the liquid-solid interface invading the bulk as $B \nearrow B_m$) and (b) at $T = 0.33 \epsilon_0 d$ (O_1 transition with the thick line corresponding to $B = B_m$).

work) and thus capable of describing the negative magnetization jump obtained in experiments.

The extension of this work to include the effect of an ab surface [44, 45] leads to the phenomenon of surface melting for which two distinct scenarios are known [95], a first-order type melting termed O_1 or surface-non-melting where the order parameter undergoes a jump to zero at the bulk melting temperature T_m , and a second-order type melting termed O_2 or surface-melting where the order parameter smoothly goes to zero at T_m (Fig. 13). Starting from the microscopic interaction between pancake vortices, the density functional theory in the mean-field substrate approach is used to derive a Landau-type theory describing surface melting. Both scenarios, O_1 and O_2 , turn out to be realized in the pancake vortex system of a layered superconductor, with the O_1 behavior realized at very low and high magnetic fields. In the most important intermediate field regime, the transition is continuous (O_2), in agreement with the asymmetric hysteresis observed in the experiment (absence of an overheated solid, see Ref. [96]). The two regimes (O_1 versus O_2) are separated via multicritical points.

2.2 Quantum instability in a dynamically asymmetric dc-SQUID

A classical system cannot escape out of a metastable state at zero temperature. However, a composite system made from both classical and quantum degrees of freedom may drag itself out of the metastable state by a sequential process. This sequence starts with the tun-

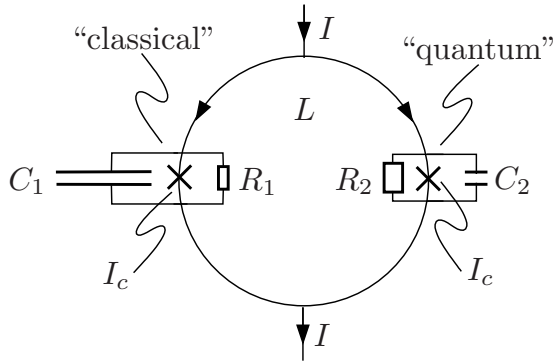


Figure 14: Schematics of the dynamically asymmetric dc-SQUID. Two Josephson-junctions are integrated in a current (I) biased superconducting loop with inductance L . The two junctions have equal critical current I_c , but strongly asymmetric (shunt) capacitance C_j and (shunt) normal resistance R_j ; the parameters are chosen such that junction 1 behaves classically, whereas junction 2 is subject to quantum effects.

neling of the quantum component which then triggers a distortion of the trapping potential holding the classical part; provided this distortion is large enough to turn the metastable state into an unstable one, the classical component can escape (the ‘Münchhausen effect’).

A device where this physics can be implemented and observed experimentally is the dynamically asymmetric dc-SQUID (Superconducting Quantum Interference Device), see Fig. 14, where the capacitances play the role of effective masses, the kinetic energy of junction j is $\mathcal{T}_j = (\hbar/2e)^2 C_j \dot{\phi}_j^2 / 2$ with $\dot{\phi}_j$ the time derivative of the relative phases of the superconducting order parameter across the two junctions.

The coupling of the two junctions via the loop inductance L produces the interaction energy, whereas the external driving current I couples to the absolute coordinate. Small junctions exhibiting quantum behavior in the form of quantum tunnelling [97, 98] and even quantum coherence [99, 100] can be routinely fabricated today.

The result of the theoretical analysis is conveniently expressed in a dynamical phase diagram involving the inductive coupling L between the junctions and the bias current I through the SQUID loop (Fig. 15). A small inductance L strongly couples the ‘light’ and ‘heavy’ junctions and the transport through the SQUID turns dissipative close to the maximal critical current $2I_c$. On the other hand, a large inductance L in a large loop allows the ‘light’ junction to decay violently and a large number of flux quanta enter the loop, redirect-

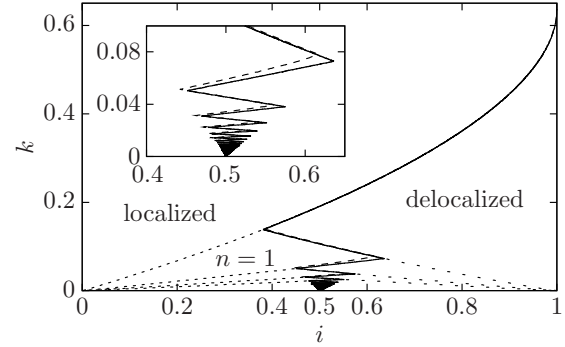


Figure 15: Phase diagram of the dynamically asymmetric dc-SQUID as a function of bias current $i = I/2I_c$ and inductive coupling $k = \Phi_0 c / 2\pi L I_c$ with both junctions overdamped. The critical current $i_c(k)$ (solid line) marks the boundary between a localized classical junction ($i < i_c$) and a delocalized classical junction ($i > i_c$), which corresponds to a finite voltage state of the SQUID; branches with negative slope (dashed lines) are triggered by a classical pathway, while those with positive slope (dotted lines) are determined by the quantum instability of the light junction. The inset shows a comparison between the approximate analytical result (solid line) and the exact numerical result (dashed).

ing the current over the classical ‘heavy’ junction — as a consequence, the maximal current transported across the SQUID loop is limited to I_c , half the critical current expected in a classical setting. The complex zig-zag boundary in the I - L diagram separating the dissipation-free- (localized) from the finite voltage (delocalized) regime is the consequence of a delicate competition between the stepwise increase in flux-quanta entering the loop with increasing inductance L , while the concomitant decrease in coupling $\propto 1/L$ reduces the ability of the flux quanta in redirecting the current.

For a classical junction with massive dynamics, the kinetic energy has to be accounted for in the decay process and the transition line in Fig. 15 is shifted towards smaller currents. Replacing the quantum junction by an underdamped junction as well (as is relevant in experiments attempting to observe this effect), effects of quantum coherence and avoided level crossings have been accounted for in this model [46]. Experiments with typical parameters as chosen for superconducting flux qubits and with a dynamical anisotropy of order 300 in the capacitances are under way.

2.3 STS study of vortices in KO_2O_6 and RbO_2O_6

Fischer and collaborators have mapped the vortices for different applied fields on KO_2O_6

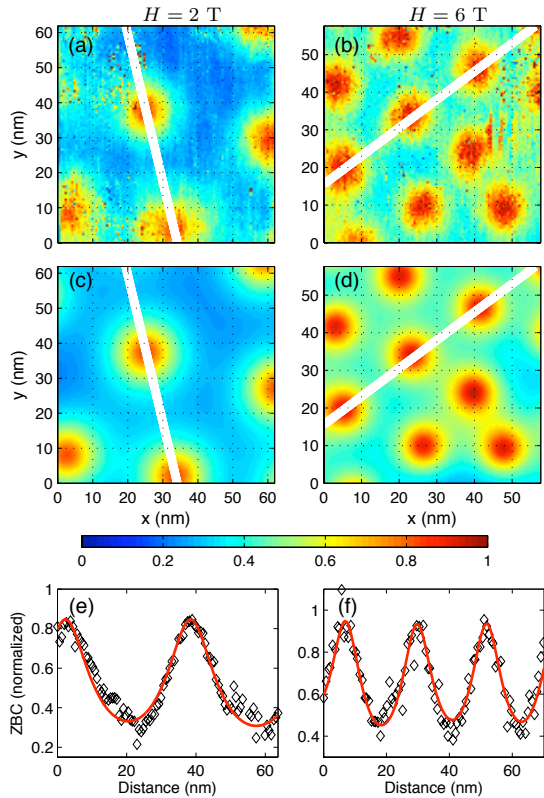


Figure 16: Vortices mapped by STS through ZBC maps on KOs_2O_6 . (a), (b) Experimental ZBC maps for 2 and 6 T respectively with corresponding fits (c), (d); large values (red) correspond to normal regions (i.e. vortex cores) and low values (blue) to superconducting (gapped) regions. (e), (f) Experimental ZBC profiles across vortex centers together with the corresponding profiles from the 2D fits (red lines).

and demonstrated that they are arranged in an hexagonal lattice with spacings consistent with those of an Abrikosov vortex lattice. The outstanding agreement between the experimental and theoretical Zero Bias Conductance (ZBC) maps (Fig. 16) allowed to extract the coherence length ξ of 31–40 Å showing a slight field-dependence. This value, obtained through a microscopic probe, confirms previous thermodynamic estimates. The absence of a zero bias conductance peak, the apparent field dependence of ξ and the precise radial dependence of the LDOS all call for deeper exploration. Another member of the β -pyrochlore family, $RbOs_2O_6$, has a slightly lower T_c and a significantly smaller upper critical field [82]. STM measurements revealed gapped spectra, with well-developed coherence peaks and a flat background at high energies (inset of Fig. 17). Spectra taken at different temperatures show that the gap closes progressively (Fig. 17), but remains measurable above the bulk T_c (5.5 K for this sample) and only completely disap-

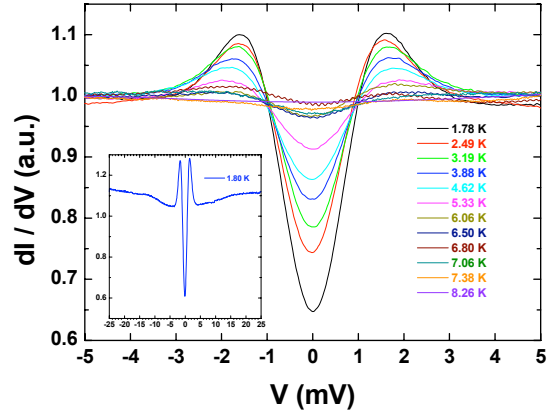


Figure 17: Tunnelling Spectra of $RbOs_2O_6$ taken at temperatures from 1.78 K to 8.26 K. Inset: spectrum at 1.80 K.

pears at about 7.5 K.

2.4 Effects of oxygen doping on $Bi_2Sr_2Ca_2Cu_3O_{10+\delta}$ vortex matter

Understanding the extremely-anisotropic electronic and magnetic properties of layered cuprates requires to unveil the nature of the coupling mechanisms between the superconducting Cu-O planes [91, 101]. Fischer *et al.* studied the effect of oxygen doping on the critical temperature T_c , the vortex matter phase diagram and the nature of the coupling between Cu-O planes in the three-layered $Bi_2Sr_2Ca_2Cu_3O_{10+\delta}$ (Bi-2223) compound [47, 48].

Contrary to previous reports [102, 103], in the overdoped regime, T_c varies with the annealing pressure, though less significant than in the bi-layer parental compound $Bi_2Sr_2CaCu_2O_{10+\delta}$ (Bi-2212). As shown in the insert of Fig. 18, magnetic measurements reveal that increasing oxygen concentration produces a reduction of the liquid vortex region. The second-peak field H_{SP} associated with the order-disorder transition between the quasi-crystalline Bragg glass and the disordered vortex glass also increases with oxygen concentration. These findings imply that the interlayer coupling (anisotropy) between Cu-O planes monotonously increases (decreases) with δ . The main panel of Fig. 18 shows that the anisotropy parameter varies between 50 ($T_c/T_c^{\max} \sim 0.9$) and 15 ($T_c/T_c^{\max} \sim 0.96$) when increasing oxygen concentration ($s = 18$ Å). These data were obtained from in and out-of-plane first-penetration field measurements. On the contrary, the in-plane penetration depth λ_{ab} presents a boomerang-like behavior with δ , having a minimum

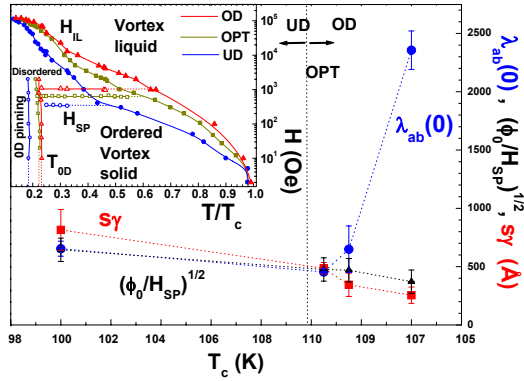


Figure 18: London penetration depth $\lambda_{ab}(0)$, $\sqrt{\Phi_0/H_{SP}}$ and anisotropy times the interlayer spacing, $s\gamma$, as a function of T_c for the underdoped (UD), optimally-doped (OPT) and overdoped (OD) regimes of $\text{Bi}_2\text{Sr}_2\text{Ca}_2\text{Cu}_3\text{O}_{10}$. Insert: vortex phase diagram for the same sample in UD (\circ symbols), OPT (\square symbols) and extremely OD (\triangle symbols) regimes. The irreversibility, $H_{IL}(T)$ (full symbols), second peak $H_{SP}(T)$ (open symbols) and zero-dimensional pinning T_{0D} (gray-filled symbols) lines are shown.

value close to optimal doping. In spite of Bi-2223 being roughly three times less anisotropic than Bi-2212, these effects lead to a crossover from a Josephson(overdoped)- to an electromagnetic(underdoped)-dominating interlayer coupling in the vicinity of optimal doping.

2.5 Competition between high T_c superconductivity and ferromagnetism in $\text{YBa}_2\text{Cu}_3\text{O}_y/\text{SrRuO}_3$ multilayers

The LE- μ SR technique [49] was applied to explore on the depth-resolved scale (of nanometers) the magnetic properties of superconducting YBCO layers that are part of a superconductor/ferromagnet ($\text{YBa}_2\text{Cu}_3\text{O}_y/\text{SrRuO}_3$) superlattice.

As shown in Fig. 19 well defined sidebands below T_{Curie} highlight that the ferromagnetic phase transition in the SrRuO₃ (SRO) layers gives rise to induced magnetic moments within the $\text{YBa}_2\text{Cu}_3\text{O}_y$ (YBCO) layer that have a fairly well defined spatial order. Similar phenomena have been observed experimentally in classical Fe/Ag/Fe and Fe/Pb/Fe multilayers and corresponding superconductor/ferromagnet multilayers with conventional superconductors and ferromagnets [104][50, 51]. However, while in the latter systems the spin-density-wave propagates along the direction perpendicular to the film plane, the analyses of Morenzoni and Bernhard seems to imply that in the YBCO/SRO superlattice the spin-density

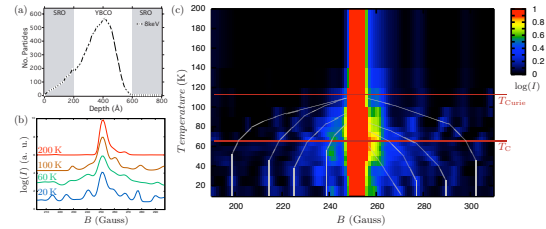


Figure 19: (a) Depth of the muon implantation with 8 keV muon energy. (b) Magnetic field distribution as seen by the muons at different temperatures. (c) Temperature dependent magnetic field distribution as seen by the muons. Note the peaks on both sides of the applied magnetic field $B_{ext} = 252$ G whose evolution is indicated by the gray lines.

wave is oriented along the CuO_2 planes.

2.6 Neutron reflectometry of $\text{YBa}_2\text{Cu}_3\text{O}_7/\text{La}_{2/3}\text{Ca}_{1/3}\text{MnO}_3$ superlattices

Superlattices consisting of individual layers (of equal thickness of 10 nm) of the high-temperature superconductor $\text{YBa}_2\text{Cu}_3\text{O}_7$ ferromagnet $\text{La}_{2/3}\text{Ca}_{1/3}\text{MnO}_3$ (LCMO) exhibit a wealth of interesting phenomena related to the competition between ferromagnetism and superconductivity. For example, a ferromagnetic (FM) moment is induced within the superconducting (SC) YBCO layers that is antiparallel to the one of the LCMO layers [52, 53].

Recently Bernhard and Morenzoni observed a superconductivity induced modulation of the ferromagnetic moment along the vertical direction in similar multilayers with strongly underdoped $\text{Y}_{0.6}\text{Pr}_{0.4}\text{Ba}_2\text{Cu}_3\text{O}_7$ ($\text{Y}_{0.6}\text{Pr}_{0.4}\text{BCO}$) layers. In particular a peak appears at the position of the 0.5th Bragg peak in the reflectivity curve right below the superconducting transition temperature of the $\text{Y}_{0.6}$ ($T_c = 40$ K). The data indicate that the magnitude of the FM moment in the LCMO layers becomes modulated along the vertical direction with a periodicity of twice the one of the bilayers when the $\text{Y}_{0.6}\text{Pr}_{0.4}\text{BCO}$ layers enter the superconducting state.

2.7 Superconductivity and magnetism in $\text{YBa}_2\text{Cu}_3\text{O}_7/\text{PrBa}_2\text{Cu}_3\text{O}_7$ multi-layers

The critical temperature of superlattices composed of one unit cell thick layers $\text{YBa}_2\text{Cu}_3\text{O}_7$ (YBCO) separated by $\text{PrBa}_2\text{Cu}_3\text{O}_7$ (PBCO) layers of variable thickness has been found to decrease continuously as the PBCO thickness is increased, indicating that coupling persists

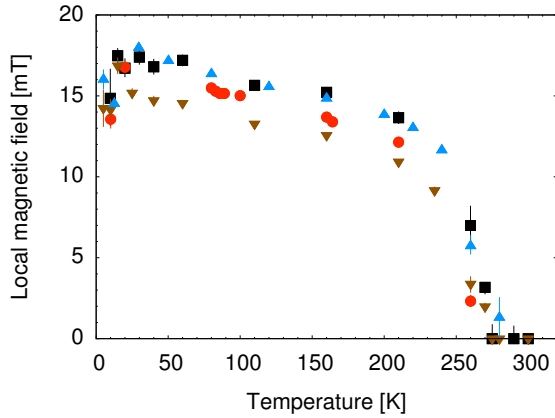


Figure 20: Internal magnetic fields measured by Zero Field- μ SR in a bulk powder sample (blue triangles), a single PBCO layer (black squares), inside a PBCO layer in a tri-layer (red circles) and in a bi-layer (brown nablas).

over distances of approximately 10 nm [105]. Spin polarized low energy muons were used to investigate the local superconducting and magnetic properties of c -axis oriented YBCO/PBCO/YBCO tri-layers, YBCO/PBCO bi-layers and single layer films. The magnetic properties of the PBCO layers have been investigated by zero field μ SR. Fig. 20 shows the local magnetization for a single layer with a thickness of 50 nm, as part of the YBCO(75nm)/PBCO(75nm) bi-layer and embedded in two YBCO layers in a YBCO(75nm)/PBCO(50nm)/YBCO(75nm) structure. The energy of the muons has been chosen so that they stop in the center of the particular PBCO layers. In all investigated single layer and multi-layer film structures the antiferromagnetic ordering is similar to bulk samples, as shown from the evolution of the internal field and the muon depolarization rate with temperature.

When a magnetic field is applied parallel to the ab -planes of a YBCO/PBCO/YBCO trilayer, a sizeable fraction of the PBCO buffer layer displays a diamagnetic shift characteristic of the superconducting state. This fraction coexists with an antiferromagnetic fraction exhibiting the same ordering as described above for the zero field experiment. A typical depth profile of the diamagnetically shifted field component is depicted in Fig 21 at a temperature below the critical temperature of YBCO. In the trilayer film the monotonic decrease of the screened field in the top superconducting layer and the large shift in PBCO imply that unexpected large dissipation free supercurrents are flowing through a 50 nm AF barrier to the bottom YBCO layer, which sustains the return flow. By

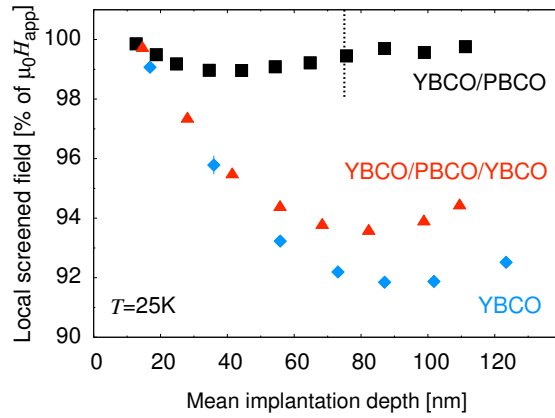


Figure 21: Depth dependence of the local screened magnetic field in the bi-layer (black squares) and tri-layer (red triangles) samples at $T = 25$ K in the Meissner state. The dotted line indicates the top YBCO/PBCO interface. For comparison the depth profile of a 200 nm thick single layer of YBCO is also shown (blue diamonds).

applying a magnetic field perpendicular to the film the field distribution becomes characteristic for a rigid vortex state in the top and bottom superconducting layer, reflecting the vortex supercurrents flowing in the ab -planes. These results present the signature of a large proximity effect between two compounds with different electronic ground state, not expected on the base of conventional proximity theory.

3 Microscopic properties of the cuprates

3.1 Modelling the asymmetric tunnelling spectra in Bi-based cuprates

This program aims to unveil clues on the microscopic mechanisms of superconductivity from modelling STM spectra of high- T_c cuprates [54, 12]. Previous works [54] [106, 107, 108] have focused on the particularities of the dip-hump structure observed in Bi-based compounds. The present study follows this program by modelling the spectra measured on $\text{Bi}_2\text{Sr}_2\text{CaCu}_2\text{O}_8$ (Bi-2212) and $\text{Bi}_2\text{Sr}_2\text{Ca}_2\text{Cu}_3\text{O}_{10}$ (Bi-2223) single crystals.

The group of Fischer measured nanometer-size maps of dI/dV spectra and sort them by their peak-to-peak energy-separation. The spectra with smaller (larger) Δ_p are associated to an overdoped (underdoped) local doping level. As an example, Fig. 22 shows optimally-doped (OPT) Bi-2223 and underdoped (UD) Bi-2212 spectra. Spectra of both materials present an asymmetric background (becoming more pronounced in the UD regime), a significant asymmetry in the height of the coherence peaks and a strongly developed dip-hump feature.

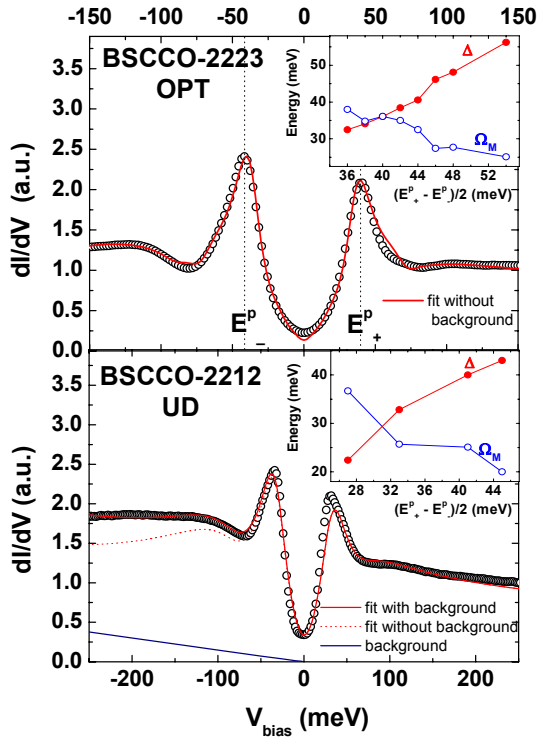


Figure 22: *Top panel:* average spectrum of optimally-doped $\text{Bi}_2\text{Sr}_2\text{Ca}_2\text{Cu}_3\text{O}_{10}$ fitted without the asymmetric background term. *Bottom panel:* average spectrum of under-doped $\text{Bi}_2\text{Sr}_2\text{CaCu}_2\text{O}_8$ fitted considering an asymmetric background term. The background contribution is depicted in blue. *Inserts:* evolution of the superconducting gap, Δ , and the collective mode energy, Ω_M , with the peak-to-peak gap Δ_p for $\text{Bi}_2\text{Sr}_2\text{Ca}_2\text{Cu}_3\text{O}_{10}$ (top) and $\text{Bi}_2\text{Sr}_2\text{CaCu}_2\text{O}_8$ (bottom).

Using the strong-coupling model introduced in Ref. [108], which takes into account the d -wave BCS pairing, the two-dimensional band structure of the Cu-O planes and an interaction of the quasiparticles with the (π, π) spin resonance observed in neutron-scattering experiments [109, 110, 111], excellent were obtained of the STM spectra in both Bi-2212 [54] and Bi-2223 [12] in the optimally- and over-doped regimes (top panel of Fig. 22).

However, the model does not properly fit the UD spectra where the asymmetry is more pronounced (bottom panel of Fig. 22). Therefore an asymmetric slowly-varying background was introduced, associated to the incoherent part of the spectral function as suggested by a slave-boson theory [112]. This resulted in excellent fits of the UD spectra as well, and allowed to follow the trend of the microscopic parameters also in the UD regime (bottom panel of Fig. 22). The trends are in agreement with measurements done by other non-local

techniques ([113][55]). In particular, the energy of the collective mode decreases as a function of increasing Δ_p (inset of the figure).

Therefore robust evidence was obtained that the dip-hump feature in the electron excitation spectra of high- T_c superconductors is due to a collective bosonic mode like the (π, π) spin resonance. Whether this collective mode is at the origin of the superconducting pairing deserves further studies.

3.2 Scanning Tunneling Spectroscopy on $\text{YBa}_2\text{Cu}_3\text{O}_{7-x}$

Unlike the Bi-based cuprate family, $\text{YBa}_2\text{Cu}_3\text{O}_{7-x}$ (Y123) does not offer natural cleaving planes, making surface measurements quite challenging. Up to now, the best scanning tunneling spectroscopic measurements were obtained on optimally-doped single crystals, along the (001) crystallographic direction. Measurements were done on the (100) or (010) facets of a thick optimally-doped single crystal *in situ* fractured. Two kinds of spectra have been measured, both spatially reproducible over tens of nanometers: superconducting-like spectra showing mostly small gaps of the order of 10 meV, and spectra with a sharp zero-bias conductance peak (ZBCP). All spectra can be fitted using a d -wave based Blonder, Tinkham and Klapwijk (BTK) model [114] mixing tunneling into the (001), (100) and (110) directions. For the spectra with a ZBCP the superconducting gap is of the order of 20 meV, similar to the one detected in (001) tunneling. The topography roughness by STM is consistent with the possibility to inject charge carriers into the (110) direction while position the tip perpendicularly to a (100) or (010) crystal edge.

While a lot of studies have been reported on the doping dependence of the spectra in the Bi-based cuprates, very few measurements have been successfully performed on Y123 with non-optimal doping. The Fischer group has carried out the first STS studies on a Y123 single crystal presenting a very broad superconducting transition ($> 40\text{K}$). Contrary to measurements done on homogenous samples, the measurements reveal here spectra with a large distribution of gaps. Fig. 23 show spectra acquired at different locations, and ordered by decreasing gap amplitude. As the gaps increase (from 20 meV to more than 50 meV) the height of the gap-edge peaks (coherence peaks) decrease, similarly to what is observed for Bi-based cuprates. Spectra showing the largest gaps have almost no coherence peaks, and re-

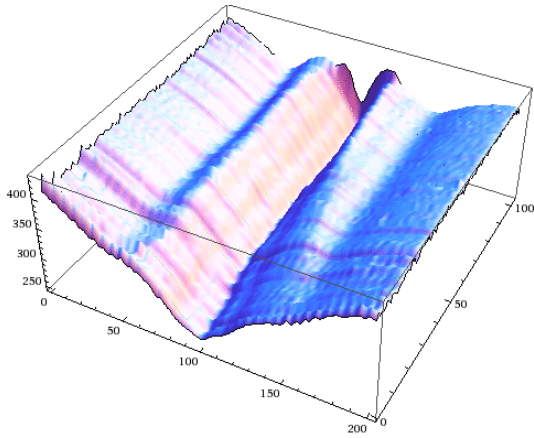


Figure 23: STM spectra of $\text{YBa}_2\text{Cu}_3\text{O}_7$ at different locations, and ordered by decreasing gap amplitude.

flect a possible pseudo-gap state like in BSSCO. A temperature dependence of these spectra is under study, and may confirm these assumptions.

3.3 $\text{La}_{2-x}\text{Sr}_x\text{CuO}_4$ and $\text{YBa}_2\text{Cu}_4\text{O}_8$

The existence of an extended pseudogap phase in both $\text{La}_{2-x}\text{Sr}_x\text{CuO}_4$ (LSCO) and $\text{YBa}_2\text{Cu}_4\text{O}_8$ (Y124) compounds has been claimed from magnetic and transport bulk measurements [115]. However, the local electron spectroscopic properties of this pseudogap phase have not been thoroughly explored [56]. For optimally-doped $\text{La}_{1.85}\text{Sr}_{0.15}\text{CuO}_4$ ($T_c = 38$ K, *in situ* fractured in UHV), and $\text{YBa}_2\text{Cu}_4\text{O}_8$, spectra were acquired in two regimes: high (true tunneling) and low (pseudo point-contact) tunneling resistance regimes. In the true tunneling regime, spectra are gapped-like with a finite zero-bias conductance and faint gap-edge peaks. In the pseudo point-contact regime, spectra reveal sharp zero-bias conductance peaks, consistent with theoretical predictions of electrons injected in the nodal in-plane directions. For the two compounds, fits of conductance curves using a BTK-like model assuming a *d*-wave density of states [114] give the same superconducting gap in both regimes: $\Delta = (7 \pm 1.5)$ meV for LSCO, and $\Delta = (14 \pm 2)$ meV for Y124 [57]. The ratio $2\Delta/k_B T_c$ is 4.3 for LSCO, and 4.1 for Y124, within the *d*-wave BCS value but in contrast with results obtained for cuprates with an extended pseudogap phase such the BiSrCaCuO family [56].

The first temperature dependence of the tunneling spectra were also performed (Fig. 24). For both compounds, the low-bias conductance dip progressively vanishes with temperature, and no gap is measured at T_c . The

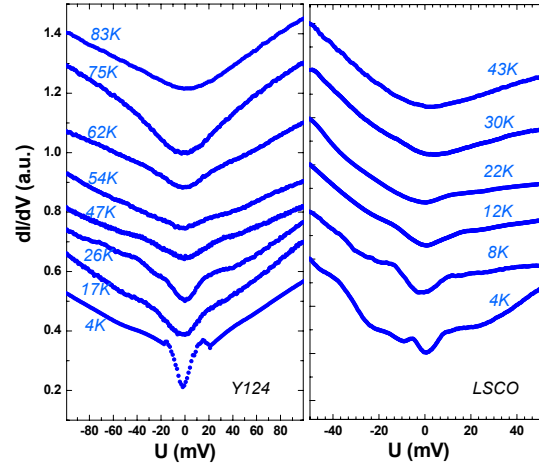


Figure 24: Temperature evolution of the tunneling spectra for Y124 (left panel) and LSCO (right panel). T_c is 78K for Y124, and 38K for LSCO.

tunneling-detected pseudogap phase is therefore restrained to a region close to T_c . For LSCO, this $T^* \approx T_c = 38$ K is 3–5 times smaller than values reported from various bulk techniques [115]. For Y124, $T^* \approx T_c = 78$ K, in contrast with nuclear magnetic resonance and transport measurements which report a $T^* \sim 180 - 240$ K.

These results stress the need to clarify the differences between the pseudogap phases detected by charge and spin sensitive techniques. However, surface effects cannot be completely ruled out: the gap values provided from the measurements are compatible with a slightly overdoped and pseudogap-less surface.

3.4 Local correlations between the superconducting gap size and the superstructure in $\text{Bi}_2\text{Sr}_2\text{Ca}_2\text{Cu}_3\text{O}_{10+\delta}$

The interplay of inhomogeneities and superconductivity in high-temperature superconductors is an highly debated subject. For example, the well-known structural modulation in BiSrCaCuO compounds and its influence on superconducting properties is currently unclear. This modulation has a period of nearly 5 unit cells [58]. All metal atoms are modulated parallel to the *c*-axis. In addition, both the bismuth and strontium atoms also vary from their ideal rocksalt positions in the *a*-*b* plane [116]. In Fig. 25A scanning tunneling spectroscopy (STS) measurements are represented on $\text{Bi}_2\text{Sr}_2\text{Ca}_2\text{Cu}_3\text{O}_{10+\delta}$ (Bi-2223), which reveal a modulation of the superconducting gap magnitude, Δ , in correlation with the structural modulation.

The dI/dV spectrum shown in Fig. 25B is an

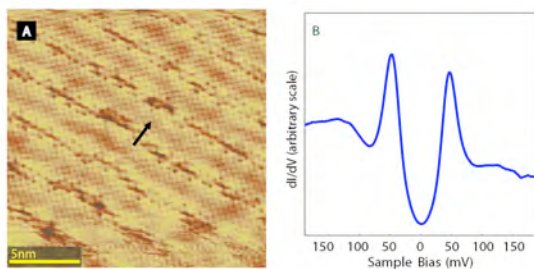


Figure 25: (A) Typical topography of the $\text{Bi}_2\text{Sr}_2\text{Ca}_2\text{Cu}_3\text{O}_{10+\delta}$ sample ($U = 0.4 \text{ V}$, $I = 0.2 \text{ nA}$). The supermodulation is 45° from the Bi sublattice (black arrow). (B) Normalized average dI/dV spectrum over a 30 nm square region. The average gap value is 48 meV .

average of thousands of spectra acquired over a $30 \times 30 \text{ nm}^2$ surface. It shows all of the typical features of an underdoped Bi-2223 surface: large gap, asymmetry of the peak height and background.

Studying the variation of the superconducting gap on the atomic scale shows a striking relation between the size of the gap and the position relative to the superstructure. Fig. 26B is an image of the local superconducting gap magnitude in each spectrum of a 255×255 pixel low-temperature spectroscopic map. Bright areas indicate regions with a large Δ . Fig. 26A is the simultaneously acquired topography. Dark areas indicate regions with lower apparent height. The bright lines running diagonally downwards in the gapmap correspond to the dark lines running in the same direction in the topography. Fig. 26C is the cross-correlation of the gapmap and topography.

To quantify the magnitude of the gap variation, all gap values lying at a given distance from the superstructure were averaged and then plotted in Fig. 27 (blue line). The green line shows a similar averaging of the topography. The gap value varies sinusoidally by roughly 8–10 per-

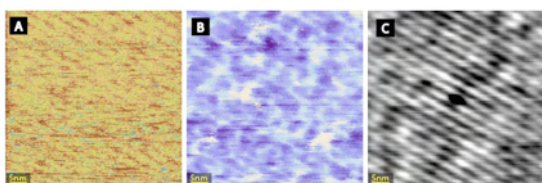


Figure 26: (A) 255×255 pixel topographic map acquired on a Bi-2223 single-crystal at low temperature. (B) 255×255 pixel image of the local gap magnitude over the area seen in (A). Bright areas indicate regions of large gap. (C) Cross-correlation of (A) and (B) shows that the gapmap and topography are anticorrelated.

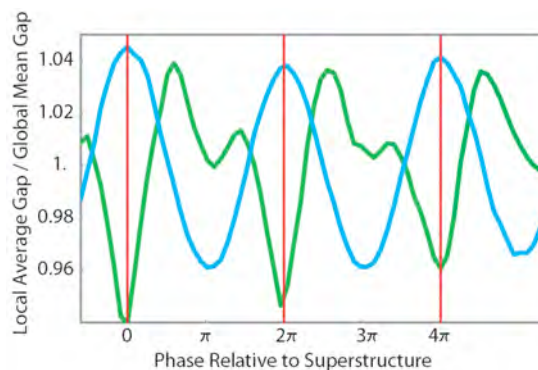


Figure 27: Average value of the superconducting gap (blue line) and topography (green line) as a function of distance from the superstructure (phase offset from the minimum of the superstructure). The topography units are not shown.

cent from its mean value, being maximal at the minimum of the superstructure.

3.5 Isotope shift of the STM of cuprate superconductors

The recent series of scanning tunneling microscopy (STM) experiments on cuprate superconductors by the Davis group has received a lot of attention. The STM spectra they obtained cover large surface areas, show strong variations on an atomic scale and yield spectacular pictures [117]. However, there has been relatively little theory of the physics underlying these pictures and their interpretation. The group of Rice has investigated three issues raised by these STM spectra.

First, the spectra showed structures consistent with an O-phonon sideband. In conventional superconductors such phonon structure in tunneling spectra can be nicely explained within BCS-Eliashberg theory and is the most direct confirmation of this microscopic theory. In the present case Pilgram and collaborators [59] proposed an alternative explanation arising from inelastic tunneling processes as electrons tunnel through the insulating barrier between the STM tip and the conducting CuO_2 -planes (Fig. 28).

Second, a prominent feature of the spectra in underdoped cuprates is a modulated pattern when the STM tip is above O-sites in the CuO_2 -plane with enhanced and reduced signal strengths on opposite O-pairs in a $(\text{CuO})_4$ -plane (Fig. 29). This pattern was interpreted as evidence for a strong charge modulation on O-sites in the CuO_2 -planes. Chen *et al.* [60] showed that interference effects occur exactly when the tip is in this position, which depend on the relative phase for tunneling processes

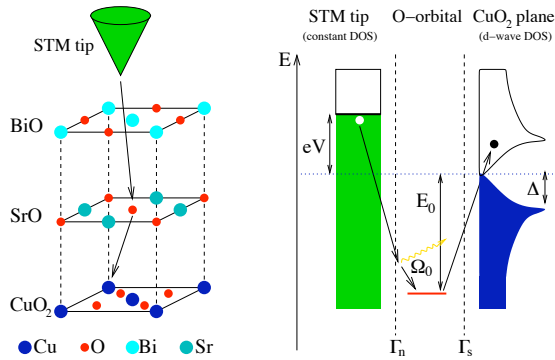


Figure 28: Left panel: geometry relevant for the STM experiment with the superconducting CuO_2 plane lying below BiO and SrO layers. Right panel: proposed inelastic cotunneling process via the apical oxygen atom which leads to phonon satellites in the current-voltage characteristics in the electron-energy scheme.

through the apical O-ions lying above the two Cu-neighbors of a planar O-ion. Further they found a similar interference pattern generated by hole states localized around the dopant acceptors. These calculations demonstrate that the STM patterns do not simply measure local density variations but contain phase information about the underlying many-body wavefunction of the holes doped into the CuO_2 -planes.

Lastly the tunneling spectra on superconducting BiSrCaCuO cuprates showed a simultaneous modulation of the superconducting gap and the phonon feature in phase with the known structural superlattice in the BiO layers of these compounds. At first this was claimed

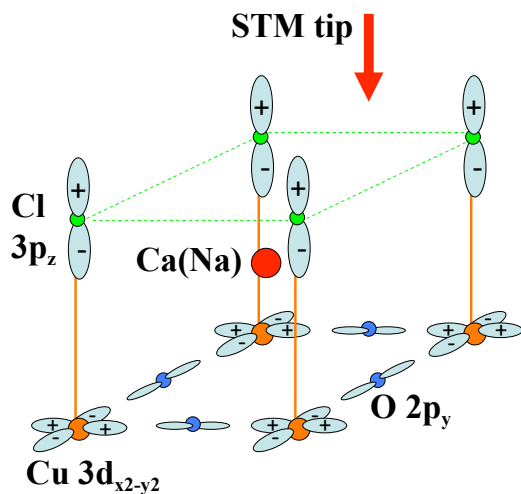


Figure 29: Schematic crystal structure of $\text{Ca}_{2-x}\text{Na}_x\text{CuO}_2\text{Cl}_2$ around a Ca^{2+} ion or a doped Na^+ ion. The sign represents the phase of the Cu- and Cl-orbital wavefunction.

to be evidence that exchange of this phonon was a key component in the microscopic origin of the superconductivity. However Yang *et al.* [61] demonstrated that both modulations directly follow from the structural displacements induced in the CuO_2 -planes within the strong correlation t - J -model and do not imply a causal relation between the superconducting gap and the phonon.

3.6 Variational wavefunction approach to the Hubbard model in two dimensions

The Hubbard model plays a key role in the analysis of correlated electron systems, and it is widely used for describing quantum antiferromagnetism, the Mott metal-insulator transition and, ever since Anderson's suggestion [118], also for describing superconductivity in the layered cuprates. While the one-dimensional case can be treated exactly, approximate techniques have been developed to determine the various phases of the two-dimensional Hubbard model. For very weak coupling, the perturbative Renormalization Group has allowed to extract the dominant instabilities in an unbiased way, namely antiferromagnetism at half filling and d -wave superconductivity for moderate doping [62]. Quantum Monte Carlo simulations have been successful in extracting the antiferromagnetic correlations at half filling, but in the presence of holes the numerical procedure is plagued by the fermionic minus sign problem. This problem appears to be less severe in dynamic cluster Monte Carlo simulations, which exhibit a clear tendency towards d -wave superconductivity for intermediate values of U [119].

Variational techniques address directly the ground state and thus offer an alternative to quantum Monte Carlo simulations, which are limited to relatively high temperatures. Previous variational wave functions include mean-field trial states from which configurations with doubly occupied sites are either completely eliminated (full Gutzwiller projection) [120, 121, 122] or at least partially suppressed [123]. Recently, more sophisticated wave functions have been proposed, which include, besides the Gutzwiller projector, non-local operators related to charge and spin densities [124, 125]. Eichenberger and Baeriswyl's variational wave function [5, 6] is based on the idea that for intermediate values of U the best ground state is a compromise between the conflicting requirements of low potential energy (small double occupancy) and low kinetic energy (delocalization). It is known that the ad-

dition of an operator involving the kinetic energy yields an order of magnitude improvement of the ground state energy with respect to a wave function with a Gutzwiller projector alone [126, 127].

In its most simple form, the 2D Hubbard model is composed of two terms, $\hat{H} = t\hat{T} + U\hat{D}$, with

$$\hat{T} = - \sum_{\langle i,j \rangle, \sigma} (c_{i\sigma}^\dagger c_{j\sigma} + c_{j\sigma}^\dagger c_{i\sigma}) \quad (1)$$

$$\hat{D} = \sum_i n_{i\uparrow} n_{i\downarrow} \quad (2)$$

Here $c_{i\sigma}^\dagger$ creates an electron at site i with spin σ , the summation is restricted to nearest-neighbour sites and $n_{i\sigma} = c_{i\sigma}^\dagger c_{i\sigma}$. Beariswyl and collaborators considered a square lattice with periodic-antiperiodic boundary conditions and choose U to be equal to the bandwidth, $U = 8t$. The ansatz

$$|\Psi\rangle = e^{-h\hat{T}} e^{-g\hat{D}} |\Psi_0\rangle \quad (3)$$

is linked to a mean-field ground state $|\Psi_0\rangle$ with either a (d -wave) superconducting or an antiferromagnetic order parameter. The operator $e^{-g\hat{D}}$ partially suppresses double occupancy for $g > 0$, while $e^{-h\hat{T}}$ promotes both hole motion and kinetic exchange (close to half filling). In the limit $h \rightarrow 0$ the Gutzwiller ansatz is recovered [123]. For $g \rightarrow \infty$ and $h \ll 1$ the present variational problem is equivalent to that of the t - J Hamiltonian with respect to a fully Gutzwiller-projected mean-field state. The calculations for $h > 0$ are carried out in momentum space where the operator \hat{D} is not diagonal. Therefore a discrete Hubbard-Stratonovich transformation is applied to decouple the terms $n_{i\uparrow} n_{i\downarrow}$ in the operator $e^{-g\hat{D}}$ by introducing an Ising spin at each site. Expectation values are obtained using a Monte Carlo simulation with respect to the Ising spin configurations.

For an average site occupation $n = 1$ (half-filling) the ground state is expected to exhibit long-range antiferromagnetic order. A mean-field reference state $|\Psi_0\rangle$ is therefore chosen with a finite staggered order parameter. There is indeed an energy minimum for a finite staggered magnetization. The order parameter is reduced with respect to both the unrestricted Hartree-Fock approximation and the Gutzwiller ansatz, although it is still larger than the value expected in the large U limit (the Heisenberg model).

Away from half filling a BCS wave function is used with d -wave symmetry as mean-field reference state, characterized by a gap parame-

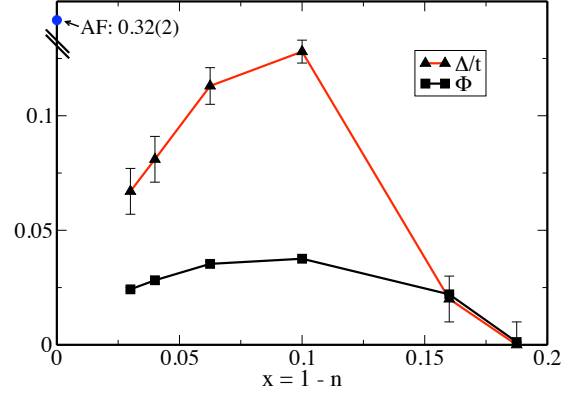


Figure 30: Gap (triangles) and order parameter (squares) as functions of the doping for $U = 8t$ and an 8×8 lattice.

ter Δ describing pairing and a “chemical potential” μ fixing the average electron density n . For such a “grand canonical” trial state the problems with the fermionic minus sign, which show up strongly for a fixed particle number, are greatly reduced and allow to obtain reliable results for both rather large system sizes and a realistic value of the interaction parameter ($U = 8t$).

The minimization of the energy with respect to the variational parameters Δ , g , h for a given average density is very time consuming. The initial results [6] for $n \approx 0.8$ were not conclusive, but the more recent results [63] clearly exhibit both a finite gap parameter Δ and a finite superconducting order parameter Φ for $0.8 < n < 0.95$, as shown in Fig. 30.

For some densities three different lattice sizes were studied (6×6 , 8×8 and 10×10). The results do not change much between the larger lattice sizes, at least for densities where Δ is not too small.

The “kinetic” and potential energies were also calculated separately (see section 3.7 for the experimental data). Quite generally the condensation energy is found to be to a large extent due to a decrease in kinetic energy and to a much lesser extent to a decrease in potential energy.

The Fermi surface determined by ARPES data for hole-doped cuprates suggests that the restriction to nearest-neighbor hopping in Eq. (1) is not adequate and that next-nearest-neighbor hopping (parameter t') cannot be neglected. It is straightforward to include such a term in this variational procedure. The first results for $t' = -0.3t$ indicate that d -wave superconductivity remains stable and even persists up to higher doping ($n_c \approx 0.75$) than for the simple Hubbard model.

3.7 Optical spectral weight and free carrier kinetic energy in high T_c cuprates

Many-body electronic correlations play a dominant role in the physics of cuprate materials. The main optical feature associated with the free charge carriers (electrons or holes) of a metallic system is the zero-frequency mode, which for non-interacting electrons becomes a Lorentzian centered at zero frequency, the width of which is due to impurity scattering. Electrons in a solid have in general a more complex lineshape due to the interactions, which can be formally decomposed in a zero-frequency mode and one or several oscillators, the latter representing the ‘incoherent’ transport of a charge carrier while the former represents the propagation the Landau Fermi liquid quasi-particles. The total free carrier spectral weight is defined as the total (coherent + incoherent) free charge carrier spectral weight, which is obtained by integrating the optical conductivity

$$W(T) = \int_0^{\Omega_c} \sigma_1(\omega, T) d\omega \quad (4)$$

where the value of the cutoff up to a frequency Ω_c (typically ≈ 1 eV) chosen to separate the free carrier response from the interband transitions. In all cuprate compounds investigated so far $W(T)$ is seen to increase when the temperature is decreased. This increase is 5 to 10 times larger than the temperature dependence expected from the Local Density Approximation (LDA) bandstructure, and neglecting the effect of electron-electron interactions [128][64]. The observed large increase is on the other hand consistent with cluster Dynamical Mean-Field Theory (DMFT) calculations within the framework of the repulsive Hubbard model [128][9].

At the normal-to-superconducting phase transition, the free charge carrier spectral weight $W(T)$ shows a kink-like anomaly. The sign and the size of the superconductivity-induced change $\Delta W = W_s - W_n$ are related to the change of the electronic kinetic energy E_{kin} (in the simple tight binding model with nearest neighbor hopping, $\Delta W \propto -\Delta E_{kin}$). This allows, in principle, distinguishing between a BCS-like mechanism, where the increase of the kinetic energy is overcompensated by a decrease of the potential energy and the opposite scenario where the condensation energy is due to the gain in kinetic energy in the superconducting state. ΔW was determined for several superconducting cuprates (Hg-1201 [11], Bi-2212 [8, 9], Bi-2223 [10]) in order to establish its dependence on doping, the number of the

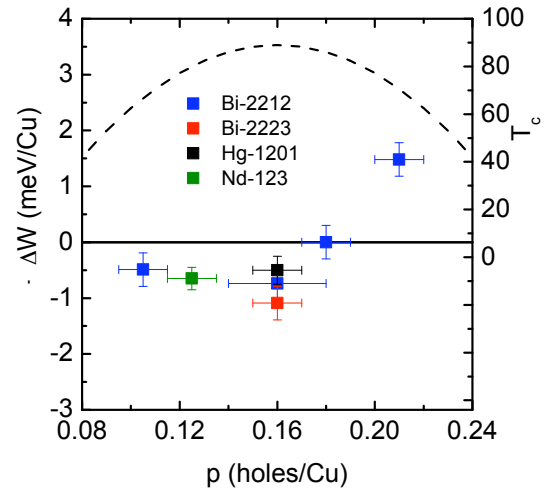


Figure 31: The doping dependence of the negative of the superconductivity induced change of free carrier optical spectral weight of several cuprate compounds, which is approximately proportional to ΔE_{kin} . The critical temperature is indicated for $Bi_2Sr_2CaCu_2O_{10+\delta}$.

CuO_2 planes and the chemical composition. Since the energetic changes are rather small, spectroscopic ellipsometry was used in combination with reflectivity measurements and advanced methods of the analysis of optical spectra (as described below) in order to improve the accuracy of ΔW . The results of these studies are summarized in Fig. 31.

The cuprates from the studied families appear to follow the same trend: ΔE_{kin} is negative (not BCS like) at low doping levels but crosses over to positive, i.e. BCS-consistent, values for the overdoped regime. Intuitively this can be associated with the fact that the quasiparticles in the normal state are much more coherent, or Fermi-liquid like, for the overdoped samples than for the underdoped ones, which make the energetics more conventional.

Two issues regarding the interpretation of these experimental results have been addressed: first of all the truncation at finite Ω_c introduces a systematic underestimation of the free carrier spectral weight. This was investigated in collaboration with M. Norman, A. Chubukov and F. Marsiglio, using a strong coupling model fitted to the experimental optical data (see section 3.8). In the normal state the strong temperature dependence of $W(T)$ can be largely accounted for by the cutoff [13, 65]. However, at any finite impurity scattering, the same model predicts a superconductivity induced decrease of $W(T)$ [65], which contradicts the observations on underdoped and optimally doped samples. The second is-

sue is that the simple relation $\Delta W \propto -\Delta E_{kin}$ is valid only for a simple tight-binding band with nearest-neighbor hopping only. The relation between ΔW and ΔE_{kin} was studied theoretically, taking into account a realistic band structure of the cuprates, which is consistent with ARPES experiments. In the relevant doping regime (below about 0.28 holes/Cu), the change of the spectral weight due to superconductivity is $\Delta W < 0$ [64].

This confirms that BCS theory cannot account for the experimental observations of the superconductivity induced spectral weight change, in that for the underdoped and optimally doped cuprates the kinetic energy of the charge carriers decreases when the material becomes superconducting. On the other hand, these observations agree with cluster DMFT calculations [9] and variational ansatz calculations [5, 6] within the framework of the repulsive Hubbard model.

3.8 Electron-boson coupling function from optical spectra

Although the discovery of high-temperature superconductivity in the cuprates raised doubts about the applicability of the Fermi-liquid description of these materials, there is growing evidence that quasiparticles exist at low energies, and that they interact with bosonic degrees of freedom. These observations have given rise to a renewed interest in the analysis of experiments in terms of the more conventional Fermi Liquid based approaches. Therefore the optical spectra of a large number of different high T_c superconducting materials were measured and analyzed using a strong coupling model. The goal is to obtain a boson spectral density $\alpha^2 F(\omega)$ which can then be compared to spectral densities obtained by other techniques. The analysis is based on the Kubo expression for the optical conductivity,

$$\sigma(\omega, T) = \frac{\omega_p^2}{4\pi i} \frac{1}{\omega} \times \int_{-\infty}^{\infty} \frac{n_F(\omega + \omega') - n_F(\omega')}{\Sigma(\omega + \omega', T) - \Sigma^*(\omega', T) - \omega} d\omega'$$

The self-energy $\Sigma(\omega, T)$ is related to $\alpha^2 F(\omega)$ via,

$$\Sigma(\omega, T) = \int d\epsilon \int \alpha^2 F(\omega') \left[\frac{n_B(\omega') + n_F(\epsilon)}{\omega - \epsilon + \omega' + i\delta} + \frac{n_B(\omega') + 1 - n_F(\epsilon)}{\omega - \epsilon - \omega' + i\delta} \right] d\epsilon \quad (5)$$

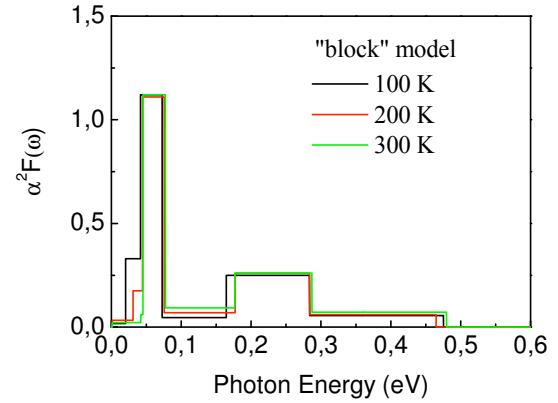


Figure 32: The electron-boson coupling function $\alpha^2 F(\omega)$ obtained by fitting of optical data of the single layer high T_c superconductor Hg-1201 ($T_c = 97$ K), in the normal state.

An analytical function was chosen for $\alpha^2 F(\omega)$ with a few parameters that are to be optimized. In view of the double integral linking $\alpha^2 F(\omega)$ to the self-energy, which in turn is linked to the optical conductivity through an integral expression, it is not realistic to try to fit any details of $\alpha^2 F(\omega)$. Instead $\alpha^2 F(\omega)$ is represented as a sum of square blocks, the width and height of which are adjustable parameters of a numerical fitting routine.

This idea was tested for Bi-2212 at various dopings, Bi-2223 and Hg-1201. In all cases it turns out that $\alpha^2 F(\omega)$ has two main features: a low energy feature around 50 meV and a much broader one centered around 250 meV. An example of this is shown in Fig. 32, which in this case corresponds to the single-layer Hg-1201 ($T_c = 97$ K). This is in good agreement with the observations made by ARPES experiments where one finds the low energy kink at the same binding energy and a “waterfall” like feature at high binding energy.

3.9 Momentum anisotropy of the scattering rate in cuprate superconductors

Mesot and collaborators examined the momentum and energy dependence of the scattering rate of the high-temperature cuprate superconductors using angle-resolved photoemission spectroscopy. The scattering rate is of the form $a+b\omega$ around the Fermi surface for under- and optimal doping. The inelastic coefficient b is found to be isotropic. The elastic term a , however, is found to be highly anisotropic for under- and optimally doped samples, with an anisotropy which correlates with that of the pseudogap. This is contrasted with heavily overdoped samples, which show an isotropic

scattering rate and an absence of the pseudo-gap above T_c . This was found to be a generic property for both single- and double-layer compounds [66].

3.10 Dual character of the electronic structure of $\text{YBa}_2\text{Cu}_4\text{O}_8$: the conduction bands of CuO_2 planes and CuO chains

Microprobe angle-resolved photoemission spectroscopy (ARPES) was used by the Mesot group to separately investigate the electronic properties of CuO_2 planes and CuO chains in the high temperature superconductor, $\text{YBa}_2\text{Cu}_4\text{O}_8$. For the CuO_2 planes, a two-dimensional (2D) electronic structure is observed and, in contrast to $\text{Bi}_2\text{Sr}_2\text{CaCu}_2\text{O}_{8+\delta}$, the bilayer splitting is almost isotropic and 50% larger, which strongly suggests that bilayer splitting has no direct effect on the superconducting properties. In addition, the scattering rate for the bonding band is about 1.5 times stronger than the antibonding band and is independent of momentum. For the CuO chains, the electronic structure is quasi-one-dimensional and consists of a conduction and insulating band. Finally, the conduction electrons are well confined within the planes and chains with a nontrivial hybridization [67].

3.11 When low- and high-energy electronic responses meet in cuprate superconductors

The existence of coherent quasiparticles near the Fermi energy in the low-temperature state of high-temperature superconductors has been well established by angle-resolved photoemission spectroscopy (ARPES). The group of Mesot has studied $\text{La}_{1.83}\text{Sr}_{0.17}\text{CuO}_4$ in the su-

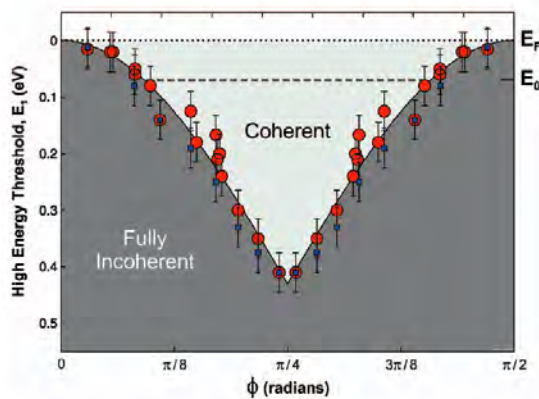


Figure 33: Dispersion of E_1 (boundary between low- and high-energy features) as a function of the Fermi surface angle ϕ .

perconducting state, and reported an abrupt change in the quasiparticle spectral function, as the dispersion of the ARPES signal was followed from the Fermi energy to 0.6 eV. The interruption in the quasiparticle dispersion separates coherent quasiparticle peaks at low energies from broad incoherent excitations at high energies. The boundary between these low-energy and high-energy features exhibits a cosine-shaped momentum dependence (Fig. 33), reminiscent of the superconducting d -wave gap. Further intriguing similarities between characteristics of the incoherent excitations and quasiparticle properties suggest a close relation between the electronic response at high and low energies in cuprate superconductors [14].

3.12 ARPES study of triple-layer $\text{Bi}_2\text{Sr}_2\text{Ca}_2\text{Cu}_3\text{O}_{10+\delta}$

A collaboration of the groups of Mesot, Griani and van der Marel has studied the electronic structure of the three-layer compound $\text{Bi}_2\text{Sr}_2\text{Ca}_2\text{Cu}_3\text{O}_{10+\delta}$ (Bi-2223) by high-resolution ARPES studies. Experiments have been performed with a UV source at Lausanne, and with synchrotron radiation at the Swiss Light Source on optimally doped (OPT; $T_c = 110$ K) and slightly overdoped (OD; $T_c = 108$ K) high-quality samples grown by E. Gianini (UniGe).

The ARPES data illustrate the opening of a d -wave superconducting gap ($\Delta_0 = 76 \pm 4$ meV for the OPT sample). The measured dispersion exhibits clear signatures of renormalization on two different energy scales: a low-energy kink (at ~ 60 meV) and a high-energy waterfall, in

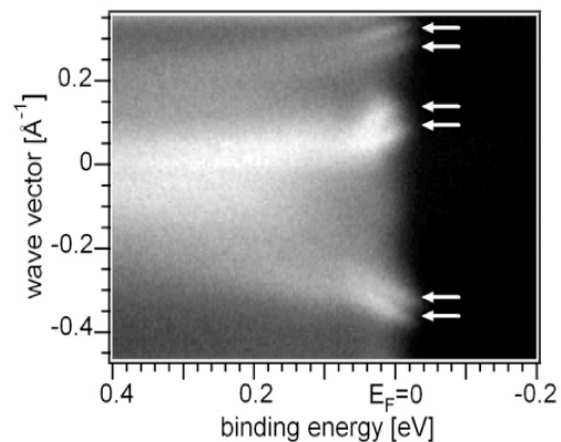


Figure 34: ARPES (SLS data) of an optimally doped $\text{Bi}_2\text{Sr}_2\text{Ca}_2\text{Cu}_3\text{O}_{10+\delta}$ sample, measured near the antinodal point, showing the splitting of the conduction band.

agreement with recent ARPES literature [129]. The present data unambiguously show that the Cu-O band is split by a coupling between CuO planes within each 3-layer block (Fig. 34). Remarkably only two branches are observed instead of three, as would be expected from a simple model of three coupled metallic layers. This is likely to be a manifestation of different doping levels in the outer and inner planes of the tri-layer, as was previously suggested by NMR data [130]. These new ARPES data will therefore provide a stringent test for realistic band structure calculations for this material.

3.13 ARPES study of single-layer $\text{Bi}_2\text{Sr}_2\text{CuO}_{6+\delta}$ thin films

While almost all ARPES studies of cuprates are performed on the cleaved surfaces of single crystal samples, artificially grown thin film samples are of clear interest. Thin films offer the possibility of introducing a controlled

strain in the lattice, which is known to have a considerable effect on the superconducting properties [131]. Moreover, they may enable a better control over the stoichiometry and the surface conditions than bulk samples.

Thin films were grown using pulsed laser deposited and immediately transferred under ultra high vacuum to the ARPES chamber. Fully relaxed underdoped (UD) films of Bi-2201 showed sharp superconducting transitions with $T_c < 10$ K. The LEED images show the presence of the pseudo 5×1 periodicity, and the coexistence of two equivalent domains in the ab plane. The presence of domains is verified also in the ARPES results, where two sets of superlattice bands, symmetric around the ΓM direction, are observed (Fig. 35). The normal state data show quasiparticle (QP) peaks that are consistent with the best single crystal spectra of Bi-2201, which confirms the good quality of the films. They also exhibit the typical low energy *kink* from the coupling of the QPs to a bosonic mode. Close to the nodal direction the high-energy *waterfall* anomaly was clearly visible (Fig. 36).

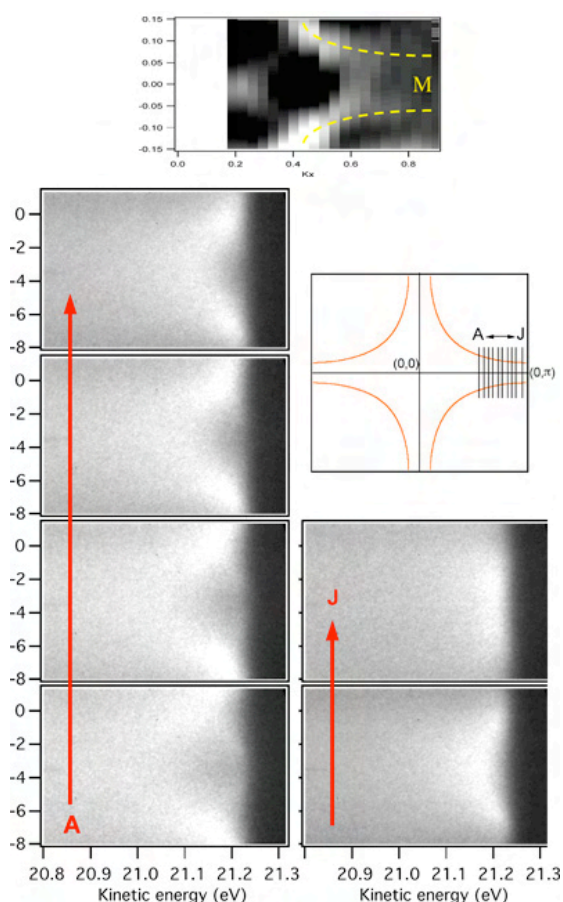


Figure 35: (top) The Fermi surface of an UD Bi-2201 film in a narrow momentum range around the $M(0,\pi)$ point. Besides the main sheets (dashed lines) two symmetric superlattice arcs are visible. (bottom) ARPES intensity plots showing the evolution of the dispersion for various cuts along the ΓM direction.

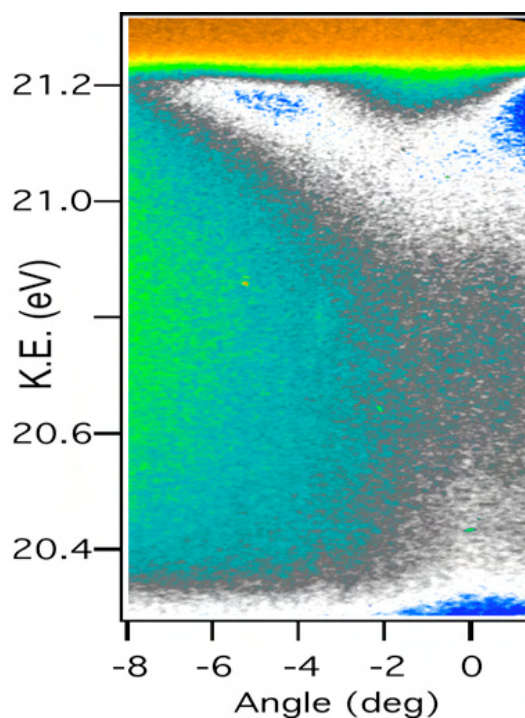


Figure 36: ARPES intensity plot of an UD Bi-2201 film near the nodal point, showing both the low-energy kink and high-energy waterfall features.

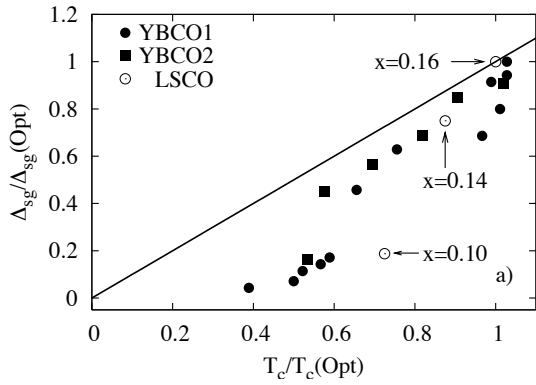


Figure 37: Normalized Δ_{sg} versus normalized T_c for LSCO (open symbols) and YBCO (filled circles and filled squares).

3.14 Magnetic-field-induced spin excitations and renormalized spin gap of the Underdoped $\text{La}_{1.895}\text{Sr}_{0.105}\text{CuO}_4$ Superconductor

High-resolution neutron inelastic scattering experiments in applied magnetic fields have been performed on $\text{La}_{1.895}\text{Sr}_{0.105}\text{CuO}_4$ (LSCO). In zero field, the temperature dependence of the low-energy peak intensity at the incommensurate momentum transfer $\text{QIC}=(0.5,0.5\pm\delta,0),(0.5\pm\delta,0.5,0)$ exhibits an anomaly at the superconducting T_c which broadens and shifts to lower temperature upon the application of a magnetic field along the c -axis. A field-induced enhancement of the spectral weight is observed, but only at finite energy transfers and in an intermediate temperature range. These observations establish the opening of a strongly downward renormalized spin gap in the underdoped regime of LSCO (Fig. 37). This behavior contrasts with the observed doping dependence of most electronic energy features [68].

3.15 Nature of the magnetic order in the charge-ordered cuprate $\text{La}_{1.48}\text{Nd}_{0.4}\text{Sr}_{0.12}\text{CuO}_4$

Using polarized neutron scattering the magnetic order in $\text{La}_{1.48}\text{Nd}_{0.4}\text{Sr}_{0.12}\text{CuO}_4$ was shown to be either (i) one dimensionally modulated and collinear, consistent with the stripe model or (ii) two dimensionally modulated with a novel noncollinear structure. The measurements rule out a number of alternative models characterized by 2D electronic order or 1D helical spin order (Fig. 38). The low-energy spin excitations are found to be primarily transversely polarized relative to the stripe ordered state, consistent with conventional spin waves [69].

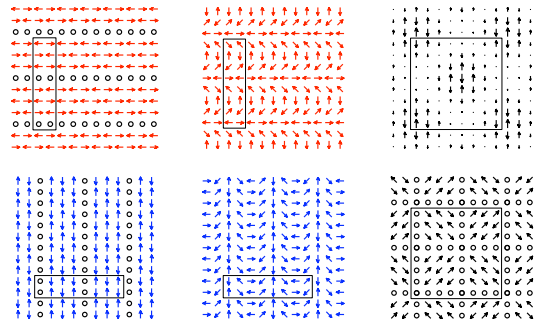


Figure 38: Four models that yield magnetic diffraction patterns with principal Fourier components $\mathbf{Q} = (1/2, 1/2) \pm \mathbf{q}_1$ and $(1/2, 1/2) \pm \mathbf{q}_2$ and equivalent wavevectors, as observed experimentally. Two stripe domains, two spiral domains, one “diagonal stripe” domain and one complex 8×8 unit cell domain.

3.16 Two-gap superconductivity in cuprate superconductors

The crystal structure of Hg1201 and Tl2201 , being tetragonal, has an ideal fourfold symmetry, and consequently the symmetry of the superconducting gap can have, among other possibilities, s -wave or d -wave symmetry. The admixture of the form $\Delta = a\Delta_s + ib\Delta_d$ is also allowed by symmetry. The latter state is fully gapped (there are no nodes), and it has broken time-reversal symmetry.

In most other cuprates superconductors the crystal symmetry is orthorhombic. Due to the low symmetry of the crystal the ground state of the system can not have a pure d or s -wave symmetry, and consequently the gap will be of the form $\Delta = a\Delta_s + b\Delta_d$, with the nodes shifted away from 45 degrees relative to the copper-oxygen bond direction.

Different order parameter symmetries can also occur simultaneously when the Fermi energy is crossed by several bands, each one having a different order parameter. The superfluid density $\sigma(T)$ can then be decomposed into two components having d -wave and s -wave symmetry as $\sigma(T) = \sigma^s(T) + \sigma^d(T)$. Keller and collaborators used the latter — multi component — model to analyze μSR data of $\text{YBa}_2\text{Cu}_4\text{O}_8$ [70] and $\text{YBa}_2\text{Cu}_3\text{O}_{7-\delta}$ [71, 72, 73]. The main results are summarized in Fig. 39 where the a , b , and c components of the muon-spin depolarization rate ($\sigma_i \propto \lambda_i^{-2}$) are plotted as a function of temperature. The temperature dependence of the c -axis related superfluid density closely follows the one expected for a single s -wave gap (Fig. 39c and f), which emphasizes the distinct role of the third dimension for high T_c superconductors. Since mixed

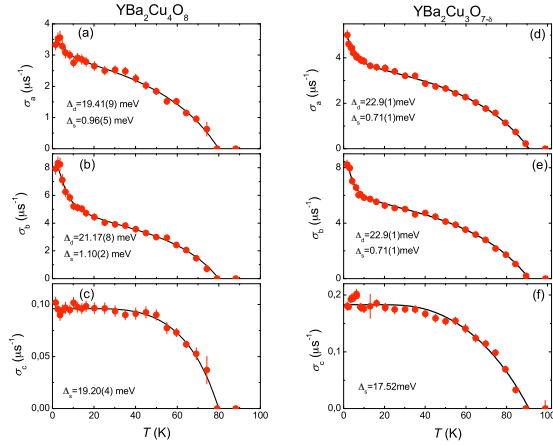


Figure 39: Temperature dependences of $\sigma_a \propto \lambda_a^{-2}$, $\sigma_b \propto \lambda_b^{-2}$, and $\sigma_c \propto \lambda_c^{-2}$ of $\text{YBa}_2\text{Cu}_4\text{O}_8$ [panels (a), (b), and (c)] and $\text{YBa}_2\text{Cu}_3\text{O}_{7-\delta}$ [panels (d), (e), and (f)]. Lines represent results of the analysis within two-component and one-component models.

s and d -wave symmetries of the superconducting order parameter were observed previously in various cuprate families by various different techniques, the present μSR data support the idea that this behavior is intrinsic and possibly universal for the cuprates.

3.17 Doped Cu-O ladders

Recently the question of whether orbital currents could exist in the pseudogap regime of cuprate materials has received much attention, with the proposal that for a three band model of the copper-oxygen planes orbital currents could exist while absent for the single band one. Of course the situation in the high T_c context is still quite open and reliable calculations on this issue are quite challenging.

In order to tackle this question in a more controlled situation, Giamarchi and collaborators have looked at the case of a two leg ladder. For a simple Hubbard ladder, the phase diagram is now well established, with a superconducting phase with d -wave like pairing for repulsive interactions. Orbital currents can exist [132] but only for more complicated and somewhat unrealistic interactions. The case of a three band ladder was thus examined, using bosonization and renormalization techniques for weak interactions [74]. For this case where the calculation can be controlled, for intermediate doping the three band ladder presents, contrarily to the single band one, a gapless phase with orbital currents. In this regime, the ground state consists of a pattern of orbital currents plus a spin density wave (SDW) structure. This is a quite surprising result, suggesting that deep

differences between the one and three band model can exist. Of course, given the difference in geometry and strength of interactions, extrapolations to the case of the cuprates would be quite hasty, and would certainly require more than a grain of salt. Independently of the cuprates, the above results could be applied to compounds such as $\text{Sr}_{14-x}\text{Ca}_x\text{Cu}_{24}\text{O}_{41}$ where the hole concentration can be somewhat varied. The NMR consequences of such patterns of currents were calculated, a prediction which now awaits experimental testing.

3.18 Layered superconductors

Much attention has been devoted to the effect of phase fluctuations in quasi 2D superfluid systems. Thin films are natural candidates for the observation of the “universal” (i.e. sample-independent) behavior characteristic of the Beresinsky-Kosterlitz-Thouless (BKT) physics, as the universal jump of the superfluid density, measured in ^4He superfluid films, or the non-linear $I - V$ characteristic, observed in thin films of conventional superconductors. Signatures of BKT physics can be expected also in layered superconductors with weak interplane coupling. A remarkable example of systems belonging to this class are underdoped samples of high T_c superconductors. Recently, various experimental data, ranging from finite-frequency conductivity, Nernst signal and non-linear magnetization, have been interpreted as signatures of BKT phase fluctuations. Nonetheless, several experiments failed to observe any effect reminiscent of the universal jump of the superfluid density at the critical temperature, which would be the most direct probe of BKT physics in these systems. Until now, the 2D-3D crossover in anisotropic layered superconductors has been discussed mainly within the theoretical framework of the anisotropic 3D XY model. Within this model a finite interlayer coupling J_c stabilizes the superconducting phase, by cutting the vortex potential. However the superfluid phase has a critical temperature T_c at most a few percents above T_{BKT} . This would be inconsistent with several recent measurements of the superfluid density in strongly underdoped $\text{YBa}_2\text{Cu}_3\text{O}_{6+x}$ (YBCO) samples.

Giamarchi and collaborators [75] have thus re-analyzed the role played by the interlayer coupling and the vortex-core energy at the crossover from 2D BKT to 3D superconducting behavior in layered superconductors. In particular, focus was on the behavior of the superfluid density below T_c and of the phase fluc-

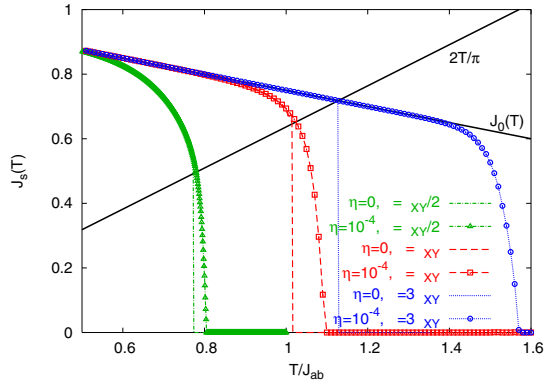


Figure 40: Temperature dependence of the superfluid density in a layered superconductor. In presence of interlayer coupling the discontinuous jump of the BKT transition is replaced by a smooth crossover. The shift is strongly dependent on the vortex core energy μ .

tuation correlation length above T_c . To perform this analysis, renormalization group techniques were used which were developed and used in the context of the metal-insulator transition in the quantum 1D sine-Gordon model for the cold atomic gases described in MaNEP Project 1. In these systems the interchain tunneling amplitude plays the same role as the Josephson coupling in layered superconductors. In the presence of a finite interlayer coupling the superfluid density loses its universal character. The jump in the superfluid density at T_{BKT} observed in the pure 2D system is replaced by a downturn curvature at a temperature T_d which is determined by the vortex-core energy, as shown in Fig. 40. To account for the data, a larger vortex core energy than the one of a simple XY model is needed. Using the recent data on bilayer systems the T_c dependence of this core energy could be determined [76] and, from this phenomenological model it was seen to scale roughly as T_c .

In addition to the above results, a similar mapping to the sine-Gordon model was used to investigate the properties of a 2D superconductor under magnetic field [77]. This is directly relevant for the various superconducting films, as well as the novel 2D superconductors found at the interface between insulating materials. Due to the strong interest of such a question, this problem has been addressed in the past but, unfortunately, contrarily to the case of the $B = 0$ transition, the efforts have been largely unsatisfactory. In particular most of the literature on the subject rested on extending the mapping to the Coulomb gas to incorporate the effects of the magnetic field, i.e., in the Coulomb gas language, of an ex-

cess of positive charges. However this mapping is not as transparent as in the neutral case, and leaves some ambiguities in the definition of the physical observables (like the magnetization) and in their dependence on the magnetic induction instead of the magnetic field. Using the mapping to sine-Gordon provides a very simple and physically transparent way to deal with the finite magnetic field case. In the present scheme the physical observables have a straightforward definition, regardless the approximation method used to compute them, and the role of both magnetic induction and magnetic field is clarified.

4 Collaborative efforts

There are many collaborative efforts within this project. Crystals and thin films which have been prepared at the ETHZ, the EPFL, the University of Geneva, and the PSI, have been studied by several groups in several other laboratories participating to the MaNEP network. The list of examples is too long to spell out in detail here, since this is the case for almost all of the projects described above in this report. The Bi2223 crystals prepared at Geneva are a typical and representative example. These materials have been studied at Geneva (STM and IRS), EPFL (ARPES) and PSI (ARPES and RIXS). The results obtained with different techniques, as well as theoretical calculations are discussed in frequent sessions (every three months) by the five teams involved in these studies. Similar exchanges of samples, ideas and experimental or theoretical data take place for pure and doped MgB_2 , potassium and rubidium osmates, SC/FM multilayers, several cuprate superconducting materials, to give a few examples.

5 Goals for the next year

- ARPES, optical and STM studies will be carried out on copper-oxychlorides single crystals.
- STM studies of $K_xRb_{1-x}Os_2O_6$ will be continued.
- STM experiments will be carried out on the temperature dependence of STS spectra in a magnetic field.
- A detailed study will be carried out of elastic manifold subject to a random force. The physics of thermal depinning and the disorder potential generating the pinning landscape for the vortices will be addressed using the Larkin model.

- A theory will be developed describing the influence of spin-orbit coupling on the superconducting phase in non-centrosymmetric superconductors around defects like twin-boundaries, and the frustration effects in Sr_2RuO_4 with Ru-metal inclusions.
- Low-energy μSR and neutron reflectometry measurements on the oxide multilayers from cuprate high T_c superconductors and ferromagnets down to the scale of single monolayers will be performed.
- Electron-doped cuprate superconductors will be studied with μSR .
- The proximity effects in cuprate heterostructures (YBCO/PBCO/YBCO) will be studied using LE- μSR .
- The local order in the pseudogap state will be studied with STM.
- The theory which has been developed to describe the properties of one dimensional chains of bosons will be applied to layered superconductors such as the high T_c .
- The effects of the next-nearest neighbor hopping, on electron doping and long-range order in the 2D Hubbard model will be studied.
- Bi2223 and Bi2201 high T_c films will be studied for different doping levels with ARPES.
- The optical properties of Bi2201 will be investigated for a series of doping concentrations.
- The doping dependence of the superconducting gap in LSCO will be studied by ARPES.

MaNEP-related publications

- [1] C. Iniotakis, S. Fujimoto, and M. Sigrist, arXiv:0801.1373 (2008).
- ▶ [2] R. Lortz, Y. Wang, A. Demuer, M. Böttger, B. Bergk, G. Zwicknagel, Y. Nakazawa, and J. Wosnitzer, *Phys. Rev. Lett.* **99**, 187002 (2007).
- ▶ [3] A. D. Bianchi, M. Kenzelmann, L. DeBeer-Schmitt, J. S. White, E. M. Forgan, J. Mesot, M. Zolliker, J. Kohlbrecher, R. Movshovich, E. D. Bauer, J. L. Sarrao, Z. Fisk, C. Petrovic, and M. R. Eskildsen, *Science* **319**, 177 (2008).
- ▶ [4] N. Reyren, S. Thiel, A. D. Caviglia, L. F. Kourkoutis, G. Hammerl, C. Richter, C. W. Schneider, T. Kopp, A.-S. Ruetschi, D. Jaccard, M. Gabay, D. A. Müller, J.-M. Triscone, and J. Mannhart, *Science* **317**, 1196 (2007).
- [5] D. Eichenberger and D. Baeriswyl, *Physica C* **460-462**, 1153 (2007).
- [6] D. Baeriswyl, D. Eichenberger, and B. Gut, *Phys. Stat. Sol. (b)* **244**, 2299 (2007).
- [7] H. J. A. Molegraaf, C. Presura, D. van der Marel, P. H. Kes, and M. Li, *Science* **295**, 2239 (2002).
- [8] A. B. Kuzmenko, H. J. A. Molegraaf, F. Carbone, and D. van der Marel, *Phys. Rev. B* **72**, 144503 (2005).
- [9] F. Carbone, A. B. Kuzmenko, H. Molegraaf, E. van Heumen, V. Lukovac, F. Marsiglio, D. van der Marel, K. Haule, G. Kotliar, H. Berger, C. S., P. H. Kes, and M. Li, *Phys. Rev. B* **74**, 064510 (2006).
- [10] F. Carbone, A. B. Kuzmenko, H. J. A. Molegraaf, E. van Heumen, E. Giannini, and D. van der Marel, *Phys. Rev. B* **74**, 024502 (2006).
- [11] E. van Heumen, R. Lortz, A. B. Kuzmenko, F. Carbone, D. van der Marel, X. Zhao, G. Yu, Y. Cho, N. Barisic, M. Greven, C. C. Homes, and S. V. Dordevic, *Phys. Rev. B* **75**, 054522 (2007).
- [12] G. Levy de Castro, C. Berthod, A. Piriou, E. Giannini, and Ø. Fischer, cond-mat/0703131 (2007).
- [13] M. R. Norman, A. V. Chubukov, E. van Heumen, A. B. Kuzmenko, and D. van der Marel, *Phys. Rev. B* **76**, 220509 (2007).
- ▶ [14] J. Chang, S. Pailhès, M. Shi, M. Mansson, T. Claesson, O. Tjernberg, J. Voigt, V. Perez, L. Patthey, N. Momono, M. Oda, M. Ido, A. Schnyder, C. Mudry, and J. Mesot, *Phys. Rev. B* **75**, 224508 (2007).
- [15] P. A. Frigeri, D. F. Agterberg, I. Milat, and M. Sigrist, *Eur. Phys. J. B* **54**, 435 (2007).
- [16] C. Iniotakis, N. Hayashi, Y. Sawa, T. Yokoyama, U. May, Y. Tanaka, and M. Sigrist, *Phys. Rev. B* **76**, 012501 (2007).
- [17] N. Hayashi, C. Iniotakis, M. Machida, and M. Sigrist, arXiv:0711.3241 (2007).
- [18] P. A. Frigeri, D. F. Agterberg, and M. Sigrist, *New J. Phys.* **6**, 115 (2004).
- ▶ [19] Y. Yanase and M. Sigrist, *J. Phys. Soc. Jpn.* **76**, 043712 (2007).
- [20] Y. Yanasa and M. Sigrist, *J. Phys. Soc. Jpn.* **76**, 124709 (2007).
- [21] F. P. Mena, D. van der Marel, and J. L. Sarrao, *Phys. Rev. B* **72**, 045119 (2005).
- [22] C. Dallera, E. Annese, J.-P. Rueff, M. Grioni, G. Vanko, L. Braicovich, A. Barla, J.-P. Sanchez, R. Gusmeroli, A. Palenzona, L. Degiorgi, and G. Lapertot, *J. Phys.: Cond. Mat.* **17**, S849 (2005).
- [23] C. Dallera, O. Wessely, M. Colarieti-Tosti, O. Eriksson, R. Ahuja, B. Johansson, M. I. Katsnelson, E. Annese, J.-P. Rueff, G. Vankó, L. Braicovich, and M. Grioni, *Phys. Rev. B* **74**, 081101(R) (2006).
- [24] L. Moreschini, C. Dallera, J. J. Joyce, J. L. Sarrao, E. D. Bauer, V. Fritsch, S. Bobev, E. Carpena, S. Huotari, G. Vankó, G. Monaco, P. Lacovig, G. Panaccione, A. Fondacaro, G. Paolicelli, P. Torelli, and M. Grioni, *Phys. Rev. B* **75**, 035113 (2007).
- [25] V. Guritanu, A. B. Kuzmenko, D. van der Marel, S. M. Kazakov, N. D. Zhigadlo, and J. Karpinski, *Phys. Rev. B* **73**, 104509 (2006).
- [26] A. V. Sologubenko, J. Jun, S. M. Kazakov, J. Karpinski, and H. R. Ott, *Phys. Rev. B* **66**, 014504 (2002).
- [27] A. V. Sologubenko, N. D. Zhigadlo, J. Karpinski, and H. R. Ott, *Phys. Rev. B* **74**, 184523 (2006).
- [28] A. V. Sologubenko, N. D. Zhigadlo, S. M. Kazakov, J. Karpinski, and H. R. Ott, *Phys. Rev. B* **71**, 020501 (2005).

- [29] J. Teyssier, A. B. Kuzmenko, D. van der Marel, F. Marsiglio, A. B. Liashchenko, V. Filippov, and N. Shitsevalova, *Phys. Rev. B* **75**, 134503 (2007).
- [30] R. Lortz, Y. Wang, U. Tutsch, S. Abe, C. Meingast, P. Popovich, W. Knafo, N. Shitsevalova, Y. Paderno, and A. Junod, *Phys. Rev. B* **73**, 024512 (2006).
- [31] Y. Wang, R. Lortz, Y. Paderno, V. Filippov, S. Abe, U. Tutsch, and A. Junod, *Phys. Rev. B* p. 024548 (2005).
- [32] R. Lortz, Y. Wang, S. Abe, C. Meingast, Y. Paderno, V. Filippov, and A. Junod, *Phys. Rev. B* **72**, 024547 (2005).
- [33] G. Schuck, S. Kazakov, K. Rogacki, N. Zhigadlo, and J. Karpinski, *Phys. Rev. B* **73**, 144506 (2006).
- [34] P. A. Frigeri, D. F. Agterberg, A. Koga, and M. Sigrist, *Phys. Rev. Lett.* **92**, 097001 (2004).
- [35] P. A. Frigeri, D. F. Agterberg, A. Koga, and M. Sigrist, *Phys. Rev. Lett.* **93**, 099903 (2004).
- [36] N. Hayashi, Y. Kato, P. A. Frigeri, K. Wakabayashi, and M. Sigrist, *Physica C* **437-38**, 96 (2006).
- [37] C. Dubois, P. E. Bisson, A. A. Manuel, Ø. Fischer, and S. Reymond, *Rev. Sci. Instr.* **77**, 043712 (2006).
- [38] C. Dubois, G. Santi, I. Cuttat, C. Berthod, N. Jenkins, A. P. Petrović, A. A. Manuel, Ø. Fischer, S. M. Kazakov, Z. Bukowski, and J. Karpinski, arXiv:0704.0529 (2007).
- [39] C. Dubois, A. P. Petrovic, G. Santi, C. Berthod, A. A. Manuel, M. Decroux, Ø. Fischer, M. Potel, and R. Chevrel, *Phys. Rev. B* **75**, 104501 (2007).
- [40] A. P. Petrović, Y. Fasano, R. Lortz, M. Decroux, M. Potel, R. Chevrel, and Ø. Fischer, *Physica C* **460-462**, 702 (2007).
- [41] A. P. Petrović, R. Lortz, G. Santi, M. Decroux, H. Monnard, Ø. Fischer, L. Boeri, O. Andersen, J. Kortus, D. Salloum, P. Gougeon, and M. Potel, Phonon Mode Spectroscopy and Electron-Phonon Coupling in the Quasi-One-Dimensional $M_2Mo_6Se_6$ family: Competing Instabilities, Ultra-Strong Coupling and "Phonon-Boosted" Superconductivity (2008), submitted to *Phys. Rev. B*.
- ▶ [42] K. S. Takahashi, M. Gabay, D. Jaccard, K. Shibuya, T. Ohnishi, M. Lippmaa, and J.-M. Triscone, *Nature* **441**, 195 (2006).
- ▶ [43] A. De Col, G. I. Menon, and G. Blatter, *Phys. Rev. B* **75**, 014518 (2007).
- ▶ [44] A. De Col, G. I. Menon, V. B. Geshkenbein, and G. Blatter, *Phys. Rev. Lett.* **96**, 177001 (2006).
- [45] A. De Col, G. I. Menon, V. B. Geshkenbein, and G. Blatter, *Phys. Rev. B* **75**, 184532 (2007).
- ▶ [46] A. U. Thomann, V. B. Geshkenbein, and G. Blatter, *Physica C* (2008).
- [47] A. Piriou, Y. Fasano, E. Giannini, and O. Fischer, *Physica C* **460-462**, 408 (2007).
- [48] A. Piriou, Y. Fasano, E. Giannini, and O. Fischer, Effect of oxygen-doping on $Bi_2Sr_2Ca_2Cu_3O_{10+\delta}$ vortex matter: Crossover from electromagnetic to Josephson interlayer coupling (2008), submitted to *Phys. Rev. B*.
- [49] E. Morenzoni, T. Prokscha, A. Suter, H. Luetkens, and R. Khasanov, *J. Phys.: Cond. Mat.* **16**, S4583 (2004).
- [50] H. Luetkens, J. Korecki, E. Morenzoni, T. Prokscha, M. Birke, H. Glöckler, R. Khasanov, H.-H. Klauss, T. Ślezak, A. Suter, E. M. Forgan, C. Niedermayer, and F. J. Litterst, *Phys. Rev. Lett.* **91**, 017204 (2003).
- [51] A. J. Drew, S. L. Lee, D. Charalambous, A. Potenza, C. Marrows, H. Luetkens, A. Suter, T. Prokscha, K. R., E. Morenzoni, D. Ucko, and E. M. Forgan, *Phys. Rev. Lett.* **95**, 197201 (2005).
- [52] J. Stahn, J. Chakhalian, C. Niedermayer, J. Hoppler, T. Gutberlet, J. Voigt, F. Treubel, H.-U. Habermeier, G. Cristiani, B. Keimer, and C. Bernhard, *Phys. Rev. B* **71**, R140509 (2005).
- [53] J. Chakhalian, J. W. Freeland, G. Srajer, J. Strempler, G. Khaliullin, J. C. Cezar, T. Charlton, R. Dalgliesh, C. Bernhard, G. Cristiani, H.-U. Habermeier, and K. B., *Nature Phys.* **2**, 244 (2006).
- [54] B. W. Hoogenboom, C. Berthod, M. Peter, Ø. Fischer, and A. A. Kordyuk, *Phys. Rev. B* **67**, 224502 (2003).
- [55] J. Mesot, M. Randeria, M. R. Norman, A. Kaminski, H. M. Fretwell, J. C. Campuzano, H. Ding, T. Takeuchi, T. Sato, T. Yokoya, T. Takahashi, I. Chong, T. Terashima, M. Takano, T. Mochiku, and K. Kadowaki, *Phys. Rev. B* **63**, 224516 (2001).
- ▶ [56] Ø. Fischer, M. Kugler, I. Maggio-Aprile, C. Berthod, and C. Renner, *Rev. Mod. Phys.* **79**, 353 (2007).
- [57] Y. Fasano, I. Maggio-Aprile, J. Karpinski, and Ø. Fischer, *Physica C* **460-462**, 958 (2007).
- [58] E. Giannini, R. Gladyshevskii, N. Clayton, N. Musolino, V. Garnier, A. Piriou, and R. Flükiger, *Curr. Appl. Phys.* **8**, 115 (2008).
- ▶ [59] S. Pilgram, T. M. Rice, and M. Sigrist, *Phys. Rev. Lett.* **97**, 117003 (2006).
- ▶ [60] Y. Chen, T. M. Rice, and F. C. Zhang, *Phys. Rev. Lett.* **97**, 237004 (2006).
- [61] K.-Y. Yang, T. M. Rice, and F.-C. Zhang, *Phys. Rev. B* **76**, 100501 (2007).
- [62] B. Binz, D. Baeriswyl, and B. Douçot, *Ann. Phys. (Leipzig)* **12**, 704 (2003).
- [63] D. Eichenberger and D. Baeriswyl, *Phys. Rev. B* **76**, 180504(R) (2007).
- [64] F. Marsiglio, F. Carbone, A. B. Kuzmenko, and D. van der Marel, *Phys. Rev. B* **74**, 174516 (2006).
- [65] F. Marsiglio, E. van Heumen, and A. B. Kuzmenko, arXiv:0710.5941 (2007).
- [66] A. Kaminski, H. M. Fretwell, M. R. Norman, M. Randeria, S. Rosenkranz, U. Chatterjee, J. C. Campuzano, J. Mesot, T. Sato, T. Takahashi, T. Terashima, M. Takano, K. Kadowaki, Z. Z. Li, and H. Raffy, *Phys. Rev. B* **71**, 014517 (2005).
- ▶ [67] T. Kondo, R. Khasanov, J. Karpinski, S. M. Kazakov, N. D. Zhigadlo, T. Ohta, H. M. Fretwell, A. D. Palczewski, J. D. Koll, J. Mesot, E. Rotenberg, H. Keller, and A. Kaminski, *Phys. Rev. Lett.* **98**, 157002 (2007).
- ▶ [68] J. Chang, A. P. Schnyder, R. Gilardi, H. M. Rønnow, S. Pailhes, N. B. Christensen, C. Niedermayer, D. F. McMorrow, A. Hiess, A. Stunault, M. Enderle, B. Lake, O. Sobolev, N. Momono, M. Oda, M. Ido, C. Mudry, and J. Mesot, *Phys. Rev. Lett.* **98**, 077004 (2007).
- ▶ [69] N. B. Christensen, H. M. Rønnow, J. Mesot, R. A. Ewings, N. Momono, M. Oda, M. Ido, M. Enderle, D. F. McMorrow, and A. T. Boothroyd, *Phys. Rev. Lett.* **98**, 197003 (2007).
- [70] R. Khasanov, A. Shengelaya, A. Bussmann-Holder, J. Karpinski, H. Keller, and K. A. Müller, arXiv:0705.0577 (2007).
- ▶ [71] R. Khasanov, A. Shengelaya, A. Maisuradze, F. La Mattina, A. Bussmann-Holder, H. Keller, and K. A. Müller, *Phys. Rev. Lett.* **98**, 057007 (2007).
- [72] R. Khasanov, A. Shengelaya, A. Bussmann-Holder, and H. Keller, in *High- T_c Superconductors and Related Transition Metal Compounds*, A. Bussmann-Holder and H. Keller, eds. (Springer, Berlin, 2007), p. 177.

- ▶ [73] R. Khasanov, S. Strässle, D. Di Castro, T. Masui, S. Miyasaka, S. Tajima, A. Bussmann-Holder, and H. Keller, *Phys. Rev. Lett.* **99**, 237601 (2007).
- ▶ [74] P. Chudzinski, M. Gabay, and T. Giamarchi, *Phys. Rev. B* **76**, 161101(R) (2007).
- ▶ [75] L. Benfatto, C. Castellani, and T. Giamarchi, *Phys. Rev. Lett.* **98**, 117008 (2007).
- [76] L. Benfatto, C. Castellani, and T. Giamarchi, *Phys. Rev. B* **77**, 100506(R) (2008).
- ▶ [77] L. Benfatto, C. Castellani, and T. Giamarchi, *Phys. Rev. Lett.* **99**, 207002 (2007).

Other references

- [78] A. Sumiyama, K. Nakatsuji, Y. Tsuji, Y. Oda, T. Yasuda, R. Settai, and Y. Onuki, *J. Phys. Soc. Jpn.* **74**, 3041 (2005).
- [79] N. Kimura, Y. Muro, and H. Aoki, *J. Phys. Soc. Jpn.* **76**, 051010 (2007).
- [80] N. D. Mathur, F. M. Grosche, S. R. Julian, I. R. Walker, D. M. Freye, R. K. W. Haselwimmer, and G. G. Lonzarich, *Nature* **394**, 39 (1998).
- [81] S. Yonezawa, Y. Muraoka, Y. Matsushita, and Z. Hiroi, *J. Phys.: Cond. Mat.* **16**, L9 (2004).
- [82] S. Yonezawa, Y. Muraoka, Y. Matsushita, and Z. Hiroi, *J. Phys. Soc. Jpn.* **73**, 819 (2004).
- [83] S. Yonezawa, Y. Muraoka, and Z. Hiroi, *J. Phys. Soc. Jpn.* **73**, 1655 (2004).
- [84] P. W. Anderson, *Mat. Res. Bull.* **8**, 153 (1973).
- [85] H. Aoki, *J. Phys.: Cond. Mat.* **16**, V1 (2004).
- [86] T. M. Mishonov, G. V. Pachov, I. N. Genchev, L. A. Atanasova, and D. C. Damianov, *Phys. Rev. B* **68**, 054525 (2003).
- [87] R. Brusetti, A. J. Dianoux, P. Gougeon, M. Potel, E. Bonjour, and R. Calemczuk, *Phys. Rev. B* **41**, 6315 (1990).
- [88] C. S. Koonce, M. L. Cohen, J. F. Schooley, W. R. Hosler, and E. R. Pfeiffer, *Phys. Rev.* **163**, 380 (1967).
- [89] A. Ohtomo and H. Y. Hwang, *Nature* **427**, 423 (2004).
- [90] S. Thiel, G. Hammerl, A. Schmehl, C. W. Schneider, and J. Mannhart, *Science* **313**, 1942 (2006).
- [91] G. Blatter, M. V. Feigel'man, V. B. Geshkenbein, A. I. Larkin, and V. M. Vinokur, *Rev. Mod. Phys.* **66**, 1125 (1994).
- [92] J. Clem, *Phys. Rev. B* **43**, 7837 (1991).
- [93] M. J. W. Dodgson, A. E. Koshelev, V. B. Geshkenbein, and G. Blatter, *Phys. Rev. Lett.* **84**, 2698 (2000).
- [94] T. V. Ramakrishnan and M. Yussouf, *Phys. Rev. B* **19**, 2775 (1979).
- [95] R. Lipowsky and W. Speth, *Phys. Rev. B* **28**, 3983 (1983).
- [96] A. Soibel, E. Zeldov, M. Rappaport, Y. Myasoedov, T. T. Tamegai, S. Ooi, M. Konczykowski, and V. B. Geshkenbein, *Nature* **406**, 282 (2000).
- [97] A. O. Caldeira and A. J. Leggett, *Phys. Rev. Lett.* **46**, 211 (1981).
- [98] J. M. Martnis, M. H. Devoret, and J. Clarke, *Phys. Rev. B* **35**, 4682 (1987).
- [99] S. Chakravart and A. J. Leggett, *Phys. Rev. Lett.* **52**, 5 (1984).
- [100] I. Chiorescu, Y. Nakamura, C. J. P. M. Harmans, and J. E. Mooji, *Science* **299**, 1869 (2003).
- [101] A. E. Koshelev and V. M. Vinokur, *Phys. Rev. B* **57**, 8026 (1998).
- [102] T. Fujii, I. Terasaki, T. Watanabe, and A. Matsuda, *Phys. Rev. B* **66**, 024507 (2002).
- [103] B. Liang, C. Bernhard, T. Wolf, and C. Lin, *Supercond. Sci. Technol.* **17**, 731 (2004).
- [104] P. Bruno and C. Chappert, *Phys. Rev. B* **46**, 261 (1992).
- [105] J.-M. Triscone and O. Fischer, *Rep. Prog. Phys.* **60**, 1673 (1997).
- [106] J. C. Campuzano, H. Ding, M. R. Norman, H. M. Fretwell, M. Randeria, A. Kaminski, J. Mesot, T. Takeuchi, T. Sato, T. Yokoya, T. Takahashi, T. Mochiku, K. Kadowaki, P. Guptasarma, D. G. Hinks, Z. Konstantinovic, Z. Z. Li, and H. Raffy, *Phys. Rev. Lett.* **83**, 3709 (1999).
- [107] J. F. Zasadzinski, L. Coffey, P. Romano, and Z. Yusof, *Phys. Rev. B* **68**, 180504 (2003).
- [108] M. Eschrig and M. R. Norman, *Phys. Rev. Lett.* **85**, 3261 (2000).
- [109] J. Mesot, N. Metoki, M. Böhm, A. Hiess, and K. Kadowaki, *Physica C* **341**, 2105 (2000).
- [110] H. F. Fong, P. Bourges, Y. Sidis, L. P. Regnault, A. Ivanov, G. D. Gu, N. Koshizuka, and B. Keimer, *Nature* **398**, 588 (1999).
- [111] H. He, Y. Sidis, P. Bourges, G. D. Gu, A. Ivanov, N. Koshizuka, B. Liang, C. T. Lin, L. P. Regnault, E. Schoenherr, and B. Keimer, *Phys. Rev. Lett.* **86**, 1610 (2001).
- [112] W. Rantner and X.-G. Wen, *Phys. Rev. Lett.* **85**, 3692 (2000).
- [113] M. R. Norman, *Phys. Rev. B* **61**, 14751 (2000).
- [114] Y. Tanaka and S. Kashiwaya, *Phys. Rev. Lett.* **74**, 3451 (1995).
- [115] T. Timusk and B. Statt, *RPP* **62**, 61 (1999).
- [116] P. Lee, Y. Gao, H. S. Sheu, V. Petricek, R. Restori, P. Coppens, A. Darovskikh, J. C. Phillips, A. W. Sleight, and M. A. Subramanian, *Science* **244**, 62 (1989).
- [117] J. Lee, K. Fujita, K. McElroy, J. A. Slezak, M. Wang, Y. Aiura, H. Bando, M. Ishikado, T. Masui, J.-X. Zhu, A. V. Balatsky, H. Eisaki, S. Uchida, and J. C. Davis, *Nature* **442**, 546 (2006).
- [118] P. W. Anderson, *Science* **235**, 1196 (1987).
- [119] T. A. Maier, M. Jarrell, and D. J. Scalapino, *Phys. Rev. B* **74**, 094513 (2006).
- [120] C. Gros, *Phys. Rev. B* **38**, 931 (1988).
- [121] H. Yokoyama and H. Shiba, *J. Phys. Soc. Jpn.* **57**, 2482 (1988).
- [122] A. Paramekanti, M. Randeria, and N. Trivedi, *Phys. Rev. B* **70**, 054504 (2004).
- [123] T. Giamarchi and C. Lhuillier, *Phys. Rev. B* **43**, 12943 (1991).
- [124] S. Sorella, G. B. Martins, F. Becca, C. Gazza, L. Capriotti, A. Parola, and E. Dagotto, *Phys. Rev. Lett.* **88**, 117002 (2002).
- [125] H. Yokoyama, Y. Tanaka, M. Ogata, and H. Tsuchiura, *J. Phys. Soc. Jpn.* **73**, 1119 (2004).
- [126] H. Otsuka, *J. Phys. Soc. Jpn.* **61**, 1645 (1992).
- [127] M. Dzierzawa, D. Baeriswyl, and M. Di Stasio, *Phys. Rev. B* **51**, 1993(R) (1995).
- [128] A. Toschi, M. Capone, M. Ortolani, P. Calvani, S. Lupi, and C. Castellani, *Phys. Rev. Lett.* **95**, 097002 (2005).

- [129] W. Meevasana, X. J. Zhou, S. Sahrakorpi, W. S. Lee, W. L. Yang, K. Tanaka, N. Mannella, T. Yoshida, D. H. Lu, Y. L. Chen, R. H. He, H. Lin, S. Komiya, Y. Ando, F. Zhou, W. X. Ti, J. W. Xiong, Z. X. Zhao, T. Sasagawa, T. Kakeshita, K. Fujita, S. Uchida, H. Eisaki, A. Fujimori, Z. Hussain, R. S. Markiewicz, A. Bansil, N. Nagaosa, J. Zaanen, T. P. Devereaux, and Z.-X. Shen, *Phys. Rev. B* **75**, 174506 (2007).
- [130] A. Trokiner, L. Le Noc, J. Schneck, A. M. Pougnet, R. Mellet, J. Primot, H. Savary, Y. M. Gao, and S. Aubry, *Phys. Rev. B* **44**, 2426 (1991).
- [131] J.-P. Locquet, J. Perret, J. Fompeyrine, E. Mächler, J. W. Seo, and G. Van Tendeloo, *Nature* **394**, 453 (1998).
- [132] E. Orignac and T. Giamarchi, *Phys. Rev. B* **56**, 7167 (1997).

Project 3 Crystal growth

Project leader: M. Forró (EPFL)

Participating members: J. Karpinski (ETHZ), D. van der Marel (UniGE), G. Margaritondo (EPFL), J. Mesot (PSI). Contribution from Ø. Fischer (UniGE).

Summary and highlights: During the first and the second phases of MaNEP the importance of having a co-ordinated effort on crystal growth was recognized and progressively developed in terms of infrastructure and staff. Traditionally, good crystal growth laboratories were present at ETHZ and EPFL. Very positively, strong single crystal growth programs were developed in the last period at PSI and UniGE. At PSI (group leader J. Mesot) four-mirror optical furnaces were installed, with K. Conder, as a leading scientist for synthesis. At UniGE (group leader D. van der Marel) besides the Czochralski method using Hukin crucible, a high temperature image furnace has been purchased for traveling solvent floating zone growth of the majority of materials. The leading scientist is E. Giannini. At the EPFL (group leader G. Margaritondo) the major techniques are the self-flux and the chemical vapor transport methods, and ~ 25 furnaces are used for these purposes. The leading scientist is H. Berger. At ETHZ, under the command of J. Karpinski, the high pressure crystal growth is the major specialty. Crystalline phases which cannot be synthesized otherwise are successfully prepared in this laboratory. With all these developments we can make a safe statement that crystal growth is a strength of the Swiss solid state community. Here below, a very selective list of the crystals synthesized in the last years will be presented. For an easier overview, they are divided into the following categories: 1. Novel superconducting materials; 2. Magnetic materials; 3. Low-dimensional conductors; 4. Materials beyond the foreseen plan. Over 140 materials in single crystalline form are available for internal and external collaborations, and the full list (with chemical composition, preparation method, basic properties, contact person to ask for it) can be consulted in the *Single Crystal Catalog* of MaNEP (see pages 99–101). The in-depth studies performed on these crystals are given in Projects 1 and 2.

1 Novel superconducting materials

Studying novel superconductors, from theory through experiments to applications, has an important place in the activity of the NCCR. This is especially expressed in this project, where high quality single crystals are grown with original techniques, e.g. high pressure synthesis. Lot of emphases are put on the mastering of the chemical homogeneity of optimally and underdoped cuprate superconductors, on the doping of MgB_2 and on superconducting pyrochlore osmates.

1.1 Crystal growth of Bi-based superconducting cuprates

(contribution: D. van der Marel)

The most productive crystal growth activity of the laboratory at UniGE concerns the family of superconducting compounds $\text{Bi}_2\text{Sr}_2\text{Ca}_{n-1}\text{Cu}_n\text{O}_{4+2n+\delta}$ ($n = 1, 2, 3$; abbreviated by BiSCCO 2201, 2212 and 2223, respectively). Crystals of all the members of this family have been grown (Fig. 1, right panels) by means of the Travelling Solvent Floating

Zone (TFZ) method using a 2-mirror furnace (Fig. 1, left panel). In particular, crystals of $\text{Bi}_2\text{Sr}_2\text{Ca}_2\text{Cu}_3\text{O}_{10+\delta}$ ($T_c = 110$ K) of unique size

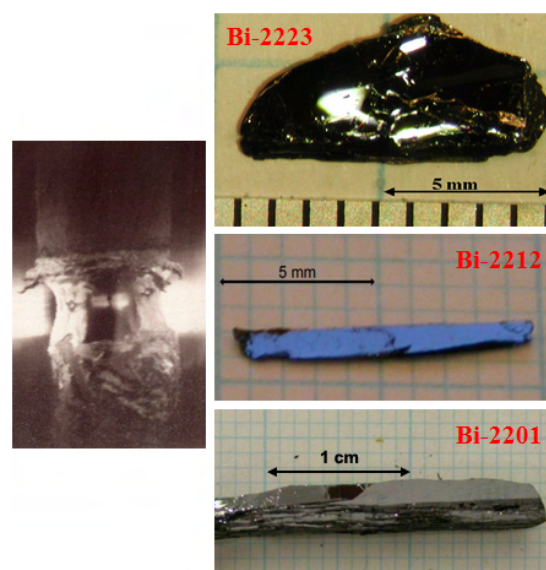


Figure 1: Crystals of BiSCCO (right panels) grown by the TFZ method in a mirror furnace (left panel).

and quality have been grown.

A wide and fruitful collaboration among various MaNEP partners is working ahead since few years on these materials and has led to outstanding experimental studies in optics, as well as in local spectroscopy, photoemission and structural investigations. From high-resolution single-crystal X-ray diffraction data, the modulated structure has been solved and conveniently described in a 5-fold orthorhombic supercell in the space group P222 [1]. The relationship between doping, structure and properties has been investigated: as-grown crystals were subjected to long (10 days) post-annealing under controlled oxygen partial pressure in order to tune and homogenize the doping level. The high homogeneity of these crystals is shown by the narrow (0.5–2 K) transitions of the susceptibility at T_c . The $n = 3$ phase (2223) is less sensitive to oxygen doping than the other two compounds of the same family, as shown in Fig. 2 [2]. The effect of oxygen doping on the superconducting properties, namely the critical temperature and the vortex lattice, has been studied. Scanning tunnelling microscopy and spectroscopy (STM/STS) have been performed on these crystals, achieving the atomic resolution and making possible the understanding of the peculiarities of the STS spectra (see Project 2 for details).

Crystals of the 1-layer compound $\text{Bi}_2\text{Sr}_2\text{CuO}_{6+\delta}$ have been grown with a maximum $T_c = 11$ K, and successfully overdoped down to a critical temperature of about 5 K. Despite of the strong effort done by several authors in growing La and/or Pb-doped $\text{Bi}_2\text{Sr}_2\text{CuO}_{6+\delta}$, the pure compound has been a little disregarded in the past, mainly because of the difficulty in crystal growth. These crystals will make possible to study the transition from the superconducting state to a FL-like state in

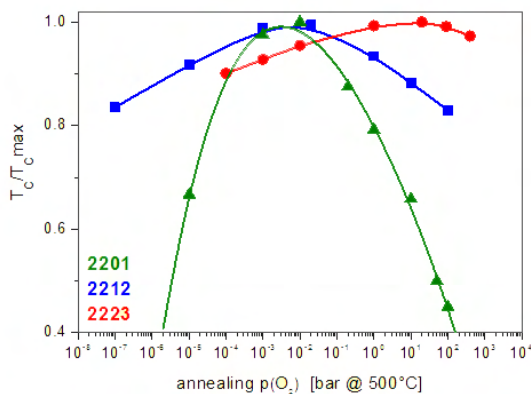


Figure 2: Oxygen doping dependence of T_c in Bi2201, Bi2212, and Bi2223 crystals.

the overdoped regime, and, thanks to the low critical field and temperature, to access the normal state at low temperatures.

1.2 Synthesis and bulk properties of oxychloride superconductor $\text{Ca}_{2-x}\text{Na}_x\text{CuO}_2\text{Cl}_2$
(contribution: J. Karpinski)

$\text{Ca}_{2-x}\text{Na}_x\text{CuO}_2\text{Cl}_2$ (Na-CCOC) is a structural analogue to the cuprate superconductor $\text{La}_{2-x}\text{Sr}_x\text{CuO}_4$ (La214) with Cl atoms replacing oxygen on the apical sites. Na-CCOC is a model system for studying the electronic state of doped CuO_2 planes and for establishing the role of the apical sites in high-temperature superconductivity. Despite of similarity to other cuprate superconductors, properties of the Na-CCOC compound are not well characterized due to difficulties in obtaining single crystals which can be grown only at high pressure and are very hygroscopic. Investigation of single crystals with oxygen and halogen atoms on the apical sites might help to clarify the origin of superconductivity in cuprates. With the aim of growing large crystals of Na-CCOC, suitable for physical measurements, we carried out a systematic investigation of the parameters controlling the growth of crystals, including temperature, pressure, composition, reaction time, and heating/cooling rate. A series of polycrystalline samples and submillimeter size single crystals of a cuprate oxychloride $\text{Ca}_{2-x}\text{Na}_x\text{CuO}_2\text{Cl}_2$ (Na-CCOC), with values of Na content ranging from underdoped to optimally doped regions, were synthesized at pressure and temperature ranges of 30–55 kbar and 1250–1700 °C (Fig. 3). Experiments performed on samples grown at 45 kbar show that the Na content depends not only on the synthesis pressure, as it was established before [23, 24], but also on the reaction temperature and time. A systematic variation of the transition temperature T_c with a maximum value of 29 K for $x \approx 0.20$ has been found as a function of Na content (Fig. 4).

In order to check the role of the apical oxygen for high-temperature superconductivity, we

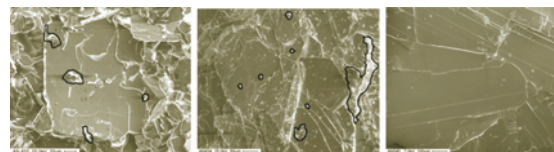


Figure 3: From left to right. SE images of $\text{Ca}_{2-x}\text{Na}_x\text{CuO}_2\text{Cl}_2$ with $x \approx 0.18$ and $T_c = 27\text{K}$; $x \approx 0.11$ and $T_c = 13\text{K}$; $x \approx 0.06$, not superconductor. Some rests of solidified flux can be seen on the surface of crystals (marked by black lines).

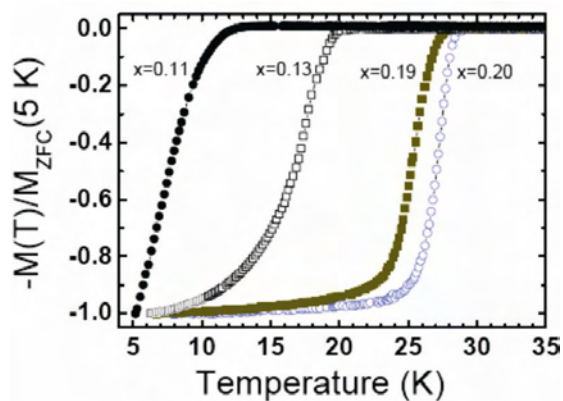


Figure 4: Normalized diamagnetic signal for a series of $\text{Ca}_{2-x}\text{Na}_x\text{CuO}_2\text{Cl}_2$ samples with various Na content (x) grown at high pressure. The highest $T_{c,on} = 29.0$ K was observed for optimally doped composition $\text{Ca}_{1.8}\text{Na}_{0.2}\text{CuO}_2\text{Cl}_2$.

performed muon-spin rotation and magnetization studies of the in-plane magnetic penetration depth λ_{ab} for $\text{Ca}_{2-x}\text{Na}_x\text{CuO}_2\text{Cl}_2$ samples with $x \approx 0.11, 0.12, 0.15, 0.18,$ and 0.19 . Based on a comparison of the present Na-CCOC data with the data of $\text{La}_{2-x}\text{Sr}_x\text{CuO}_4$ cuprate superconductors, it is concluded that replacing the apical oxygen by chlorine decreases the coupling between the superconducting CuO_2 planes, leading to an enhancement of the two-dimensionality of Na-CCOC. The torque studies imply that the anisotropy coefficient $\gamma = 84(1)$ of $\text{Ca}_{1.82}\text{Na}_{0.18}\text{CuO}_2\text{Cl}_2$ single crystals is much more enhanced compared to the structurally related $\text{La}_{1.82}\text{Sr}_{0.18}\text{CuO}_4$, where, for the same doping, γ is much lower.

1.3 $\text{La}_{2-x}\text{Sr}_x\text{CuO}_4$ (contribution: J. Mesot)

A series of single crystals of $\text{La}_{2-x}\text{Sr}_x\text{CuO}_4$ ($x = 0.08, 0.1, 0.17, 0.21$) superconductor were grown in order to study an oxygen isotope effect on a magnetic penetration depth. This work is just at the beginning and will be continued (in collaboration with a group of Prof. H. Keller, University of Zurich).

Inelastic neutron scattering study of vortex structure of $\text{La}_{1.9}\text{Sr}_{0.1}\text{CuO}_4$ (about 5 crystals have to be measured in one time) will be done in 2008.

1.4 Crystal growth and substitutions in MgB_2 (contribution: J. Karpinski)

MgB_2 crystals grow at $T > 1800$ °C. Our crystal growth experiments have been performed in the pressure range of 25–30 kbar using the

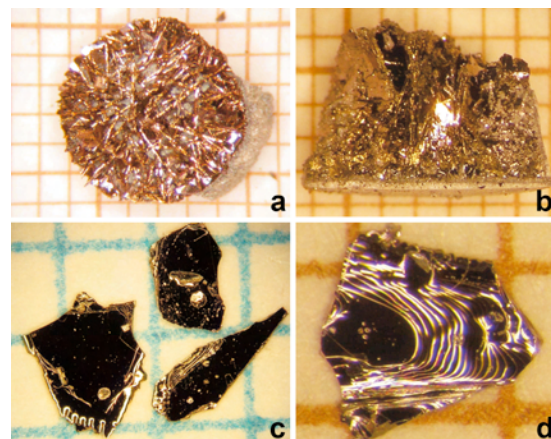


Figure 5: MgB_2 crystals grown in BN crucible: a) view from the top, b) view from the side, c) and d) crystals after separation. Scale is 1 mm.

anvil system (Fig. 5). A doping/substitution dependence of the superconducting properties was performed for a large variety of elements. Magnetic (Mn, Fe) and non-magnetic (Al, C, Li) ions have been substituted during crystal growth. Various levels of substitutions have been done with a goal to obtain homogeneous crystals for physical studies. This is a difficult task due to complicated chemistry leading to precipitation of different phases in the crystals. In the case of Mn and C substitution it was possible to grow single phase crystals in a substitution range up to $x = 0.07$ and $x = 0.3$ in $\text{Mg}_{1-x}\text{Mn}_x\text{B}_2$ and $\text{MgB}_{2-x}\text{C}_x$ respectively, while Al substitution turns out to be more difficult and single phase crystals of $\text{Mg}_{1-x}\text{Al}_x\text{B}_2$ were grown up to $x = 0.3$. Fe substitution was possible up to $x = 0.03$, but many $\text{Mg}_{1-x}\text{Fe}_x\text{B}_2$ crystals contain intergrowth of non-superconducting phase with larger content of Fe. Li up to $x = 0.12$ has been substituted in $\text{Mg}_{1-x}\text{Li}_x\text{B}_2$ crystals. Double Li and C as well as Li and Al substitutions have been performed in order to investigate the effects of hole and electron doping effects. Li and C contents have been determined from the single crystal X-ray refinement, while Al, Mn and Fe content have been determined with EDX analysis.

Substitutions change the electronic structure, the superconducting gap value, the type of defects and their density, the inter- and intra-band scattering, and thus the superconducting properties such as T_c , the upper critical field, H_{c2} , and its anisotropy. Figure 6a summarizes our results on the influence of substitutions in MgB_2 single crystals on T_c . Doping with electrons, introduced by C or Al substitution, decreases T_c as a result of increase of carrier con-

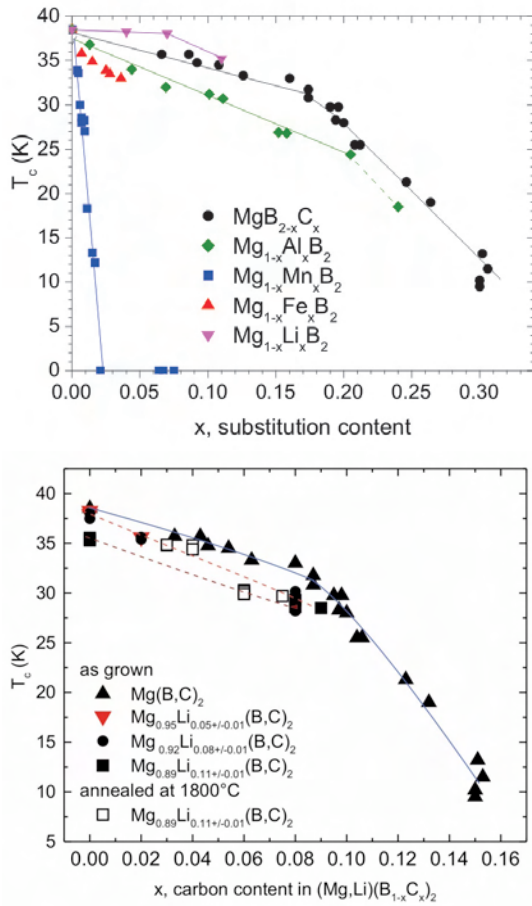


Figure 6: a) T_c as a function of various substitutions in MgB_2 . Aluminum and carbon dope MgB_2 with electrons. Li^{+1} dopes MgB_2 with holes, while isovalent Mn^{+2} is a magnetic ion. b) T_c dependence on substitution of C (triangles) or co-substitution of C and Li (reversed triangles, circles, and squares). Dash lines show the same level of Li content for various level of C substitution.

tent as well as a result of the introduction of new scattering centers. For the Li substitution, T_c also decreases with the increasing Li content, however the rate of this decrease is much lower than for C or Al substitutions. This reduction of T_c , which is accompanied by the increased or decreased number of charge carriers, seems to reveal MgB_2 as the close to optimally doped compound. For the Mn substitution the change is much more rapid because of the magnetic pair breaking. Co-doping with holes and electrons is a very interesting case, because it can bring new information about the role of electronic band doping and of intra- and interband scattering. In the crystals where Li and C are substituted simultaneously one can expect the compensation of the electron doping effect and an increase of T_c . However, the T_c reduction in co-doped crystals is a sum of

the T_c reduction of separate C and Li doping (Fig. 6a and b). The observed behavior can be explained as a result of two effects, influencing both T_c and H_{c2} . The first one is the doping related to the changes in the carrier concentration, which may lead to the decrease or to the increase of T_c . The second one is related to the introduction of new scattering centers leading to the modification of the interband and/or intraband scattering and therefore, to changes in the gap structure and to the reduction of T_c . Electrical transport measurements have shown an increase of resistivity in Li doped crystals and even an higher increase of resistivity in crystals co-doped with Li and C. This indicates an enhanced scattering due to defects introduced by substitutions including distortion of the lattice. In the crystals substituted with Li and C, the increase of T_c as a result of annealing at 1800 °C is observed. This leads to the conclusion that distortion of the lattice being a result of Li substitution plays an important role in the modification of superconducting properties, and that not only the band filling effect is important.

We studied the influence of high temperature vacuum annealing on the crystal structure and superconducting properties of MgB_2 single crystals, as well. MgB_2 single crystals were annealed in vacuum (4×10^{-6} mbar) at various temperatures between 800 and 1000 °C for 2 hrs followed by cooling to room temperature. The present results imply that MgB_2 is a stable phase up to 975 °C.

1.5 Crystal growth of superconducting pyrochlore osmates (contribution: J. Karpinski)

We were investigating the growth of single crystals of osmates AOs_2O_6 ($A = K, Rb$) with the β -pyrochlore structure. Single crystals of superconducting KOs_2O_6 , and $RbOs_2O_6$ with sizes up to 0.4 mm have been grown in sealed quartz ampoule starting from Os metal and KO_2 or Rb_2O respectively. The process of crystal growth of $RbOs_2O_6$ has been optimized by using a temperature gradient. Single crystal X-ray diffraction studies have shown that both KOs_2O_6 and $RbOs_2O_6$ crystallize in the β -pyrochlore structure [3, 4]. Magnetic moment measurements show superconducting transitions at $T_c = 9.65$ K and $T_c = 6.18$ K for KOs_2O_6 and $RbOs_2O_6$ respectively. These compounds and their synthesis are extensively studied in Project 4.

2 Magnetic materials

Within MaNEP there is a strong interest for magnetic materials both for experimental and theoretical studies. In the second phase of the NCCR the crystal growers made a considerable progress at PSI, EPFL and UniGE in synthesis of high quality crystals of a broad range of magnetic materials.

2.1 Crystal growth of doped $\text{Sr}_{14}\text{Cu}_{24}\text{O}_{41}$ “ladder” compounds

(contribution: D. van der Marel)

Doping the Sr atomic site in $\text{Sr}_{14}\text{Cu}_{24}\text{O}_{41}$ with one or more elements (Ca, Bi, Y, Pb, ...) is expected to modify the coupling between the CuO chains and Cu_2O_3 ladders and change the carrier doping, thus inducing superconductivity in ladder compounds [25]. Doping with either Bi, Pb, or Y was found to modify the incommensurately modulated structure of the “ladder” compound. This study was carried out in collaboration with the University of L’viv, Ukraine [5]. Crystals of Bi- and Ca-doped $\text{Sr}_{14}\text{Cu}_{24}\text{O}_{41}$ were successfully grown at UniGE by using the floating zone technique in a 2-mirror furnace. An overpressure of flowing pure oxygen ($p(\text{O}_2) = 3$ bar, 0.5 l/h) was applied during crystal growth. Typically 3–5 mm-size crystals of $(\text{Sr}_{5.6}\text{Ca}_{7.6}\text{Bi}_{0.7})\text{Cu}_{24}\text{O}_{41}$ are cleaved from the crystallized seed rod.

2.2 Transition Metal Monosilicides

(contribution: D. van der Marel)

Transition Metal Monosilicides TMSi ($\text{TM} = \text{Cr}, \text{Mn}, \text{Fe}, \text{Co}$) with the FeSi -type structure “B20” attract a lot of attention because of the intriguing electronic properties related to the spin-singlet formation and various ground states. So far, the most studied TMSi compounds are MnSi , an itinerant helimagnetic metal, FeSi , a small gap semiconductor, and the solid solution $(\text{Fe},\text{Co})\text{Si}$, a helimagnetic material with a half-metallic behaviour. We have undertaken a study of the whole family of TMSi and the solid solutions $\text{TM}'\text{-TM}''\text{-Si}$, aiming at the full understanding of their transport and magnetic properties. When doping the TMSi compounds with Ni, a structural transition occurs from the “B20” to the MnP-type “B31” structure. We have investigated the stability of the Ni-doped B20 structure and the pseudo-binary phase diagram of the Co-Ni-Si system. Single crystals of CoSi , $(\text{Fe},\text{Co})\text{Si}$, and $(\text{Co},\text{Mn})\text{Si}$ have been grown.

a) *The $\text{Co}_{1-x}\text{Ni}_x\text{Si}$ solid solution* A complete set of samples of the series $\text{Co}_{1-x}\text{Ni}_x\text{Si}$ has

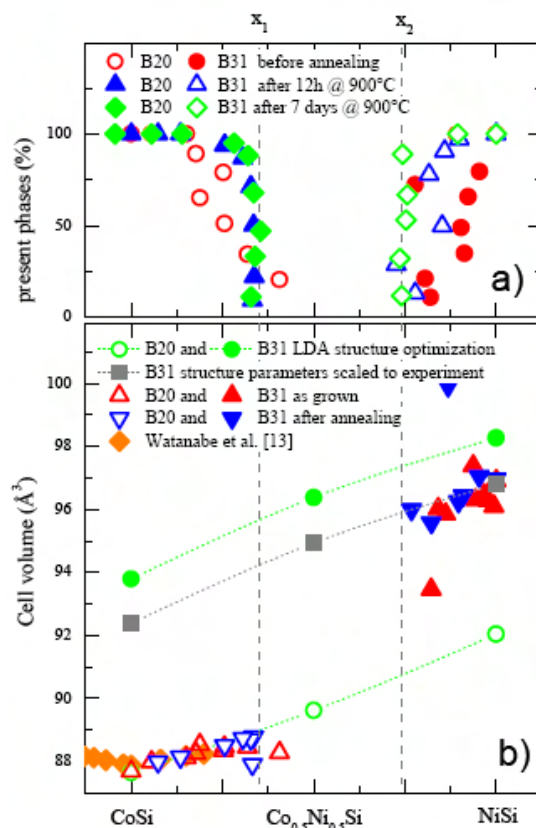


Figure 7: (a) Molar fraction of the B20 and B31 phases in the sample. (b) Experimental and LDA predicted values of the cell volume for B20 (open symbols) and B31 (closed symbols) structures.

been synthesized and a systematic study of phase formation under various annealing conditions has been carried out in order to understand the reason of the structural transition when x goes from 0 to 1. Our study has revealed a limit in the solubility of Ni in the CoSi B20 structure of about 17.5 at.%, and of Co in the NiSi B31 structure of about 13 at.%. For $0.35 < x < 0.74$ both the B20 and B31 phases are present in the samples at their respective limits of solubility. The experimental study was supported by first principle calculations of the structural parameters, which well predict the structural instability. The molar fractions of the B20 and B31 phases as a function of the composition are shown in Fig. 7. [6]

b) *Crystal growth of $\text{Fe}_{1-x}\text{Co}_x\text{Si}$* Large and pure crystals of TMSi are needed for the investigation of the magnetic properties of such family of compounds. The availability of single crystals guarantees the chemical order of the solid solutions and allows performing neutron scattering experiments. Single crystals of $\text{Fe}_{1-x}\text{Co}_x\text{Si}$ have been grown with the Czochralski crystal pulling technique from a



Figure 8: Crystal growth of $(\text{Fe,Co})\text{Si}$ from levitating melt (left). As-grown crystal boule of $\text{Fe}_{0.6}\text{Co}_{0.4}\text{Si}$ (right).

levitating melt using an RF-induction furnace. This growth technique has proved to be very useful for these materials, because it prevents the crystal from reacting with the crucible materials and allows us to grow larger crystals than the floating zone method. An example of the as-grown crystal of $\text{Fe}_{0.6}\text{Co}_{0.4}\text{Si}$ is shown in Fig. 8. The study of the electronic properties of these compounds has been carried out by optical spectroscopy (as reported in Project 1).

2.3 $\text{R}\text{BaCo}_2\text{O}_{5+x}$ (R = Rare earth element) (contribution: J. Mesot)

Layered cobalt oxides have a perovskite-derived structure similar to those of high temperature superconductors. Despite being not superconducting, these compounds have interesting physical properties (magnetoresistance, metal-insulator transition, ionic conductivity) [7]. We made lots of experiments to optimize growth conditions in order to obtain big single crystals of good quality [8]. By increasing the diameter of a feeding rod and decreasing a growth rate (0.5 mm/h) crystals of a good quality can be obtained. We have grown single crystals of $\text{TbBaCo}_2\text{O}_{5+x}$, $\text{Tb}_{0.9}\text{Dy}_{0.1}\text{BaCo}_2\text{O}_{5+x}$ and $\text{NdBaCo}_2\text{O}_{5+x}$. Oxygen stoichiometry was adjusted to 5.5 by annealing in different gas-atmospheres and temperatures depending on the rare earth in the structure. Magnetic and electric transport measurements in external magnetic fields were performed on $\text{TbBaCo}_2\text{O}_{5.5}$ single crystal [9], crystal and magnetic structure were studied by means of X-ray and neutron powder diffraction and muon spin spectroscopy.

2.4 $\text{R}\text{BaMn}_2\text{O}_6$ (contribution: J. Mesot)

$\text{R}\text{BaMn}_2\text{O}_6$ is an interesting candidate for which the magnetic and orbital degrees of freedom are strongly linked to each other. The material shows a charge and orbital ordering transitions similar as other half doped manganates. In this case however, an orbital reorientation is proposed to occur at the antiferromagnetic transition temperatures, indicative of strong correlations between the two order parameters. Using resonant soft x-diffraction in combination with resonant hard X-ray diffraction, it will allow to entangle the different effects between orbitals, Jahn-Teller distortion, structure and magnetism in this material, and to test recent prediction on the driving force of these phase transitions. First resonant soft X-ray powder diffraction study to determine the orbital ordering in A-site ordered $\text{Sm}\text{BaMn}_2\text{O}_6$ were already successfully done [10] and will be continued on a single crystal (already grown) of the same composition and with another rare earth (to be grown in 2008).

2.5 LaCoO_3 , $\text{La}_{1-x}\text{Sr}_x\text{CoO}_3$ (contribution: J. Mesot)

Large single crystals of LaCoO_3 and $\text{La}_{1-x}\text{Sr}_x\text{CoO}_3$ were grown (Fig. 9) for studying Co spin-state transitions using resonant X-ray absorption at the Co K edge [11] and inelastic neutron scattering [12]. A novel inelastic excitation in LaCoO_3 was observed, which is due to a thermally excited magnetic state in Co^{3+} . This confirms the presence of a thermally induced spin-state transition at $T \sim 100$ K from the low spin (LS) Co^{3+} to a magnetic high spin (HS) or intermediate spin (IS) state. Further inelastic neutron scattering study of low energy field excitations were performed on the lightly Sr doped $\text{La}_{0.998}\text{Sr}_{0.002}\text{CoO}_3$ [13]. In contrast to the parent compound LaCoO_3 an inelastic peak at energy transfer ~ 0.75 meV was found. This can be explained assuming that the hole doping of LaCoO_3 leads to the creation of a magnetic polaron and hence to the low-to-high spin state transition on the relevant Co sites.



Figure 9: Single crystal of LaCoO_3 .

2.6 YMnO₃

(contribution: J. Mesot)

YMnO₃ is a geometrically frustrated two-dimensional (2D) antiferromagnet, which consists of weakly coupled triangular layers of $S = 2$ spins. Our inelastic neutron scattering studies [14] done on single crystal of YMnO₃ have found evidence for coexisting three-dimensional (3D) and 2D fluctuations. More recent neutron studies done on powder [15] show that the ordered moment decreases with increasing hydrostatic pressure. Later magnetism in geometrically frustrated YMnO₃ (single crystal) under hydrostatic pressure was studied with muon spin relaxation [26]. Below $T_N \approx 70$ K muon-spin relaxation data show two oscillatory relaxing signals due to magnetic order, with no purely relaxing signals resolvable (which would require different coexisting spin distributions). The transition temperature T_N increases with applied hydrostatic pressure, even though the ordered moment decreases. These results suggest that pressure increases both the exchange coupling between the layers and the frustration within the layers.

2.7 SrCu₂(BO₃)₂

(contribution: J. Mesot)

Large single crystals of SrCu₂(BO₃)₂ were grown by applying a very small growth rate (0.25 mm/h). The structure of this compound is a physical realization of the Shastry-Sutherland model. It is a quasi-two dimensional spin system with a singlet dimer ground state. The magnetic phase diagram of the system was studied by means of inelastic neutron scattering, muon spin resonance and magnetization measurements under different pressures. Crystal structure modification under hydrostatic pressure was studied with neutron diffraction. Additional experiments with a newly designed piston-cell up to ~ 20 kbar will be done in 2008 to complete a phase diagram and publish the data (in collaboration with a group of Prof. H. M. Ronnøw, EPFL).

2.8 LuFe₂O₄

(contribution: J. Mesot)

The ferroelectricity of this multiferroic material appears to result from Fe²⁺ and Fe³⁺ ions. In order to understand the field dependence of a magnetic order and to determine the magnetic structure, neutron diffraction experiments (in collaboration with a group of Prof. M. Kenzelmann, ETHZ) and resonant soft x-diffraction experiments (in collaboration with a group of

Dr. U. Staub (SLS, PSI)) were already done. Different field and temperature dependent behavior of two magnetic peaks have been observed. This fact allows to conclude that two magnetic order parameters exist in this system. This work will be continued in 2008.

2.9 Na_xCoO₂

(contribution: J. Mesot)

X-ray photoelectron diffraction measurements have been performed on Na_xCoO₂ single crystal at room temperature to study the atomic structure near the surface. Data are compared with single scattering simulations based on the P6₃/mmc and the R $\bar{3}m$ unit cells which are bulk atomic structures proposed in the literature for different dopings x . The R $\bar{3}m$ symmetry was discarded and the P6₃/mmc symmetry was validated for surface unit cells. This is in contradiction with bulk measurements, revealing a drastic change in the surface structure. This work (in collaboration with a group of Prof. Ph. Aebi, Neuchatel) will be continued in 2008.

2.10 Single crystals of LiCu₂O₂

(contribution: G. Margaritondo)

Large specimens ($4 \times 4 \times 2$ mm³) of LiCu₂O₂ helimagnet, an antiferromagnetic $S = 1/2$ spin-chain quasi-one-dimensional compound were synthesized by H. Berger (Fig. 10). The ARPES spectra show several dispersive branches associated with hybrid copper-oxygen states. The occurrence of the valence band maximum halfway between the center and the edge of the Brillouin zone, and the complex spectral line shapes are not reproduced by the existing calculations of the electronic structure. They can be interpreted within a one-dimensional scenario of strongly

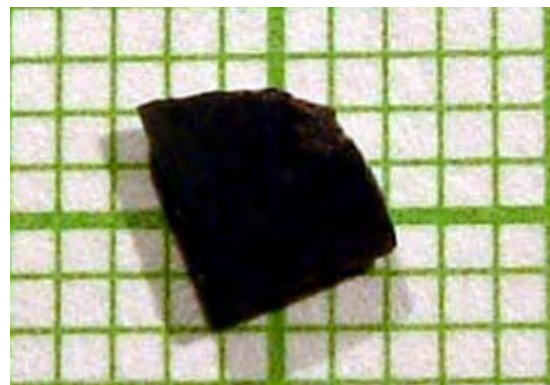


Figure 10: Large single crystals of LiCu₂O₂ grown by chemical vapor transport method.

correlated antiferromagnetic insulators. The combination of ARPES and optics allowed us to determine the 1.95 eV charge-transfer gap. Moreover, the temperature-dependent optical conductivity bears signatures of the three different magnetic phases of this material. The field dependence of the electron spin resonance of LiCu_2O_2 was also investigated for the first time [16].

2.11 Single crystals of diverse magnetic compounds

(contribution: G. Margaritondo)

Lately, a lot of attention has been devoted to oxohalides (e.g. $\text{Cu}_2\text{Te}_2\text{O}_5\text{X}_2$ ($\text{X} = \text{Cl}, \text{Br}$)) with their rather puzzling magnetic properties. The compounds of interest include, among others: $\text{Ni}_5(\text{TeO}_3)_4\text{Cl}_2$, $\text{Ni}_5(\text{TeO}_3)_4\text{Br}_2$, $\text{Co}_5(\text{TeO}_3)_4\text{X}_2$ ($\text{X} = \text{Cl}, \text{Br}$), $\text{Cu}_3(\text{SeO}_3)_2\text{Cl}_2$ (Fig. 11). Initially, mainly of interest to theorists (F. Mila), oxohalides were in the past two years also systematically studied by the group of J. Mesot (PSI). Moreover, the arrival of a new professor (H. Rønnow) to the IPMC-EPFL added an additional impetus to this activity.

Specifically, Rønnow *et al.* [17] have performed single crystal inelastic neutron scattering to study the excitation spectrum of the coupled tetrahedra system $\text{Cu}_2\text{Te}_2\text{O}_5\text{X}_2$ ($\text{X} = \text{Cl}, \text{Br}$). While the spectrum of $\text{Cu}_2\text{Te}_2\text{O}_5\text{Cl}_2$ behaves very similarly to the one of ordered low-dimensional antiferromagnet, the excitations of $\text{Cu}_2\text{Te}_2\text{O}_5\text{Br}_2$ have an unusual temperature dependence. They have established a qualitative relationship with previous bulk and transport measurements and proposed reminiscences of singlet-triplet energy levels as responsible for the unusual Br-compound spec-

trum above the ordering temperature.

Rønnow *et al.* [17] have also performed the SQUID magnetometry on $\text{Ni}_2\text{CuTe}_4\text{O}_{12}\text{Br}_2$ and $\text{Ni}_4\text{CuTe}_4\text{O}_{12}\text{Br}_2$, both new compounds, synthesised by vapor transport. The SQUID magnetometry was done on a 28.7 mg single crystal with one of the crystal axes parallel to the field. A cusp characteristic of antiferromagnetic ordering is observed at approximately 29 K. There is no apparent difference between the low and high field curves or the ZFC and FC curves, also implying the antiferromagnetic order. A Curie-Weiss fit of the inverse susceptibility gives a magnetic moment of $3.45\mu_B$, which is slightly larger than the spin only formula prediction of $3.26\mu_B$ for 1 Ni^{2+} and 0.25 Cu^{2+} moments. The Weiss constant is found to be $\Theta = -50$ K, consistent with the ordering temperature.

3 Low-dimensional conductors

The competition between several collective electronic states remains one of the main mechanisms for the formation of novel electronic phases. The quasi one- and two-dimensional compounds are a prime example of materials, where collective phenomena compete forming new phases. Several groups within MaNEP are interested in the study of competing interactions in such low-dimensional materials and they are served by high quality single crystal.

3.1 Transition metal dichalcogenides

(contribution: G. Margaritondo)

The weak interlayer interaction in transition metal dichalcogenides (TMD) renders them a rich playground for tuning with pressure. Structurally, the two most common types of TMD are the 2H and 1T polytypes. The main difference between these two types is the arrangement of the chalcogen atoms within the layers, which results in diverse electronic structures. Superconductivity was encountered in 2H-NbS₂ and 2H-TaS₂ among several others, all belonging to the 2H polytype [27]. Recently one of the 1T polytype compounds 1T-TiSe₂ was found to develop superconductivity upon doping with copper [28]. The phase diagram reported in this latter work bears a significant resemblance to the cuprate high-temperature superconductors, with the commensurate charge density wave (CDW) phase replacing antiferromagnetism. This provides additional parallels to the already observed link between the cuprate superconductors and some organic CDW systems [29, 30]. In both type of compounds the correlations due to the

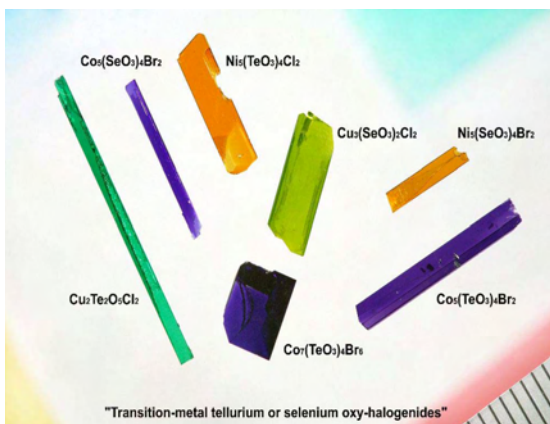


Figure 11: Selection of large single crystals of transition metal tellurium or selenium oxy-halide magnetic chain systems grown by chemical vapor transport method.

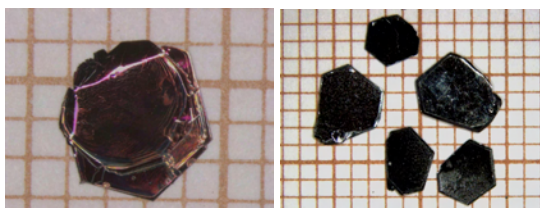


Figure 12: Crystals of $1T\text{-TiSe}_2$ and $2H\text{-NbSe}_2$ grown by chemical vapor transport method.

melting of the commensurate density-wave order are regarded as essential for the development of the superconductivity as well as peculiar normal state properties.

A large variety of TMD was synthesized. They include $1T\text{-TaS}_2$, $1T\text{-TaSe}_2$, $2H\text{-NbSe}_2$, $1T\text{-TiSe}_2$, $1T\text{-Ti}_{1-x}\text{Cu}_x\text{Se}_2$, $2H\text{-TaSe}_2$ (Fig. 12). It has resulted a strong collaboration between several groups within MaNEP, e.g. with the groups of L. Degiorgi, P. Aebi, M. Grioni and L. Forró. The scientific highlights are given in Projects 1 and 2.

3.2 BaVS_3 and BaVSe_3 single crystals (contribution: G. Margaritondo)

BaVS_3 consists of linear chains of vanadium atoms, surrounded by face-sharing sulfur octahedra, running parallel to the c -axis. Barium ions serve as spacers, separating the chains. The room temperature space group is $P6_3/mmc$ with two formula units per cell. At lower temperatures (at 240 K) a transition from a hexagonal to an orthorhombic cell was observed. The separation between the two nearest neighboring vanadium ions on the same chain at room temperature is 2.805 \AA , which is close to the atomic distance (2.624 \AA) in pure metallic BCC vanadium. The much larger distance between the chains, 6.73 \AA , suggests a quasi-one-dimensionality of the compound. At 70 K the sample shows a MI transition preserving some short range magnetic character. Further down in temperature, at $T_x = 30 \text{ K}$, a long range magnetic order sets in. The phase diagram is complex and the full understanding is missing. The physical properties are strongly affected by the impurity content. It is also known that BaVS_3 begins to lose sulfur at approximately 370 K under vacuum. In order to elucidate the intrinsic electrical and magnetic properties of this material, a strong effort was devoted to produce large ($5 \times 0.3 \times 0.3 \text{ mm}^3$) but homogeneous single crystals. It was achieved with chemical vapor transport method at EPFL (Fig. 13). In the last years their quality and size have been significantly improved, which enabled the first ARPES study

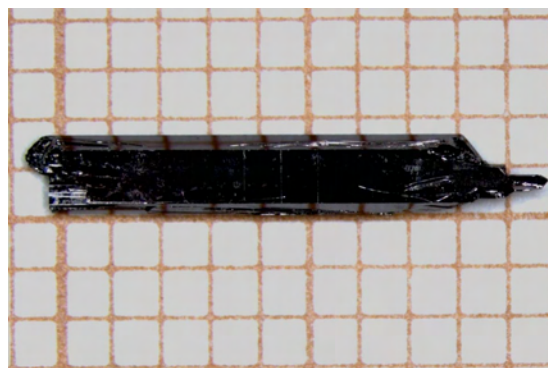


Figure 13: Large single crystals of BaVS_3 grown in tellurium flux.

of this compound [18] and the group of H.R. Ott has started detailed NMR study of a single crystal.

Replacing sulfur in BaVS_3 by isovalent but slightly bigger selenium brings a change in the overlap integrals of vanadium. BaVSe_3 has smaller direct overlap of V ions along the c -axis than BaVS_3 , and increased ligand-mediated overlap between chains. The enhanced dimensionality of the system leads to the absence of the MI transition. Instead, there is metal-metal phase transition at 43 K, accompanied by a ferromagnetic ground state.

Using newly synthesized single crystals of BaVSe_3 , high pressure measurements of resistivity and Seebeck coefficient were performed in the group of L. Forró. The crystals are of high quality, which reflects in the residual resistivity ratio of 30–50. As it is expected, the temperature and pressure dependence of the thermopower are different from what we have previously observed on the ceramic samples.

3.3 Synthesis of Chevrel phases and molybdenum chalcogenide cluster-based compounds (contribution: Ø. Fischer)

Recent STM [19], transport [20] and specific heat [21] experiments have re-awakened a long-dormant interest in the physics of Mo_6X_8 ($X = \text{S}, \text{Se}, \text{Te}$) cluster-based materials. This family of superconductors was intensively studied in the 1970s and 80s, falling out of favour following the discovery of the high- T_c cuprates. However, questions remain over the nature of superconductivity in these compounds, particularly in view of the extremely short coherence lengths and high upper critical fields exhibited by the Chevrel phases.

In collaboration with the Mineral Chemistry group at the University of Rennes, we have synthesised numerous molybdenum chalcogenide cluster compounds exhibiting a wide

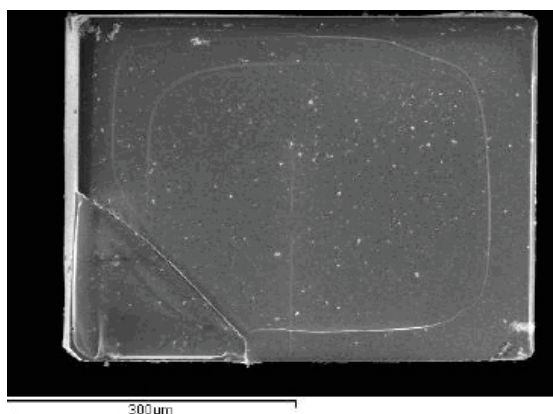


Figure 14: Photograph of a typical single crystal of $PbMo_6S_8$.

range of physical properties. Our initial priorities lay amongst the Chevrel phases MMo_6X_8 . Using molybdenum crucibles at high temperature (1600–1650 °C), we succeeded in producing high-quality large (0.5–2 mm) homogeneous single crystals of $PbMo_6S_8$ (Fig. 14) and $SnMo_6S_8$ with transition temperatures between 14 and 15 K, as well the solid solutions $Pb_xSn_{1-x}Mo_6S_8$ ($x = 0.2$ and 0.35) and $SnMo_6Se_2$.

Other related compounds with lower critical temperatures, including $InMo_6S_8$, Mo_6S_8 , Mo_6Se_8 , $Mo_6S_6Br_2$, $AgMo_6S_8$ and $LaMo_6S_8$, have also been synthesised. It is hoped that STM and high-resolution specific heat studies on these materials will finally reveal the mysteries of superconductivity in the Chevrel phases which have eluded researchers for over 30 years.

In contrast to quasi-3D MMo_6X_8 , the Mo_6X_8 clusters may also be stacked end-to-end to form $Mo_{6n}X_{6n+2}$ columns. An infinite-length condensation of molybdenum selenide clusters produces the $M_2Mo_6Se_6$ family, which includes the most strongly one-dimensional superconductors currently known: $Tl_2Mo_6Se_6$ ($T_c = 3 - 6$ K) and $In_2Mo_6Se_6$ ($T_c = 2.9$ K). For $M =$ Group IA metal (Na, K, Cs, Rb), the compounds become semiconducting at low temperature — it is unclear whether this is due to a Mott transition or the formation of a charge density wave. All quasi-one-dimensional compounds are synthesised in molybdenum crucibles at 1700 °C, except $In_2Mo_6Se_6$ which is made in a sealed silica tube at 1075 °C (Fig. 15). The related $Rb_{2n}(Mo_9S_{11})(Mo_{6n}S_{6n+2})$ ($n = 1 - 5$) family comprises finite-length cluster stacks with an intrinsic dimensionality therefore lying between the quasi-3D Chevrel phases and quasi-1D $M_2Mo_6Se_6$. These materials become superconducting at low temperature with T_c

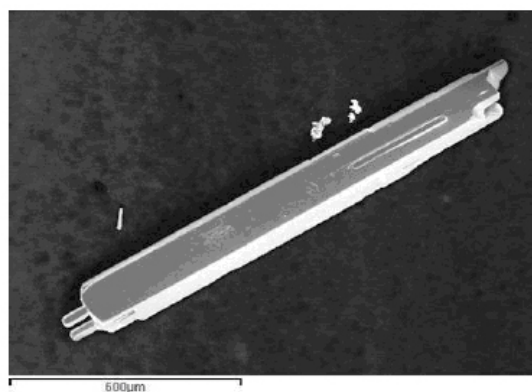


Figure 15: Photograph of a typical single crystal of $In_2Mo_6Se_6$.

between 4.2 and 11 K; they also boast high upper critical fields between 30 and 40 T. By varying the length of the cluster stacks, it is possible to chemically tune the dimensionality of these materials, offering a unique opportunity to examine the interplay between low dimensionality, superconductivity and other competing instabilities without applying pressure or uniaxial strain.

Two other cluster-based compounds have also been synthesised: $CsMo_{12}S_{14}$ and $Ba_4Mo_{12}S_{18}$ which become superconducting at $T_c = 7.5$ K and 5 K respectively. $CsMo_{12}S_{14}$ has trigonal symmetry (space group $P-31c$): unusually, it is composed of infinite-length chains of Mo_6S_8 units sharing two sulphur atoms, separated by channels in which the Cs ions are randomly distributed over two half-filled sites. A structural phase transition resulting in the ordering of the Cs ions takes place below room temperature.

In contrast, $Ba_4Mo_{12}S_{18}$ is hexagonal and crystallises with space group $P63/mmc$. It is formed from dimeric $(Mo_6)_2$ clusters, exhibits metallic behavior at room temperature and is not believed to undergo any structural phase transition prior to superconductivity. Using sealed molybdenum crucibles at 1500 °C, we have succeeded in producing high-quality single crystals of size approximately 1 mm. It is hoped that these new materials will enhance our understanding of the factors influencing superconductivity throughout the molybdenum chalcogenide cluster family.

4 Materials beyond the foreseen plan

4.1 Crystal growth of elemental bismuth (contribution: D. van der Marel)

Bismuth is a semimetal with exceptional properties like large magnetoresistance and

pressure-induced metal-to-insulator transitions. This is due to its very low carrier density and effective mass of the electrons. Single-crystal bismuth was grown by a modified Bridgman-Stockbarger technique in a vertical three-zone furnace. A silica tube filled with 5N-pure Bi powder and sealed under vacuum was heated above the melting point of Bi and slowly cooled in a temperature gradient of 10-15 °C/cm at a rate of 30 °C/h. Bismuth is a very soft material and the quality of the samples is strongly affected by mechanical stress during handling and cutting. The crystals were cleaved from the as-grown boule along a plane perpendicular to the trigonal direction [001] at LN₂ temperature. X-ray diffraction revealed that the mirrorlike cleavage surfaces were planes perpendicular to the trigonal axis which were subsequently used as reflecting surfaces for optical experiments. A detailed optical study of these crystals has been performed using reflectivity and ellipsometry, and has provided the evidence of electron-plasmon scattering [22] (see MaNEP Project 1).

4.2 Single crystals of TiO₂

(contribution: G. Margaritondo)

Titanium dioxide occurs in three crystalline modifications: rutile (tetragonal), brookite (orthorhombic) and anatase (tetragonal). The last two less dense phases are metastable and slowly convert to rutile on annealing. Most sample preparation and growth techniques directly yield the rutile phase so that rutile is the most extensively investigated form. Nevertheless, anatase works much better in photovoltaic applications and as a dilute magnetic semiconductor. Especially for this latter purpose we have re-lunched its synthesis in single crystalline form, together with rutile with different dopings (Fig. 16).



Figure 16: Large single crystals of anatase (left) and rutile (right) phases of TiO₂.



Figure 17: Typical single crystals of rubrene organic molecular crystal prepared by chemical vapor transport method.

4.3 Semiconducting organic molecular crystals (contribution: G. Margaritondo)

These materials are very attractive as the essential part for organic light emitting diodes, and organic field effect transistor applications. Nevertheless, they are also interesting for basic science, e.g. for the understanding of the electronic transport in polaronic materials. A large variety of semiconducting organic crystals were successfully synthesized: pentacene, rubrene, coronene, perylene (Fig. 17). Their in-depth study is foreseen in the final stage of the present MaNEP program.

5 Conclusions

During the elapsed period of the second phase of MaNEP, the single crystal growing activity had a remarkable productivity. It has contributed strongly to the coherence of the pool, reinforcing collaborations between various groups. It has enhanced the international visibility of the MaNEP members, as well.

6 Collaborative efforts

Within the solid state chemists, the members of the project, the collaboration and the communication were at a very good level. The exchange of ideas and know-hows have happened during the meetings in Lausanne, topical meetings in Neuchâtel, and at the Diablerets workshop. The collaboration with other projects is at an enviable level, which is testified by numerous joint publications. This high output was possible due to the active interaction of the physicists with the crystal growers which very often delivered “custom designed” samples.

7 Goals for the next year

For the remaining period of Phase II the goals are the following: i) synthesis and crystal growth of new superconductor $\text{La}(\text{O}_{1-x}\text{F}_x)\text{FeAs}$ ($T_c = 26$ K) and related compounds from the same family; ii) high pressure synthesis and crystal growth of MgCNi_3 superconductor and of oxichlorides; iii) study the influence of Mg vacancies and hole doping with Li on properties of MgB_2 single crystals; iv) growth of high quality LSCO crystals for neutron, ARPES and STM studies; v) growth of the 2-D spin 1/2 frustrated quantum magnet $\text{SrCu}_2(\text{BO}_3)_2$ for neutron scattering studies; vi) improvement of the stoichiometry and the crystal size of BaVS_3 and BaVSe_3 crystals.

MaNEP-related publications

- [1] E. Giannini, R. Gladyshevskii, N. Clayton, N. Musolino, V. Garnier, A. Piriou, and R. Flükiger, *Curr. Appl. Phys.* **8**, 115 (2008).
- [2] A. Piriou, Y. Fasano, E. Giannini, and O. Fischer, *Physica C* **460-462**, 408 (2007).
- [3] G. Schuck, S. Kazakov, K. Rogacki, N. Zhigadlo, and J. Karpinski, *Phys. Rev. B* **73**, 144506 (2006).
- [4] K. Rogacki, G. Schuck, Z. Bukowski, N. D. Zhigadlo, and J. Karpinski, *Phys. Rev. B* (2008).
- [5] O. Zaremba, O. Shcherban, R. Gladyshevskii, F. Banfi, and E. Giannini, *to be published in J. All. Comp.* (2008).
- [6] J. Teyssier, R. Viennois, J. Salamin, E. Giannini, and D. van der Marel, *to be published in J. All. Comp.* (2008).
- ▶ [7] A. Podlesnyak, K. Conder, E. Pomjakushina, and A. Mirmelstein, in *Frontal Semiconductor Research*, O. T.Chang, ed. (Nova Publishers, 2006), p. 171.
- [8] M. Stingaciu, E. Pomjakushina, H. Grimmer, M. Trottmann, and K. Conder, *J. Cryst. Growth* **310**, 1239 (2008).
- [9] A. Podlesnyak, A. Karkin, K. Conder, E. Pomjakushina, M. Stingaciu, and P.Allenspach, *J. Mag. Mat.* **316**, e710 (2007).
- ▶ [10] M. García-Fernández, U. Staub, Y. Bodenthin, S. M. Lawrence, A. M. Mulders, C. E. Buckley, S. Weyeneth, E. Pomjakushina, and K. Conder, *Phys. Rev. B* **77**, 060402 (2008).
- [11] M. Medarde, C. Dallera, M. Grioni, J. Voigt, A. Podlesnyak, E. Pomjakushina, K. Conder, T. Neisius, O. Tjernberg, and S. N. Barilo, *Phys. Rev. B* **73**, 054424 (2006).
- ▶ [12] A. Podlesnyak, S. Streule, J. Mesot, M. Medarde, E. Pomjakushina, K. Conder, A. Tanaka, M. Haverkort, and D. I. Homsikii, *Phys. Rev. Lett.* **97**, 247208 (2006).
- [13] A. Podlesnyak, K. Conder, E. Pomjakushina, A. Mirmelstein, P. Allenspach, and D. Khomskii, *J. Mag. Mat.* **310**, 1552 (2007).
- [14] B. Roessli, S. N. Gvasaliya, E. Pomjakushina, and K. Conder, *JETP Lett.* **81**, 287 (2005).
- [15] M. Janoschek, B. Roessli, L. Keller, S. N. Gvasaliya, K. Conder, and E. Pomjakushina, *J. Phys.: Cond. Mat.* **17**, L425 (2005).
- ▶ [16] L. Mihály, B. Dóra, A. Ványolos, H. Berger, and L. Forró, *Phys. Rev. Lett.* **97**, 067206 (2006).
- [17] H. Rønnow *et al.*, unpublished (2008).
- [18] S. Mitrovic, P. Fazekas, C. Söndergaard, D. Ariosa, N. Barisic, H. Berger, D. Cloetta, L. Forró, H. Höchst, I. Kupcic, D. Pavuna, and G. Margaritondo, *Phys. Rev. B* **75**, 153103 (2007).
- [19] C. Dubois, A. P. Petrovic, G. Santi, C. Berthod, A. A. Manuel, M. Decroux, Ø. Fischer, M. Potel, and R. Chevrel, *Phys. Rev. B* **75**, 104501 (2007).
- [20] A. P. Petrović, Y. Fasano, R. Lortz, M. Decroux, M. Potel, R. Chevrel, and Ø. Fischer, *Physica C* **460-462**, 702 (2007).
- [21] A. P. Petrović, R. Lortz, G. Santi, M. Decroux, H. Monnard, Ø. Fischer, L. Boeri, O. Andersen, J. Kortus, D. Salloum, P. Gougeon, and M. Potel, *Phonon Mode Spectroscopy and Electron-Phonon Coupling in the Quasi-One-Dimensional $\text{M}_2\text{Mo}_6\text{Se}_6$ family: Competing Instabilities, Ultra-Strong Coupling and "Phonon-Boosted" Superconductivity* (2008), submitted to *Phys. Rev. B*.
- ▶ [22] R. Tediosi, N. P. Armitage, E. Giannini, and D. van der Marel, *Phys. Rev. Lett.* **99**, 016406 (2007).

Other references

- [23] Z. Hiroi, N. Kobayashi, and M. Takano, *Nature* **371**, 139 (1994).
- [24] M. Azuma, T. Saito, I. Yamada, Y. Kohsaka, H. Takagi, and M. Takano, *J. Low Temp. Phys.* **131**, 671 (2003).
- [25] M. Uehara, T. Nagata, J. Akimitsu, H. Takahashi, N. Mori, and K. Kinoshita, *J. Phys. Soc. Jpn.* **65**, 2764 (1996).
- [26] T. Lancaster, S. J. Blundell, D. Andreica, M. Janoschek, B. Roessli, S. N. Gvasaliya, K. Conder, E. Pomjakushina, M. L. Brooks, P. J. Baker, D. Prabhakaran, W. Hayes, and F. L. Pratt, *Phys. Rev. Lett.* **98**, 197203 (2007).
- [27] R. Friend and A. Yoffe, *Adv. Phys.* **36**, 1 (1987).
- [28] E. Morosan, H. Zandbergen, B. Dennis, J. Bos, Y. Onose, T. Klimczuk, A. Ramirez, N. Ong, and R. Cava, *Nature Phys.* **2**, 544 (2006).
- [29] J. Merino and R. McKenzie, *Phys. Rev. Lett.* **87**, 237002 (2001).
- [30] A. M. Gabovich, A. I. Voitenko, and M. Ausloos, *Phys. Rep.* **367**, 583 (2002).

Single Crystal Catalog of MaNEP

Material	Growth technique	Furnace	Conductor	Insulator	Magnetic	Responsible
Various elemental metals	Bridgman, Zone melting	RF induction, Electronic bombardment	yes			Giannini (022.3796076, enrico.giannini@physics.unige.ch)
MgB2	Mg-flux under HP	cubic anvil hot press	yes, T _c =39K			Giannini (022.3796076, enrico.giannini@physics.unige.ch)
TiMnSi (TiM=Transition Metal: Co, Fe, Mn, ...)	Czochralski, TSFZ	RF induction, Mirror image furnace	yes/no		some	Giannini (022.3796076, enrico.giannini@physics.unige.ch)
Sm14Cu24O41	TSFZ	Mirror image furnace	No			Giannini (022.3796076, enrico.giannini@physics.unige.ch)
(Sr,M1,M2)14Cu24O41-x (M1, M2 = Ca, Bi, Y, ...)	TSFZ	Mirror image furnace	No			Giannini (022.3796076, enrico.giannini@physics.unige.ch)
Bi2Sr2Ca2Cu3O10	TSFZ	Mirror image furnace	Yes, T _c =110 K			Giannini (022.3796076, enrico.giannini@physics.unige.ch)
Bi2-xPbxSr2CaCu3O10+d	TSFZ	Mirror image furnace	Yes, T _c =110 K			Giannini (022.3796076, enrico.giannini@physics.unige.ch)
Bi2Sr2CaCu2O8	TSFZ	Mirror image furnace	Yes, T _c =91 K			Giannini (022.3796076, enrico.giannini@physics.unige.ch)
Bi2-xPbxSr2CaCu2O8	TSFZ	Mirror image furnace	Yes, T _c =93 K			Giannini (022.3796076, enrico.giannini@physics.unige.ch)
Bi2Sr2CuO6	TSFZ	Mirror image furnace	Yes, T _c =8 K			Giannini (022.3796076, enrico.giannini@physics.unige.ch)
REBa2Cu3O7	self flux	3-zone furnace, Top seeded growth	Yes, T _c =90 K			Giannini (022.3796076, enrico.giannini@physics.unige.ch)
MgB2	Mg-flux under HP	cubic anvil hot press	yes, T _c =39K			Karpinski(044.6332254, karpinski@phys.ethz.ch)
Mg(1-x)AlxB2	Mg-flux under HP	cubic anvil hot press	yes			Karpinski(044.6332254, karpinski@phys.ethz.ch)
MgB2-xCx	Mg-flux under HP	cubic anvil hot press	yes			Karpinski(044.6332254, karpinski@phys.ethz.ch)
Mg(1-x)MnxB2	Mg-flux under HP	cubic anvil hot press	yes			Karpinski(044.6332254, karpinski@phys.ethz.ch)
Mn(1-x)FexB2	Mg-flux under HP	cubic anvil hot press	yes			Karpinski(044.6332254, karpinski@phys.ethz.ch)
KO32O6	ampoule method	resistive furnace	yes, T _c =9.6K			Karpinski(044.6332254, karpinski@phys.ethz.ch)
Na2O82O6.5	HP	cubic anvil hot press	no			Karpinski(044.6332254, karpinski@phys.ethz.ch)
YBa2Cu4O8	HP	high O2 pressure	yes, T _c =80K			Karpinski(044.6332254, karpinski@phys.ethz.ch)
Ca(2-x)NaxCuO2Cl2	HP	cubic anvil hot press	yes, T _c =13-25K			Karpinski(044.6332254, karpinski@phys.ethz.ch)
YBa(2-x)SrxCu4O8	HP	high O2 pressure	yes			Karpinski(044.6332254, karpinski@phys.ethz.ch)
YmNO3	TSFZ	Mirror image furnace		stacked-triangular AF		Kazimierz Corder@psi.ch
DyMnO3	TSFZ	Mirror image furnace		AF T _n -40K, ferroelectric T<19K		ekaterina.pomjakushina@psi.ch
LaCoO3	TSFZ	Mirror image furnace		magnetic and spin state transitions		Kazimierz Corder/Ekaterina Pomjakushina
La(1-x)SrxCoO3	TSFZ	Mirror image furnace		magnetic and spin state transitions		Kazimierz Corder/Ekaterina Pomjakushina
SrCu2(BCO3)2	TSFZ	Mirror image furnace		2D spin system		Kazimierz Corder/Ekaterina Pomjakushina
LaFeO3	TSFZ	Mirror image furnace		valence transition in t		Kazimierz Corder/Ekaterina Pomjakushina
EuNi2(Si(1-x)Gex)2	TSFZ	Mirror image furnace		magneto-optical Faraday effect		Kazimierz Corder/Ekaterina Pomjakushina
La(1-x)SrxFeO3	TSFZ	Mirror image furnace		magneto-optical Faraday effect		Kazimierz Corder/Ekaterina Pomjakushina
ErFeO3	TSFZ	Mirror image furnace		magneto-optical Faraday effect		Kazimierz Corder/Ekaterina Pomjakushina
YFeO3	TSFZ	Mirror image furnace		magneto-optical Faraday effect		Kazimierz Corder/Ekaterina Pomjakushina
TbBaCo2O(5+x)	TSFZ	Mirror image furnace		magnetic, metal-insulator, spin state transition		Kazimierz Corder/Ekaterina Pomjakushina
LuFe2O4	TSFZ	Mirror image furnace		FM, AFM, MI transitions		Kazimierz Corder/Ekaterina Pomjakushina
NaxCoO2 (x=0.7, 0.75, 1)	TSFZ	Mirror image furnace		magnetic, metal-insulator, spin state transition		Kazimierz Corder/Ekaterina Pomjakushina
NdBaCo2O(5+x)	TSFZ	Mirror image furnace	superconductor			Kazimierz Corder/Ekaterina Pomjakushina
La(2-x)SrxCuO4	TSFZ	Mirror image furnace		AFM		Kazimierz Corder/Ekaterina Pomjakushina
La2CuO4	TSFZ	Mirror image furnace	metal below 1K	AFM, charge disproportionation		Kazimierz Corder/Ekaterina Pomjakushina
Nd1/3Si2/3FeO3	TSFZ	Mirror image furnace	superconductor			Kazimierz Corder/Ekaterina Pomjakushina
CaVO3	TSFZ	Mirror image furnace		charge ordering, orbital ordering		Kazimierz Corder/Ekaterina Pomjakushina
SmBaMn2O6	TSFZ	Mirror image furnace		magnetic, metal-insulator, spin state transition		Kazimierz Corder/Ekaterina Pomjakushina
YBa2Cu3O(6+x), x=0-1, 160-180	solid state synthesis	Mirror image furnace		AFM		Kazimierz Corder/Ekaterina Pomjakushina
LnBaCo2O9+x, x=0-1, 160-180	solid state synthesis	Mirror image furnace		AFM, charge disproportionation		Kazimierz Corder/Ekaterina Pomjakushina
Ln(2-x)SrxCuO4, 160-180	solid state synthesis	Mirror image furnace		charge ordering, orbital ordering		Kazimierz Corder/Ekaterina Pomjakushina
Ca3Cu(3-x)NiX(PO4)4	solid state synthesis	Mirror image furnace		magnetic, metal-insulator, spin state transition		Kazimierz Corder/Ekaterina Pomjakushina
NdNi2B2C	arc melting	Mirror image furnace	superconductor		quantum spin trimer	Kazimierz Corder/Ekaterina Pomjakushina
(La(1-x)Prx)1-yCayMnO3, 160-180	solid state synthesis	Mirror image furnace	superconductor		AF, FM	Kazimierz Corder/Ekaterina Pomjakushina
Bi1.6Pb0.4Sr2CaCu2O8 P1,Y doped Bi,Pb-2212	Flux grown	1-zone furnace with temp.gradient	Yes			Berger 021.693.4484, helmuth.berger@epfl.ch
Bi1.6Pb0.4Sr2CaCu2O8	Flux grown	1-zone furnace with temp.gradient	Yes			Berger 021.693.4484, helmuth.berger@epfl.ch
Bi2Sr2CaCu2O8	Flux grown	1-zone furnace with temp.gradient	Yes			Berger 021.693.4484, helmuth.berger@epfl.ch
Bi2Sr2CaCu2O8 Ni, Co doped	Flux grown	1-zone furnace with temp.gradient	Yes Tc 123K			Berger 021.693.4484, helmuth.berger@epfl.ch
Fe3O4	CVT	2-zone furnace	Yes Tc 121K		ferromagnetic	Berger 021.693.4484, helmuth.berger@epfl.ch
CoS2	CVT	1-zone furnace	Yes			Berger 021.693.4484, helmuth.berger@epfl.ch
BaV5S3	Flux grown	1-zone furnace with temp.gradient	Yes			Berger 021.693.4484, helmuth.berger@epfl.ch
LiCu2O2	Flux grown	1-zone furnace with temp.gradient	No	Insulator		Berger 021.693.4484, helmuth.berger@epfl.ch

Single Crystal Catalog of MaNEP

Material	Growth technique	Furnace	Conductor	Insulator	Magnetic	Responsible
NbSe2	CVT	2-zone furnace	Yes Tc 7.2K			Berger 021 693 4484, heilmuth.berger@epfl.ch)
Cu3TeO6	CVT and flux grown	2-zone furnace	No			Berger 021 693 4484, heilmuth.berger@epfl.ch)
Na0.75CoO2	Flux grown	1-zone furnace with temp.gradient	Yes			Berger 021 693 4484, heilmuth.berger@epfl.ch)
CuSb2O5	CVT	2-zone furnace	No			Berger 021 693 4484, heilmuth.berger@epfl.ch)
CdCr2S4	CVT	2-zone furnace	Tc		ferromagnetic	Berger 021 693 4484, heilmuth.berger@epfl.ch)
CdCr2Se4	CVT	2-zone furnace	Yes		ferromagnetic	Berger 021 693 4484, heilmuth.berger@epfl.ch)
C-60	Sublimation	10-zone furnace	No	Insulator		Berger 021 693 4484, heilmuth.berger@epfl.ch)
NbTe2	CVT	2-zone furnace	Yes Tc= 86K		ferromagnetic	Berger 021 693 4484, heilmuth.berger@epfl.ch)
TaTe2	CVT	2-zone furnace	Yes Tc=130K		ferromagnetic	Berger 021 693 4484, heilmuth.berger@epfl.ch)
TiTe2	CVT	2-zone furnace	Yes		ferromagnetic	Berger 021 693 4484, heilmuth.berger@epfl.ch)
alpha.TeVO4	CVT	2-zone furnace	No		magnetic properties	Berger 021 693 4484, heilmuth.berger@epfl.ch)
beta TeVO4	CVT	2-zone furnace	No		magnetic properties	Berger 021 693 4484, heilmuth.berger@epfl.ch)
ZnO	CVT	2-zone furnace	No		magnetic properties	Berger 021 693 4484, heilmuth.berger@epfl.ch)
Ni5(SeO3)4Cl2	CVT	2-zone furnace	No		magnetic properties	Berger 021 693 4484, heilmuth.berger@epfl.ch)
Ni5(SeO3)4Br2	CVT	2-zone furnace	No		magnetic properties	Berger 021 693 4484, heilmuth.berger@epfl.ch)
Ni5(TeO3)4Br2	CVT	2-zone furnace	No		magnetic properties	Berger 021 693 4484, heilmuth.berger@epfl.ch)
Cu2Te2O5Br2	CVT	2-zone furnace	No		magnetic properties	Berger 021 693 4484, heilmuth.berger@epfl.ch)
Co6(TeO3)2(TeO6)Cl2	CVT	2-zone furnace	No		magnetic properties	Berger 021 693 4484, heilmuth.berger@epfl.ch)
Co6(TeO3)2(TeO6)Br2	CVT	2-zone furnace	No		magnetic properties	Berger 021 693 4484, heilmuth.berger@epfl.ch)
CdRe2O7	CVT	2-zone furnace	Yes Tc=1k		antiferromagnetic	Berger 021 693 4484, heilmuth.berger@epfl.ch)
Co2TeO3Cl2	CVT	2-zone furnace	No		magnetic properties	Berger 021 693 4484, heilmuth.berger@epfl.ch)
Co2TeO3Br2	CVT	2-zone furnace	No		magnetic properties	Berger 021 693 4484, heilmuth.berger@epfl.ch)
Ni5(TeO3)4Cl2	CVT	2-zone furnace	No		magnetic properties	Berger 021 693 4484, heilmuth.berger@epfl.ch)
Ni5(TeO3)4Br2	CVT	2-zone furnace	No		magnetic properties	Berger 021 693 4484, heilmuth.berger@epfl.ch)
Ni5(TeO3)4Br2-xClx	Flux grown and CVT	2-zone furnace	No		magnetic properties	Berger 021 693 4484, heilmuth.berger@epfl.ch)
CuWO4	CVT	2-zone furnace	No		magnetic properties	Berger 021 693 4484, heilmuth.berger@epfl.ch)
Co7Te4O12Br6	CVT	2-zone furnace	No		magnetic properties	Berger 021 693 4484, heilmuth.berger@epfl.ch)
CuSbTeO3Cl2	CVT	2-zone furnace	No	Insulator		Berger 021 693 4484, heilmuth.berger@epfl.ch)
Cu3(SeO3)4Cl2	CVT	2-zone furnace	No		magnetic properties	Berger 021 693 4484, heilmuth.berger@epfl.ch)
CuTe2O5	CVT	2-zone furnace	No		magnetic properties	Berger 021 693 4484, heilmuth.berger@epfl.ch)
CuSe2O5	CVT	2-zone furnace	No		magnetic properties	Berger 021 693 4484, heilmuth.berger@epfl.ch)
Pentacene	CVT	2-zone furnace	No	Insulator		Berger 021 693 4484, heilmuth.berger@epfl.ch)
Rubrene	CVT	2-zone furnace	No	Insulator		Berger 021 693 4484, heilmuth.berger@epfl.ch)
Coronene	CVT	2-zone furnace	No	Insulator		Berger 021 693 4484, heilmuth.berger@epfl.ch)
Tetracene	CVT	2-zone furnace	No	Insulator		Berger 021 693 4484, heilmuth.berger@epfl.ch)
Anthracene	CVT	2-zone furnace	No	Insulator		Berger 021 693 4484, heilmuth.berger@epfl.ch)
TCNQ	CVT	2-zone furnace	No	Insulator		Berger 021 693 4484, heilmuth.berger@epfl.ch)
TTF-TCNQ	CVT	2-zone furnace	No	Organic Conductor		Berger 021 693 4484, heilmuth.berger@epfl.ch)
Perylene	CVT	2-zone furnace	No	Insulator		Berger 021 693 4484, heilmuth.berger@epfl.ch)
TCNQ-Phenylene complexe	CVT	2-zone furnace	No	Insulator		Berger 021 693 4484, heilmuth.berger@epfl.ch)
Copper Phthalocyanine	CVT	2-zone furnace	No	p-type semiconductor		Berger 021 693 4484, heilmuth.berger@epfl.ch)
FeTe2O5Cl	CVT	2-zone furnace	No	Insulator	magnetic properties	Berger 021 693 4484, heilmuth.berger@epfl.ch)
FeTe2O5Br	CVT	2-zone furnace	No	Insulator	magnetic properties	Berger 021 693 4484, heilmuth.berger@epfl.ch)
Na0.70CoO2	Flux grown	1-zone furnace with temp.gradient	No		magnetic properties	Berger 021 693 4484, heilmuth.berger@epfl.ch)
Ca3Co2O6	Flux grown	1-zone furnace with temp.gradient	No		magnetic properties	Berger 021 693 4484, heilmuth.berger@epfl.ch)
Ca3Co4O9	Flux grown	1-zone furnace with temp.gradient	No		magnetic properties	Berger 021 693 4484, heilmuth.berger@epfl.ch)
In2VO5	CVT	2-zone furnace	No		magnetic properties	Berger 021 693 4484, heilmuth.berger@epfl.ch)
Co4Te4O11Cl4	CVT	2-zone furnace	No		magnetic properties	Berger 021 693 4484, heilmuth.berger@epfl.ch)
Co4(TeO3)X2 (X = Cl, Br).	CVT	2-zone furnace	No	Insulator	magnetic properties	Berger 021 693 4484, heilmuth.berger@epfl.ch)
Co4(SeO3)X2 (X = Cl, Br).	CVT	2-zone furnace	No	Insulator	magnetic properties	Berger 021 693 4484, heilmuth.berger@epfl.ch)
Ni5SiO3	CVT	2-zone furnace	No	Insulator	magnetic properties	Berger 021 693 4484, heilmuth.berger@epfl.ch)
ZrS3	CVT	2-zone furnace	No	Semiconductor		Berger 021 693 4484, heilmuth.berger@epfl.ch)
ZrSe3	CVT	2-zone furnace	No	Semiconductor		Berger 021 693 4484, heilmuth.berger@epfl.ch)
ZrTe3	CVT	2-zone furnace	No	Semiconductor		Berger 021 693 4484, heilmuth.berger@epfl.ch)

Single Crystal Catalog of MaNEP

Material	Growth technique	Furnace	Conductor	Insulator	Magnetic	Responsible
HfS ₃	CTV	2-zone furnace	No	Semiconductor		Berger: 021.693.4484, helmuth.berger@epfl.ch
HfTe ₃	CTV	2-zone furnace	No	Semiconductor	magnetic properties	Berger: 021.693.4484, helmuth.berger@epfl.ch
TiOBr	CTV	2-zone furnace	No	Insulator	diamagnetic	Berger: 021.693.4484, helmuth.berger@epfl.ch
Pd ₃ (PS) ₄ I ₂	CTV	2-zone furnace	No	Semiconductor	magnetic properties	Berger: 021.693.4484, helmuth.berger@epfl.ch
MnPS ₃	CTV	2-zone furnace	No	Semiconductor	magnetic properties	Berger: 021.693.4484, helmuth.berger@epfl.ch
MnPS ₃	CTV	2-zone furnace	No	Semiconductor	magnetic properties	Berger: 021.693.4484, helmuth.berger@epfl.ch
NiPS ₃	CTV	2-zone furnace	No	Semiconductor	magnetic properties	Berger: 021.693.4484, helmuth.berger@epfl.ch
NiPS ₃	CTV	2-zone furnace	No	Semiconductor	magnetic properties	Berger: 021.693.4484, helmuth.berger@epfl.ch
FePS ₃	CTV	2-zone furnace	No	Semiconductor	magnetic properties	Berger: 021.693.4484, helmuth.berger@epfl.ch
FePS ₃	CTV	2-zone furnace	No	Semiconductor	magnetic properties	Berger: 021.693.4484, helmuth.berger@epfl.ch
Ni ₃ TeO ₆	CTV	2-zone furnace	No	Semiconductor	magnetic properties	Berger: 021.693.4484, helmuth.berger@epfl.ch
Co ₃ TeO ₆	CTV	2-zone furnace	No	Semiconductor	magnetic properties	Berger: 021.693.4484, helmuth.berger@epfl.ch
Li ₂ CoTeO ₆	Flux grown	1-zone furnace with temp.gradient	No	Semiconductor	magnetic properties	Berger: 021.693.4484, helmuth.berger@epfl.ch
LiCu ₂ O ₂	Flux grown	1-zone furnace with temp.gradient	No	Semiconductor	magnetic properties	Berger: 021.693.4484, helmuth.berger@epfl.ch
PbMo ₆ S ₈	solid state synthesis		No	Semiconductor		Petrovic (022.3796287, Alexander.Petrovic@physics.unige.ch)
PbMo ₆ S ₈ + 3% O ₂	solid state synthesis		Yes Tc = 15K			Petrovic (022.3796287, Alexander.Petrovic@physics.unige.ch)
SnMo ₆ S ₈	solid state synthesis		Yes Tc = 11K			Petrovic (022.3796287, Alexander.Petrovic@physics.unige.ch)
Sn(1-x)PbxMo ₆ S ₈	solid state synthesis		Yes Tc = 14K			Petrovic (022.3796287, Alexander.Petrovic@physics.unige.ch)
LaMo ₆ S ₈	solid state synthesis		Yes Tc = 7-12K			Petrovic (022.3796287, Alexander.Petrovic@physics.unige.ch)
LaMo ₆ S ₈	solid state synthesis		Yes Tc = 7K			Petrovic (022.3796287, Alexander.Petrovic@physics.unige.ch)
Mo ₆ Se ₈	solid state synthesis		Yes Tc = 6K			Petrovic (022.3796287, Alexander.Petrovic@physics.unige.ch)
Mo ₆ S ₈	solid state synthesis		Yes Tc = 1K			Petrovic (022.3796287, Alexander.Petrovic@physics.unige.ch)
Mo ₆ S ₈ Br ₂	solid state synthesis		Yes Tc = 13.5K			Petrovic (022.3796287, Alexander.Petrovic@physics.unige.ch)
InMo ₆ S ₈	solid state synthesis		Yes			Petrovic (022.3796287, Alexander.Petrovic@physics.unige.ch)
Ti ₂ Mo ₆ Se ₆	solid state synthesis		Yes Tc = 4.2K	Metal-Insulator		Petrovic (022.3796287, Alexander.Petrovic@physics.unige.ch)
In ₂ Mo ₆ Se ₆	solid state synthesis		Yes Tc = 2.9K	Metal-Insulator		Petrovic (022.3796287, Alexander.Petrovic@physics.unige.ch)
Na ₂ Mo ₆ Se ₆	solid state synthesis		No	Metal-Insulator		Petrovic (022.3796287, Alexander.Petrovic@physics.unige.ch)
K ₂ Mo ₆ Se ₆	solid state synthesis		No	Metal-Insulator		Petrovic (022.3796287, Alexander.Petrovic@physics.unige.ch)
Ru ₂ Mo ₆ Se ₆	solid state synthesis		No	Metal-Insulator		Petrovic (022.3796287, Alexander.Petrovic@physics.unige.ch)
Cs ₂ Mo ₆ Se ₆	solid state synthesis		No			Petrovic (022.3796287, Alexander.Petrovic@physics.unige.ch)
Mo ₆ Se ₆	solid state synthesis		No			Petrovic (022.3796287, Alexander.Petrovic@physics.unige.ch)
CsMo ₁₂ S ₁₄	solid state synthesis		Yes Tc = 7K			Fischer (022.3796270, Oystein.Fischer@physics.unige.ch)
Ba ₂ Mo ₆ S ₉	solid state synthesis		Yes Tc = 5K			Fischer (022.3796270, Oystein.Fischer@physics.unige.ch)
Rb(2n)Mo(6n+9)S(6n+13) (n = 1-4)	solid state synthesis		Yes Tc = 4-10K			Fischer (022.3796270, Oystein.Fischer@physics.unige.ch)

Project **4** **Novel materials**

Project leader: J. Hulliger (UniBE)

Participating members: L. Forró (EPFL), J. Hulliger (UniBE), J. Karpinski (ETHZ), R. Nesper (ETHZ), A. Schilling (UniZH), L. Schlapbach (Empa), J.W. Seo (EPFL).

Summary and highlights: During the three years of MaNEP phase II, the search for new materials featuring physical properties of interest to other projects within MaNEP was intensified and resulted in roughly 30 new compounds and 15 new modifications of known materials. Although physical characterization is still ongoing, success emerged from different directions: oxynitrides are materials gaining interest for heterostructures, showing e.g. a giant Seebeck effect. These new materials exhibit other interesting properties which can be tuned by substitution of O by N. The search for superconductivity in Ni-based rare earth compounds has produced four new metallic compounds (LMNiO_4 , where L = Dy, Ho, Nd or Sm and M = Sr or Ca). Along this series only LaBaNiO_4 shows a variable-range hopping type conductivity and becomes an insulator at $T = 0$, showing no magnetic ordering down to 1.5 K. In the field of spintronics, the controversy on room temperature ferromagnetism in oxides such as doped ZnO is ongoing. Homogeneously doped ZnO:Mn(II) bulk material was prepared, showing antiferromagnetic ordering at low temperature and no evidence for Mn(II) cluster formation down to concentrations of a few percent. The search for novel pyrochlore compounds using low and high pressure syntheses including ion exchange reactions has produced new compounds as well. Upper critical fields of KOs_2O_6 and RbOs_2O_6 and the temperature dependence of the superconducting transition at various fields were investigated. Nanostructured oxidic fibers of molybdates and tungstates were explored. Such nanofibers have demonstrated enhanced sensing properties, better than corresponding classical materials. The development of new strategies for finding superconductors has reached a level, which will allow in a near future to explore known and new classes of cuprates for grains showing a higher T_c than known by today. The most essential achievement is a high sensitive separation technique for superconducting particles down to one ppm. More close to applications, the MgB_2 wire formation was continued and hole doping for related compounds was successfully achieved. A collaborative project on the possibility of superconductivity in d^1 – vanadium oxide was started.

1 **Synthesis of new bulk materials at ambient and high pressure**

1.1 **Anionic substitutions in perovskites**

Perovskite type materials still attract great interest due to the varieties of their properties and applications. The most common way to tune the material properties is the substitution of different elements in the perovskite crystal structure. While most research efforts on oxide compounds have been focused on modifications of the cationic composition, a less explored approach was to investigate modifications of the anionic composition. The group at Empa/PSI (A. Weidenkaff, T. Lippert, L. Schlapbach) showed that the substitution of oxygen with nitrogen to form perovskite type oxynitrides is changing the properties in a profound way. These new materials exhibit promising electrical and optical properties, which can be tuned by continuous substitution of O with N. At Empa/PSI, the oxyni-

tride perovskites were prepared by two different approaches: a two step process, which implies the preparation of the corresponding oxide precursors and subsequent thermal or plasma ammonolysis; or direct deposition of oxynitride films by pulsed laser deposition (PLD). Strontium and calcium titanates were chosen as model systems to investigate the influence of different ammonolysis parameters on the crystal structure, chemical composition, and properties. In oxynitride titanates, the optical band gap width is modified by the nitrogen content in a broad range, making the material interesting as potential new pigments.

Oxynitrides with the general formula $\text{La}_{1-x}\text{Ca}_x\text{TiO}_{2+x}\text{N}_{1-x}$ ($x = 0, 0.3, 0.5, 0.7, 1.0$) were synthesized by thermal ammonolysis of oxide precursors produced by a soft chemistry method. The crystallographic structure, the optical properties and the thermal stability of the compounds were studied with X-ray and neutron diffraction, UV/VIS and Raman

spectroscopy. All materials crystallized in a perovskite type pseudo cubic unit cell. The lattice parameters decrease with increasing Ca content, while the optical band gap width increases from 2.3 to 3.7 eV with increasing x . Thin films of pure STO:N (0.7% N) revealed only a slight increase of the band gap from 3.2 to 3.25 eV.

1.2 Surface plasma ammonolysis of single crystals

In this work, the Empa's group partially substituted oxygen by nitrogen in a microwave induced quasi neutrally glow discharge plasma of reactive ammonia (NH_3). SrTiO_3 monocystals with (111) orientation were used as starting material since the exposed (111) surface is assumed to be more reactive than the non-polar (100) surface. The studies on chemical compositions and structures of the products were performed by X-ray diffraction (XRD), in-depth profile X-ray photoelectron spectroscopy (XPS) of core level binding energies, and elastic recoil detection analysis (ERDA), all confirming a perovskite type structure with a nitrogen con-

tent up to about 8%.

Novel nitrogenated heterostructures and oxynitride single crystals were successfully prepared by a microwave induced plasma (MIP) from STO single crystals. These heterostructures showed interesting physical properties such as a giant Seebeck effect and superconductivity. The analysis of the heterostructures with varying nitrogen content showed that they consist of a hundred of micrometer reduced strontium titanate layer (blue), covered with a STON layer of tenths of microns (yellow) and a few nm thick layer of TiN (Fig. 1 bottom). The superconductivity at $T < 5$ K shown in Fig. 1 top (probably related to a thin TiN layer) and the giant Seebeck effect of -465 V/K at 300 K will need theoretical work for understanding.

Pure oxynitride single crystals with a nitrogen content of 3–4% could be obtained by optimizing the MIP conditions. However, present attempts to increase the nitrogen content resulted in a Sr depletion from the surface and TiN phase formation. Single crystals revealed a metallic-like behavior.

1.3 Cation and anion substitutions in LaBaNiO_4

Stoichiometric La_2CuO_4 is antiferromagnetic at room temperature, with Cu in a $3d^9$ (spin $s = 1/2$) configuration, and it is regarded to be a Mott-Hubbard insulator. These main features ($s = 1/2$ antiferromagnet, Mott-Hubbard insulator) are generally believed to be important ingredients for the occurrence of superconductivity on subsequent doping the compound with charge carriers. By contrast, stoichiometric LaSrNiO_4 is metallic, although a $3d^7$ configuration of Ni in a low-spin $s = 1/2$ state might be expected to also lead to a Mott-Hubbard-type insulating state. For this reason LaSrNiO_4 has not been considered to be a serious candidate as a "parent compound" for superconductors. Doping experiments over a wide range ($0.4 \leq x \leq 1$) in $\text{La}_{1+x}\text{Sr}_{1-x}\text{NiO}_4$, with the aim to find a superconductor, have indeed not been successful [16].

To modify the electronic structure of LaSrNiO_4 and drive it to an insulating state, the group of A. Schilling (UniZH) has attempted to apply chemical pressure, e.g. by the substitution of Sr by Ba (stretching of the lattice [17, 18]), or Sr by Ca and La by rare earths with smaller ionic radii, respectively (lattice compression). By analogy with other known oxyhalides and oxynitrides with the K_2NiF_4 structure where the apical oxygen in the oxygen octahedra could be successfully replaced by

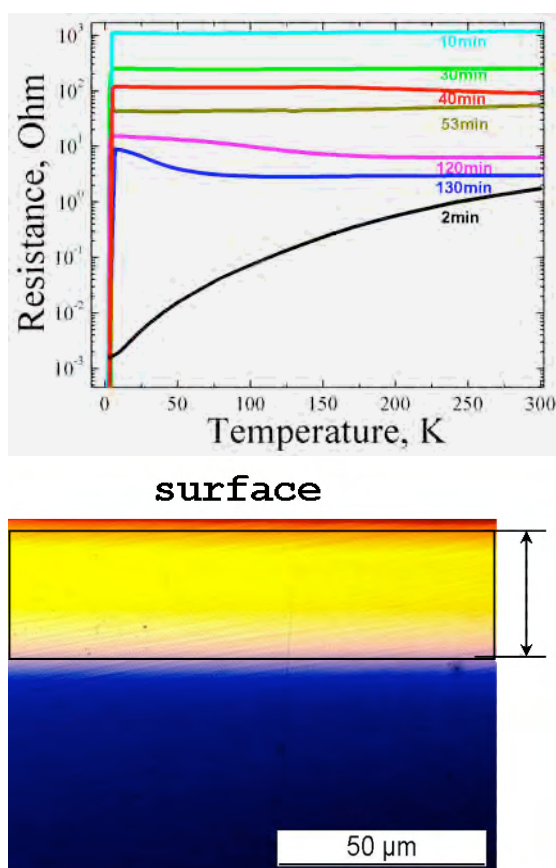


Figure 1: Top: Resistance of plasma treated samples. Bottom: Cross sectional view of an ammonolysed crystal.

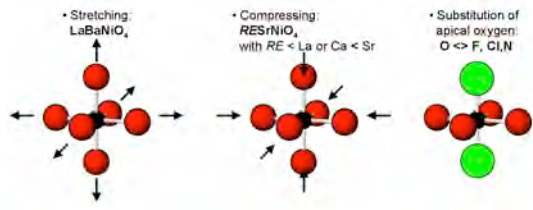


Figure 2: Strategy to modify the electronic structure of LaSrNiO_4 .

halogen atoms or nitrogen, they have also attempted to substitute oxygen by F, Cl and N (Fig. 2).

a) LaBaNiO_4 Very little is known about $\text{LaBaNiO}_{4-\delta}$ which has been reported to be semiconducting [17]. It has also been claimed that this compound shows a crossover from a high-spin to a low-spin state of Ni upon cooling below $T = 100$ K [17]. The questions Schilling wanted to clarify were: (i) is stoichiometric LaBaNiO_4 really an insulator at $T = 0$ K? And (ii) is Ni in a low spin $s = 1/2$ state, and if yes, is there antiferromagnetic ordering at finite temperature?

Consequently, they have prepared polycrystalline samples of $\text{LaSr}_{1-x}\text{Ba}_x\text{NiO}_{4-\delta}$ by a standard wet chemical procedure (dissolving metal

nitrate in nitric acid with subsequent evaporation, firing the product at 900°C for several hours and finally at 1100°C in form of pressed pellets during 3 days in air). The product was characterized by X-ray diffraction (S. Siegrist, UniZH), neutron diffraction (M. Medarde, Laboratory for neutron scattering at the PSI Villigen), chemical analysis (K. Pomjakushina, PSI Villigen), resistivity, thermal conductivity, magnetic susceptibility, specific heat (S. Siegrist and R. Dell'Amore, UniZH), and UV-excited photoemission (T. Brugger, UniZH). Chemical analysis and neutron diffraction clearly showed that as prepared $\text{LaBaNiO}_{4-\delta}$ is always oxygen deficient with $\delta \approx 0.15$, in contradiction to results reported in [17, 18]. Samples of LaBaNiO_4 and $\text{LaSr}_{0.5}\text{Ba}_{0.5}\text{NiO}_{4-\delta}$ were therefore post-annealed at 400°C at an O_2 pressure of 880 bar (J. Karpinski, ETHZ). Only after such a treatment, an oxygen content of 4.03(1) could be achieved. In Fig. 3 they show the electrical conductivity, the magnetic susceptibility and the low temperature specific heat of $\text{LaBaNiO}_{4-\delta}$ ($a = 3.869 \text{ \AA}$, $c = 12.880 \text{ \AA}$), in comparison with corresponding data from metallic LaSrNiO_4 ($a = 3.826 \text{ \AA}$, $c = 12.862 \text{ \AA}$).

The electrical conductivity of LaBaNiO_4 shows a pronounced variable-range hopping VRH-type dependence over a wide range of temperatures (Fig. 3 top). Therefore, it is clear that the electrical transport in LaBaNiO_4 is indeed different from LaSrNiO_4 , and LaBaNiO_4 is an insulator at $T = 0$. Corresponding thermal conductivity data show a slightly higher thermal conductivity ($\sigma \approx 1.9 \text{ W/Km}$ at $T = 300 \text{ K}$) for LaSrNiO_4 than for LaBaNiO_4 ($\approx 1.7 \text{ W/Km}$). In contrast to these transport data, the magnetic susceptibilities of all stoichiometric samples are almost temperature independent like in a metal, and a metal-like linear term in the specific heat at low temperatures, $\gamma \approx 10 \text{ mJ/moleK}^2$, is measured both in metallic LaSrNiO_4 and in insulating LaBaNiO_4 . A similarly paradoxical situation as in LaBaNiO_4 is met in a so called Fermi-glass [19], where the density of states at the Fermi level is finite, but these states are localized. This typically leads to a VRH transport property as it has been observed in LaBaNiO_4 , but resulting in a Pauli-like paramagnetism typical of a metal. Further neutron diffraction experiments on fully oxygenated LaBaNiO_4 (M. Medarde, PSI Villigen) did not show any sign of magnetic ordering of the Ni magnetic moments down to $T = 1.5 \text{ K}$. From all these facts, Schilling concludes that LaBaNiO_4 , although an insulator at $T = 0$, does not represent the sought analogue to

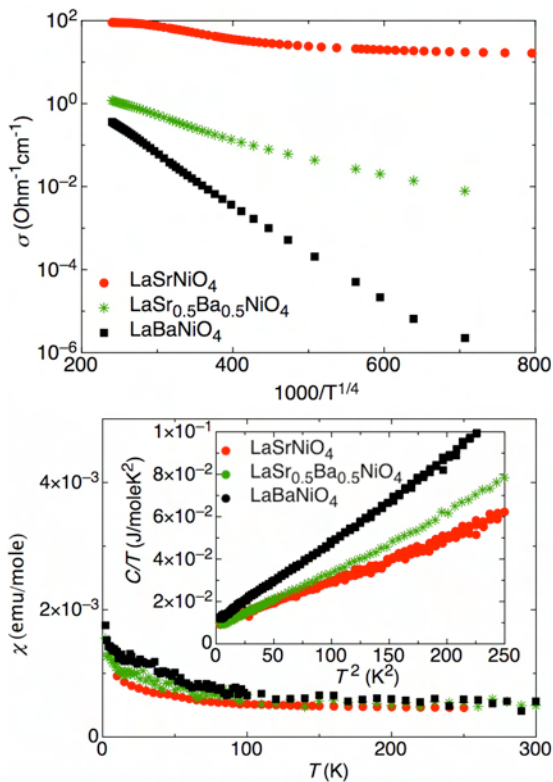


Figure 3: physical properties of LaBaNiO_4 in comparison with LaSrNiO_4 .

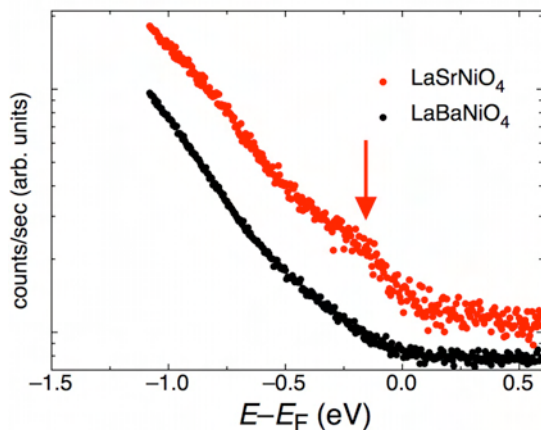


Figure 4: UV excited photoemission data on polycrystalline LaSrNiO_4 and LaBaNiO_4 at $T = 300$ K.

La_2CuO_4 . Doping experiments on LaBaNiO_4 ($\text{La} \leftrightarrow \text{Ca}$, $\text{La} \leftrightarrow \text{Ba}$, both hole and electron doping) indeed did not result in metallic transport properties of the substituted samples.

To clarify whether electrically insulating LaBaNiO_4 does show a finite electronic density of states (DOS) at its Fermi level E_F or not, Schilling's group have performed preliminary UV excited photoemission experiments (T. Brugger, UniZH, see Fig. 4). A comparison with corresponding data from metallic LaSrNiO_4 shows that in both compounds the total measured DOS must be small. However, the data also showed a slightly enhanced DOS near E_F in LaSrNiO_4 when compared to respective data of LaBaNiO_4 . This result is in agreement with bandstructure calculations [20] that clearly show a finite DOS near E_F for LaSrNiO_4 (corresponding calculations are not available for LaBaNiO_4).

b) *LaSrNiO₄, lattice compression, substitution of Sr by Ca or La by a rare earth* In a different approach, Schilling argued that the substitution of La or Sr with elements of smaller ionic radii, i.e. the application of chemical pressure, might distort the crystal structure of LaSrNiO_4 in a way that a transition to an insulating state can be achieved. This argument is based on the observation that in some perovskite oxides an increasing distortion of the oxygen octahedra around the transition metal atoms is indeed accompanied by such a transition [21]. To achieve this, they have made a number of experiments, substituting La in LaSrNiO_4 by rare earth elements and Sr by Ca. Up to now, only the stoichiometric compounds LaSrNiO_4 , NdSrNiO_4 , SmSrNiO_4 , EuSrNiO_4 , and GdSrNiO_4 have been reported to exist [22, 23] (all metallic, see Tab. 1). A partial substitution has been achieved for $\text{Dy}_{0.5}\text{Sr}_{1.5}\text{NiO}_4$

and $\text{Nd}_{1.4}\text{Ca}_{0.6}\text{NiO}_4$ [24, 25].

While their conventional synthesis procedure at ambient pressure always produced multiphased samples, the preparation under elevated oxygen pressure (1 kbar at 1000 °C, J. Karpinski, ETHZ) resulted in the formation of four new compounds: DySrNiO_4 , HoSrNiO_4 , NdCaNiO_4 and SmCaNiO_4 . While the as prepared samples were semiconducting, a post-annealing procedure at ~ 1 kbar oxygen pressure resulted in a drop of their room temperature resistivity by almost two orders of magnitude, and the temperature dependence became very similar to LaSrNiO_4 , i.e., metallic. The results of all these experiments are summarized in Tab. 1.

Subsequent substitution experiments ($\text{Nd}_{0.82}\text{Ca}_{1.18}\text{NiO}_4$, $\text{Nd}_{1.15}\text{Ca}_{0.85}\text{NiO}_4$ and $\text{Dy}_{0.83}\text{Sr}_{1.17}\text{NiO}_4$) had only a marginal effect on the temperature dependence of the resistivity as compared to the unsubstituted samples. From these investigations they conclude that the lattice compression of LaSrNiO_4 by chemical substitution alone does not produce an insulating phase analogous to the "parent compound" La_2CuO_4 , and subsequent doping does not result in superconducting matter.

c) *Anion substitution* A number of attempts have been made to change the electronic structure of LaSrNiO_4 by replacing the apical oxygen in the oxygen octahedra by halogen atoms. This substitution has been reported to be possible in several transition metal perovskites with the K_2NiF_4 structure. In the case of the cuprates, for example, full or partial substitution with F, Cl or Br has been achieved [26, 27]. In analogy to these structures one might expect the existence of compounds such as $\text{Sr}_2\text{NiO}_3\text{X}$ or $\text{Ca}_2\text{NiO}_3\text{X}$ with $\text{X} = \text{F}, \text{Cl}$ or Br . Among the several possible synthesis techniques described in the literature Schilling's group chose to fluorinate with NH_4F and to try a direct solid state reaction using NiCl_2 . In none of these experiments compounds featuring the K_2NiF_4 structure, containing halogen atoms, were formed.

Schilling's group has also attempted to substitute the oxygen in La_2NiO_4 by nitrogen, as has been reported to be possible in oxynitrides such as $\text{Sr}_2\text{TaO}_3\text{N}$ [28]. To achieve this, they mixed polycrystalline La_2NiO_4 with Ca_2N and heat treated this mixture at 750 °C for 2 h in Nb ampoules (D. Widmer, Laboratory for Inorganic Chemistry, ETHZ). Preliminary X-ray diffraction data indicate a partial decomposition, but at the same time small changes in the diffraction pattern of the remaining K_2NiF_4 phase are clearly detectable. Whether these

Composition	a (Å)	c (Å)	Preparation	Metallic
LaSrNiO ₄	3.826	12.862	ambient pressure	yes
LaBaNiO ₄	3.869	12.880	ambient pressure post annealed 400 °C O ₂ 880 bar	no
NdSrNiO ₄ [22]	3.786	12.26	ambient pressure	yes
SmSrNiO ₄ [22]	3.777	12.25	ambient pressure	yes
EuSrNiO ₄ [22]	3.772	12.24	ambient pressure	yes
GdSrNiO ₄ [22]	3.768	12.23	ambient pressure	yes
TbSrNiO ₄	–	–	K ₂ NiF ₄ did not form	–
DySrNiO ₄	≈ 3.755	≈ 12.15	1000 °C 1 kbar O ₂	yes
HoSrNiO ₄	≈ 3.755	≈ 12.15	1000 °C 1 kbar O ₂	yes
ErSrNiO ₄	–	–	K ₂ NiF ₄ did not form	–
YSrNiO ₄	–	–	K ₂ NiF ₄ did not form	–
LaCaNiO ₄	–	–	K ₂ NiF ₄ did not form	–
NdCaNiO ₄	≈ 3.77	≈ 12.15	950 °C 900 bar O ₂	yes
SmCaNiO ₄	≈ 3.75	≈ 11.95	950 °C 900 bar O ₂	yes
GdCaNiO ₄	–	–	950 °C 900 bar O ₂ , belt type 30 kbar, K ₂ NiF ₄ did not form	–
DyCaNiO ₄	–	–	950 °C 900 bar O ₂ , belt type 30 kbar, K ₂ NiF ₄ did not form	–

Table 1: Summary of the syntheses of the lattice compression type.

changes are due to an incorporation of N or to a substitution of La by Ca is, however, unknown at present. Magnetization measurements on the resulting powders showed the presence of a ferromagnetic phase that they have not yet identified.

In the remaining time of MaNEP phase II, Schilling's group is planning to complete their investigations on LaBaNiO₄, i.e. to more precisely determine its electronic structure, for example by resonant inelastic X-ray scattering using soft X-rays. The research group of T. Schmitt (SLS, PSI Villigen) is planning to do such experiments on single crystalline LaSrNiO₄, therefore the results on their polycrystalline LaSrNiO₄ and LaBaNiO₄ samples may yield valuable complementary information.

While the application of hydrostatic chemical pressure on LaSrNiO₄, i.e. the simultaneous reduction of all the lattice parameters, did not result in the desired insulating phase, it will be worthwhile to consider the application of uniaxial chemical pressure, e.g. experiments on epitaxial films with compressive strain on LaSrAlO₄ substrates. Uniaxial deformations are expected to have a subtle effect on the electronic structure of transition metal oxides, as has been recently calculated for the case of Sr₂VO₄ [29]. This work may initiate further collaboration within MaNEP.

1.4 Magnetically diluted semiconducting ZnO

Spintronics was launched by Sato and coworkers [30] who first predicted theoretically that diluted magnetic semiconductors (DMS) doped with 3d transition metal ions, such as V, Cr, Fe, Co and Ni may exhibit ferromagnetism. This was followed by Dietl et al. [31] having claimed that Mn(II) doped p-type ZnO should be ferromagnetic above room temperature. Ferromagnetic coupling is assumed to be mediated via RKKY interactions, and thus a sample may show a bulk ferromagnetic state. These predictions, with the promise that DMS may be the basis of semiconducting spintronics devices, have triggered a vivid research in this field. To confirm the predictions, a number of experiments have been performed on ZnO substituted with transition metals. Some of these materials exhibit ferromagnetism at room temperature and above. The origin of the ferromagnetism is, however, still not identified and often ascribed to synthesis artifacts. For critical reviews on this field, see [32, 33]. In many cases, the synthesis involves complex solid state chemistry based on high temperature heat treatment leading to clustering of transition metal ions or formation of magnetic secondary phases. Indeed, samples with the same nominal composition seem to have different magnetic properties when prepared by different groups. To accurately identify the origin of the magnetism, the observation of room



Figure 5: Synthesis of ZnO doped with transition metals by the nitrate route. The process is consisting in three steps: melting of nitrates (a), quenching to preserve the homogeneity of Mn distribution in a powder form (b), fast decomposition to produce the oxides (c).

temperature ferromagnetism must be accompanied by a careful identification of the phases and structures that are present in the material. The objective of the work in the group of J.M. Seo (continued by L. Forró in 2007, EPFL) is to tune the material to achieve ferromagnetism in a clear, controllable and reproducible way. For the synthesis of high quality materials, their strategy is based on the decomposition of precursors homogeneously doped with transition metal ions at low temperature.

At first, they developed the nitrate route (Fig. 5): zincnitrate, homogeneously doped with transition metals was obtained by melting a stoichiometric mixture of zincnitrate and transition metal nitrate below 100 °C. In order to preserve homogeneity, liquid nitrates were quenched, followed by a fast decomposition by heating the powder above the decomposition temperature of nitrates (400 °C). During the decomposition of the nitrate, strongly oxidizing NO₂ (g) is produced. An unforeseen oxidation of the transition metal leads to the formation of a second phase. When Mn doped ZnO is prepared, the presence of a ZnMnO₃ impurity (needle like particles) has been observed by electron microscopy. The oxidation could not be avoided by introducing additional H₂ or carbon in the reactor during the decomposition.

A more promising method is based on

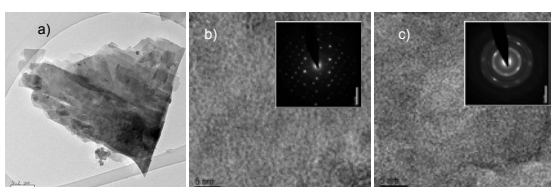


Figure 6: TEM and HRTEM micrographs of Mn doped hydrozincite particles (a and b). 5 nm particles of Mn doped ZnO are obtained in the TEM by decomposition due to beam irradiation (c).

hydrozincite as precursor. Hydrozincite are zinhydroxocarbonate materials (Zn₅(OH)_{6-2n}(CO₃)_{1+n}) with a low decomposition temperature. At 150 °C, the decomposition produces CO₂ and H₂O species with a lower potential of oxidation than NO₂. Mn(II) doped hydrozincite materials can be produced by a reaction between nitrate and urea which can be summarized by the following equation:

$$15 \text{ Zn}_{0.98}\text{Mn}_{0.02}(\text{NO}_3)_2 + 25 \text{ CO}(\text{NH}_2)_2 \rightarrow 3 (\text{Zn}_{0.98}\text{Mn}_{0.02})_5(\text{OH})_{6-2n}(\text{CO}_3)_{1+n} + x \text{ CO}_2 + y \text{ H}_2\text{O} + z \text{ N}_2$$

The exothermic reaction originating from the field of explosives and propellants can be performed in hydrothermal conditions producing flakelike nanoparticles. The poor stability of hydrozincite materials has been demonstrated by the decomposition *in situ* occurring during the TEM observations (Fig. 6). Indeed, uniformly doped zincoxide along with Mn nanoparticles have been obtained by the interaction of hydrozincite particles in the electron beam. In addition, single phase materials of uniformly doped ZnO have been produced by low temperature heat treatment (150 °C). Magnetic measurements showed that the response of this homogeneously doped DMS is antiferromagnetic. In conclusion, the group at EPFL has produced ZnO bulk material being uniformly doped up to about 2% Mn(II). Electron spin resonance showed single ion hyperfine splitting, confirming well dispersed Mn(II) ions. SQUID measurements indicated antiferromagnetic coupling of the Mn(II) cations.

As immediate perspectives to increase the doping level, they plan to dope ZnO with other transition metal, in particular Fe or Co, which exhibit an ionic radius closer to Zn than Mn. Furthermore, codoping by Li is also envisaged.

1.5 A new approach to search for superconducting materials

The general effort for finding new materials featuring similarly high T_c values or surpassing those known for the Bi, Tl, and Hg cuprates has not encountered new superconductors for some years now (for a US government report on “basic research needs for superconductivity”, see www.sc.doe.gov/bes/reports/list.html). This might have reasons such as: either almost all of what is possible has already been found or what can be prepared quite easily has been produced. However, it could well be that, among compositions using elements which most frequently are leading to high T_c materials or by involving other elements,

normal or high pressure ceramic reactions might produce small amounts of difficult to obtain phases. Such phases may form under kinetic control or are very unlikely to nucleate. Taking for a working hypothesis that among many phase systems involving preferentially copper oxide there are still opportunities, the group of J. Hulliger (UniBE) has elaborated a systematic view on how to use ceramic reactions to produce what thermodynamically or in some cases kinetically can be anticipated to form. Producing superconducting phases in the presence of a large excess of normal state matter is, however, very demanding in view of phase separation. Consequently, the group has put forward a great effort on the development of a high sensitivity technique to separate superconducting grains originating in normal state multiphase ceramic samples.

a) *Combinatorial ceramic synthesis* The base of the chemical approach they apply in Berne is essentially combinatorial and thermodynamic: assume a reaction mixture made of e.g. CuO, BaO and Y₂O₃ particles of the micrometer size pressed into a pellet. Locally, the stoichiometry of primary components follows an inhomogeneous distribution. Consequently, for short reaction times transient phases may be formed and only after a long reaction time and a second grinding step, YBCO as a single phase is formed. This basic behaviour of any ceramic reaction system has systematically been worked out by the group at Berne. Extended to more than three components such a combinatorial sample can produce many phases in parallel. At first they were using small starting particles of the typical size of 0.5 to 1 micrometer for combinatorial reactions. In the case of three different groups of materials, experimental results showed that local property formation is indeed taking place: (i) spot wise observation of second harmonic generation in 30 reacted oxides, (ii) luminescent spots in a reacted mixture of 16 oxides containing Eu for optical excitation, and (iii) pyroelectric peaks measured across a random ceramic pellet made of 10 oxides containing Nb and Ti for perovskite formation. Furthermore, bulk superconductivity was observed up to 100 K for reacting similarly CaO, SrO, BaO, La₂O₃, Y₂O₃, Tl₂O₃, Bi₂O₃, PbO, HgO and CuO. However, here no spatial information on the distribution could be observed (for magneto-optic results, see below). Essentials of the idea briefly summarized here are worked out in more detail in [1, 2, 3, 4, 5]. A clear drawback of using small sized starting materials is that product particles are of the same size and thus too small for magnetic sep-

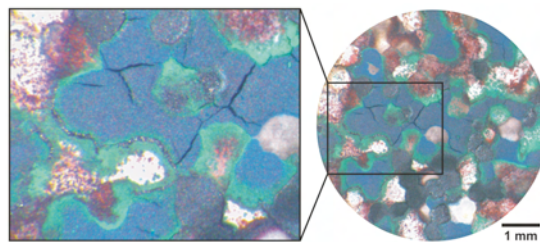


Figure 7: Test for random neck synthesis (RNS) by the YBCO system using spherical particles: the enlargement shows the formation of a green and a black phase around a white sphere that clearly indicates the reaction in the neck regions. The pellet was heated to 930 °C for 3 days in oxygen atmosphere.

aration and chemical/structural characterization. A main improvement resulted therefore from the idea of using particles of the 50–100 micrometer size, which during solid state reaction are not completely consumed up. Under these conditions and thermodynamically speaking, all phases kinetically accessible under reaction conditions are formed in between particles undergoing mass exchange. At that point it appears reasonable to use (ij) particles, i.e. starting grains composed of two metals i, j, because most known cuprate superconductors are composed of 3 to 4 metals. During local reaction of (ij) + (ik) or (ij) + (kl) starting materials, (ijk) and (ijkl) product particles may form. The feasibility of this extension of the original idea was tested by reacting BaO/Y₂O₃, CuO/BaO and CuO/Y₂O₃ particles to form phases appearing in the known phase system of YBCO. Fig. 7 shows clearly that expected phases are formed in the neck zone of interacting grains. X-ray diffraction confirmed the formation of the green phase and YBa₂Cu₃O_x. To demonstrate local formation of superconductivity, magneto-optical imaging (MOI) was ap-

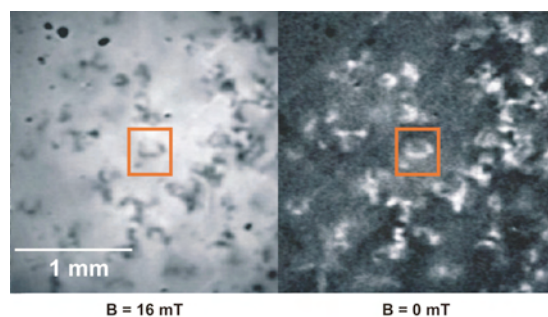


Figure 8: MOI images of a polycrystalline RNS YBCO disk measured at 10 K. Local formation of superconducting YBCO inside the pellets is clearly visible (collaboration with Dr. J. Albrecht, MPI for Metal Research, Stuttgart).

plied (collaboration with Dr. J. Albrecht, MPI for Metal Research, Stuttgart, Germany). In an external field, areas appearing black in the optical microscope turned out to be superconducting, which in zero field (remanent state) showed a contrast inversion. The magneto-optical contrast was vanishing close to 90 K (Fig. 8).

The use of starting materials in the size range of 50-100 micrometers seems to result in a feasible procedure for locally producing sufficient material of interest for characterization. Such samples were also suited to perform magnetic separation (see below). To perform various random neck syntheses in the near future, the following set of (ij) particles of proper size were made: Ca/Cu; Sr/Cu, Ba/Cu, Y/Cu, La/Cu, Bi/Cu, Ca/Sr, Ca/Ba, Sr/Ba, Ca/Bi, Sr/Bi, Ba/Bi, Y/Bi, Sr/Y, Ba/Y, Ca/Pb (all oxides).

b) *Magnetic separation* Different from general chemistry performed in gases or solutions, in solid state chemistry there are no methods for efficient separation such as chromatography. Therefore, the development of a most sensitive method to collect superconducting grains from a reaction mixture is of great importance for the type of work undertaken by Hulliger's group. Here, they have developed (i) a unique new method for phase separation in solid state chemistry (ii) and a very sensitive method to detect *in situ* traces of superconductivity [6]. The method is based on the fact that within an inhomogeneous magnetic field superimposed to gravity, a diamagnetic grain tends to move into the area of lowest potential energy. Using a ferromagnetic wire, magnetized perpendicular to its length, an optimum stray element is given: diamagnetic particles in gravitational field follow trajectories leading them to the sides of the wire (paramagnetic and ferromagnetic particles move to the top and below). Because of a large difference in the diamagnetic susceptibility of a Meissner state superconductor and a normal state piece of matter (ratio: about 10^4 , SI), the wire method is very selective, unless the external magnetic field is set to values (several Tesla) for which magnetic forces for normal state grains are also exceeding the effect of gravity.

Extensive experimentation (Fig. 9) of the group at Berne using YBCO and Bi2223 has established a great potential for using this type of magnetic separation.

(i) Fields as low as 50–100 Gauss may overcome gravity, an undoubted demonstration for a diamagnetism provided only by superconductors. (ii) At higher fields (several hundred Gauss) where at a given temperature the magnetiza-

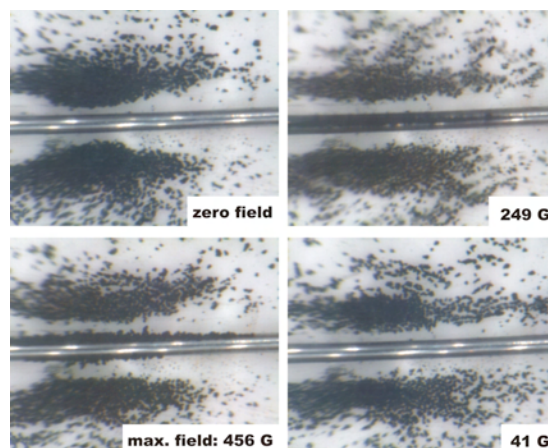


Figure 9: Attractive mode of separation for polycrystalline YBCO in a DC field after ZFC to 77 K and liquid O_2 for a medium. Magnetic field perpendicular to the image plane. Wire (Fe) diameter: 500 μm .

tion $M(H)$ is described by a hysteresis, rising and lowering the field (DC or AC) showed that particles can move from side to top and reversed. Such an observation is due to a hysteresis behavior of $M(H)$ and again a clear sign of superconductivity.

(iii) Most useful are alternating fields of a frequency matching the viscosity of the suspending medium. In case of $O_2(l)$ 25–50 Hz or alkanes(l) 5–10 Hz worked out to be optimum. At low frequency, grains can move in phase with the field, thus a further indication for a movement induced only by magnetic forces.

So far, the group at Berne has performed separation experiments at constant temperature (liquid N_2) up to fields of 600–700 Gauss. However, most interestingly is a temperature scan and the use of higher fields. Also in a vortex state, as estimated from Landau-Ginsburg theory, the capturing force is still increasing by rising the field into the range of several Tesla. An upper limit is given by the feasibility of an electromagnet operating at frequency ν and a loss of selectivity, because at high fields also normal state matter is attracted to the wire. The present solution operates with a home made new magnet rising up to 1000 Gauss and a maximum frequency of 50 Hz. The magnet was constructed as such to provide fast increase/decrease of the field (calculated: up: 9 ms; down: 12 ms, Fig. 10). Concerning the liquid for making suspensions of particles, the group has elaborated a new mixture (using thermodynamic data on pure components) allowing operation down to 80 K and upwards. A 1:1 molar mixture of propane/ethane was successfully tested, proving a viscosity suited to apply fre-

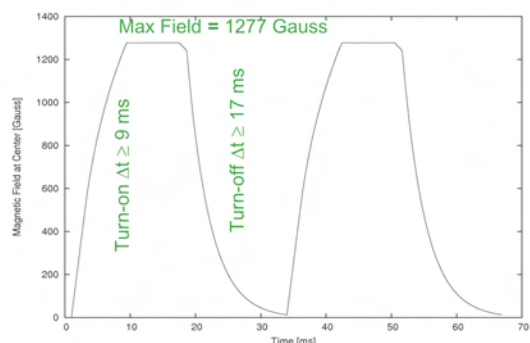


Figure 10: Simulated time dependence of field of the new electromagnet for fast attraction and release of superconducting particles.

quencies of 5–10 Hz. A further problem had to be solved: the temperature of grains under investigation is of crucial importance for any interpretation on observed T_c values. Consequently, they have developed a capturing wire system being simultaneously active as a thermocouple (type J: Fe/Ni, Cu), where the Fe part serves for magnetic purposes. To ensure absolute temperature measurements, the doubly equipped Fe-wire based thermocouple was calibrated (in collaboration with METAS, Berne, Dr. A. Steiner) to $\delta T < 0.1$ K. For future work, this capturing element will be inserted into a separation chamber (presently under construction), stabilized to $\delta T = 0.1$ K. Preliminary investigations on the temperature dependence of captured Bi(Pb)2223 grains allow to conclude that the magnetic properties of grains within a given powder sample were distributed. Therefore, it may well be that certain grains can be found which exceed the present T_c limit of the Bi-family (110 K). Indications for such a behavior from *bulk* measurements have been reported [34].

A further step was also successfully managed: a container system was attached to the wire for taking out captured grains (Fig. 11). This became possible because in the horizontal direction the field component is very low. Therefore, inclining the wire can make particles moving to the end of the wire, where a container is mounted for definitive collection.

The overall sensitivity of the separation was tested by adding some YBCO grains to Bi_2O_3 powder (100 ppm, 10 ppm, 1 ppm): within several minutes, in all cases, grains were found on the wire. This means that the present sensitivity is as high as 1 ppm. In view of using several wires in parallel and an automatic system for particle agitation, a 10 ppb limit seems feasible. Promising to notice that they were also able to capture mixed particles, where only about

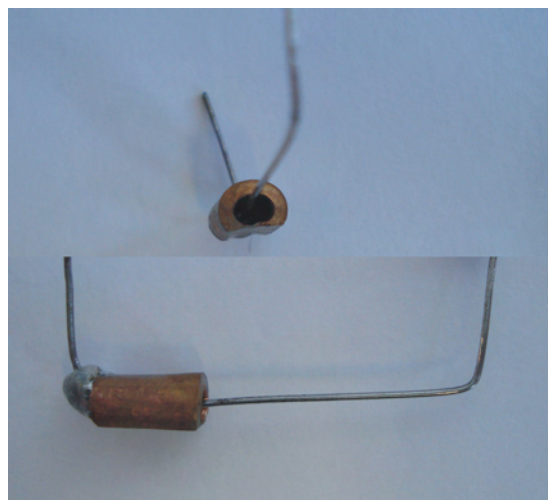


Figure 11: Deposition cup fixed at one corner of the U-shaped iron wire for *in situ* deposition and taking out of superconductive particles for further analysis. Particles move into the container by inclining the wire with respect to the horizontal line.

10% of superconducting phase was present. This is an important perspective, because random neck syntheses most likely will produce strongly intergrown particles.

In view of a bulk separator able to handle many grams of material, they have theoretically investigated a feasible geometry of a multi-wire configuration, proving a very high probability for safely capturing grains (Fig. 12).

Concerning copper oxides showing ferromagnetic behavior up to 300 K, Hulliger's group could show that any of the investigated YBCO powder samples (made at Berne or e.g. from Aldrich) exhibited a ferromagnetic hysteresis even above 300 K (Fig. 13). Such powders were passed through a magnetic separator proving 30 BFeNd magnets in vertical series. As can be seen from susceptibility mea-

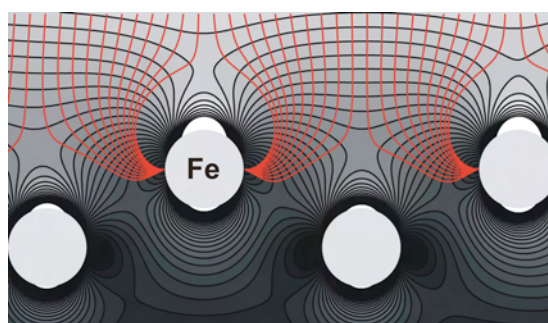


Figure 12: A zig-zag arrangement worked out to provide best results for capturing starting particles from above. The figure shows a contour plot for potential energy (greyscaled coded) and trajectories of particles (in red).

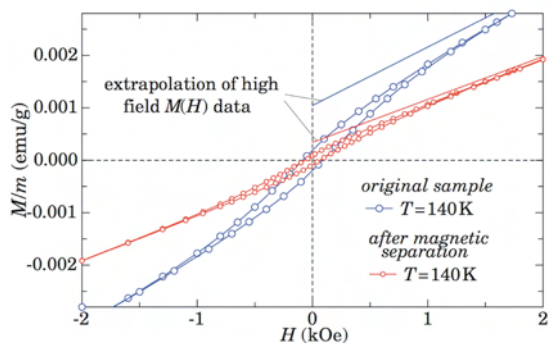


Figure 13: $M(H)$ data for a YBCO sample with ferromagnetic impurities (blue curve). The red curve shows the effect of purification from the magnetic phase by column separation at 300 K.

measurements, the content of ferromagnetic phase could be reduced. For comparison, BaCuO_2 was made, because literature [35] is reporting such effects for MCuO_2 ($M = \text{Ca}, \text{Sr}$). However, no ferromagnetism was found in this compound, undergoing the same $\text{O}_2(\text{g})$ treatment as the YBCO. At present it is anticipated that doping by Y is leading to ferromagnetic properties. During the synthesis of YBCO a certain phase segregation could thus be responsible for a small amount of ferromagnetic material.

In conclusion, the most relevant results of the group at Berne is to have developed methods to produce most inhomogeneous and phase rich ceramic reaction mixtures and an extremely sensitive technique to investigate multiphase samples for the existence of superconductivity or ferromagnetism.

Having soon elaborated necessary procedures for preparing combinatorial samples and magnetic separation including *in situ* magnetic characterization, the group will in the last year of MaNEP phase II concentrate on the following investigations: (i) search for a higher T_c of grains in Bi, Tl and Hg cuprates, than known from ceramic bulk measurements [36]; (ii) search for minor quantities of superconducting phases in reaction systems involving

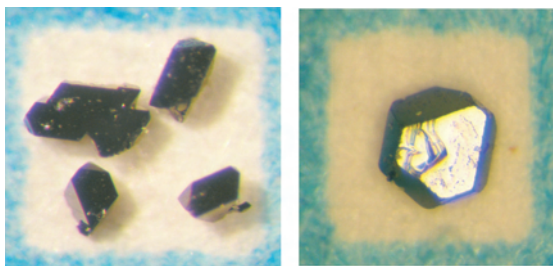


Figure 14: Single crystals of superconducting β -pyrochlore KOs_2O_6 (left) and RbOs_2O_6 (right).

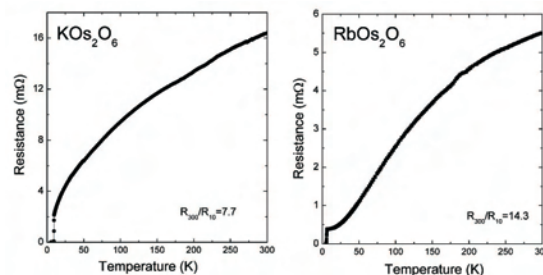


Figure 15: Temperature dependence of resistance for single crystals of β -pyrochlore KOs_2O_6 and RbOs_2O_6 .

main elements not appearing so far in known compounds; (iii) search for superconductivity in phase systems not involving Cu. Here, many of the qualitative arguments of how to make a superconductor [37, 38, 39] will be used for a guideline, however, this will mainly be done, because of a lack of advanced input which might originate from *first-principle calculations* (see US report mentioned above).

1.6 Novel pyrochlore materials

The group of J. Karpinski at ETHZ is investigating syntheses of superconducting osmates AOs_2O_6 ($A = \text{K}, \text{Rb}$) with the β -pyrochlore structure. Single crystals of superconducting β -pyrochlore KOs_2O_6 , and RbOs_2O_6 with sizes up to 0.4 mm have been grown as well in sealed quartz ampoules starting from Os metal and KO_2 (Fig. 14). The process of crystal growth of RbOs_2O_6 has been optimized by using a temperature gradient. Single crystal X-ray diffraction studies have shown that both KOs_2O_6 and RbOs_2O_6 crystallize in the non centrosymmetric space group $F\bar{4}3m$ [7, 8], while a recent Raman study indicates that the structure is centrosymmetric $Fd\bar{3}m$ [9]. Electrical resistivity measurements of the KOs_2O_6 and RbOs_2O_6 single crystals have been per-

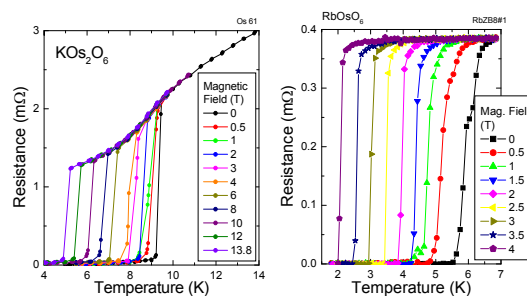


Figure 16: Temperature dependence of resistance for single crystals of β -pyrochlore KOs_2O_6 and RbOs_2O_6 measured in different magnetic fields.

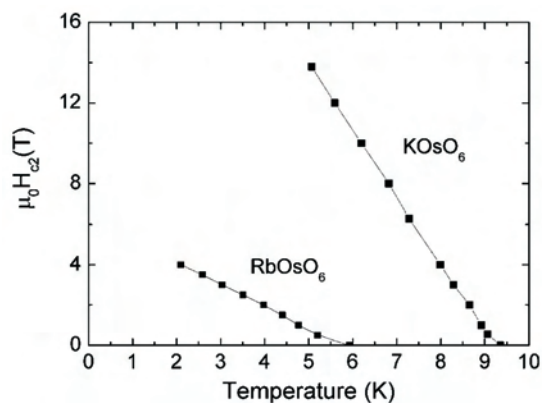


Figure 17: The upper critical fields vs temperature for β -pyrochlore KO_2O_6 and RbOs_2O_6

formed at low temperatures and in high magnetic fields (Figs. 15 and 16). The high values of the resistance ratio $R_{300}/R_{10} = 7.7$ for KO_2O_6 and $R_{300}/R_{10} = 14.3$ for RbOs_2O_6 suggest a good quality of the obtained crystals. The temperature dependence of the upper critical field H_{c2} for KO_2O_6 and RbOs_2O_6 were determined from the resistivity data and are shown in Fig. 17. Attempts to synthesize pyrochlore compounds $\text{A}_2\text{Os}_2\text{O}_7$ ($\text{A} = \text{Na}, \text{Ca}, \text{Sr}$) and $\text{A}_2\text{Re}_2\text{O}_7$ ($\text{A} = \text{Pb}, \text{Hg}, \text{Zn}$) under normal pressure were, however, unsuccessful.

It has been demonstrated that high pressure synthesis is highly effective in preparation of many pyrochlore type compounds [40]. This motivated the group to use high pressure and high temperature techniques in the search for other pyrochlore compounds in related systems. The syntheses were carried out in a cubic anvil device at 30 kbar in the temperature range of 800–1100 °C using AgO as an oxidizer. The results of their experiments are summarized in Tab. 2.



Figure 18: Single crystal of α -pyrochlore $\text{Na}_{1.6}\text{Os}_2\text{O}_{6.6}$ grown under high pressure.

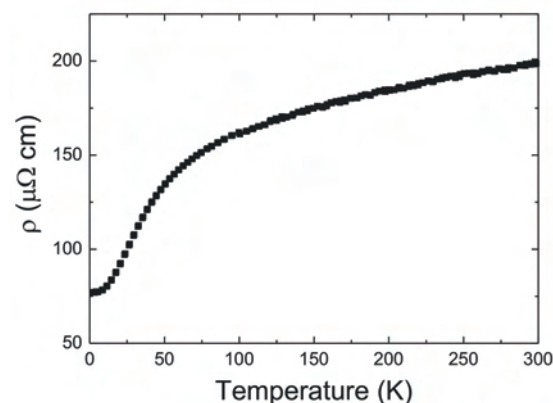
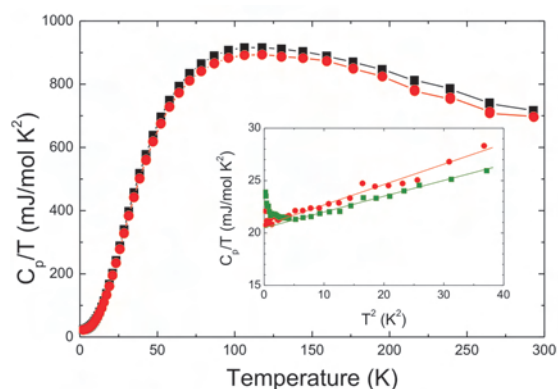


Figure 19: Heat capacity (top) and resistivity (bottom) vs temperature for a α -pyrochlore $\text{Na}_{1.6}\text{Os}_2\text{O}_{6.6}$ single crystal.

The synthesis of sodium osmate under high pressure resulted in octahedral single crystals shown in Fig. 18. From the single crystal X-ray diffraction data they have found that this compound crystallizes in the α -pyrochlore structure (Fd-3m) and exhibits high Na deficiency which leads to the composition of $\text{Na}_{1.6}\text{Os}_2\text{O}_{6.6}$. Heat capacity measurements (Fig. 19a) showed slightly enhanced value of the Sommerfeld coefficient $\gamma = 21 \text{ mJ/molK}^2$ what is roughly half of the value observed for superconducting β -pyrochlore RbOs_2O_6 [10]. The absolute value of the electrical resistivity is relatively low but, in contrast to typical metals, it is almost temperature independent (Fig. 19 bottom). The magnetic susceptibility of this compound is also temperature independent, suggesting a Pauli paramagnetism. Superconductivity has not been detected down to 0.5 K.

High-pressure synthesis of β -pyrochlore KO_2O_6 was unsuccessful, instead they have obtained a non superconducting compound of the same composition, crystallizing in the triclinic system. Using high pressure methods they were able to synthesize α -pyrochlore $\text{Ca}_{1.66}\text{Os}_2\text{O}_7$ and $\text{Ca}_{1.62}\text{Re}_2\text{O}_{6.82}$. Their phys-

Nominal composition	A-ionic radius r (Å)	Lattice parameter (Å)	Obtained compound
LiOs ₂ O ₆	0.92	no pyrochlore	LiOsO ₃
Cd ₂ Os ₂ O ₇	1.10	10.170(1)	α -Cd ₂ Os ₂ O ₇
Ca ₂ Os ₂ O ₇	1.12	10.211(1)	α -Ca _{1.5} Os ₂ O _{6.5}
(Na _{1.5} Cd _{0.5})Os ₂ O ₇	1.16	10.220(1)	α -Na _{1.7} Cd _{0.3} Os ₂ O _{6.5}
NaOs ₂ O ₆	1.18	10.170(1)	α -Na _{1.6} Os ₂ O _{6.6}
Sr ₂ Os ₂ O ₇	1.26	no pyrochlore	Sr ₃ Os ₄ O ₁₄
KOs ₂ O ₆	1.51	no pyrochlore	triclinic KOs ₂ O ₆
RbOs ₂ O ₆	1.61	10.1137(1)	β -RbOs ₂ O ₆
Ca ₂ Re ₂ O ₇	1.10	10.285(1)	α -Ca _{1.62} Re ₂ O _{6.82}
Ca ₂ Ru ₂ O ₇	1.12	10.197(1)	α -Ca ₂ Ru ₂ O ₇
Ca _{1.7} Na _{0.3} Ru ₂ O ₇	1.13	no pyrochlore	new compound (cubic)

Table 2: Summary of high pressure syntheses of the pyrochlore compounds.

ical properties have not been reported yet. These compounds have in common a substantial Ca deficiency. Measurements suggest for both compounds a metallic behavior and temperature independent paramagnetism down to 4 K.

They have also prepared α -pyrochlore Cd₂Os₂O₇ which is reported to show metal-to-insulator transition at 225 K [10]. Here, they demonstrated that by using high-pressure synthesis it is possible to prepare solid solutions Cd_{2-x}Na_xOs₂O_{7-d} which could be potentially interesting objects for further studies. They have also obtained the α -pyrochlore ruthenate Ca₂Ru₂O₇ which properties are similar to that found for Ca₂Ru₂O₇ prepared hydrothermally [41].

Karpinski's attempt to prepare strontium osmate under high pressure resulted in a novel compound Sr₃Os₄O₁₄. A collection of single crystals of this compound is shown in Fig. 20 left. The crystal structure determined using single crystal X-ray diffraction has been identified as tetragonal, isostructural to Pb₃Nb₄O₁₂F₂ [42]. The analysis of collected data suggests P4₂nm or P4₂/mnm as a possible space group. The crystal structure along [001] direction is shown in Fig. 20 right. In general, the structure may be regarded as a pyrochlore type: here, zigzag chains of BO₆ octahedra, linked to each other in the same manner, are directed along face diagonals of the cubic unit cell, forming a symmetrical framework. In this structure, such chains are retained only in one dimension. In a and b directions the chains are broken, i.e. only fragments of two octahedra remain connecting chains into a three-dimensional framework. This arrangement of a structural fragment creates another type

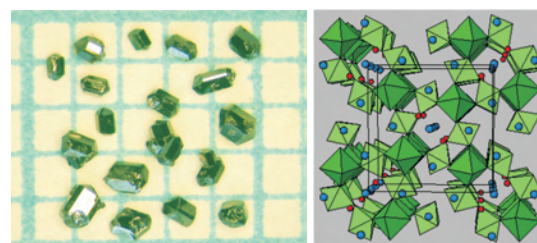


Figure 20: Left: Single crystals of Sr₃Os₄O₁₄ grown under high pressure. Right: Crystal structure of Sr₃Os₄O₁₄ along [001] direction (green octahedra – OsO₆, blue spheres – Sr, red spheres – O).

of channels, running in the same direction, namely along the c -axis. The presence of terminal oxygen atoms from Os(2)O₆ octahedra and the size of the channels allow to suggest that small cations may be intercalated in them. This compound is metallic as evidenced from resistivity measurements (Fig. 21 top) and exhibits temperature independent paramagnetism. Superconductivity has not been observed down to 2 K. The measured heat capacity is shown in Fig. 21 bottom.

An attempt to prepare lithium osmate resulted in novel compounds, e.g. LiOsO₃. This phase crystallize in rhombohedral system and presumably is isostructural with LiReO₃. Its properties are not known yet. In an attempt to substitute Ca by Na in Ca₂Ru₂O₇ under high pressure, a novel cubic Ca_{1-x}Na_xRuO₃ has been synthesized.

The pyrochlore structure contains tunnels surrounded by six BO₆ octahedra. These tunnels intersect in a three-dimensional manner. The ionic mobilities of ions in the tunnels strongly depend on the size of both the ion and the tunnel. The sodium or potassium ions in the

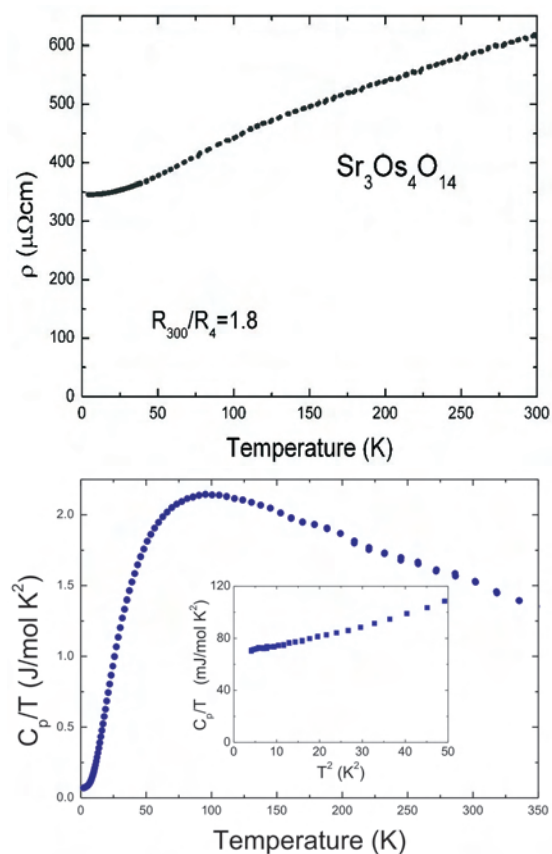


Figure 21: Temperature dependence of resistance (top) and heat capacity (bottom) for the $\text{Sr}_3\text{Os}_4\text{O}_{14}$ single crystals.

pyrochlore structure are readily exchanged by most other monovalent cations. This low temperature ion exchange allows for the formation of novel, often metastable, compounds that can not be synthesized by conventional high temperature solid state reactions.

The ionic exchange experiments were carried out by reacting pyrochlore powder with an excess of metal nitrates in air at 175–300 °C (or with 1 M HNO_3 at 80 °C); results are summarized in Tab 3. Na^+ ions in α -pyrochlore $\text{Na}_{1.6}\text{Os}_2\text{O}_{6.6}$ can be easily exchanged for K^+ or Ag^+ . Similarly, K^+ in β -pyrochlore KOs_2O_6 can be exchanged for Na^+ or Ag^+ . It is interesting to note that when Na^+ ions are exchanged for K^+ in $\text{Na}_{1.6}\text{Os}_2\text{O}_{6.6}$ the α -pyrochlore structure transforms into the β -pyrochlore one and the product become superconducting and vice versa, when K^+ ions in superconducting β -pyrochlore KOs_2O_6 are exchanged for Na^+ , non superconducting α -pyrochlore is formed. The exchange of Na^+ or K^+ ions for Ag^+ results in the formation of the α -pyrochlore $\text{Ag}_x\text{Os}_2\text{O}_{6+d}$ (non superconducting). Since the ionic radius of Ag^+ is larger than that of Na^+ , but smaller than that of K^+ , one may conclude

that, for osmates, K^+ is the smallest cation which can occupy 8b sites in the β -pyrochlore structure. All smaller cations occupy 16d sites and the α -pyrochlore structure is formed. In a reaction with 1 M HNO_3 , sodium can be completely deintercalated from $\text{Na}_{1.6}\text{Os}_2\text{O}_{6.6}$ to form $\text{Os}_2\text{O}_6 \cdot n \text{H}_2\text{O}$. Karpinski's group has found that Na^+ ions can be also exchanged for divalent Sr cations, but this process is, however, very slow. Further attempts to exchange Rb^+ , Ca^{2+} , Pb^{2+} for Na^+ , K^+ , Ag^+ or H^+ as well as Na^+ for Ba^{2+} were unsuccessful, meaning that ion exchange may practically be limited to small monovalent ions.

2 Materials by thin film methods

2.1 Pulsed laser deposition (PLD) of $\text{SrTiO}_3:\text{N}$ films

Nitrogen doped SrTiO_3 films were directly deposited by two different modifications of PLD: nitriding pulsed reactive crossed beam laser ablation (PRCLA) and RF-plasma assisted PLD (RF-PLD) developed at PSI.

PRCLA is a modification of PLD in which an additional gas pulsed synchronized with the laser is used, which crosses the ablation plume close to its origin. This geometry leads to interactions of the gas pulse molecules with the energetic ablation species, which results in the formation of the additional reactive species from the gas pulse molecules. The application of a nitrogen or ammonia gas pulse provides therefore the source of active N-containing species, which can be incorporated into the growing film.

In RF-PLD, an additional continuous RF-plasma beam is utilized, which is directed to the substrate during deposition. Using of N_2 or NH_3 for the RF-plasma leads to formation of ionized active N-containing species, which can be incorporated into the growing film. Most of the studied $\text{SrTiO}_3:\text{N}$ films revealed epitaxial growth along the (100) plane direction, even despite the relatively high lattice mismatch with $\text{MgO}(100)$ substrate of +7.8%.

The film composition was determined in two steps: first, Rutherford backscattering spectroscopy (RBS) measurements were performed to obtain the Sr:Ti:O stoichiometry. However, the sensitivity of RBS for light elements is relatively poor. Therefore, elastic recoil detection analysis (ERDA) was used to determine the N concentration. RBS analysis show stoichiometric transport of cations from the target to the growing film. The nitrogen content could be tuned within the range of 0.6–1.8 atom % by adjusting the deposition param-

Starting composition	Exchanged ions	Final composition	Lattice parameter of the pyrochlore phase (Å)
β -KOs ₂ O ₆	K ⁺ /Na ⁺	α -Na _{2-x} Os ₂ O _{6+d}	10.160
β -KOs ₂ O ₆	K ⁺ /Ag ⁺	α -Ag _x Os ₂ O _{6+d}	10.152
α -Na _{1.6} Os ₂ O _{6.6}	Na ⁺ /K ⁺	β -KOs ₂ O ₆	10.092
α -Na _{1.6} Os ₂ O _{6.6}	Na ⁺ /Ag ⁺	α -Ag _x Os ₂ O _{6+d}	10.166
α -Na _{1.6} Os ₂ O _{6.6}	Na ⁺ /Sr ²⁺	α -Sr _x Os ₂ O _{6+d}	10.232
α -Na _{1.6} Os ₂ O _{6.6}	Na ⁺ /H ₃ O ⁺	Os ₂ O ₆ ·nH ₂ O	10.199

Table 3: Summary of ionic exchange experiments.

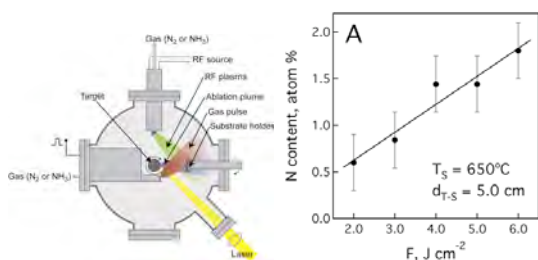


Figure 22: Left: Set-up for thin film growth. Right: Variation of the content in the films vs the laser fluence.

eters. The nitrogen concentration increased with the laser fluence, reaching a maximum value of 1.8(0.3) atom % at a laser fluence of 6.0 J cm^{-2} (Fig. 22 right). Higher laser fluences resulted in higher ablation rates, kinetic energies, and plasma ionization degrees, which led to a higher reactivity of the nitrogen species, e.g. by formation of N or N* by collisions of the energetic plasma species with N₂ molecules from the gas pulse and background.

All films deposited by PRCLA exhibited a n-type electronic conductivity, which is most probably associated with the partial reduction of the film during the deposition process. It is noteworthy to mention that homoepitaxial growth of N-doped strontium titanate films on SrTiO₃ substrates resulted in metallic-like behavior of the conductivity with very high electron mobilities, while the corresponding films deposited on MgO and LaAlO₃ substrates revealed much higher resistances and a semiconductor-to-metal transition of the conductivity with increasing temperature.

Perovskite type nitrogen substituted SrTiO₃ thin films were deposited with a one step process by RF-plasma assisted pulsed laser deposition using a N₂ plasma, while deposition with a NH₃ plasma yielded films with almost no incorporated nitrogen. The deposited films exhibited cubic perovskite type crystal structure and revealed oriented growth

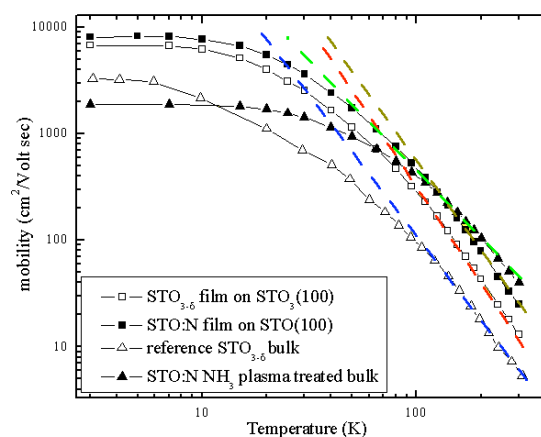


Figure 23: Mobility of films made at different conditions.

on MgO(100) substrates. The nitrogen content in the films varied from 0.2 to 0.7 atom %, which is lower compared to the corresponding films deposited by PRCLA. The amount of incorporated nitrogen in the films deposited by RF-PLD decreased with increasing RF power, while the N₂ flow rate did not have a pronounced influence on the N content. The films were insulators which is different to N-doped SrTiO₃ films deposited by PRCLA.

Comparing the carrier mobility versus temperature of the thin films with bulk materials and reduced STO showed pronounced differences. The thin films and reduced samples show a $\mu \sim T^{-2.7}$ relation (Fig. 23).

3 Preparation and modification of nanosized materials

The family of tungsten bronzes (M_xWO₃) and tungstates (M_xWO_{3+x/2}) with open structures represents an interesting and versatile target of modern materials chemistry. Their unique chemical, electrochemical and structural properties have attracted considerable research interest. They readily incorporate cations, and

the modification of the host tungstate framework opens up new options for tailoring novel materials [43]. This renders tungstates promising materials for the application as active electrodes, and they can enhance the performance of electrochromic devices, catalysts or large-scale static displays.

In the course of previous investigations, the group of R. Nesper (G. Patzke, ETHZ) has established a preparative pathway to nanoscale ammonium pyrochlore tungstates based on ammonium metatungstate (AMT, $(\text{NH}_4)_6[\text{H}_2\text{W}_{12}\text{O}_{40}] \cdot 2\text{H}_2\text{O}$) [11]. Starting from these results, they have systematically studied the morphochemistry and kinetics of the hydrothermal formation of nanostructured alkali tungstates in MCl/AMT systems ($M = \text{Li-Cs}$). In addition, they have employed microwave-hydrothermal techniques to compare the morphological behavior of selected MCl/AMT-systems under the influence of microwave irradiation to conventional hydrothermal conditions. In the next step, Nesper's group has evaluated the kinetics of nanostructured alkali HTB tungstate formation through *in situ* EXAFS and EDXRD methods.

3.1 Hydrothermal synthesis of nanoscale alkali HTB

AMT and the according alkali chloride are reacted in 25 vol. % acetic acid in a Teflon-lined stainless-steel autoclave. After 2 days of hydrothermal treatment at 180 °C, the quantitative formation of nanostructured products is completed under standard conditions [12]. The microwave-hydrothermal experiments were conducted using a MARS5 microwave digestion system (cooperation with Prof. Dr. S. Komarneni, Pennsylvania State University). For further details on the EXAFS and EDXRD measurements, see [12] (cooperations with Prof. Dr. A. Baiker/PD Dr. J.-D. Grunwaldt, ETHZ and Prof. Dr. W. Bensch, University of Kiel).

The Li- and Na-HTB tungstates readily incorporate ammonium cations from the AMT precursor, whereas the K-, Rb- and Cs-HTBs are practically ammonium-free. This has been analyzed in terms of IR spectroscopy and LA-ICP-MS analyses (cooperation with Prof. Dr. D. Günther, Laboratory of Inorganic Chemistry, ETHZ).

The alkali cations exert a distinct structure-directing influence on the phase and the morphology of the products. RbCl and CsCl tend to favor the formation of pyrochlore tungstates under hydrothermal conditions. Thus, they

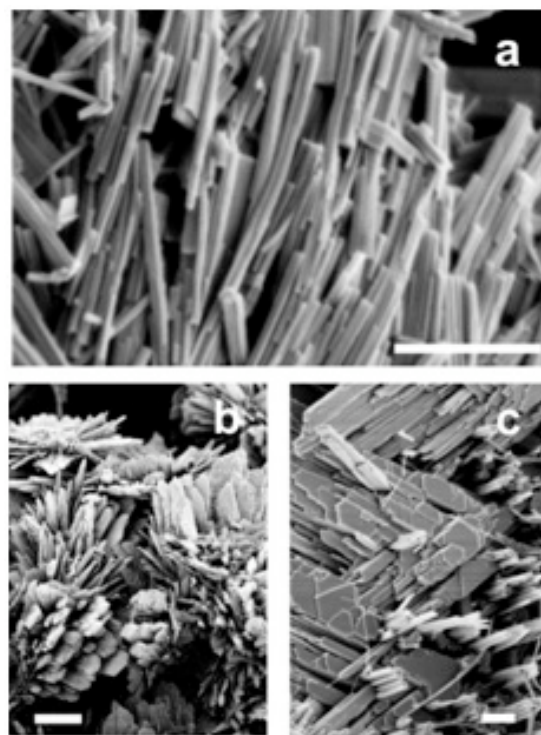


Figure 24: SEM images of lithium tungstates synthesized (a) under standard conditions (scale bar = 300 nm), (b, c) from highly diluted AMT solutions ($c(\text{W}) = 0.007 \text{ M}$; scale bar = $3 \mu\text{m}$ and 300 nm, respectively).

have conducted extensive optimization work to establish clear-cut preparative approaches to phase pure HTB tungstates that can be directly used for the production of larger quantities.

3.2 Morphology control

The aspect ratio of Li-HTB nanorods can be adjusted through the initial concentration of the AMT precursor (Fig. 24). Further dilution of the starting materials induces the growth of flower-like microscale orthorhombic lithium tungstate with HTB nanorods emerging from the flower leaves (Fig. 24b, c).

Similarly, the shape of Na-HTB tungstate nanorods can be controlled via dilution techniques. The emerging particles range from small rods with lengths around 100 nm and diameters in the 50 nm range to fibers with microscale lengths and diameters around 100 nm (Fig. 25).

Whereas the morphology of K-HTB tungstate nanorods is similar to the Na-HTB tungstate nanorods, the XRD patterns of the obtained rods reveal their almost amorphous structure. In parallel, the yields drop sharply in the K-HTB tungstate hydrothermal systems compared to their Na-based analogues.

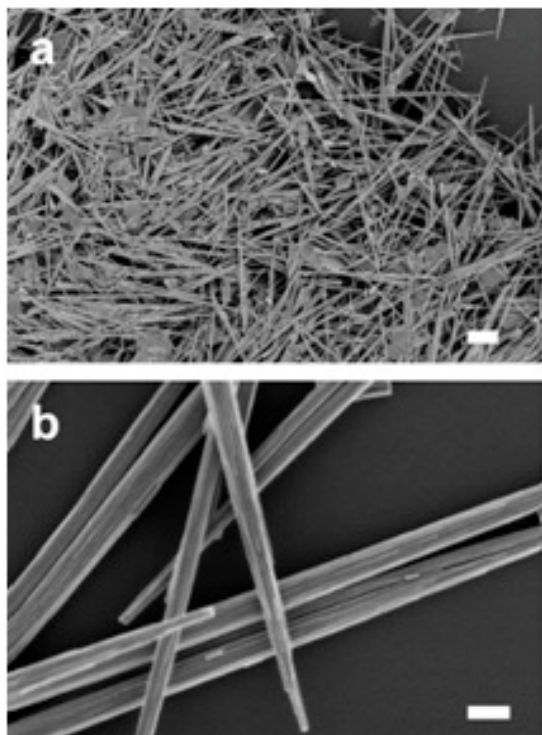


Figure 25: SEM images of Na-HTB tungstate rods synthesized from highly diluted AMT solutions ($c(W) = 0.007\text{ M}$ in H_2O). (a, b): scale bar = $3\ \mu\text{m}$ and 300 nm , respectively).

When the hydrothermal reaction of AMT was performed in the presence of RbCl, a significant morphological change was induced: the resulting Rb-HTB tungstate nanorods were very small (Fig. 26a, b), and they showed a strong tendency towards the self-assembly into cylindrical arrangements.

This effect is even more pronounced in the preparation of nanostructured Cs-HTB tungstates: they exhibit a hierarchical structure on three levels, because the above-mentioned cylindrical arrangements (Fig. 26c) tend to form microspheres.

3.3 Microwave hydrothermal experiments

The use of microwave irradiation can dramatically speed up hydrothermal reactions, and the full potential of this combined preparative approach for nanomaterials synthesis still remains to be tapped. Nesper's group has studied the effect of microwave-hydrothermal treatment on the formation of Li- and Cs-HTB tungstates. Careful adjustment of the initial Li:W ratio opens up a preparative pathway to orthorhombic tungstates with a flower-like morphology and a very low uptake of lithium. The influence of microwave treatment is even more pronounced in the CsCl-AMT hydrother-

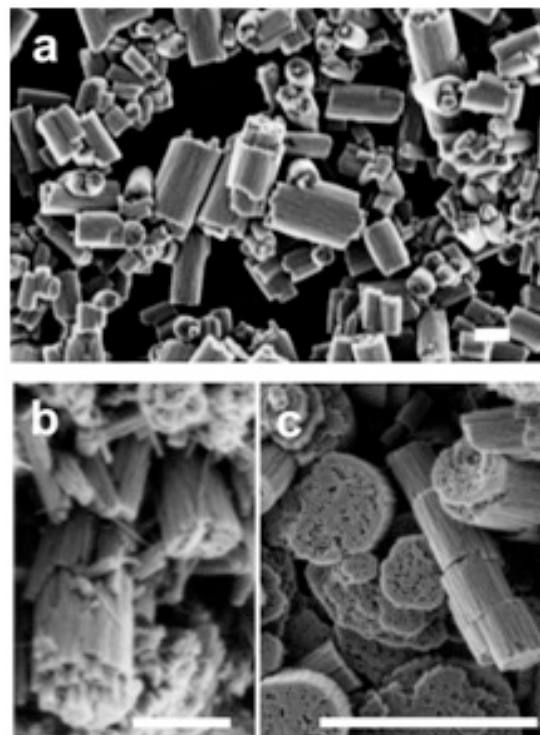


Figure 26: SEM images of nanostructured Rb-HTB tungstate rods synthesized under standard conditions (a, b): scale bar = 200 nm and of Cs-HTB tungstates (c): scale bar = 800 nm).

mal system: low Cs:W ratios favor the formation of a microcrystalline cesium tungstate with a hitherto unidentified structural motif. When an excess of CsCl is employed, phase-pure nanostructured Cs-HTB tungstates are formed: this direct preparation method saves a considerable amount of optimization work that is required for suppressing the formation of the concurring pyrochlore tungstate under conventional hydrothermal conditions.

3.4 Formation of carbon nanotubes and other carbon nanospecies

The procedure of growing carbon nanotube carpets on the surface of Si/B/C/N, the high temperature polymer Si/B/C/N ($T_{max.decomp.} = 1700\text{--}2300\text{ K}$) was further developed. The amorphous polymer which is free of grain boundaries has semiconducting properties ($E_G \sim 0.5\text{ eV}$) and a good conductivity already at room temperature due to a large number of dangling bonds in the glass matrix. It can directly be heated through a current and remains inert to air moisture. On Ni doping carbon nanotubes grow on the surface through the polymerization thermolysis in a one step process [13] [44]. This process showed to be reproducible (Fig. 27).

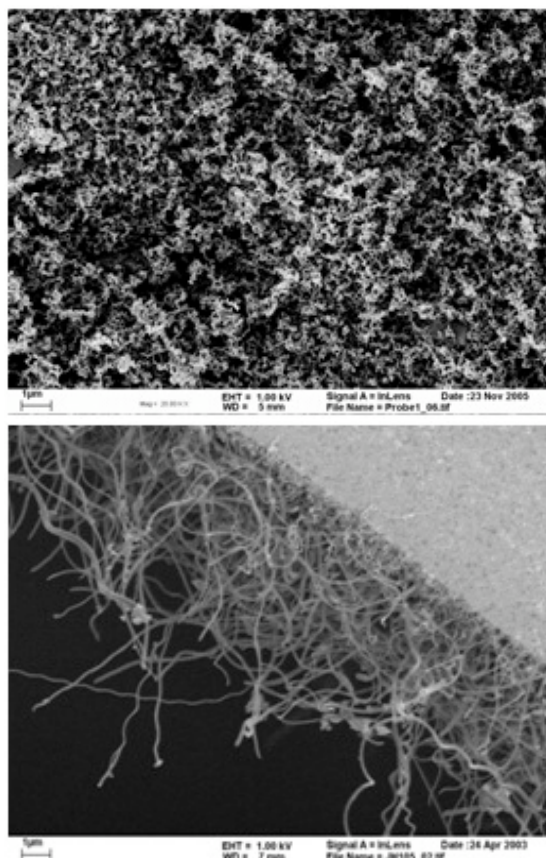
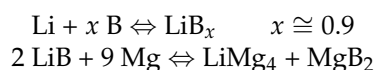


Figure 27: SEM picture of two samples of carbon NT coated Si/B/C/N polymer ceramics.

4 MgB₂ wire formation

MgB₂ wire formation was driven through a method which the group of R. Nesper (ETHZ) has sent in for patent in 2002. In 2006, the patent was granted for the EU [14], specifically the countries CH, D, E, F, GB, and I; the US version is ready for acceptance and will be granted in 2007, while the Japanese version is still in the checking phase. The method utilizes a low-melting ductile pre-alloy which may be a binary Li/B or a ternary Li/Mg/B form. Such alloy may be cast, coated or shaped into any form and thereafter transformed into MgB₂. The two steps reaction schemes at 650 °C may be written as follows:



The Li/B and the Li/Mg/B melts capture some of the impurities which may be brought into the system through many ways, mainly through impurities of the source materials, especially boron, as well as through the inert atmosphere. The procedure was primarily used to coat wires, i.e. (\varnothing 0.5 – 1 mm): Mo, Pt, Ni, Cu, W, Ag, Kanthal, stainless steel. While Pt,

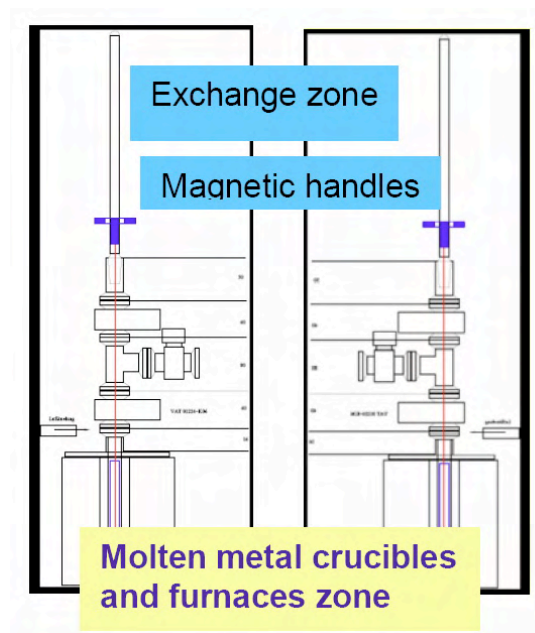


Figure 28: Small volume inert gas Schlenk line for MgB₂ wire production.

Ag and Cu react with the alloys, coating of Ni, W, Kanthal and stainless steel was successful and led to very pure MgB₂ films. However, due to shrinking effects (30% volume loss) cracks occur which have to be filled through multiple coating cycles. While the magnetic susceptibility confirmed very pure MgB₂, conductivity was inferior due to grain boundary impurities (mainly MgO and Mg₃N₂). For this reason a new small volume Schlenk apparatus was constructed (Fig. 28) which allows to perform all manipulations under inert atmosphere. By the help of a valve system, coated wires (Fig. 29) at different stages of the procedure can be transferred from one reaction tube to the next one, for example from furnace 1 to 2 or to 3 (for final tempering up to 1100 °C).

Prior to use, they introduced a carbon pre-coating for two reasons: (i) reduction of surface oxygen on the substrate wires; (ii) to enhance carbon doping into MgB₂. In addition, prior to all experiments, lithium and magnesium were distilled and boron was treated in high vacuum at 900 °C for 24 h. Measured current densities of wires are shown in Fig. 30.

4.1 Investigation on MgB₂ related hole-doped compounds

Underdoped Li_{1-x}BC and Mg_{1-y}(BC)₂ have been prepared and investigated with respect to superconductivity already a year ago [14]. Samples can be prepared up to $x = 0.5$ and $y = 0.78$ but did not show superconductivity down

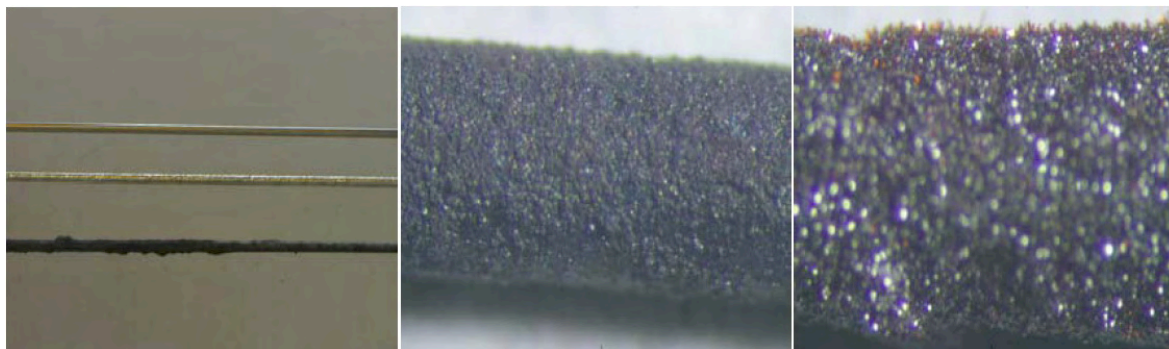


Figure 29: (left) Steps of wire coating: top — uncoated (metal Kanthal) wire; middle — LiB_x coated; bottom — MgB_2 coated; wire thickness ~ 1 mm. (right) Picture height ~ 1 mm, red transparent crystals on the surface of the wire have been identified as Li_3N .

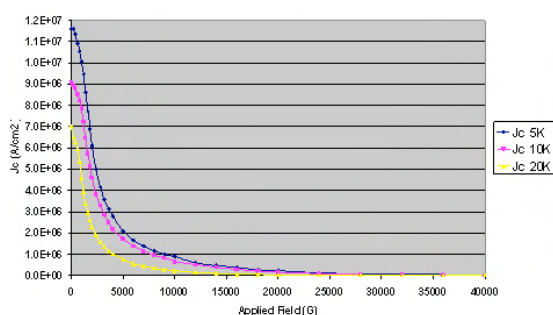


Figure 30: Current densities of a free-standing 10×1 mm MgB_2 rod prepared according to the three-step method from zero to four Tesla and 5, 10 and 20 K (blue, red and yellow curves).

to 4 K in magnetic measurements. According to theoretical investigations hole doping could increase the superconducting T_c to ~ 90 K for $\text{Li}_{0.5}\text{BC}$ [15]. Aiming at underdoped samples different techniques of Mg deintercalation have been applied to $\text{Mg}_{1-x}\text{B}_2\text{C}_2$ which led to compositions from $0 < x < 0.25$. The thermal decomposition under vacuum resulted in the formation of graphite and borocarbides above 900°C as reported already. Synthesis at reduced Mg ratios yielded hole doped MgB_2C_2 samples which could also be reintercalated by either Mg or Li-metal under preservation of the structure. None of these samples did show a Meissner effect down to 4 K.

5 Collaborative efforts

Members of Project 4 have many collaborations to groups outside MaNEP (see report). Collaboration within MaNEP are the following: (i) Schilling, Hulliger Karpinski cooperate in the field of high pressure syntheses, (ii) Nesper and Flückiger work on MgB_2 wire formation, (iii) Nesper and Fischer cooperate on the development of sensor materials. A collabora-

tive project was started between van der Marel and Hulliger on possible d1-vanadium oxide superconductors.

6 Goals for the next year

Forró: further improvement of the doping in ZnO by magnetic ions, increasing also the carrier density by codoping.

Hulliger: final construction and use of a new separation equipment. Investigation of Bi, Tl, Hg families for superconducting grains featuring a higher T_c than known. Investigation of new compositions, not known to show superconductivity so far.

Karpinski: synthesis of a new superconductor $\text{La}(\text{O}_{1-x}\text{F}_x)\text{FeAs}$ and related compounds. Electron and hole doping of Y124 crystals. High pressure synthesis of $\text{Ca}_{14}\text{Cu}_{24}\text{O}_{41}$, a spin ladder compound.

Nesper: synthesis of $\text{Ca}_x\text{B}_x\text{C}$ compounds, single graphene layer preparation.

Schilling: completing the electronic investigation on LaBaNiO_4 . Growth of epitaxial films for LaSrNiO_4 to apply compressive strain.

Schlapbach: further characterization of $\text{SrTiO}_3:\text{N}$ films and heterostructures (resistivity switching and dielectric properties). Deposition of strontium molybdate oxynitride films (high N loading).

MaNEP-related publications

- [1] J. Hulliger and M. A. Awan, Chem.-Eur. J. **10**, 4694 (2004).
- [2] J. Hulliger and M. A. Awan, J. Comb. Chem. **7**, 73 (2005).
- [3] J. Hulliger, M. A. Awan, B. Trusch, and T. A. Samtleben, Z. Anorg. Allg. Chem. **631**, 1255 (2005).
- [4] J. Hulliger, L. Dessauges, and T. A. Samtleben, J. Am. Ceram. Soc. **89**, 1072 (2006).
- [5] G. Couderc, J. B. Willems, B. Trusch, and J. Hulliger, Mat. Res. Bull. **42**, 1845 (2007).

- [6] L. Dessauges, J. B. Willems, D. Favre, C. Bohrer, F. Helbling, and J. Hulliger, *Supercond. Sci. Technol.* **19**, 748 (2006).
- [7] G. Schuck, S. Kazakov, K. Rogacki, N. Zhigadlo, and J. Karpinski, *Phys. Rev. B* **73**, 144506 (2006).
- [8] K. Rogacki, G. Schuck, Z. Bukowski, N. D. Zhigadlo, and J. Karpinski, *Phys. Rev. B* (2008).
- [9] J. Schoenes, A.-M. Racu, K. Doll, Z. Bukowski, and J. Karpinski, Phonons and crystal structure in the beta-pyrochlore superconductors KOs_2O_6 and RbOs_2O_6 (2008), unpublished.
- [10] M. Brühwiler, S. M. Kazakov, J. Karpinski, and B. Batlogg, *Phys. Rev. B* **73**, 094518 (2006).
- [11] A. Michailovski, F. Krumeich, and G. R. Patzke, *Mat. Res. Bull.* **39**, 887 (2004).
- [12] A. Michailovski, R. Kiebach, W. Bensch, J.-D. Grunwaldt, A. Baiker, S. Komarneni, and G. R. Patzke, *Chem. Mater.* **19**, 185 (2007).
- [13] J. Haberecht, F. Krumeich, M. Stalder, and R. Nesper, *Catalysis Today* **102**, 40 (2005).
- [14] R. Nesper, F. Ottinger, M. Reinoso, and M. Wörle, Method for producing a superconducting material made of MgB_2 , European Patent EP 1 368 840 (2006).
- [15] I. S. Costanza, Synthesis and Structures of Selected Layered Materials, and their Magnetic and electrochemical Properties, Ph.D. thesis, ETH-Zürich (2006).
- [16] R. J. Cava, B. Batlogg, T. T. Palstra, J. J. Krajewski, W. F. Peck, A. P. Ramirez, and L. W. Rupp, *Phys. Rev. B* **43**, 1229 (1991).
- [17] G. Demazeau, J. L. Marty, B. Buffat, J. M. Dance, M. Pouchard, P. Dordor, and B. Chevalier, *Mat. Res. Bull.* **17**, 37 (1982).
- [18] J. A. Alonso, J. Amador, E. Gutiérrez-Puebla, M. A. Monge, I. Rasines, C. Ruíz-Valero, and J. A. Campá, *Sol. State Com.* **76**, 1327 (1990).
- [19] P. W. Anderson, *Comm. Sol. St. Phys.* **2**, 193 (1970).
- [20] V. I. Anisimov, D. Bukhvalov, and T. M. Rice, *Phys. Rev. B* **59**, 7901 (1999).
- [21] J. B. Torrance, P. Lacorre, A. I. Nazzal, E. J. Ansaldo, and C. Niedermayer, *Phys. Rev. B* **45**, 8209 (1992).
- [22] G. Demazeau, M. Pouchard, and P. Hagenmuller, *J. Sol. State Chem.* **18**, 159 (1976).
- [23] M. James and J. P. Attfield, *J. Mater. Chem.* **6**, 57 (1996).
- [24] G. Lu, L. Cao, H. Lou, and F. Ma, *Acta Chim. Sin.* **54**, 667 (1996).
- [25] Y. Takeda, M. Nishijima, N. Imanishi, R. Kanno, O. Yamamoto, and M. Takano, *J. Sol. State Chem.* **96**, 72 (1992).
- [26] M. Al-Mamouri, P. P. Edwards, C. Greaves, and M. Slaski, *Nature* **369**, 382 (1994).
- [27] B. Grande and H. Müller-Buschbaum, *Z. Anorg. Allg. Chem.* **429**, 88 (1977).
- [28] N. Diot, R. Marchand, J. Haines, J. M. Léger, P. Macaudière, and S. Hull, *J. Sol. State Chem.* **146**, 390 (1999).
- [29] R. Arita, A. Yamasaki, K. Held, J. Matsuno, and K. Kuroki, *Phys. Rev. B* **75**, 174521 (2007).
- [30] K. Sato and H. Katayama-Yoshida, *Jap. J. Appl. Phys.* **39**, L555 (2000).
- [31] T. Dietl, H. Ohno, F. Matsukura, J. Cibert, and D. Ferrand, *Science* **287**, 1019 (2000).
- [32] R. Seshadri, *Curr. Op. Sol. St. Mat. Sci.* **9**, 1 (2005).
- [33] J. M. D. Coey, *Curr. Op. Sol. St. Mat. Sci.* **10**, 83 (2006).
- [34] J. Hagberg, E. Lähderanta, G. Zsolt, S. Leppävuori, I. Kirschner, R. Laiho, A. Uusimäki, T. Porjesz, I. Dódon, G. Kovács, J. Levoska, and T. Kármán, *J. Less Comm. Met.* **164–165**, 730 (1990).
- [35] R. S. Burrows, D. H. McDaniel, and M. Abdelgadir, *J. Mag. Mag. Mat.* **125**, 269 (1993).
- [36] C. Poole, H. Farach, and R. Creswick, *Handbook of Superconductivity* (Academic Press, San Diego, 2000).
- [37] T. H. Geballe, *Science* **259**, 1550 (1993).
- [38] T. H. Geballe and G. Koster, in *Strongly Correlated Electron Materials: Physics and Nanoengineering*, I. Bozovic and D. Pavuna, eds. (SPIE, San Diego, 2005), vol. 5932, p. 59321S.
- [39] A. W. Sleight, *Acc. Chem. Res.* **28**, 103 (1995).
- [40] M. A. Subramanian, G. Aravamudan, and G. V. Subba Rao, *Progr. Sol. State Chem.* **15**, 55 (1983).
- [41] A. W. Sleight, J. L. Gillson, J. F. Weiher, and W. Bindloss, *Sol. State Com.* **14**, 357 (1974).
- [42] T. Munenaka and H. Sato, *J. Phys. Soc. Jpn.* **75**, 103801 (2006).
- [43] K. P. Reis, A. Ramanan, and M. S. Whittingham, *Chem. Mater.* **2**, 219 (1990).
- [44] M. Holzapfel, C. Jost, A. Prodi-Schwab, F. Krumeich, A. Würsig, H. Buqa, and P. Novák, *Carbon* **43**, 1488 (2005).

Other references

Project 5

Thin films, artificial materials and novel devices

Project leader: J.-M. Triscone (UniGE)

Participating members: P. Aebi (UniNE), Ø. Fischer (UniGE), G. Margaritondo (EPFL), G. Blatter (ETHZ), A. Schilling (UniZH), J.-M. Triscone (UniGE), D. van der Marel (UniGE).

Introduction: This report is summarizing our last three years efforts in the field of thin films, artificial materials and novel devices. The report describes our studies, as stated in the proposal, on: 1. “Epitaxial ferroelectric films and artificial insulating superlattices for basic studies and future applications”; 2. “Oxide thin films and heterostructures as model systems for spectroscopic, field effect and transport studies”; 3. “Novel single photon detectors using low and high- T_c superconducting nanostructures”. The main goals of the project are to produce high quality materials in thin film form which are essential for some applications and may be particularly useful for specific studies and novel devices. The use of advanced deposition techniques to fabricate heterostructures and novel oxide superlattices allowed the creation of new materials with designed properties and also new phenomena to be generated at oxide interfaces. In the summary below we describe the main results obtained in the project. It is followed by a detailed description of each sub-project.

Summary and highlights

Sub-project 1

(Aebi-Triscone)

Epitaxial ferroelectric films and artificial insulating superlattices for basic studies and future applications.

- The important issue of size effects in ferroelectrics has been studied. Several series of epitaxial ferroelectric films of PbTiO_3 were grown. X-ray diffraction and X-ray photoelectron diffraction were used to probe the non-central symmetry of the material and the material tetragonality (which can be related to the polarization) as a function of film thickness. The results point to a progressive reduction of the polarization as the film thickness is reduced due to an imperfect screening of the polarization. Films as thin as three unit cells ($\sim 12 \text{ \AA}$) are found to be ferroelectric. Also, it is found that the polar distortion is controlled, as the film thickness is reaching the unit cell level, by surface relaxation and rumpling.
- The project has initiated a substantial development of photoemission based methods for probing ferroelectric thin films. Using the chemical sensitivity of X-ray photoemission spectroscopy and the angular intensity distribution of core level emission lines ultra-thin ferroelectric PbTiO_3 films grown on Nb-SrTiO_3 have been studied at the atomic scale. This is an important progress since it allows an atom

specific view of these significant materials which was previously not possible.

- In $\text{Pb}(\text{Zr,Ti})\text{O}_3$ films, atomic force microscopy was used to demonstrate that 2D ferroelectric domain wall motion is a creep process controlled by random bond disorder in the presence of dipolar interactions (this part is not described in the report, details can be found in [1]).
- Superlattices based on ferroelectric PbTiO_3 and paraelectric SrTiO_3 have been realized. In this system, the key ferroelectric properties can be tailored by changing the volume ratio between PbTiO_3 and SrTiO_3 . At short wavelengths, a new behavior is observed linked to the coupling between antiferrodistortive and polar instabilities. This very unusual coupling is leading to an improper ferroelectricity (the polarization is not the main order parameter) which manifests itself by a polarization developing linearly in temperature and a dielectric constant essentially temperature independent close to T_C but with a very large value, potentially useful for applications.

Related publications: [1, 2, 3, 4, 5, 6, 7].

Sub-project 2

(Aebi, Margaritondo, Pavuna, Fischer, van der Marel)

Oxide thin films and heterostructures as model systems for spectroscopic, field effect and

transport studies.

- In the past three years, we have continued systematic studies of direct ARPES (no cleavage of samples) on *in situ* grown compressively and tensively strained high- T_c (La, Sr)₂CuO₄ (LSCO-214) films [8]. Specifically, the electronic band structure on 12 unit cells thin epitaxial LSCO-214 films under extreme tensile strain shows anomalous features compatible with *c*-axis dispersion [9]. This result is in striking contrast with the usual quasi-two-dimensional dispersion observed up to now in most superconducting cuprates, including relaxed and compressively strained LSCO-214 films grown under the same conditions. The data were analyzed using a 3D tight-binding dispersion for a body-centered tetragonal lattice. We relate the enhancement of the *c*-axis dispersion to the significant displacement of the apical oxygen induced by the strain [9].
- In this sub-project, we also have exploited the possibility to grow thin films of various materials including manganites and cuprates with a very high degree of crystallinity and ultra flat surfaces. These films are fabricated in the form of single phase materials, where the strain induced by the substrate mismatch can be tuned by controlling the film thickness. These films have been used to investigate electronic properties, polaronic transport and superconductivity.
- The optical conductivity of thin single crystal SrTi_{1-x}Nb_xO₃, for *x* between 0 and 0.01, has been determined in the spectral range between 1.5 and 37000 cm⁻¹. This has been done by performing transmission and/or reflection measurements in

the THz and infrared range and ellipsometry in the near-infrared to ultraviolet regions. Our experimental data indicate that this mass renormalization is about a factor two.

Related publications: [8, 9, 10, 11].

Sub-project 3

(Blatter, Schilling, Fischer)

Novel single photon detectors using low and high- T_c superconducting nanostructures.

- Superconducting single photon detectors (SSPD) are a type of device combining ultimate sensitivity (single photon) with a good quantum efficiency and counting rates > GHz [24]. Recently, such superconducting single-photon detectors have attracted growing interest from diverse fields such as astronomy, spectroscopy or quantum communication.
- Here, we investigated the properties of NbN thin film superconductors, which we further structure into narrow bridges or meander lines with typical thickness $d < 10$ nm and widths $w \lesssim 100$ nm. The meander lines are of particular interest. It has been shown [25] that such structures, suitably operated, can be utilized as very fast and sensitive single-photon counters in the visible and near-infrared spectral range.
- We also have investigated high- T_c superconductors YBa₂Cu₃O_{7- δ} (YBCO)/PrBa₂Cu₃O_{7- δ} (PBCO) films in order to provide alternative materials to current state-of-the-art SSPDs, made from NbN.

Related publications: [12, 13, 14, 15, 16, 17].

1 Epitaxial ferroelectric films and artificial insulating superlattices for basic studies and future applications.

In this sub-project, the properties of ultrathin ferroelectric films and superlattices based on ferroelectric and dielectric materials have been studied. Ferroelectricity has been investigated at nanoscale using local probe techniques and X-ray photoelectron diffraction. Artificial ferroelectric materials with tailored properties have been realized. In short wavelength PbTiO₃ (PTO)/SrTiO₃ (STO) superlattices, an interfacial coupling of different instabilities is leading to a new type of ferroelectricity.

1.1 Finite size effects in thin ferroelectric PbTiO₃ thin films: a study of ferroelectricity and tetragonality in ultrathin PbTiO₃ films. (Aebi, Triscone)

This part contains the results of the active (Neuchâtel-Geneva, Aebi-Triscone) collaboration on the study of thin ferroelectric PbTiO₃ films.

Oxide materials exist in a wide variety of chemical compositions and structures and exhibit a

tremendous range of physical properties. In this work, we focus our attention on ferroelectric oxides with a perovskite structure, materials with remarkable functionalities which make them attractive for numerous applications. Thin film applications are of particular interest and therefore the study of finite size effects is important. We used two complementary approaches to study the intriguing modifications of the physical properties occurring when one or more physical lengths of the system are reaching the nanometre scale: high resolution X-ray diffraction and X-ray photoelectron diffraction.

Ferroelectric finite size effects have been probed in a series of *c*-axis oriented PbTiO₃ epitaxial perovskite films ranging from 500 down to 4 Å (1 unit cell). The samples were grown using off-axis RF magnetron sputtering on metallic (001) Nb-SrTiO₃ substrates and on La_{0.67}Sr_{0.33}MnO₃ epitaxial electrodes (typically 200-300 Å thick) prepared on insulating SrTiO₃ substrates. The experimental approach used to address the problem of size effects was to measure the tetragonality *c/a* versus thickness in these thin films using X-ray diffraction and X-ray photoelectron diffraction. The X-ray photoelectron diffraction technique was also used to study the non-centro-symmetry of the unit cells in the same samples.

For the PbTiO₃ series on Nb-SrTiO₃, the films are found to be monodomain and it is shown that the *c*-axis parameter systematically decreases with decreasing film thickness below 200 Å and down to the unit cell level. This decrease in the tetragonality *c/a* is related to a reduction of the polarization through the strain-polarization coupling. Using a first-principle model Hamiltonian approach, we demonstrated that films well below 100 Å are ferroelectric and that the progressive polarization reduction is due to the depolarizing field resulting from imperfect screening. Our analyses, combined with *ab initio* calculations, demonstrate that films down to 12 Å are ferroelectric and suggest for even thinner films are polar but non switchable structure [2, 3, 4].

On this series of samples, as discussed above, we applied the photoemission based, surface sensitive and atom specific X-ray photoelectron diffraction (XPD) method. A real space projection of the material structure is obtained by the experiment, probing directly the intracell atomic displacements associated with ferroelectricity. The local geometry around a selected atom is probed by intensity versus emission-angle scans of a given photoemission line. Owing to the chemical sensitivity of pho-

toemission, a given atom type is then chosen by selecting one of its core levels. The outgoing electrons exhibit a strongly anisotropic angular intensity distribution. This angular distribution originates from interference of directly emitted photoelectron waves with the scattered electron waves. The analysis of the interference patterns is facilitated by the so-called forward focusing effect taking place for kinetic energies greater than ~0.5 keV.

In order to theoretically model the angular distribution of photo-emitted electrons, multiple scattering calculations have been applied and compared with experiments via an R-factor (reliability factor analysis). This approach gives very good results despite of some limitations [18]. The variation of the tetragonality and polar distortion induced non-centrosymmetric O atom positions are preferentially probed via Pb 4*f* and O 1*s* emission, respectively [3].

Fig. 1 compares the evolution of the tetragonality (*c/a* ratio) as a function of film thickness for bulk sensitive X-ray diffraction (XRD) [2] and surface sensitive XPD [4]. The similar behavior observed for both measurements implies that the polarization evolves at the surface in the same way as inside the film and that there is no thick paraelectric dead layer at the surface. The fact that the XPD *c/a* ratio is larger than the one from XRD is not explained so far.

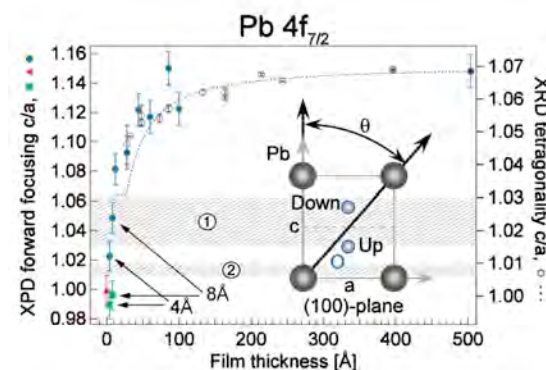


Figure 1: Tetragonality (*c/a* ratio) as a function of film thickness for PTO films (blue circles), for the Nb-SrTiO₃ substrate through PTO films of one and two unit cells (green squares) and the Nb-SrTiO₃ substrate surface (red triangle). Black open circles are X-ray diffraction data and the black dotted curve is the result from model Hamiltonian calculations. Ribbons, labeled 1 and 2, indicate regions as discussed in the text. The left scale indicates the *c/a* values extracted from the XPD experiment. The inset shows the crystallographic plane used to extract the *c/a* ratio. Pb-Pb scattering dominates compared to Pb-O scattering allowing θ to be determined via Pb-Pb forward focusing.

The XPD measurement shows a continuous decrease of tetragonality down to the thickness of one unit cell. Two ribbons are drawn in Fig. 1, labeled with 1 and 2, indicating regions where c/a values of 1.03 (value expected at the bulk level for the paraelectric phase, resulting from the mechanical constraint imposed by the substrate) and 1.01 (value expected from surface relaxation and rumpling as shown by the *ab initio* calculations [4]) are crossed with respect to both c/a scales. This observation implies, via the polarization-strain coupling, that the films have a finite — although progressively reduced — spontaneous polarization. At thicknesses of one or two unit cells, the macroscopic elasticity no longer applies and surface relaxation and rumpling dominates, suggesting the absence of any additional ferroelectric distortion at these thicknesses.

Fig. 2 shows energy shifts observed for the core level photoemission lines of the PTO films as a function of thickness. Such shifts are related to changes of the electrostatic potential of the films (band bending, charging). It is striking to see that the evolution is identical to the one observed for the tetragonality and it is obvious to try to link the shifts to the electrostatic potential drop created by the ferroelectric polarization across the screened ferroelectric films. Therefore, if the shifts are attributed to this potential drop it is possible from a simple electrostatic model to extract the effective screening length of the ferroelectric films with the substrate as the bottom electrode and the exposed-to-air surface with C and O related species (H_2O , C-O groups, O-H groups, etc.) as the top electrode. However, recent, detailed experiments on these energy shifts show a rich phenomenology and suggest a more complicated scenario. As a matter of fact, the experiments show energy shifts of core level photoemission lines not

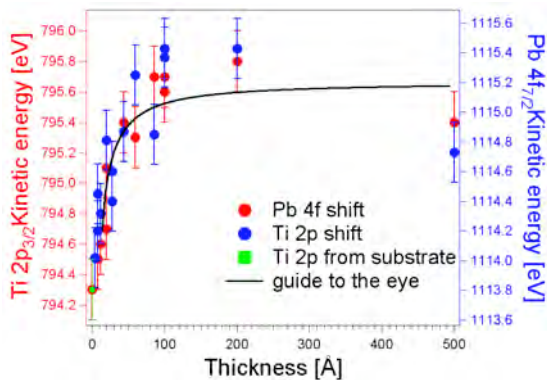


Figure 2: Kinetic energy shifts of the Pb 4f and Ti 2p core level photoemission lines as a function of the PTO film thickness.

only as a function of thickness: a partial removal of carbon related species at the top electrode shifts the spectra to lower kinetic energies (E_{kin}) whereas the complete removal induces a shift to higher E_{kin} . Furthermore, lowering the temperature decreases E_{kin} (with an amplitude depending on the thickness of the film) and regions close to the surface emit electrons with decreased E_{kin} .

A simple electrostatic model as suggested above does not explain all these phenomena and a more elaborate model has to be found including screened ferroelectricity but also charge carrying surface/interface states.

All the experiments described above have been performed on $PbTiO_3$ films prepared on metallic Nb-doped STO substrates. The behavior observed for the series of $PbTiO_3$ films on $La_{0.67}Sr_{0.33}MnO_3$ electrodes prepared on insulating substrates is however strikingly different [19]. Using X-ray diffraction, a decrease in tetragonality is first observed as the film thickness is reduced but is followed by a recovery for the thinnest films studied as can be seen on Fig. 3. This behavior is accompanied by a change from a monodomain to a polydomain configuration of the polarization with 180° alternating polarization domains. This transition was confirmed by piezoresponse atomic force microscopy measurements, also allowing a direct demonstration of the ferroelectric switching of the polarization in $PbTiO_3$ films as thin as 28 Å (Fig. 4). Using X-ray photoelectron diffraction however, all samples were found to be monodomain, with a tetragonality value in good agreement with the values found for the $PbTiO_3$ thin films of similar thickness prepared

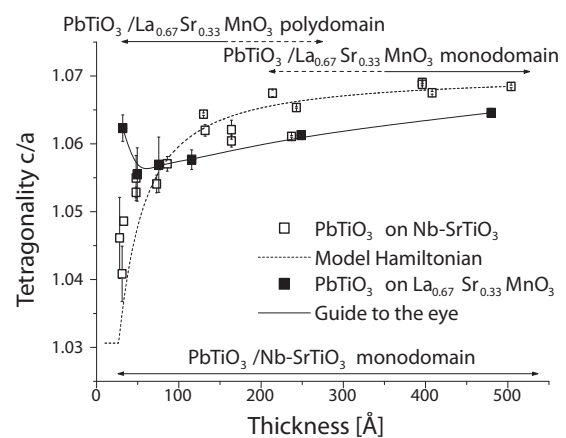


Figure 3: Tetragonality as a function of film thickness for $PbTiO_3$ films grown on $La_{0.67}Sr_{0.33}MnO_3$ (black squares), compared to what was obtained in the case of $PbTiO_3$ films grown on Nb-SrTiO₃ (open squares).

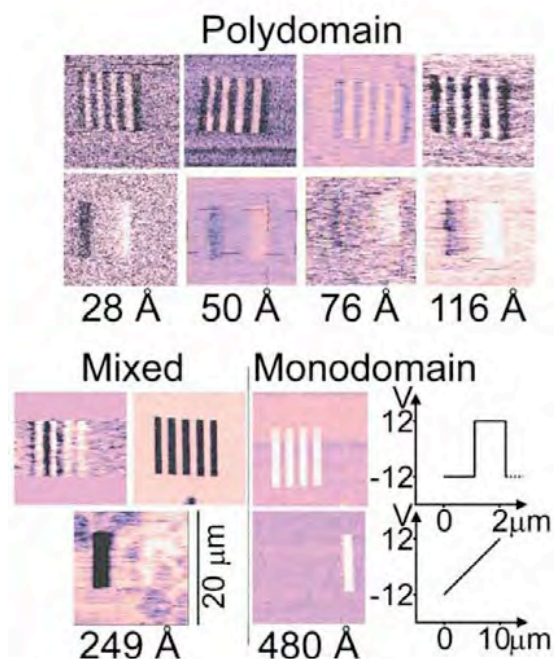


Figure 4: Top: piezoresponse signals obtained after alternate -12 V and $+12$ V voltages were applied between the metallic tip and the conducting $\text{La}_{0.67}\text{Sr}_{0.33}\text{MnO}_3$ layer to polarize nine stripes over a 10×10 mm² area. Bottom: piezoresponse signal obtained after application over a 10×10 mm² square of a voltage gradually ramped from -12 V up to $+12$ V. These data also demonstrate ferroelectric switching of the polarization in PbTiO_3 films as thin as 28 Å.

on Nb- SrTiO_3 substrates. It appears that during the X-ray photoelectron diffraction measurements, the samples are forced to be in a monodomain configuration, causing a reduction of the polarization (for very thin films) and a concomitant decrease of the tetragonality. Once the X-ray photoelectron diffraction measurements are finished, the samples return to their more stable state, which for the thinner film is a polydomain state, allowing a recovery of the polarization and therefore also of the tetragonality, as was checked by repeating the X-ray diffraction and piezoelectric measurements.

All the samples being epitaxially strained to the substrates, the main difference between the two PbTiO_3 series is the change of the bottom electrical boundary conditions. The results presented here thus demonstrate the key role of the electrical boundary conditions on ferroelectricity and on the ferroelectric domain structure of very thin PbTiO_3 films, and reveal in thin films the direct relationship between the tetragonality value and the domain configuration.

1.2 Artificially layered ferroelectric superlattices: tailored properties and “new” ferroelectricity. (Triscone)

Artificial superlattices and complex heterostructures are in principle interesting systems where one hopes to develop controlled properties and/or new functionalities. Here we have studied $\text{PbTiO}_3/\text{SrTiO}_3$ superlattices and discovered that in this, *a priori* simple combination of paraelectric and ferroelectric materials, the properties can be tuned over a wide range of thicknesses but also, that, for short wavelength superlattices, a new type of ferroelectricity develops.

Experimentally we have developed the ability to produce superlattice structures of high crystalline and surface qualities. We have demonstrated that the key ferroelectric parameters, polarization and critical temperature, can be tuned over a very large range in $\text{PbTiO}_3/\text{SrTiO}_3$ superlattices. Polarization can be tuned from 0 – 60 $\mu\text{C}/\text{cm}^2$ and the transition temperature from room temperature to 700 °C while maintaining a perfect crystal structure and low leakage currents in these heterostructures. We developed a simple model based on Landau theory that would guide straightforward production of samples with ferroelectric properties designed for particular applications. As electrostatic considerations force the two materials in the superlattice to have near identical polarizations, the PbTiO_3 volume fraction, $x = l_p/(l_p + l_s)$, where l_p and l_s are the thicknesses of the PbTiO_3 and SrTiO_3 layers respectively in the superlattice, is the key parameter

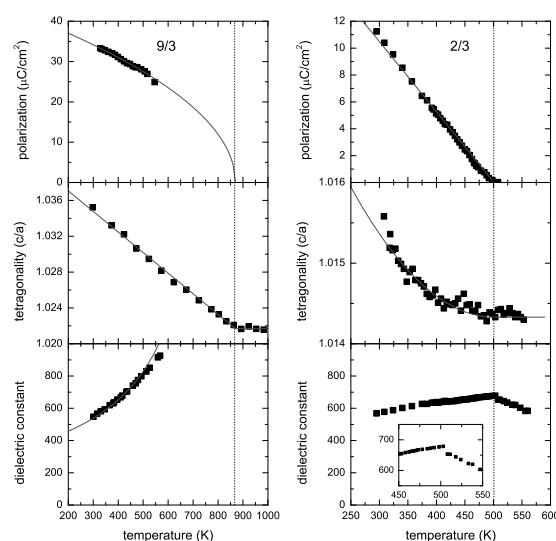


Figure 5: Polarization, tetragonality and dielectric constant as a function of temperature for two samples at high ($9/3$) and low ($2/3$) PTO volume fraction.

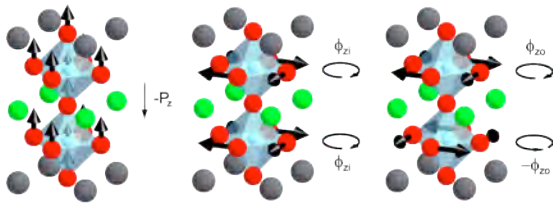


Figure 6: Three instabilities (ferroelectric and antiferrodistortive) present at the interface between PbTiO_3 and SrTiO_3 .

in controlling the properties of the system. For short wavelength superlattices, we, however, have discovered a different behavior with striking “ferroelectric” properties: a polarization developing linearly in temperature and a dielectric constant not diverging at T_C as shown in Fig. 5 where the behavior of a “normal” superlattice is compared to the one of a short wavelength one. We believe that this anomalous behavior is a signature of an improper ferroelectricity (the polarization is not the main order parameter) driven by the very special coupling of three instabilities, two antiferrodistortive ones and a polar mode. The three instabilities are schematically shown in Fig. 6. The new properties of these artificial materials, in particular the high, temperature independent, dielectric constant, might be interesting for applications. Also, this approach opens the road to a new way of designing properties using coupling of instabilities at interfaces. This interface engineering might be a way to realize new ferroelectrics and new multiferroic materials.

2 Oxide thin films and heterostructures as model systems for spectroscopic, field effect and transport studies.

In this sub-project, complex oxides such as doped $(\text{La,Sr})\text{CuO}_4$, SrTiO_3 and manganites thin films are investigated. On $(\text{La,Sr})\text{CuO}_4$ films, *in situ* ARPES measurements have been successfully realized. In doped SrTiO_3 and manganites, the nature of the transport properties is investigated.

2.1 ARPES on $(\text{La, Sr})_2\text{CuO}_4$ (LSCO-214) thin films (Margaritondo, Pavuna)

In the past three years, we have continued systematic studies of direct ARPES (no cleavage of samples) on *in situ* grown compressively and tensively strained high- T_C $(\text{La, Sr})_2\text{CuO}_4$ (LSCO-214) films [8]. Specifically, the electronic band structure on 12 unit cells thin epitaxial LSCO-214 films under extreme tensile strain

shows anomalous features compatible with c -axis dispersion [9]. This result is in striking contrast with the usual quasi-two-dimensional dispersion observed up to now in most superconducting cuprates, including relaxed and compressively strained LSCO-214 films grown under the same conditions. The data were analyzed using a 3D tight-binding dispersion for a body-centered tetragonal lattice. We relate the enhancement of the c -axis dispersion to the significant displacement of the apical oxygen induced by the strain [9].

In 2007 we have successfully directly linked our EPFL laser ablation system to an XPS-Scienta set-up. Subsequently we have fabricated thin, superconducting La-doped Bi-2201 films and performed *in situ* ARPES measurements. We have developed a simple model for the nucleation of random intercalates during the growth of high-temperature superconductor films [10, 11] by laser deposition (PLD). The model predicts a very particular spatial distribution of defects: a Markovian-like sequence of displacements along the growth direction (c -axis), as well as a two-component in-plane correlation function, characteristic of self-organized intercalates. A model for X-ray diffraction (XRD) on such structures is also developed and accounts for both c -axis and in-plane anomalies observed in XRD experiments. Our method constitutes a useful characterization tool in the optimization of deposition parameters for the growth of similar oxide films [10]. The very first ARPES spectra measured on as grown La-doped Bi-2201 thin high- T_C film shown on Fig. 7 are rather striking as films are not cleaved, and yet exhibit pronounced quasi-particle peaks directly observed from the as-made film surface.

We also note that following our successful demonstration of the concept of direct ARPES (DARPES: no film cleavage) on *in situ* grown films, several other groups are now trying to adopt our approach.

2.2 Correlated oxides epitaxial growth: a study of manganites, cuprates and doped SrTiO_3

a) *Manganites thin films* Doped rare-earth manganese oxides (manganites) have been the focus of intensive research since the discovery of “colossal” magnetoresistance in thin films [26]. This effect, present also in bulk samples, is related to a field-induced shift of the insulator-to-metal transition (MIT) temperature. Intrinsic phase separation has been proposed to play a major role at the MIT [27], but scanning tunneling spectroscopy (STS) experiments per-

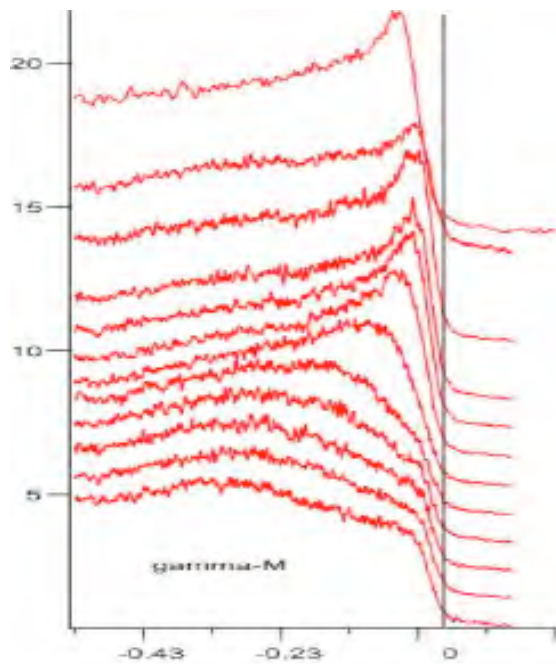


Figure 7: As measured ‘raw’ ARPES spectrum on non-cleaved (as grown) La-doped Bi-2201 thin high- T_c film.

formed on films of the same nominal composition have shown both the presence [28] and absence [29] of electronic inhomogeneities in the sub-micron scale.

We have grown and carefully characterized films of the paradigmatic $\text{La}_{0.67}\text{Ca}_{0.33}\text{MnO}_3$ (LCMO) manganite on (100) SrTiO_3 (STO), (100) LaAlO_3 (LAO) and (110) NdGaO_3 (NGO) substrates. Details on the growth procedure are presented in Ref. [20]. Structural analysis using X-ray diffraction in Fig. 8 shows that films grown on substrates with a large ($\gtrsim 1\%$) lattice-parameter mismatch to LCMO are fully strained at thicknesses below roughly 100 nm. On increasing thickness, a partial relaxation of the film lattice parameters towards bulk values takes place but a substantial part of the film remains in a high-strain state. At large thickness, films are thus structurally inhomogeneous: regions with different degrees of structural strain coexist within the film. In the case of films grown on NGO, considered often as “bulk-like” [30, 31] because of the small mismatch ($\lesssim 0.1\%$), we observed the presence of compressive strain at small thickness and its relaxation on increasing thickness [20]. Unlike for large-mismatch substrates, no signature of the coexistence of strained and relaxed domains was observed at large thickness, the relaxation appears to be homogeneous throughout the film [20].

In manganites, lattice, charge and magnetism

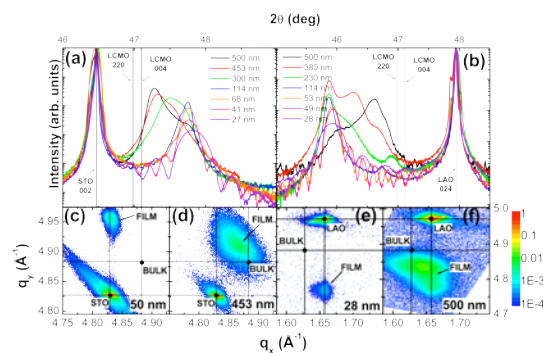


Figure 8: Second order reflection for the out-of-plane parameter of LCMO films grown on (a) STO and (b) LAO. Reciprocal space maps around the (303) pseudocubic reflection (c) for a 50 and (d) a 453 nm film grown on STO. Reciprocal space maps around the (103) pseudocubic reflection for (e) 28 and (f) 500 nm thick LCMO films grown on LAO. Films are fully strained at low thickness and as thickness is increased an inhomogeneous relaxation of strain occurs.

are strongly coupled, so modifications in structure due to biaxial strain are expected to give rise to changes in the transport properties. Fig. 9 presents a comparison of transport properties for films grown on STO and NGO at different thicknesses. The polaron activation energy, E_a , obtained from a fit of the high-temperature resistivity with an adiabatic small-polaron model [32] $\rho = AT \exp(E_a/kT)$ is plotted in Fig. 9a. The activation energy is roughly a half of the polaron binding energy. Fig. 9b shows the insulator-to-metal transition temperature obtained as the temperature at which $d\rho/dT$ changes sign (full

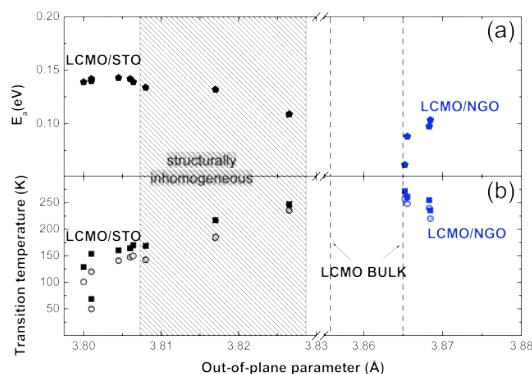


Figure 9: Transport properties of LCMO films grown on STO and NGO: (a) polaronic activation energy and (b) metal-insulator transition temperature (full symbols) and Curie temperature (hollow symbols) obtained from resistivity measurements (see text).

symbols) and the ferromagnetic Curie temperature obtained from the maximum slope in the resistivity curve. The behavior of both activation energy and transition temperature is independent of the sign of the substrate-induced strain. The transition temperature decreases and the polaron activation energy increases as strain is increased for films grown on STO (tensile strain) as well as for films grown on NGO (slightly compressive strain). The hatched zone represents the structurally inhomogeneous films on STO, for which the plotted lattice parameter corresponds to the maximum intensity in Fig. 8a. The structural anisotropy induced by the biaxial strain breaks the degeneracy of e_g orbitals, favoring carrier localization [33]. Strain provides thus a way to control transport properties. However, the coexistence of regions with different strain states in the same sample implies the coexistence of regions with different (local) transport properties. In investigations regarding ‘intrinsic’ inhomogeneities, films grown on NGO or homogeneously strained samples on large-mismatch substrates should be favored. The local electronic properties of homogeneously strained films measured by scanning tunneling spectroscopy are shown under Project 1.

b) *Growth and properties of $La_{1.9}Sr_{0.1}CuO_4$ thin films* We have studied properties of thin films of $La_{1.9}Sr_{0.1}CuO_4$ (LSCO) grown on $SrLaAlO_4$ substrates, with a Pulsed Laser Deposition system. We have grown films of different thicknesses, from 38.8 nm down to 3.9 nm (3 unit cells), without any buffer or cap layer. For ev-

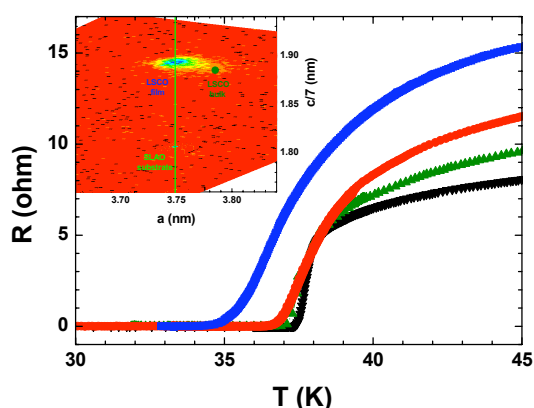


Figure 10: Resistance vs temperature measured for samples of different thicknesses: 3.9, 6.5, 13.3, 38.8 nm. Inset: reciprocal space map measured by X-ray diffraction on the 38.8 nm thick film. The large spot represents the film, the small spot represents the substrate. The dot is the theoretical position of bulk LSCO.

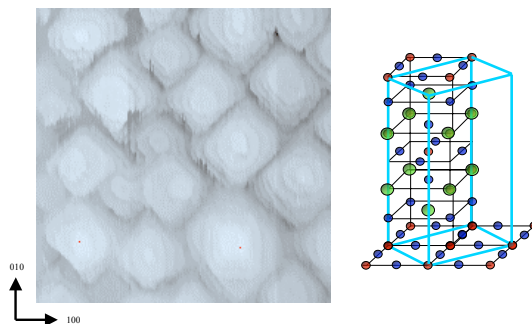


Figure 11: Topographic 400 nm by 400 nm image obtained by STM on a 35 nm thick film. Terraces are separated by 0.65 nm steps.

ery thickness we obtained a high crystalline quality, as shown by X-ray diffraction. Inset of Fig. 10 shows the reciprocal space map of a film of 38.8 nm. The spot shows that the a -axis parameter of the film is equal to that of the substrate, with only a slight dispersion towards the value of bulk LSCO. This proves that the films are strained by the substrate (compressive strain), up to thicknesses of 38.8 nm.

The transition temperatures T_c of the films measured by resistivity are shown on Fig. 10. A remarkable result is that the T_c remains very high for a 3.9 nm film, i.e. only 3 unit cells thin. One year later, the T_c value was unchanged, proving that the films are very stable and do not alter with time. Hall effect studies also revealed that the number of carriers was similar to that found on bulk samples.

An STM topographic image of a 35 nm thin film (Fig. 11) shows islands of piled up terraces separated by steps of 0.65 nm height (half a unit cell). The islands are oriented 45° from the substrate main axis. This shows that the grains grow along the [110] axis, which is consistent with an orthorhombic structure of the unit cell. On these films, superconducting properties could not be probed using scanning tunneling spectroscopy, possibly because of surface contamination during the film transfer.

c) *Growth of $Nd_{1+x}Ba_{2-x}Cu_3O_{7+\delta}$ (NBCO) and $YBa_2Cu_3O_{7-\delta}$ (YBCO) films* We produced NBCO films by RF magnetron sputtering deposition on (100) $SrTiO_3$ substrates, who met our criteria beyond our best expectations. For example, the flatness of our 40 nm thick films was 2-3 unit cells, peak-to-peak, for $2.6 \mu m^2$ (Fig. 12), and the observed density of particles was very low thus allowing a patterning process to be performed. However it appeared that oxygen’s stoichiometry in this compound is highly unstable, meaning that superconducting properties are partially to totally lost with

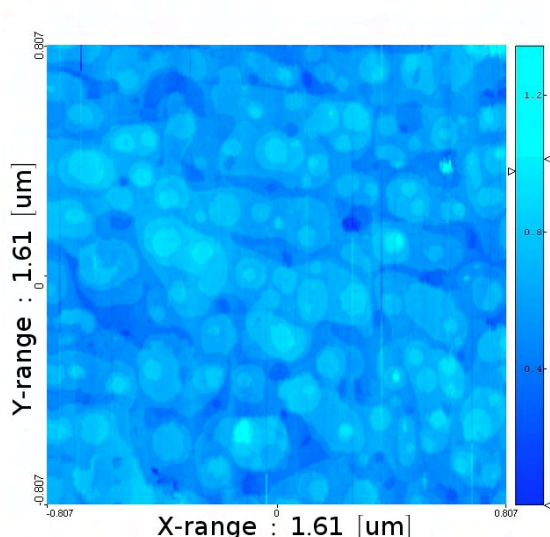


Figure 12: STM surface topography of a 40 nm thick $\text{Nd}_{1+x}\text{Ba}_{2-x}\text{Cu}_3\text{O}_{7+\delta}$ film grown on SrTiO_3 . Two successive color levels correspond to a unit cell. Unlike YBCO, no screw dislocations are present on the NBCO films, which present an exceptional flatness inside the 123 family.

time or treatments. Unlike YBCO, where the cation's solubility cannot fluctuate, in NBCO x can easily reach up to 0.4, leading consequently to more inhomogeneities in the films. Moreover Nd ions are magnetic, hence not suitable for muons measurements. For this reason, 13 nm thick YBCO films with $T_{c0} = 85$ K and very nice finite size oscillations in the Bragg diffraction pattern were grown. These good crystallographic properties were also found in thick bilayers dedicated to slow muons measurements. Fig. 13 shows a (001) diffraction peak for a 75 nm/75 nm thick bilayer. Two series of oscillations are clearly distinguished, constituting the signature of a nearly perfect bilayer. To attenuate the reduction of the critical temperature occurring during the patterning process, an amorphous $\text{PrBa}_2\text{Cu}_3\text{O}_{7-\delta}$ (PBCO) top layer was deposited *in situ* by sputtering to protect the surface of the YBCO phase. Additionally, in order to secure electrical contacts we adapted an *in situ* gold evaporation deposition system involving a mechanical mask to obtain some patterned gold structures between the YBCO and the protective layer.

d) *Nanoscale field-effect studies with STM* Finally, we report here on the use of ferroelectric/doped SrTiO_3 structures to perform local, STM controlled ferroelectric field effect.

Control of the density of mobile charge carriers using electric fields is widely used in a variety of metal-insulator-semiconductor struc-

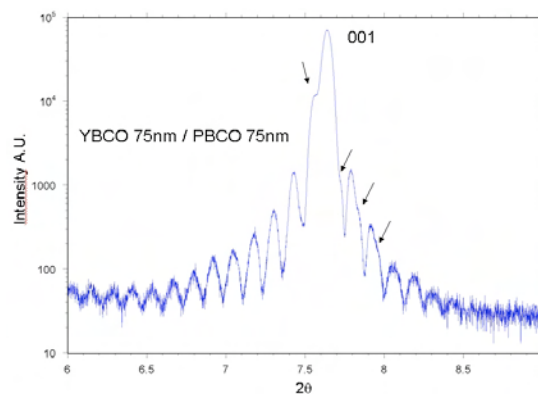


Figure 13: (001) X-ray diffraction pattern of a YBCO/PBCO 75nm/75nm thick bilayer used for slow muons measurements. The arrows point out the double periodicity of the oscillations due to the nearly perfect bilayer structure.

tures and is the governing principle behind the operation of field-effect transistors. Ferroelectric materials possessing a switchable and non-volatile polarization field can be used as insulating layers, revealing new opportunities for device applications. Advances in material processing and in particular complex oxide thin-film growth mean that high quality field-effect devices can be based on ferroelectric/metallic oxide heterostructures [21]. In addition, advances in local probe techniques such as atomic force microscopy allow them to be used in the imaging and study of small ferroelectric domain structures in bulk crystals and thin films. In this work, a scanning tunnelling microscope is used to investigate the ferroelectric field effect in all perovskite heterostructures. Scanning tunnelling spectroscopy allows us to probe the local electronic properties of the polarized channel of a ferroelectric field-effect device as a function of the field orientation. This technique can be used to read and write ferroelectric field-induced with a size as low as 20 nm [22].

2.3 Electron-phonon interaction and charge carrier mass enhancement in an archetypal perovskite

One of the major questions in the physics of high temperature superconductors [34] and colossal magnetoresistance materials [35, 36] is to what extent electron-phonon coupling is important for the transport anomalies and superconductivity. A major obstacle in addressing this issue has been the complexity of these materials. In order to separate out the electron-phonon coupling we have studied the relatively simpler perovskite compound

$\text{SrTi}_{1-x}\text{Nb}_x\text{O}_3$ with $0.001 \leq x \leq 0.02$. The lowest unoccupied bands of pristine SrTiO_3 are Ti $3d$ bands of t_{2g} character, which become occupied with electrons upon substituting Nb for Ti. Here we report a comprehensive study of this system using THz, infrared, and optical spectroscopies, as well as DC conductivity and Hall effect measurements. An optical characterization of the electron-phonon coupling in SrTiO_3 is also interesting in its own right, as it can be considered as a model system for polaron formation [37]. Our THz spectra at 7K (Fig. 14) show the presence of a very narrow (less than 2 meV) Drude peak, the spectral weight of which reveals a moderate mass enhancement of about three times the unrenormalized band mass, independent of

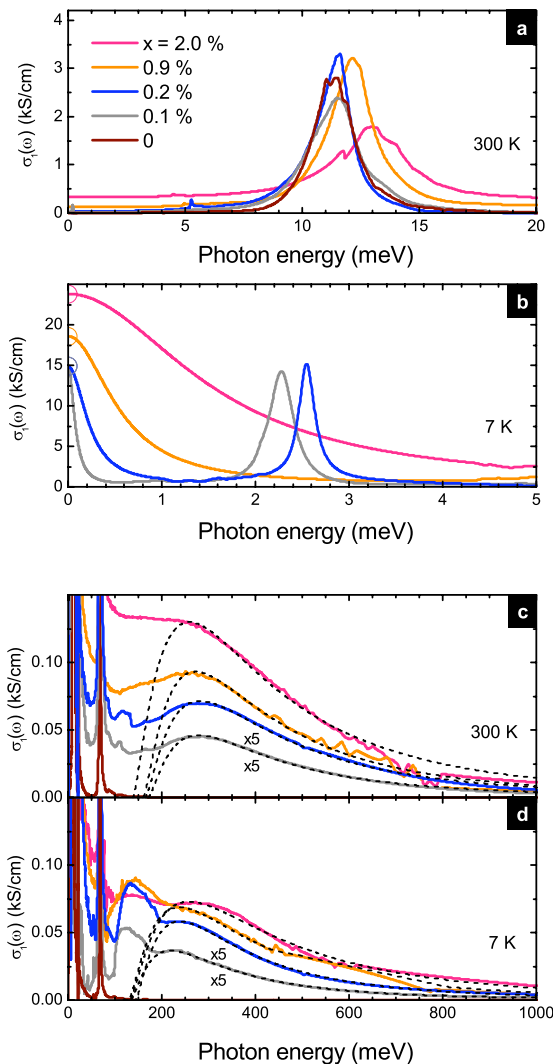


Figure 14: (a-d) The optical conductivity of $\text{SrTi}_{1-x}\text{Nb}_x\text{O}_3$ for $x = 0, 0.1\%, 0.2\%, 0.9\%$ and 2% at 300 and 7 K. Open symbols are the experimental DC conductivities. (c-d) For clarity, the mid-infrared conductivities of $x = 0.1\%$ and 0.2% are magnified by a factor 5.

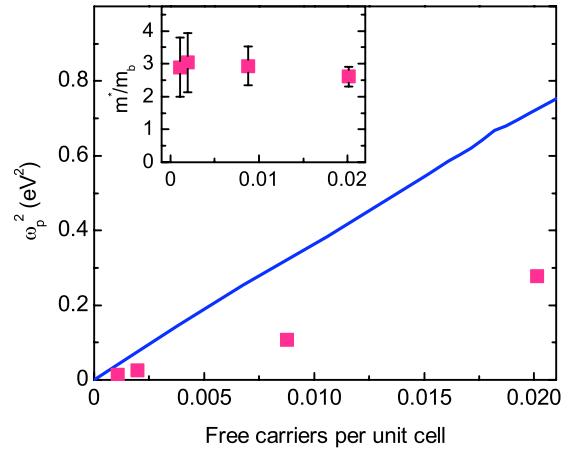


Figure 15: Experimental plasma frequency derived from the spectral weight $W(\omega)$ of the Drude peak (squares) as a function of the free carrier concentration (from Hall effect) together with the plasma frequency obtained from LDA band structure calculations (solid line). The inset shows the corresponding effective carrier mass m^*/m_b .

the carrier concentration (Fig. 15). The deficit in spectral weight is observed to be gained back by a broad ‘mid-infrared’ band, which can be understood to originate from the polaronic character of the charge carriers. Analysis of the Drude spectral weight and of the mid-infrared band indicates that the electron-phonon coupling parameter, $\alpha=4$, is of intermediate strength.

3 Novel single photon detectors using low and high- T_c superconducting nanostructures. (Blatter, Fischer, Schilling)

This part reports first on the efforts realized in Geneva on cuprates films before to describe the Zurich efforts on detectors based on nitride films.

3.1 Patterning of YBCO thin films for Superconducting Single Photon Detectors applications

Superconducting Single Photon Detectors (SSPD) are a type of device combining ultimate sensitivity (single photon) with a good quantum efficiency and counting rates $> \text{GHz}$ [24]. These properties make them an excellent candidate for single photon telecommunications and applications such as quantum cryptography. This part of the work focuses on high- T_c superconductors (YBCO/PBCO) in order to provide alternative materials to current state-of-the-art SSPDs, made from NbN. Note that LaSrCuO (see above) is a compound to consider as well in future applications.

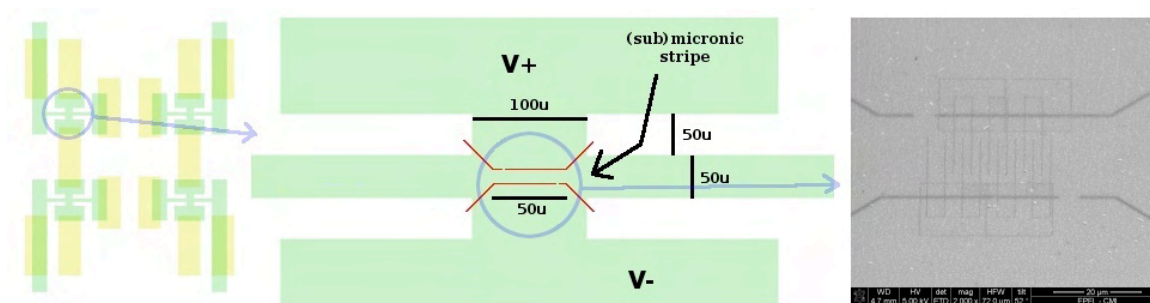


Figure 16: Scheme to pattern (sub)micronic stripes in our YBCO films – (left) design of a lithographed pattern produced chemically from a YBCO film (green): four independent structures for 4-points transport measurements; gold slots for electrical contacts are in yellow – (center) zoom in the critical area supporting the FIB-made (red) stripes, dimensions are given in micrometers – (right) SEM micrograph of a $2\ \mu\text{m}$ wide meandering stripe engineered by a $50\ \text{pA}$ focused ion beam. The stripe supporting the meander has been engineered with a higher intensity ($1\ \text{nA}$).

For this project we use YBCO/Au/PBCO structures presented in the previous section. Optical lithography being limited in resolution, a 2-step protocol was designed, involving a preliminary chemical etching followed by a focused Ga^{3+} ion beam (FIB) managed nanostructuring (Fig. 16).

It was observed that the standard FIB routines used to pattern silicon circuits cannot be carried out since they are too destructive for YBCO ultra-thin films. In this context, we began to develop a specific procedure to handle the samples. We obtained different kinds of superconducting transitions by varying the beam current, the numerical aperture, and the number of passes. Here, the lateral contamination is a crucial parameter to consider, since it directly addresses both the issues of smallest reachable dimensions and current homogeneities. We stress out that no physical etching is necessary and that it is sufficient to implant Ga^{3+} ions into the YBCO phase during the exposure, turning it locally in an insulator. We are developing a modus operandi to create superconducting YBCO structures by implanting Ga^{3+} ions with a Focused Ion Beam. We confined current in $2\ \mu\text{m}$ wide superconducting meandering wires using a $50\ \text{pA}$ beam current. Downscaling and critical current measurements are still to be performed before to study the light response.

3.2 NbN SSPD detectors

Here, we investigated the properties of NbN thin film superconductors, which we further structure into narrow bridges or meander lines with typical thickness $d < 10\ \text{nm}$ and widths $w \lesssim 100\ \text{nm}$. The meander lines are of particular interest. It has been shown [25] that such structures, suitably operated, can be utilized as

very fast and sensitive single-photon counters in the visible and near-infrared spectral range.

a) *Refined Detection Model* The detection mechanism for single photons is based on quasi-particle multiplication after absorption of a photon and subsequent creation of a normal conducting cross-section due to a bias current that is close to the critical current. The energy $h\nu$ of the absorbed photon is many orders of magnitude larger than the superconducting gap energy Δ in conventional low-temperature superconductors. In a cascading process following the initial creation of a highly excited single electron the excess energy is shared among a large number of quasi-particles. If the quasi-particle density becomes high enough, the superconducting order parameter may be locally suppressed to zero, leading to a normal conducting core inside this hot-spot. In early detection models it was assumed that this normal conducting core is essential for the detection of photons. The superconducting cross-section of the strip would be reduced and eventually the bias current in this reduced cross-sectional area will exceed the critical current density.

In our refined detection model we suggest that the formation of a normal conducting hot-spot core is not necessary to detect single photons [23, 17]. The creation of quasi-particles leads to a local reduction of the critical current density even if no normal-conducting core develops. Applying the continuity equation to the bias current and taking into account the phase coherence in the superconducting state, one can show that the creation of a minimum number of quasi-particles in a certain volume is sufficient for the temporary transition into the normal-conducting state.

The NbN thin films of SSPD are in the

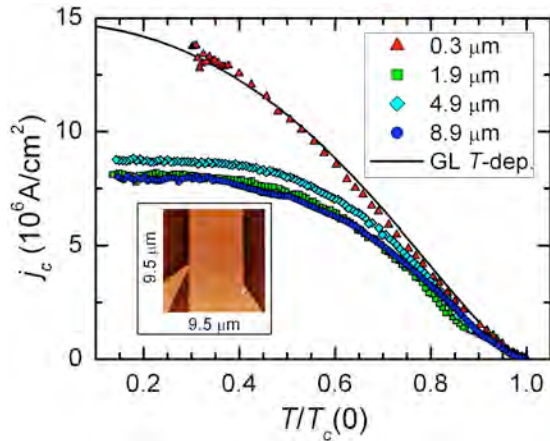


Figure 17: Critical current density j_c as a function of reduced temperature $T/T_c(0)$ for NbN bridges of different widths. The solid line is a fit of the Ginzburg-Landau depairing critical-current density to the data of the 300 nm wide bridge. The inset shows an AFM-image of the 4.9 μm wide bridge.

two-dimensional limit and their normal-state square resistance is on the order of $\text{k}\Omega$. Therefore one has to expect vortex-antivortex pairs of the Kosterlitz-Thouless type [38, 39]. Assuming vortex-antivortex pair excitations to be present in SSPD we can explain the temperature dependence of dark counts [17] and the wavelength dependence of the sensitivity and energy resolution [15, 16].

b) $j_c(T, H)$ in NbN Bridges The detection model briefly described above requires bias currents about 90% to 95% of the depairing critical-current density. Such high current densities can only be reached if the meander strip lines remain free of magnetic vortices, otherwise the dissipation-free current transport will be limited by the depinning of vortices. We have systematically measured critical current densities in NbN bridges with widths ranging from 100 nm to 10 μm to shed light on the mechanism determining the critical-current density.

We have found that the experimentally determined critical current densities in sub- μm wide bridges can be well described by the mean-field Ginzburg-Landau depairing critical current density (Fig. 17). Wider bridges deviate substantially from this temperature-dependence below a certain temperature. We interpret this reduction in critical-current density below the expectations for the depairing critical-current density as the entry of vortices due to self-field of the applied current. This can be qualitatively described with an edge-barrier model [14] taking into account edge effects analogues to the Bean-Livingston surface

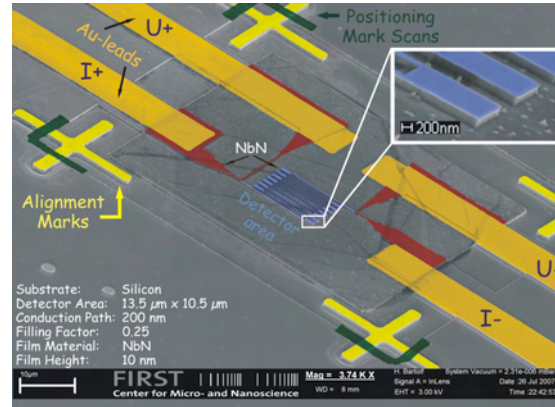


Figure 18: SEM picture of a 200 nm wide NbN meander on a Si substrate in false color representation to emphasize different elements.

barrier [40].

c) *E-beam Lithography* In order to obtain a good SSPD it is of paramount importance that the complete device is as homogeneous as possible. Already very small variations in T_c , I_c or the cross-sectional area of the strip line lead to a reduced performance or even a complete failure. This implies great demands on the production process of the device. During the last three years we have developed two alternative nanopatterning techniques of normal and superconducting thin films.

The central production step of our first technique is a lift-off process. With this technique we were able to demonstrate the production of metallic structures with minimum feature sizes down to about 10 nm [13]. However, the lift-off technique is limited to materials which can be deposited at substrate temperatures below $\approx 150^\circ\text{C}$, determined by the stability of the organic resist used.

NbN and some other interesting superconductors require substrate temperatures of several hundred degrees Celsius in order to obtain high-quality thin films. Therefore, we have developed a second e-beam lithography process that uses a reactive ion-etching step to obtain the desired nanostructures starting from an extended thin film. In Fig. 18 we show a scanning electron micrograph of a 200 nm wide NbN meander that exhibited excellent superconducting properties [12].

d) *Alternative Superconductors* So far, SSPD are sensitive in the visible and near-infrared spectral range. One way to increase the spectral range of SSPD further into the low energy range, is to use other superconductors with lower T_c . Work on thin films of TaN and MoN is already in progress.

4 Collaborative efforts

The collaboration between the Neuchâtel-Geneva groups on size effects has been crucial and has led to the use of XPD for the study of ferroelectric ultra-thin films.

On SSPD, the collaboration between Geneva and Zurich is developing.

5 Goals for the next year

Thin ferroelectric films

- We intend to elaborate the phenomenology of the shifts in kinetic energy of photoemission lines with well defined experiments. In particular, detailed measurements as a function of temperature and top electrode composition are planned. The goal is to come up with an explanation accounting for possible charging, charge transfer, surface polarization, band bending, surface and interface states.

Ferroelectric superlattices

- We plan to pursue and complete our work on PTO/STO superlattices and address questions related to the polarization instability observed on superlattices prepared on SrRuO₃. Measurements will be performed at low temperatures.
- Also, we plan to investigate in detail, the in-plane unit cell doubling linked to the AFD instability.

SSPD

- Our target is to reach submicron scale for the high T_c meanders' width. We also plan to perform optical measurements by looking for non-bolometric effects of light on the meanders' critical current.
- We will also set up an optical 3 He-cryostat to test the SSPD.
- We will realize NbN SSPD using in-house lithography process and characterize them in details.
- Finally, we will study the properties of other nitride thin films.

MaNEP-related publications

- ▶ [1] P. Paruch, T. Giamarchi, and J.-M. Triscone, *Phys. Rev. Lett.* **94**, 197601 (2005).
- ▶ [2] C. Lichtensteiger, J.-M. Triscone, J. Junquera, and P. Ghosez, *Phys. Rev. Lett.* **94**, 047603 (2005).
- [3] L. Despont, C. Lichtensteiger, F. Clerc, M. G. Garnier, F. J. Garcia de Abajo, M. A. Van Hove, J.-M. Triscone, and P. Aebi, *Eur. Phys. J. B* **49**, 141 (2006).

- ▶ [4] L. Despont, C. Koitzsch, F. Clerc, M. G. Garnier, P. Aebi, C. Lichtensteiger, J.-M. Triscone, F. J. G. de Abajo, E. Bousquet, and P. Ghosez, *Phys. Rev. B* **73**, 094110 (2006).
- ▶ [5] M. Dawber, C. Lichtensteiger, M. Cantoni, M. Veithen, P. Ghosez, K. Johnston, K. M. Rabe, and J.-M. Triscone, *Phys. Rev. Lett.* **95**, 177601 (2005).
- [6] M. Dawber, N. Stucki, C. Lichtensteiger, S. Gariglio, P. Ghosez, and J.-M. Triscone, *Adv. Mater.* **19**, 4153 (2007).
- ▶ [7] E. Bousquet, M. Dawber, N. Stucki, C. Lichtensteiger, P. Hermet, S. Gariglio, J.-M. Triscone, and P. Ghosez, *Nature* (2008).
- [8] D. Cloetta, D. Ariosa, M. Abrecht, C. Cancellieri, S. Mitrovic, M. Papagno, and D. Pavuna, in *Correlated Electron Systems* (SPIE, 2005), vol. 5932.
- [9] D. Cloetta, D. Ariosa, C. Cancellieri, M. Abrecht, M. S., and D. Pavuna, *Phys. Rev. B* **74**, 014519 (2006).
- [10] D. Ariosa, C. Cancellieri, P. H. Lin, and D. Pavuna, *Phys. Rev. B* **75**, 184505 (2007).
- [11] C. Cancellieri, P.-H. Lin, D. Ariosa, and D. Pavuna, *J. Phys.: Cond. Mat.* **19**, 246214 (2007).
- ▶ [12] H. Bartolf, A. Engel, A. Schilling, K. Il'in, and M. Siegel, *Physica C* (2008).
- [13] H. Bartolf, A. Engel, and A. Schilling, *Superconducting Single Photon Detectors*, Raith application note, Physics Institute of the University of Zurich, Switzerland (2006).
- ▶ [14] A. Engel, H. Bartolf, A. Schilling, A. Semenov, H.-W. Hübers, K. Il'in, and M. Siegel, *J. Mod. Opt.* (2008).
- [15] P. Haas, A. Semenov, H.-W. Hübers, J. Beyer, A. Kirste, T. Schurig, K. Il'in, M. Siegel, A. Engel, and A. Smirnov, *IEEE Trans. Appl. Supercond.* **17**, 298 (2007).
- [16] A. Semenov, P. Haas, K. Il'in, H.-W. Hübers, M. Siegel, A. Engel, and A. Smirnov, *Physica C* **460-462**, 1491 (2007).
- [17] A. Engel, A. D. Semenov, H.-W. Hübers, K. Il'in, and M. Siegel, *Physica C* **444**, 12 (2006).
- [18] L. Despont, D. Naumovic, F. Clerc, C. Koitzsch, M. G. Garnier, F. J. Garcia de Abajo, M. A. Van Hove, and P. Aebi, *Surf. Sci.* **600**, 380 (2006).
- ▶ [19] C. Lichtensteiger, M. Dawber, N. Stucki, J.-M. Triscone, J. Hoffman, J.-B. Yau, C. H. Ahn, L. Despont, and P. Aebi, *Appl. Phys. Lett.* **90**, 052907 (2007).
- ▶ [20] S. Seiro, E. Koller, Y. Fasano, and Ø. Fischer, *Appl. Phys. Lett.* **91**, 091913 (2007).
- [21] O. Kuffer and Ø. Fischer, *J. App. Phys.* **97**, 014103 (2005).
- ▶ [22] O. Kuffer, I. Maggio-Aprile, and Ø. Fischer, *Nature Mat.* **4**, 378 (2005).
- ▶ [23] A. Semenov, A. Engel, H.-W. Hübers, K. Il'in, and M. Siegel, *Eur. Phys. J. B* **47**, 495 (2005).

Other references

- [24] G. N. Gol'tsman, O. Okunev, G. Chulkova, A. Lipatov, A. Semenov, K. Smirnov, B. Voronov, A. Dzardanov, C. Williams, and R. Sobolewski, *Appl. Phys. Lett.* **79**, 705 (2001).
- [25] A. D. Semenov, G. N. Gol'tsman, and A. A. Korneev, *Physica C* **351**, 349 (2001).
- [26] S. Jin, T. H. Tiefel, M. McCormack, R. A. Fastnacht, R. Ramesh, and L. H. Chen, *Science* **264**, 413 (1994).

- [27] E. Dagotto, *Nanoscale Phase Separation and Colossal Magnetoresistance* (Springer-Verlag, Berlin, 2003).
- [28] M. Fäth, S. Freisem, A. A. Menovsky, Y. Tomioka, J. Aarts, and J. A. Mydosh, *Science* **285**, 1540 (1999).
- [29] J. Mitra, M. Paranjape, A. K. Raychaudhuri, N. D. Mathur, and M. G. Blamire, *Phys. Rev. B* **71**, 094426 (2005).
- [30] M. Bibes, S. Valencia, L. Balcells, B. Martínez, J. Fontcuberta, M. Wojcik, S. Nadolski, and E. Jedryka, *Phys. Rev. B* **66**, 134416 (2002).
- [31] S. Valencia, A. Gaupp, W. Gudat, L. Abad, L. Balcells, A. Cavallaro, B. Martínez, and F. J. Palomares, *Phys. Rev. B* **73**, 104402 (2006).
- [32] M. Jaime, M. B. Salamon, M. Rubinstein, R. E. Treece, J. S. Horwitz, and D. B. Chrisey, *Phys. Rev. B* **54**, 11914 (1996).
- [33] A. J. Millis, T. Darling, and A. Migliori, *J. App. Phys.* **83**, 1588 (1998).
- [34] A. Lanzara, P. V. Bogdanov, X. J. Zhou, S. A. Kellar, D. L. Feng, E. D. Lu, T. Yoshida, H. Eisaki, A. Fujimori, K. Kishio, J.-I. Shimoyama, T. Noda, S. Uchida, Z. Hussain, and Z.-X. Shen, *Nature* **412**, 510 (2001).
- [35] H. Y. Hwang, S.-W. Cheong, P. G. Radaelli, M. Marezio, and B. Batlogg, *Phys. Rev. Lett.* **75**, 914 (1995).
- [36] N. Mannella, W. L. Yang, X. J. Zhou, H. Zheng, J. F. Mitchell, J. Zaanen, T. P. Devereaux, N. Nagaosa, Z. Hussain, and Z.-X. Shen, *Nature* **438**, 474 (2005).
- [37] P. Calvani, *Nuovo Cimento* **24**, 1 (2001).
- [38] V. L. Berezinskii, *Sov. Phys.-JETP* **61**, 1144 (1971).
- [39] J. M. Kosterlitz and D. J. Thouless, *J. Phys. C* **6**, 1181 (1973).
- [40] C. P. Bean and J. D. Livingston, *Phys. Rev. Lett.* **12**, 14 (1964).

Project 6

Industrial applications and pre-application development

Project leader: Ø. Fischer (UniGE)

Participating members: M. Abplanalp (ABB), D. Eckert (BRUKER BIOSPIN), Ø. Fischer (UniGE), R. Flükiger (UniGE), L. Forró (EPFL), M. Hasler (EPFL), J. Mesot (PSI), R. Nesper (ETHZ), J.-M. Triscone (UniGE).

Introduction: Project 6 aims to bridge the gap between fundamental and applied research, and to develop projects with industry based on know-how available in MaNEP. The project covers the topics of applied superconductivity, MaNEP materials for sensors and security applications, and applications of thin film technology. We first present the main highlights of the research activities, followed by detailed reports on each sub-topic.

Summary and highlights

Applied Superconductivity

Superconducting wires This MaNEP sub-project (a collaboration between R. Flükiger (UniGe) and Bruker Biospin with contributions from R. Nesper (ETHZ)) targets the improvement of the performance of superconducting wires for industrial applications. Nb₃Sn-based wires still show room for improvement in high-field regimes, and MgB₂ appears as an interesting candidate for lower fields applications. Important results are:

- TEM measurements have revealed a strong Sn gradient in the A15 filaments of Nb₃Sn Bronze Route wires, the Sn content varying from 18 at.% in columnar grains to 24 at.% in equiaxial grains. A high resolution TEM/EELS study has revealed that inside A15 filaments, Cu is equally distributed at the grain boundaries over the whole filament volume, its amount being < 1 at%.
- We have introduced low temperature specific heat measurements as a powerful mean for determining the real T_c profile in the filaments of industrial Nb₃Sn and MgB₂ wires. In Nb₃Sn wires prepared by the Bronze Route, the width ΔT_c reached 4 K, in agreement with the TEM results. In industrial Nb₃Al wires, the measured width of $\Delta T_c = 6$ K suggests that improvements are still possible. In MgB₂ alloyed with carbon, calorimetry has shown a strong T_c distribution, revealing a strong C inhomogeneity throughout the filament.
- The variation of J_c of Nb₃Sn and Nb₃Al wires under uniaxial tensile stress was

measured up to 21 T by means of a modified Walter Spiral. Bronze Route Nb₃Sn wires have been found to be less sensitive than wires produced by competing processes and are found to be considerably more robust against transverse stresses than Internal Sn and PIT wires. This result is important in view of the construction of large magnets with strong Lorentz forces, e.g. high field dipoles or Tokamak coils for ITER.

- MgB₂ wires and tapes: By simultaneous addition of B₄C and SiC submicro-size powders to the initial B and Mg powders, a substantial enhancement of J_c was reached: at 4.2 K, $J_c = 1 \cdot 10^4$ A/cm² was obtained at values as high as 11.3 T. At 20 K, this J_c value was achieved at 4.7 T, which is among the highest reported so far. Two processes have been established to produce clean sub micron boron for MgB₂ generation.
- The relaxation rates measured on a series of superconducting wires and tapes have revealed a high potential for Y-123 Coated Conductor tapes and MgB₂ wires for persistent mode operation.

Superconducting Fault Current Limiter This sub-project covers collaborative work between the group of Ø. Fischer and M. Decroux (UniGe) with ABB, and is supported by numerical simulations carried out in the group of M. Hasler and B. Dutoit at EPFL. Superconducting Fault Current Limiters (FCLs) are based on the principle that superconductors turn into a highly resistive state when a certain critical current is exceeded. FCLs are intended to improve the actual devices present on electrical grids and to protect sensitive components

when a fault occurs on the network (i.e. short circuits, lightning strokes or any sudden excessive current bursts). Main results achieved so far are:

- We developed a new meander design to improve the switching behavior of the HTSC thin film FCL. Using this design, we have successfully tested a 10kW FCL made of two sapphire wafers connected in parallel.
- A notched-constriction design was implemented for the critical asymmetrical (low voltage) short circuits. Tests with 5 kW FCLs have confirmed the positive effect of this design. The switching behavior was further improved by implementing a thermally assisted transition mechanism. The thin-film FCL that combines the notches design together with a thermally assisted transition shows all lines switching within 2 ms of the short circuit.
- The switching behavior of Coated Conductor (CC) lines has been studied and compared to the thin film FCL. The results suggest that by tuning the grain-dominated thermal conductivity of CC lines, a FCL of technical and commercial interest can be built.
- A model has been developed to simulate the superconducting transition of the FCL. The simulation reproduces correctly the experimental fault current limitation of the thin film FCL.
- A geometrical model of 4-layer coated HTS tape was developed to perform thermal stability simulations. The model allows for accurate computations of the thermal response of the conductor to the current amplitude.

Actively shielded 16T-Magnet This work initially started between Bruker Biospin and PSI. The goal is to build a self shielded magnet for use in neutron scattering facilities. Such self shielded magnets with high magnetic fields have never been realized before.

- The actively shielded 16T-Magnet will be operational in early summer 2009 at the research at SNS — the world's strongest pulsed neutron source. Bruker Biospin as the manufacturer of this innovative magnet opens up a new field of technology aside from the application of actively shielded magnets for NMR.

MaNEP Sensors and security applications

This sub-project aims to explore the use of new materials in the field of sensing devices (contributions from L. Forró (EPFL), Ø. Fischer and J. Cors (UniGe) and G. Patzke (ETHZ, UniZH)). Also, since mid-2007, we are developing a marking technology for security applications in the framework of a CTI-MaNEP project. The sensor part covers the preparation of materials with narrow ESR line for low-field magnetic field sensing, as well as gas detection with semiconducting oxides and electrochemical sensors. The main highlights are:

- We have identified a family of quasi-one dimensional organic metals, which have very narrow ESR linewidths. These compounds are compatible with the target application of a low magnetic field sensor based on ESR technique.
- We have found that multiwire MoO₃ nanorod sensors are very sensitive to gases like NO₂ and NH₃. Their response time is faster compared to standard MoO₃ powder-based sensors.
- For Clark-type electrochemical sensors, we have obtained experimental evidence that the detection limit can be improved. The maximum cathodic current, at a given oxygen concentration, can be substantially increased by working on the microstructure of the gold surface.
- Using a modified STM setup, we have carried out first tests of a marking technology for small metal objects. A feasibility grant from CTI was obtained, as well as letters of interest from several industries.

Thin film preparation and applications

This section of Project 6 targets thin-film-based applications. The group of J. Mesot (PSI) studies the use of multilayers for supermirrors and monochromators, together with the company SwissNeutronics. The group of J.-M. Triscone (UniGE) explores the potential interest of epitaxial ferroelectric films and heterostructures for applications in oxide electronics, high frequency applications and micro-electro-mechanical systems (MEMS) devices. The main results are:

- Neutron supermirrors were prepared by reactive sputtering of Ni in Ar/N₂, at different N₂ contents in the sputter gas. It was found that supermirrors coated on

glass are stable when the generated tensile stress is below 750 GPa-nmm.

- Polarizing supermirrors based on FeCoV/TiN_x multilayers deposited on Ti-Gd/Ti absorbers have been optimized. As well, a multilayer system for neutron monochromators was investigated. For certain layer-thickness ratio, a distinct inhibition of undesired harmonics in the scattered beam was observed.
- A MBE deposition system for the growth of epitaxial SrTiO₃ buffer layers is operational. This system can accommodate 4" silicon wafers.
- Experimental results show that the ferroelectric phase transition temperature T_c in epitaxial PZT films can be substantially

higher than for the bulk, opening interesting perspectives for applications.

- PbTiO₃/SrTiO₃ superlattices offer the possibility to tune the ferroelectric properties. In the same system, for short wavelength superlattices, we have observed a high dielectric constant independent of temperature. This feature appears as the signature of an improper ferroelectricity originating of a coupling of instabilities at the PbTiO₃/SrTiO₃ interfaces.
- We have shown that the high frequency properties of epitaxial PZT films are excellent and suitable for devices based on such films. Also, the realization of MEMS on silicon with fully epitaxial oxide structures is under way.

1 Applied Superconductivity

1.1 Wires for high field applications

a) *Microstructure in Nb₃Sn filaments* A progress has been achieved in understanding the Nb₃Sn reaction mechanism in multifilamentary wires, thanks to collaboration with Dr. Marco Cantoni at the EPFL, who performed a very detailed TEM/EELS investigation. This study revealed that inside A15 filaments, Cu is equally distributed at the grain boundaries over the whole filament volume (Fig. 1) [1]. The amount of Cu is very low, < 1 at%. It is known that a small amount of Cu is nec-

essary for the formation of the Nb₃Sn phase at temperatures as low as 600–650 °C. It has been possible to establish a clear formation sequence of the equiaxed and the columnar grains (Fig. 2). We have shown that these two grain types are correlated to the local Sn content in the filaments [2]. The equiaxed grains having a high Sn content (close to 25 at.%) form at the interface with the Cu-Sn bronze (the Sn source), whereas the columnar grains with Sn contents < 22 at.% form at the growth front towards the Nb core. The dual grain structure with different Sn contents [2] is

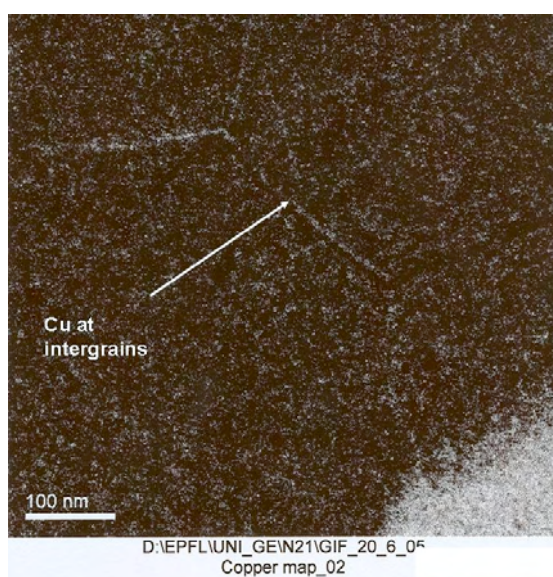


Figure 1: Visualization by TEM/EELS of the Cu present at the boundaries of equiaxed Nb₃Sn grains in a Bronze Route wire.

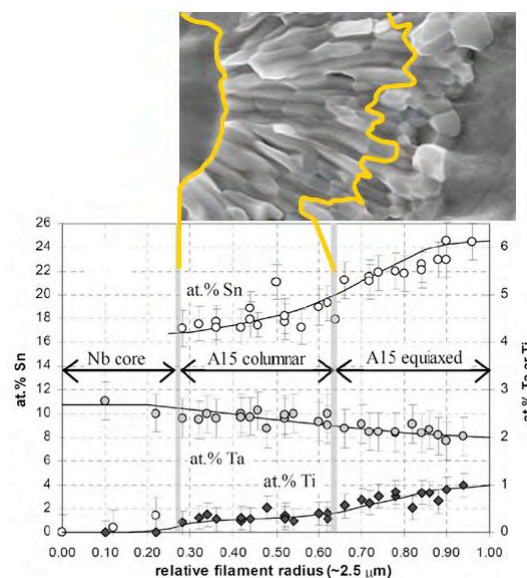


Figure 2: TEM/EDX profiles of Sn, Ta and Ti over a single filament for a Bronze Route Nb₃Sn wire.

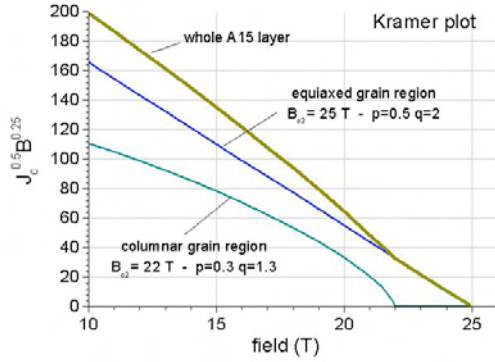


Figure 3: Kramer plot for the equiaxed and columnar grain regions of a Bronze Route Nb_3Sn wire. The Kramer plot for the whole A15 layer is obtained by summing the two contributions.

only observed in Bronze Route Nb_3Sn wires, in contrast to Internal Sn and Powder-in-Tube (PIT) wires, where the filaments are entirely composed by equiaxed grains. Based on the presence of the dual grain structure in Bronze Route wires, it was possible to give an answer to the old question why the Kramer relationship $J_c^{0.5} B^{0.25}$ vs. B is linear and gives a correct extrapolation for B_{c2} for Internal Sn and PIT wires, whereas it undergoes a downward curvature in Bronze Route wires [3, 4]. We have shown by quantitative calculation that this nonlinearity is in reality a pinning effect. Indeed, the Kramer plot for the large grains in the columnar grain layer in Bronze Route wires shows a downward curvature in the range 10–21 T, in contrast to the small equiaxed grains (< 180 nm size), which are described by a linear plot. The sum of both contributions also yields a nonlinear plot, with a downward curvature (Fig. 3).

b) T_c profiles in Nb_3Sn wires A systematical work was undertaken for determining the T_c profiles of Nb_3Sn wires by low temperature specific heat measurements, by the deconvolution of the jump at the superconducting transition [5, 6]. Measurements were performed on industrial multifilamentary Nb_3Sn wires prepared either by the Bronze Route, Internal Sn Diffusion and Powder-In-Tube technique. It is seen from Fig. 4 that the centre of the T_c distribution in the filaments of the different wires is shifted to lower temperatures in the order PIT \rightarrow Internal Sn \rightarrow Bronze Route [5]. The difference in the position of T_{max} of the distribution with respect to the onset T_c reflects the different Sn distributions for the 3 wire types. A TEM investigation has revealed strong differences between the localization of

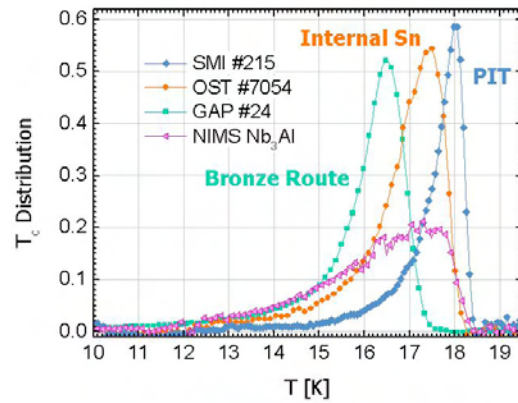


Figure 4: Distribution of T_c for Bronze Route, Internal Sn and PIT wires obtained by the deconvolution of the calorimetric data. The T_c distribution for a Nb_3Al multifilamentary wire is shown for comparison.

Nb_3Sn grains with varying T_c (which is connected to the Sn content): in Bronze Route wires, T_c decreases radially towards the center of the filament [2], whereas in Internal Sn and in PIT wires the grains with different T_c are randomly distributed throughout the whole filament. The T_c distribution in Nb_3Al wires prepared by the quenching technique at NIMS (Tsukuba, Japan) was determined for the first time and is also shown in Fig. 4. As expected, the T_c distribution width is rather large ($\Delta T_c \approx 6$ K), which indicates that further progress is still possible in Nb_3Al wires.

c) T_c profiles in MgB_2 wires Specific heat measurements have been performed on bulk and filamentary MgB_2 samples, with and without the addition of Carbon. In the case of $MgB_{1.9}C_{0.1}$, specific heat measurements show that the C substitution on the B sites modifies the low temperature shoulder related to the second gap [6]. This effect is not visible in the sample doped with SiC. From the distribution of T_c , we argue that SiC leads to an inhomogeneous distribution of C. Our goal is to develop MgB_2 wires with improved formation kinetics and a narrow T_c distribution, as determined by calorimetry (Fig. 5).

d) The effect of uniaxial tensile stress In view of NMR magnets with fields > 22 T, but also of fusion magnets (ITER), large Lorentz forces are expected, and a particular importance was given to the variation of the critical current I_c of the 3 main industrial Nb_3Sn wire types under the effect of mechanical load. The critical current I_c was measured as a function of ϵ , the uniaxial applied strain, by means of a modified Walter spiral [7]. It was found that the slope

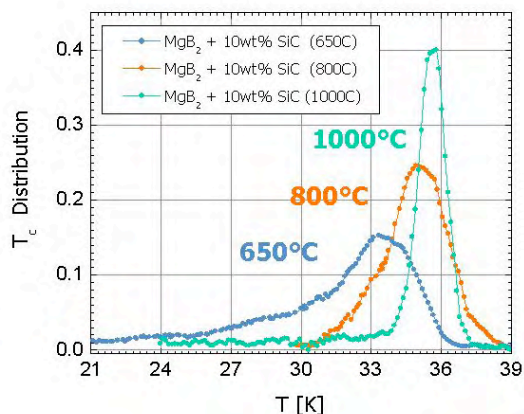


Figure 5: Dependence on the annealing temperature of the T_c distribution for SiC doped MgB_2 .

of the $I_c(\epsilon)$ curve is steeper for the Powder-In-Tube (PIT) and the Internal Sn wires than for the Bronze Route wire [3]. It is thought that the smaller filament size ($5 \mu\text{m}$) of Bronze Route wires contributes to the higher mechanical stability with respect to Internal Sn and PIT wires ($50 \mu\text{m}$). The comparison between the 3 wire types is shown in Fig. 6, where the $I_c(\epsilon)$ curves at 4.2 K, 19 T are plotted. An additional argument in favor of a higher stability for smaller filament diameters is given by the fact that the irreversible strain, ϵ_{irr} , in Bronze Route wires is higher by at least 0.2%. A series of Walter Spirals have been fabricated for the measurement of round or rectangular wires, but also of flat tapes. In particular, the WASP was also used for measuring J_c vs. ϵ of Y-123 Coated Conductor tapes, where an irreversible strain of 0.54% was found [8].

e) *Compressive transverse stress* A new device for measuring the effect of transverse compressive stresses on J_c of Nb_3Sn wires developed

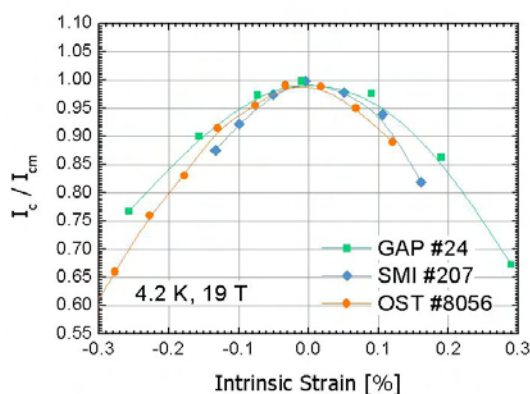


Figure 6: Reduced critical current vs intrinsic strain at 19 T for Bronze Route, Internal Sn and PIT wires.

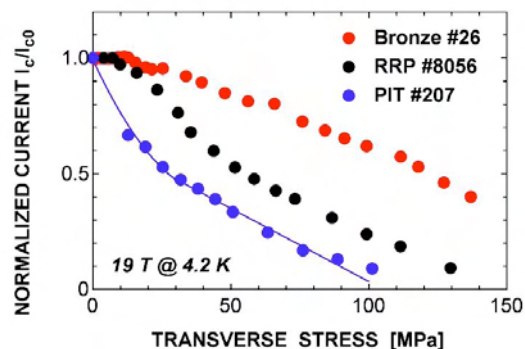


Figure 7: Reduced critical current vs compressive stress at 19 T for Bronze Route, Internal Sn and PIT wires.

in the frame of a collaboration with CERN was successfully tested up to 21 T and at currents up to 1'000 A: the compressive WASP [9]. A very different behavior was found for the 3 wire types mentioned above. After applying a compressive stress of 120 MPa, I_c of the Bronze wire is reduced to 50% of its initial value, whereas Internal Sn and PIT wires exhibit a reduction to 20% and 10%, respectively (Fig. 7). After releasing the compressive stress from 120 MPa, I_c of Bronze Route wires recovers to 95% of the initial value, which is in sharp contrast to the other two wire types, where only 30% of the initial value, I_{c0} , are recovered. This difference is attributed to the presence of voids in the "tubular" filaments of Internal Sn and PIT wires, which could favor the formation of nanocracks. Further experiments will be carried out to determine whether the particular, "tubular" configuration favors the formation of nanocracks, responsible for irreversibility effects. The present results are important in view of the modelization of the behavior of Nb_3Sn wires in large magnets with strong Lorentz forces, e.g. Tokamak coils for ITER and multipole magnets for CERN.

f) *Enhanced J_c values in MgB_2 wires from simultaneous simultaneous additives (codoping)* It is well known that the addition of 10 wt.% SiC nanopowders to the initial Mg + B powder mixture enhances the value of B_{c2} and B_{irr} and thus leads to an increase of J_c at 4.2 K and at fields exceeding 10 T. In an earlier article, we have reported an enhancement of J_c for B_4C additives [10]. Based on this result, we have introduced the simultaneous addition of various Carbon based additives (in the present case B_4C + SiC) to Mg and B powders as a new concept in view of further enhancing the superconducting parameters B_{c2} , B_{irr} and J_c values of *in*

situ Fe/MgB₂ wires [11]. The observed difference between the slopes for SiC alloyed and the binary wires at lower fields suggests the presence of two different mechanisms:

1. the enhancement of the normal state resistivity ρ_0 due to the substitution of Boron by Carbon leads to an increase of B_{irr} and a decrease of T_c ,
2. the presence of defects, e.g. grain boundaries or precipitations, leads to enhanced pinning. We have proposed that the simultaneous introduction of two different additives (one of them containing Carbon) could have a cumulative effect on J_c .

g) *Critical current densities in MgB₂ at 4.2 K* A series of Fe sheathed monofilamentary wires of 1.1 mm diameter with a MgB₂ core of 600 μ m diameter was prepared with various B₄C:SiC ratios. After reaction of 1 hour at 760 °C, the wire containing 7.5 wt.% B₄C and 2.5 wt.% SiC powders exhibited a J_c value of $1 \cdot 10^4$ A/cm² at 11.3 T and 4.2 K (Fig. 8) [11]. Although only 2.5 wt.% SiC were added, these values are considerably above those of ternary wires with B₄C additions, where the same J_c value is obtained at 9.6 T [10]. The slope J_c vs. B for the B₄C + SiC wires is steeper than for SiC additives, the J_c values at 4.2 K being superior at fields below 9 T. The lattice parameters a of the B₄C + SiC added wires exhibit lower values than ternary wires with the same nominal C content, suggesting a higher C content in the MgB₂ phase. With the simultaneous introduction of B₄C + SiC, a strong improvement of J_c and B_{irr} has been obtained with respect to B₄C additions. A further enhancement of J_c is expected when using combinations of additives with and without Carbon, aiming for a

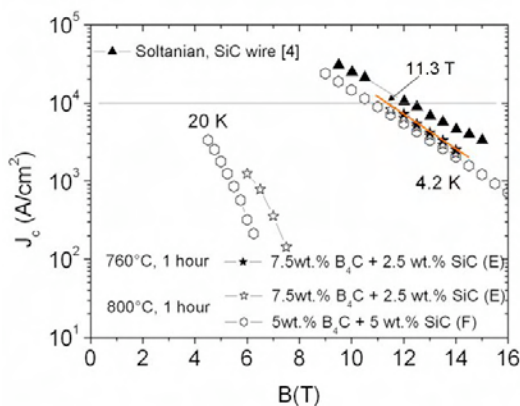


Figure 8: Critical current densities of MgB₂ wires with 7.5 wt.% B₄C + 2.5 wt.% SiC at 4.2 K and 20 K.

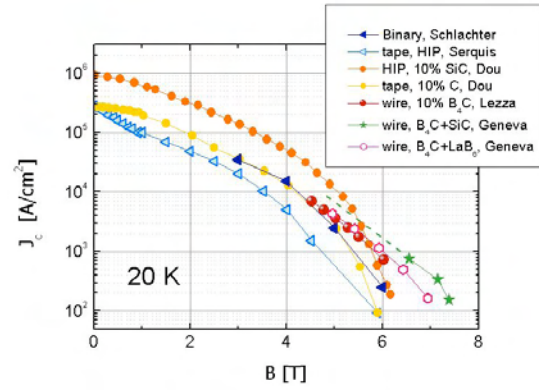


Figure 9: Comparison between the curves $J_c(B)$ at 20 K for MgB₂ wires with additive combinations B₄C + SiC and B₄C + LaB₆ and MgB₂ wires with SiC or C additives.

further raise of J_c in wires with multiple additives, as a result of the combination of different mechanisms. We have also investigated another combination of additives where SiC is absent: B₄C + LaB₆. At 4.2 K these additive combinations lead to an increase of J_c over binary MgB₂ wires [4].

h) *Critical current densities in MgB₂ at 20 K* Both combinations, B₄C + SiC and B₄C + LaB₆, show considerable enhancements of J_c at 20 K: the value of 1×10^4 A/cm² is reached at 4.7 and 4.5 T, respectively [4], i.e. higher than 4.2 T, the highest value for B₄C additions. In Fig. 9 the critical current densities at 20 K of the wires with additive combinations B₄C + SiC and B₄C + LaB₆ are compared with those of MgB₂ wires with SiC additives. The situation at 20 K is different from that one at 4.2 K, the J_c values at the higher fields being now higher for simultaneous additives than for SiC additives. This indicates that the critical field at 20 K is higher for wires with the combined additives than for SiC added wires, i.e. there is a cross-over of the $B_{irr}(T)$ for these two wire types, reflecting the slight, but significant difference in T_c : 35 K for the present combined additives with respect to 33 K for SiC additives.

i) *Relaxation rates* In the context of the applications of superconductors in high-field NMR magnets, the most stringent condition is the ability to operate in persistent mode, which requires a low relaxation rate as a function of time for the supercurrent. Magnetic relaxation studies have been performed on Nb₃Sn and Nb₃Al (multifilamentary wires), Chevrel phase Pb_{1,2}Mo₆S₈ (bulk samples), MgB₂ (*ex situ* Fe sheathed tapes and bulk samples), Bi-2212 (multifilamentary wires and single crys-

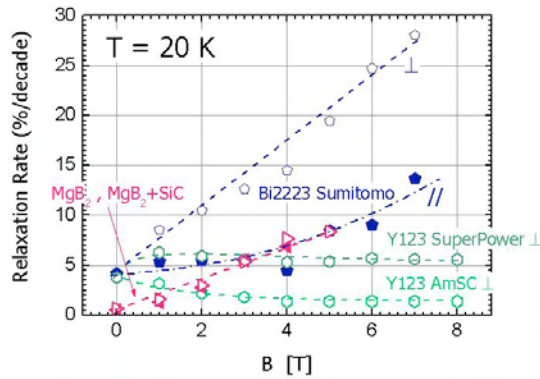


Figure 10: Comparison of the relaxation rates at 20 K for Y-123 Coated Conductors, Bi-2223 multifilamentary tapes and MgB_2 wires.

tals), Bi-2223 (multifilamentary tapes and single crystals) and Y-123 (Coated Conductors) in DC magnetic field up to 9 T and at temperatures varying from 5 to 50 K [12, 13]. The results show that Y-123 Coated Conductors exhibit very low relaxation rates in this temperature range. They appear thus as a promising candidate for NMR magnets with fields > 25 T, as soon as the sufficient lengths will be available. Nevertheless, the properties of the tapes are strongly dependent on the fabrication technique, as shown in Fig. 10 where two different industrial Coated Conductor tapes are compared at 20 K [13]. We found that at 20 K, the relaxation rate of MgB_2 is sufficiently low to allow operation in the persistent mode, as required for Magnetic Resonance Imaging (MRI).

1.2 Thin film based Fault Current Limiter

a) *Investigations on epitaxial films on sapphire*
The Fault Current Limiter (FCL) is a device which limits the current in the electrical network during a short circuit. Thanks to the fast superconducting to normal transition the FCL can limit the current in less than a ms. Even if there are several types of FCL the most promising and developed FCL is the resistive one based on high T_c thin films. For instance Siemens has built a 1.25 MVA (AC) and a 0.9MW (DC) FCL based on YBCO films grown onto sapphire wafer. We use in this project a meander of a Au(45nm)/YBCO(300nm)/CeO structure epitaxially grown onto two inches sapphire wafers ($T_c = 88$ K, $J_c(77K) = 3$ MA/cm²).

One of the problem often encountered in this type of FCL occurs at the beginning of the short circuit where only a fraction of the meander switches. This implies that only this part of the

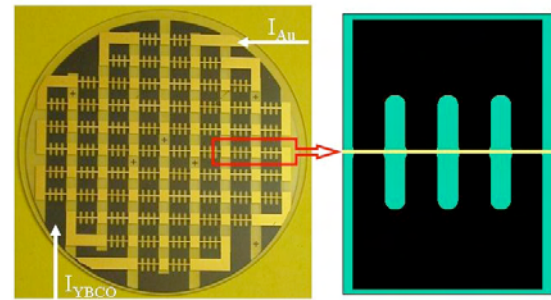


Figure 11: Left: view of the backside of a wafer. The white meander is the gold line used for the heating of the superconducting meander. The later is seen, in black, through the transparent substrate. Right: schematic blow up of one region of the wafer. The heating region (in white) lies exactly underneath the constricted region of the superconducting meander.

meander is acting as a FCL and all the power is concentrated in this region leading to possible irreversible damages. During this project we have developed several new designs of the meander in order to solve this problem and therefore to improve the performance of the FCL.

To be able to propose a new design of the meander we have carefully characterized the behavior of a YBCO line at high current densities. During a short circuit our measurements show that the current is limited in few μ s, the peak current reaches values of 3–4 I_c and the current is limited after 25–50 μ s to 1.5–2 I_c [14]. We also observed that at the beginning of a short circuit the initial dissipative length is proportional to the applied voltage [14]. The basic idea of this design is to split this initial dissipative length into several small regions homogeneously distributed along the meander [15]. This is done by locally decreasing the width of the line (and therefore the critical current), i.e. by including constrictions along the meander as presented in Fig. 11. The benefit of the constrictions has been confirmed during AC test on a 5 kW FCL (340 V/16 A). All the constrictions switch at the beginning of the short circuit starting at the maximum voltage and therefore the dissipated power is homogeneously distributed over the whole wafer [16]. We have successfully tested, using this design, a 10kW FCL made of two wafers connected in parallel.

However the behavior of our FCL was not optimal during asymmetrical short circuits (short circuit starting at voltages close to zero) which is the most critical condition for the FCL. At this voltage the initial dissipative length is very small and then only a small fraction of the constrictions will switch into the normal state. After this initial switching, the increase of both the meander resistance and the applied volt-

age keep the current around $1.5 J_c$ for a too long time (few ms). This current is too small to quickly switch the other constrictions into the dissipative state but too large to be safely sustained by the connecting path. This can lead, as we have observed few times, to a local burn out of the FCL.

To solve this problem one needs to find a way to speed up the transition into the normal state of the other parts of the meander during short circuits at low voltages. A possible solution is to locally decrease the critical current of the line in such a way that the limited current density of the line ($1.5-2 J_c$) becomes high enough to quickly switch these parts of the wafer. This can be obtained in two ways; by decreasing the width of the line or by heating the line locally.

For the first solution we have modified the constrictions by including notches within the constrictions. These notches represent a five percent local decrease of I_c and their total length is determined in such a way that they should all switch for an applied voltage of 30 V (maximum voltage = 340V). The effects of these modified constrictions have been confirmed during low voltage pulses. For instance, already for an applied voltage of only 5V (1.5% of the maximum voltage) there are notches switching in each of the 8 lines of the meander showing that these modified constrictions lead to a better homogenization of the initial normal state. During AC asymmetrical short circuits, we have also observed a different behavior of the FCL depending on J_c inhomogeneities of the wafer. The modified constrictions are efficient only if the variation of J_c across the wafer is less than 5%. This underlines the importance to have wafers with a good homogeneity of the critical current density. We have tested several 5 KW FCLs (300 V/16 A) and they have all sustained several short circuits starting at zero voltage without any burning, confirming the positive effect of these modified constrictions.

The other solution consists in heating the line locally (but within the constrictions) in order to decrease the critical current density. The heating is obtained by applying a current to a heater line in good thermal contact with the superconducting line; this is what we called the thermal assisted transition. Since the sapphire wafer is an excellent thermal conductor the current (heat pulse) can be applied from the backside of the wafer. We have then grown, by using a lift-off process, a 80 nm thick gold layer on the backside of the wafer as shown in Fig. 11.

To focus the heat on the superconducting constrictions located on the opposite side, the Au-

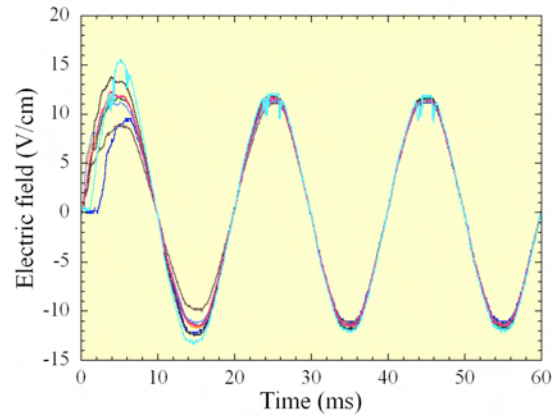


Figure 12: Averaged electric field across each line of the wafer during a 60 ms AC short circuit starting at $U \sim 0$ V ($t = 0$ ms). The heat pulse ($P = 350$ W) starts also at $t = 0$ ms.

meander is narrowed at these locations i.e. exactly underneath the constrictions. The heat pulse is obtained by discharging capacitors into this Au line. We have developed an electronic set-up which allows us to precisely choose the charging voltage of the capacitors and the delay between the start of the short circuit and the start of the heat pulse. To highlight the effect of this thermal transition, we have tested the behavior of the FCL during constant current pulses and low voltage pulses. We observe that the effect of heat pulses on the superconducting line is very fast, less than $100 \mu\text{s}$. For low voltage pulses the benefit of the thermally assisted transition is clearly confirmed. During a 26 V pulse (8% of U_{max}), the results show that 5 lines have partially switched at the beginning of the short circuit with the heat pulse instead of only two without the heat pulse [17]. Finally we have extensively studied the behavior of the FCL, using a design with notches and thermal assisted transition, during asymmetrical short circuits. A typical result is shown on Fig. 12 [17] for a 340V/12A FCL during a 60ms short circuit starting at $U=0$ V. All the lines switch in the normal state within 2ms after the start of the short circuit and 6 of the 8 lines switch almost instantaneously. This demonstrates the benefits that can be obtained by this thermally assisted transition.

b) *Results on coated conductors* The results reported in the first part of the report show that we have improved the performance of the FCL based on high- T_c film grown onto sapphire wafer. However, the major drawback for the commercialization of this type of FCL is their production costs. To reduce these costs the most promising and investigated way is to

use the second generation (2G) HTS wires (the so called coated conductors (CC)) for fault current limiter application. Based on CC produced by AMSC, Siemens has already built a 2 MW FCL. However measurements during short circuits highlighted the poor thermal behavior of these CC leading to very low quench mechanism and very low electric field, typically below 1 V/cm. This electric field (maximum applied voltage divided by the length of the CC) is one of the key parameter for the production cost. To improve these characteristics one need to understand the behavior of the CC at high current densities. It also important to compare this behavior with the characteristics of the FCL on sapphire. We then bought CC from Theva and Superpower. We mainly tested the CC from Theva: these tapes are 1cm wide with a structure Ag(40nm)/DyBCO(300nm or 2.4μ)/MgO(90μ m)/Hastelloy and $J_c = 0.9 - 1.8$ MA/cm². We have patterned the CC in order to get a line or a constriction of 1mm width. We first measured the $I - V$ (or $\rho - J$) characteristics of this DyBCO line by recording the voltage along the line during short current pulses. The $\rho - J$ characteristics at 77 K for CC and for a YBCO film grown on sapphire are presented in Fig. 13. This figure highlights the important difference in the flux flow resistivities between these two different types of thin films: the flux flow resistivity of CC is almost 3 orders of magnitude higher than in the film on sapphire. This difference in resistivities might be explained by a different variety of interfaces present in these films; for film grown onto sapphire these interfaces are mainly twin boundaries while in CC there are in addition grain

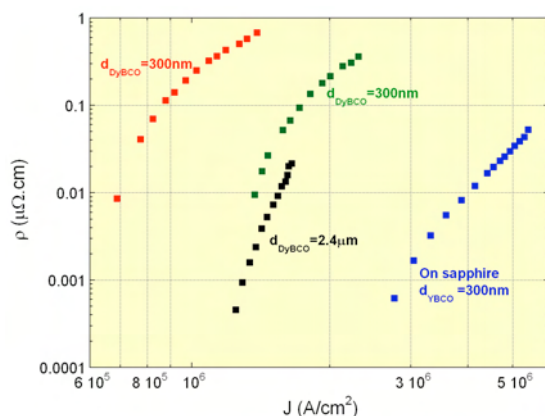


Figure 13: Flux flow resistivity as a function of the applied current for a 300 nm CC (circle), a 2.4 mm (triangle) and a 300 nm YBCO thin film grown onto sapphire (diamond). The squared symbol represents the resistivity of the 300 nm CC perpendicular to the length of the tape.

boundaries. These grain boundaries might influence several characteristics of the CC as the thermal conductivity or the switching behavior. We have indeed observed a clear difference in the switching behavior of the CC and of the film grown onto sapphire. In the latter the line stays in a very low dissipative state until a quick transition into a highly dissipative state appears while in CC the line is in a high dissipative state and then there is a heating of the line up to the normal state.

An important parameter for FCLs is the quench propagation, i.e. the propagation of the normal zone along the meander. Fast quench propagation is a crucial issue for the homogenization of the dissipated power distribution along the tape. We have estimated this propagation in our CC by measuring the voltage on different adjacent sections of the line during current pulses. The results are reported and compared with the propagation velocities in YBCO films grown on sapphire [14] in Fig. 14. This figure highlights the large difference between the propagation velocities; in films grown on sapphire the velocities are in the range of 20 m/s while in CC they are around 0.03 m/s, i.e. almost 3 orders of magnitude lower. On the same figure we have reported the prediction of an adiabatic model. The velocities calculated from the model are ~ 35 higher than the velocities we observe in the CC. The velocities in this model depend on the applied current, the resistivity of the Au/DyBCO bilayer, its heat capacity, the temperature and the thermal conductivity of the film. All these parameters are not supposed to change with the quality of the superconducting layer, except for the thermal conductivity. Therefore this model will give

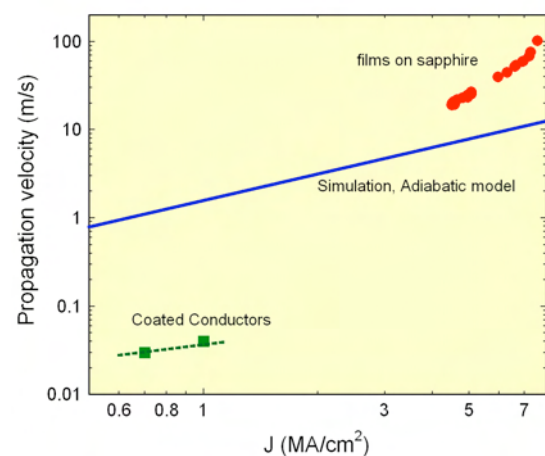


Figure 14: Propagation velocity of the normal zone in film grown on sapphire and in CC as a function of the applied current.

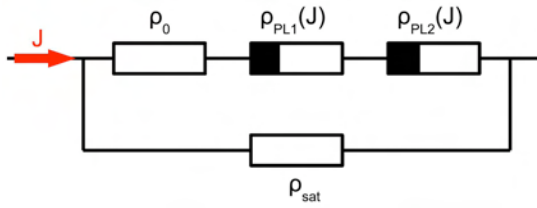


Figure 15: Equivalent electrical circuit for the transition regimes.

correct velocities if the thermal conductivity is decreased by 3 order of magnitude which is also the difference we observe in the flux flow resistivities between the CC and the film on sapphire. This suggests that grains boundaries might strongly reduce the thermal conductivity of the DyBCO film. In conclusion, our results show that to improve the behavior of a CC based FCL, it will be very important to investigate what are the parameters which govern the propagation velocities of the superconducting layer. If one can modify these parameters, there is a good chance that the coated conductors will offer a sufficiently cheap solution for a commercial viable FCL.

c) *Modeling of YBCO FCLs* In order to take into account of thermal phenomena during a fault, coupling between electromagnetic and thermal models has been implemented. Based on measurements [14], different regimes have been distinguished. The electrical behavior related to these regimes has been modeled with the equivalent electrical circuit given in Fig. 15, where each component describes a different part of the resistivity curve:

- For $0 < J < J_c$, the electrical resistivity is very low, and has not been measured. In this regime, the superconducting material can be considered as an almost perfect conductor. For reasons of numerical stability of the solving algorithm, for avoiding division by zero, a residual resistivity ρ_0 is used for current densities lower than or equal to J_c , i.e. when the resistivity of the superconducting material has not been measured. This correspond to the TAFF phenomenon.
- For $J_c < J < 3J_c$, the resistivity of the material has been modeled by a power law relation $\rho = (E_0/J)(J/J_c - 1)^{n_1}$, where n_1 and E_0 are two fitting parameters. It has to be noted that E_0 is not the critical electric field E_c used in the usual E-J power-law relation. The element ρ_{PL1} represents this power law in the circuit of Fig. 15.

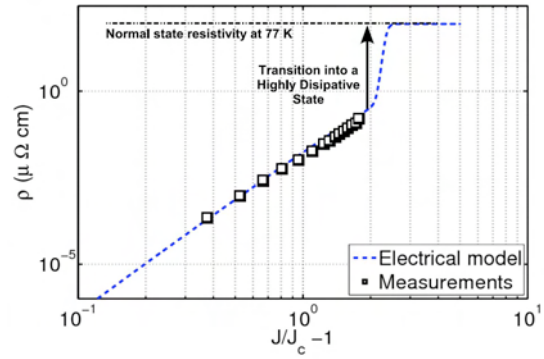


Figure 16: YBCO thin film resistivity vs reduced current density J/J_c at 77 K: pulse current measurements and equivalent electrical model.

- When the current density reaches $3J_c$, the material loses its superconducting properties and goes to normal state, where its behavior is similar to a conventional material. This sharp transition has been modeled with an additional power-law $E = E_0(J/J_c - \gamma)^{n_2}$ where $n_2 > n_1$. This power-law is not linked with a physical phenomenon, but is used for avoiding discontinuities in the $\rho - J$ relation. In the electrical equivalent circuit, it is represented by the element ρ_{PL2} . This correspond to the avalanche phenomenon.
- For $J > 3J_c$, and since the two power-laws are not limited functions, a resistive parallel branch ρ_{sat} is inserted in order to have a constant resistivity at very large current densities. This resistivity represents the normal state resistivity. Fig. 16 presents the succession of these behavior as the current increases.

In particular, this model allows describing the high current range where the transition from the superconducting to the normal state takes place.

The practical value of any simulation is based on its capability to reproduce or even predict experimental data. Our FEM model can reproduce the global behavior of FCLs, and allows studying the effects occurring during a fault caused by the temperature increase. Measurements have been made by the University of Geneva [14], where the total current flowing through a 5 kW FCL (2 inch sapphire wafer composed of a 300 nm YBCO thin film covered by a 125 nm gold layer) has been recorded. We have used those experimental data to test our model. Fig. 17 shows the total current flowing through the device. The simulation reproduces correctly the fault current limitation, i.e.

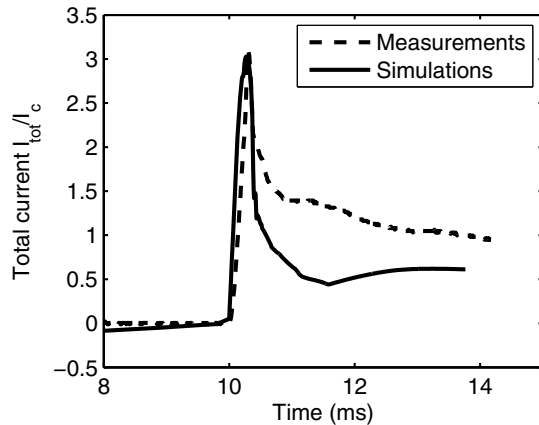


Figure 17: Total current flowing through the FCL: comparison with measurements.

the presence of a current peak and of a limitation phase (between 10 and 10.5 ms). Nevertheless, some differences appear between the curves (after 10.5 ms). These inaccuracies are due to incorrect values of the external electrical components such as circuit inductance which need to be estimated more carefully in a future work.

d) *Thermal stability simulation* To simulate correctly various situations of thermal stability we have introduced the thermal exchange with the nitrogen bath, called pool boiling. When the surface temperature T_s is close to the boiling temperature of the fluid T_0 , heat transfer is mostly governed by free convection. A further increase of temperature causes the apparition of vapor bubbles that nucleate on the CC surface. Due to the latent heat, large thermal exchange occurs in this range of temperature. However, when the vapor covers more areas on the heated surface, a considerable degradation of the heat transfer is observed due to the fact that thermal conductivity of the vapor is much less than that of the liquid. At large temperature differences, the solid-liquid interface becomes notably weak and a vapor film completely covers the heated surface. In this final stage, the heat transfer is very low and the tape becomes almost thermally isolated from its surroundings.

For this section, our geometrical model was based on the parameters of commercial coated conductors available from Theva (www.theva.com). The coated HTS tapes are made of four layers. A thick conductive substrate layer made of Hastelloy C276, which is usually electrically isolated from the HTS; a MgO buffer layer; a superconductive film made of DyBCO ($\text{DyBa}_2\text{Cu}_3\text{O}_7$) and a silver stabilizer in electrical contact with the superconductor.

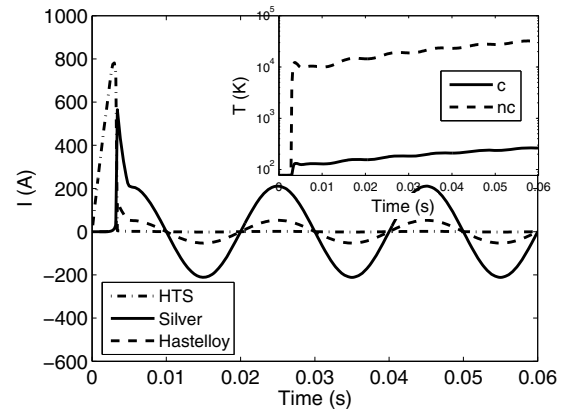


Figure 18: Distribution of the current ($I_{peak}=810\text{ A}$) in the subdomains for a shunted tape (substrate and stabilizer). The inset is the temperature of the tape for a shunted (c) and non-shunted (nc) device. For a non-shunted configuration, all the current goes in the HTS which has a high resistivity in the normal state. This has a direct effect on the temperature increase.

Using coated superconductors allows us to attain higher critical current density than massive conductors. Nevertheless, the small thickness of CCs makes them very sensitive to temperature excursions.

Therefore, a rapid recovery seems impossible once the HTS has switched to its normal state. This is particularly true if the tape does not have a shunt resistance (i.e. Ag and/or Hastelloy) to absorb a part of the dissipated energy. This is what we can observe in Fig. 18. The normal resistance of the HTS, which is higher than that of the substrate and stabilizer (we do not introduce a temperature dependence for the resistivity of these layers), makes the power generated within the DyBCO practically negligible in comparison to that in the silver film. In this case, the superconducting state will be recovered only if the stabilizer film succeeds in trading the generated heat with the nitrogen bath before the next current peak is reached.

Since silver is a better conductor than Hastelloy, it is interesting to study the influence of the stabilizer thickness on the heat dissipation. The Ag/HTS thickness ratio, to be thermally stable, depends on I_{peak} . However, an increase of the silver thickness (relatively to the HTS thickness) can favor the thermal stability by acting as a buffer zone to absorb heat and reduce the current density responsible of the heat generation within the stabilizer.

In spite of the positive effects on thermal stability, using a thicker stabilizer has a side effect on the limitation capability of the device. As a matter of fact, if there is an electrical contact be-

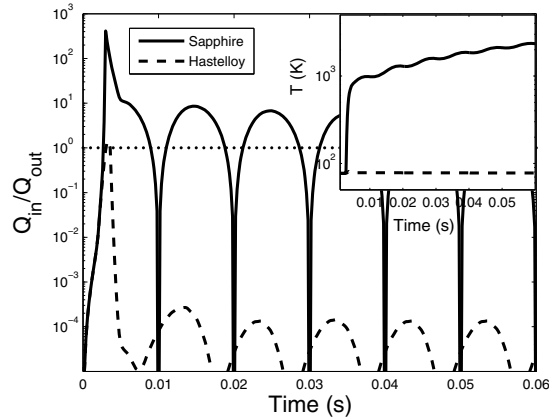


Figure 19: Comparison of the heat balance for different substrate material. The heat generated in the tape made of sapphire is not evacuated at all. The temperature is continuously increasing until the device burned out. Inset is the temperature for both samples. $I_{peak}=800.355$ A.

tween the HTS film and a conducting layer, the layer shunts the film in the normal state, and a part of the current flows through the other electrically connected part of the tape, as simple parallel resistors. Adding a parallel resistance lowers the global resistance of the tape, so that more current can flow in the tape without attenuation. This leads to a decrease of losses in the HTS film and, on the other hand, produces Joule losses in the conductive parallel paths. Accordingly, the shunted limiter requires more tape length to limit the same imposed current.

The materials constituting the tape have an important influence on the thermal exchange between the coolant and the tape surface. By comparing two usual CC substrates, such as Hastelloy and sapphire, we observe that a rapid increase of the surface temperature induces a huge drop on the thermal flux within the tape-coolant interface. The combination of a low heat capacity and a high thermal conductivity gives sapphire a thermal diffusivity (defined as $\alpha_d = k/\rho_m C_p$) that is more than 1000 times larger than Hastelloy. However, the heat, which is not readily stored in the sapphire substrate, can not be released due to a kind of bottleneck effect.

Fig. 19 allows us to observe the stability criteria for these two cases (i.e. Hastelloy and sapphire substrate). Stability recovery occurs when the heat removed to the substrate and coolant (Q_{out}) is greater than that generated within the superconductor (Q_{in}). The dot line plotted in Fig. 19 is the graphical illustration of this criteria which is defined as:

$$\frac{Q_{in}}{Q_{out}} = \frac{\left(\int_A E \cdot J dA'\right)_{HTS} + \left(\int_A E \cdot J dA'\right)_{Ag}}{\oint h(T_s - T_0) dl}$$

We can see that samples made on sapphire have a notable energy gain at each half-cycle which also produces the continuous increase of the temperature (see inset of Fig. 19). For this particular case, we can observe that the tape burned out almost instantaneously at the first current peak. The Hastelloy curve let us observe that the denominator of equation d), which is the LN2 exchange term, rapidly gets higher than the heat generation term (numerator). This leads to a fast thermal equilibrium with the surrounding coolant. Moreover, we observe in this figure that a “phase shift” exists between the produced energy within the Hastelloy-made tape and the imposed current to the device. This comes from the flux diffusion phenomenon in the superconducting state, in which losses continue to occur within the sample through magnetic relaxation even if the source current is zero. In the case with sapphire, the temperature gets so high that superconductivity is rapidly lost, therefore no relaxation process exists.

Finally, we observe that an increase of the thermal diffusivity is not a synonym of success to attain readily the thermal stability. Indeed, the key factor is the heat capacity instead of the thermal conductivity. This apparent discrepancy with the experiments on coated conductors is related to the importance of the local instabilities and will be further investigated.

1.3 Actively shielded 16 T split-coil magnet

Self shielded solenoid magnets for high magnetic fields are today readily available for NMR with maximum fields up to 21 T and a room temperature bore of a few centimeters. However, for scattering methods (X-rays and neutrons) an axial access and room temperature is by far not satisfactory since these techniques and the problems to be investigated ask for access to most of the scattering plane and temperatures well below or beyond room temperature. In addition, such magnets have to be operated in an environment with many other field-sensitive instruments, which can tolerate very low stray fields. Moreover, magnetic material from the neutron source and instrument shielding might cause environmental magnetic forces that can lead to a significant degradation of unshielded magnet. “Off-the-shelf” split coil

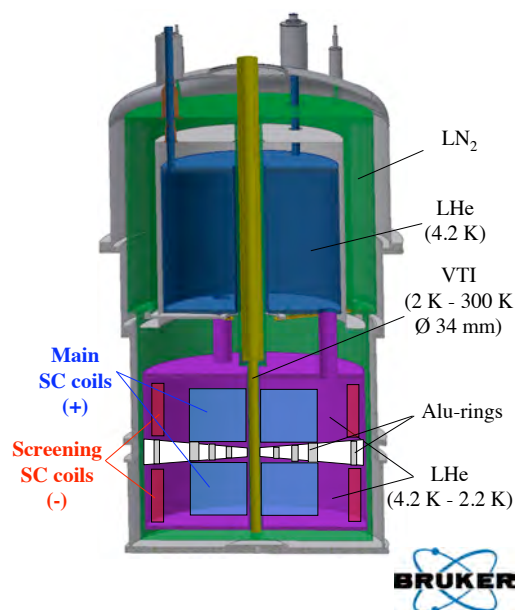


Figure 21: Layout of the self shielded 16 T split coil magnet system.

magnets nowadays reach 15 T but in most of the cases can only be operated at fields well below the maximum field due to the reasons mentioned above. The combination of a neutron laboratory with a large experience in magnetic scattering experiments and a manufacturer of commercial self shielded NMR magnets provides a unique possibility to realize this demanding combination of self shielding, high magnetic field and access to the scattering plane by a split coil arrangement. The first magnet of this kind will finally be installed at the first 3rd generation neutron source (SNS, Oak Ridge, USA) and will there be available for Swiss users. The delivery of the magnet is expected in spring 2009 for neutron tests at PSI and a final delivery to SNS two months later. The whole process is displayed in Fig. 20 (p. 155) together with the spending profile.

During the design engineering phase the specific problems of such a magnet which is different from previously manufactured NMR or non-shielded split coil magnets have been investigated and solved: split region (design, stability, radiation shielding, neutron transparency, activation), coil design (magnetic shielding, asymmetric mode, field distribution, stay fields) and the VTI which has to be able to accommodate a wide range of custom made inserts (high and low temperatures). In Fig. 21 the schematic layout of the magnet system and in Fig. 22 the resulting stray fields are shown.

For the near future more investigations of neutron absorbing steel coatings for the split plates

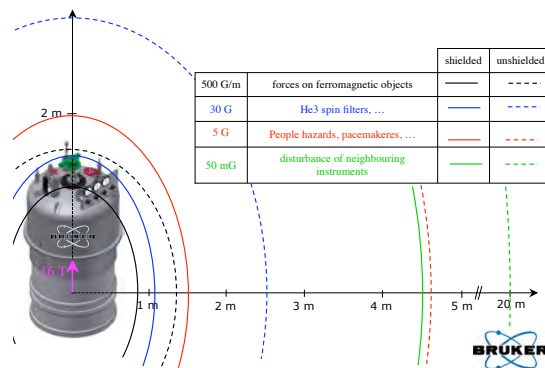


Figure 22: Comparison of magnetic stray fields for shielded and unshielded magnets.

are planned (transmission/reflection measurements, magnetization measurements, mechanical stability at very low temperatures and neutron activation experiments).

2 MaNEP sensors and security applications

2.1 Recent progress in material preparation with narrow ESR line for low-field magnetic field sensing

Magnetic sensors can be classified according to low-, medium-, and high-field sensing range. Devices that detect magnetic fields $< 1\mu\text{G}$ (microgauss) are considered low-field sensors; those with a range of $1\mu\text{G}$ to 10 G are Earth's field sensors; and detectors that sense fields > 10 G are referred to as bias magnet field sensors. Low-field sensors tend to be bulky and costly compared to other magnetic devices. Care must be taken to account for the effects of the Earth's field, whose daily variations may exceed the sensor's measurement range. The devices are used for medical, geological applications and military surveillance. The magnetic range of medium-field sensors lends itself well to using the Earth's magnetic field to determine compass headings for navigation, detect anomalies in it for vehicle sensing, and measure the derivative of the change in field to determine yaw rate. This project is the fruit of collaboration between the group of Forró and Metrolab SA (which has a commercial product for high-field sensors) for elaborating a low magnetic field sensor based on ESR technique. Such a sensor needs a material with very narrow ESR line which position would indicate the magnetic field value. The criteria for having a good ESR probe with narrow ESR line are the following:

- ESR linewidth < 100 mG (ideal 20 mG)
- Spin density $\geq 10^{26} \text{ m}^{-3}$

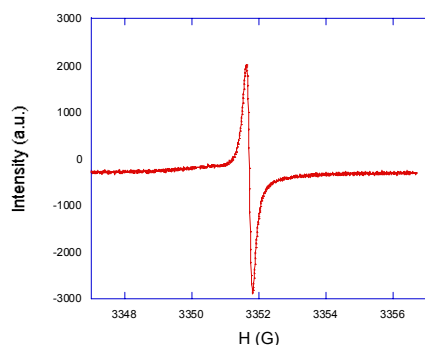


Figure 23: ESR linewidth of Perylen-AsF₆ quasi-one-dimensional conductor. The peak-to-peak linewidth is 0.07 G.

- Sample quantity 1–10 mm³
- Isotropic line
- Working temperature 10–40 °C
- Stable composition: Δg is defined better than 10 ppm
- Time stability (but it is not a high priority)
- Price < 1000 CHF

Organic samples can satisfy these requirements, because of the weak spin-orbit coupling, the spin relaxation is slow. However, the test of several organic compounds (electron irradiated kapton, NMP-TCNQ, Qn(TCNQ)₂, KC₆₀, Na@C₆₀, Mg₅C₆₀, carbon nanotubes, nanohorns, Perylene-AsF₆ have revealed, that only the electrically conducting are appropriate. In samples with localized electrons, either the spin concentration is too low, or because of the dipolar interaction the linewidth is too broad. The highlight of these studies is that we have found the family of quasi-one-dimensional organic metal, Perylene-AsF₆ and Fluoranthene-AsF₆ which have an ESR linewidth of 0.07 G and 0.02 G, respectively at 300 K (Fig. 23). These compounds were synthesized by a guest scientist, Dr. Dmitry Konarev from Chernogolovka (Russia) and by a visiting student Barbara Korbely from Szeged (Hungary). A positive development is that an external consultant of Metrolab, Dr. Giovanni Boero, expert in miniaturization of ESR devices, has joined the project.

2.2 Gas detection with semiconducting oxides

The field of resistive gas sensors is in fast and consistent growth. These devices are based on

gas-induced changes in the electronic properties of a sensing material. They show a large number of applications in the industrial and environmental fields, and are the subject of a great effort of research (For a recent review on the subject, see [20]). For example, semiconducting oxides like SnO₂ and WO₃ exhibit dramatic changes of the electrical resistance when exposed to oxidizing (NO₂, O₃) or reducing (H₂) gases. Several promising sensing materials are available within the MaNEP network. In this project we have developed the experimental tools and facilities required for applied research in this field. In a first step, we have focused our work on the MoO₃ compound which is now available in the shape of nanorods [18]. MoO₃ is a wide band *n*-type semiconductor. In recent years MoO₃ films have attracted interest as active elements in resistance-type sensors [21]. Growth techniques like sputtering, CVD [22], and flash evaporation [23] have been used. The properties of the films appear to be dependent on the deposition technique and the deposition parameters.

1D structures offer new possibilities due to the larger surface to volume ratio. Their electrical conductivity may be strongly influenced by surface reactions. The nanorods were deposited by wet techniques on alumina substrates with IDT gold electrodes. In these multiwire devices bulk nanorods quantities (10² – 10³) are contacted by the electrodes (Figs. 24 and 25). The resistance was measured in a test chamber with a regulated hot plate. Tests were carried out around 300 °C with both NO₂ and NH₃ in a synthetic air background. The sensing properties of the nanorods were compared to commercially available MoO₃ powder (Fluka).

We have found that the response time of multiwire nanorod sensor is faster compared to

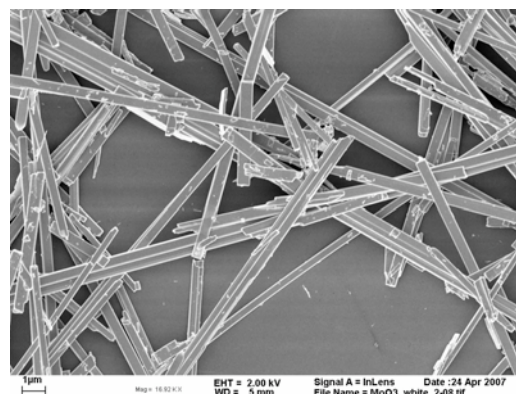


Figure 24: SEM images of MoO₃ nanorods grown in a neutral ionic media [18].

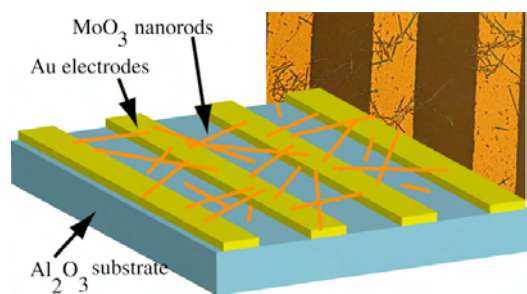


Figure 25: *MoO₃ nano-fibers deposited on an alumina substrate with gold interdigitated electrodes (IDTs). Width of the electrodes is 25 μm , and spacing is also 25 μm .*

standard 3D MoO₃ grains. When compared to 'standard' MoO₃, the nanorods display two main differences. They become conducting at a somewhat higher temperature (250 °C instead of 200 °C), and their response to the presence of NO₂ or NH₃ is about two to three times faster. A typical response of a nanorod sensor to the injection of a reducing gas is shown in Fig. 26. The measured response time (baseline to 90% signal saturation) is less than 6 s. This time corresponds approximately to the response time of the gas flow system used for the experiment, and it represents an upper limit to the real response time of these multiwire sensors. The same sensor showed a similar behavior upon the injection of a mixture of 5% NO₂ in N₂. The recovery times, that depend on the desorption process, appear to be longer. Whether this is an intrinsic property of the material or related to the rinsing dynamics is not yet clear. The particular morphology of nanorod-based sensors may be responsible for the fast response

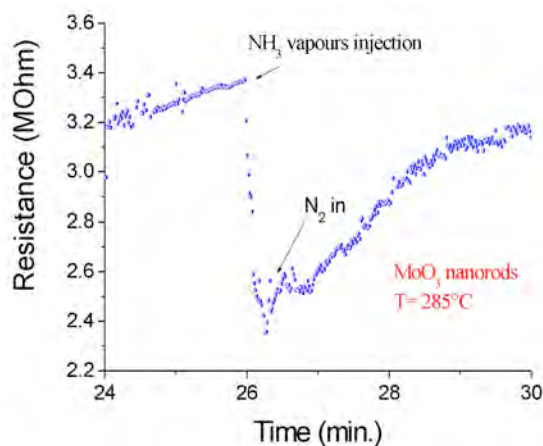


Figure 26: *Response of MoO₃ nanorods to the injection of NH₃ vapors in the test chamber, and to the subsequent rinsing inflow of dry nitrogen.*

time [24]. The nanorod/nanorod junctions between the metal electrodes are more accessible and there is a better gas diffusion. This makes them good candidates for gas sensing applications. In the framework of this project, we have also developed 40MHz surface acoustic wave (SAW) microbalances. These devices are powerful tools for measuring non-percolative electrical conductivity changes in nano-materials [25], and adsorption/desorption in gas sensing compounds. SAW devices are ideal platforms for H₂ detection in energy management applications. At this point this project can lead to a CTI proposal with an industrial partner, where cross-sensitivity and poisoning by other gases must be investigated.

3 Thin film preparation and applications

3.1 Neutron supermirrors

Neutron supermirrors are depth graded multilayers e.g. of Ni and Ti, which are applied as reflecting surfaces in guides to transport neutrons over large distances and in optical devices to define the neutron beam adequately for experiments. In particular, focusing of neutron beams is requiring high reflection angles. In order to obtain high reflectivity at large reflection angles, low interfacial roughness and suppression of interdiffusion are of crucial importance. For the investigation of the influence of the preparation conditions on the performance of supermirrors, systematic series of samples could be produced using the sputter plants at PSI (ETHZ) and SwissNeutronics. Characterization with neutron reflectometry, X-ray diffraction and reflectometry, and stress measurements were performed at the laboratories of PSI. Here, the new neutron reflectometer NARZISS dedicated to test neutron optics was successfully commissioned, jointly by PSI and SwissNeutronics.

The work was focused on the investigation of reactive sputtering of Ni in an Ar/N₂ atmosphere in comparison to previous work using an Ar/synthetic air mixture [26]. Series of supermirrors with varying number of layers were prepared at different contents of N₂ in the sputter gas. Fig. 27 depicts the neutron reflectivity data of supermirrors with $m = 3.6$ (m denotes the maximum reflection angle in units of the critical angle for total reflection). It shows the variation of the neutron reflectivity as function of the N₂ flow rate during the sputtering process. The generated tensile stress of the multilayer system causes forces acting on the glass substrate which lead to a peel of the supermirror. Over all series of supermirrors it was

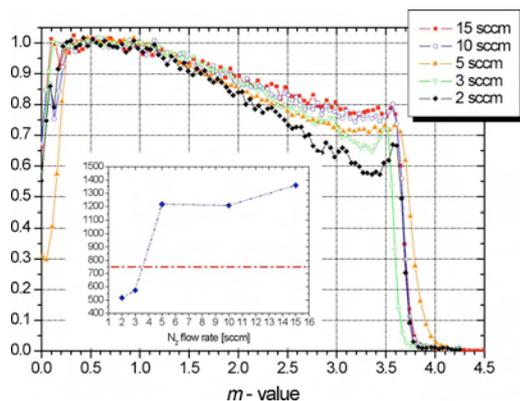


Figure 27: Reflectivity of supermirrors $m = 3.6$. Ni layers prepared in a Ar (35 sccm) / N_2 (x sccm) atmosphere. The inset shows the force acting on the glass surface dependent on the N_2 flow rate (see text).

found that the mirrors are stable when the force is below 750 GPa-nm. This limit is apparently valid for supermirrors up to $m = 3.6$ and presumably in general, too. This experience establishes an essential condition for supermirrors coated on glass substrates as usual.

3.2 Polarizing supermirrors

Polarizing supermirrors based on various multilayer systems such as Fe/Si and FeCoV/TiN_x are used in neutron instrumentation to provide a polarized neutron beam and to analyze the polarization of the scattered beam. Multilayer consisting of magnetic and non-magnetic layers can be used to polarize neutrons due to the different scattering contrasts for neutrons with either up or down polarization. Moreover, the internal stress of the thin films can be manipulated in such a way as to create an anisotropic distribution, which results in a magnetic anisotropy via magneto-elastic coupling [27]. Due to the magnetic anisotropy the polarizer/analyzer can be used in its "remanent" state. This feature enables to switch the neutron polarization in the experiment by switching the magnetization of the mirror [27, 28]. The use of TiGd/Ti multilayer absorbers shows considerable improvement of the polarizing properties of the supermirrors. The range of high polarization ($P \geq 95\%$) could be expanded down to $m \approx 0.7$. The intensity of the reflected neutrons of a $m=3.0$ mirror composed of 300 layers is shown in Fig. 28 (p. 155). We implemented the optimized FeCoV/TiN_x supermirrors in a analyzer-prototype for the HYSPEC-Spectrometer at the SNS (Oak Ridge, USA).

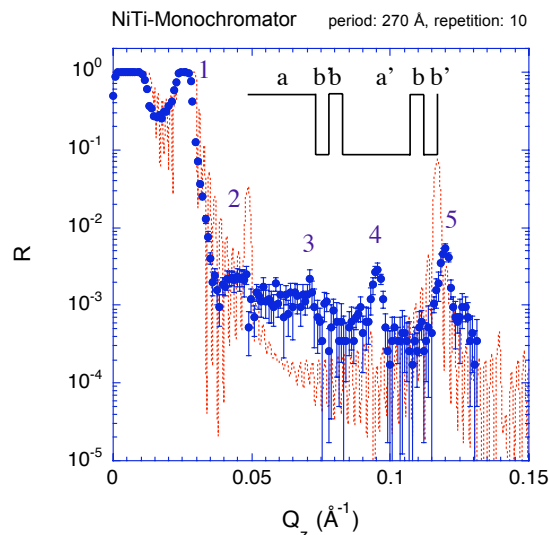


Figure 29: Neutron reflectivity of a multilayer system (period of 270 Å) measured on the reflectometer NARZISS at SINQ, PSI. The 6-layer system shows a distinct inhibition of the 2nd, 3rd and 4th order peaks.

3.3 Multilayer monochromators

For neutron- or X-ray-scattering multilayer monochromators are used to select a certain wavelength (band) [19][29]. For many applications the contamination of the scattered beam with higher harmonics is undesired. Based on Fourier-series expansion of scattering length density profiles we tailored multilayer systems in order to prevent selected higher order peaks in the neutron reflectivity from appearing. We investigated a multilayer system with periods of 6-layers and 10-layers, respectively. We were able to show (Fig. 29), that for a certain layer-thickness ratio within a period the 3rd harmonic in the tested multilayer system could be suppressed as expected from the Fourier-series expansion. We choose an anti-symmetric periodic function and therefore for symmetry reasons the even higher order peaks are canceled out. It is sufficient to avoid the 2nd, 3rd and 4th harmonic because the intensity of the 5th order peak is negligible due to the spectrum of the primary neutron beam. To inhibit the 3rd order we have to solve the integral equation for the respective term in the Fourier-series expansion. We are going to implement such a multilayer monochromator on the reflectometer NARZISS (SINQ, PSI) in April 2008.

3.4 Large area deposition on silicon

To develop applications of epitaxial ferroelectric films, epitaxial layers over large surfaces and on industrial substrates are necessary. These requirements led us to develop

the growth of epitaxial perovskite thin films on Si wafers. We have set-up a molecular beam epitaxy (MBE) deposition system able to accommodate large (up to 4") Si wafer for the growth of epitaxial SrTiO₃ buffer layers. This home-made chamber, equipped with *in situ* surface analysis to monitor the growth (RHEED), is operational. Based on our know-how on the growth of epitaxial perovskite thin films, we have also designed an off-axis reactive magnetron sputtering chamber suited for the growth over large area substrates. We have recently focused our interest on the thickness homogeneity that can be achieved with a 90° 3" off-axis target-substrate geometry. Homogeneity measurements based on optical spectroscopy allowing the layer thickness in a non-destructive way to be measured have revealed thickness variations of the order of 10% over a 3" wafer.

3.5 Ferroelectric properties of epitaxial PZT thin films

A series of studies on epitaxial ferroelectric oxide thin films has shown that mechanical constraints can deeply modify the ferroelectric properties. Under certain conditions, these constraints, due to the epitaxial growth, can induce a large increase in the polarization and in the critical temperature in prototype ferroelectric perovskites such as BaTiO₃ and PbTiO₃, and are thus of potential interest for applications. We have studied the effect of epitaxial constraints on the structural and physical properties of epitaxial PZT thin films in order to better understand the interplay between strain and ferroelectricity. Using X-ray diffraction, the crystallographic structure and the ferroelectric phase transition temperatures were studied in a series of ferroelectric PZT thin films grown onto metallic 0.5% Nb-doped SrTiO₃ (Nb-STO) (001) substrates, with thicknesses ranging from 150 Å to 1230 Å.

Fig. 30 shows the evolution of the lattice parameters at room temperature as a function of film thickness. A 150 Å thick film is found to be pseudomorphic with the Nb-STO substrate: the PZT in-plane lattice parameter reduces to that of STO while the *c*-axis parameter elongates. Increasing the film thickness induces a progressive relaxation of the strain which is partially relaxed for a 200 Å thick film, and fully relaxed for a 400 Å thick film. Because of the large strain-polarization coupling, the modification of the mechanical boundary conditions should induce substantial changes in the T_c of the films: we could expect a T_c

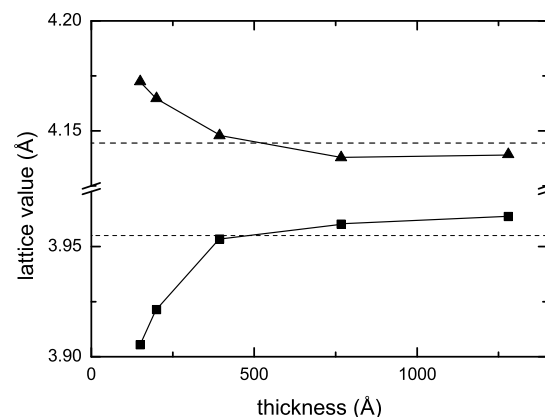


Figure 30: *a* (square) and *c* (triangle) -lattice parameters of PZT vs film thickness. Dashed lines indicate the bulk values.

of 1000 °C for the thinnest films (bulk T_c is 450 °C). As the film thickness is increased and the strain progressively released, the T_c should approach the value of 680 °C for the thickest "relaxed" films.

Fig. 31A shows the temperature evolution of the *c* value for a 1230 Å thick relaxed film. The *c*-axis shrinks up to 680 °C and then expands. The change in behavior is ascribed to the ferroelectric-paraelectric transition with an estimated T_c of about 680 °C. The results for all the samples are reported in Fig. 31B: the transition temperature does not vary significantly with thickness: strained and relaxed films display a rather similar transition temperature. These experimental results demonstrate that T_c in thin films can be much higher than the bulk (450 °C), a particularly interesting result for applications. The thickness independence of T_c is not fully understood at this point.

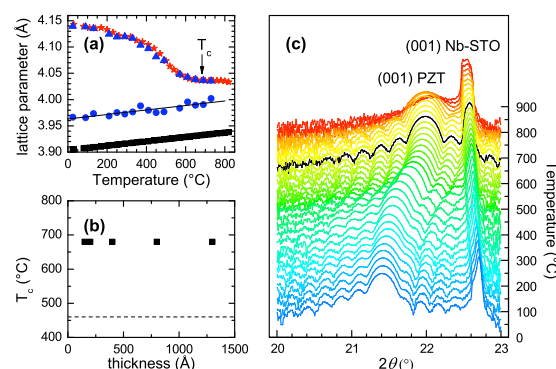


Figure 31: (A) *c*-axis parameter evolution vs temperature for PZT (triangle) and STO (square) (B) T_c vs PZT film thickness (C) $\theta - 2\theta$ scan for a 1230 Å thick film vs temperature.

3.6 High frequency surface acoustic wave devices on epitaxial PZT thin films

In this collaboration, we pursued our effort on SAW devices based on epitaxial PZT thin films. Finite element simulations have been performed to investigate different transduction configurations for thin piezoelectric and ferroelectric layers on single crystal substrates with lithographically defined electrodes and a classical inter-digital configuration has been experimentally tested. We fabricated inter-digital transducers (IDT) directly in one process step, by using focused ion beam (FIB) etching techniques on epitaxial PZT layers deposited on SrTiO₃ single crystal substrates. For that purpose, the FEMTO-ST Institute in Besançon has used its FIB machine to directly etch the aluminum layer deposited on top the PZT film. Test devices have been fabricated on PZT epitaxial layers of thicknesses ranging from 100 to 200 nm, allowing for the excitation of 1 micron wavelength Rayleigh-like waves.

These devices (Fig. 32) correspond to a single-port resonator operating at frequencies ranging from 3 to 5 GHz, depending on the mode order. Electro-mechanical coupling factors varying from 0.5 to 1.6 % for the first mode and from 0.8 % to 2.8 % for the second mode have been measured, whereas Q factors in the range of 30-90 were obtained, which are very promising figures according to the literature and to the used device configuration, far from the optimal one. The temperature coefficient of the resonance frequency (TCF) was also measured for this device. A negative TCF of -85 ppm/K was experimentally found, probably due to the thermoelastic behavior of SrTiO₃.

Fig. 33 shows the superimposition of the experimental admittance of one device and the harmonic admittance computed considering the expected shape of the strip. One can note that resonance frequencies are correctly predicted.

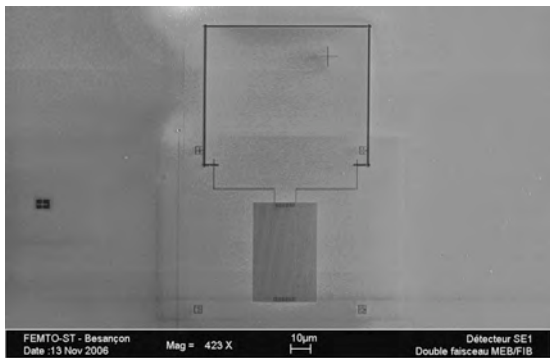


Figure 32: SEM view of a SAW device fabricated by FIB.

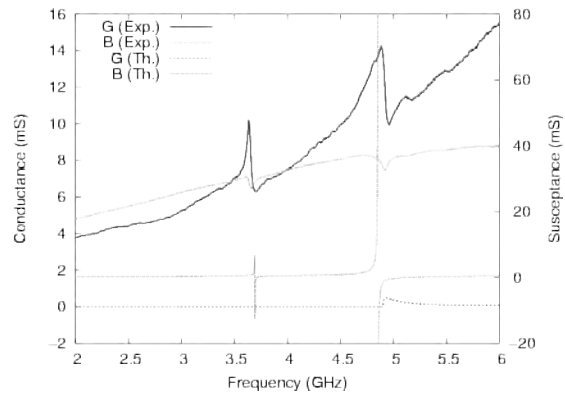


Figure 33: Admittance of a PZT resonator as a function of frequency. The experimental and theoretical results are displayed.

(Project in collaboration with Dr. S. Ballandras, FEMTO-ST, LPMO, Besançon)

3.7 MEMS fabrication based on epitaxial piezoelectric thin films on silicon

The aim of this part of the project is the realization of novel micro-electro-mechanical systems (MEMS) based on epitaxial piezoelectric thin films grown directly on silicon. These epitaxial ferroelectric films should display superior piezoelectric coefficients over conventional sol-gel like piezoelectric thin films. Using SrTiO₃-buffered silicon substrates, it is possible to grow epitaxial thin films of PbZr_{0.2}Ti_{0.8}O₃ and Pb(MgNb)O₃-PbTiO₃ and take advantage of their high piezoelectric coefficients as actuating/sensing layers in MEMS.

Since piezoelectric microcantilevers have attracted much attention due to their potential as actuating/sensing platforms, theoretical analysis and computational simulation have been performed to study the behavior of a cantilever deflected by the piezoelectric layer as a function of various parameters (piezoelectric coefficient, film thickness, applied voltage, cantilever size, electrode configuration, and operating modes). The results show that the epitaxial piezoelectric cantilevers can give higher deflection (actuating mode) and higher voltage sensitivity (sensing mode) compared to conventional piezoelectric cantilevers.

We defined the etching procedure for the fabrication of a cantilever that requires, on the silicon side, to define the desirable cantilever thickness down to few micrometers while on the thin film side, the piezoelectric layer has to be patterned to electrically contact the top and bottom electrodes. Several wet and dry etching experiments have been performed to establish the different etching procedures for the

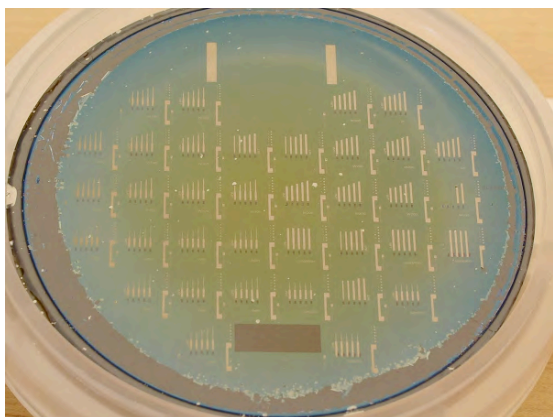


Figure 34: Photograph of a partially processed wafer revealing cantilevers of different sizes.

different materials and their reciprocal compatibility. The current situation of the project is illustrated in Fig. 34. On a 2" Si wafer, a sequence of SrTiO₃ (5 nm thick)/SrRuO₃ (30 nm thick)/PZT (150 nm thick) layers has been grown. After a metallization step, the layers have been etched, defining cantilevers of different shapes and lengths. The Si side has also to be processed by reactive ion etching. (Project in collaboration with Prof. de Rooij, IMT, Université de Neuchâtel, Prof. C. B. Eom, University of Wisconsin and Prof. C. Ahn, University of Yale)

4 Collaborative efforts

Project 6 is largely based on collaborative work for two main reasons. First, the applied projects are essentially cross-disciplinary. Each sub-topic requires input and expertise from different teams. Second, applied projects need the active participation of industrial partners. Therefore a MaNEP scientist working in Project 6 is naturally brought to use and sometimes to learn skills from other MaNEP teams and projects, as well as to gather a good understanding of the needs of the end-user and the market. This brings the added benefit of finding new applied research opportunities. In the framework of Project 6, we can outline collaborative work between MaNEP teams as follows

- Superconducting wires: R. Flükiger (UniGE), R. Nesper (ETHZ) and D. Eckert, Bruker Biospin.
- Fault Current Limiter: Ø. Fischer, M. Decroux (UniGE), M. Hasler (EPFL) and M. Abplanalp, ABB.
- Sensors: Ø. Fischer (UniGE), J. Cors (UniGE), G. Patzke (ETHZ, UniZH) and Mecsens SA. L. Forro and Metrolab SA

- Thin film preparation: J. Mesot (PSI), J.-M. Triscone and Swissneutronics, J.-M. Triscone (UniGE) and N. de Rooij (UniNE).

5 Goals for the next year

The main goals for the last year of MaNEP phase II are the following

5.1 Applied Superconductivity

1. The production of the first 50m of multifilamentary wires by the Internal Sn diffusion technique.
2. Systematical search for new ternary and quaternary additions to MgB₂ wires, to enhance the upper critical field and the critical current density.
3. Detection of internal stresses in MgB₂ filaments by studying the calorimetric transition at T_c .
4. Test of coated conductors on various substrates for FCL applications, and FEM testing of new coated conductor geometries.
5. Dynamic Hall probe field mapping development, and probe field mapping of current limiter.

5.2 MaNEP Sensors and security applications

1. Synthesis and test of ESR materials for weak field measurements.
2. Measurement of reference gas samples, in particular H₂ with sensitive coatings on a 40 MHz SAW device.
3. Integration of optimized electrochemical cathodes (coating and surface morphology) in working sensors, and field test at end-user site.
4. Demonstration of the industrial feasibility of the marking technology. Launch of a new CTI project with at least one industrial partner.

5.3 Thin film preparation and applications

1. Investigation of substrates and coatings by X-rays and local probes. Fabrication of polarizing multilayers of type FeCo/Ti, and exploration of controlled interdiffusion on magnetization.

2. Realization of epitaxial SrTiO₃ buffer layers on silicon and of epitaxial piezoelectric layers on buffered silicon.
3. Realization of a pyroelectric sensor using epitaxial PZT films on silicon, and of PIT-SAW devices on SrTiO₃-doped SrTiO₃/PZT structures. Demonstration of the frequency doubling capability of the PIT-SAW technology. Realization of a PIT-SAW device on silicon.
4. High frequency characterization of epitaxial PZT films.

MaNEP-related publications

- [1] R. Flükiger, D. Uglietti, C. Senatore, F. Buta, and B. Seeber, in *Special Issues on Superconductivity*, L. Botura and R. Heller, eds. (Elsevier, Amsterdam, 2008, to be published), Cryogenics.
- [2] V. Abächerli, D. Uglietti, P. Lezza, B. Seeber, R. Flükiger, M. Cantoni, and P.-A. Buffat, *IEEE Trans. Appl. Supercond.* **15**, 3482 (2005).
- [3] D. Uglietti, B. Seeber, V. Abächerli, M. Cantoni, and R. Flükiger, *Adv. Cryo. Eng.* **824**, 528 (2006).
- [4] R. Flükiger, C. Senatore, M. Cesaretti, F. Buta, D. Uglietti, and B. Seeber, *to be published in Supercond. Sci. Technol.* (2008).
- [5] C. Senatore, D. Uglietti, V. Abächerli, A. Junod, and R. Flükiger, *IEEE Trans. Appl. Supercond.* **17**, 2611 (2007).
- [6] C. Senatore, P. Lezza, R. Lortz, O. Shcherbakova, W. K. Yeoh, S. X. Dou, and R. Flükiger, *IEEE Trans. Appl. Supercond.* **17**, 2941 (2007).
- [7] B. Seeber, D. Uglietti, V. Abächerli, P. A. Bovier, D. Eckert, G. Kübler, P. Lezza, A. Pollini, and R. Flükiger, *Rev. Sci. Inst.* **76**, 093901 (2005).
- [8] D. Uglietti, B. Seeber, and R. Flükiger, *Supercond. Sci. Technol.* **19**, 869 (2006).
- [9] B. Seeber, A. Ferreira, V. Abächerli, T. Boutboul, L. Oberli, and R. Flükiger, *IEEE Trans. Appl. Supercond.* **17**, 2643 (2007).
- [10] P. Lezza, C. Senatore, and R. Flükiger, *Supercond. Sci. Technol.* **19**, 1030 (2006).
- [11] R. Flükiger, P. Lezza, M. Cesaretti, C. Senatore, and R. Gladyshevski, *IEEE Trans. Appl. Supercond.* **17**, 2846 (2007).
- [12] C. Senatore, P. Lezza, and R. Flükiger, *Adv. Cryo. Eng.* **824**, 654 (2006).
- [13] C. Senatore and R. Flükiger, *to be published in Supercond. Sci. Technol.* (2008).
- ▶ [14] M. Decroux, L. Antognazza, N. Musolino, E. de Chambrier, S. Reymond, J.-M. Triscone, Ø. Fischer, W. Paul, and M. Chen, *IEEE Trans. Appl. Supercond.* **11**, 2046 (2001).
- [15] M. Decroux, L. Antognazza, S. Reymond, W. Paul, M. Chen, and Ø. Fischer, *IEEE Trans. Appl. Supercond.* **13**, 1988 (2003).
- [16] L. Antognazza, M. Decroux, M. Therasse, M. Abplanalp, and Ø. Fischer, *IEEE Trans. Appl. Supercond.* **15**, 1990 (2005).
- ▶ [17] L. Antognazza, M. Decroux, M. Therasse, M. Abplanalp, J. Duron, B. Dutoit, and Ø. Fischer, *IEEE Trans. Appl. Supercond.* **17**, 3463 (2007).
- [18] G. R. Patzke, A. Michailovski, F. Krumeich, R. Nesper, J. Grunwaldt, and A. Baiker, *Chem. Mater.* **16**, 1126 (2004).
- [19] J. Padiyath, J. Stahn, P. Allenspach, M. Horisberger, M. Gupta, T. Gutberlet, and P. Böni, *Physica B* **357**, 218 (2005).

Other references

- [20] X.-J. Huang and Y.-K. Choi, *Sens. Actu. B: Chem.* **122**, 659 (2007).
- [21] C. Imawan, H. Steffes, F. Solzbacher, and E. Obermeier, *Sens. Actu. B: Chem.* **77**, 346 (2001).
- [22] T. Maruyama and T. Kanagawa, *J. Electrochem. Soc.* **142**, 1644 (1995).
- [23] C. Julien, B. Yebka, and G. Nazri, *Mat. Sci. Eng. B* **38**, 65 (1996).
- [24] J. W. Gardner, *Sens. Actu. B: Chem.* **1**, 166 (1990).
- [25] A. J. Ricco, S. J. Martin, and T. E. Zipperian, *Sens. Actu. B*, 319 (1985).
- [26] M. Senthil Kumar, P. Böni, and S. Tixier, *Physica B* **248**, 53 (1998).
- [27] P. Böni, *Physica B* **234**, 1038 (1999).
- [28] M. Senthil Kumar and P. Böni, *J. App. Phys.* **91**, 3750 (2002).
- [29] A. A. van Well, V. O. de Haan, H. Fredrikze, and D. Clemens, *Physica B* **283**, 282 (2000).

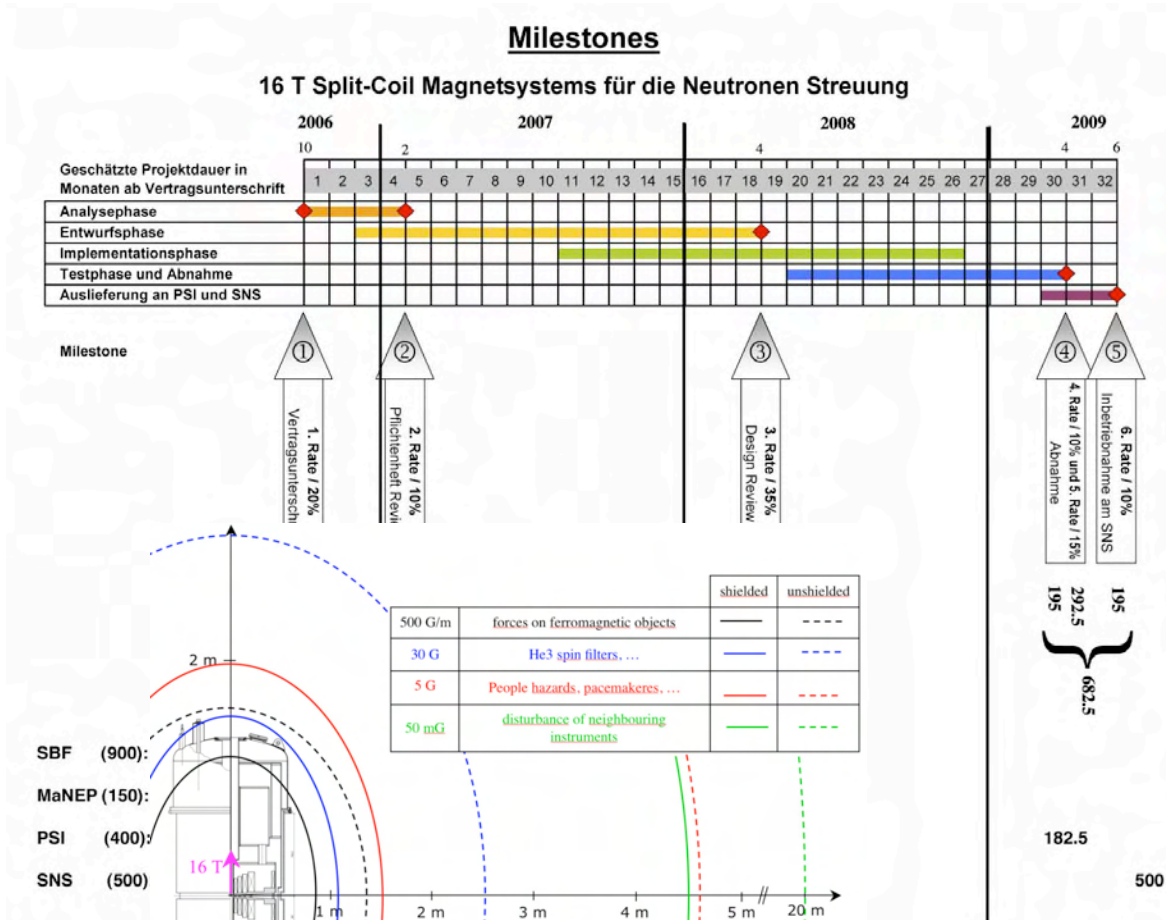


Figure 20: Planning chart and spending profile for the project based on the contracted milestones.

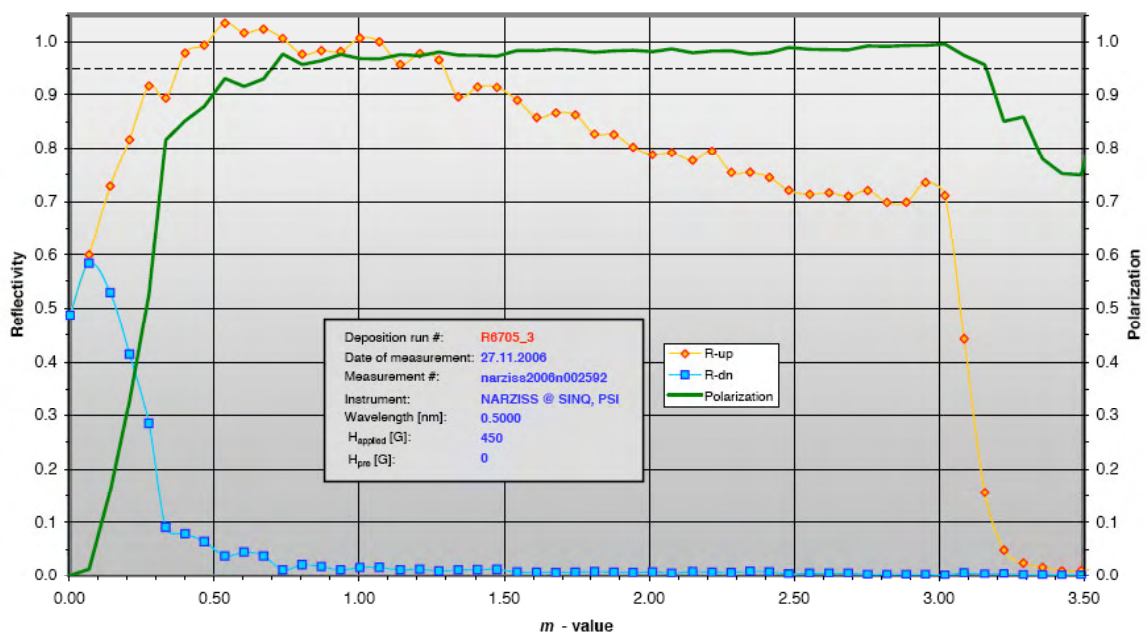


Figure 28: Neutron reflectivity data of a $m = 3.0$ FeCoV/TiN_x supermirror deposited on [Ti(1.3nm)/TiGd(5nm)]₂₅ multilayer absorber. This remanent multilayer system shows a polarization up to 98% for a wide range of the supermirror regime.

3 Three years of MaNEP's life

3.1 Communication

In 2007, the main highlight in communication was the *SupraFête*, an ambitious MaNEP public event dedicated to the discovery of high- T_c superconductivity. It lasted for three days and attracted an estimated 1500 visitors (Fig. 1). This event was the best example of our pragmatic approach which consists of “making the most” out of every public relation opportunity. In this case, the idea was to fulfill our mission to share science with the public, while drawing the media’s attention on MaNEP and creating a series of state-of-the-art branded tools. These tools were meant to be premiered during the event and then be used on other occasions, both inside and outside MaNEP. They consist of the following:

3.1.1 A 15-minute introduction movie on superconductivity

Superconductivity: a short story of an enduring enigma is an introduction to superconductivity covering the scientific explanation, the main historical milestones of research, an overview of today’s applications and perspectives for the future. The movie was praised and was later shown not only to high-school students, but also physics students at the CNRS in Paris, the



Figure 1: *The new generation taking up scientific challenges at the SupraKids.*



Figure 2: *The SupraSurf: a new and unique large-scale levitating device developed for the SupraFête and now installed at the Physiscope.*

EPFL and the Paul Scherrer Institute (PSI) in Switzerland. In 2008, it was also shown at CERN’s Open Days in April. Initially made in French, the movie was translated in English and German and released on a 3-language DVD.

3.1.2 The SupraSurf : a large-scale levitating device

Levitating devices used for demonstrations are usually model trains or cars. We decided it would be more impressive for people to experience the levitation physically by making them glide on a magnetic rail supported by superconductors. It would illustrate the power of the phenomenon – lifting a human body and not only a toy! The challenge was taken up by MaNEP’s engineering team in Geneva who conceived the SupraSurf (Fig. 2).

This unique set up proved very successful and was later used at the PSI’s Open Day in October and on several other occasions. It is now permanently installed in the Geneva Physiscope, a MaNEP initiated-outreach project (see below).

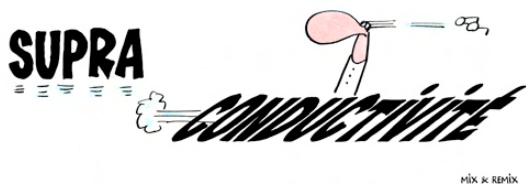


Figure 3: One of the 20 drawings created by cartoonist Mix & Remix for the exhibition.

3.1.3 Exhibition : superconductivity (re)viewed by Swiss cartoonist

Hard science is often seen by the general public as being “beyond their understanding”, making them shy away from it. We thus thought it would put everybody at ease to ask a true non-scientist to explain superconductivity. The idea of illustrating the key facts with humorous drawings emerged and we asked Swiss cartoonist Mix&Remix to take up the challenge. It resulted in 20 large and colorful panels including a central drawing designed to raise people’s curiosity enough as to make them read the related text (Fig. 3).

To make the exhibition “portable” we printed a leaflet which is especially valued by physics teachers and visitors. Like the movie and the SupraSurf, the exhibition was displayed at CERN in 2008, once during the Open Day in April and then at The Globe (CERN’s visitors center) during a special exhibition on superconductivity from October 2008 to January 2009.

3.2 Education and training

3.2.1 Physiscope Genève

The Physiscope is an original outreach initiative to rekindle the interest for science among the young of Geneva and beyond, through an interactive and playful discovery of physics (Figs. 4 and 5). It was inaugurated on October 3rd, 2008 in the presence of Charles Beer, the head of the Geneva department of education, and over 120 invited guests. The Physiscope is a modern seminar and exhibition area designed by the scenographic department of the *Télévision Suisse Romande*. It is located in the basement of the Physics section, thereby bringing the visitors into close contact with active scientists and modern research. Each session lasts about one hour during which the visitor is taken from a basic physics concept to some of the most modern research by a young scientist.



Figure 4: High-school students at the Physiscope experiencing electron transport hands on (October 2007).

Selected themes have been developed in close collaboration with high-school and pre high-school teachers. These presentations are designed to become an integral part of the student’s curriculum, the ultimate goal being to reach beyond a simple repetition of concepts introduced in class. The ambition of the Physiscope is to build a bridge to modern research likely to trigger the interest for a scientific career amongst the visitors. New presentations are continuously developed, not only for our target audience (12–19 year old students), but also for the general public. The aim is to expand our offer and be able to respond in a timely and original fashion to science related questions of the public, for example the implications of the LHC.

3.2.2 Doctoral School

A MaNEP doctoral School is being installed at the University of Geneva and the first courses started in autumn 2008.



Figure 5: High-school students at the Physiscope mastering the mysteries of superconducting levitation (October 2007).



Figure 6: Participants to the 2006 MaNEP Summer school in Saas Fee

3.2.3 Summer schools

After having co-organised a summer school with PSI in 2002 in Zuoz, Manep organized two successful summer schools at Saas-Fee (2004 and 2006). About 70 students followed lectures given by international experts (Fig. 6). A large part of the students were MaNEP doctoral students, but the schools also admitted students from other countries. The most recent event in this series was the winter school in January 11-16, 2009 in Saas Fee.

3.2.4 Conferences

Every two years since 2001, MaNEP organizes the Swiss Workshop on Materials with Novel Electronic Properties in Les Diablerets. The fifth conference will take place on August 26-28, 2009. This conference usually gathers about 200 physicists and presentations cover a broad range of current topics in condensed matter physics. A lot of care is taken to organize attractive poster sessions in order to give a certain visibility to the important work done by the young researchers (Fig. 7).

In February 2006 and March 2008, the three NCCR in physics were invited to contribute to



Figure 7: Poster session at the 2005 Swiss Workshop on MaNEP.

the general meeting of the Swiss Physical Society. MaNEP was strongly present in both editions with about 140 scientists, including almost 60 PhD students.

On September 27, 2006, 150 researchers attended a one day topical meeting on the subject of Novel Superconductors which ended by the second "Martin Peter colloquium" given by the Nobel Prize winner P.W. Anderson, from Princeton University.

3.3 Advancement of women

Since summer 2004, MaNEP proposes a dedicated program for the female students in physics to encourage them to continue their cursus at the highest level. This program consists of a summer internship of one month for students from the third year of study (Fig. 8). Since then, 7 to 13 students in the different universities and federal institutes in MaNEP carried out their internship each year during summertime on very interesting projects. These internships not only immerse the students within the reality of the research with all its constraints, but also reveal their ability to feel comfortable in this working environment. In several cases, it has convinced both parties to continue their collaboration at the PhD level.

2007 saw the nomination in the person of Patrycja Paruch of the first female professor at the Condensed Matter Physics Department of the University of Geneva since its creation. It is a great pleasure to see the presence of women in physics strengthened at this higher level.

3.4 Knowledge and Technology Transfer (KTT)

Whereas Phase 1 of MaNEP comprised significant energy to structure KTT and build promotional documents (Fig. 9), Phase 2 focused KTT efforts on the industry. The goal was to establish new collaborations with the industry. To this end, direct contacts were taken with companies using newly prepared marketing material. Several dozen companies were contacted and visited. At the same time, a strong and strategic relationship was put in place between MaNEP and the Geneva Economic Promotion. This organization's role is to attract new companies on the Geneva territory. As a consequence of MaNEP efforts, this organization has now become an important ambassador for MaNEP promoting MaNEP both internationally and locally with existing companies.

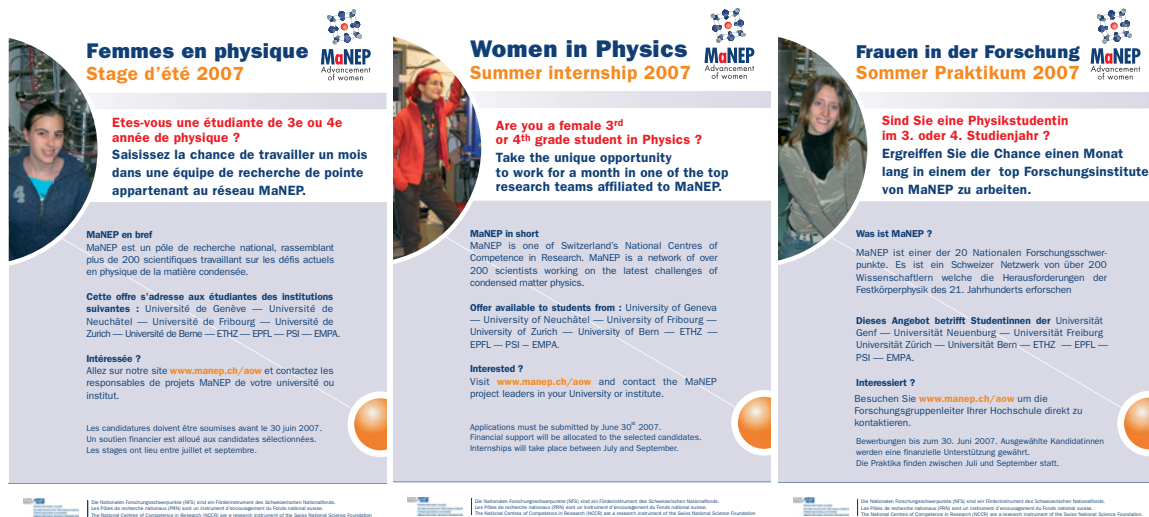


Figure 8: Posters for the announcement of the Advancement of Women program.

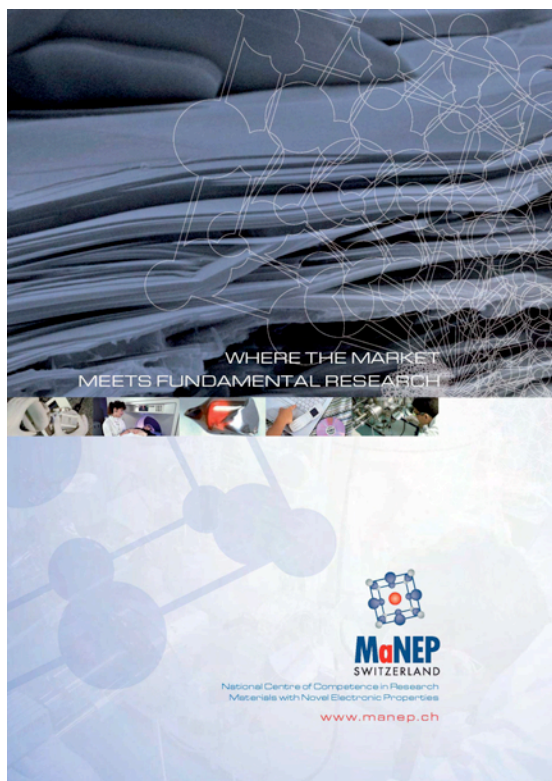


Figure 9: Cover page for the KTT promotional brochure.

The canton of Geneva, in addition to being attractive for its quality of life also offers an ideal set up for companies needing academic R&D input. With nine intention letters from companies to collaborate over phase III, MaNEP is in well geared to continue fulfilling its Knowledge and Technology Transfer (KTT) mission.

4 Three years of publications

The following lists cover the period from July 1st, 2005 to March 31st, 2008:

1. Scientific articles in journals with peer review
2. Scientific articles in journals without peer review
3. Books and scientific articles in anthologies

The lists are sorted by the name of the group leaders, and the most important publications are outlined by a red mark.

4.1 Scientific articles in journals with peer review

Group of Ph. Aebi

C. BATTAGLIA, H. CERCELLIER, L. DESPONT, C. MONNEY, M. PRESTER, H. BERGER, L. FORRÓ, M. G. GARNIER, AND P. AEBI
Non-uniform doping across the Fermi surface of NbS₂ intercalates

The European Physical Journal B **57**, 385 (2007).

Groups: Aebi, Margaritondo, Forró / Projects: 1, 3

C. BATTAGLIA, H. CERCELLIER, C. MONNEY, M. G. GARNIER, AND P. AEBI
Stabilization of silicon honeycomb chains by trivalent adsorbates

Europhysics Letters **77**, 36003 (2007).

Group: Aebi / Project: 5

- ▶ H. CERCELLIER, C. MONNEY, F. CLERC, C. BATTAGLIA, L. DESPONT, M. G. GARNIER, H. BECK, P. AEBI, L. PATTHEY, H. BERGER, AND L. FORRÓ
Evidence for an Excitonic Insulator Phase in 1T-TiSe₂

Physical Review Letters **99**, 146403 (2007).

Groups: Aebi, Margaritondo, Forró / Projects: 1, 3

F. CLERC, C. BATTAGLIA, H. CERCELLIER, C. MONNEY, H. BERGER, L. DESPONT, M. G. GARNIER, AND P. AEBI

Fermi surface of layered compounds and bulk charge density wave systems

Journal of Physics: Condensed Matter **19**,

335002 (2007).

Groups: Aebi, Margaritondo / Projects: 1, 3

- ▶ D. HOFSTETTER, L. DESPONT, M. G. GARNIER, E. BAUMANN, F. R. GIORGETTA, P. AEBI, L. KIRSTE, H. LU, AND W. J. SCHAFF
Structural investigations of epitaxial InN by x-ray photoelectron diffraction and x-ray diffraction

Applied Physics Letters **90**, 191912 (2007).

Group: Aebi / Project: 5

- ▶ C. LICHTENSTEIGER, M. DAWBER, N. STUCKI, J.-M. TRISCONE, J. HOFFMAN, J.-B. YAU, C. H. AHN, L. DESPONT, AND P. AEBI
Monodomain to polydomain transition in ferroelectric PbTiO₃ thin films with La_{0.67}Sr_{0.33}MnO₃ electrodes

Applied Physics Letters **90**, 052907 (2007).

Groups: Aebi, Triscone / Project: 5

P. STAROWICZ, C. BATTAGLIA, F. CLERC, L. DESPONT, A. PRODAN, H. J. P. VAN MIDDEN, U. SZERER, A. SZYTULA, M. G. GARNIER, AND P. AEBI

Electronic structure of ZrTe₃

Journal of Alloys and Compounds **442**, 268 (2007).

Group: Aebi / Project: 1

F. CLERC, C. BATTAGLIA, M. BOVET, L. DESPONT, C. MONNEY, H. CERCELLIER, M. GARNIER, P. AEBI, H. BERGER, AND L. FORRÓ

Lattice-distortion-enhanced electron-phonon coupling and Fermi surface nesting in 1T-TaS₂

Physical Review B **74**, 155114 (2006).

Groups: Margaritondo, Aebi, Forró / Projects: 1, 2, 3

L. DESPONT, F. CLERC, M. G. GARNIER, H. BERGER, L. FORRÓ, AND P. AEBI

Multiple scattering investigation of the 1T-TaS₂ surface termination

The European Physical Journal B **52**, 421 (2006).

Groups: Aebi, Margaritondo, Forró / Projects: 3, 5

- ▶ L. DESPONT, C. KOITZSCH, F. CLERC, M. G. GARNIER, P. AEBI, C. LICHTENSTEIGER, J.-M. TRISCONE, F. J. GARCIA DE ABAJO, E. BOUSQUET, AND P. GHOSEZ

Direct evidence for ferroelectric polar distortion in ultrathin lead titanate perovskite films

Physical Review B **73**, 094110 (2006).

Groups: Aebi, Triscione / Project: 5

L. DESPONT, C. LICHTENSTEIGER, F. CLERC, M. G. GARNIER, F. J. GARCIA DE ABAJO, M. A. VAN HOVE, J.-M. TRISCONE, AND P. AEBI

X-ray photoelectron diffraction study of ultrathin PbTiO₃ films

The European Physical Journal B **49**, 141 (2006).

Groups: Aebi, Triscione / Project: 5

L. DESPONT, D. NAUMOVIC, F. CLERC, C. KOITZSCH, M. G. GARNIER, F. J. GARCIA DE ABAJO, M. A. VAN HOVE, AND P. AEBI

X-ray photoelectron diffraction study of Cu(111): Multiple scattering investigation

Surface Science **600**, 380 (2006).

Group: Aebi / Project: 5

C. BATTAGLIA, H. CERCELLIER, F. CLERC, L. DESPONT, M. G. GARNIER, C. KOITZSCH, P. AEBI, H. BERGER, L. FORRÓ, AND C. AMBROSCH-DRAXL

Fermi surface induced lattice distortion in NbTe₂

Physical Review B **72**, 195114 (2005).

Groups: Margaritondo, Aebi, Forró / Projects: 1, 3

- ▶ C. KOITZSCH, C. BATTAGLIA, F. CLERC, L. DESPONT, M. G. GARNIER, AND P. AEBI

Photoemission of a Quantum Cavity with a Nonmagnetic Spin Separator

Physical Review Letters **95**, 126401 (2005).

Group: Aebi / Project: 1

D. POPOVIC, M. BOVET, H. BERGER, AND P. AEBI

Fingerprinting substitution sites in Pb, Dy-Bi₂Sr₂Ca₁Cu₂O_{8+δ} using X-ray Photoelectron Diffraction

The European Physical Journal – Applied Physics **30**, 171 (2005).

Groups: Aebi, Margaritondo / Projects: 2, 3

Group of D. Baeriswyl

D. BAERISWYL, D. EICHENBERGER, AND B. GUT

Superconductivity in the two-dimensional Hubbard model?

Physica Status Solidi (b) **244**, 2299 (2007).

Group: Baeriswyl / Project: 2

D. EICHENBERGER AND D. BAERISWYL

Superconducting ground state of the two-dimensional Hubbard model: A variational study

Physica C **460-462**, 1153 (2007).

Group: Baeriswyl / Project: 2

D. EICHENBERGER AND D. BAERISWYL

Superconductivity and antiferromagnetism in the two-dimensional Hubbard model: A variational study

Physical Review B **76**, 180504(R) (2007).

Group: Baeriswyl / Project: 2

- ▶ G. I. JAPARIDZE, R. M. NOACK, D. BAERISWYL, AND L. TINCANI

*Phases and phase transitions in the half-filled *t-t'* Hubbard chain*

Physical Review B **76**, 115118 (2007).

Group: Baeriswyl / Project: 1

Group of Ch. Bernhard

C. BERNHARD, L. YU, A. DUBROKA, K. W. KIM, M. RÖSSLE, D. MUNZAR, J. CHALOUKKA, C. T. LIN, AND T. WOLF

Broad-band infrared ellipsometry measurements of the c-axis response of underdoped YBa₂Cu₃O₇: Spectroscopic distinction between the normal state pseudogap and the superconducting gap

to be published in Journal of the Physics and Chemistry of Solids (2008).

Group: Bernhard / Project: 2

- ▶ V. HINKOV, D. HAUG, P. BOURGES, B. FAUQUÉ, Y. SIDIS, A. IVANOV, C. BERNHARD, B. KEIMER, AND C. T. LIN

Electronic Liquid Crystal State in the High-Temperature Superconductor YBa₂Cu₃O_{6.45}

Science **319**, 597 (2008).

Group: Bernhard / Project: 2

C. BERNHARD, C. NIEDERMAYER, A. DREW, G. KHALIULLIN, S. BAYRAKCI, J. STREMPFER,

- R. K. KREMER, D. P. CHEN, C. T. LIN, AND B. KEIMER
Muon-spin rotation study of magnetism in Na_xCoO_2 single crystals with $0.78 \leq x \leq 0.97$
 Europhysics Letters **80**, 27005 (2007).
 Group: Bernhard / Project: 2
- N. N. KOVALEVA, A. V. BORIS, P. YORDANOV, A. MALJUK, E. BRÜCHER, J. STREMPFER, M. KONUMA, I. ZEGKINOGLU, C. BERNHARD, A. M. STONEHAM, AND B. KEIMER
Optical response of ferromagnetic YTiO_3 studied by spectral ellipsometry
 Physical Review B **76**, 155125 (2007).
 Group: Bernhard / Project: 2
- ▶ S. S. A. SEO, W. S. CHOI, H. N. LEE, L. YU, K. W. KIM, C. BERNHARD, AND T. W. NOH
Optical Study of the Free Carrier Response of $\text{LaTiO}_3/\text{SrTiO}_3$ superlattices
 Physical Review Letters **99**, 266801 (2007).
 Group: Bernhard / Project: 2
- P. ADLER, A. LEBON, V. DAMLJANOVIĆ, C. ULRICH, C. BERNHARD, A. V. BORIS, A. MALJUK, C. T. LIN, AND B. KEIMER
Magnetoresistance effects in $\text{SrFeO}_{3-\delta}$: Dependence on phase composition and relation to magnetic and charge order
 Physical Review B **73**, 094451 (2006).
 Group: Bernhard / Project: 2
- J. CHAKHALIAN, J. W. FREELAND, G. SRAJER, J. STREMPFER, G. KHALIULLIN, J. C. CEZAR, T. CHARLTON, R. DALGLIESH, C. BERNHARD, G. CRISTIANI, H.-U. HABERMEIER, AND B. KEIMER
Magnetism at the interface between ferromagnetic and superconducting oxides
 Nature Physics **2**, 244 (2006).
 Group: Bernhard / Project: 2
- ▶ Y. KROCKENBERGER, I. FRITSCH, G. CRISTIANI, H.-U. HABERMEIER, L. YU, C. BERNHARD, B. KEIMER, AND L. ALFF
Superconductivity in epitaxial thin films of $\text{Na}_x\text{CoO}_2.y\text{D}_2\text{O}$
 Applied Physics Letters **88**, 162501 (2006).
 Group: Bernhard / Project: 2
- H. E. MOHOTTALA, B. O. WELLS, J. I. BUDNICK, W. A. HINES, C. NIEDERMAYER, L. UDBY, C. BERNHARD, A. R. MOODENBAUGH, AND F. C. CHOU
Phase separation in superoxygenated $\text{La}_{2-x}\text{Sr}_x\text{CuO}_{4+y}$
 Nature Materials **5**, 377 (2006).
 Groups: Bernhard, Mesot / Projects: 1, 2, 3, 6
- A. TRAJNEROWICZ, A. GOLNIK, C. BERNHARD, L. MACHTOUB, C. ULRICH, J. L. TALLON, AND M. CARDONA
Isotope effect on the optical phonons of $\text{YBa}_2\text{Cu}_4\text{O}_8$ studied by far-infrared ellipsometry and Raman scattering
 Physical Review B **74**, 104513 (2006).
 Group: Bernhard / Project: 2
- ▶ A. V. PIMENOV, A. V. BORIS, L. YU, V. HINKOV, T. WOLF, J. L. TALLON, B. KEIMER, AND C. BERNHARD
Nickel Impurity-Induced Enhancement of the Pseudogap of Cuprate High- T_c Superconductors
 Physical Review Letters **94**, 227003 (2005).
 Group: Bernhard / Project: 2
- J. STAHN, J. CHAKHALIAN, C. NIEDERMAYER, J. HOPPLER, T. GUTBERLET, J. VOIGT, F. TREUBEL, H.-U. HABERMEIER, G. CRISTIANI, B. KEIMER, AND C. BERNHARD
Magnetic proximity effect in Perovskite Superconductor/Ferromagnet Multilayers
 Physical Review B **71**, R140509 (2005).
 Group: Bernhard / Project: 2
- Group of G. Blatter**
- ▶ V. DOTSSENKO, L. B. IOFFE, V. B. GESHKENBEIN, S. E. KORSHUNOV, AND G. BLATTER
Joint Free-Energy Distribution in the Random Directed Polymer Problem
 Physical Review Letters **100**, 050601 (2008).
 Group: Blatter / Project: 1
- ▶ S. D. HUBER, B. THEILER, E. ALTMAN, AND G. BLATTER
Amplitude Mode in the Quantum Phase Model
 Physical Review Letters **100**, 050404 (2008).
 Group: Blatter / Project: 1
- ▶ A. U. THOMANN, V. B. GESHKENBEIN, AND G. BLATTER
The dynamically asymmetric SQUID: Münchhausen effect
 Physica C (2008).
 Group: Blatter / Project: 1
- ▶ A. DE COL, G. I. MENON, AND G. BLATTER
Density functional theory of vortex lattice melting in layered superconductors: A mean-field substrate approach
 Physical Review B **75**, 014518 (2007).
 Group: Blatter / Project: 1

A. DE COL, G. I. MENON, V. B. GESHKENBEIN, AND G. BLATTER

Surface melting of the vortex lattice in layered superconductors: Density functional theory

Physical Review B **75**, 184532 (2007).

Group: Blatter / Project: 1

- ▶ S. D. HUBER, E. ALTMAN, H. P. BÜCHLER, AND G. BLATTER

Dynamical properties of ultracold bosons in an optical lattice

Physical Review B **75**, 085106 (2007).

Group: Blatter / Project: 1

- ▶ A. DE COL, G. I. MENON, V. B. GESHKENBEIN, AND G. BLATTER

Surface Melting of the Vortex Lattice

Physical Review Letters **96**, 177001 (2006).

Group: Blatter / Project: 1

T. SHIBAUCHI, L. KRUSIN-ELBAUM, Y. KASHIHARA, Y. SHIMONO, Y. MATSUDA, R. D. McDONALD, C. H. MIELKE, S. YONEZAWA, Z. HIROI, M. ARAI, T. KITA, G. BLATTER, AND M. SIGRIST

Uncommonly high upper critical field of the pyrochlore superconductor KOs_2O_6 below the enhanced paramagnetic limit

Physical Review B **74**, 220506 (2006).

Groups: Rice, Sigrist, Blatter / Project: 2

- ▶ H. P. BÜCHLER, M. HERMELE, S. D. HUBER, M. P. A. FISHER, AND P. ZOLLER

Atomic Quantum Simulator for Lattice Gauge Theories and Ring Exchange Models

Physical Review Letters **95**, 040402 (2005).

Group: Blatter / Project: 1

Group of M. Büttiker

- ▶ M. MOSKALETS, P. SAMUELSSON, AND M. BÜTTIKER

Quantized Dynamics of a Coherent Capacitor

Physical Review Letters **100**, 086601 (2008).

Group: Büttiker / Project: 1

- ▶ S. E. NIGG AND M. BÜTTIKER

Quantum to Classical Transition of the Charge Relaxation Resistance of a Mesoscopic Capacitor

Physical Review B **77**, 085312 (2008).

Group: Büttiker / Project: 1

M. BÜTTIKER AND S. E. NIGG

Mesoscopic Capacitance Oscillations

Nanotechnology **18**, 044029 (2007).

Group: Büttiker / Project: 1

M. BÜTTIKER AND P. SAMUELSSON

Interference of independently emitted electrons in quantum shot noise

Annalen der Physik (Leipzig) **16**, 751 (2007).

Group: Büttiker / Project: 1

H. FÖRSTER, P. SAMUELSSON, S. PILGRAM, AND M. BÜTTIKER

Voltage and dephasing probes in mesoscopic conductors: A study of full-counting statistics

Physical Review B **75**, 035340 (2007).

Group: Büttiker / Project: 1

- ▶ A. N. JORDAN, A. N. KOROTKOV, AND M. BÜTTIKER

Leggett-Garg Inequality with a Kicked Quantum Pump

Physical Review Letters **97**, 026805 (2006).

Group: Büttiker / Project: 1

- ▶ S. E. NIGG, R. LÓPEZ, AND M. BÜTTIKER

Mesoscopic Charge Relaxation

Physical Review Letters **97**, 206804 (2006).

Group: Büttiker / Project: 1

- ▶ S. PILGRAM, P. SAMUELSSON, H. FÖRSTER, AND M. BÜTTIKER

Full-Counting Statistics for Voltage and Dephasing Probes

Physical Review Letters **97**, 066801 (2006).

Group: Büttiker / Project: 1

- ▶ P. SAMUELSSON AND M. BÜTTIKER

Quantum state tomography with quantum shot noise

Physical Review B **73**, 041305 (2006).

Group: Büttiker / Project: 1

Group of L. Degiorgi

- ▶ F. PFUNER, L. DEGIORGI, H. R. OTT, A. BIANCHI, AND Z. FISK

Magneto-optical behavior of $EuIn_2P_2$

Physical Review B **77**, 024417 (2008).

Groups: Degiorgi, Ott / Project: 1

D. PACILÉ, M. PAPAGNO, M. LAVAGNINI, H. BERGER, L. DEGIORGI, AND M. GRIONI

Photoemission and optical studies of $ZrSe_3$, $HfSe_3$, and ZrS_3

Physical Review B **76**, 155406 (2007).

Groups: Margaritondo, Degiorgi, Grioni / Projects: 1, 3

- ▶ A. SACCHETTI, E. ARCANGELETTI, A. PERUCCHI, P. POSTORINO, S. LUPI, N. RU, I. R. FISHER, AND L. DEGIORGI

Pressure Dependence of the Charge-Density-Wave Gap in Rare-Earth Tritellurides

- Physical Review Letters **98**, 026401 (2007).
Group: Degiorgi / Project: 1
- G. CAIMI, L. DEGIORGI, H. BERGER, AND L. FORRÓ
Optical evidence for a magnetically driven structural transition in the spin web Cu_3TeO_6
Europhysics Letters **75**, 496 (2006).
Groups: Margaritondo, Degiorgi, Forró / Projects: 1, 3
- G. CAIMI, L. DEGIORGI, H. BERGER, AND L. FORRÓ
Phonon analysis of the $S = 1$ quantum spin systems $\text{Ni}_5\text{Te}_4\text{O}_{12}\text{X}_2$ ($X = \text{Cl}$ and Br)
Journal of Physics: Condensed Matter **18**, 4065 (2006).
Groups: Margaritondo, Degiorgi, Forró / Projects: 1, 3
- G. CAIMI, A. PERUCCHI, L. DEGIORGI, H. R. OTT, V. M. PEREIRA, A. H. CASTRO NETO, A. D. BIANCHI, AND Z. FISK
Magneto-Optical Evidence of Double Exchange in a Percolating Lattice
Physical Review Letters **96**, 016403 (2006).
Groups: Degiorgi, Ott / Project: 1
- L. DEGIORGI
The Drude model in correlated systems
Annalen der Physik **15**, 571 (2006).
Group: Degiorgi / Project: 1
- L. DEGIORGI AND D. JEROME
Transport and Optics in Quasi-One-Dimensional Organic Conductors
Journal of the Physical Society of Japan **75**, 051004 (2006).
Group: Degiorgi / Project: 1
- M. PAPAGNO, D. PACILÉ, G. CAIMI, H. BERGER, L. DEGIORGI, AND M. GRIONI
Electronic structure of one-dimensional copper oxide chains in LiCu_2O_2 from angle-resolved photoemission and optical spectroscopy
Physical Review B **73**, 115120 (2006).
Groups: Margaritondo, Degiorgi, Grioni / Projects: 1, 3
- A. PERUCCHI, L. DEGIORGI, R. HU, C. PETROVIC, AND V. F. MITROVIC
Optical investigation of the metal-insulator transition in FeSb_2
The European Physical Journal B **54**, 175 (2006).
Group: Degiorgi / Project: 1
- A. SACCHETTI, L. DEGIORGI, T. GIAMARCHI, N. RU, AND I. R. FISHER
Chemical pressure and hidden one-dimensional behavior in rare-earth tri-telluride charge-density wave compounds
Physical Review B **74**, 125115 (2006).
Groups: Degiorgi, Giamarchi / Project: 1
- C. DALLERA, E. ANNESE, J.-P. RUEFF, M. GRIONI, G. VANKO, L. BRAICOVICH, A. BARLA, J.-P. SANCHEZ, R. GUSMEROLI, A. PALENZONA, L. DEGIORGI, AND G. LAPERTOT
Intermediate valence behaviour under pressure: how precisely can we probe it by means of resonant inelastic x-ray emission?
Journal of Physics: Condensed Matter **17**, S849 (2005).
Groups: Degiorgi, Grioni / Project: 1
- A. PERUCCHI, L. DEGIORGI, AND H. BERGER
Infrared signature of the charge-density-wave gap in ZrTe_3
The European Physical Journal B **48**, 489 (2005).
Groups: Margaritondo, Degiorgi / Project: 3
- ### Group of Ø. Fischer
- A. P. PETROVIĆ, R. LORTZ, G. SANTI, M. DECROUX, H. MONNARD, Ø. FISCHER, L. BOERI, O. ANDERSEN, J. KORTUS, D. SALLOUM, P. GOUGEON, AND M. POTEI
Phonon Mode Spectroscopy and Electron-Phonon Coupling in the Quasi-One-Dimensional $\text{M}_2\text{Mo}_6\text{Se}_6$ family: Competing Instabilities, Ultra-Strong Coupling and "Phonon-Boosted" Superconductivity
submitted to Physical Review B (2008).
Group: Fischer / Projects: 1, 2
- A. PIRIOU, Y. FASANO, E. GIANNINI, AND O. FISCHER
Effect of oxygen-doping on $\text{Bi}_2\text{Sr}_2\text{Ca}_2\text{Cu}_3\text{O}_{10+\delta}$ vortex matter: Crossover from electromagnetic to Josephson interlayer coupling
submitted to Physical Review B (2008).
Groups: Fischer, van der Marel / Projects: 2, 5
- S. SEIRO, Y. FASANO, I. MAGGIO-APRILE, E. KOLLER, O. KUFFER, AND Ø. FISCHER
Polaronic signature in the metallic phase of $\text{La}_{0.7}\text{Ca}_{0.3}\text{MnO}_3$ films detected by scanning tunneling spectroscopy
Physical Review B **77**, 020407(R) (2008).
Group: Fischer / Project: 1
- L. ANTOGNAZZA, M. DECROUX, M. THERASSE, M. ABPLANALP, J. DURON, B. DUTOIT, AND Ø. FISCHER
Thermally Assisted Transition in Thin Film Based FCL: A Way to Speed Up the Normal Transition Across the Wafer

IEEE Transactions on Applied Superconductivity **17**, 3463 (2007).

Groups: Fischer, Hasler / Project: 6

- ▶ C. DUBOIS, A. P. PETROVIĆ, G. SANTI, C. BERTHOD, A. A. MANUEL, M. DECROUX, Ø. FISCHER, M. POTEI, AND R. CHEVREL

Node-like excitations in superconducting $PbMo_6S_8$ probed by scanning tunneling spectroscopy

Physical Review B **75**, 104501 (2007).

Groups: Fischer, Giamarchi / Projects: 1, 2

- ▶ J. DURON, F. GRILLI, L. ANTOGNAZZA, M. DECROUX, B. DUTOIT, AND Ø. FISCHER

Finite-element modelling of YBCO fault current limiter with temperature dependent parameters

Superconductor Science & Technology **20**, 338 (2007).

Groups: Hasler, Fischer / Project: 6

- ▶ J. DURON, B. DUTOIT, F. GRILLI, M. DECROUX, L. ANTOGNAZZA, AND Ø. FISCHER

Computer Modeling of YBCO Fault Current Limiter Strips Lines in Over-Critical Regime With Temperature Dependent Parameters

IEEE Transactions on Applied Superconductivity **17**, 1839 (2007).

Groups: Hasler, Fischer / Project: 6

Y. FASANO, I. MAGGIO-APRILE, J. KARPINSKI, AND Ø. FISCHER

Tunneling and pseudo point-contact spectroscopy on $YBa_2Cu_4O_8$

Physica C **460-462**, 958 (2007).

Groups: Fischer, Karpinski / Projects: 2, 3, 4

- ▶ Ø. FISCHER, M. KUGLER, I. MAGGIO-APRILE, C. BERTHOD, AND C. RENNER

Scanning tunneling spectroscopy of high-temperature superconductors

Reviews of Modern Physics **79**, 353 (2007).

Groups: Fischer, Giamarchi / Project: 2

A. P. PETROVIĆ, Y. FASANO, R. LORTZ, M. DECROUX, M. POTEI, R. CHEVREL, AND Ø. FISCHER

Unconventional resistive transitions in the extreme type-II superconductor $Tl_2Mo_6Se_6$

Physica C **460-462**, 702 (2007).

Groups: Fischer, Triscone, van der Marel / Projects: 1, 2

A. PIRIOU, Y. FASANO, E. GIANNINI, AND Ø. FISCHER

Doping-dependence of the vortex phase diagram of $Bi_2Sr_2Ca_2Cu_3O_{10+\delta}$

Physica C **460-462**, 408 (2007).

Groups: Fischer, van der Marel / Projects: 2, 3, 5

S. SEIRO, Y. FASANO, I. MAGGIO-APRILE, O. KUFFER, AND Ø. FISCHER

Homogeneous Spectroscopic Properties in Manganite Films

Journal of Magnetism and Magnetic Materials **310**, e243 (2007).

Group: Fischer / Project: 1

- ▶ S. SEIRO, E. KOLLER, Y. FASANO, AND Ø. FISCHER

Homogeneous strain-relaxation effects in $La_{0.67}Ca_{0.33}MnO_3$ films grown on $NdGaO_3$

Applied Physics Letters **91**, 091913 (2007).

Group: Fischer / Projects: 1, 5

D. SHALTIEL, H.-A. K. VON NIDDA, B. Y. SHAPIRO, I. SHAPIRO, A. LOIDL, T. KURZ, B. BOGOSLAVSKY, T. TAMAGAI, Ø. FISCHER, A. PIRIOU, E. GIANNINI, T. WATANABE, T. FUJII, AND A. MATSUDA, B. ROSENSTEIN

Interaction of AC magnetic field with Josephson vortices in high anisotropy superconductors $Bi2212$ and $Bi2223$

Physica C **460-462**, 1238 (2007).

Groups: van der Marel, Fischer / Project: 3

- ▶ C. DUBOIS, P. E. BISSON, A. A. MANUEL, Ø. FISCHER, AND S. REYMOND

Compact design of a low temperature XY stage scanning tunneling microscope

Review of Scientific Instruments **77**, 043712 (2006).

Group: Fischer / Project: 2

C. DUBOIS, N. JENKINS, A. A. MANUEL, N. D. ZHIGADLO, J. KARPINSKI, AND Ø. FISCHER

Crystal-edge scanning tunnelling spectroscopy on aluminium-doped magnesium diboride

Superconductor Science & Technology **19**, 695 (2006).

Groups: Fischer, Karpinski / Projects: 2, 3, 4

- ▶ J. DURON, F. GRILLI, L. ANTOGNAZZA, M. DECROUX, S. STAVREV, B. DUTOIT, AND Ø. FISCHER

Finite-element modeling of superconductors in over-critical regime with temperature dependent resistivity.

Journal of Physics: Conference Series **43**, 1076 (2006).

Groups: Fischer, Hasler / Project: 6

M. KUGLER, G. L. DE CASTRO, E. GIANNINI, A. PIRIOU, A. A. MANUEL, C. HESS, AND Ø. FISCHER

Scanning tunneling spectroscopy on $Bi_2Sr_2Ca_2Cu_3O_{10+\delta}$ single crystals

Journal of the Physics and Chemistry of Solids

67, 353 (2006).

Groups: van der Marel, Fischer / Project: 3

L. ANTOGNAZZA, M. DECROUX, M. THERASSE, M. ABPLANALP, AND Ø. FISCHER

Test of YBCO thin films based Fault Current Limiters with a newly designed meander.

IEEE Transactions on Applied Superconductivity **15**, 1990 (2005).

Group: Fischer / Project: 6

J. DURON, L. ANTOGNAZZA, M. DECROUX, F. GRILLI, S. STAVREV, B. DUTOIT, AND ØS. FISCHER

3D finite element Simulations of strip lines in a YBCO/Au fault current limiter.

IEEE Transactions on Applied Superconductivity **15**, 1998 (2005).

Groups: Fischer, Hasler / Project: 6

J. DURON, L. ANTOGNAZZA, M. DECROUX, F. GRILLI, S. STAVREV, B. DUTOIT, AND Ø. FISCHER

3-D finite element Simulations of strip lines in a YBCO/Au fault current limiter

in *IEEE, Applied Superconductivity Conference 2004* (2005), vol. 15, pp. 1998–2002.

Groups: Hasler, Fischer / Project: 6

O. KUFFER AND Ø. FISCHER

Low temperature growth of pseudocubic perovskites by off-axis rf magnetron sputtering for the realization of epitaxial ferroelectric-based heterostructures

Journal of Applied Physics **97**, 014103 (2005).

Group: Fischer / Project: 5

► O. KUFFER, I. MAGGIO-APRILE, AND Ø. FISCHER

Nanoscale ferroelectric field-effect writing and reading using scanning tunneling spectroscopy

Nature Materials **4**, 378 (2005).

Group: Fischer / Project: 5

Group of R. Flükiger

R. FLÜKIGER, C. SENATORE, M. CESARETTI, F. BUTA, D. UGLIETTI, AND B. SEEBER

Optimization of Nb₃Sn and MgB₂ wires

to be published in *Superconductor Science & Technology* (2008).

Group: Flükiger / Project: 6

E. GIANNINI, R. GLADYSHEVSKII, N. CLAYTONA, N. MUSOLINO, V. GARNIER, A. PIRIOU, AND R. FLÜKIGER

Growth, structure and physical properties of single crystals of pure and Pb-doped Bi-based high-T_c superconductors

Current Applied Physics **8**, 115 (2008).

Groups: Flükiger, van der Marel / Project: 3

C. SENATORE AND R. FLÜKIGER

Relaxation rates of Y-123 and Bi-based tapes compared to low T_c and MgB₂ superconductors in view of persistent mode high field magnets

to be published in *Superconductor Science & Technology* (2008).

Group: Flükiger / Project: 6

V. ABÄCHERLI, F. BUTA, D. UGLIETTI, C. SENATORE, B. SEEBER, AND R. FLÜKIGER

Investigation on the Effect of Ta Additions on J_c and n of (Nb, Ti)₃Sn Bronze Processed Multifilamentary Wires at High Magnetic Fields

IEEE Transactions on Applied Superconductivity **17**, 2564 (2007).

Group: Flükiger / Project: 6

M. G. ADESSO, R. FLÜKIGER, D. UGLIETTI, M. POLOCHETTI, AND S. PACE

Influence of grain boundaries and Sn distribution on the H-T phase diagram of Nb₃Sn

IEEE Transactions on Applied Superconductivity **17**, 2619 (2007).

Group: Flükiger / Project: 6

M. G. ADESSO, M. POLOCHETTI, D. ZOLA, S. PACE, D. UGLIETTI, AND R. FLÜKIGER

Effect of the amplitude of the AC magnetic field on the vortex dynamics: a quantitative analysis in Nb and NbTi polycrystalline samples

Physica C **460**, 1286 (2007).

Group: Flükiger / Project: 6

S. X. DOU, O. SHCHERBAKOVA, W. K. YEOH, J. H. KIM, S. SOLTANIAN, X. L. WANG, C. SENATORE, R. FLÜKIGER, M. DHALLE, O. HUSNJAK, AND E. BABIC

Mechanism of enhancement in electromagnetic properties of MgB₂ by nano SiC doping

Physical Review Letters **98**, 097002 (2007).

Group: Flükiger / Project: 6

R. FLÜKIGER, P. LEZZA, M. CESARETTI, C. SENATORE, AND R. GLADYSHEVSKI

Simultaneous Addition of B₄C+SiC to MgB₂ wires and consequences for J_c and B_{irr}

IEEE Transactions on Applied Superconductivity **17**, 2846 (2007).

Group: Flükiger / Project: 6

P. LEZZA, C. SENATORE, R. GLADYSHEVSKII, AND R. FLÜKIGER

Critical Current Anisotropy and Texture Gradients in ex situ MgB₂/Fe Tapes

- IEEE Transactions on Applied Superconductivity **17**, 2834 (2007).
Group: Flükiger / Project: 6
- S. OH, C. LEE, K. W. CHO, K. KIM, D. UGLIETTI, AND R. FLÜKIGER
Field dependence of the n -value and its relation with the critical current of Nb_3Sn strands
Superconductor Science & Technology **20**, 851 (2007).
Group: Flükiger / Project: 6
- B. SEEBER, A. FERREIRA, V. ABÄCHERLI, T. BOUTBOUL, L. OBERLI, AND R. FLÜKIGER
Transport Properties up to 1000 A of Nb_3Sn Wires Under Transverse Compressive Stress
IEEE Transactions on Applied Superconductivity **17**, 2643 (2007).
Group: Flükiger / Project: 6
- B. SEEBER, A. FERREIRA, V. ABÄCHERLI, AND R. FLÜKIGER
Critical current of a Nb_3Sn bronze route conductor under uniaxial tensile and transverse compressive stress
Superconductor Science & Technology **20**, S184 (2007).
Group: Flükiger / Project: 6
- C. SENATORE, V. ABÄCHERLI, D. CANTONI, AND R. FLÜKIGER
Distribution of T_c from calorimetry and the determination of Sn gradients in Bronze Route Nb_3Sn wires with internal and external Ti source
Superconductor Science & Technology **20**, S217 (2007).
Group: Flükiger / Project: 6
- C. SENATORE, P. LEZZA, R. LORTZ, O. SHCHERBAKOVA, W. K. YEOH, S. X. DOU, AND R. FLÜKIGER
Specific heat and magnetic relaxation analysis of MgB_2 bulk samples with and without additives
IEEE Transactions on Applied Superconductivity **17**, 2941 (2007).
Group: Flükiger / Project: 6
- C. SENATORE, D. UGLIETTI, V. ABÄCHERLI, A. JUNOD, AND R. FLÜKIGER
Specific heat, a method to determine the T_c distribution in industrial Nb_3Sn wires prepared by various techniques
IEEE Transactions on Applied Superconductivity **17**, 2611 (2007).
Group: Flükiger / Project: 6
- D. UGLIETTI, V. ABÄCHERLI, M. CANTONI, AND R. FLÜKIGER
Grain growth, Morphology and Composition Profiles in Industrial Nb_3Sn wires
IEEE Transactions on Applied Superconductivity **17**, 2615 (2007).
Group: Flükiger / Project: 6
- M. G. ADESSO, D. UGLIETTI, V. ABÄCHERLI, R. FLÜKIGER, M. POLICHIETTI, AND S. PACE
Investigations of magnetic behaviour in various type of Nb_3Sn multifilamentary wires by means of the 1st and 3rd harmonics of the AC magnetic susceptibility
IEEE Transactions on Applied Superconductivity **16**, 1241 (2006).
Group: Flükiger / Project: 6
- M. G. ADESSO, D. UGLIETTI, R. FLÜKIGER, P. M., AND S. PACE
Phase Transition between the Bragg Glass and a Disordered Phase in Nb_3Sn , as detected by 3rd harmonics of the AC magnetic susceptibility
Physical Review B **73**, 092513 (2006).
Group: Flükiger / Project: 6
- M. G. ADESSO, D. UGLIETTI, R. FLÜKIGER, AND S. PACE
 Nb_3Sn single crystals, polycrystals and multifilamentary wires: common and different features in the magnetic response
Journal of Physics: Conference Series **43**, 22 (2006).
Group: Flükiger / Project: 6
- M. G. ADESSO, D. UGLIETTI, N. MUSOLINO, R. FLÜKIGER, AND S. PACE
 $H(T)$ Phase Diagram in Nb_3Sn : A Different Behavior in Single Crystals, Polycrystalline Samples and Multifilamentary Wires
Advances in Cryogenic Engineering **52**, 473 (2006).
Group: Flükiger / Project: 6
- P. LEZZA, R. GLADYSHEVSKII, V. ABÄCHERLI, AND R. FLÜKIGER
Texture gradients in Fe-sheathed ex situ MgB_2 tapes
Superconductor Science & Technology **19**, 286 (2006).
Group: Flükiger / Project: 6
- P. LEZZA, C. SENATORE, AND R. FLÜKIGER
Improved critical current densities in B_4C doped MgB_2 based wires
Superconductor Science & Technology **19**, 1030 (2006).
Group: Flükiger / Project: 6
- C. SENATORE, P. LEZZA, AND R. FLÜKIGER

- Critical Current Anisotropy, Pinning Properties and Relaxation Rate of ex situ MgB₂/Fe Tapes*
Advances in Cryogenic Engineering **824**, 654 (2006).
Group: Flükiger / Project: 6
- C. SENATORE, P. LEZZA, AND R. FLÜKIGER
Determination of the texturing gradient in ex situ MgB₂/Fe tapes examined by X ray diffraction and its effects on the pinning force
Journal of Applied Physics **100**, 113913 (2006).
Group: Flükiger / Project: 6
- D. UGLIETTI, V. ABÄCHERLI, B. SEEBER, AND R. FLÜKIGER
The effect of Ti addition on critical Parameters and Transport Properties of Quaternary (Nb, Ta, Ti)₃Sn Wires
Superconductor Science & Technology **19**, 1185 (2006).
Group: Flükiger / Project: 6
- D. UGLIETTI, B. SEEBER, V. ABÄCHERLI, M. CANTONI, AND R. FLÜKIGER
Strain and Field Scaling Laws for Internal Sn and Bronze Route Nb₃Sn Wires up to 21 T
Advances in Cryogenic Engineering **824**, 528 (2006).
Group: Flükiger / Project: 6
- D. UGLIETTI, B. SEEBER, AND R. FLÜKIGER
Critical Currents versus Applied Strain for Industrial Y-123 Coated Conductors at Various Temperatures and Magnetic Fields up to 19 T
Superconductor Science & Technology **19**, 869 (2006).
Group: Flükiger / Project: 6
- J. WANG, J. L. JORDA, A. PISCH, AND R. FLÜKIGER
Experimental Study of the CeNi₅-CeCu₅ System
Intermetallics **14**, 869 (2006).
Group: Flükiger / Project: 6
- Y. WANG, C. SENATORE, V. ABÄCHERLI, D. UGLIETTI, AND R. FLÜKIGER
Specific Heat of Nb₃Sn Wires
Superconductor Science & Technology **19**, 2030 (2006).
Group: Flükiger / Project: 6
- V. ABÄCHERLI, D. UGLIETTI, P. LEZZA, B. SEEBER, R. FLÜKIGER, M. CANTONI, AND P.-A. BUFFAT
The Influence of Ti doping Methods on the High Field Performance of (Nb, Ta, Ti)₃Sn Multifilamentary Wires Using Ospray Bronze
IEEE Transactions on Applied Superconductivity **15**, 3482 (2005).
Group: Flükiger / Project: 6
- N. BANNO, D. UGLIETTI, B. SEEBER, T. TAKEUCHI, AND R. FLÜKIGER
Field and strain dependence of critical current in technical Nb₃Al superconductors
Superconductor Science & Technology **18**, S338 (2005).
Group: Flükiger / Project: 6
- N. BANNO, D. UGLIETTI, B. SEEBER, T. TAKEUCHI, AND R. FLÜKIGER
Strain dependence of superconducting characteristics in technical Nb₃Al superconductors
Superconductor Science & Technology **18**, 284 (2005).
Group: Flükiger / Project: 6
- R. FLÜKIGER, D. UGLIETTI, V. ABÄCHERLI, AND B. SEEBER
Asymmetric Behaviour of J_c(ε) in Nb₃Sn Wires and correlation with the stress induced elastic tetragonal distortion
Superconductor Science & Technology **18**, S416 (2005).
Group: Flükiger / Project: 6
- E. GIANNINI, N. CLAYTON, N. MUSOLINO, A. PIRIOU, R. GLADYSHEVSKII, AND R. FLÜKIGER
Growth and superconducting properties of Pb-free and Pb-doped Bi-2223 crystals
IEEE Transactions on Applied Superconductivity **15**, 3102 (2005).
Groups: van der Marel, Flükiger / Project: 3
- P. LEZZA, R. GLADYSHEVSKII, H. L. SUO, AND R. FLÜKIGER
Quantitative study of the inhomogeneous distribution of phases in Fe-sheathed ex situ MgB₂ tapes
Superconductor Science & Technology **18**, 753 (2005).
Group: Flükiger / Project: 6
- B. SEEBER, D. UGLIETTI, V. ABÄCHERLI, P. A. BOVIER, D. ECKERT, G. KÜBLER, P. LEZZA, A. POLLINI, AND R. FLÜKIGER
Critical Current vs. Strain Measurement up to 21 T and 1'000 A of Long Length Superconducting Wires and Tapes
Review of Scientific Instruments **76**, 093901 (2005).
Group: Flükiger / Project: 6
- X. SU, E. GIANNINI, AND R. FLÜKIGER

Improvement of the critical current density of Bi-2223 tapes by introducing Ag Layers inside individual filaments

Superconductor Science & Technology **18**, 830 (2005).

Groups: Flükiger, van der Marel / Project: 6

Group of L. Forró

A. AKRAP, N. BARIŠIĆ, L. FORRÓ, D. MANDRUS, AND B. C. SALES

High-pressure resistivity and thermoelectric power in $\text{Yb}_{14}\text{MnSb}_{11}$

Physical Review B **76**, 085203 (2007).

Group: Forró / Project: 1

A. AKRAP, N. BARIŠIĆ, R. GAAL, AND L. FORRÓ

Pressure-induced tuning of phase transition and role of disorder in electrical transport properties of $\beta\text{-Sr}_x\text{V}_6\text{O}_{15}$

Physical Review B **76**, 235111 (2007).

Group: Forró / Project: 1

A. AKRAP, E. TUTIŠ, S. M. KAZAKOV, N. D. ZHIGADLO, J. KARPINSKI, AND L. FORRÓ

Manifestations of fine features of the density of states in the transport properties of KOs_2O_6

Physical Review B **75**, 172501 (2007).

Groups: Forró, Karpinski / Projects: 1, 3, 4

A. AKRAP, T. WELLER, M. ELLERBY, S. S. SAXENA, G. CSÁNYI, AND L. FORRÓ

C_6Yb and graphite: A comparative high-pressure transport study

Physical Review B **76**, 045426 (2007).

Group: Forró / Project: 1

C. BATTAGLIA, H. CERCELLIER, L. DESPONT, C. MONNEY, M. PRESTER, H. BERGER, L. FORRÓ, M. G. GARNIER, AND P. AEBI

Non-uniform doping across the Fermi surface of NbS_2 intercalates

The European Physical Journal B **57**, 385 (2007).

Groups: Aebi, Margaritondo, Forró / Projects: 1, 3

- ▶ H. CERCELLIER, C. MONNEY, F. CLERC, C. BATTAGLIA, L. DESPONT, M. G. GARNIER, H. BECK, P. AEBI, L. PATTHEY, H. BERGER, AND L. FORRÓ

Evidence for an Excitonic Insulator Phase in 1T-TiSe_2

Physical Review Letters **99**, 146403 (2007).

Groups: Aebi, Margaritondo, Forró / Projects: 1, 3

P. FAZEKAS, N. BARISIC, I. KEZSMARKI, L. DEMKO, H. BERGER, L. FORRÓ, AND G. MIHALY

Magnetic-field-induced transition in BaVS_3

Physical Review B **75**, 035128 (2007).

Groups: Margaritondo, Forró / Projects: 1, 3

P. FAZEKAS, K. PENC, K. RADNÓCZI, N. BARIŠIĆ, H. BERGER, L. FORRÓ, S. MITROVIĆ, A. GAUZZI, L. DEMKÓ, I. KÉZSMÁRKI, AND G. MIHÁLY

The electronic structure and the phases of BaVS_3

Journal of Magnetism and Magnetic Materials **310**, 928 (2007).

Groups: Margaritondo, Forró / Project: 3

L. V. GASPAROV, K.-Y. CHOI, G. GÜNTHERODT, H. BERGER, AND L. FORRÓ

Electronic Raman scattering in magnetite

Journal of Applied Physics **101**, 09G108 (2007).

Groups: Margaritondo, Forró / Project: 3

I. KÉZSMÁRKI, R. GAÁL, C. C. HOMES, B. SÍPOS, H. BERGER, S. BORDÁCS, G. MIHÁLY, AND L. FORRÓ

High-pressure infrared spectroscopy: tuning of the low-energy excitations in correlated electron systems

Physical Review B **76**, 205114 (2007).

Groups: Margaritondo, Forró / Projects: 1, 3

S. MITROVIC, P. FAZEKAS, C. SÖNDERGAARD, D. ARIOSA, N. BARISIC, H. BERGER, D. CLOETTA, L. FORRÓ, H. HÖCHST, I. KUPCIC, D. PAVUNA, AND G. MARGARITONDO

Experimental electronic structure and Fermi-surface instability of the correlated 3d sulphide BaVS_3 : High-resolution angle-resolved photoemission spectroscopy

Physical Review B **75**, 153103 (2007).

Groups: Margaritondo, Forró / Projects: 1, 3

F. SIMON, F. MURÁNYI, T. FEHÉR, A. JÁNOSSY, L. FORRÓ, C. PETROVIC, S. L. BUD'KO, AND P. C. CANFIELD

Spin-lattice relaxation time of conduction electrons in MgB_2

Physical Review B **76**, 024519 (2007).

Group: Forró / Project: 1

B. SIPOS, N. BARISIC, R. GAAL, L. FORRÓ, J. KARPINSKI, AND F. RULLIER-ALBENQUE

Matthiessen's rule in MgB_2 : Resistivity and T_c as a function of point defect concentration

Physical Review B **76**, 132504 (2007).

Groups: Forró, Karpinski / Projects: 1, 3, 4

G. CAIMI, L. DEGIORGI, H. BERGER, AND L. FORRÓ

- Optical evidence for a magnetically driven structural transition in the spin web Cu_3TeO_6*
 Europhysics Letters **75**, 496 (2006).
 Groups: Margaritondo, Degiorgi, Forró / Projects: 1, 3
- G. CAIMI, L. DEGIORGI, H. BERGER, AND L. FORRÓ
Phonon analysis of the $S = 1$ quantum spin systems $\text{Ni}_5\text{Te}_4\text{O}_{12}\text{X}_2$ ($X = \text{Cl}$ and Br)
 Journal of Physics: Condensed Matter **18**, 4065 (2006).
 Groups: Margaritondo, Degiorgi, Forró / Projects: 1, 3
- F. CLERC, C. BATTAGLIA, M. BOVET, L. DESPONT, C. MONNEY, H. CERCELLIER, M. GARNIER, P. AEBI, H. BERGER, AND L. FORRÓ
Lattice-distortion-enhanced electron-phonon coupling and Fermi surface nesting in 1T-TaS_2
 Physical Review B **74**, 155114 (2006).
 Groups: Margaritondo, Aebi, Forró / Projects: 1, 2, 3
- L. DESPONT, F. CLERC, M. G. GARNIER, H. BERGER, L. FORRÓ, AND P. AEBI
Multiple scattering investigation of the 1T-TaS_2 surface termination
 The European Physical Journal B **52**, 421 (2006).
 Groups: Aebi, Margaritondo, Forró / Projects: 3, 5
- ▶ I. KÉZSMÁRKI, G. MIHÁLY, R. GAÁL, N. BARIŠIĆ, A. AKRAP, H. BERGER, L. FORRÓ, C. C. HOMES, AND L. MIHÁLY
Separation of orbital contributions to the optical conductivity of BaVS_3
 Physical Review Letters **96**, 186402 (2006).
 Groups: Margaritondo, Forró / Projects: 1, 3
- H. L. LIU, M. QUIJADA, D. B. ROMERO, D. B. TANNER, A. ZIBOLD, G. L. CARR, H. BERGER, L. FORRÓ, L. MIHALY, G. CAO, B.-H. O, J. T. MARKERT, J. P. RICE, M. J. BURNS, AND K. A. DELIN
Drude behavior in the far-infrared conductivity of cuprate superconductors
 Annalen der Physik **15**, 606 (2006).
 Groups: Margaritondo, Forró / Project: 3
- P. MATUS, H. ALLOUL, G. KRIZA, V. BROUET, P. M. SINGER, S. GARAJ, AND L. FORRÓ
Influence of local fullerene orientation on the electronic properties of $\text{Na}_2\text{AC}_{60}$ ($A = \text{Cs}, \text{Rb}, \text{K}$) compounds
 Physical Review B **74**, 214509 (2006).
 Group: Forró / Project: 1
- L. MIHÁLY, T. FEHÉR, B. DÓRA, B. NÁFRÁDI, H. BERGER, AND L. FORRÓ
Spin resonance in the ordered magnetic state of $\text{Ni}_5(\text{TeO}_3)_4\text{Cl}_2$
 Physical Review B **74**, 174403 (2006).
 Groups: Margaritondo, Forró / Projects: 1, 3
- ▶ L. MIHÁLY, B. DÓRA, A. VÁNYOLOS, H. BERGER, AND L. FORRÓ
Spin-Lattice Interaction in the Quasi-One-Dimensional Helimagnet LiCu_2O_2
 Physical Review Letters **97**, 067206 (2006).
 Groups: Margaritondo, Forró / Projects: 1, 3
- ▶ F. SIMON, H. KUZMANY, B. NÁFRÁDI, T. FEHÉR, L. FORRÓ, F. FÜLÖP, A. JÁNOSSY, L. KORECZ, A. ROCKENBAUER, F. HAUKE, AND A. HIRSCH
Magnetic Fullerenes inside Single-Wall Carbon Nanotubes
 Physical Review Letters **97**, 136801 (2006).
 Group: Forró / Project: 1
- R. P. SMITH, A. KUSMARTSEVA, Y. T. C. KO, S. S. SAXENA, A. AKRAP, L. FORRÓ, M. LAAD, T. E. WELLER, M. ELLERBY, AND N. T. SKIPPER
Pressure dependence of the superconducting transition temperature in C_6Yb and C_6Ca
 Physical Review B **74**, 024505 (2006).
 Group: Forró / Project: 1
- C. BATTAGLIA, H. CERCELLIER, F. CLERC, L. DESPONT, M. G. GARNIER, C. KOITZSCH, P. AEBI, H. BERGER, L. FORRÓ, AND C. AMBROSCH-DRAXL
Fermi surface induced lattice distortion in NbTe_2
 Physical Review B **72**, 195114 (2005).
 Groups: Margaritondo, Aebi, Forró / Projects: 1, 3
- L. V. GASPAROV, D. ARENAS, K.-Y. CHOI, G. GÜNTHERODT, H. BERGER, L. FORRÓ, G. MARGARITONDO, V. V. STRUZHKIN, AND R. HEMLEY
Magnetite: Raman study of the high-pressure and low-temperature effects
 Journal of Applied Physics **97**, 10A922 (2005).
 Groups: Margaritondo, Forró / Project: 3
- I. KÉZSMÁRKI, G. MIHÁLY, R. GAÁL, N. BARIŠIĆ, H. BERGER, L. FORRÓ, C. C. HOMES, AND L. MIHÁLY
Pressure-induced suppression of the spin-gapped insulator phase in BaVS_3 : An infrared optical study
 Physical Review B **71**, 193103 (2005).
 Groups: Margaritondo, Forró / Project: 3
- J.-P. SALVETAT, T. FEHÉR, C. L'HUILLIER, F. BEUNEU, AND L. FORRÓ
Anomalous electron spin resonance behavior of single-walled carbon nanotubes
 Physical Review B **72**, 075440 (2005).
 Group: Forró / Project: 1

F. SIMON, A. JÁNOSSY, T. FEHÉR, F. MURÁNYI, S. GARAJ, L. FORRÓ, C. PETROVIC, S. BUD'KO, R. A. RIBEIRO, AND P. C. CANFIELD

Magnetic-field-induced density of states in MgB₂: Spin susceptibility measured by conduction-electron spin resonance

Physical Review B **72**, 012511 (2005).

Group: Forró / Project: 1

Group of T. Giamarchi

L. BENFATTO, C. CASTELLANI, AND T. GIAMARCHI

Doping dependence of the vortex-core energy in bilayer films of cuprates

Physical Review B **77**, 100506(R) (2008).

Group: Giamarchi / Project: 2

T. GIAMARCHI, C. RÜEGG, AND O. TCHERNYSHYOV

Bose-Einstein Condensation in Magnetic Insulators

Nature Physics **4**, 198 (2008).

Groups: Giamarchi, Mesot / Project: 1

A. KLEINE, C. KOLLATH, I. P. MCCULLOCH, T. GIAMARCHI, AND U. SCHOLLWÖCK

Excitations in two-component Bose-gases

to be published in New Journal of Physics (2008).

Group: Giamarchi / Project: 1

▶ C. KOLLATH, J. S. MEYER, AND T. GIAMARCHI

Dipolar bosons in a planar array of one-dimensional tubes

to be published in Physical Review Letters (2008), accepted in Phys. Rev. Lett. (2008).

Group: Giamarchi / Project: 1

▶ L. BENFATTO, C. CASTELLANI, AND T. GIAMARCHI

Kosterlitz-Thouless Behavior in Layered Superconductors: The Role of the Vortex Core Energy

Physical Review Letters **98**, 117008 (2007).

Group: Giamarchi / Project: 2

▶ L. BENFATTO, C. CASTELLANI, AND T. GIAMARCHI

Sine-Gordon Description of Beresinskii-Kosterlitz-Thouless Vortices in Superconductors Immersed in an External Magnetic Field

Physical Review Letters **99**, 207002 (2007).

Group: Giamarchi / Project: 2

M. A. CAZALILLA, A. IUCCI, AND T. GIAMARCHI

Competition between vortex unbinding and tunneling in an optical lattice

Physical Review A **75**, 051603(R) (2007).

Group: Giamarchi / Project: 1

▶ P. CHUDZINSKI, M. GABAY, AND T. GIAMARCHI

Phase diagram of hole doped two-leg Cu-O ladders

Physical Review B **76**, 161101(R) (2007).

Group: Giamarchi / Project: 2

M. CORTI, F. CARBONE, M. FILIBIAN, T. JARLBORG, A. A. NUGROHO, AND P. CARRETTA

Spin dynamics in a weakly itinerant magnet from ²⁹Si NMR in MnSi

Physical Review B **75**, 115111 (2007).

Group: Giamarchi / Project: 1

▶ C. DUBOIS, A. P. PETROVIĆ, G. SANTI, C. BERTHOD, A. A. MANUEL, M. DECROUX, Ø. FISCHER, M. POTEL, AND R. CHEVREL

Node-like excitations in superconducting PbMo₆S₈ probed by scanning tunneling spectroscopy

Physical Review B **75**, 104501 (2007).

Groups: Fischer, Giamarchi / Projects: 1, 2

▶ Ø. FISCHER, M. KUGLER, I. MAGGIO-APRILE, C. BERTHOD, AND C. RENNER

Scanning tunneling spectroscopy of high-temperature superconductors

Reviews of Modern Physics **79**, 353 (2007).

Groups: Fischer, Giamarchi / Project: 2

▶ V. GURITANU, D. VAN DER MAREL, J. TEYSSIER, T. JARLBORG, H. WILHELM, M. SCHMIDT, AND F. STEGLICH

Optical evidence for heavy charge carriers in FeGe

Physical Review B **75**, 155114 (2007).

Groups: Giamarchi, van der Marel / Project: 1

A. IUCCI, G. A. FIETE, AND T. GIAMARCHI
Fourier transform of the 2k_F Luttinger liquid density correlation function with different spin and charge velocities

Physical Review B **75**, 205116 (2007).

Group: Giamarchi / Project: 1

T. JARLBORG

Effects of spin-phonon interaction within the CuO plane of high-T_c superconductors

Physica C **454**, 5 (2007).

Group: Giamarchi / Project: 1

T. JARLBORG

Importance of thermal disorder and electronic occupation for temperature dependence of optical conductivity in FeSi and MnSi

- Physical Review B **76**, 205105 (2007).
Group: Giamarchi / Project: 1
- T. JARLBORG
Properties of high- T_c copper oxides from the nearly-free-electron model
Physical Review B **76**, 140504(R) (2007).
Group: Giamarchi / Project: 1
- T. JEONG AND T. JARLBORG
Varying Cu-Ti hybridization near the Fermi energy in Cu_xTiSe_2 : Results from supercell calculations
Physical Review B **76**, 153103 (2007).
Group: Giamarchi / Project: 1
- A. KLEINE, C. KOLLATH, I. P. MCCULLOCH, T. GIAMARCHI, AND U. SCHOLLWÖCK
Spin-charge separation in two-component Bose gases
Physical Review A **77**, 013607 (2007).
Group: Giamarchi / Project: 1
- ▶ C. KOLLATH, M. KÖHL, AND T. GIAMARCHI
Scanning tunneling microscopy for ultracold atoms
Physical Review A **76**, 063602 (2007).
Group: Giamarchi / Project: 1
- C. KOLLATH, A. M. LÄUCHLI, AND E. ALTMAN
Quench Dynamics and Nonequilibrium Phase Diagram of the Bose-Hubbard Model
Physical Review Letters **98**, 180601 (2007).
Group: Giamarchi / Project: 1
- G. LEÓN, C. BERTHOD, AND T. GIAMARCHI
Hall effect in strongly correlated low-dimensional systems
Physical Review B **75**, 195123 (2007).
Group: Giamarchi / Project: 1
- E. ORIGNAC, R. CITRO, AND T. GIAMARCHI
Critical properties and Bose-Einstein condensation in dimer spin systems
Physical Review B **75**, 140403(R) (2007).
Group: Giamarchi / Project: 1
- ▶ P. PEDRAZZINI, H. WILHELM, D. JACCARD, T. JARLBORG, M. SCHMIDT, M. HANFLAND, L. AKSELRUD, H. Q. YUAN, U. SCHWARZ, Y. GRIN, AND F. STEGLICH
Metallic State in Cubic FeGe Beyond Its Quantum Phase Transition
Physical Review Letters **98**, 047204 (2007).
Group: Giamarchi / Project: 1
- ▶ M. B. ZVONAREV, V. V. CHEIANOV, AND T. GIAMARCHI
Spin Dynamics in a One-Dimensional Ferromagnetic Bose Gas
Physical Review Letters **99**, 240404 (2007).
Group: Giamarchi / Project: 1
- ▶ C. BERTHOD, T. GIAMARCHI, S. BIERMANN, AND A. GEORGES
Breakup of the Fermi Surface Near the Mott Transition in Low-Dimensional Systems
Physical Review Letters **97**, 136401 (2006).
Group: Giamarchi / Project: 1
- ▶ M. A. CAZALILLA, A. F. HO, AND T. GIAMARCHI
Interacting Bose gases in quasi-one-dimensional optical lattices
New Journal of Physics **8**, 158 (2006).
Group: Giamarchi / Project: 1
- ▶ L. F. CUGLIANDOLO, T. GIAMARCHI, AND P. LE DOUSSAL
Dynamic Compressibility and Aging in Wigner Crystals and Quantum Glasses
Physical Review Letters **96**, 217203 (2006).
Group: Giamarchi / Project: 1
- A. IUCCI, M. A. CAZALILLA, A. F. HO, AND T. GIAMARCHI
Energy absorption of a Bose gas in a periodically modulated optical lattice
Physical Review A **73**, 041608 (2006).
Group: Giamarchi / Project: 1
- ▶ C. KOLLATH, A. IUCCI, T. GIAMARCHI, W. HOFSTETTER, AND U. SCHOLLWÖCK
Spectroscopy of Ultracold Atoms by Periodic Lattice Modulations
Physical Review Letters **97**, 050402 (2006).
Group: Giamarchi / Project: 1
- C. KOLLATH, A. IUCCI, I. P. MCCULLOCH, AND T. GIAMARCHI
Modulation spectroscopy with ultracold fermions in an optical lattice
Physical Review A **74**, 041604(R) (2006).
Group: Giamarchi / Project: 1
- U. LONDON, T. GIAMARCHI, AND D. ORGAD
Disorder effects in fluctuating one-dimensional interacting systems
Physical Review B **73**, 134201 (2006).
Group: Giamarchi / Project: 2
- E. ORIGNAC, A. ROSSO, R. CHITRA, AND T. GIAMARCHI
Coulomb disorder in periodic systems: Effect of unscreened charged impurities
Physical Review B **73**, 035112 (2006).
Group: Giamarchi / Project: 1

P. PARUCH, T. GIAMARCHI, T. TYBELL, AND J.-M. TRISCONI

Nanoscale studies of domain wall motion in epitaxial ferroelectric thin films

Journal of Applied Physics **100**, 051608 (2006).

Groups: Triscone, Giamarchi / Project: 5

► A. SACCHETTI, L. DEGIORGI, T. GIAMARCHI, N. RU, AND I. R. FISHER

Chemical pressure and hidden one-dimensional behavior in rare-earth tri-telluride charge-density wave compounds

Physical Review B **74**, 125115 (2006).

Groups: Degiorgi, Giamarchi / Project: 1

C. WEBER, A. LÄUCHLI, F. MILA, AND T. GIAMARCHI

Magnetism and superconductivity of strongly correlated electrons on the triangular lattice

Physical Review B **73**, 014519 (2006).

Groups: Mila, Giamarchi / Project: 1

► M. A. CAZALILLA, A. F. HO, AND T. GIAMARCHI

Two-Component Fermi Gas on Internal-State-Dependent Optical Lattices

Physical Review Letters **95**, 226402 (2005).

Group: Giamarchi / Project: 1

► P. PARUCH, T. GIAMARCHI, AND J.-M. TRISCONI

Domain Wall Roughness in Epitaxial Ferroelectric $PbZr_{0.2}Ti_{0.8}O_3$ Thin Films

Physical Review Letters **94**, 197601 (2005).

Groups: Triscone, Giamarchi / Project: 5

Group of M. Grioni

► C. R. AST, J. HENK, A. ERNST, L. MORESCHINI, M. C. FALUB, D. PACILÉ, P. BRUNO, K. KERN, AND M. GRIONI

Giant Spin Splitting through Surface Alloying

Physical Review Letters **98**, 186807 (2007).

Group: Grioni / Project: 1

C. R. AST, G. WITTICH, P. WAHL, R. VOGELGESANG, D. PACILÉ, M. C. FALUB, L. MORESCHINI, M. PAPAGNO, M. GRIONI, AND K. KERN

Local detection of spin-orbit splitting by scanning tunneling spectroscopy

Physical Review B **75**, 201401(R) (2007).

Group: Grioni / Project: 1

L. MORESCHINI, C. DALLERA, J. J. JOYCE, J. L. SARRAO, E. D. BAUER, V. FRITSCH, S. BOBEV, E. CARPENE, S. HUOTARI, G. VANKÓ, G. MONACO, P. LACOVIG, G. PANACCIONE,

A. FONDACARO, G. PAOLICELLI, P. TORELLI, AND M. GRIONI

Comparison of bulk-sensitive spectroscopic probes of Yb valence in Kondo systems

Physical Review B **75**, 035113 (2007).

Group: Grioni / Project: 1

D. PACILÉ, M. PAPAGNO, M. LAVAGNINI, H. BERGER, L. DEGIORGI, AND M. GRIONI

Photoemission and optical studies of $ZrSe_3$, $HfSe_3$, and ZrS_3

Physical Review B **76**, 155406 (2007).

Groups: Margaritondo, Degiorgi, Grioni / Projects: 1, 3

X. WANG, H. MICHOR, AND M. GRIONI

Probing the nature of the Ce 4f states in CeX_9Si_4 ($X=Ni, Co$) by high-energy electron spectroscopies

Physical Review B **75**, 035127 (2007).

Group: Grioni / Project: 1

C. R. AST, D. PACILÉ, M. PAPAGNO, T. GLOOR, F. MILA, S. FEDRIGO, G. WITTECH, K. KERN, H. BRUNE, AND M. GRIONI

Orbital selective overlayer-substrate hybridization in a Pb monolayer on Ag(111)

Physical Review B **73**, 245428 (2006).

Groups: Grioni, Mila / Project: 1

► S. G. CHIUZBĂIAN, G. GHIRINGHELLI, C. DALLERA, M. GRIONI, P. AMANN, X. WANG, L. BRAICOVICH, AND L. PATTHEY

Localized Electronic Excitations in NiO Studied with Resonant Inelastic X-Ray Scattering at the Ni M Threshold: Evidence of Spin Flip

Physical Review Letters **95**, 197402 (2006).

Group: Grioni / Project: 1

S. COLONNA, F. RONCI, A. CRICENTI, L. PERFETTI, H. BERGER, AND M. GRIONI

Scanning tunneling microscopy observation of a mott-insulator phase at the 1T-TaSe₂ surface

Japanese Journal of Applied Physics **45**, 1950 (2006).

Groups: Margaritondo, Grioni / Projects: 1, 3

C. DALLERA, O. WESSELY, M. COLARIETI-TOSTI, O. ERIKSSON, R. AHUJA, B. JOHANSSON, M. I. KATSNELSON, E. ANNESE, J.-P. RUFFE, G. VANKÓ, L. BRAICOVICH, AND M. GRIONI

Understanding mixed valent materials: Effects of dynamical core-hole screening in high-pressure x-ray spectroscopy

Physical Review B **74**, 081101(R) (2006).

Group: Grioni / Project: 1

G. GHIRINGHELLI, A. PIAZZALUNGA, C. DALLERA, G. TREZZI, L. BRAICOVICH,

- T. SCHMITT, V. N. STROCOV, R. BETEMPS, L. PATTHEY, X. WANG, AND M. GRIONI
SAXES, a high resolution spectrometer for resonant x-ray emission in the 400–1600 eV energy range
Review of Scientific Instruments **77**, 113108 (2006).
Group: Grioni / Project: 1
- M. MEDARDE, C. DALLERA, M. GRIONI, J. VOIGT, A. PODLESNYAK, E. POMJAKUSHINA, K. CONDER, T. NEISIUS, O. TJERNBERG, AND S. BARILO
Low-temperature spin-state transition in LaCoO₃ investigated using resonant x-ray absorption at the Co K edge
Physical Review B **73**, 054424 (2006).
Groups: Mesot, Grioni / Projects: 1, 3
- D. PACILÉ, C. R. AST, M. PAPAGNO, C. DA SILVA, L. MORESCHINI, M. FALUB, A. P. SEITSONEN, AND M. GRIONI
Electronic structure of an ordered Pb/Ag(111) surface alloy: Theory and experiment
Physical Review B **73**, 245429 (2006).
Group: Grioni / Project: 1
- M. PAPAGNO, D. PACILÉ, G. CAIMI, H. BERGER, L. DEGIORGI, AND M. GRIONI
Electronic structure of one-dimensional copper oxide chains in LiCu₂O₂ from angle-resolved photoemission and optical spectroscopy
Physical Review B **73**, 115120 (2006).
Groups: Margaritondo, Degiorgi, Grioni / Projects: 1, 3
- S. COLONNA, F. RONCI, A. CRICENTI, L. PERFETTI, H. BERGER, AND M. GRIONI
Mott phase at the surface of 1T-TaSe₂ observed by scanning tunneling microscopy
Physical Review Letters **94**, 036405 (2005).
Groups: Margaritondo, Grioni / Project: 3
- C. DALLERA, E. ANNESE, J.-P. RUEFF, M. GRIONI, G. VANKO, L. BRAICOVICH, A. BARLA, J.-P. SANCHEZ, R. GUSMEROLI, A. PALENZONA, L. DEGIORGI, AND G. LAPERTOT
Intermediate valence behaviour under pressure: how precisely can we probe it by means of resonant inelastic x-ray emission?
Journal of Physics: Condensed Matter **17**, S849 (2005).
Groups: Degiorgi, Grioni / Project: 1
- M. GRIONI, C. R. AST, D. PACILE, M. PAPAGNO, H. BERGER, AND L. PERFETTI
Photoemission as a probe of coexisting and conflicting periodicities in low-dimensional solids
New Journal of Physics **7**, 106 (2005).
Groups: Margaritondo, Grioni / Projects: 1, 3
- N. KOCH, F. JÄCKEL, J. GHIJSEN, M. C. ROJAS, M. GRIONI, J. P. RABE, R. L. JOHNSON, A. KAHN, AND J.-J. PIREAUX
Observation of filled states at the Fermi-level in alkali-metal intercalated organic films: dependence on substrate work function
Journal of Electron Spectroscopy and Related Phenomena **144-147**, 495 (2005).
Group: Grioni / Project: 1
- G. PANACCIONE, G. CAUTERO, M. CAUTERO, A. FONDACARO, M. GRIONI, P. LACOVIG, G. MONACO, F. OFFI, G. PAOLICELLI, M. SACCHI, N. STOJIC, G. STEFANI, R. TOMMASINI, AND P. TORELLI
High-energy photoemission in silver: resolving d and sp contributions in valence band spectra
Journal of Physics: Condensed Matter **17**, 2671 (2005).
Group: Grioni / Project: 1
- G. PAOLICELLI, A. FONDACARO, F. OFFI, G. STEFANI, G. CAUTERO, M. CAUTERO, B. KRASTANOV, P. LACOVIG, P. PITTANA, R. SERGO, R. TOMMASINI, P. TORELLI, M. SACCHI, M. GRIONI, G. MONACO, AND G. PANACCIONE
Bulk sensitive photoemission: first results of VOLPE project at ESRF
Journal of Electron Spectroscopy and Related Phenomena **144-147**, 963 (2005).
Group: Grioni / Project: 1
- L. PERFETTI, T. A. GLOOR, F. MILA, H. BERGER, AND M. GRIONI
Unexpected periodicity in the quasi-two-dimensional Mott insulator 1T-TaS₂ revealed by angle-resolved photoemission
Physical Review B **71**, 153101 (2005).
Groups: Margaritondo, Mila, Grioni / Projects: 1, 3
- M. SACCHI, F. OFFI, P. TORELLI, A. FONDACARO, C. SPEZZANI, M. CAUTERO, G. CAUTERO, S. HUOTARI, M. GRIONI, R. DELAUNAY, M. FABRIZIOLI, G. VANKÓ, G. MONACO, G. PAOLICELLI, G. STEFANI, AND G. PANACCIONE
Quantifying the effective attenuation length in high energy photoemission experiments
Physical Review B **71**, 155117 (2005).
Group: Grioni / Project: 1

Group of M. Hasler

- F. ROY, B. DUTOIT, F. GRILLI, AND F. SIROIS
Magneto-thermal finite element modeling of 2nd generation HTS for FCL design purposes
in *8th European Conference on Applied Superconductivity* (2008), Conference Series.
Group: Hasler / Project: 6
- F. ROY, B. DUTOIT, F. GRILLI, AND F. SIROIS
Magneto-Thermal Modeling of Second-Generation HTS for Resistive Fault Current Limiter Design Purposes
IEEE Transactions on Applied Superconductivity **18**, 29 (2008).
Group: Hasler / Project: 6
- F. SIROIS, D. MOUHAMADOU, F. ROY, F. GRILLI, AND B. DUTOIT
Evaluation of two commercial finite element packages for calculating AC losses in 2-D high temperature superconducting strips
in *8th European Conference on Applied Superconductivity* (2008), Conference Series.
Group: Hasler / Project: 6
- L. ANTOGNAZZA, M. DECROUX, M. THERASSE, M. ABPLANALP, J. DURON, B. DUTOIT, AND Ø. FISCHER
Thermally Assisted Transition in Thin Film Based FCL: A Way to Speed Up the Normal Transition Across the Wafer
IEEE Transactions on Applied Superconductivity **17**, 3463 (2007).
Groups: Fischer, Hasler / Project: 6
- J. DURON, F. GRILLI, L. ANTOGNAZZA, M. DECROUX, B. DUTOIT, AND Ø. FISCHER
Finite-element modelling of YBCO fault current limiter with temperature dependent parameters
Superconductor Science & Technology **20**, 338 (2007).
Groups: Hasler, Fischer / Project: 6
- J. DURON, B. DUTOIT, F. GRILLI, M. DECROUX, L. ANTOGNAZZA, AND Ø. FISCHER
Computer Modeling of YBCO Fault Current Limiter Strips Lines in Over-Critical Regime With Temperature Dependent Parameters
IEEE Transactions on Applied Superconductivity **17**, 1839 (2007).
Groups: Hasler, Fischer / Project: 6
- F. SIROIS AND F. ROY
Computation of 2-D Current Distribution in Superconductors of Arbitrary Shapes Using a New Semi-Analytical Method
IEEE Transactions on Applied Superconductivity **17**, 3836 (2007).
Group: Hasler / Project: 6
- J. DURON, F. GRILLI, L. ANTOGNAZZA, M. DECROUX, S. STAVREV, B. DUTOIT, AND Ø. FISCHER
Finite-element modeling of superconductors in over-critical regime with temperature dependent resistivity.
Journal of Physics: Conference Series **43**, 1076 (2006).
Groups: Fischer, Hasler / Project: 6
- S. STAVREV, F. GRILLI, B. DUTOIT, AND S. ASHWORTH
Finite-element analysis and comparison of the AC loss performance of BSCCO and YBCO conductors
in *7th European Conference on Applied Superconductivity* (2006), vol. 43 of *J. Phys.: Conf. Ser.*, p. 581.
Group: Hasler / Project: 6
- J. DURON, L. ANTOGNAZZA, M. DECROUX, F. GRILLI, S. STAVREV, B. DUTOIT, AND Ø. FISCHER
3D finite element Simulations of strip lines in a YBCO/Au fault current limiter.
IEEE Transactions on Applied Superconductivity **15**, 1998 (2005).
Groups: Fischer, Hasler / Project: 6
- J. DURON, L. ANTOGNAZZA, M. DECROUX, F. GRILLI, S. STAVREV, B. DUTOIT, AND Ø. FISCHER
3-D finite element Simulations of strip lines in a YBCO/Au fault current limiter
in *IEEE, Applied Superconductivity Conference 2004* (2005), vol. 15, pp. 1998–2002.
Groups: Hasler, Fischer / Project: 6
- B. DUTOIT, J. DURON, S. STAVREV, AND F. GRILLI
Dynamic field mapping for obtaining the current distribution in high-temperature superconducting tapes
in *IEEE, Applied Superconductivity Conference 2004* (2005), vol. 15, pp. 3644–3647.
Group: Hasler / Project: 6
- F. GRILLI, L. MARTINI, B. DUTOIT, S. STAVREV, AND R. BRAMBILLA
Analysis of magnetic field and geometry effects for the design of HTS devices for AC power applications
in *IEEE, Applied Superconductivity Conference 2004* (2005), vol. 15, pp. 2074–2077.
Group: Hasler / Project: 6
- S. STAVREV, F. GRILLI, B. DUTOIT, AND

S. P. ASHWORTH

Comparison of the AC losses of BSCCO and YBCO conductors by means of numerical analysis

Superconductor Science & Technology **18**, 1300 (2005).

Group: Hasler / Project: 6

Group of J. Hulliger

I. L. LANDAU, J. B. WILLEMS, AND J. HULLIGER

Detailed magnetization study of superconducting properties of $YBa_2Cu_3O_{7-x}$ ceramic spheres

Journal of Physics: Condensed Matter **20**, 095222 (2008).

Group: Hulliger / Project: 4

G. COUDERC, J. B. WILLEMS, B. TRUSCH, AND J. HULLIGER

Optical recognition of local reaction products in ceramic combinatorial syntheses

Materials Research Bulletin **42**, 1845 (2007).

Group: Hulliger / Project: 4

- ▶ L. DESSAUGES, J. B. WILLEMS, D. FAVRE, C. BOHRER, F. HELBLING, AND J. HULLIGER

Theory of high gradient attractive magnetic separation of superconducting materials and its experimental verification by $YBa_2Cu_3O_x$ particles

Superconductor Science & Technology **19**, 748 (2006).

Group: Hulliger / Project: 4

J. HULLIGER, L. DESSAUGES, AND T. A. SAMTLEBEN

Analysis of Compositional Distributions for Exploring the Phase Space by the Single Sample Concept in Ceramic Combinatorial Chemistry

Journal of the American Ceramic Society **89**, 1072 (2006).

Group: Hulliger / Project: 4

J. HULLIGER AND M. A. AWAN

Single Sample Concept: Theoretical Model for a Combinatorial Approach to Solid-State Inorganic Materials

Journal of Combinatorial Chemistry **7**, 73 (2005).

Group: Hulliger / Project: 4

J. HULLIGER, M. A. AWAN, B. TRUSCH, AND T. A. SAMTLEBEN

Chemical Diversity in View of Property Generation by a New Combinatorial Approach

Zeitschrift für Anorganische und Allgemeine Chemie **631**, 1255 (2005).

Group: Hulliger / Project: 4

Group of J. Karpinski

D. DAGHERO, D. DELAUDE, A. CALZOLARI, M. TORTELLO, G. A. UMMARINO, R. GONNELLI, V. STEPANOV, N. ZHIGADLO, S. KATRYCH, AND J. KARPINSKI

Point-contact Andreev-reflection spectroscopy in segregation-free $Mg_{1-x}Al_xB_2$ single crystals up to $x = 0.32$

Journal of Physics: Condensed Matter **20**, 085225 (2008).

Group: Karpinski / Projects: 3, 4

R. KHASANOV, A. SHENGELAYA, J. KARPINSKI, A. BUSSMANN-HOLDER, H. KELLER, AND K. A. MÜLLER

s-wave symmetry along the c-axis and s + d in-plane superconductivity in bulk $YBa_2Cu_4O_8$

Journal of Superconductivity and Novel Magnetism **21**, 81 (2008).

Groups: Keller, Karpinski / Project: 2, 3, 4

- ▶ K. ROGACKI, G. SCHUCK, Z. BUKOWSKI, N. D. ZHIGADLO, AND J. KARPINSKI

Structural and superconducting properties of $RbOs_2O_6$ single crystals

Physical Review B (2008).

Group: Karpinski / Projects: 3, 4

S. WEYENETH, T. SCHNEIDER, N. ZHIGADLO, J. KARPINSKI, AND H. KELLER

Probing Superconductivity in MgB_2 confined to magnetic field tuned cylinders by means of critical fluctuations

Journal of Physics: Condensed Matter **20**, 135208 (2008).

Groups: Karpinski, Keller / Projects: 3, 4

M. D'ASTUTO, M. CALANDRA, S. REICH, A. SHUKLA, M. LAZZERI, F. MAURI, J. KARPINSKI, N. D. ZHIGADLO, A. BOSSAK, AND M. KRISCH

Weak anharmonic effects in MgB_2 : A comparative inelastic x-ray scattering and Raman study

Physical Review B **75**, 174508 (2007).

Group: Karpinski / Projects: 3, 4

A. AKRAP, E. TUTIŠ, S. M. KAZAKOV, N. D. ZHIGADLO, J. KARPINSKI, AND L. FORRÓ

Manifestations of fine features of the density of states in the transport properties of KOs_2O_6

Physical Review B **75**, 172501 (2007).

Groups: Forró, Karpinski / Projects: 1, 3, 4

- ▶ G. BLUMBERG, A. MIALITSIN, B. S. DENNIS, M. V. KLEIN, N. D. ZHIGADLO, AND J. KARPINSKI

Observation of Leggett's Collective Mode in a Multiband MgB_2 Superconductor

- Physical Review Letters **99**, 227002 (2007).
Group: Karpinski / Projects: 3, 4
- G. BLUMBERG, A. MIALITSIN, B. S. DENNIS, N. D. ZHIGADLO, AND J. KARPINSKI
Multi-gap superconductivity in MgB₂: Magneto-Raman spectroscopy
Physica C **456**, 75 (2007).
Group: Karpinski / Projects: 3, 4
- M. BRÜHWILER, T. SCHULZE, S. M. KAZAKOV, Z. BUKOWSKI, R. PUZNIAK, N. D. ZHIGADLO, J. KARPINSKI, AND B. BATLOGG
Superconductivity in the β -pyrochlore osmates
Physica C **460**, 62 (2007).
Group: Karpinski / Projects: 3, 4
- D. DAGHERO, A. CALZOLARI, D. DELAUDE, R. S. GONNELLI, M. TORTELLO, G. A. UMMARINO, V. A. STEPANOV, N. D. ZHIGADLO, J. KARPINSKI, AND M. PUTTI
Point-contact study of the role of non-magnetic impurities and disorder in the superconductivity of MgB₂
Physica C **460**, 975 (2007).
Group: Karpinski / Projects: 3, 4
- D. DAGHERO, A. CALZOLARI, M. TORTELLO, G. A. UMMARINO, R. S. GONNELLI, V. A. STEPANOV, N. D. ZHIGADLO, K. ROGACKI, AND J. KARPINSKI
Point-Contact Spectroscopy in Mn-Doped MgB₂ Single Crystals: Effects of Magnetic Impurities in a Two-Band Superconductor
Journal of Superconductivity **20**, 523 (2007).
Group: Karpinski / Projects: 3, 4
- M. EISTERER, C. KRUTZLER, M. ZEHETMAYER, H. W. WEBER, S. M. KAZAKOV, AND J. KARPINSKI
Influence of carbon doping on the reversible magnetization of MgB₂ single crystals
Physica C **460**, 606 (2007).
Group: Karpinski / Projects: 3, 4
- Y. FASANO, I. MAGGIO-APRILE, J. KARPINSKI, AND Ø. FISCHER
Tunneling and pseudo point-contact spectroscopy on YBa₂Cu₄O₈
Physica C **460-462**, 958 (2007).
Groups: Fischer, Karpinski / Projects: 2, 3, 4
- F. GIUBILEO, F. BOBBA, A. SCARFATO, A. M. CUCOLO, A. KOHEN, D. RODITCHEV, N. D. ZHIGADLO, AND J. KARPINSKI
Local tunneling study of three-dimensional order parameter in the π band of Al-doped MgB₂ single crystals
Physical Review B **76**, 024507 (2007).
Group: Karpinski / Projects: 3, 4
- F. GIUBILEO, F. BOBBA, A. SCARFATO, D. RODITCHEV, N. ZHIGADLO, J. KARPINSKI, AND A. M. CUCOLO
Nanoscale spatial non-homogeneity of 3D in $\Delta\pi$ Mg_{0.9}Al_{0.1}B₂ single crystals
Physica C **460**, 585 (2007).
Group: Karpinski / Projects: 3, 4
- R. S. GONNELLI, A. CALZOLARI, D. DAGHERO, D. DELAUDE, M. TORTELLO, G. A. UMMARINO, V. A. STEPANOV, N. D. ZHIGADLO, J. KARPINSKI, AND P. MANFRINETTI
Effect of Heavy Al Doping on MgB₂: A Point-Contact Study of Crystals and Polycrystals
Journal of Superconductivity **20**, 555 (2007).
Group: Karpinski / Projects: 3, 4
- R. S. GONNELLI, D. DAGHERO, G. A. UMMARINO, M. TORTELLO, D. DELAUDE, V. A. STEPANOV, AND J. KARPINSKI
Point-contact Andreev-reflection spectroscopy in MgB₂: The role of substitutions
Physica C **456**, 134 (2007).
Group: Karpinski / Projects: 3, 4
- J. KARPINSKI, N. D. ZHIGADLO, S. KATRYCH, R. PUZNIAK, K. ROGACKI, AND R. GONNELLI
Single crystals of MgB₂: Synthesis, substitutions and properties
Physica C **456**, 3 (2007).
Group: Karpinski / Projects: 3, 4
- ▶ R. KHASANOV, A. SHENGELAYA, D. DI CASTRO, D. G. ESHCHENKO, I. M. SAVIĆ, K. CONDER, E. POMJAKUSHINA, J. KARPINSKI, S. KAZAKOV, AND H. KELLER
Magnetic-field dependence of the oxygen isotope effect on the magnetic penetration depth of hole-doped cuprate superconductors
Physical Review B **75**, 060505 (2007).
Groups: Keller, Karpinski / Projects: 2, 3, 4
- ▶ R. KHASANOV, N. D. ZHIGADLO, J. KARPINSKI, AND H. KELLER
In-plane magnetic penetration depth λ_{ab} in Ca_{2-x}Na_xCuO₂Cl₂: Role of the apical sites
Physical Review B **76**, 094505 (2007).
Groups: Keller, Karpinski / Projects: 2, 3, 4
- ▶ T. KONDO, R. KHASANOV, J. KARPINSKI, S. M. KAZAKOV, N. D. ZHIGADLO, T. OHTA, H. M. FRETWELL, A. D. PALCZEWSKI, J. D. KOLL, J. MESOT, E. ROTENBERG, H. KELLER, AND A. KAMINSKI

- Dual character of the electronic structure of $YBa_2Cu_4O_8$: The conduction bands of CuO_2 planes and CuO chains*
Physical Review Letters **98**, 157002 (2007).
Groups: Keller, Karpinski, Mesot / Projects: 2, 3, 4
- C. KRUTZLER, M. ZEHETMAYER, M. EISTERER, H. W. WEBER, N. D. ZHIGADLO, AND J. KARPINSKI
Comparative study of neutron irradiation and carbon doping in MgB_2 single crystals
Physical Review B **75**, 224510 (2007).
Group: Karpinski / Projects: 3, 4
- C. KRUTZLER, M. ZEHETMAYER, M. EISTERER, H. W. WEBER, N. D. ZHIGADLO, AND J. KARPINSKI
Modification of the defect structure in MgB_2 single crystals by carbon doping and neutron irradiation
Physica C **460**, 555 (2007).
Group: Karpinski / Projects: 3, 4
- A. MIALITSIN, B. S. DENNIS, N. D. ZHIGADLO, J. KARPINSKI, AND G. BLUMBERG
Anharmonicity and self-energy effects of the E_{2g} phonon in MgB_2
Physical Review B **75**, 020509 (2007).
Group: Karpinski / Projects: 3, 4
- P. PARIASDES, D. LAMPAKIS, D. PALLES, E. LIAROKAPIS, AND J. KARPINSKI
The relation of the broad band with the E_{2g} phonon and superconductivity in the $Mg(B_{1-x}C_x)_2$ compound
Journal of Magnetism and Magnetic Materials **310**, E110 (2007).
Group: Karpinski / Projects: 3, 4
- B. PEDRINI, S. WESSEL, J. L. GAVILANO, H. R. OTT, S. M. KAZAKOV, AND J. KARPINSKI
Quenching of the Haldane gap in $LiVSi_2O_6$ and related compounds
The European Physical Journal B **55**, 219 (2007).
Groups: Karpinski, Ott / Projects: 1, 3, 4
- M. PISSAS, D. STAMOPOULOS, N. ZHIGADLO, AND J. KARPINSKI
Influence of aluminum substitution on the vortex matter properties of MgB_2
Physical Review B **75**, 184533 (2007).
Group: Karpinski / Projects: 3, 4
- R. PUZNIAK, A. WISNIEWSKI, A. SZEWCZYK, K. KAPCIA, J. JUN, N. D. ZHIGADLO, S. M. KAZAKOV, AND J. KARPINSKI
Anisotropic upper critical field of chemically substituted MgB_2 single crystals studied by torque magnetometry
Physica C **460**, 616 (2007).
Group: Karpinski / Projects: 3, 4
- B. SIPOS, N. BARISIC, R. GAAL, L. FORRÓ, J. KARPINSKI, AND F. RULLIER-ALBENQUE
Matthiessen's rule in MgB_2 : Resistivity and T_c as a function of point defect concentration
Physical Review B **76**, 132504 (2007).
Groups: Forró, Karpinski / Projects: 1, 3, 4
- S. STRÄSSLE, J. ROOS, M. MALI, H. KELLER, AND J. KARPINSKI
 ^{11}B NMR study of single-crystal MgB_2 in the normal conducting phase
Physica C **466**, 168 (2007).
Groups: Keller, Karpinski / Projects: 2, 3, 4
- A. WISNIEWSKI, R. PUZNIAK, A. BIENIAS, M. BARAN, J. JUN, N. D. ZHIGADLO, AND J. KARPINSKI
Anisotropy of the lower and of the upper critical fields in $Mg_{1-x}Al_xB_2$ single crystals
Physica C **460**, 614 (2007).
Group: Karpinski / Projects: 3, 4
- A. WISNIEWSKI, R. PUZNIAK, J. JUDEK, C. KRUTZLER, M. EISTERER, H. W. WEBER, J. JUN, S. M. KAZAKOV, AND J. KARPINSKI
Comparison of the influence of carbon substitution and neutron-induced defects on the upper critical field and flux pinning in MgB_2 single crystals
Superconductor Science & Technology **20**, 256 (2007).
Group: Karpinski / Projects: 3, 4
- S. WU, P. GEISER, J. JUN, J. KARPINSKI, AND R. SOBOLEWSKI
Femtosecond optical generation and detection of coherent acoustic phonons in GaN single crystals
Physical Review B **76**, 085210 (2007).
Group: Karpinski / Projects: 3, 4
- S. WU, P. GEISER, J. JUN, J. KARPINSKI, D. WANG, AND R. SOBOLEWSKIA
Time-resolved intervalley transitions in GaN single crystals
Journal of Applied Physics **101**, 043701 (2007).
Group: Karpinski / Projects: 3, 4
- S. WU, J. ZHANG, A. BELOUSOV, J. KARPINSKI, AND R. SOBOLEWSKI
Ultra-long-lived coherent acoustic phonons in GaN single crystals
Journal of Physics: Conference Series **92**,

012021 (2007).

Group: Karpinski / Projects: 3, 4

M. ZEHETMAYER, M. EISTERER, C. KRUTZLER, J. JUN, S. M. KAZAKOV, J. KARPINSKI, AND H. W. WEBER

Order-disorder transition in the flux line lattice of superconducting MgB₂ single crystals with artificially introduced defects: comparison with theory

Superconductor Science & Technology **20**, S247 (2007).

Group: Karpinski / Projects: 3, 4

N. D. ZHIGADLO AND J. KARPINSKI

High-pressure synthesis and superconductivity of Ca_{2-x}Na_xCuO₂Cl₂

Physica C **460**, 372 (2007).

Group: Karpinski / Projects: 3, 4

M. BRUHWILER, B. BATLOGG, S. M. KAZAKOV, C. NIEDERMAYER, AND J. KARPINSKI

Na_xCoO₂: Enhanced low-energy excitations of electrons on a 2d triangular lattice

Physica B **378-80**, 630 (2006).

Group: Karpinski / Projects: 3, 4

M. BRÜHWILER, S. M. KAZAKOV, J. KARPINSKI, AND B. BATLOGG

Large mass enhancement in RbOs₂O₆

Physica B **378-80**, 880 (2006).

Group: Karpinski / Projects: 3, 4

M. BRÜHWILER, S. M. KAZAKOV, J. KARPINSKI, AND B. BATLOGG

Mass enhancement, correlations, and strong-coupling superconductivity in the β-pyrochlore KO₅O₆

Physical Review B **73**, 094518 (2006).

Group: Karpinski / Projects: 3, 4

R. CUBITT, C. D. DEWHURST, M. R. ESKILDSEN, S. J. LEVETT, A. MATADEEN, J. JUN, S. M. KAZAKOV, J. KARPINSKI, S. L. BUD'KO, N. E. ANDERSON, AND P. C. CANFIELD

Penetration depth anisotropy in MgB₂ single crystals and powders

Journal of the Physics and Chemistry of Solids **67**, 493 (2006).

Group: Karpinski / Projects: 3, 4

D. DAGHERO, R. S. GONNELLI, G. A. UMMARINO, A. CALZOLARI, V. DELLAROCCHA, V. A. STEPANOV, S. M. KAZAKOV, J. JUN, AND J. KARPINSKI

Effect of the magnetic field on the gaps of MgB₂: A directional point-contact study

Journal of the Physics and Chemistry of Solids

67, 424 (2006).

Group: Karpinski / Projects: 3, 4

D. DI CASTRO, M. ORTOLANI, E. CAPPELLUTI, U. SCHADE, N. D. ZHIGADLO, AND J. KARPINSKI

Infrared properties of Mg_{1-x}Al_x(B_{1-y}C_y)₂ single crystals in the normal and superconducting state

Physical Review B **73**, 174509 (2006).

Group: Karpinski / Projects: 3, 4

C. DUBOIS, N. JENKINS, A. A. MANUEL, N. D. ZHIGADLO, J. KARPINSKI, AND Ø. FISCHER

Crystal-edge scanning tunnelling spectroscopy on aluminium-doped magnesium diboride

Superconductor Science & Technology **19**, 695 (2006).

Groups: Fischer, Karpinski / Projects: 2, 3, 4

J. L. GAVILANO, B. PEDRINI, K. MAGISHI, J. HINDERER, M. WELLER, H. R. OTT, S. M. KAZAKOV, AND J. KARPINSKI

Localized versus itinerant magnetic moments in Na_{0.7}CoO₂

Physical Review B **74**, 064410 (2006).

Groups: Karpinski, Ott / Projects: 1, 3, 4

R. S. GONNELLI, D. DAGHERO, A. CALZOLARI, G. A. UMMARINO, M. TORTELLO, V. A. STEPANOV, N. D. ZHIGADLO, K. ROGACKI, J. KARPINSKI, C. PORTESI, E. MONTICONE, D. MIJATOVIC, D. VELDHUIS, AND A. BRINKMAN

Recent achievements in MgB₂ physics and applications: A large-area SQUID magnetometer and point-contact spectroscopy measurements

Physica C **435**, 59 (2006).

Group: Karpinski / Projects: 3, 4

R. S. GONNELLI, D. DAGHERO, G. A. UMMARINO, A. CALZOLARI, V. DELLAROCCHA, V. A. STEPANOV, S. M. KAZAKOV, J. JUN, AND J. KARPINSKI

A point-contact study of the superconducting gaps in Al-substituted and C-substituted MgB₂ single crystals

Journal of the Physics and Chemistry of Solids **67**, 360 (2006).

Group: Karpinski / Projects: 3, 4

▶ R. S. GONNELLI, D. DAGHERO, G. A. UMMARINO, A. CALZOLARI, M. TORTELLO, V. A. STEPANOV, N. D. ZHIGADLO, K. ROGACKI, J. KARPINSKI, F. BERNARDINI, AND S. MASSIDA

Effect of Magnetic Impurities in a Two-Band Superconductor: A Point-Contact Study of Mn-Substituted MgB₂ Single Crystals

- Physical Review Letters **97**, 037001 (2006).
Group: Karpinski / Projects: 3, 4
- V. GURITANU, A. B. KUZMENKO, D. VAN DER MAREL, S. M. KAZAKOV, N. D. ZHIGADLO, AND J. KARPINSKI
Anisotropic optical conductivity and two colors of MgB₂
Physical Review B **73**, 104509 (2006).
Groups: Karpinski, van der Marel / Projects: 2, 3, 4
- R. KHASANOV, A. SHENGELAYA, K. CONDER, E. MORENZONI, I. M. SAVIĆ, J. KARPINSKI, AND H. KELLER
Correlation between oxygen isotope effects on transition temperature and magnetic penetration depth in high-temperature superconductors close to optimal doping
Physical Review B **74**, 064504 (2006).
Groups: Keller, Karpinski / Projects: 2, 3, 4
- V. G. KOGAN, R. PROZOROV, S. L. BUD'KO, P. C. CANFIELD, J. R. THOMPSON, J. KARPINSKI, N. D. ZHIGADLO, AND P. MIRANOVIĆ
Effect of field-dependent core size on reversible magnetization of high- κ superconductors
Physical Review B **74**, 184521 (2006).
Group: Karpinski / Projects: 3, 4
- A. KOHEN, T. CREN, Y. NOAT, T. PROSLIER, F. GIUBILEO, F. BOBBA, A. M. CUCOLO, N. ZHIGADLO, S. M. KAZAKOV, J. KARPINSKI, W. SACKS, AND D. RODITCHEV
Recent progress in vortex studies by tunneling spectroscopy
Physica C **437-38**, 145 (2006).
Group: Karpinski / Projects: 3, 4
- A. KOHEN, F. GIUBILEO, F. BOBBA, T. PROSLIER, N. ZHIGADLO, S. M. KAZAKOV, J. KLEIN, J. KARPINSKI, A. M. CUCOLO, AND D. RODITCHEV
"Lazy Fisherman" method of vortex analysis: application to MgB₂
Journal of the Physics and Chemistry of Solids **67**, 442 (2006).
Group: Karpinski / Projects: 3, 4
- C. KRUTZLER, M. ZEHETMAYER, M. EISTERER, H. W. WEBER, N. D. ZHIGADLO, J. KARPINSKI, AND A. WISNIEWSKI
Anisotropic reversible mixed-state properties of superconducting carbon-doped Mg(B_{1-x}C_x)₂ single crystals
Physical Review B **74**, 144511 (2006).
Group: Karpinski / Projects: 3, 4
- G. LAMURA, A. GAUZZI, S. M. KAZAKOV, J. KARPINSKI, AND A. ANDREONE
High-resolution measurements of the magnetic penetration depth on Yba₂Cu₄O₈ single crystals
Journal of the Physics and Chemistry of Solids **67**, 447 (2006).
Group: Karpinski / Projects: 3, 4
- E. LIAROKAPIS, D. LAMPAKIS, D. PALLES, J. KARPINSKI, AND C. PANAGOPOULOS
A Raman view of local lattice distortions and charge transfer in cuprates
Journal of the Physics and Chemistry of Solids **67**, 2065 (2006).
Group: Karpinski / Projects: 3, 4
- D. PAL, L. DEBEER-SCHMITT, T. BERA, R. CUBITT, C. D. DEWHURST, J. JUN, N. D. ZHIGADLO, J. KARPINSKI, V. G. KOGAN, AND M. R. ESKILDSEN
Measuring the penetration depth anisotropy in MgB₂ using small-angle neutron scattering
Physical Review B **73**, 012513 (2006).
Group: Karpinski / Projects: 3, 4
- B. PEDRINI, S. WEYENETH, J. L. GAVILANO, J. HINDERER, M. WELLER, H. R. OTT, S. M. KAZAKOV, AND J. KARPINSKI
Magnetic transition in Na_{0.5}CoO₂ at 88 K
Physica B **378-80**, 861 (2006).
Groups: Karpinski, Ott / Projects: 1, 3, 4
- K. ROGACKI, B. BATLOGG, J. KARPINSKI, N. D. ZHIGADLO, G. SCHUCK, S. M. KAZAKOV, P. WAGLI, R. PUŻNIAK, A. WIŚNIEWSKI, F. CARBONE, A. BRINKMAN, AND D. VAN DER MAREL
Strong magnetic pair breaking in Mn-substituted MgB₂ single crystals
Physical Review B **73**, 174520 (2006).
Groups: Karpinski, van der Marel / Projects: 2, 3, 4
- G. SCHUCK, S. M. KAZAKOV, K. ROGACKI, N. D. ZHIGADLO, AND J. KARPINSKI
Crystal growth, structure, and superconducting properties of the β -pyrochlore KOs₂O₆
Physical Review B **73**, 144506 (2006).
Group: Karpinski / Projects: 3, 4
- A. V. SOLOGUBENKO, N. D. ZHIGADLO, J. KARPINSKI, AND H. R. OTT
Thermal conductivity of Al-doped MgB₂: Impurity scattering and the validity of the Wiedemann-Franz law
Physical Review B **74**, 184523 (2006).
Groups: Karpinski, Ott / Projects: 2, 3, 4
- S. STREULE, M. MEDARDE, A. PODLESNYAK, E. POMJAKUSHINA, K. CONDER, S. KAZAKOV,

- J. KARPINSKI, AND J. MESOT
Short-range charge ordering in $\text{Ho}_{0.1}\text{Sr}_{0.9}\text{CoO}_{3-x}$ ($0.15 \leq x \leq 0.49$)
Physical Review B **73**, 024423 (2006).
Groups: Karpinski, Mesot / Projects: 1, 3, 4, 6
- S. WU, P. GEISER, J. JUN, J. KARPINSKI, J. R. PARK, AND R. SOBOLEWSKI
Long-lived, coherent acoustic phonon oscillations in GaN single crystals
Applied Physics Letters **88**, 041917 (2006).
Group: Karpinski / Projects: 3, 4
- M. ZEHETMAYER, M. EISTERER, R. MÜLLER, M. WEIGAND, J. JUN, S. M. KAZAKOV, J. KARPINSKI, AND H. W. WEBER
Flux Pinning in Neutron Irradiated MgB_2 Single Crystals
Journal of Physics: Conference Series **43**, 651 (2006).
Group: Karpinski / Projects: 3, 4
- M. ZEHETMAYER, C. KRUTZLER, M. EISTERER, J. JUN, S. M. KAZAKOV, J. KARPINSKI, AND H. W. WEBER
Effect of disorder on the irreversible magnetic properties of single crystalline MgB_2 : comparison of carbon doping and neutron irradiation
Physica C **445**, 65 (2006).
Group: Karpinski / Projects: 3, 4
- M. BRÜHWILER, S. M. KAZAKOV, J. KARPINSKI, AND B. BATLOGG
Intrinsic thermodynamic properties of the pyrochlore superconductor RbOs_2O_6 extracted by condensation energy analysis
Physical Review B **71**, 214517 (2005).
Group: Karpinski / Projects: 3, 4
- P. CARRETTA, A. KEREN, J. S. LORD, I. ZUCCA, S. M. KAZAKOV, AND J. KARPINSKI
Anomaly in $\text{YBa}_2\text{Cu}_4\text{O}_8$ charge distribution below T_c : A zero-field muon spin relaxation study
Physical Review B **71**, 052507 (2005).
Group: Karpinski / Projects: 3, 4
- A. CARRINGTON, J. D. FLETCHER, J. R. COOPER, O. J. TAYLOR, L. BALICAS, N. D. ZHIGADLO, S. M. KAZAKOV, J. KARPINSKI, J. P. H. CHARMANT, AND J. KORTUS
de Haas-van Alphen effect investigation of the electronic structure of Al-substituted MgB_2
Physical Review B **72**, 060507 (2005).
Group: Karpinski / Projects: 3, 4
- D. DAGHERO, R. S. GONNELLI, A. CALZOLARI, G. A. UMMARINO, V. DELLARocca,
- V. A. STEPANOV, N. ZHIGADLO, S. M. KAZAKOV, AND J. KARPINSKI
The superconducting gaps of C-substituted and Al-substituted MgB_2 single crystals by point-contact spectroscopy
Physica Status Solidi (c) **2**, 1656 (2005).
Group: Karpinski / Projects: 3, 4
- D. DI CASTRO, R. KHASANOV, C. GRIMALDI, J. KARPINSKI, S. M. KAZAKOV, R. BRÜTSCH, AND H. KELLER
Pressure effect on the magnetic penetration depth in MgB_2
Physical Review B **72**, 094504 (2005).
Groups: Keller, Karpinski / Projects: 2, 3, 4
- M. EISTERER, M. ZEHETMAYER, H. W. WEBER, AND J. KARPINSKI
Reversible magnetization of the two-band MgB_2 superconductor: A phenomenological approach
Physical Review B **72**, 134525 (2005).
Group: Karpinski / Projects: 3, 4
- J. D. FLETCHER, A. CARRINGTON, O. J. TAYLOR, S. M. KAZAKOV, AND J. KARPINSKI
Temperature-Dependent Anisotropy of the Penetration Depth and Coherence Length of MgB_2
Physical Review Letters **95**, 097005 (2005).
Group: Karpinski / Projects: 3, 4
- S. GALAMBOSI, J. A. SOININEN, A. MATTILA, S. HUOTARI, S. MANNINEN, G. VANKO, N. D. ZHIGADLO, J. KARPINSKI, AND K. HÄMÄLÄINEN
Inelastic x-ray scattering study of collective electron excitations in MgB_2
Physical Review B **71**, 060504 (2005).
Group: Karpinski / Projects: 3, 4
- J. L. GAVILANO, D. RAU, B. PEDRINI, K. MAGISHI, M. WELLER, J. HINDERER, H. R. OTT, S. M. KAZAKOV, AND J. KARPINSKI
Unconventional charge ordering in $\text{Na}_{0.70}\text{CoO}_2$ below 300 K?
Physica B **359**, 1237 (2005).
Groups: Karpinski, Ott / Projects: 3, 4
- P. GEISER, J. JUN, S. M. KAZAKOV, P. WÄGLI, J. KARPINSKI, B. BATLOGG, AND L. KLEMM
 $\text{Al}_x\text{Ga}_{1-x}\text{N}$ bulk single crystals
Applied Physics Letters **86**, 081908 (2005).
Group: Karpinski / Projects: 3, 4
- R. S. GONNELLI, D. DAGHERO, A. CALZOLARI, G. A. UMMARINO, V. DELLARocca, V. A. STEPANOV, S. M. KAZAKOV, N. ZHIGADLO, AND J. KARPINSKI

- Evidence for single-gap superconductivity in $Mg(B_{1-x}C_x)_2$ single crystals with $x = 0.132$ from point-contact spectroscopy*
Physical Review B **71**, 060503 (2005).
Group: Karpinski / Projects: 3, 4
- R. S. GONNELLI, D. DAGHERO, G. A. UMMARINO, A. CALZOLARI, M. TORTELLO, V. A. STEPANOV, N. ZHIGADLO, S. M. KAZAKOV, AND J. KARPINSKI
Evidence for One-Gap Superconductivity in $Mg(B_{1-x}C_x)_2$ Single Crystals at $x = 0.132$ by Point-Contact Spectroscopy
Journal of Superconductivity **18**, 681 (2005).
Group: Karpinski / Projects: 3, 4
- J. KARPINSKI, N. D. ZHIGADLO, G. SCHUCK, S. M. KAZAKOV, B. BATLOGG, K. ROGACKI, R. PUZNIAK, J. JUN, E. MÜLLER, P. WÄGLI, R. GONNELLI, D. DAGHERO, G. A. UMMARINO, AND V. A. STEPANOV
Al substitution in MgB_2 crystals: Influence on superconducting and structural properties
Physical Review B **71**, 174506 (2005).
Group: Karpinski / Projects: 3, 4
- S. M. KAZAKOV, R. PUZNIAK, K. ROGACKI, A. V. MIRONOV, N. D. ZHIGADLO, J. JUN, C. SOLTSMANN, B. BATLOGG, AND J. KARPINSKI
Carbon substitution in MgB_2 single crystals: Structural and superconducting properties
Physical Review B **71**, 024533 (2005).
Group: Karpinski / Projects: 3, 4
- ▶ R. KHASANOV, D. G. ESHCHENKO, D. DI CASTRO, A. SHENGELAYA, F. LA MATTINA, A. MAISURADZE, C. BAINES, H. LUETKENS, J. KARPINSKI, S. M. KAZAKOV, AND H. KELLER
Magnetic penetration depth in $RbOs_2O_6$ studied by muon spin rotation
Physical Review B **72**, 104504 (2005).
Groups: Keller, Karpinski, Mesot / Projects: 1, 2, 3, 4
- R. KHASANOV, J. KARPINSKI, AND H. KELLER
Pressure effect on the in-plane magnetic penetration depth in $YBa_2Cu_4O_8$
Journal of Physics: Condensed Matter **17**, 2453 (2005).
Groups: Keller, Karpinski, Mesot / Projects: 1, 2, 3, 4
- ▶ A. KOHEN, T. CREN, T. PROSLIER, Y. NOAT, W. SACKS, D. RODITCHEV, F. GIUBILEO, F. BOBBA, A. M. CUCOLO, N. ZHIGADLO, S. M. KAZAKOV, AND J. KARPINSKI
Superconducting vortex profile from fixed point measurements the "Lazy Fisherman" tunneling microscopy method
Applied Physics Letters **86**, 212503 (2005).
Group: Karpinski / Projects: 3, 4
- D. LAMPAKIS, D. PALLES, E. LIAROKAPIS, S. M. KAZAKOV, AND J. KARPINSKI
Hydrostatic-pressure-induced phase separation in the $YBa_2Cu_4O_8$ superconductor
Physical Review B **72**, 014539 (2005).
Group: Karpinski / Projects: 3, 4
- K. MAGISHI, J. L. GAVILANO, B. PEDRINI, J. HINDERER, M. WELLER, H. R. OTT, S. M. KAZAKOV, AND J. KARPINSKI
Evidence for s-wave superconductivity in the β -pyrochlore oxide $RbOs_2O_6$
Physical Review B **71**, 024524 (2005).
Groups: Karpinski, Ott / Projects: 3, 4
- ▶ A. MATTILA, J. A. SOININEN, S. GALAMBOSI, S. HUOTARI, G. VANKÓ, N. D. ZHIGADLO, J. KARPINSKI, AND K. HÄMÄLÄINEN
Local Electronic Structure of MgB_2 by X-Ray Raman Scattering at the boron K edge
Physical Review Letters **94**, 247003 (2005).
Group: Karpinski / Projects: 3, 4
- J. D. MOORE, G. K. PERKINS, A. D. CAPLIN, J. JUN, S. M. KAZAKOV, J. KARPINSKI, AND L. F. COHEN
Angular dependence of the order-disorder transition in proton irradiated single crystal MgB_2
Physical Review B **71**, 224509 (2005).
Group: Karpinski / Projects: 3, 4
- B. PEDRINI, J. L. GAVILANO, S. WEYENETH, E. FELDER, J. HINDERER, M. WELLER, H. R. OTT, S. M. KAZAKOV, AND J. KARPINSKI
Magnetic phase transition at 88 K in $Na_{0.5}CoO_2$ revealed by ^{23}Na NMR investigations
Physical Review B **72**, 214407 (2005).
Groups: Karpinski, Ott / Projects: 1, 3, 4
- V. SCAGNOLI, U. STAUB, M. JANOUSCH, A. M. MULDER, M. SHI, G. I. MEIJER, S. ROSENKRANZ, S. B. WILKINS, L. PAOLASINI, J. KARPINSKI, S. M. KAZAKOV, AND S. W. LOVESEY
Charge disproportionation and search for orbital ordering in $NdNiO_3$ by use of resonant x-ray diffraction
Physical Review B **72**, 155111 (2005).
Group: Karpinski / Projects: 3, 4
- A. V. SOLOGUBENKO, N. D. ZHIGADLO, S. M. KAZAKOV, J. KARPINSKI, AND H. R. OTT
Influence of carbon substitution on the heat transport in single crystalline MgB_2
Physical Review B **71**, 020501 (2005).
Groups: Karpinski, Ott / Projects: 2, 3, 4

M. ZEHETMAYER, M. EISTERER, S. SPONAR, H. W. WEBER, A. WISNIEWSKI, R. PUZNIAK, P. PANTA, S. M. KAZAKOV, AND J. KARPINSKI
Magnetic properties of superconducting $\text{HgBa}_2\text{CuO}_{4+\delta}$ single crystals in the overdoped state before and after particle irradiation
 Physica C **418**, 73 (2005).

Group: Karpinski / Projects: 3, 4

Group of H. Keller

R. KHASANOV, A. SHENGELAYA, J. KARPINSKI, A. BUSSMANN-HOLDER, H. KELLER, AND K. A. MÜLLER
s-wave symmetry along the c-axis and s + d in-plane superconductivity in bulk $\text{YBa}_2\text{Cu}_4\text{O}_8$
 Journal of Superconductivity and Novel Magnetism **21**, 81 (2008).

Groups: Keller, Karpinski / Project: 2, 3, 4

- ▶ R. KHASANOV, A. SHENGELAYA, A. MAISURADZE, D. DI CASTRO, R. ESCAMILLA, AND H. KELLER
Correlation between the transition temperature and the superfluid density in BCS superconductor NbB_{2+x}
 Physical Review B **77**, 064506 (2008).

Group: Keller / Project: 2

S. WEYENETH, T. SCHNEIDER, N. ZHIGADLO, J. KARPINSKI, AND H. KELLER
Probing Superconductivity in MgB_2 confined to magnetic field tuned cylinders by means of critical fluctuations
 Journal of Physics: Condensed Matter **20**, 135208 (2008).

Groups: Karpinski, Keller / Projects: 3, 4

A. R. BISHOP, A. BUSSMANN-HOLDER, O. V. DOLGOV, A. FURRER, H. KAMIMURA, H. KELLER, R. KHASANOV, D. KREMER, R. KANS MANSKE, K. A. MÜLLER, AND A. SIMON
Real and marginal isotope effects in cuprate superconductors
 Journal of Superconductivity and Novel Magnetism **20**, 393 (2007).

Group: Keller / Project: 2

A. BUSSMANN-HOLDER, H. KELLER, AND K. A. MÜLLER
Entscheidende Rolle des Gitters
 Physik Journal **6**, 16 (2007).

Group: Keller / Project: 2

A. BUSSMANN-HOLDER, R. KHASANOV, A. SHENGELAYA, A. MAISURADZE, F. LA MATTINA, H. KELLER, AND K. A. MÜLLER

Mixed order parameter symmetries in cuprate superconductors

Europhysics Letters **77**, 27002 (2007).

Group: Keller / Project: 2

- ▶ R. KHASANOV, A. SHENGELAYA, D. DI CASTRO, D. G. ESHCHENKO, I. M. SAVIĆ, K. CONDER, E. POMJAKUSHINA, J. KARPINSKI, S. KAZAKOV, AND H. KELLER
Magnetic-field dependence of the oxygen isotope effect on the magnetic penetration depth of hole-doped cuprate superconductors

Physical Review B **75**, 060505 (2007).

Groups: Keller, Karpinski / Projects: 2, 3, 4

- ▶ R. KHASANOV, A. SHENGELAYA, A. MAISURADZE, F. LA MATTINA, A. BUSSMANN-HOLDER, H. KELLER, AND K. A. MÜLLER
Experimental Evidence for Two Gaps in the High-Temperature $\text{La}_{1.83}\text{Sr}_{0.17}\text{CuO}_4$ Superconductor

Physical Review Letters **98**, 057007 (2007).

Group: Keller / Project: 2

- ▶ R. KHASANOV, S. STRÄSSLE, D. DI CASTRO, T. MASUI, S. MIYASAKA, S. TAJIMA, A. BUSSMANN-HOLDER, AND H. KELLER
Multiple Gap Symmetries for the Order Parameter of Cuprate Superconductors from Penetration Depth Measurements

Physical Review Letters **99**, 237601 (2007).

Group: Keller / Project: 2

- ▶ R. KHASANOV, N. D. ZHIGADLO, J. KARPINSKI, AND H. KELLER
In-plane magnetic penetration depth λ_{ab} in $\text{Ca}_{2-x}\text{Na}_x\text{CuO}_2\text{Cl}_2$: Role of the apical sites

Physical Review B **76**, 094505 (2007).

Groups: Keller, Karpinski / Projects: 2, 3, 4

S. KOHOUT, T. SCHNEIDER, J. ROOS, H. KELLER, T. SASAGAWA, AND H. TAKAGI
Vortex states and magnetic anisotropy in single-crystal $\text{La}_{2-x}\text{Sr}_x\text{CuO}_4$ studied by torque magnetometry

Physical Review B **76**, 064513 (2007).

Group: Keller / Project: 2

- ▶ T. KONDO, R. KHASANOV, J. KARPINSKI, S. M. KAZAKOV, N. D. ZHIGADLO, T. OHTA, H. M. FRETWELL, A. D. PALCZEWSKI, J. D. KOLL, J. MESOT, E. ROTENBERG, H. KELLER, AND A. KAMINSKI
Dual character of the electronic structure of $\text{YBa}_2\text{Cu}_4\text{O}_8$: The conduction bands of CuO_2 planes and CuO chains

Physical Review Letters **98**, 157002 (2007).

Groups: Keller, Karpinski, Mesot / Projects: 2, 3, 4

- I. L. LANDAU AND H. KELLER
On the interpretation of muon-spin-rotation experiments in the mixed state of type-II superconductors
Physica C **466**, 131 (2007).
Group: Keller / Project: 2
- I. L. LANDAU AND H. KELLER
Two types of $H_{c2}(T)$ dependences in $Bi_2Sr_2Ca_{1-x}Y_xCu_2O_{8+\delta}$ with different Yttrium content
Physica C **458**, 38 (2007).
Group: Keller / Project: 2
- E. MORENZONI, H. LUETKENS, S. A., D. G. ESHCHENKO, R. KHASANOV, A. AMATO, T. PROKSCHA, AND R. SCHEUERMANN
 μ SR studies of hydrogen-bonded ferroelectrics and antiferroelectrics
Physica B **388**, 274 (2007).
Group: Keller / Project: 2
- ▶ T. PROKSCHA, E. MORENZONI, D. G. ESHCHENKO, N. GARIFIANOV, H. GLÜCKLER, R. KHASANOV, H. LUETKENS, AND S. A.
Formation of Hydrogen Impurity States in Silicon and Insulators at Low Implantation Energies
Physical Review Letters **98**, 227401 (2007).
Group: Keller / Project: 2
- S. STRÄSSLE, J. ROOS, M. MALI, K. CONDER, E. POMJAKUSHINA, AND H. KELLER
 ^{139}La NMR and NQR investigations of the superconductor $\text{LaBa}_2\text{Cu}_3\text{O}_{7-\delta}$
Physica C **460-462**, 890 (2007).
Group: Keller / Project: 2
- S. STRÄSSLE, J. ROOS, M. MALI, H. KELLER, AND J. KARPINSKI
 ^{11}B NMR study of single-crystal MgB_2 in the normal conducting phase
Physica C **466**, 168 (2007).
Groups: Keller, Karpinski / Projects: 2, 3, 4
- R. V. YUSUPOV, R. KABANOV, D. MIHAILOVIC, K. CONDER, H. KELLER, AND K. A. MÜLLER
Surface nanomagnetism of La_2CuO_4 particles
Physica C **460-462**, 801 (2007).
Group: Keller / Project: 2
- R. V. YUSUPOV, R. KABANOV, D. MIHAILOVIC, K. CONDER, K. A. MÜLLER, AND H. KELLER
Spontaneous ferromagnetic spin ordering at the surface of La_2CuO_4
Physical Review B **76**, 024428 (2007).
Group: Keller / Project: 2
- R. V. YUSUPOV, T. MERTELJ, D. MIHAILOVIC, K. CONDER, H. KELLER, AND K. A. MÜLLER
Oxygen isotope effect on the polaronic infrared photo-induced absorption spectra of surface nanomagnetism of La_2CuO_4
Physica C **460-462**, 920 (2007).
Group: Keller / Project: 2
- A. ZORKOVSKÁ, A. BARAN, I. BRADARIĆ, I. SAVIĆ, J. ŠEBEK, E. ŠANTAVÁ, D. MARINČEV, S. KOHOUT, H. KELLER, AND A. FEHER
Influence of Ti^{4+} on the magnetic state of $\text{CaRu}_{1-x}\text{Ti}_x\text{O}_3$
Journal of Magnetism and Magnetic Materials **316**, e699 (2007).
Group: Keller / Project: 2
- ▶ R. KHASANOV, P. S. HÄFLIGER, N. SHITSEVALOVA, A. DUKHNENKO, AND H. KELLER
Pressure effect on the Ginzburg-Landau parameter $\kappa = \lambda/\xi$ in YB_6
Physical Review Letters **97**, 157002 (2006).
Group: Keller / Project: 2
- ▶ R. KHASANOV, I. L. LANDAU, F. BAINES, C. LA MATTINA, A. MAISURADZE, K. TOGANO, AND H. KELLER
Muon-spin-rotation measurements of the penetration depth in $\text{Li}_2\text{Pd}_3\text{B}$
Physical Review B **73**, 214528 (2006).
Group: Keller / Project: 2
- ▶ R. KHASANOV, A. SHENGELAYA, K. CONDER, E. MORENZONI, I. M. SAVIĆ, J. KARPINSKI, AND H. KELLER
Correlation between oxygen isotope effects on transition temperature and magnetic penetration depth in high-temperature superconductors close to optimal doping
Physical Review B **74**, 064504 (2006).
Groups: Keller, Karpinski / Projects: 2, 3, 4
- I. L. LANDAU, R. KHASANOV, K. TOGANO, AND H. KELLER
Temperature dependences of the upper critical field and the Ginzburg-Landau parameter of $\text{Li}_2\text{Pd}_3\text{B}$ from magnetization measurements
Physica C **451**, 134 (2006).
Group: Keller / Project: 2
- E. MORENZONI, R. KHASANOV, T. LUETKENS, H. PROKSCHA, AND A. SUTER
Surface and thin film studies with polarized low energy muons
Journal of Neutron Research **14**, 269 (2006).
Group: Keller / Project: 2
- T. PROKSCHA, E. MORENZONI, K. DEITERS, F. FOROUGHI, D. GEORGE, R. KOBLER,

- A. SUTER, AND V. VRANKOVIC
The new high-intensity surface muon beam $\mu E4$ for the generation of low-energy muons at PSI
Physica B **374-375**, 460 (2006).
Group: Keller / Project: 2
- V. G. STORCHAK, D. G. ESHCHENKO, AND J. H. BREWER
Quantum diffusion of muonium atoms in solids: Localization vs. band-like propagation
Physica B **374-375**, 347 (2006).
Group: Keller / Project: 2
- V. G. STORCHAK, D. G. ESHCHENKO, J. H. BREWER, AND S. P. COTTREL
Formation and dynamics of muonium centers in semiconductors
Physica B **374-375**, 398 (2006).
Group: Keller / Project: 2
- ▶ V. G. STORCHAK, D. G. ESHCHENKO, J. H. BREWER, S. P. COTTREL, AND R. L. LICHTI
Muonium in InSb: Shallow acceptor versus deep trap or recombination center
Physical Review B **73**, 081203 (2006).
Group: Keller / Project: 2
- V. G. STORCHAK, D. G. ESHCHENKO, H. LUETKENS, E. MORENZONI, R. L. LICHTI, S. F. MARENKIN, O. N. PASHKOVA, AND J. H. BREWER
Room temperature ferromagnetism in III-V and II-IV- V_2 dilute magnetic semiconductors
Physica B **374-375**, 430 (2006).
Group: Keller / Project: 2
- A. SUTER, E. MORENZONI, N. GARIFIANOV, R. KHASANOV, E. KIRK, H. LUETKENS, T. PROKSCHA, AND M. HORISBERGER
Nonlocal Meissner screening
Physica B **374-375**, 243 (2006).
Group: Keller / Project: 2
- A. BUSSMANN-HOLDER AND H. KELLER
Polaron formation as origin of unconventional isotope effects in cuprate superconductors
The European Physical Journal B **44**, 487 (2005).
Group: Keller / Project: 2
- A. BUSSMANN-HOLDER, H. KELLER, A. R. BISHOP, A. SIMON, R. MICNAS, AND K. A. MÜLLER
Unconventional isotope effects as evidence for polaron formation in cuprates
Europhysics Letters **72**, 423 (2005).
Group: Keller / Project: 2
- D. DI CASTRO, R. KHASANOV, C. GRIMALDI, J. KARPINSKI, S. M. KAZAKOV, R. BRÜTSCH, AND H. KELLER
Pressure effect on the magnetic penetration depth in MgB_2
Physical Review B **72**, 094504 (2005).
Groups: Keller, Karpinski / Projects: 2, 3, 4
- ▶ A. DREW, S. L. LEE, D. CHARALAMBOUS, A. POTENZA, C. MARROWS, H. LUETKENS, A. SUTER, T. PROKSCHA, R. KHASANOV, E. MORENZONI, D. UCKO, AND E. M. FORGAN
Coexistence and Coupling of Superconductivity and Magnetism in Thin Film Structures
Physical Review Letters **95**, 197201 (2005).
Groups: Keller, Mesot / Projects: 1, 2
- ▶ R. KHASANOV, D. G. ESHCHENKO, D. DI CASTRO, A. SHENGELAYA, F. LA MARTINA, A. MAISURADZE, C. BAINES, H. LUETKENS, J. KARPINSKI, S. M. KAZAKOV, AND H. KELLER
Magnetic penetration depth in $RbOs_2O_6$ studied by muon spin rotation
Physical Review B **72**, 104504 (2005).
Groups: Keller, Karpinski, Mesot / Projects: 1, 2, 3, 4
- R. KHASANOV, J. KARPINSKI, AND H. KELLER
Pressure effect on the in-plane magnetic penetration depth in $YBa_2Cu_4O_8$
Journal of Physics: Condensed Matter **17**, 2453 (2005).
Groups: Keller, Karpinski, Mesot / Projects: 1, 2, 3, 4
- ▶ R. KHASANOV, T. SCHNEIDER, AND H. KELLER
Pressure effects on the superconducting properties of $YBa_2Cu_4O_8$
Physical Review B **72**, 014524 (2005).
Groups: Mesot, Keller / Projects: 1, 2
- S. KOHOUT, J. ROOS, AND H. KELLER
Automated operation of a homemade torque magnetometer using LabVIEW
Measurement Science & Technology **16**, 2240 (2005).
Group: Keller / Project: 2
- F. L. PRATT, T. LANCASTER, M. L. BROOKS, S. L. BLUNDELL, T. PROKSCHA, E. MORENZONI, A. SUTER, H. LUETKENS, R. KHASANOV, K. SHINOTSUKA, AND H. E. ASSENDER
Surface dynamics of a thin polystyrene film probed by low energy muons
Physical Review B **72**, 121401 (2005).
Group: Keller / Project: 2
- ▶ T. SCHNEIDER, R. KHASANOV, AND H. KELLER

Evidence for charged critical behavior in the pyrochlore superconductor RbOs_2O_6

Physical Review Letters **94**, 077002 (2005).

Group: Keller / Project: 2

- ▶ A. SHENGELAYA, R. KHASANOV, D. G. ESHCHENKO, D. DI CASTRO, I. M. SAVIĆ, M. S. PARK, K. H. KIM, S.-I. LEE, K. A. MÜLLER, AND H. KELLER

Muon-spin-rotation measurements of the penetration depth of the infinite-layer electron-doped $\text{Sr}_{0.9}\text{La}_{0.1}\text{CuO}_2$ cuprate superconductor

Physical Review Letters **94**, 127001 (2005).

Group: Keller / Project: 2

- ▶ V. G. STORCHAK, D. G. ESHCHENKO, J. H. BREWER, B. HITTI, R. L. LICHTI, AND B. A. ARONZON

Magnetic freezeout of electrons into muonium atoms in GaAs

Physical Review B **71**, 113202 (2005).

Group: Keller / Project: 2

A. SUTER, E. MORENZONI, N. GARIFIANOV, R. KHASANOV, E. KIRK, H. LUETKENS, T. PROKSCHA, AND M. HORISBERGER

Observation of nonexponential magnetic penetration profiles in the Meissner state: A manifestation of nonlocal effects in superconductors

Physical Review B **72**, 024506 (2005).

Group: Keller / Project: 2

Group of D. van der Marel

E. GIANNINI, R. GLADYSHEVSKII, N. CLAYTONA, N. MUSOLINO, V. GARNIER, A. PIRIOU, AND R. FLÜKIGER

Growth, structure and physical properties of single crystals of pure and Pb-doped Bi-based high- T_c superconductors

Current Applied Physics **8**, 115 (2008).

Groups: Flükiger, van der Marel / Project: 3

- ▶ A. B. KUZMENKO, E. VAN HEUMEN, F. CARBONE, AND D. VAN DER MAREL

Universal dynamical conductance in graphite to be published in Physical Review Letters (2008).

Group: van der Marel / Project: 1

A. PIRIOU, Y. FASANO, E. GIANNINI, AND O. FISCHER

Effect of oxygen-doping on $\text{Bi}_2\text{Sr}_2\text{Ca}_2\text{Cu}_3\text{O}_{10+\delta}$ vortex matter: Crossover from electromagnetic to Josephson interlayer coupling

submitted to Physical Review B (2008).

Groups: Fischer, van der Marel / Projects: 2, 5

J. TEYSSIER, R. VIENNOIS, J. SALAMIN, E. GIANNINI, AND D. VAN DER MAREL

Experimental and First principle calculation of $\text{Co}_x\text{Ni}_{1-x}\text{Si}$ solid solution structural stability to be published in Journal of Alloys and Compounds (2008).

Group: van der Marel / Projects: 1, 3

O. ZAREMBA, O. SHCHERBAN, R. GLADYSHEVSKII, F. BANFI, AND E. GIANNINI

The 5:7 member of the spin-ladder series in the Bi-Sr-Ca-Cu-O system to be published in Journal of Alloys and Compounds (2008).

Group: van der Marel / Project: 3

K. S. BURCH, S. V. DORDEVIC, F. P. MENA, A. B. KUZMENKO, D. VAN DER MAREL, J. L. SARRAO, J. R. JEFFRIES, E. D. BAUER, M. B. MAPLE, AND D. N. BASOV

Optical signatures of momentum-dependent hybridization of the local moments and conduction electrons in Kondo lattices

Physical Review B **75**, 054523 (2007).

Group: van der Marel / Projects: 1, 2

C. FILIPIC, Z. KUTNJAK, R. LORTZ, M. DAUBER, AND J. F. SCOTT

Low temperature phase transitions in barium sodium niobate

Journal of Physics: Condensed Matter **19**, 236206 (2007).

Groups: Triscone, van der Marel / Project: 2

- ▶ V. GURITANU, D. VAN DER MAREL, J. TEYSSIER, T. JARLBORG, H. WILHELM, M. SCHMIDT, AND F. STEGLICH

Optical evidence for heavy charge carriers in FeGe

Physical Review B **75**, 155114 (2007).

Groups: Giamarchi, van der Marel / Project: 1

E. VAN HEUMEN, R. LORTZ, A. B. KUZMENKO, F. CARBONE, D. VAN DER MAREL, X. ZHAO, G. YU, Y. CHO, N. BARISIC, M. GREVEN, C. C. HOMES, AND S. V. DORDEVIC

Optical and thermodynamic properties of the high-temperature superconductor $\text{HgBa}_2\text{CuO}_{4+\delta}$

Physical Review B **75**, 054522 (2007).

Group: van der Marel / Project: 2

A. B. KUZMENKO

Multiband and impurity effects in infrared and optical spectra of MgB_2

Physica C **456**, 63 (2007).

Group: van der Marel / Projects: 2, 3

- A. B. KUZMENKO, D. VAN DER MAREL, F. CARBONE, AND F. MARSIGLIO
Model-independent sum rule analysis based on limited-range spectral data
New Journal of Physics **9**, 229 (2007).
Group: van der Marel / Projects: 1, 2
- R. LORTZ, C. MEINGAST, A. I. RYKOV, AND S. TAJIMA
Fragile Superconductivity and a kinetic glass transition in the vortex matter of the high-temperature superconductor $YBa_2Cu_3O_{7-\delta}$
Journal of Low Temperature Physics **147**, 365 (2007).
Groups: Triscone, van der Marel / Project: 2
- R. LORTZ, N. MUSOLINO, Y. WANG, A. JUNOD, AND N. TOYOTA
Origin of the magnetization peak effect in the superconductor Nb_3Sn
Physical Review B **75**, 094503 (2007).
Groups: Triscone, van der Marel / Project: 2
- ▶ R. LORTZ, Y. WANG, A. DEMUER, M. BÖTTGER, B. BERGK, G. ZWICKNAGEL, Y. NAKAZAWA, AND J. WOSNITZA
Calorimetric evidence for a novel superconducting state in the layered organic superconductor κ -(BEDT) $_2$ Cu(NCS) $_2$
Physical Review Letters **99**, 187002 (2007).
Groups: Triscone, van der Marel / Project: 2
- R. LORTZ, Y. WANG, A. JUNOD, AND N. TOYOTA
Thermal fluctuations in the classical superconductor Nb_3Sn from high-resolution specific-heat measurements
Physica C **460-462**, 149 (2007).
Groups: Triscone, van der Marel / Project: 2
- M. R. NORMAN, A. V. CHUBUKOV, E. VAN HEUMEN, A. B. KUZMENKO, AND D. VAN DER MAREL
Optical integral in the cuprates and the question of sum-rule violation
Physical Review B **76**, 220509 (2007).
Group: van der Marel / Project: 2
- A. P. PETROVIĆ, Y. FASANO, R. LORTZ, M. DECROUX, M. POTEL, R. CHEVREL, AND Ø. FISCHER
Unconventional resistive transitions in the extreme type-II superconductor $Tl_2Mo_6Se_6$
Physica C **460-462**, 702 (2007).
Groups: Fischer, Triscone, van der Marel / Projects: 1, 2
- A. PIRIOU, Y. FASANO, E. GIANNINI, AND O. FISCHER
Doping-dependence of the vortex phase diagram of $Bi_2Sr_2Ca_2Cu_3O_{10+\delta}$
Physica C **460-462**, 408 (2007).
Groups: Fischer, van der Marel / Projects: 2, 3, 5
- F. RONNING, C. CAPAN, N. O. MORENO, J. D. THOMPSON, L. N. BULAEVSKII, R. MOVSHOVICH, AND D. VAN DER MAREL
Magnetic excitations of the 2-D Sm spin layers in $Sm(La, Sr)CuO_4$
Journal of Magnetism and Magnetic Materials **310**, e392 (2007).
Group: van der Marel / Projects: 1, 2
- D. SHALTIEL, H.-A. K. VON NIDDA, B. Y. SHAPIRO, I. SHAPIRO, A. LOIDL, T. KURZ, B. BOGOSLAVSKY, T. TAMAGAI, Ø. FISCHER, A. PIRIOU, E. GIANNINI, T. WATANABE, T. FUJII, AND A. MATSUDA, B. ROSENSTEIN
Interaction of AC magnetic field with Josephson vortices in high anisotropy superconductors $Bi2212$ and $Bi2223$
Physica C **460-462**, 1238 (2007).
Groups: van der Marel, Fischer / Project: 3
- ▶ R. TEDIOSI, N. P. ARMITAGE, E. GIANNINI, AND D. VAN DER MAREL
Charge Carrier Interaction with a Purely Electronic Collective Mode: Plasmarons and the Infrared Response of Elemental Bismuth
Physical Review Letters **99**, 016406 (2007).
Group: van der Marel / Project: 1
- J. TEYSSIER, A. B. KUZMENKO, D. VAN DER MAREL, F. MARSIGLIO, A. B. LIASHCHENKO, V. FILIPPOV, AND N. SHITSEVALOVA
Optical study of electronic structure and electron-phonon coupling in ZrB_{12}
Physical Review B **75**, 134503 (2007).
Group: van der Marel / Project: 2
- R. VIENNOIS, E. GIANNINI, M. KOZA, AND J. L. SAUVAJOL
Lattice dynamics of Sr_2TiO_4
Journal of Physics: Conference Series **92**, 012172 (2007).
Group: van der Marel / Project: 3
- F. CARBONE, A. B. KUZMENKO, H. J. A. MOLEGRAAF, E. VAN HEUMEN, E. GIANNINI, AND D. VAN DER MAREL
In-plane optical spectral weight transfer in optimally doped $Bi_2Sr_2Ca_2Cu_3O_{10}$
Physical Review B **74**, 024502 (2006).
Group: van der Marel / Projects: 2, 3
- F. CARBONE, A. B. KUZMENKO, H. J. A. MOLEGRAAF, E. VAN HEUMEN, V. LUKOVAC, F. MARSIGLIO, D. VAN DER MAREL, K. HAULE, G. KOTLIAR, H. BERGER, S. COURJAULT, P. H. KES, AND M. LI

- Doping dependence of the redistribution of optical spectral weight in $\text{Bi}_2\text{Sr}_2\text{CaCu}_2\text{O}_{8+\delta}$*
Physical Review B **74**, 064510 (2006).
Groups: van der Marel, Margaritondo / Projects: 2, 3
- F. CARBONE, M. ZANGRANDO, A. BRINKMAN, A. NICOLAOU, F. BONDINO, E. MAGNANO, A. A. NUGROHO, T. JARLBORG, F. PARMIGIANI, AND D. VAN DER MAREL
Electronic structure of MnSi: The role of electron-electron interactions
Physical Review B **73**, 085114 (2006).
Group: van der Marel / Project: 1
- J. DEISENHOFER, R. M. EREMINA, A. PIMENOV, T. GAVRILOVA, H. BERGER, M. JOHNSON, P. LEMMENS, H.-A. KRUG VON NIDDA, A. LOIDL, K.-S. LEE, AND M.-H. WHANGBO
Structural and magnetic dimers in the spin-gapped system CuTe_2O_5
Physical Review B **74**, 174421 (2006).
Groups: Margaritondo, van der Marel / Projects: 1, 3
- D. L. FENG, Z. X. SHEN, X. J. ZHOU, M. K. SHEN, D. H. LU, AND D. V. D. MAREL
Puzzles about 1/8 magic doping in cuprate
Journal of the Physics and Chemistry of Solids **67**, 198 (2006).
Group: van der Marel / Projects: 1, 2
- G. GOLL, M. MARZ, R. LORTZ, A. JUNOD, AND W. GOLDACKER
Observation of a second energy gap in Nb_3Sn break junctions
AIP Conference Proceedings **850**, 987 (2006).
Groups: Triscone, van der Marel / Project: 2
- C. GRIMALDI AND I. BALBERG
Tunneling and Nonuniversality in Continuum Percolation Systems
Physical Review Letters **96**, 066602 (2006).
Group: van der Marel / Project: 1
- C. GRIMALDI, E. CAPPELLUTI, AND F. MARSIGLIO
Off-Fermi surface cancellation effects in spin-Hall conductivity of a two-dimensional Rashba electron gas
Physical Review B **73**, 081303 (2006).
Group: van der Marel / Project: 1
- V. GURITANU, A. B. KUZMENKO, D. VAN DER MAREL, S. M. KAZAKOV, N. D. ZHIGADLO, AND J. KARPINSKI
Anisotropic optical conductivity and two colors of MgB_2
Physical Review B **73**, 104509 (2006).
Groups: Karpinski, van der Marel / Projects: 2, 3, 4
- M. KUGLER, G. L. DE CASTRO, E. GIANNINI, A. PIRIOU, A. A. MANUEL, C. HESS, AND Ø. FISCHER
Scanning tunneling spectroscopy on $\text{Bi}_2\text{Sr}_2\text{Ca}_2\text{Cu}_3\text{O}_{10+\delta}$ single crystals
Journal of the Physics and Chemistry of Solids **67**, 353 (2006).
Groups: van der Marel, Fischer / Project: 3
- R. LORTZ, F. LIN, N. MUSOLINO, Y. WANG, A. JUNOD, B. ROSENSTEIN, AND N. TOYOTA
Thermal fluctuations and vortex melting in the superconductor Nb_3Sn from high-resolution specific-heat experiments
Physical Review B **74**, 104502 (2006).
Groups: Triscone, van der Marel / Project: 2
- R. LORTZ, T. TOMITA, Y. WANG, A. JUNOD, J. S. SCHILLING, T. MASUI, AND S. TAJIMA
On the Origin of the Double Superconducting Transition in overdoped $\text{YBa}_2\text{Cu}_3\text{O}_x$
Physica C **194-198**, 434 (2006).
Groups: Triscone, van der Marel / Project: 2
- R. LORTZ, Y. WANG, U. TUTSCH, S. ABE, C. MEINGAST, P. POPOVICH, W. KNAFO, N. SHITSEVALOVA, Y. PADERNO, AND A. JUNOD
Superconductivity mediated by a soft phonon mode: specific heat and resistivity and thermal expansion and magnetization of YB_6
Physical Review B **73**, 024512 (2006).
Groups: Triscone, van der Marel / Project: 2
- D. VAN DER MAREL
Superconductors: Electrons living apart together
Nature Physics **2**, 585 (2006).
Group: van der Marel / Project: 2
- D. VAN DER MAREL, F. CARBONE, A. B. KUZMENKO, AND E. GIANNINI
Scaling properties of the optical conductivity of Bi-based cuprates
Annalen der Physik **321**, 1716 (2006).
Group: van der Marel / Project: 2
- F. MARSIGLIO
Sum rule anomaly from suppression of inelastic scattering in the superconducting state
Physical Review B **73**, 064507 (2006).
Group: van der Marel / Project: 2
- F. MARSIGLIO, F. CARBONE, A. B. KUZMENKO, AND D. VAN DER MAREL
Intraband optical spectral weight in the presence of a van Hove singularity: Application to $\text{Bi}_2\text{Sr}_2\text{CaCu}_2\text{O}_{8+\delta}$
Physical Review B **74**, 174516 (2006).
Group: van der Marel / Project: 2

F. P. MENA, J. F. DiTUSA, D. VAN DER MAREL, G. AEPPLI, D. P. YOUNG, A. DAMASCELLI, AND J. A. MYDOSH

Suppressed reflectivity due to spin-controlled localization in a magnetic semiconductor

Physical Review B **73**, 085205 (2006).

Group: van der Marel / Project: 1

► K. ROGACKI, B. BATLOGG, J. KARPINSKI, N. D. ZHIGADLO, G. SCHUCK, S. M. KAZAKOV, P. WAGLI, R. PUŻNIAK, A. WIŚNIEWSKI, F. CARBONE, A. BRINKMAN, AND D. VAN DER MAREL

Strong magnetic pair breaking in Mn-substituted MgB₂ single crystals

Physical Review B **73**, 174520 (2006).

Groups: Karpinski, van der Marel / Projects: 2, 3, 4

P. ROMANIELLO, P. L. DE BOEIJ, F. CARBONE, AND D. VAN DER MAREL

Optical properties of bcc transition metals in the range 0–40 eV

Physical Review B **73**, 075115 (2006).

Group: van der Marel / Project: 1

J. TEYSSIER, A. KUZMENKO, D. VAN DER MAREL, R. LORTZ, A. JUNOD, V. FILIPPOV, AND N. SHITSEVALOVA

Electronic and optical properties of ZrB₁₂ and YB₆. Discussion on electron-phonon coupling

Physica Status Solidi (c) **3**, 3114 (2006).

Group: van der Marel / Project: 2

E. GIANNINI, N. CLAYTON, N. MUSOLINO, A. PIRIOU, R. GLADYSHEVSKII, AND R. FLÜKIGER

Growth and superconducting properties of Pb-free and Pb-doped Bi-2223 crystals

IEEE Transactions on Applied Superconductivity **15**, 3102 (2005).

Groups: van der Marel, Flükiger / Project: 3

A. B. KUZMENKO

Kramers-Kronig constrained variational analysis of optical spectra

Review of Scientific Instruments **76**, 083108 (2005).

Group: van der Marel / Projects: 1, 2

A. B. KUZMENKO, H. J. A. MOLEGRAAF, F. CARBONE, AND D. VAN DER MAREL

Temperature-modulation analysis of superconductivity-induced transfer of in-plane spectral weight in Bi₂Sr₂CaCu₂O₈

Physical Review B **72**, 144503 (2005).

Group: van der Marel / Project: 2

R. LORTZ, S. ABE, Y. WANG, F. BOUQUET, U. TUTSCH, AND A. JUNOD

Modulated-bath AC calorimetry using modified commercial Peltier elements

Review of Scientific Instruments **76**, 103902 1 (2005).

Groups: Triscone, van der Marel / Project: 2

R. LORTZ, A. JUNOD, D. JACCARD, Y. WANG, S. TAJIMA, AND T. MASUI

Evolution of the specific-heat anomaly of the high-temperature superconductor YBa₂Cu₃O₇ under influence of charge transfer through application of high pressure up to 10 GPa

Journal of Physics: Condensed Matter **17**, 4135 (2005).

Groups: Triscone, van der Marel / Project: 2

R. LORTZ, Y. WANG, S. ABE, C. MEINGAST, Y. PADERNO, V. FILIPPOV, AND A. JUNOD

Specific heat and magnetic susceptibility and resistivity and thermal expansion of the superconductor ZrB₁₂

Physical Review B **72**, 024547 (2005).

Groups: Triscone, van der Marel / Project: 2

► F. P. MENA, A. B. KUZMENKO, A. HADIPOUR, J. L. M. VAN MECHELEN, D. VAN DER MAREL, AND N. A. BABUSHKINA

Oxygen isotope effect and phase separation in the optical conductivity of (La_{0.5}Pr_{0.5})_{0.7}Ca_{0.3}MnO₃ thin films

Physical Review B **72**, 134422 (2005).

Group: van der Marel / Projects: 1, 5

F. P. MENA, D. VAN DER MAREL, AND J. L. SARRAO

Optical conductivity of CeMIn₅ (M = Co, Rh, Ir)

Physical Review B **72**, 045119 (2005).

Group: van der Marel / Projects: 1, 2

T. PLACKOWSKI, Y. WANG, R. LORTZ, A. JUNOD, AND T. WOLF

Reversible and irreversible magnetocaloric effect in the NdBa₂Cu₃O₇ superconductor in relation with specific heat and magnetization

Journal of Physics: Condensed Matter **17**, 6871 (2005).

Groups: Triscone, van der Marel / Project: 2

X. SU, E. GIANNINI, AND R. FLÜKIGER

Improvement of the critical current density of Bi-2223 tapes by introducing Ag Layers inside individual filaments

Superconductor Science & Technology **18**, 830 (2005).

Groups: Flükiger, van der Marel / Project: 6

Y. WANG, R. LORTZ, Y. PADERNO, V. FILIPPOV, S. ABE, U. TUTSCH, AND A. JUNOD

Specific heat and magnetization of a ZrB_{12} single crystal: characterization of a type II/1 superconductor

Physical Review B **72**, 024548 (2005).

Groups: Triscone, van der Marel / Project: 2

Group of G. Margaritondo

D. ARCON, A. ZORKO, M. PREGELJ, J. DOLINSEK, H. BERGER, A. OZAROWSKI, H. VAN TOOL, AND L. C. BRUNEL

High field ESR in a two-dimensional $S = 1$ spin system $Ni_5(TeO_3)_4Br_2$

Journal of Magnetism and Magnetic Materials **316**, E349 (2007).

Group: Margaritondo / Project: 3

D. ARIOSA, C. CANCELLIERI, P. H. LIN, AND D. PAVUNA

Self ordering of random intercalates in thin films of cuprate superconductors: Growth model and x-ray diffraction diagnosis

Physical Review B **75**, 184505 (2007).

Group: Margaritondo / Project: 5

C. BATTAGLIA, H. CERCELLIER, L. DESPONT, C. MONNEY, M. PRESTER, H. BERGER, L. FORRÓ, M. G. GARNIER, AND P. AEBI

Non-uniform doping across the Fermi surface of NbS_2 intercalates

The European Physical Journal B **57**, 385 (2007).

Groups: Aebi, Margaritondo, Forró / Projects: 1, 3

R. BECKER, H. BERGER, AND M. JOHNSON
Monoclinic $Cu_3(SeO_3)_2Cl_2$: an oxohalide with an unusual CuO_4Cl trigonal-bipyramidal coordination

Acta Crystallographica C **63**, i4 (2007).

Group: Margaritondo / Project: 3

R. BECKER, M. JOHNSON, AND H. BERGER
Crystal Structure of the New Cobalt Tellurite Chloride $Co_5Te_4O_{11}Cl_4$

Zeitschrift für Anorganische und Allgemeine Chemie **633**, 422 (2007).

Group: Margaritondo / Project: 3

R. BECKER, M. PRESTER, H. BERGER, M. JOHNSON, D. DROBAC, AND I. ZIVKOVIC
Crystal structure and magnetic properties of the new cobalt tellurite halide $Co_5(TeO_3)_4X_2$ ($X = Cl, Br$)

Solid State Sciences **9**, 223 (2007).

Group: Margaritondo / Project: 3

R. BECKER, M. PRESTER, H. BERGER, P. H. LIN, M. JOHNSON, D. DROBAC, AND

I. ZIVKOVIC

Crystal structure and magnetic properties of two new cobalt selenite halides $Co_5(SeO_3)_4X_2$ ($X = Cl, Br$)

Journal of Solid State Chemistry **180**, 1051 (2007).

Group: Margaritondo / Project: 3

C. CANCELLIERI, P.-H. LIN, D. ARIOSA, AND D. PAVUNA

Dopant rearrangement and superconductivity in $Bi_2Sr_{2-x}La_xCuO_6$ thin films under annealing

Journal of Physics: Condensed Matter **19**, 246214 (2007).

Group: Margaritondo / Project: 5

▶ H. CERCELLIER, C. MONNEY, F. CLERC, C. BATTAGLIA, L. DESPONT, M. G. GARNIER, H. BECK, P. AEBI, L. PATTHEY, H. BERGER, AND L. FORRÓ

Evidence for an Excitonic Insulator Phase in $1T-TiSe_2$

Physical Review Letters **99**, 146403 (2007).

Groups: Aebi, Margaritondo, Forró / Projects: 1, 3

F. CLERC, C. BATTAGLIA, H. CERCELLIER, C. MONNEY, H. BERGER, L. DESPONT, M. G. GARNIER, AND P. AEBI

Fermi surface of layered compounds and bulk charge density wave systems

Journal of Physics: Condensed Matter **19**, 335002 (2007).

Groups: Aebi, Margaritondo / Projects: 1, 3

P. FAZEKAS, N. BARISIC, I. KEZSMARKI, L. DEMKO, H. BERGER, L. FORRÓ, AND G. MIHALY

Magnetic-field-induced transition in $BaVS_3$

Physical Review B **75**, 035128 (2007).

Groups: Margaritondo, Forró / Projects: 1, 3

P. FAZEKAS, K. PENC, K. RADNÓCZI, N. BARIŠIĆ, H. BERGER, L. FORRÓ, S. MITROVIĆ, A. GAUZZI, L. DEMKÓ, I. KÉZSMÁRKI, AND G. MIHÁLY

The electronic structure and the phases of $BaVS_3$

Journal of Magnetism and Magnetic Materials **310**, 928 (2007).

Groups: Margaritondo, Forró / Project: 3

L. V. GASPAROV, K.-Y. CHOI, G. GÜNTHERODT, H. BERGER, AND L. FORRÓ

Electronic Raman scattering in magnetite

Journal of Applied Physics **101**, 09G108 (2007).

Groups: Margaritondo, Forró / Project: 3

- ▶ J. GECK, S. V. BORISENKO, H. BERGER, H. ESCHRIG, J. FINK, M. KNUPFER, K. KOEPERNIK, A. KOITZSCH, A. A. KORDYUK, V. B. ZABOLOTNYY, AND B. BÜCHNER
Anomalous Quasiparticle Renormalization in $\text{Na}_{0.73}\text{CoO}_2$: Role of Interorbital Interactions and Magnetic Correlations
Physical Review Letters **99**, 046403 (2007).
Group: Margaritondo / Project: 3
- C. L. HUANG, J. Y. LIN, Y. T. CHANG, C. P. SUN, H. Y. SHEN, C. C. CHOU, H. BERGER, T. K. LEE, AND H. D. YANG
Experimental evidence for a two-gap structure of superconducting NbSe_2 : A specific-heat study in external magnetic fields
Physical Review B **76**, 212504 (2007).
Group: Margaritondo / Project: 3
- D. S. INOSOV, S. V. BORISENKO, I. EREMIN, A. A. KORDYUK, V. B. ZABOLOTNYY, J. GECK, A. KOITZSCH, J. FINK, M. KNUPFER, B. BÜCHNER, H. BERGER, AND R. FOLLATH
Relation between the one-particle spectral function and dynamic spin susceptibility of superconducting $\text{Bi}_2\text{Sr}_2\text{CaCu}_2\text{O}_{8-\delta}$
Physical Review B **75**, 172505 (2007).
Group: Margaritondo / Project: 3
- ▶ D. S. INOSOV, J. FINK, A. A. KORDYUK, S. V. BORISENKO, V. B. ZABOLOTNYY, R. SCHUSTER, M. KNUPFER, B. BÜCHNER, R. FOLLATH, H. A. DÜRR, W. EBERHARDT, V. HINKOV, B. KEIMER, AND H. BERGER
Momentum and energy dependence of the anomalous high-energy dispersion in the electronic structure of high temperature superconductors
Physical Review Letters **99**, 237002 (2007).
Group: Margaritondo / Project: 3
- E. E. KRASOVSKII, V. N. STROCOV, N. BARRATT, H. BERGER, W. SCHATTKE, AND R. CLAESSEN
Band mapping in the one-step photoemission theory: Multi-Bloch-wave structure of final states and interference effects
Physical Review B **75**, 045432 (2007).
Group: Margaritondo / Project: 3
- T. KROLL, A. A. ALIGIA, M. KNUPFER, J. GECK, C. HESS, T. SCHWIEGER, G. KRABBES, C. SEKAR, D. R. BATCHELOR, H. BERGER, G. A. SAWATZKY, AND B. BÜCHNER
Spectroscopic investigations on layered sodium cobaltates
Physica C **460-462**, 487 (2007).
Group: Margaritondo / Project: 3
- I. KÉZSMÁRKI, R. GAÁL, C. C. HOMES, B. SÍPOS, H. BERGER, S. BORDÁCS, G. MIHÁLY, AND L. FORRÓ
High-pressure infrared spectroscopy: tuning of the low-energy excitations in correlated electron systems
Physical Review B **76**, 205114 (2007).
Groups: Margaritondo, Forró / Projects: 1, 3
- M. MILJAK, R. BECKER, M. HERAK, M. PRESTER, O. MILAT, M. JOHNSON, AND H. BERGER
A new modification of nickel selenite NiSeO_3 — crystal structure and magnetic properties
Journal of Physics: Condensed Matter **19**, 196203 (2007).
Group: Margaritondo / Project: 3
- S. MITROVIC, P. FAZEKAS, C. SÖNDERGAARD, D. ARIOSA, N. BARISIC, H. BERGER, D. CLOETTA, L. FORRÓ, H. HÖCHST, I. KUPCIC, D. PAVUNA, AND G. MARGARITONDO
Experimental electronic structure and Fermi-surface instability of the correlated 3d sulphide BaVS_3 : High-resolution angle-resolved photoemission spectroscopy
Physical Review B **75**, 153103 (2007).
Groups: Margaritondo, Forró / Projects: 1, 3
- D. PACILÉ, M. PAPAGNO, M. LAVAGNINI, H. BERGER, L. DEGIORGI, AND M. GRIONI
Photoemission and optical studies of ZrSe_3 , HfSe_3 , and ZrS_3
Physical Review B **76**, 155406 (2007).
Groups: Margaritondo, Degiorgi, Grioni / Projects: 1, 3
- M. PREGELJ, A. ZORKO, H. BERGER, H. VAN TOL, L. C. BRUNEL, A. OZAROWSKI, S. NELLUTLA, Z. JAGLIČIČ, O. ZAHARKO, P. TREGENNA-PIGGOTT, AND D. ARČON
Magnetic structure of the $S = 1 \text{Ni}_5(\text{TeO}_3)_4\text{Br}_2$ layered system governed by magnetic anisotropy
Physical Review B **76**, 144408 (2007).
Group: Margaritondo / Project: 3
- ▶ R. SCHUSTER, M. KNUPFER, AND H. BERGER
Exciton band structure of pentacene molecular solids: Breakdown of the frenkel exciton model
Physical Review Letters **98**, 037402 (2007).
Group: Margaritondo / Project: 3
- R. SCHUSTER, M. KNUPFER, D. R. ZAHN, AND H. BERGER
Anisotropic dynamic response of pentacene single crystals

- The European Physical Journal B **59**, 25 (2007).
Group: Margaritondo / Project: 3
- F. SOTO, H. BERGER, L. CABO, C. CARBALLEIRA, J. MOSQUEIRA, D. PAVUNA, P. TOIMIL, AND F. VIDAL
Electric and magnetic characterization of NbSe₂ single crystals: Anisotropic superconducting fluctuations above T_c
Physica C **460-462**, 789 (2007).
Group: Margaritondo / Project: 3
- F. SOTO, H. BERGER, L. CABO, C. CARBALLEIRA, J. MOSQUEIRA, D. PAVUNA, AND F. VIDAL
In-plane and transverse superconducting fluctuation diamagnetism in the presence of charge-density waves in 2H-NbSe₂ single crystals
Physical Review B **75**, 094509 (2007).
Group: Margaritondo / Project: 3
- D. STOLTZ, M. BIELMANN, M. BOVET, L. SCHLAPBACH, AND H. BERGER
Tunneling evidence for spatial location of the charge-density-wave induced band splitting in 1T-TaSe₂
Physical Review B **76**, 073410 (2007).
Groups: Margaritondo, Schlapbach / Project: 3
- V. B. ZABOLOTNYY, S. V. BORISENKO, A. A. KORDYUK, J. FINK, J. GECK, A. KOITZSCH, M. KNUPFER, B. BÜCHNER, H. BERGER, A. ERB, C. T. LIN, B. KEIMER, AND R. FOLLATH
Effect of Zn and Ni impurities on the quasiparticle renormalization in Bi₂Sr₂CaCu₂O_{8+δ}
Physica C **460-462**, 882 (2007).
Group: Margaritondo / Project: 3
- V. B. ZABOLOTNYY, S. V. BORISENKO, A. A. KORDYUK, J. GECK, D. S. INOSOV, A. KOITZSCH, J. FINK, M. KNUPFER, B. BÜCHNER, S.-L. DRECHSLER, H. BERGER, A. ERB, M. LAMBACHER, L. PATTHEY, V. HINKOV, AND B. KEIMER
Momentum and temperature dependence of renormalization effects in the high-temperature superconductor YBa₂Cu₃O_{7-δ}
Physical Review B **76**, 064519 (2007).
Group: Margaritondo / Project: 3
- A. ZORKO, D. ARCON, J. DOLINSEK, Z. JAGLICIC, A. JEROMEN, H. VAN TOL, L. C. BRUNEL, AND H. BERGER
Magnetism in the novel spin system Ni₅(TeO₃)₄Br₂ with two-dimensional frustrated geometry
Journal of Physics: Condensed Matter **19**, 145278 (2007).
Group: Margaritondo / Project: 3
- R. BECKER AND H. BERGER
Cu₂CoTeO₆
Acta Crystallographica E **62**, i261 (2006).
Group: Margaritondo / Project: 3
- R. BECKER AND H. BERGER
Reinvestigation of CuSe₂O₅
Acta Crystallographica E **62**, i256 (2006).
Group: Margaritondo / Project: 3
- R. BECKER AND H. BERGER
Reinvestigation of Ni₃TeO₆
Acta Crystallographica E **62**, i222 (2006).
Group: Margaritondo / Project: 3
- R. BECKER, H. BERGER, M. JOHNSON, M. PRESTER, Z. MAROHNIC, M. MILJAK, AND M. HERAK
Crystal structure and magnetic properties of Co₂TeO₃Cl₂ and Co₂TeO₃Br₂
Journal of Solid State Chemistry **179**, 836 (2006).
Group: Margaritondo / Project: 3
- R. BECKER, M. JOHNSON, AND H. BERGER
A new synthetic cobalt tellurate: Co₃TeO₆
Acta Crystallographica C **62**, I67 (2006).
Group: Margaritondo / Project: 3
- R. BECKER, M. JOHNSON, H. BERGER, M. PRESTER, I. ZIVKOVIC, D. DROBAC, M. MILJAK, AND M. HERAK
Crystal structure and magnetic properties of Co₇(TeO₃)₄Br₆ – A new cobalt tellurite bromide
Solid State Sciences **8**, 836 (2006).
Group: Margaritondo / Project: 3
- M. BIMBI, G. ALLODI, R. DE RENZI, G. MAZZOLI, H. BERGER, AND A. AMATO
The Verwey transition in Fe₃O₄: A single crystal muon investigation
Physica B **374**, 51 (2006).
Group: Margaritondo / Project: 3
- S. V. BORISENKO, A. A. KORDYUK, A. KOITZSCH, J. FINK, J. GECK, V. ZABOLOTNYY, M. KNUPFER, B. BÜCHNER, H. BERGER, M. FALUB, M. SHI, J. KREMPASKY, AND L. PATTHEY
Parity of the pairing bosons in a high-temperature Pb-Bi₂Sr₂CaCu₂O₈ bilayer superconductor by angle-resolved photoemission spectroscopy
Physical Review Letters **96**, 067001 (2006).
Group: Margaritondo / Project: 3
- G. CAIMI, L. DEGIORGI, H. BERGER, AND L. FORRÓ

- Optical evidence for a magnetically driven structural transition in the spin web Cu_3TeO_6*
 Europhysics Letters **75**, 496 (2006).
 Groups: Margaritondo, Degiorgi, Forró / Projects: 1, 3
- G. CAIMI, L. DEGIORGI, H. BERGER, AND L. FORRÓ
Phonon analysis of the $S = 1$ quantum spin systems $\text{Ni}_5\text{Te}_4\text{O}_{12}\text{X}_2$ ($X = \text{Cl}$ and Br)
 Journal of Physics: Condensed Matter **18**, 4065 (2006).
 Groups: Margaritondo, Degiorgi, Forró / Projects: 1, 3
- F. CARBONE, A. B. KUZMENKO, H. J. A. MOLEGRAAF, E. VAN HEUMEN, V. LUKOVAC, F. MARSIGLIO, D. VAN DER MAREL, K. HAULE, G. KOTLIAR, H. BERGER, S. COURJAULT, P. H. KES, AND M. LI
Doping dependence of the redistribution of optical spectral weight in $\text{Bi}_2\text{Sr}_2\text{CaCu}_2\text{O}_{8+\delta}$
 Physical Review B **74**, 064510 (2006).
 Groups: van der Marel, Margaritondo / Projects: 2, 3
- F. CLERC, C. BATTAGLIA, M. BOVET, L. DESPONT, C. MONNEY, H. CERCELLIER, M. GARNIER, P. AEBI, H. BERGER, AND L. FORRÓ
Lattice-distortion-enhanced electron-phonon coupling and Fermi surface nesting in 1T-TaS_2
 Physical Review B **74**, 155114 (2006).
 Groups: Margaritondo, Aebi, Forró / Projects: 1, 2, 3
- D. CLOETTA, D. ARIOSA, C. CANCELLIERI, M. ABRECHT, M. S., AND D. PAVUNA
Three-dimensional dispersion induced by extreme tensile strain in $\text{La}_{2-x}\text{Sr}_x\text{CuO}_4$ films
 Physical Review B **74**, 014519 (2006).
 Group: Margaritondo / Project: 5
- S. COLONNA, F. RONCI, A. CRICENTI, L. PERFETTI, H. BERGER, AND M. GRIONI
Scanning tunneling microscopy observation of a mott-insulator phase at the 1T-TaSe_2 surface
 Japanese Journal of Applied Physics **45**, 1950 (2006).
 Groups: Margaritondo, Grioni / Projects: 1, 3
- S. J. CROWE, M. R. LEES, D. M. K. PAUL, R. I. BEWELY, J. TAYLOR, G. MCINTYRE, O. ZAHARKO, AND H. BERGER
Effect of externally applied pressure on the magnetic behavior of $\text{Cu}_2\text{Te}_2\text{O}_5(\text{Br}_x\text{Cl}_{1-x})_2$
 Physical Review B **73**, 144410 (2006).
 Groups: Mesot, Margaritondo / Projects: 1, 3, 6
- J. DEISENHOFER, R. M. EREMINA, A. PIMENOV, T. GAVRILOVA, H. BERGER, M. JOHNSON, P. LEMMENS, H.-A. KRUG VON NIDDA, A. LOIDL, K.-S. LEE, AND M.-H. WHANGBO
Structural and magnetic dimers in the spin-gapped system CuTe_2O_5
 Physical Review B **74**, 174421 (2006).
 Groups: Margaritondo, van der Marel / Projects: 1, 3
- L. DESPONT, F. CLERC, M. G. GARNIER, H. BERGER, L. FORRÓ, AND P. AEBI
Multiple scattering investigation of the 1T-TaS_2 surface termination
 The European Physical Journal B **52**, 421 (2006).
 Groups: Aebi, Margaritondo, Forró / Projects: 3, 5
- D. V. EVTUSHINSKY, A. A. KORDYUK, S. V. BORISENKO, V. B. ZABOLOTNYY, M. KNUPFER, J. FINK, B. BÜCHNER, A. PAN, A. ERB, C. T. LIN, AND H. BERGER
Unadulterated spectral function of low-energy quasiparticles in $\text{Bi}_2\text{Sr}_2\text{CaCu}_2\text{O}_{8+\delta}$
 Physical Review B **74**, 172509 (2006).
 Group: Margaritondo / Project: 3
- J. FINK, A. KOITZSCH, J. GECK, V. ZABOLOTNYY, M. KNUPFER, B. BÜCHNER, A. CHUBUKOV, AND H. BERGER
Reevaluation of the coupling to a bosonic mode of the charge carriers in $(\text{Bi}, \text{Pb})_2\text{Sr}_2\text{CaCu}_2\text{O}_{8+\delta}$ at the antinodal point
 Physical Review B **74**, 165102 (2006).
 Group: Margaritondo / Project: 3
- J. GECK, M. V. ZIMMERMANN, H. BERGER, S. V. BORISENKO, H. ESCHRIG, K. KOEPERNIK, M. KNUPFER, AND B. BÜCHNER
Stripe correlations in $\text{Na}_{0.75}\text{CoO}_2$
 Physical Review Letters **97**, 106403 (2006).
 Group: Margaritondo / Project: 3
- M. GROBOSCH, R. SCHUSTER, T. PICHLER, M. KNUPFER, AND H. BERGER
Analysis of the anisotropy of excitons in pentacene single crystals using reflectivity measurements and electron energy-loss spectroscopy
 Physical Review B **74**, 155202 (2006).
 Group: Margaritondo / Project: 3
- Z. JAGLIČIĆ, J. DOLINŠEK, A. BILUŠIĆ, A. SMONTARA, Z. TRONTELJ, AND H. BERGER
Searching for magnetic frustration-like properties in tetrahedral spin systems $\text{Cu}_2\text{Te}_2\text{O}_5(\text{Br}_{1-x}\text{Cl}_x)_2$
 Physica B **382**, 209 (2006).
 Group: Margaritondo / Project: 3
- Z. JAGLIČIĆ, S. EL SHAWISH, A. JEROMEN, A. BILUŠIĆ, A. SMONTARA, Z. TRONTELJ, J. BONČA, J. DOLINŠEK, AND H. BERGER

- Magnetic ordering and ergodicity of the spin system in the $\text{Cu}_2\text{Te}_2\text{O}_5\text{X}_2$ family of quantum magnets*
Physical Review B **73**, 214408 (2006).
Group: Margaritondo / Project: 3
- M. KNUPFER AND H. BERGER
Dispersion of electron-hole excitations in pentacene along (100)
Chemical Physics **325**, 92 (2006).
Group: Margaritondo / Project: 3
- ▶ A. KOHEN, T. PROSLIER, T. CREN, Y. NOAT, W. SACKS, H. BERGER, AND D. RODITCHEV
Probing the superfluid velocity with a superconducting tip: the Doppler shift effect
Physical Review Letters **97**, 027001 (2006).
Group: Margaritondo / Project: 3
- A. A. KORDYUK, S. V. BORISENKO, A. KOITZSCH, J. FINK, M. KNUPFER, B. BÜCHNER, AND H. BERGER
Life of the nodal quasiparticles in Bi-2212 as seen by ARPES
Journal of the Physics and Chemistry of Solids **67**, 201 (2006).
Group: Margaritondo / Project: 3
- ▶ A. KORDYUK, S. V. BORISENKO, V. B. ZABOLOTNYY, J. GECK, M. KNUPFER, J. FINK, B. BÜCHNER, C. T. LIN, B. KEIMER, H. BERGER, A. PAN, S. KOMIYA, AND Y. ANDO
Constituents of the quasiparticle spectrum along the nodal direction of high- T_c cuprates
Physical Review Letters **97**, 017002 (2006).
Group: Margaritondo / Project: 3
- T. KROLL, M. KNUPFER, J. GECK, C. HESS, T. SCHWIEGER, G. KRABBES, C. SEKAR, D. R. BATCHELOR, H. BERGER, AND B. BÜCHNER
X-ray absorption spectroscopy of Na_xCoO_2 layered cobaltates
Physical Review B **74**, 115123 (2006).
Group: Margaritondo / Project: 3
- ▶ I. KÉZSMÁRKI, G. MIHÁLY, R. GAÁL, N. BARIŠIĆ, A. AKRAP, H. BERGER, L. FORRÓ, C. C. HOMES, AND L. MIHÁLY
Separation of orbital contributions to the optical conductivity of BaVS_3
Physical Review Letters **96**, 186402 (2006).
Groups: Margaritondo, Forró / Projects: 1, 3
- H. L. LIU, M. QUIJADA, D. B. ROMERO, D. B. TANNER, A. ZIBOLD, G. L. CARR, H. BERGER, L. FORRÓ, L. MIHALY, G. CAO, B.-H. O, J. T. MARKERT, J. P. RICE, M. J. BURNS, AND K. A. DELIN
Drude behavior in the far-infrared conductivity of cuprate superconductors
Annalen der Physik **15**, 606 (2006).
Groups: Margaritondo, Forró / Project: 3
- ▶ A. MANS, I. SANTOSO, Y. HUANG, W. K. SIU, S. TAVADDOD, V. ARPIAINEN, M. LINDROSS, H. BERGER, V. N. STROCOV, M. SHI, L. PATTHEY, AND M. S. GOLDEN
Experimental Proof of a Structural Origin for the Shadow Fermi Surface of $\text{Bi}_2\text{Sr}_2\text{CaCu}_2\text{O}_{8+\delta}$
Physical Review Letters **96**, 107007 (2006).
Group: Margaritondo / Project: 3
- L. MIHÁLY, T. FEHÉR, B. DÓRA, B. NÁFRÁDI, H. BERGER, AND L. FORRÓ
Spin resonance in the ordered magnetic state of $\text{Ni}_5(\text{TeO}_3)_4\text{Cl}_2$
Physical Review B **74**, 174403 (2006).
Groups: Margaritondo, Forró / Projects: 1, 3
- ▶ L. MIHÁLY, B. DÓRA, A. VÁNYOLOS, H. BERGER, AND L. FORRÓ
Spin-Lattice Interaction in the Quasi-One-Dimensional Helimagnet LiCu_2O_2
Physical Review Letters **97**, 067206 (2006).
Groups: Margaritondo, Forró / Projects: 1, 3
- M. PAPAGNO, D. PACILÉ, G. CAIMI, H. BERGER, L. DEGIORGI, AND M. GRIONI
Electronic structure of one-dimensional copper oxide chains in LiCu_2O_2 from angle-resolved photoemission and optical spectroscopy
Physical Review B **73**, 115120 (2006).
Groups: Margaritondo, Degiorgi, Grioni / Projects: 1, 3
- ▶ L. PERFETTI, P. LOUKAKOS, M. LISOWSKI, U. BOVENSIEPEN, H. BERGER, S. BIERMANN, P. S. CORNAGLIA, A. GEORGES, AND M. WOLF
Time evolution of the electronic structure of 1T-TaS_2 through the insulator-metal transition
Physical Review Letters **97**, 067402 (2006).
Group: Margaritondo / Project: 3
- V. N. STROCOV, E. E. KRASOVSKII, W. SCHATTKE, N. BARRETT, H. BERGER, D. SCHRUPP, AND R. CLAESSEN
Three-dimensional band structure in layered TiTe_2 : Photoemission final-state effects
Physical Review B **74**, 195125 (2006).
Group: Margaritondo / Project: 3
- ▶ V. B. ZABOLOTNYY, S. V. BORISENKO, A. A. KORDYUK, J. FINK, J. GECK, A. KOITZSCH, M. KNUPFER, B. BÜCHNER, H. BERGER, A. ERB, C. T. LIN, B. KEIMER, AND R. FOLLATH

Effect of Zn and Ni impurities on the quasi-particle renormalization of superconducting Bi-2212

Physical Review Letters **96**, 037003 (2006).

Group: Margaritondo / Project: 3

O. ZAHARKO, H. RØNNOW, J. MESOT, S. CROWE, D. PAUL, P. BROWN, A. DAOUD-ALADINE, A. MEENTS, A. WAGNER, M. PRESTER, AND H. BERGER

Incommensurate magnetic ordering in $\text{Cu}_2\text{Te}_2\text{O}_5\text{X}_2$ ($\text{X} = \text{Cl}, \text{Br}$) studied by single crystal neutron diffraction

Physical Review B **73**, 064422 (2006).

Groups: Margaritondo, Mesot / Projects: 2, 3

C. BATTAGLIA, H. CERCELLIER, F. CLERC, L. DESPONT, M. G. GARNIER, C. KOITZSCH, P. AEBI, H. BERGER, L. FORRÓ, AND C. AMBROSCH-DRAXL

Fermi surface induced lattice distortion in NbTe_2

Physical Review B **72**, 195114 (2005).

Groups: Margaritondo, Aebi, Forró / Projects: 1, 3

► S. COLONNA, F. RONCI, A. CRICENTI, L. PERFETTI, H. BERGER, AND M. GRIONI

Mott phase at the surface of 1T-TaSe_2 observed by scanning tunneling microscopy

Physical Review Letters **94**, 036405 (2005).

Groups: Margaritondo, Grioni / Project: 3

L. V. GASPAROV, D. ARENAS, K.-Y. CHOI, G. GÜNTHERODT, H. BERGER, L. FORRÓ, G. MARGARITONDO, V. V. STRUZHKIN, AND R. HEMLEY

Magnetite: Raman study of the high-pressure and low-temperature effects

Journal of Applied Physics **97**, 10A922 (2005).

Groups: Margaritondo, Forró / Project: 3

M. GRIONI, C. R. AST, D. PACILE, M. PAPANAGNO, H. BERGER, AND L. PERFETTI

Photoemission as a probe of coexisting and conflicting periodicities in low-dimensional solids

New Journal of Physics **7**, 106 (2005).

Groups: Margaritondo, Grioni / Projects: 1, 3

M. HERAK, H. BERGER, M. PRESTER, M. MILJAK, I. ZIVKOVIC, O. MILAT, D. DROBAC, S. POPOVIC, AND O. ZAHARKO

Novel spin lattice in Cu_3TeO_6 : an antiferromagnetic order and domain dynamics

Journal of Physics: Condensed Matter **17**, 7667 (2005).

Groups: Margaritondo, Mesot / Projects: 1, 3

A. A. KORDYUK, S. V. BORISENKO, A. KOITZSCH, J. FINK, M. KNUPFER, AND H. BERGER

Bare electron dispersion from experiment: Self-consistent self-energy analysis of photoemission data

Physical Review B **71**, 214513 (2005).

Group: Margaritondo / Project: 3

I. KÉZSMÁRKI, G. MIHÁLY, R. GAÁL, N. BARIŠIĆ, H. BERGER, L. FORRÓ, C. C. HOMES, AND L. MIHÁLY

Pressure-induced suppression of the spin-gapped insulator phase in BaVS_3 : An infrared optical study

Physical Review B **71**, 193103 (2005).

Groups: Margaritondo, Forró / Project: 3

L. PERFETTI, T. A. GLOOR, F. MILA, H. BERGER, AND M. GRIONI

Unexpected periodicity in the quasi-two-dimensional Mott insulator 1T-TaS_2 revealed by angle-resolved photoemission

Physical Review B **71**, 153101 (2005).

Groups: Margaritondo, Mila, Grioni / Projects: 1, 3

A. PERUCCHI, L. DEGIORGI, AND H. BERGER

Infrared signature of the charge-density-wave gap in ZrTe_3

The European Physical Journal B **48**, 489 (2005).

Groups: Margaritondo, Degiorgi / Project: 3

D. POPOVIC, M. BOVET, H. BERGER, AND P. AEBI

Fingerprinting substitution sites in $\text{Pb}, \text{Dy-Bi}_2\text{Sr}_2\text{Ca}_1\text{Cu}_2\text{O}_{8+\delta}$ using X-ray Photoelectron Diffraction

The European Physical Journal – Applied Physics **30**, 171 (2005).

Groups: Aebi, Margaritondo / Projects: 2, 3

A. SMONTARA, A. BILUSIC, Z. JAGLICIC, A. ZORKO, J. DOLINSEK, AND H. BERGER

Anomalous thermal conductivity of single crystal $\text{Cu}_2\text{Te}_2\text{O}_5\text{Cl}_2$

Applied Magnetic Resonance **29**, 261 (2005).

Group: Margaritondo / Project: 3

O. ZAHARKO, H. M. RØNNOW, A. DAOUD-ALADINE, S. STREULE, F. JURANYI, J. MESOT, H. BERGER, AND P. BROWN

Incommensurate magnetism in the coupled spin tetrahedra system $\text{Cu}_2\text{Te}_2\text{O}_5\text{Cl}_2$

Low Temperature Physics **31**, 814 (2005).

Groups: Mesot, Margaritondo / Projects: 1, 3

O. ZAHARKO, H. M. RØNNOW, A. DAOUD-ALADINE, S. STREULE, F. JURANYI, J. MESOT, H. BERGER, AND P. J. BROWN

Incommensurate magnetism in the coupled spin tetrahedra system $\text{Cu}_2\text{Te}_2\text{O}_5\text{Cl}_2$

Fizika Nizkikh Temperatur **31**, 1068 (2005).

Groups: Margaritondo, Mesot / Projects: 1, 3

Group of J. Mesot

- ▶ A. D. BIANCHI, M. KENZELMANN, L. DEBEER-SCHMITT, J. S. WHITE, E. M. FORGAN, J. MESOT, M. ZOLLIKER, J. KOHLBRECHER, R. MOVSHOVICH, E. D. BAUER, J. L. SARRAO, Z. FISK, C. PETROVIC, AND M. R. ESKILDSEN
Superconducting Vortices in CeCoIn₅: Toward the Pauli-Limiting Field
Science **319**, 177 (2008).
Group: Mesot / Project: 2
- ▶ M. GARCÍA-FERNAÁNDEZ, U. STAUB, Y. BODENTHIN, S. M. LAWRENCE, A. M. MULDER, C. E. BUCKLEY, S. WEYENETH, E. POMJAKUSHINA, AND K. CONDER
Resonant soft x-ray powder diffraction study to determine the orbital ordering in A-site ordered SmBaMn₂O₆
Physical Review B **77**, 060402 (2008).
Group: Mesot / Project: 3
- T. GIAMARCHI, C. RÜEGG, AND O. TCHERNYSHYOV
Bose-Einstein Condensation in Magnetic Insulators
Nature Physics **4**, 198 (2008).
Groups: Giamarchi, Mesot / Project: 1
- ▶ C. RÜEGG, B. NORMAND, M. MATSUMOTO, A. FÜRER, D. MCMORROW, K. KRÄMER, H.-U. GÜDEL, S. N. GVASALIYA, H. MUTKA, AND M. BOEHM
Pressure-induced quantum phase transition in the spin-liquid TICuCl₃
Physical Review Letters (2008).
Group: Mesot / Project: 1
- M. STINGACIU, E. POMJAKUSHINA, H. GRIMMER, M. TROTTMANN, AND K. CONDER
Crystal Growth of Tb_{0.9}Dy_{0.1}BaCo₂O_{5+δ} using travelling solvent floating zone method
Journal of Crystal Growth **310**, 1239 (2008).
Group: Mesot / Project: 3
- ▶ J. CHANG, S. PAILHÉS, M. SHI, M. MANSOON, T. CLAESSON, O. TJERNBERG, J. VOIGT, V. PEREZ, L. PATTHEY, N. MOMONO, M. ODA, M. IDO, A. SCHNYDER, C. MUDRY, AND J. MESOT
When low- and high-energy electronic responses meet in cuprate superconductors
Physical Review B **75**, 224508 (2007).
Group: Mesot / Project: 2
- ▶ J. CHANG, A. P. SCHNYDER, R. GILARDI, H. M. RØNNOW, S. PAILHES, N. B. CHRISTENSEN, C. NIEDERMAYER, D. F. MCMORROW, A. HIESS, A. STUNAUT, M. ENDERLE, B. LAKE, O. SOBOLEV, N. MOMONO, M. ODA, M. IDO, C. MUDRY, AND J. MESOT
Magnetic-Field-Induced Spin Excitations and Renormalized Spin Gap of the Underdoped La_{1.895}Sr_{0.105}CuO₄ Superconductor
Physical Review Letters **98**, 077004 (2007).
Group: Mesot / Projects: 1, 3, 6
- N. B. CHRISTENSEN, H. M. RØNNOW, D. F. MCMORROW, A. HARRISON, T. G. PERRING, M. ENDERLE, R. COLDEA, L. P. REGNAULT, AND G. AEPPLI
Quantum dynamics and entanglement of spins on a square lattice
Proceedings of the National Academy of Science of the USA **104**, 15264 (2007).
Group: Mesot / Project: 1
- ▶ N. B. CHRISTENSEN, H. M. RØNNOW, J. MESOT, R. A. EWINGS, N. MOMONO, M. ODA, M. IDO, M. ENDERLE, D. F. MCMORROW, AND A. T. BOOTHROYD
Nature of the Magnetic Order in the Charge-Ordered Cuprate La_{1.48}Nd_{0.4}Sr_{0.12}CuO₄
Physical Review Letters **98**, 197003 (2007).
Group: Mesot / Project: 2
- ▶ T. KONDO, R. KHASANOV, J. KARPINSKI, S. M. KAZAKOV, N. D. ZHIGADLO, T. OHTA, H. M. FRETWELL, A. D. PALCZEWSKI, J. D. KOLL, J. MESOT, E. ROTENBERG, H. KELLER, AND A. KAMINSKI
Dual character of the electronic structure of YBa₂Cu₄O₈: The conduction bands of CuO₂ planes and CuO chains
Physical Review Letters **98**, 157002 (2007).
Groups: Keller, Karpinski, Mesot / Projects: 2, 3, 4
- A. PODLESNYAK, K. CONDER, E. POMJAKUSHINA, A. MIRMELSTEIN, P. ALLENSPACH, AND D. KHOMSKII
Effect of light Sr doping on the spin-state transition in LaCoO₃
Journal of Magnetism and Magnetic Materials **310**, 1552 (2007).
Group: Mesot / Project: 3
- A. PODLESNYAK, A. KARKIN, K. CONDER, E. POMJAKUSHINA, M. STINGACIU, AND P. ALLENSPACH
Magnetic and electric transport properties of TbBaCo₂O_{5.5} single crystal
Journal of Magnetism and Magnetic Materials **316**, e710 (2007).
Group: Mesot / Project: 3

- A. PODLESNYAK, V. POMJAKUSHIN, E. V. POMJAKUSHINA, K. CONDER, AND A. FURRER
Magnetic excitations in the spin-trimer compounds $\text{Ca}_3\text{Cu}_{3-x}\text{Ni}_x(\text{PO}_4)_4$ ($x = 0, 1, 2$)
 Physical Review B **76**, 064420 (2007).
 Group: Mesot / Project: 1
- V. Y. POMJAKUSHIN, A. FURRER, D. V. SHEPTYAKOV, E. V. POMJAKUSHINA, AND K. CONDER
Crystal and magnetic structures of the spin-trimer compounds $\text{Ca}_3\text{Cu}_{3-x}\text{Ni}_x(\text{PO}_4)_4$ ($x = 0, 1, 2$)
 Physical Review B **76**, 174433 (2007).
 Group: Mesot / Project: 1
- H. M. RØNNOW, J. JENSEN, R. PARTHASARATHY, G. AEPPLI, T. F. ROSENBAUM, D. MCMORROW, AND C. KRAEMER
Magnetic excitations near the quantum phase transition in the Ising ferromagnet LiHoF_4
 Physical Review B **75**, 054426 (2007).
 Group: Mesot / Project: 1
- J. CHANG, J. MESOT, R. GILARDI, J. KOHLBRECHER, A. J. DREW, U. DIVAKAR, S. J. LISTER, S. L. LEE, S. P. BROWN, D. CHARALAMBOUS, E. M. FORGAN, C. D. DEWHURST, R. CUBITT, N. MONOMO, AND M. ODA
Neutron scattering investigations of the Abrikosov state of high-temperature superconductors
 Physica B **385-386**, 35 (2006).
 Group: Mesot / Projects: 1, 3, 6
- S. J. CROWE, M. R. LEES, D. M. K. PAUL, R. I. BEWELY, J. TAYLOR, G. MCINTYRE, O. ZAHARKO, AND H. BERGER
Effect of externally applied pressure on the magnetic behavior of $\text{Cu}_2\text{Te}_2\text{O}_5(\text{Br}_x\text{Cl}_{1-x})_2$
 Physical Review B **73**, 144410 (2006).
 Groups: Mesot, Margaritondo / Projects: 1, 3, 6
- A. J. DREW, D. O. G. HERON, U. K. DIVAKAR, S. L. LEE, R. GILARDI, J. MESOT, F. Y. OGRIN, D. CHARALAMBOUS, N. MONOMO, M. ODA, AND C. BAINES
 μSR measurements on the vortex lattice of $\text{La}_{1.83}\text{Sr}_{0.17}\text{CuO}_4$
 Physica B **374-375**, 203 (2006).
 Group: Mesot / Projects: 1, 3, 6
- A. FURRER AND C. RÜEGG
Bose-Einstein condensation in magnetic materials
 Physica B **385-386**, 295 (2006).
 Group: Mesot / Projects: 1, 3, 6
- P. S. HÄFLIGER, A. PODLESNYAK, K. CONDER, AND A. FURRER
Pressure effect on the pseudogap in the optimally doped high-temperature superconductor $\text{La}_{1.81}\text{Sr}_{0.15}\text{Ho}_{0.04}\text{Cu}_{16}\text{O}_4$
 Europhysics Letters **73**, 260 (2006).
 Group: Mesot / Projects: 1, 3, 6
- P. S. HÄFLIGER, A. PODLESNYAK, K. CONDER, E. POMJAKUSHINA, AND A. FURRER
Pseudogap of the high-temperature superconductor $\text{La}_{1.96-x}\text{Sr}_x\text{Ho}_{0.04}\text{CuO}_4$ as observed by neutron crystal-field spectroscopy
 Physical Review B **74**, 184520 (2006).
 Group: Mesot / Projects: 1, 3, 6
- M. MEDARDE, C. DALLERA, M. GRIONI, J. VOIGT, A. PODLESNYAK, E. POMJAKUSHINA, K. CONDER, T. NEISIUS, O. TJERNBERG, AND S. BARILO
Low-temperature spin-state transition in LaCoO_3 investigated using resonant x-ray absorption at the Co K edge
 Physical Review B **73**, 054424 (2006).
 Groups: Mesot, Grioni / Projects: 1, 3
- G. I. MENON, A. DREW, U. DIVAKAR, S. LEE, R. GILARDI, J. MESOT, F. OGRIN, D. CHARALAMBOUS, E. FORGAN, N. MOMONO, M. ODA, C. DEWHURST, AND C. BAINES
Muons as Local Probes of Three-Body Correlations in the Mixed State of Type-II Superconductors
 Physical Review Letters **97**, 177004 (2006).
 Group: Mesot / Projects: 1, 3, 6
- H. E. MOHOTTALA, B. O. WELLS, J. I. BUDNICK, W. A. HINES, C. NIEDERMAYER, L. UDBY, C. BERNHARD, A. R. MOODENBAUGH, AND F. C. CHOU
Phase separation in superoxygenated $\text{La}_{2-x}\text{Sr}_x\text{CuO}_{4+y}$
 Nature Materials **5**, 377 (2006).
 Groups: Bernhard, Mesot / Projects: 1, 2, 3, 6
- J. PADIYATH, J. STAHN, AND M. HORISBERGER
Multilayers with tailored blurred interfaces
 Applied Physics Letters **89**, 113123 (2006).
 Group: Mesot / Projects: 1, 3, 6
- A. PODLESNYAK, S. STREULE, K. CONDER, E. POMJAKUSHINA, J. MESOT, A. MIRMELSTEIN, P. SCHÜTZENDORF, R. LENGSDORF, AND M. M. ABD-ELMEGUID
Pressure effects on crystal structure, magnetic and transport properties of layered perovskite $\text{TbBaCo}_2\text{O}_{5.5}$
 Physica B **378-380**, 537 (2006).
 Group: Mesot / Projects: 1, 3, 6

- ▶ A. PODLESNYAK, S. STREULE, J. MESOT, M. MEDARDE, E. POMJAKUSHINA, K. CONDER, A. TANAKA, M. HAVERKORT, AND D. I. HOMSKII
Spin-state transition in LaCoO₃: direct neutron spectroscopic evidence of excited magnetic states
Physical Review Letters **97**, 247208 (2006).
Group: Mesot / Projects: 1, 3, 6
- E. POMJAKUSHINA, K. CONDER, AND V. POMJAKUSHIN
Orbital order-disorder transition with volume collapse in HoBaCo₂O_{5.5}: A high-resolution neutron diffraction study
Physical Review B **73**, 113105 (2006).
Group: Mesot / Projects: 1, 3, 6
- ▶ H. M. RØNNOW, C. RENNER, G. AEPPLI, T. KIMURA, AND Y. TOKURA
Polarons and confinement of electronic motion to two dimensions in a layered manganite
Nature **440**, 1025 (2006).
Group: Mesot / Projects: 1, 3, 6
- V. R. SHAH, C. SCHANZER, P. BÖNI, AND H. B. BRAUN
Interface and magnetic characterization of FM/AF/FM multilayers
Proceedings of the NATO Advanced Research Workshop p. 179 (2006).
Group: Mesot / Project: 6
- S. STREULE, M. MEDARDE, A. PODLESNYAK, E. POMJAKUSHINA, K. CONDER, S. KAZAKOV, J. KARPINSKI, AND J. MESOT
Short-range charge ordering in Ho_{0.1}Sr_{0.9}CoO_{3-x} (0.15 ≤ x ≤ 0.49)
Physical Review B **73**, 024423 (2006).
Groups: Karpinski, Mesot / Projects: 1, 3, 4, 6
- S. STREULE, A. PODLESNYAK, E. POMJAKUSHINA, K. CONDER, D. SHEPTYAKOV, M. MEDARDE, AND J. MESOT
Oxygen order-disorder phase transition in PrBaCo₂O_{5.48} at high temperature
Physica B **378-380**, 539 (2006).
Group: Mesot / Projects: 1, 3, 6
- S. STREULE, A. PODLESNYAK, D. SHEPTYAKOV, E. POMJAKUSHINA, M. STINGACIU, K. CONDER, M. MEDARDE, M. V. PATRAKEEV, I. A. LEONIDOV, V. L. KOZHEVNIKOV, AND J. MESOT
High-temperature order-disorder transition and polaronic conductivity in PrBaCo₂O_{5.48}
Physical Review B **73**, 094203 (2006).
Group: Mesot / Projects: 1, 3, 6
- O. ZAHARKO, H. RØNNOW, J. MESOT, S. CROWE, D. PAUL, P. BROWN, A. DAOU-ALADINE, A. MEENTS, A. WAGNER, M. PRESTER, AND H. BERGER
Incommensurate magnetic ordering in Cu₂Te₂O₅X₂ (X = Cl, Br) studied by single crystal neutron diffraction
Physical Review B **73**, 064422 (2006).
Groups: Margaritondo, Mesot / Projects: 2, 3
- S. N. BARILO, S. SHIRYAEV, G. L. BYCHKOV, V. P. PLAKHTY, A. S. SHESTAK, A. G. SOLDATOV, A. PODLESNYAK, K. CONDER, M. BARAN, W. R. FLAVELL, AND A. FURRER
Sub-liquidus co-crystallization in the Ln₂O₃-BaO-CoO system: growth of large LnBaCo₂O_{5+x} (Ln = Eu, Gd, Tb, Dy) single crystals
Journal of Crystal Growth **275**, 120 (2005).
Group: Mesot / Project: 3
- ▶ S. BAYRAKCI, I. MIREBEAU, P. BOURGES, Y. SIDIS, M. ENDERLE, J. MESOT, D. CHEN, C. LIN, AND B. KEIMER
Magnetic ordering and spin waves in Na_{0.82}CoO₂
Physical Review Letters **94**, 157205 (2005).
Group: Mesot / Project: 1
- G. L. BYCHKOV, S. V. SHIRYAEV, A. G. SOLDATOV, A. S. SHESTAK, S. BARILO, D. V. SHEPTYAKOV, K. CONDER, E. POMJAKUSHINA, A. PODLESNYAK, A. FURRER, AND R. BRUETSCH
Crystal growth features and properties of layered rare earth and barium cobaltates
Crystal Research and Technology **40**, 395 (2005).
Group: Mesot / Project: 3
- K. CONDER, E. POMJAKUSHINA, V. POMJAKUSHIN, M. STINGACIU, S. STREULE, AND A. PODLESNYAK
Oxygen isotope effect on metal-insulator transition in layered cobaltites RBaCo₂O_{5.5} (R = Pr, Dy, Ho, and Y)
Journal of Physics: Condensed Matter **17**, 5813 (2005).
Group: Mesot / Project: 3
- K. CONDER, E. POMJAKUSHINA, A. SOLDATOV, AND E. MITBERG
Oxygen content determination in perovskite-type cobaltates
Materials Research Bulletin **40**, 257 (2005).
Group: Mesot / Project: 3
- ▶ A. DREW, S. L. LEE, D. CHARALAMBOUS, A. POTENZA, C. MARROWS, H. LUETKENS,

- A. SUTER, T. PROKSCHA, R. KHASANOV, E. MORENZONI, D. UCKO, AND E. M. FORGAN
Coexistence and Coupling of Superconductivity and Magnetism in Thin Film Structures
 Physical Review Letters **95**, 197201 (2005).
 Groups: Keller, Mesot / Projects: 1, 2
- J. EMERY, D. MASSIOT, P. LACORRE, Y. LALIGANT, AND K. CONDER
 ^{17}O NMR in room temperature phase of $\text{La}_2\text{Mo}_2\text{O}_9$ fast oxide ionic conductor
 Magnetic Resonance in Chemistry **43**, 366 (2005).
 Group: Mesot / Project: 3
- M. ENDERLE, C. MUKHERJEE, B. FAK, R. KREMER, J.-M. BROTO, H. ROSNER, S.-L. DRECHSLER, J. RICHTER, J. MALEK, A. PROKOFIEV, W. ASSMUS, S. PUJOL, J.-L. RAGGAZZONI, H. RAKOTO, M. RHEINSTADTER, AND H. RØNNOW
Quantum helimagnetism of the frustrated spin-1/2 chain LiCuVO_4
 Europhysics Letters **70**, 237 (2005).
 Group: Mesot / Project: 1
- R. GILARDI, S. STREULE, N. MOMONO, M. ODA, AND J. MESOT
Doping dependence of the vortex glass and sublimation transitions in the high- T_c superconductor $\text{La}_{2-x}\text{Sr}_x\text{CuO}_4$ as determined from macroscopic measurements
 The European Physical Journal B **47**, 231 (2005).
 Group: Mesot / Project: 1
- M. HERAK, H. BERGER, M. PRESTER, M. MILJAK, I. ZIVKOVIC, O. MILAT, D. DROBAC, S. POPOVIC, AND O. ZAHARKO
Novel spin lattice in Cu_3TeO_6 : an antiferromagnetic order and domain dynamics
 Journal of Physics: Condensed Matter **17**, 7667 (2005).
 Groups: Margaritondo, Mesot / Projects: 1, 3
- M. JANOSCHEK, B. ROESSLI, L. KELLER, S. N. GVASALIYA, K. CONDER, AND E. POMJAKUSHINA
Reduction of the ordered magnetic moment in YMnO_3 with hydrostatic pressure
 Journal of Physics: Condensed Matter **17**, L425 (2005).
 Group: Mesot / Project: 3
- A. KAMINSKI, H. M. FRETWELL, M. R. NORMAN, M. RANDERIA, S. ROSENKRANZ, U. CHATTERJEE, J. C. CAMPUZANO, J. MESOT, T. SATO, T. TAKAHASHI, T. TERASHIMA, M. TAKANO, K. KADOWAKI, Z. Z. LI, AND H. RAFFY
Momentum anisotropy of the scattering rate in cuprate superconductors
 Physical Review B **71**, 014517 (2005).
 Group: Mesot / Project: 1
- ▶ R. KHASANOV, D. G. ESHCHENKO, D. DI CASTRO, A. SHENGELAYA, F. LA MARTINA, A. MAISURADZE, C. BAINES, H. LUETKENS, J. KARPINSKI, S. M. KAZAKOV, AND H. KELLER
Magnetic penetration depth in RbOs_2O_6 studied by muon spin rotation
 Physical Review B **72**, 104504 (2005).
 Groups: Keller, Karpinski, Mesot / Projects: 1, 2, 3, 4
- R. KHASANOV, J. KARPINSKI, AND H. KELLER
Pressure effect on the in-plane magnetic penetration depth in $\text{YBa}_2\text{Cu}_4\text{O}_8$
 Journal of Physics: Condensed Matter **17**, 2453 (2005).
 Groups: Keller, Karpinski, Mesot / Projects: 1, 2, 3, 4
- ▶ R. KHASANOV, T. SCHNEIDER, AND H. KELLER
Pressure effects on the superconducting properties of $\text{YBa}_2\text{Cu}_4\text{O}_8$
 Physical Review B **72**, 014524 (2005).
 Groups: Mesot, Keller / Projects: 1, 2
- B. LAKE, K. LEFMANN, N. B. CHRISTENSEN, G. AEPPLI, D. F. MCMORROW, H. M. RØNNOW, P. VORDERWISCH, P. SMEIBIDL, N. MANGKORNTONG, T. SASAGAWA, M. NOHARA, AND H. TAKAGI
Three-dimensionality of field-induced magnetism in a high-temperature superconductor
 Nature Materials **4**, 658 (2005).
 Group: Mesot / Project: 1
- S. LEE, A. A. PODLESNYAK, K. PROKES, V. E. SIKOLENKO, A. S. ERMOLENKO, E. G. GERASIMOV, Y. A. DOROFEEV, A. P. VOKHMYANIN, J.-G. PARK, AND A. N. PIROGOV
Magnetic phase transitions in TbNi_5 single crystal: Bulk properties and neutron diffraction studies
 Journal of Experimental and Theoretical Physics Letters **82**, 34 (2005).
 Group: Mesot / Project: 1
- E. LIAROKAPIS, D. PALLES, D. LAMPAKIS, G. BÖTTGER, K. CONDER, AND E. KALDIS
Phase separation in fully oxygenated $\text{Y}_{1-y}\text{Ca}_y\text{Ba}_2\text{Cu}_3\text{O}_x$ compounds
 Physical Review B **71**, 014303 (2005).
 Group: Mesot / Project: 3

- J. MESOT, J. CHANG, J. KOHLBRECHER, R. GILARDI, A. J. DREW, U. DIVAKAR, D. HERON, S. J. LISTER, S. L. LEE, S. P. BROWN, D. CHARALAMBOUS, E. M. FORGAN, F. Y. OGRIN, G. I. MENON, C. D. DEWHURST, R. CUBITT, C. BAINES, N. MOMONO, M. ODA, T. UEFUJI, AND K. YAMADA
Combined neutron scattering and muon-spin rotation investigations of the Abrikosov state of high-temperature superconductors
Proceedings of SPIE **5932**, 59322D (2005).
Group: Mesot / Project: 1
- J. PADIYATH, J. STAHN, P. ALLENSPACH, M. HORISBERGER, M. GUPTA, T. GUTBERLET, AND P. BÖNI
Smooth interfaces of multilayer monochromators
Physica B **357**, 218 (2005).
Group: Mesot / Project: 6
- A. PODLESNYAK, P. S. HÄFLIGER, K. CONDER, AND A. FURRER
Neutron spectroscopic study of the pseudogap formation in $\text{La}_{1.81}\text{Sr}_{0.15}\text{Ho}_{0.04}\text{CuO}_4$ at ambient and elevated pressure
Journal of Physics: Condensed Matter **17**, S801 (2005).
Group: Mesot / Project: 1
- A. PODLESNYAK, S. STREULE, M. MEDARDE, K. CONDER, E. POMJAKUSHINA, AND J. MESOT
Effect of oxygen nonstoichiometry on structural and magnetic properties of $\text{PrBaCo}_2\text{O}_{5+\delta}$
Physica B **359-361**, 1348 (2005).
Group: Mesot / Project: 1
- C. RENNEN, G. AEPPLI, AND H. M. RØNNOW
Charge ordering, stripes and phase separation in manganese perovskite oxides: an STM/STS study
Materials Science and Engineering **C25**, 775 (2005).
Group: Mesot / Project: 1
- B. ROESSLI, S. N. GVASALIYA, E. POMJAKUSHINA, AND K. CONDER
Spin fluctuations in the stacked-triangular antiferromagnet YMnO_3
Journal of Experimental and Theoretical Physics Letters **81**, 287 (2005).
Group: Mesot / Project: 3
- ▶ C. RÜEGG, B. NORMAND, M. MATSUMOTO, C. NIEDERMAYER, A. FURRER, K. W. KRÄMER, H. U. GÜDEL, P. BOURGES, Y. SIDIS, AND H. MUTKA
Quantum Statistics of Interacting Dimer Spin Systems
Physical Review Letters **95**, 267201 (2005).
Group: Mesot / Project: 1
- ▶ H. M. RØNNOW, R. PARTHASARATHY, J. JENSEN, G. AEPPLI, T. F. ROSENBAUM, AND D. MCMORROW
Quantum phase transition of a magnet in a spin bath
Science **308**, 389 (2005).
Group: Mesot / Project: 1
- C. SCHANZER, V. R. SHAH, T. GUTBERLET, M. GUPTA, P. BÖNI, AND H. B. BRAUN
Magnetic depth profiling of FM/AF/FM trilayers by PNR
Physica B **356**, 46 (2005).
Group: Mesot / Project: 6
- V. R. SHAH, C. SCHANZER, P. BÖNI, AND H. B. BRAUN
Magnetization reversal in FM/AF/FM trilayers: dependence of AF thickness
Journal of Magnetism and Magnetic Materials **286**, 484 (2005).
Group: Mesot / Project: 6
- ▶ U. STAUB, A. M. MULDER, O. ZAHARKO, S. JANSSEN, T. NAKAMURA, AND S. W. LOVESEY
Orbital Dynamics of the 4f Shell in DyB_2C_2
Physical Review Letters **94**, 036408 (2005).
Group: Mesot / Project: 1
- S. STREULE, A. PODLESNYAK, J. MESOT, M. MEDARDE, K. CONDER, E. POMJAKUSHINA, E. MITBERG, AND V. KOZHEVNIKOV
Effect of oxygen ordering on the structural and magnetic properties of the layered perovskites $\text{PrBaCo}_2\text{O}_{5+\delta}$
Journal of Physics: Condensed Matter **17**, 3317 (2005).
Group: Mesot / Project: 3
- O. ZAHARKO, H. M. RØNNOW, A. DAOUD-ALADINE, S. STREULE, F. JURANYI, J. MESOT, H. BERGER, AND P. BROWN
Incommensurate magnetism in the coupled spin tetrahedra system $\text{Cu}_2\text{Te}_2\text{O}_5\text{Cl}_2$
Low Temperature Physics **31**, 814 (2005).
Groups: Mesot, Margaritondo / Projects: 1, 3
- O. ZAHARKO, H. M. RØNNOW, A. DAOUD-ALADINE, S. STREULE, F. JURANYI, J. MESOT, H. BERGER, AND P. J. BROWN
Incommensurate magnetism in the coupled spin tetrahedra system $\text{Cu}_2\text{Te}_2\text{O}_5\text{Cl}_2$
Fizika Nizkikh Temperatur **31**, 1068 (2005).
Groups: Margaritondo, Mesot / Projects: 1, 3

Group of F. Mila

A. GELLÉ, A. M. LÄUCHLI, B. KUMAR, AND F. MILA

Two-dimensional quantum antiferromagnet with a fourfold degenerate dimer ground state

Physical Review B **77**, 014419 (2008).

Group: Mila / Project: 1

G. MISGUICH AND F. MILA

Quantum Dimer Model on the triangular lattice: Semiclassical and variational approaches to vison dispersion and condensation

Physical Review B (2008).

Group: Mila / Project: 1

- ▶ K. P. SCHMIDT, J. DORIER, A. LAEUCHLI, AND F. MILA

Supersolid phase induced by correlated hopping in spin-1/2 frustrated quantum magnets

Physical Review Letters **100**, 090401 (2008).

Group: Mila / Project: 1

- ▶ N. LAFLORENCIE AND F. MILA
- Quantum and Thermal Transitions Out of the Supersolid Phase of a 2D Quantum Antiferromagnet*

Physical Review Letters **99**, 027202 (2007).

Group: Mila / Project: 1

A. LÄUCHLI, S. DOMMANGE, B. NORMAND, AND F. MILA

Static impurities in the $S = 3/2$ kagome lattice: Exact diagonalization calculations on small clusters

Physical Review B **76**, 144413 (2007).

Group: Mila / Project: 1

F. MILA, F. VERNAY, A. RALCO, F. BECCA, P. FAZEKAS, AND K. PENC

The emergence of resonating valence bond physics in spin-orbital models

Journal of Physics: Condensed Matter **19**, 145201 (2007).

Group: Mila / Project: 1

S. MIYAHARA, J.-B. FOUET, S. R. MANMANA, R. M. NOACK, H. MAYAFFRE, I. SHEIKIN, C. BERTHIER, AND F. MILA

Uniform and staggered magnetizations induced by Dzyaloshinskii-Moriya interactions in isolated and coupled spin-1/2 dimers in a magnetic field

Physical Review B **75**, 184402 (2007).

Group: Mila / Project: 1

- ▶ K. PENC, J.-B. FOUET, S. MIYAHARA, O. TCHERNYSHYOV, AND F. MILA

Ising Phases of Heisenberg Ladders in a Magnetic Field

Physical Review Letters **99**, 117201 (2007).

Group: Mila / Project: 1

D. POILBLANC, M. MAMBRINI, A. LÄUCHLI, AND F. MILA

Exotic phenomena in doped quantum magnets

Journal of Physics: Condensed Matter **19**, 145205 (2007).

Group: Mila / Project: 1

D. POILBLANC, C. WEBER, F. MILA, AND M. SIGRIST

Checkerboard order in the t - J model on the square lattice

Journal of Magnetism and Magnetic Materials **310**, 523 (2007).

Groups: Rice, Mila, Sigrist / Project: 1

A. RALCO, M. FERRERO, F. BECCA, D. IVANOV, AND F. MILA

Crystallization of the resonating valence bond liquid as vortex condensation

Physical Review B **76**, 140404 (2007).

Group: Mila / Project: 1

- ▶ A. RALCO, F. MILA, AND D. POILBLANC
- Phase Separation and Flux Quantization in the Doped Quantum Dimer Model on Square and Triangular Lattices*

Physical Review Letters **99**, 127202 (2007).

Group: Mila / Project: 1

C. R. AST, D. PACILÉ, M. PAPAGNO, T. GLOOR, F. MILA, S. FEDRIGO, G. WITICH, K. KERN, H. BRUNE, AND M. GRIONI

Orbital selective overlayer-substrate hybridization in a Pb monolayer on Ag(111)

Physical Review B **73**, 245428 (2006).

Groups: Grioni, Mila / Project: 1

- ▶ M. CLÉMANCEY, H. MAYAFFRE, C. BERTHIER, M. HORVATIĆ, J.-B. FOUET, S. MIYAHARA, F. MILA, B. CHIARI, AND O. PIOVESANA

Field-Induced Staggered Magnetization and Magnetic Ordering in $\text{Cu}_2(\text{C}_5\text{H}_{12}\text{N}_2)_2\text{Cl}_4$

Physical Review Letters **97**, 167204 (2006).

Group: Mila / Project: 1

J.-B. FOUET, A. LÄUCHLI, S. PILGRAM, R. M. NOACK, AND F. MILA

Frustrated three-leg spin tubes: From spin 1/2 with chirality to spin 3/2

Physical Review B **73**, 014409 (2006).

Group: Mila / Project: 1

J.-B. FOUET, F. MILA, D. CLARKE, H. YOUK, O. TCHERNYSHYOV, P. FENDLEY, AND R. M. NOACK

Condensation of magnons and spinons in a frustrated ladder

- Physical Review B **73**, 214405 (2006).
Group: Mila / Project: 1
- J. L. GAVILANO, E. FELDER, D. RAU, H. R. OTT, P. MILLET, F. MILA, T. CICHOREK, AND A. C. MOTA
Na₂V₃O_{0.7}: An unusual low-dimensional quantum magnet
Physica B **378-380**, 123 (2006).
Groups: Ott, Mila / Project: 1
- ▶ A. LÄUCHLI, F. MILA, AND K. PENC
Quadrupolar Phases of the S = 1 Bilinear-Biquadratic Heisenberg Model on the Triangular Lattice
Physical Review Letters **97**, 087205 (2006).
Group: Mila / Project: 1
- M. MAMBRINI, A. LÄUCHLI, D. POILBLANC, AND F. MILA
Plaquette valence-bond crystal in the frustrated Heisenberg quantum antiferromagnet on the square lattice
Physical Review B **74**, 144422 (2006).
Group: Mila / Project: 1
- V. V. MAZURENKO, F. MILA, AND V. I. ANISIMOV
Electronic structure and exchange interactions of Na₂V₃O₇
Physical Review B **73**, 014418 (2006).
Group: Mila / Project: 1
- D. POILBLANC, F. ALET, F. BECCA, A. RALCO, F. TROUSSELET, AND F. MILA
Doping quantum dimer models on the square lattice
Physical Review B **74**, 014437 (2006).
Group: Mila / Project: 1
- D. POILBLANC, A. LÄUCHLI, M. MAMBRINI, AND F. MILA
Spinon deconfinement in doped frustrated quantum antiferromagnets
Physical Review B **73**, 100403 (2006).
Group: Mila / Project: 1
- A. RALCO, M. FERRERO, F. BECCA, D. IVANOV, AND F. MILA
Dynamics of the quantum dimer model on the triangular lattice: Soft modes and local resonating valence-bond correlations
Physical Review B **74**, 134301 (2006).
Group: Mila / Project: 1
- K. P. SCHMIDT, J. DORIER, A. LÄUCHLI, AND F. MILA
Single-particle versus pair condensation of hard-core bosons with correlated hopping
Physical Review B **73**, 214405 (2006).
Group: Mila / Project: 1
- F. VERNAY, A. RALCO, F. BECCA, AND F. MILA
Identification of an RVB liquid phase in a quantum dimer model with competing kinetic terms
Physical Review B **74**, 054402 (2006).
Group: Mila / Project: 1
- C. WEBER, A. LÄUCHLI, F. MILA, AND T. GIAMARCHI
Magnetism and superconductivity of strongly correlated electrons on the triangular lattice
Physical Review B **73**, 014519 (2006).
Groups: Mila, Giamarchi / Project: 1
- C. WEBER, D. POILBLANC, S. CAPPONI, F. MILA, AND C. JAUDET
Bond-order-modulated staggered-flux phase of the tJ model on a square lattice
Physical Review B **74**, 104506 (2006).
Group: Mila / Project: 1
- ▶ R. BENDJAMA, B. KUMAR, AND F. MILA
Absence of Single-Particle Bose-Einstein Condensation at Low Densities for Bosons with Correlated Hopping
Physical Review Letters **95**, 110406 (2005).
Group: Mila / Project: 1
- J. DORIER, F. BECCA, AND F. MILA
Quantum compass model on the square lattice
Physical Review B **72**, 024448 (2005).
Group: Mila / Project: 1
- M. ELHAJAL AND F. MILA
Dynamic spin Jahn-Teller effect in small magnetic clusters
The European Physical Journal B **47**, 185 (2005).
Group: Mila / Project: 1
- J. L. GAVILANO, E. FELDER, D. RAU, H. R. OTT, P. MILLET, F. MILA, T. CICHOREK, AND A. C. MOTA
Unusual magnetic properties of the low-dimensional quantum magnet Na₂V₃O₇
Physical Review B **72**, 064431 (2005).
Groups: Mila, Ott / Project: 1
- V. N. KOTOV, M. ELHAJAL, M. E. ZHITOMIRSKY, AND F. MILA
Dzyaloshinsky-Moriya-induced order in the spin-liquid phase of the S = 1/2 pyrochlore antiferromagnet
Physical Review B **72**, 014421 (2005).
Group: Mila / Project: 1
- S. MIYAHARA AND F. MILA

The effects of Dzyaloshinsky-Moriya interaction in the orthogonal dimer Heisenberg model for SrCu₂(BO₃)₂

Progress of Theoretical Physics **159**, 33 (2005).
Group: Mila / Project: 1

L. PERFETTI, T. A. GLOOR, F. MILA, H. BERGER, AND M. GRIONI

Unexpected periodicity in the quasi-two-dimensional Mott insulator 1T-TaS₂ revealed by angle-resolved photoemission

Physical Review B **71**, 153101 (2005).
Groups: Margaritondo, Mila, Grioni / Projects: 1, 3

C. WEBER, F. BECCA, AND F. MILA

Finite-temperature properties of frustrated classical spins coupled to the lattice

Physical Review B **72**, 024449 (2005).
Group: Mila / Project: 1

Group of R. Nesper

- ▶ A. MICHAILOVSKI, R. KIEBACH, W. BENSCH, J.-D. GRUNWALDT, A. BAIKER, S. KOMARNENI, AND G. R. PATZKE

Morphological and Kinetic Studies on Hexagonal Tungstates

Chemistry of Materials **19**, 185 (2007).
Group: Nesper / Projects: 4, 6

M. WÖRLE, R. NESPER, G. MAIR, AND H. G. VON SCHNERING

Li₆B₁₈(Li₂O)_x – A boride with a porous framework of B₆ octahedra

Solid State Sciences **9**, 459 (2007).
Group: Nesper / Projects: 4, 6

M. J. HEIGHT, L. MÄDLER, S. E. PRATSINIS, AND F. KRUMEICH

Nanorods of ZnO Made by Flame Spray Pyrolysis

Chemistry of Materials **18**, 572 (2006).
Group: Nesper / Projects: 4, 6

F. KRUMEICH AND R. NESPER

Oxidation products of the niobium tungsten oxide Nb₄W₁₃O₄₇: A high-resolution scanning transmission electron microscopy study

Journal of Solid State Chemistry **179**, 1857 (2006).
Group: Nesper / Projects: 4, 6

A. MICHAILOVSKI AND G. R. PATZKE

Hydrothermal Synthesis of Molybdenum Oxide Based Materials: Strategy and Structural Chemistry

Chemistry–A European Journal **12**, 9122 (2006).
Group: Nesper / Projects: 4, 6

A. MICHAILOVSKI, H. RÜEGGER, D. SHEPTYAKOV, AND G. R. PATZKE

Synthesis and characterization of Novel Fluorinated Poly(oxomolybdates)

Inorganic Chemistry **45**, 5641 (2006).
Group: Nesper / Projects: 4, 6

R. NESPER, A. IVANTCHENKO, AND F. KRUMEICH

Synthesis and Characterization of Carbon-Based Nanoparticles and Highly Magnetic Nanoparticles with Carbon Coatings

Advanced Functional Materials **16**, 296 (2006).
Group: Nesper / Projects: 4, 6

- ▶ A. M. TAURINO, A. FORLEO, L. FRANCIOSO, P. SICILIANO, M. STALDER, AND R. NESPER

Synthesis, electrical characterization and gas sensing properties of molybdenum oxide nanorods

Applied Physics Letters **88**, 152111 (2006).
Group: Nesper / Projects: 4, 6

M. WÖRLE, R. NESPER, AND T. CHATTERJI

LiB_x (0.82 < x ≤ 1.0) – an incommensurate Composite Structure below 150 K

Zeitschrift für Anorganische und Allgemeine Chemie **632**, 1737 (2006).
Group: Nesper / Projects: 4, 6

Q. XIE AND R. NESPER

Structural and Electronic Characterization of Eu₂LiSi₃, Eu₂LiGe₃ and Eu_xSr_{2-x}LiGe₃ Mixed Crystals

Zeitschrift für Anorganische und Allgemeine Chemie **632**, 1743 (2006).
Group: Nesper / Projects: 4, 6

J. HABERRECHT, F. KRUMEICH, M. STALDER, AND R. NESPER

Carbon nanostructures on high-temperature ceramics – a novel composite material and its functionalization

Catalysis Today **102**, 40 (2005).
Group: Nesper / Projects: 4, 6

J. HABERRECHT, R. NESPER, AND H. GRÜTZMACHER

A Construction Kit for Si-B-C-N Ceramic Materials Based on Borazine Precursors

Chemistry of Materials **17**, 2340 (2005).
Group: Nesper / Projects: 4, 6

C. KUBATA, F. KRUMEICH, M. WÖRLE, AND R. NESPER

The Real Structure of YbSi_{1.4} – Commensurately and Incommensurately Modulated Silicon Substructures

Zeitschrift für Anorganische und Allgemeine

Chemie **631**, 546 (2005).

Group: Nesper / Projects: 4, 6

F. OTTINGER, I. KROSLAKOVA, K. HAMETNER, E. REUSSER, R. NESPER, AND D. GÜNTHER

Analytical evidence of amorphous microdomains within nitridosilicate and nitridoaluminosilicate single crystals

Analytical & Bioanalytical Chemistry **383**, 489 (2005).

Group: Nesper / Projects: 4, 6

F. OTTINGER AND R. NESPER

Synthesis and Crystal Structure of the Nitridosilicates $Ca_5[Si_2N_6]$ and $Ca_7[NbSi_2N_9]$

Zeitschrift für Anorganische und Allgemeine Chemie **631**, 1597 (2005).

Group: Nesper / Projects: 4, 6

S. PIOTTO AND R. NESPER

CURVIS: a program to study and analyse crystallographic structures and phase transitions

Journal of Applied Crystallography **38**, 223 (2005).

Group: Nesper / Projects: 4, 6

H. G. VON SCHNERING, M. SCHWARZ, J.-H. CHANG, K. PETERS, E. M. PETERS, AND R. NESPER

Refinement of the crystal structures of the tetrahedro-tetrasilicides K_4Si_4 , Rb_4Si_4 and CS_4Si_4

Zeitschrift für Kristallographie – New Crystal Structures **220**, 525 (2005).

Group: Nesper / Projects: 4, 6

Group of H.-R. Ott

- ▶ F. PFUNER, L. DEGIORGI, H. R. OTT, A. BIANCHI, AND Z. FISK

Magneto-optical behavior of $EuIn_2P_2$

Physical Review B **77**, 024417 (2008).

Groups: Degiorgi, Ott / Project: 1

M. WELLER, J. L. GAVILANO, A. SACCHETTI, AND H. R. OTT

Low temperature NMR study of $CeAl_3$ under hydrostatic pressure

Physica B **403**, 834 (2008).

Group: Ott / Project: 1

M. WELLER, J. L. GAVILANO, A. SACCHETTI, AND H. R. OTT

Pressure induced variation of the ground state of $CeAl_3$

Physical Review B **77**, 132402 (2008).

Group: Ott / Project: 1

B. PEDRINI, S. WESSEL, J. L. GAVILANO, H. R. OTT, S. M. KAZAKOV, AND J. KARPINSKI

Quenching of the Haldane gap in $LiVSi_2O_6$ and related compounds

The European Physical Journal B **55**, 219 (2007).

Groups: Karpinski, Ott / Projects: 1, 3, 4

A. V. SOLOGUBENKO, T. LORENZ, H. R. OTT, AND A. FREIMUTH

Thermal Conductivity via Magnetic Excitations in Spin-Chain Materials

Journal of Low Temperature Physics **174**, 387 (2007).

Group: Ott / Project: 2

G. A. WIGGER, E. FELDER, M. WELLER, S. STREULE, H. R. OTT, A. D. BIANCHI, AND Z. FISK

Percolation limited magnetic order in $Eu_{1-x}Ca_xB_6$

The European Physical Journal B **46**, 231 (2007).

Group: Ott / Project: 1

- ▶ G. CAIMI, A. PERUCCHI, L. DEGIORGI, H. R. OTT, V. M. PEREIRA, A. H. CASTRO NETO, A. D. BIANCHI, AND Z. FISK

Magneto-Optical Evidence of Double Exchange in a Percolating Lattice

Physical Review Letters **96**, 016403 (2006).

Groups: Degiorgi, Ott / Project: 1

J. L. GAVILANO, E. FELDER, D. RAU, H. R. OTT, P. MILLET, F. MILA, T. CICHOREK, AND A. C. MOTA

$Na_2V_3O_{0.7}$: An unusual low-dimensional quantum magnet

Physica B **378-380**, 123 (2006).

Groups: Ott, Mila / Project: 1

J. L. GAVILANO, B. PEDRINI, K. MAGISHI, J. HINDERER, M. WELLER, H. R. OTT, S. M. KAZAKOV, AND J. KARPINSKI

Localized versus itinerant magnetic moments in $Na_{0.7}CoO_2$

Physical Review B **74**, 064410 (2006).

Groups: Karpinski, Ott / Projects: 1, 3, 4

J. HINDERER, S. M. WEYENETH, M. WELLER, J. L. GAVILANO, E. FELDER, F. HULLIGER, AND H. R. OTT

NMR study of $CeTe$ at low temperatures

Physica B **378-380**, 765 (2006).

Group: Ott / Project: 1

H. R. OTT

Heavy electrons and non-Fermi liquids, the early times

- Physica B **378-380**, 1 (2006).
Group: Ott / Project: 1
- B. PEDRINI, S. WEYENETH, J. L. GAVILANO, J. HINDERER, M. WELLER, H. R. OTT, S. M. KAZAKOV, AND J. KARPINSKI
Magnetic transition in $\text{Na}_{0.5}\text{CoO}_2$ at 88 K
Physica B **378-80**, 861 (2006).
Groups: Karpinski, Ott / Projects: 1, 3, 4
- A. V. SOLOGUBENKO, N. D. ZHIGADLO, J. KARPINSKI, AND H. R. OTT
Thermal conductivity of Al-doped MgB_2 : Impurity scattering and the validity of the Wiedemann-Franz law
Physical Review B **74**, 184523 (2006).
Groups: Karpinski, Ott / Projects: 2, 3, 4
- M. WELLER, J. HINDERER, J. L. GAVILANO, B. PEDRINI, D. RAU, I. SHEIKIN, M. CHIAO, AND H. R. OTT
NQR studies of CePd_2In under hydrostatic pressure
Physica B **378-380**, 892 (2006).
Group: Ott / Project: 1
- J. L. GAVILANO, E. FELDER, D. RAU, H. R. OTT, P. MILLET, F. MILA, T. CICHOREK, AND A. C. MOTA
Unusual magnetic properties of the low-dimensional quantum magnet $\text{Na}_2\text{V}_3\text{O}_7$
Physical Review B **72**, 064431 (2005).
Groups: Mila, Ott / Project: 1
- J. L. GAVILANO, D. RAU, B. PEDRINI, K. MAGISHI, M. WELLER, J. HINDERER, H. R. OTT, S. M. KAZAKOV, AND J. KARPINSKI
Unconventional charge ordering in $\text{Na}_{0.70}\text{CoO}_2$ below 300 K?
Physica B **359**, 1237 (2005).
Groups: Karpinski, Ott / Projects: 3, 4
- K. MAGISHI, J. L. GAVILANO, B. PEDRINI, J. HINDERER, M. WELLER, H. R. OTT, S. M. KAZAKOV, AND J. KARPINSKI
Evidence for s-wave superconductivity in the β -pyrochlore oxide RbOs_2O_6
Physical Review B **71**, 024524 (2005).
Groups: Karpinski, Ott / Projects: 3, 4
- B. PEDRINI, J. L. GAVILANO, S. WEYENETH, E. FELDER, J. HINDERER, M. WELLER, H. R. OTT, S. M. KAZAKOV, AND J. KARPINSKI
Magnetic phase transition at 88 K in $\text{Na}_{0.5}\text{CoO}_2$ revealed by ^{23}Na NMR investigations
Physical Review B **72**, 214407 (2005).
Groups: Karpinski, Ott / Projects: 1, 3, 4
- A. V. SOLOGUBENKO, N. D. ZHIGADLO, S. M. KAZAKOV, J. KARPINSKI, AND H. R. OTT
Influence of carbon substitution on the heat transport in single crystalline MgB_2
Physical Review B **71**, 020501 (2005).
Groups: Karpinski, Ott / Projects: 2, 3, 4
- G. A. WIGGER, E. FELDER, R. MONNIER, H. R. OTT, L. PHAM, AND Z. FISK
Low-temperature phase transitions in the induced-moment system PrB_4
Physical Review B **72**, 014419 (2005).
Group: Ott / Project: 1
- Group of P. Paruch**
- ▶ G. CATALAN, H. BÉA, S. FUSIL, M. BIBES, P. PARUCH, A. BARTHÉLÉMY, AND J. F. SCOTT
Fractal Dimension and Size Scaling of Domains in Thin Films of Multiferroic BiFeO_3
Physical Review Letters **100**, 027602 (2008).
Group: Paruch / Project: 5
- ▶ P. PARUCH AND J.-M. TRISCONI
High-temperature ferroelectric domain stability in epitaxial $\text{PbZr}_{0.2}\text{Ti}_{0.8}\text{O}_3$ thin films
Applied Physics Letters **88**, 162907 (2006).
Groups: Triscone, Paruch / Project: 5
- Group of Ch. Renner**
- S. HEUTZ, C. MITRA, W. WU, A. J. FISHER, A. KERRIDGE, M. STONEHAM, A. H. HARKER, J. GARDENER, H.-H. TSENG, T. S. JONES, C. RENNER, AND G. AEPPLI
Molecular Thin Films: A New type of Magnetic Switch
Advanced Materials **19**, 3618 (2007).
Group: Renner / Project: 1
- S. DE SANTIS, B. BRYANT, M. WARNER, H. WANG, T. KIMURA, Y. TOKURA, C. RENNER, A. BIANCONI, AND G. AEPPLI
Imaging of Polarons in Ferromagnetic Bilayered Manganites by Scanning Tunnelling Microscopy
Journal of Superconductivity and Novel Magnetism **20**, 531 (2007).
Group: Renner / Project: 1
- Group of T. M. Rice**
- Y. CHEN, T. M. RICE, AND F. C. ZHANG
Atomic scale rotational symmetry breaking in lightly doped $\text{Ca}_{2-x}\text{Na}_x\text{CuO}_2\text{Cl}_2$
Physica C **460-462**, 234 (2007).
Groups: Rice, Sigrist / Project: 2

- P. A. FRIGERI, D. F. AGTERBERG, I. MILAT, AND M. SIGRIST
Phenomenological theory of the 's-wave' state in superconductors without an inversion center
The European Physical Journal B **54**, 435 (2007).
Groups: Rice, Sigrist / Project: 2
- M. INDERGAND, C. HONERKAMP, A. LÄUCHLI, D. POILBLANC, AND M. SIGRIST
Plaquette bond order wave in the quarter-filled extended Hubbard model on the checkerboard lattice
Physical Review B **75**, 045105 (2007).
Groups: Rice, Sigrist / Project: 1
- M. INDERGAND AND M. SIGRIST
Existence of Long-Range Magnetic Order in the Ground State of Two-Dimensional spin-1/2 Heisenberg antiferromagnets
Progress of Theoretical Physics **117**, 1 (2007).
Groups: Rice, Sigrist / Project: 1
- C. INIOTAKIS
Andreev bound states in rounded corners of d-wave superconductors
Physica C **460-462**, 1143 (2007).
Groups: Rice, Sigrist / Project: 2
- C. INIOTAKIS, N. HAYASHI, Y. SAWA, T. YOKOYAMA, U. MAY, Y. TANAKA, AND M. SIGRIST
Andreev bound states and tunneling characteristics of a noncentrosymmetric superconductor
Physical Review B **76**, 012501 (2007).
Groups: Rice, Sigrist / Project: 2
- ▶ Y. KASAHARA, T. IWASAWA, H. SHISHIDO, T. SHIBAUCHI, K. BEHNIA, Y. HAGA, T. D. MATSUDA, Y. ONUKI, M. SIGRIST, AND Y. MATSUDA
Exotic Superconducting Properties in the Electron-Hole-Compensated Heavy-Fermion 'semimetal' URu₂Si₂
Physical Review Letters **99**, 116402 (2007).
Groups: Rice, Sigrist / Project: 2
- R. M. KONIK AND T. M. RICE
Orbital dependence of quasiparticle lifetimes in Sr₂RuO₄
Physical Review B **76**, 104501 (2007).
Groups: Rice, Sigrist / Project: 1
- D. POILBLANC, C. WEBER, F. MILA, AND M. SIGRIST
Checkerboard order in the t-J model on the square lattice
Journal of Magnetism and Magnetic Materials **310**, 523 (2007).
Groups: Rice, Mila, Sigrist / Project: 1
- T. M. RICE
Twenty years of RVB theory
Journal of Magnetism and Magnetic Materials **310**, 454 (2007).
Groups: Rice, Sigrist / Project: 2
- T. M. RICE, K.-Y. YANG, AND F.-C. ZHANG
A Phenomenological Theory of the Pseudogap State
Physica C **460-462**, 252 (2007).
Groups: Rice, Sigrist / Project: 2
- A. RÜEGG, S. PILGRAM, AND M. SIGRIST
Strongly renormalized quasi-two-dimensional electron gas in a heterostructure with correlation effects
Physical Review B **75**, 195117 (2007).
Groups: Rice, Sigrist / Project: 1
- M. SIGRIST, D. F. AGTERBERG, P. A. FRIGERI, N. HAYASHI, R. P. KAUR, A. KOGA, I. MILAT, K. WAKABAYASHI, AND Y. YANASE
Superconductivity in non-centrosymmetric materials
Journal of Magnetism and Magnetic Materials **310**, 536 (2007).
Groups: Rice, Sigrist / Project: 2
- ▶ K. WAKABAYASHI, Y. TAKANE, AND M. SIGRIST
Perfectly Conducting Channel and Universality Crossover in Disordered Graphene Nanoribbons
Physical Review Letters **99**, 036601 (2007).
Groups: Rice, Sigrist / Project: 1
- S. WEHRLI AND M. SIGRIST
Jahn-Teller effect versus Hund's rule coupling in C₆₀^{N-}
Physical Review B **76**, 125419 (2007).
Groups: Rice, Sigrist / Project: 1
- Y. YANASA AND M. SIGRIST
Magnetic Properties in Non-centrosymmetric Superconductors with and without Antiferromagnetic Order
Journal of the Physical Society of Japan **76**, 124709 (2007).
Groups: Rice, Sigrist / Project: 2
- ▶ Y. YANASE AND M. SIGRIST
Non-centrosymmetric Superconductivity and Antiferromagnetic Order: Microscopic Discussion of CePt₃Si
Journal of the Physical Society of Japan **76**, 043712 (2007).
Groups: Rice, Sigrist / Project: 2
- K.-Y. YANG, T. M. RICE, AND F.-C. ZHANG

Effect of superlattice modulation of electronic parameters on the density of states of cuprate superconductors

Physical Review B **76**, 100501 (2007).

Groups: Rice, Sigrist / Project: 2

D. F. AGTERBERG, P. A. FRIGERI, R. P. KAUR, A. KOGA, AND M. SIGRIST

Magnetic fields and superconductivity without inversion symmetry in CePt₃Si

Physica B **378-380**, 351 (2006).

Groups: Rice, Sigrist / Project: 2

E. BASCONES AND T. M. RICE

Spin susceptibility of underdoped cuprates: The case of ortho-II YBa₂Cu₃O_{6.5}

Physical Review B **74**, 134501 (2006).

Groups: Rice, Sigrist / Project: 2

E. BAUER, I. BONALDE, A. EICHLER, G. HILSCHER, Y. KITAOKA, R. LACKNER, S. LAUMANN, H. MICHOR, M. NICKLAS, P. ROGL, E. W. SCHEIDT, M. SIGRIST, AND M. YOGI

CePt₃Si: Heavy Fermion Superconductivity and Magnetic Order without Inversion Symmetry

AIP Conference Proceedings **850**, 695 (2006).

Groups: Rice, Sigrist / Project: 2

► B. BINZ, H. B. BRAUN, T. M. RICE, AND M. SIGRIST

Magnetic Domain Formation in Itinerant Metamagnets

Physical Review Letters **96**, 196406 (2006).

Groups: Rice, Sigrist / Project: 1

► Y. CHEN, T. M. RICE, AND F. C. ZHANG

Rotational Symmetry Breaking in the Ground State of Sodium-Doped Cuprate Superconductors

Physical Review Letters **97**, 237004 (2006).

Groups: Rice, Sigrist / Project: 2

P. A. FRIGERI, M. SIGRIST, AND D. F. AGTERBERG

Characterization of the s-wave state in parity-violating superconductors

Physica B **378-380**, 900 (2006).

Groups: Rice, Sigrist / Project: 2

P. GENTILE, C. NOCE, AND M. SIGRIST

Role of spin exchange on the coexistence of superconductivity and itinerant ferromagnetism in a two carrier model

Physica B **378-380**, 550 (2006).

Groups: Rice, Sigrist / Project: 2

N. HAYASHI, Y. KATO, P. A. FRIGERI, K. WAKABAYASHI, AND M. SIGRIST

Basic properties of a vortex in a noncentrosymmetric superconductor

Physica C **437-438**, 96 (2006).

Groups: Rice, Sigrist / Project: 2

N. HAYASHI, K. WAKABAYASHI, P. A. FRIGERI, Y. KATO, AND M. SIGRIST

Spatially resolved NMR relaxation rate in a noncentrosymmetric superconductor

Physica B **378-380**, 388 (2006).

Groups: Rice, Sigrist / Project: 2

► N. HAYASHI, K. WAKABAYASHI, P. A. FRIGERI, AND M. SIGRIST

Nuclear magnetic relaxation rate in a noncentrosymmetric superconductor

Physical Review B **73**, 092508 (2006).

Groups: Rice, Sigrist / Project: 2

N. HAYASHI, K. WAKABAYASHI, P. A. FRIGERI, AND M. SIGRIST

Temperature dependence of the superfluid density in a noncentrosymmetric superconductor

Physical Review B **73**, 024504 (2006).

Groups: Rice, Sigrist / Project: 2

M. INDERGAND, A. LÄUCHLI, S. CAPPONI, AND M. SIGRIST

Modeling bond-order wave instabilities in doped frustrated antiferromagnets: Valence bond solids at fractional filling

Physical Review B **74**, 064429 (2006).

Groups: Rice, Sigrist / Project: 1

► R. M. KONIK, T. M. RICE, AND A. M. TSVELIK

Doped Spin Liquid: Luttinger Sum Rule and Low temperature order

Physical Review Letters **96**, 086407 (2006).

Groups: Rice, Sigrist / Project: 2

A. V. LUKOYANOV, V. V. MAZURENKO, V. I. ANISIMOV, M. SIGRIST, AND T. M. RICE

The semiconductor-to-ferromagnetic-metal transition in FeSb₂

The European Physical Journal B **53**, 205 (2006).

Groups: Rice, Sigrist / Project: 1

A. P. SCHNYDER, D. MANSKE, C. MUDRY, AND M. SIGRIST

Theory for inelastic neutron scattering in orthorhombic high-T_c superconductors

Physical Review B **73**, 224523 (2006).

Groups: Rice, Sigrist / Project: 2

► S. PILGRAM, T. M. RICE, AND M. SIGRIST

Role of Inelastic Tunneling through the Insulating Barrier in Scanning-Tunneling-Microscope Experiments on Cuprate Superconductors

- Physical Review Letters **97**, 117003 (2006).
Groups: Rice, Sigrist / Project: 2
- T. M. RICE AND H. TSUNETSUGU
A simple model for the checkerboard pattern of modulated hole densities in underdoped cuprates
The European Physical Journal B **49**, 1 (2006).
Groups: Rice, Sigrist / Project: 2
- T. SHIBAUCHI, L. KRUSIN-ELBAUM, Y. KASAHARA, Y. SHIMONO, Y. MATSUDA, R. D. McDONALD, C. H. MIELKE, S. YONEZAWA, Z. HIROI, M. ARAI, T. KITA, G. BLATTER, AND M. SIGRIST
Uncommonly high upper critical field of the pyrochlore superconductor KOs_2O_6 below the enhanced paramagnetic limit
Physical Review B **74**, 220506 (2006).
Groups: Rice, Sigrist, Blatter / Project: 2
- A. O. SHORIKOV, V. I. ANISIMOV, AND M. SIGRIST
A band structure analysis of the coexistence of superconductivity and magnetism in $(Ho, Dy)Ni_2B_2C$
Journal of Physics: Condensed Matter **18**, 5973 (2006).
Groups: Rice, Sigrist / Project: 2
- A. O. SHORIKOV, I. A. NEKRASOV, V. I. ANISIMOV, AND M. SIGRIST
A band-structure analysis of the coexistence of superconductivity and magnetism in $(Ho, Dy)Ni_2B_2C$
The Physics of Metals and Metallography **101**, S21 (2006).
Groups: Rice, Sigrist / Project: 2
- M. SIGRIST, D. F. AGTERBERG, P. A. FRIGERI, N. HAYASHI, R. P. KAUR, A. KOGA, I. MILAT, AND K. WAKABAYASHI
Unconventional superconductivity in non-centrosymmetric materials
AIP Conference Proceedings **816**, 124 (2006).
Groups: Rice, Sigrist / Project: 2
- S. TREBST, H. MONIEN, A. GRZESIK, AND M. SIGRIST
Quasiparticle dynamics in the Kondo lattice model at half filling
Physical Review B **73**, 165101 (2006).
Groups: Rice, Sigrist / Project: 1
- K.-Y. YANG, T. M. RICE, AND F.-C. ZHANG
Phenomenological theory of the pseudogap state
Physical Review B **73**, 174501 (2006).
Groups: Rice, Sigrist / Project: 2
- ▶ H. Q. YUAN, D. F. AGTERBERG, N. HAYASHI, P. BADICA, D. VANDERVELDE, K. TOGANO, M. SIGRIST, AND M. B. SALAMON
S-Wave Spin-Triplet Order in Superconductors without Inversion Symmetry: Li_2Pd_3B and Li_2Pt_3B
Physical Review Letters **97**, 017006 (2006).
Groups: Rice, Sigrist / Project: 2
- E. BASCONES, T. M. RICE, A. O. SHORIKOV, A. V. LUKOYANOV, AND V. I. ANISIMOV
Optical conductivity of ortho-II $YBa_2Cu_3O_{6.5}$
Physical Review B **71**, 012505 (2005).
Groups: Rice, Sigrist / Project: 2
- A. KOGA, N. KAWAKAMI, T. M. RICE, AND M. SIGRIST
Spin, charge and orbital fluctuations in a multi-orbital Mott insulator
Physical Review B **72**, 045128 (2005).
Groups: Rice, Sigrist / Project: 1
- A. RÜEGG, M. INDERGAND, S. PILGRAM, AND M. SIGRIST
Slave-boson mean-field theory of the Mott transition in the two-band Hubbard model
The European Physical Journal B **48**, 55 (2005).
Groups: Rice, Sigrist / Project: 1
- K. WAKABAYASHI, T. M. RICE, AND M. SIGRIST
Enhanced coherence of antinodal quasiparticles in a dirty d-wave superconductor
Physical Review B **72**, 214517 (2005).
Groups: Rice, Sigrist / Project: 2
- Group of A. Schilling**
- ▶ H. BARTOLF, A. ENGEL, A. SCHILLING, K. IL'IN, AND M. SIEGEL
Fabrication of metallic structures with lateral dimensions less than 15 nm and $j_c(T)$ -measurements in NbN micro- and nanobridges
Physica C (2008).
Group: Schilling / Project: 5
- ▶ A. ENGEL, H. BARTOLF, A. SCHILLING, K. IL'IN, M. SIEGEL, A. SEMENOV, AND H.-W. HÜBERS
Temperature- and field-dependence of critical currents in NbN microbridges
Journal of Physics: Conference Series **97**, 012152 (2008).
Group: Schilling / Project: 5
- ▶ A. ENGEL, H. BARTOLF, A. SCHILLING, A. SEMENOV, H.-W. HÜBERS, K. IL'IN, AND M. SIEGEL

Magnetic Vortices in Superconducting Photon Detectors

Journal of Modern Optics (2008).

Group: Schilling / Project: 5

K. IL'IN, R. SCHNEIDER, D. GERTHSEN, A. ENGEL, H. BARTOLF, A. SCHILLING, A. SEMENOV, H.-W. HÜBERS, B. FREITAG, AND M. SIEGEL

Ultra-thin NbN films on Si: crystalline and superconducting properties

Journal of Physics: Conference Series **97**, 012045 (2008).

Group: Schilling / Project: 5

K. IL'IN, M. SIEGEL, A. ENGEL, H. BARTOLF, A. SCHILLING, A. SEMENOV, AND H.-W. HÜBERS

Current-Induced Critical State in NbN Thin-Film Structures

Journal of Low Temperature Physics **151**, 585 (2008).

Group: Schilling / Project: 5

P. HAAS, A. SEMENOV, H.-W. HÜBERS, J. BEYER, A. KIRSTE, T. SCHURIG, K. IL'IN, M. SIEGEL, A. ENGEL, AND A. SMIRNOV

Spectral Sensitivity and Spectral Resolution of Superconducting Single-Photon Detectors

IEEE Transactions on Applied Superconductivity **17**, 298 (2007).

Group: Schilling / Project: 5

A. SCHILLING AND M. REIBELT

Low-temperature differential-thermal analysis to measure variations in entropy

Review of Scientific Instruments **78**, 033904 (2007).

Group: Schilling / Projects: 4, 5

A. SEMENOV, P. HAAS, K. IL'IN, H.-W. HÜBERS, M. SIEGEL, A. ENGEL, AND A. SMIRNOV

Energy resolution and sensitivity of a superconducting quantum detector

Physica C **460-462**, 1491 (2007).

Group: Schilling / Project: 5

A. ENGEL, A. D. SEMENOV, H.-W. HÜBERS, K. IL'IN, AND M. SIEGEL

Fluctuation effects in superconducting nanostrips

Physica C **444**, 12 (2006).

Group: Schilling / Project: 5

A. ENGEL, A. SEMENOV, H.-W. HÜBERS, K. IL'IN, AND M. SIEGEL

Fluctuations and dark count rates in superconducting NbN single-photon detectors

Physica Status Solidi (c) **2**, 1668 (2005).

Group: Schilling / Project: 5

K. IL'IN, M. SIEGEL, A. SEMENOV, A. ENGEL, AND H.-W. HÜBERS

Critical current of Nb and NbN thin-film structures: The cross-section dependence

Physica Status Solidi (c) **2**, 1680 (2005).

Group: Schilling / Project: 5

▶ A. SEMENOV, A. ENGEL, H.-W. HÜBERS, K. IL'IN, AND M. SIEGEL

Spectral cut-off in the efficiency of the resistive state formation caused by absorption of a single-photon in current-carrying superconducting nano-strips

The European Physical Journal B **47**, 495 (2005).

Group: Schilling / Project: 5

A. SEMENOV, A. ENGEL, K. IL'IN, M. SIEGEL, AND H.-W. HÜBERS

Noise of a Superconducting Photon Detector

IEEE Transactions on Applied Superconductivity **15**, 518 (2005).

Group: Schilling / Project: 5

Group of L. Schlapbach

R. AGUIAR, D. LOGVINOVICH, A. WEIDENKAFF, H. KARL, C. SCHNEIDER, A. RELLER, AND S. G. EBBINGHAUS

Physical Properties of (La, Sr)Ti(O, N)₃ Thin Films Grown by Pulsed Laser Deposition

to be published in Materials Research Bulletin (2008).

Group: Schlapbach / Project: 4

M. H. AGUIRRE, S. CANULESCU, R. ROBERT, N. HOMAZAVA, D. LOGVINOVICH, L. BOCHER, T. LIPPERT, M. DÖBELI, AND A. WEIDENKAFF

Structure, microstructure and high temperature transport properties of La_{1-x}Ca_xMnO_{3-δ} thin films and polycrystalline bulk materials

Journal of Applied Physics **103**, 013703 (2008).

Group: Schlapbach / Project: 4

B. BALKE, G. H. FECHER, A. GLOSKOVSKII, J. BARTH, K. KROTH, C. FELSER, R. ROBERT, AND A. WEIDENKAFF

Doped Semiconductors as half-metallic materials: CoTi_{1-x}(M_xSb (M = Sc, V, Cr, Mn, Fe)

Physical Review B **77**, 045209 (2008).

Group: Schlapbach / Project: 4

L. BOCHER, R. ROBERT, M. H. AGUIRRE, S. MALO, S. HEBERT, A. MAIGNAN, AND

- A. WEIDENKAFF
Thermoelectric and magnetic properties of perovskite-type manganate phases synthesised by a Ultrasonic Spray Combustion (USC) method
to be published in *Journal of Solid State Sciences* (2008).
Group: Schlapbach / Project: 4
- S. EBBINGHAUS, R. AGUIAR, A. WEIDENKAFF, S. GSELL, AND R. RELLER
Topotactical Growth of thick Perovskite Oxynitride Layers by Ammonolysis of Single Crystalline Oxides
to be published in *Journal of Solid State Sciences* (2008).
Group: Schlapbach / Project: 4
- R. ROBERT, M. H. AGUIRRE, L. BOCHER, M. TROTTMANN, S. HEIROTH, T. LIPPERT, AND A. WEIDENKAFF
Thermoelectric properties of polycrystalline samples and epitaxial $\text{LaCo}_{1-x}\text{Ni}_x\text{O}_3$ thin films
to be published in *Journal of Solid State Sciences* (2008).
Group: Schlapbach / Project: 4
- A. WEIDENKAFF, R. ROBERT, M. AGUIRRE, L. BOCHER, T. LIPPERT, AND S. CANULESCU
Development of thermoelectric oxides for renewable energy conversion technologies
Renewable Energy **33**, 342 (2008).
Group: Schlapbach / Project: 4
- R. AGUIAR, D. LOGVINOVICH, A. WEIDENKAFF, A. RACHEL, A. RELLER, AND S. G. EBBINGHAUS
The vast colour spectrum of ternary metal oxynitride pigments
Dyes and Pigments **76**, 70 (2007).
Group: Schlapbach / Project: 4
- R. AGUIAR, A. WEIDENKAFF, C. W. SCHNEIDER, A. RELLER, AND S. G. EBBINGHAUS
Synthesis and properties of oxynitrides ($\text{La}, \text{Sr})\text{Ti}(\text{O}, \text{N})_3$ thin films
Progress in Solid State Chemistry **35**, 291 (2007).
Group: Schlapbach / Project: 4
- M. H. AGUIRRE, R. ROBERT, D. LOGVINOVICH, AND A. WEIDENKAFF
Synthesis, Crystal Structure and Microstructure Analysis of Perovskite Type compounds $\text{LnCo}_{0.95}\text{Ni}_{0.05}\text{O}_3$ ($\text{Ln} = \text{La}, \text{Pr}, \text{Nd}, \text{Sm}, \text{Gd}$ and Dy)
Inorganic Chemistry **46**, 2744 (2007).
Group: Schlapbach / Project: 4
- L. BOCHER, M. H. AGUIRRE, R. ROBERT, M. TROTTMANN, D. LOGVINOVICH, P. HUG, AND A. WEIDENKAFF
Chimie douce synthesis and thermochemical characterization of mesoporous perovskite-type titanate phases
Thermochimica Acta **457**, 11 (2007).
Group: Schlapbach / Project: 4
- ▶ G. BUCHS, A. V. KRASHENINNIKOV, P. RUFFIEUX, P. GRÖNING, A. S. FOSTER, R. M. NIEMINEN, AND O. GRÖNING
Creation of paired electron states in the gap of semiconducting carbon nanotubes by correlated hydrogen adsorption
New Journal of Physics **9**, 275 (2007).
Group: Schlapbach / Project: 1
- ▶ G. BUCHS, P. RUFFIEUX, P. GRÖNING, AND O. GRÖNING
Creation and STM/STS investigations of hydrogen ions induced defects on single-walled carbon nanotubes
Journal of Physics: Conference Series **61**, 160 (2007).
Group: Schlapbach / Project: 1
- ▶ G. BUCHS, P. RUFFIEUX, P. GRÖNING, AND O. GRÖNING
Scanning tunneling microscopy investigations of hydrogen plasma-induced electron scattering centers on single-walled carbon nanotubes
Applied Physics Letters **90**, 013104 (2007).
Group: Schlapbach / Project: 1
- S. CANULESCU, T. LIPPERT, A. WOKAUN, M. DÖBELI, A. WEIDENKAFF, R. ROBERT, AND D. LOGVINOVICH
The effect of the fluence of the plume species on the properties of La-Ca-Mn-O thin films prepared by pulsed laser deposition
Applied Surface Science **253**, 8174 (2007).
Group: Schlapbach / Project: 4
- S. CANULESCU, T. LIPPERT, A. WOKAUN, R. ROBERT, D. LOGVINOVICH, A. WEIDENKAFF, M. DÖBELI, AND S. M.
Preparation of epitaxial $\text{La}_{0.6}\text{Ca}_{0.4}\text{Mn}_{1-x}\text{Fe}_x\text{O}_3$ ($x = 0, 0.2$) thin Films: Variation of the oxygen content
Progress in Solid State Chemistry **35**, 241 (2007).
Group: Schlapbach / Project: 4
- T. LIPPERT, M. J. MONTENEGRO, M. DÖBELI, A. WEIDENKAFF, S. MÜLLER, P. R. WILLMOTT, AND A. WOKAUN
Perovskite thin films deposited by pulsed laser ablation as model systems for electrochemical applications

Progress in Solid State Chemistry **35**, 221 (2007).

Group: Schlapbach / Project: 4

D. LOGVINOVICH, R. AGUIAR, R. ROBERT, M. TROTTMANN, S. G. EBBINGHAUS, A. RELLER, AND A. WEIDENKAFF

Synthesis, Mo-valence state, thermal stability and thermoelectric properties of SrMoO_{3-x}N_x (x > 1) oxynitride perovskites

Journal of Solid State Chemistry **180**, 2649 (2007).

Group: Schlapbach / Project: 4

D. LOGVINOVICH, A. BÖRGER, M. DÖBELI, S. G. EBBINGHAUS, A. RELLER, AND A. WEIDENKAFF

Synthesis and physical chemical properties of Ca substituted LaTiO₂N

Progress in Solid State Chemistry **35**, 281 (2007).

Group: Schlapbach / Project: 4

I. MAROZAU, M. DÖBELI, T. LIPPERT, D. LOGVINOVICH, M. MALLEPELL, A. SHKABKO, A. WEIDENKAFF, AND A. WOKAUN

One-step preparation of N-doped strontium titanate films by pulsed laser deposition

Applied Physics A **89**, 933 (2007).

Group: Schlapbach / Project: 4

R. ROBERT, M. H. AGUIRRE, P. HUG, A. RELLER, AND A. WEIDENKAFF

High temperature thermoelectric properties of Ln(Co, Ni)O₃ (Ln = La, Pr, Nd, Sm, Gd, and Dy) compounds

Acta Materialia **55**, 4965 (2007).

Group: Schlapbach / Project: 4

R. ROBERT, L. BOCHER, B. SIPOS, M. DÖBELI, AND A. WEIDENKAFF

Ni-doped cobaltates as potential materials for high temperature solar thermoelectric converters

Progress in Solid State Chemistry **35**, 447 (2007).

Group: Schlapbach / Project: 4

D. STOLTZ, M. BIELMANN, M. BOVET, L. SCHLAPBACH, AND H. BERGER

Tunneling evidence for spatial location of the charge-density-wave induced band splitting in 1T-TaSe₂

Physical Review B **76**, 073410 (2007).

Groups: Margaritondo, Schlapbach / Project: 3

A. WEIDENKAFF, R. ROBERT, M. H. AGUIRRE, L. BOCHER, AND L. SCHLAPBACH

Nanostructured thermoelectric oxides with low thermal conductivity

Physica Status Solidi **6**, 247 (2007).

Group: Schlapbach / Project: 4

► P. RUFFIEUX, M. MELLE-FRANCO, O. GRÖNING, M. BIELMANN, F. ZERBETTO, AND P. GRÖNING

Charge-density oscillation on graphite induced by the interference of electron waves

Physical Review B **71**, 153403 (2005).

Group: Schlapbach / Project: 1

Group of M. Sigrist

Y. CHEN, T. M. RICE, AND F. C. ZHANG

Atomic scale rotational symmetry breaking in lightly doped Ca_{2-x}Na_xCuO₂Cl₂

Physica C **460-462**, 234 (2007).

Groups: Rice, Sigrist / Project: 2

P. A. FRIGERI, D. F. AGTERBERG, I. MILAT, AND M. SIGRIST

Phenomenological theory of the 's-wave' state in superconductors without an inversion center

The European Physical Journal B **54**, 435 (2007).

Groups: Rice, Sigrist / Project: 2

M. INDERGAND, C. HONERKAMP, A. LÄUCHLI, D. POILBLANC, AND M. SIGRIST

Plaquette bond order wave in the quarter-filled extended Hubbard model on the checkerboard lattice

Physical Review B **75**, 045105 (2007).

Groups: Rice, Sigrist / Project: 1

M. INDERGAND AND M. SIGRIST

Existence of Long-Range Magnetic Order in the Ground State of Two-Dimensional spin-1/2 Heisenberg antiferromagnets

Progress of Theoretical Physics **117**, 1 (2007).

Groups: Rice, Sigrist / Project: 1

C. INIOTAKIS

Andreev bound states in rounded corners of d-wave superconductors

Physica C **460-462**, 1143 (2007).

Groups: Rice, Sigrist / Project: 2

C. INIOTAKIS, N. HAYASHI, Y. SAWA, T. YOKOYAMA, U. MAY, Y. TANAKA, AND M. SIGRIST

Andreev bound states and tunneling characteristics of a noncentrosymmetric superconductor

Physical Review B **76**, 012501 (2007).

Groups: Rice, Sigrist / Project: 2

► Y. KASAHARA, T. IWASAWA, H. SHISHIDO, T. SHIBAUCHI, K. BEHNIA, Y. HAGA, T. D. MATSUDA, Y. ONUKI, M. SIGRIST, AND

- Y. MATSUDA
Exotic Superconducting Properties in the Electron-Hole-Compensated Heavy-Fermion 'semimetal' URu₂Si₂
Physical Review Letters **99**, 116402 (2007).
Groups: Rice, Sigrist / Project: 2
- R. M. KONIK AND T. M. RICE
Orbital dependence of quasiparticle lifetimes in Sr₂RuO₄
Physical Review B **76**, 104501 (2007).
Groups: Rice, Sigrist / Project: 1
- D. POILBLANC, C. WEBER, F. MILA, AND M. SIGRIST
Checkerboard order in the t-J model on the square lattice
Journal of Magnetism and Magnetic Materials **310**, 523 (2007).
Groups: Rice, Mila, Sigrist / Project: 1
- T. M. RICE
Twenty years of RVB theory
Journal of Magnetism and Magnetic Materials **310**, 454 (2007).
Groups: Rice, Sigrist / Project: 2
- T. M. RICE, K.-Y. YANG, AND F.-C. ZHANG
A Phenomenological Theory of the Pseudogap State
Physica C **460-462**, 252 (2007).
Groups: Rice, Sigrist / Project: 2
- A. RÜEGG, S. PILGRAM, AND M. SIGRIST
Strongly renormalized quasi-two-dimensional electron gas in a heterostructure with correlation effects
Physical Review B **75**, 195117 (2007).
Groups: Rice, Sigrist / Project: 1
- M. SIGRIST, D. F. AGTERBERG, P. A. FRIGERI, N. HAYASHI, R. P. KAUR, A. KOGA, I. MILAT, K. WAKABAYASHI, AND Y. YANASE
Superconductivity in non-centrosymmetric materials
Journal of Magnetism and Magnetic Materials **310**, 536 (2007).
Groups: Rice, Sigrist / Project: 2
- ▶ K. WAKABAYASHI, Y. TAKANE, AND M. SIGRIST
Perfectly Conducting Channel and Universality Crossover in Disordered Graphene Nanoribbons
Physical Review Letters **99**, 036601 (2007).
Groups: Rice, Sigrist / Project: 1
- S. WEHRLI AND M. SIGRIST
Jahn-Teller effect versus Hund's rule coupling in C₆₀^{N-}
Physical Review B **76**, 125419 (2007).
Groups: Rice, Sigrist / Project: 1
- Y. YANASA AND M. SIGRIST
Magnetic Properties in Non-centrosymmetric Superconductors with and without Antiferromagnetic Order
Journal of the Physical Society of Japan **76**, 124709 (2007).
Groups: Rice, Sigrist / Project: 2
- ▶ Y. YANASE AND M. SIGRIST
Non-centrosymmetric Superconductivity and Antiferromagnetic Order: Microscopic Discussion of CePt₃Si
Journal of the Physical Society of Japan **76**, 043712 (2007).
Groups: Rice, Sigrist / Project: 2
- K.-Y. YANG, T. M. RICE, AND F.-C. ZHANG
Effect of superlattice modulation of electronic parameters on the density of states of cuprate superconductors
Physical Review B **76**, 100501 (2007).
Groups: Rice, Sigrist / Project: 2
- D. F. AGTERBERG, P. A. FRIGERI, R. P. KAUR, A. KOGA, AND M. SIGRIST
Magnetic fields and superconductivity without inversion symmetry in CePt₃Si
Physica B **378-380**, 351 (2006).
Groups: Rice, Sigrist / Project: 2
- E. BASCONES AND T. M. RICE
Spin susceptibility of underdoped cuprates: The case of ortho-II YBa₂Cu₃O_{6.5}
Physical Review B **74**, 134501 (2006).
Groups: Rice, Sigrist / Project: 2
- E. BAUER, I. BONALDE, A. EICHLER, G. HILSCHER, Y. KITAOKA, R. LACKNER, S. LAUMANN, H. MICHOR, M. NICKLAS, P. ROGL, E. W. SCHEIDT, M. SIGRIST, AND M. YOGI
CePt₃Si: Heavy Fermion Superconductivity and Magnetic Order without Inversion Symmetry
AIP Conference Proceedings **850**, 695 (2006).
Groups: Rice, Sigrist / Project: 2
- ▶ B. BINZ, H. B. BRAUN, T. M. RICE, AND M. SIGRIST
Magnetic Domain Formation in Itinerant Metamagnets
Physical Review Letters **96**, 196406 (2006).
Groups: Rice, Sigrist / Project: 1
- ▶ Y. CHEN, T. M. RICE, AND F. C. ZHANG

- Rotational Symmetry Breaking in the Ground State of Sodium-Doped Cuprate Superconductors*
Physical Review Letters **97**, 237004 (2006).
Groups: Rice, Sigrist / Project: 2
- P. A. FRIGERI, M. SIGRIST, AND D. F. AGTERBERG
Characterization of the s-wave state in parity-violating superconductors
Physica B **378-380**, 900 (2006).
Groups: Rice, Sigrist / Project: 2
- P. GENTILE, C. NOCE, AND M. SIGRIST
Role of spin exchange on the coexistence of superconductivity and itinerant ferromagnetism in a two carrier model
Physica B **378-380**, 550 (2006).
Groups: Rice, Sigrist / Project: 2
- N. HAYASHI, Y. KATO, P. A. FRIGERI, K. WAKABAYASHI, AND M. SIGRIST
Basic properties of a vortex in a noncentrosymmetric superconductor
Physica C **437-438**, 96 (2006).
Groups: Rice, Sigrist / Project: 2
- N. HAYASHI, K. WAKABAYASHI, P. A. FRIGERI, Y. KATO, AND M. SIGRIST
Spatially resolved NMR relaxation rate in a noncentrosymmetric superconductor
Physica B **378-380**, 388 (2006).
Groups: Rice, Sigrist / Project: 2
- ▶ N. HAYASHI, K. WAKABAYASHI, P. A. FRIGERI, AND M. SIGRIST
Nuclear magnetic relaxation rate in a noncentrosymmetric superconductor
Physical Review B **73**, 092508 (2006).
Groups: Rice, Sigrist / Project: 2
- N. HAYASHI, K. WAKABAYASHI, P. A. FRIGERI, AND M. SIGRIST
Temperature dependence of the superfluid density in a noncentrosymmetric superconductor
Physical Review B **73**, 024504 (2006).
Groups: Rice, Sigrist / Project: 2
- M. INDERGAND, A. LÄUCHLI, S. CAPPONI, AND M. SIGRIST
Modeling bond-order wave instabilities in doped frustrated antiferromagnets: Valence bond solids at fractional filling
Physical Review B **74**, 064429 (2006).
Groups: Rice, Sigrist / Project: 1
- ▶ R. M. KONIK, T. M. RICE, AND A. M. TSVELIK
Doped Spin Liquid: Luttinger Sum Rule and Low temperature order
Physical Review Letters **96**, 086407 (2006).
Groups: Rice, Sigrist / Project: 2
- A. V. LUKOYANOV, V. V. MAZURENKO, V. I. ANISIMOV, M. SIGRIST, AND T. M. RICE
The semiconductor-to-ferromagnetic-metal transition in FeSb₂
The European Physical Journal B **53**, 205 (2006).
Groups: Rice, Sigrist / Project: 1
- A. P. SCHNYDER, D. MANSKE, C. MUDRY, AND M. SIGRIST
Theory for inelastic neutron scattering in orthorhombic high-T_c superconductors
Physical Review B **73**, 224523 (2006).
Groups: Rice, Sigrist / Project: 2
- ▶ S. PILGRAM, T. M. RICE, AND M. SIGRIST
Role of Inelastic Tunneling through the Insulating Barrier in Scanning-Tunneling-Microscope Experiments on Cuprate Superconductors
Physical Review Letters **97**, 117003 (2006).
Groups: Rice, Sigrist / Project: 2
- T. M. RICE AND H. TSUNETSUGU
A simple model for the checkerboard pattern of modulated hole densities in underdoped cuprates
The European Physical Journal B **49**, 1 (2006).
Groups: Rice, Sigrist / Project: 2
- T. SHIBAUCHI, L. KRUSIN-ELBAUM, Y. KASHIHARA, Y. SHIMONO, Y. MATSUDA, R. D. McDONALD, C. H. MIELKE, S. YONEZAWA, Z. HIROI, M. ARAI, T. KITA, G. BLATTER, AND M. SIGRIST
Uncommonly high upper critical field of the pyrochlore superconductor KO₂O₆ below the enhanced paramagnetic limit
Physical Review B **74**, 220506 (2006).
Groups: Rice, Sigrist, Blatter / Project: 2
- A. O. SHORIKOV, V. I. ANISIMOV, AND M. SIGRIST
A band structure analysis of the coexistence of superconductivity and magnetism in (Ho, Dy)Ni₂B₂C
Journal of Physics: Condensed Matter **18**, 5973 (2006).
Groups: Rice, Sigrist / Project: 2
- A. O. SHORIKOV, I. A. NEKRASOV, V. I. ANISIMOV, AND M. SIGRIST
A band-structure analysis of the coexistence of superconductivity and magnetism in (Ho, Dy)Ni₂B₂C
The Physics of Metals and Metallography **101**, S21 (2006).
Groups: Rice, Sigrist / Project: 2

- M. SIGRIST, D. F. AGTERBERG, P. A. FRIGERI, N. HAYASHI, R. P. KAUR, A. KOGA, I. MILAT, AND K. WAKABAYASHI
Unconventional superconductivity in non-centrosymmetric materials
AIP Conference Proceedings **816**, 124 (2006).
Groups: Rice, Sigrist / Project: 2
- S. TREBST, H. MONIEN, A. GRZESIK, AND M. SIGRIST
Quasiparticle dynamics in the Kondo lattice model at half filling
Physical Review B **73**, 165101 (2006).
Groups: Rice, Sigrist / Project: 1
- K.-Y. YANG, T. M. RICE, AND F.-C. ZHANG
Phenomenological theory of the pseudogap state
Physical Review B **73**, 174501 (2006).
Groups: Rice, Sigrist / Project: 2
- ▶ H. Q. YUAN, D. F. AGTERBERG, N. HAYASHI, P. BADICA, D. VANDERVELDE, K. TOGANO, M. SIGRIST, AND M. B. SALAMON
S-Wave Spin-Triplet Order in Superconductors without Inversion Symmetry: $\text{Li}_2\text{Pd}_3\text{B}$ and $\text{Li}_2\text{Pt}_3\text{B}$
Physical Review Letters **97**, 017006 (2006).
Groups: Rice, Sigrist / Project: 2
- E. BASCONES, T. M. RICE, A. O. SHORIKOV, A. V. LUKOYANOV, AND V. I. ANISIMOV
Optical conductivity of ortho-II $\text{YBa}_2\text{Cu}_3\text{O}_{6.5}$
Physical Review B **71**, 012505 (2005).
Groups: Rice, Sigrist / Project: 2
- A. KOGA, N. KAWAKAMI, T. M. RICE, AND M. SIGRIST
Spin, charge and orbital fluctuations in a multiorbital Mott insulator
Physical Review B **72**, 045128 (2005).
Groups: Rice, Sigrist / Project: 1
- A. RÜEGG, M. INDERGAND, S. PILGRAM, AND M. SIGRIST
Slave-boson mean-field theory of the Mott transition in the two-band Hubbard model
The European Physical Journal B **48**, 55 (2005).
Groups: Rice, Sigrist / Project: 1
- K. WAKABAYASHI, T. M. RICE, AND M. SIGRIST
Enhanced coherence of antinodal quasiparticles in a dirty d-wave superconductor
Physical Review B **72**, 214517 (2005).
Groups: Rice, Sigrist / Project: 2
- Group of J.-M. Triscone**
- ▶ E. BOUSQUET, M. DAWBER, N. STUCKI, C. LICHTENSTEIGER, P. HERMET, S. GARIGLIO, J.-M. TRISCONE, AND P. GHOSEZ
Improper ferroelectricity in perovskite oxide artificial superlattices
Nature (2008).
Group: Triscone / Project: 5
- M. DAWBER, N. STUCKI, C. LICHTENSTEIGER, S. GARIGLIO, P. GHOSEZ, AND J.-M. TRISCONE
Tailoring the Properties of Artificially Layered Ferroelectric Superlattices
Advanced Materials **19**, 4153 (2007).
Group: Triscone / Project: 5
- C. FILIPIC, Z. KUTNJAK, R. LORTZ, M. DAWBER, AND J. F. SCOTT
Low temperature phase transitions in barium sodium niobate
Journal of Physics: Condensed Matter **19**, 236206 (2007).
Groups: Triscone, van der Marel / Project: 2
- ▶ S. GARIGLIO, N. STUCKI, J.-M. TRISCONE, AND G. TRISCONE
Strain relaxation and critical temperature in epitaxial ferroelectric $\text{Pb}(\text{Zr}_{0.20}\text{Ti}_{0.80})\text{O}_3$ thin films
Applied Physics Letters **90**, 202905 (2007).
Group: Triscone / Project: 5
- ▶ C. LICHTENSTEIGER, M. DAWBER, N. STUCKI, J.-M. TRISCONE, J. HOFFMAN, J.-B. YAU, C. H. AHN, L. DESPONT, AND P. AEBI
Monodomain to polydomain transition in ferroelectric PbTiO_3 thin films with $\text{La}_{0.67}\text{Sr}_{0.33}\text{MnO}_3$ electrodes
Applied Physics Letters **90**, 052907 (2007).
Groups: Aebi, Triscone / Project: 5
- R. LORTZ, C. MEINGAST, A. I. RYKOV, AND S. TAJIMA
Fragile Superconductivity and a kinetic glass transition in the vortex matter of the high-temperature superconductor $\text{YBa}_2\text{Cu}_3\text{O}_{7-\delta}$
Journal of Low Temperature Physics **147**, 365 (2007).
Groups: Triscone, van der Marel / Project: 2
- R. LORTZ, N. MUSOLINO, Y. WANG, A. JUNOD, AND N. TOYOTA
Origin of the magnetization peak effect in the superconductor Nb_3Sn
Physical Review B **75**, 094503 (2007).
Groups: Triscone, van der Marel / Project: 2

- ▶ R. LORTZ, Y. WANG, A. DEMUER, M. BÖTTGER, B. BERGK, G. ZWICKNAGEL, Y. NAKAZAWA, AND J. WOSNITZA
Calorimetric evidence for a novel superconducting state in the layered organic superconductor κ -(BEDT)₂Cu(NCS)₂
Physical Review Letters **99**, 187002 (2007).
Groups: Triscone, van der Marel / Project: 2
- R. LORTZ, Y. WANG, A. JUNOD, AND N. TOYOTA
Thermal fluctuations in the classical superconductor Nb₃Sn from high-resolution specific-heat measurements
Physica C **460-462**, 149 (2007).
Groups: Triscone, van der Marel / Project: 2
- ▶ D. MATTHEY, N. REYREN, J.-M. TRISCONE, AND T. SCHNEIDER
Electric-Field-Effect Modulation of the Transition Temperature, Mobile Carrier Density, and In-Plane Penetration Depth of NdBa₂Cu₃O_{7- δ} Thin Films
Physical Review Letters **98**, 057002 (2007).
Group: Triscone / Project: 2
- A. P. PETROVIĆ, Y. FASANO, R. LORTZ, M. DECROUX, M. POTEL, R. CHEVREL, AND Ø. FISCHER
Unconventional resistive transitions in the extreme type-II superconductor Tl₂Mo₆Se₆
Physica C **460-462**, 702 (2007).
Groups: Fischer, Triscone, van der Marel / Projects: 1, 2
- ▶ N. REYREN, S. THIEL, A. D. CAVIGLIA, L. F. KOURKOUTIS, G. HAMMERL, C. RICHTER, C. W. SCHNEIDER, T. KOPP, A.-S. RUETSCHI, D. JACCARD, M. GABAY, D. A. MULLER, J.-M. TRISCONE, AND J. MANNHART
Superconducting Interfaces Between Insulating Oxides
Science **317**, 1196 (2007).
Group: Triscone / Project: 2
- R. SALUT, W. DANIAU, S. BALLANDRAS, S. GARIGLIO, G. TRISCONE, AND J.-M. TRISCONE
Direct Writing of High Frequency Surface Acoustic Wave Devices on Epitaxial Pb(Zr_{0.20}Ti_{0.80})O₃ Thin Layers using Focus Ion Beam Etching
in *Proc. of the IEEE IFCS* (2007).
Group: Triscone / Project: 6
- D. G. SCHLOM, L.-Q. CHEN, C.-B. EOM, K. M. RABE, S. K. STREIFFER, AND J.-M. TRISCONE
Strain Tuning of Ferroelectric Thin Films
Annual Review of Materials Research **37**, 589 (2007).
Group: Triscone / Project: 5
- ▶ C. H. AHN, A. BHATTACHARYA, M. D. VENTRA, J. N. ECKSTEIN, C. D. FRISBIE, M. E. GERSHENSON, A. M. GOLDMAN, I. H. INOUE, J. MANNHART, A. J. MILLIS, A. F. MORPURGO, D. NATELSON, AND J.-M. TRISCONE
Electrostatic modification of novel materials
Reviews of Modern Physics **78**, 1185 (2006).
Group: Triscone / Project: 5
- E. COURJON, N. BODIN, G. LENGAIGNE, L. GAUTHIER-MANUEL, W. DANIAU, S. BALLANDRAS, P. PARUCH, J.-M. TRISCONE, AND J. HAUDEN
Fabrication of periodically poled domains transducers on LiNbO₃
in *Proc. of the 2006 IEEE IFCS* (2006), pp. 831–834.
Group: Triscone / Project: 6
- M. DAWBER, C. LICHTENSTEIGER, P. PARUCH, AND J.-M. TRISCONE
Advanced Fabrication and Characterization of Epitaxial Ferroelectric Thin Films and Multilayers
in *Proc. of the 2006 IEEE TUFFC* (2006), vol. 53, pp. 2261–2269.
Group: Triscone / Project: 5
- ▶ L. DESPONT, C. KOITZSCH, F. CLERC, M. G. GARNIER, P. AEBI, C. LICHTENSTEIGER, J.-M. TRISCONE, F. J. GARCIA DE ABAJO, E. BOUSQUET, AND P. GHOSEZ
Direct evidence for ferroelectric polar distortion in ultrathin lead titanate perovskite films
Physical Review B **73**, 094110 (2006).
Groups: Aebi, Triscone / Project: 5
- L. DESPONT, C. LICHTENSTEIGER, F. CLERC, M. G. GARNIER, F. J. GARCIA DE ABAJO, M. A. VAN HOVE, J.-M. TRISCONE, AND P. AEBI
X-ray photoelectron diffraction study of ultrathin PbTiO₃ films
The European Physical Journal B **49**, 141 (2006).
Groups: Aebi, Triscone / Project: 5
- G. GOLL, M. MARZ, R. LORTZ, A. JUNOD, AND W. GOLDACKER
Observation of a second energy gap in Nb₃Sn break junctions
AIP Conference Proceedings **850**, 987 (2006).
Groups: Triscone, van der Marel / Project: 2
- R. LORTZ, F. LIN, N. MUSOLINO, Y. WANG, A. JUNOD, B. ROSENSTEIN, AND N. TOYOTA

- Thermal fluctuations and vortex melting in the superconductor Nb₃Sn from high-resolution specific-heat experiments*
Physical Review B **74**, 104502 (2006).
Groups: Triscone, van der Marel / Project: 2
- R. LORTZ, T. TOMITA, Y. WANG, A. JUNOD, J. S. SCHILLING, T. MASUL, AND S. TAJIMA
On the Origin of the Double Superconducting Transition in overdoped YBa₂Cu₃O_x
Physica C **194-198**, 434 (2006).
Groups: Triscone, van der Marel / Project: 2
- R. LORTZ, Y. WANG, U. TUTSCH, S. ABE, C. MEINGAST, P. POPOVICH, W. KNAFO, N. SHITSEVALOVA, Y. PADERNO, AND A. JUNOD
Superconductivity mediated by a soft phonon mode: specific heat and resistivity and thermal expansion and magnetization of YB₆
Physical Review B **73**, 024512 (2006).
Groups: Triscone, van der Marel / Project: 2
- P. PARUCH, T. GIAMARCHI, T. TYBELL, AND J.-M. TRISCONE
Nanoscale studies of domain wall motion in epitaxial ferroelectric thin films
Journal of Applied Physics **100**, 051608 (2006).
Groups: Triscone, Giamarchi / Project: 5
- ▶ P. PARUCH AND J.-M. TRISCONE
High-temperature ferroelectric domain stability in epitaxial PbZr_{0.2}Ti_{0.8}O₃ thin films
Applied Physics Letters **88**, 162907 (2006).
Groups: Triscone, Paruch / Project: 5
- ▶ K. S. TAKAHASHI, M. GABAY, D. JACCARD, K. SHIBUYA, T. OHNISHI, M. LIPPMAA, AND J.-M. TRISCONE
Local switching of two-dimensional superconductivity using the ferroelectric field effect
Nature **441**, 195 (2006).
Group: Triscone / Project: 2
- ▶ M. DAWBER, C. LICHTENSTEIGER, M. CANTONI, M. VEITHEN, P. GHOSEZ, K. JOHNSTON, K. M. RABE, AND J.-M. TRISCONE
Unusual Behavior of the Ferroelectric Polarization in PbTiO₃/SrTiO₃ Superlattices
Physical Review Letters **95**, 177601 (2005).
Group: Triscone / Project: 5
- ▶ C. LICHTENSTEIGER, J.-M. TRISCONE, J. JUNQUERA, AND P. GHOSEZ
Ferroelectricity and Tetragonality in Ultrathin PbTiO₃ Films
Physical Review Letters **94**, 047603 (2005).
Group: Triscone / Project: 5
- R. LORTZ, S. ABE, Y. WANG, F. BOUQUET, U. TUTSCH, AND A. JUNOD
Modulated-bath AC calorimetry using modified commercial Peltier elements
Review of Scientific Instruments **76**, 103902 1 (2005).
Groups: Triscone, van der Marel / Project: 2
- R. LORTZ, A. JUNOD, D. JACCARD, Y. WANG, S. TAJIMA, AND T. MASUI
Evolution of the specific-heat anomaly of the high-temperature superconductor YBa₂Cu₃O₇ under influence of charge transfer through application of high pressure up to 10 GPa
Journal of Physics: Condensed Matter **17**, 4135 (2005).
Groups: Triscone, van der Marel / Project: 2
- R. LORTZ, Y. WANG, S. ABE, C. MEINGAST, Y. PADERNO, V. FILIPPOV, AND A. JUNOD
Specific heat and magnetic susceptibility and resistivity and thermal expansion of the superconductor ZrB₁₂
Physical Review B **72**, 024547 (2005).
Groups: Triscone, van der Marel / Project: 2
- ▶ P. PARUCH, T. GIAMARCHI, AND J.-M. TRISCONE
Domain Wall Roughness in Epitaxial Ferroelectric PbZr_{0.2}Ti_{0.8}O₃ Thin Films
Physical Review Letters **94**, 197601 (2005).
Groups: Triscone, Giamarchi / Project: 5
- T. PLACKOWSKI, Y. WANG, R. LORTZ, A. JUNOD, AND T. WOLF
Reversible and irreversible magnetocaloric effect in the NdBa₂Cu₃O₇ superconductor in relation with specific heat and magnetization
Journal of Physics: Condensed Matter **17**, 6871 (2005).
Groups: Triscone, van der Marel / Project: 2
- K. S. TAKAHASHI, D. JACCARD, K. SHIBUYA, T. OHNISHI, M. LIPPMAA, AND J.-M. TRISCONE
Epitaxial growth and transport properties of Nb-doped SrTiO₃ thin films
in *Proceedings of the SPIE*, I. BOZOVIC AND D. PAVUNA, eds. (2005), vol. 5932, pp. 267–274.
Group: Triscone / Project: 2
- Y. WANG, R. LORTZ, Y. PADERNO, V. FILIPPOV, S. ABE, U. TUTSCH, AND A. JUNOD
Specific heat and magnetization of a ZrB₁₂ single crystal: characterization of a type II/1 superconductor
Physical Review B **72**, 024548 (2005).
Groups: Triscone, van der Marel / Project: 2

Group of M. Troyer

P. CORBOZ, M. TROYER, A. KLEINE, I. P. MCCULLOCH, U. SCHOLLWOCK, AND F. F. ASSAAD

Systematic errors in Gaussian quantum Monte Carlo and a systematic study of the symmetry projection method

Physical Review B **77**, 085108 (2008).

Group: Troyer / Project: 1

- ▶ A. F. ALBUQUERQUE, F. ALET, P. CORBOZ, P. DAYAL, A. FEIGUIN, S. FUCHS, L. GAMPER, E. GULL, S. GÜRTLER, A. HONECKER, R. IGARASHI, M. KÖRNER, M. KOZHEVNIKOV, A. LÄUCHLI, S. R. MANMANA, M. MATSUMOTO, I. P. MCCULLOCH, F. MICHEL, R. M. NOACK, G. PAWLOWSKI, L. POLLET, T. PRUSCHKE, U. SCHOLLWÖCK, S. TODO, S. TREBST, M. TROYER, P. WERNER, AND S. WESSEL

The ALPS project release 1.3: Open-source software for strongly correlated systems

Journal of Magnetism and Magnetic Materials **310**, 1187 (2007).

Group: Troyer / Project: 1

D. BERGMAN, J. ALICEA, E. GULL, S. TREBST, AND L. BALENTS

Order-by-disorder and spiral spin-liquid in frustrated diamond-lattice antiferromagnets

Nature Physics **3**, 487 (2007).

Group: Troyer / Project: 1

- ▶ M. BONINSEGNI, A. KUKLOV, L. POLLET, N. PROKOF'EV, B. V. SVISTUNOV, AND M. TROYER

Luttinger Liquid in the Core of a Screw Dislocation in Helium-4

Physical Review Letters **99**, 035301 (2007).

Group: Troyer / Project: 1

P. CORBOZ, A. M. LÄUCHLI, K. TOTSUKA, AND H. TSUNETSUGU

Spontaneous trimerization in a bilinear-biquadratic $S = 1$ zig-zag chain

Physical Review B **76**, 220404(R) (2007).

Group: Troyer / Project: 1

- ▶ A. FEIGUIN, S. TREBST, A. W. W. LUDWIG, M. TROYER, A. KITAEV, Z. WANG, AND M. H. FREEDMAN

Interacting Anyons in Topological Quantum Liquids: The Golden Chain

Physical Review Letters **98**, 160409 (2007).

Group: Troyer / Project: 1

C. GILS, L. POLLET, A. VERNIER, F. HEBERT, G. G. BATROUNI, AND M. TROYER

Quantum Monte Carlo study of a one-dimensional phase-fluctuating condensate

Physical Review A **75**, 063631 (2007).

Group: Troyer / Project: 1

E. GULL, P. WERNER, A. MILLIS, AND M. TROYER

Performance analysis of continuous-time solvers for quantum impurity models

Physical Review B **76**, 235123 (2007).

Group: Troyer / Project: 1

- ▶ K. HARADA, N. KAWASHIMA, AND M. TROYER

Dimer-Quadrupolar Quantum Phase Transition in the Quasi-One-Dimensional Heisenberg Model with Biquadratic Interaction

Journal of the Physical Society of Japan **76**, 013703 (2007).

Group: Troyer / Project: 1

F. HÉBERT, F. HAUDIN, L. POLLET, AND G. G. BATROUNI

Mott insulators and correlated superfluids in ultracold Bose-Fermi mixtures

Physical Review A **76**, 043619 (2007).

Group: Troyer / Project: 1

C. P. MAY, K. ENSSLIN, AND M. TROYER

Self-consistent simulation of quantum wires defined by local oxidation of Ga[Al]As heterostructures

Physical Review B **76**, 235321 (2007).

Group: Troyer / Project: 1

- ▶ L. POLLET, M. BONINSEGNI, A. B. KUKLOV, N. V. PROKOF'EV, B. V. SVISTUNOV, AND M. TROYER

Superfluidity of Grain Boundaries in Solid ^4He

Physical Review Letters **98**, 135301 (2007).

Group: Troyer / Project: 1

- ▶ S. TREBST, P. WERNER, M. TROYER, K. SHTENGL, AND C. NAYAK

Breakdown of a Topological Phase: Quantum Phase Transition in a loop Gas Model with Tension

Physical Review Letters **98**, 070602 (2007).

Group: Troyer / Project: 1

- ▶ S. WESSEL, N. STOOP, E. GULL, S. TREBST, AND M. TROYER

Optimized broad-histogram ensembles for the simulation of quantum systems

Journal of Statistical Mechanics p. P12005 (2007).

Group: Troyer / Project: 1

- ▶ M. BONINSEGNI, A. B. KUKLOV, L. POLLET, N. PROKOF'EV, B. V. SVISTUNOV, AND

- M. TROYER
Fate of Vacancy-Induced supersolidity in ^4He
Physical Review Letters **97**, 080401 (2006).
Group: Troyer / Project: 1
- E. BUROVSKI, N. V. PROKOF'EV, B. SVIS-TUNOV, AND M. TROYER
The Fermi-Hubbard model at unitarity
New Journal of Physics **8**, 153 (2006).
Group: Troyer / Project: 1
- ▶ E. BUROVSKI, N. V. PROKOF'EV, B. V. SVIS-TUNOV, AND M. TROYER
Critical Temperature and Thermodynamics of Attractive Fermions at Unitarity
Physical Review Letters **96**, 160402 (2006).
Group: Troyer / Project: 1
- O. GYGI, H. G. KATZGRABER, M. TROYER, S. WESSEL, AND G. G. BATROUNI
Simulations of ultracold bosonic atoms in optical lattices with anharmonic traps
Physical Review A **73**, 063606 (2006).
Group: Troyer / Project: 1
- H. G. KATZGRABER, A. ESPOSITO, AND M. TROYER
Ramping fermions in optical lattices across a Feshbach resonance
Physical Review A **74**, 043602 (2006).
Group: Troyer / Project: 1
- H. G. KATZGRABER, S. TREBST, D. HUSE, AND M. TROYER
Feedback-optimized parallel tempering Monte Carlo
Journal of Statistical Mechanics p. P03018 (2006).
Group: Troyer / Project: 1
- ▶ A. B. KUKLOV, N. V. PROKOF'EV, B. V. SVIS-TUNOV, AND M. TROYER
Deconfined criticality, runaway flow in the two-component scalar electrodynamics and weak first-order superfluid-solid transitions
Annalen der Physik **321**, 1602 (2006).
Group: Troyer / Project: 1
- L. POLLET, C. KOLLATH, M. TROYER, AND S. ULRICH
Mixture of bosonic and spin-polarized fermionic atoms in an optical lattice
Physical Review A **77**, 023608 (2006).
Group: Troyer / Project: 1
- ▶ L. POLLET, M. TROYER, K. VAN HOUCKE, AND S. M. A. ROMBOUTS
Phase Diagram of Bose-Fermi Mixtures in One-Dimensional Optical lattices
Physical Review Letters **96**, 190402 (2006).
Group: Troyer / Project: 1
- ▶ S. TREBST, U. SCHOLLWÖCK, M. TROYER, AND P. ZOLLER
d-Wave Resonating Valence Bond States of Fermionic Atoms in Optical Lattices
Physical Review Letters **96**, 250402 (2006).
Group: Troyer / Project: 1
- ▶ P. WERNER, A. COMANAC, L. DE MEDICI, A. J. MILLIS, AND M. TROYER
Continuous-Time Solver for Quantum Impurity Models
Physical Review Letters **97**, 076405 (2006).
Group: Troyer / Project: 1
- F. F. ASSAAD, P. WERNER, P. CORBOZ, E. GULL, AND M. TROYER
Symmetry projection schemes for Gaussian Monte Carlo methods
Physical Review B **72**, 224518 (2005).
Group: Troyer / Project: 1
- ▶ A. LÄUCHLI, J. C. DOMENGE, C. LHUILLIER, P. SINDZINGRE, AND M. TROYER
Two-Step Restoration of $SU(2)$ Symmetry in a Frustrated Ring-Exchange Magnet
Physical Review Letters **95**, 137206 (2005).
Group: Troyer / Project: 1
- P. WERNER, G. REFAEL, AND M. TROYER
Simulation results for an interacting pair of resistively shunted Josephson junctions
Journal of Statistical Mechanics p. P12003 (2005).
Group: Troyer / Project: 1
- ▶ P. WERNER AND M. TROYER
Efficient Simulation of Resistively Shunted Josephson Junctions
Physical Review Letters **95**, 060201 (2005).
Group: Troyer / Project: 1
- ▶ S. WESSEL AND M. TROYER
Supersolid Hard-Core Bosons on the Triangular Lattice
Physical Review Letters **95**, 127205 (2005).
Group: Troyer / Project: 1

4.2 Scientific articles in journals without peer review

Group of D. Baeriswyl

D. BAERISWYL AND S. FRATINI

Fate of the Wigner crystal on the square lattice

Journal de Physique IV **131**, 247 (2005).

Group: Baeriswyl / Project: 2

Group of Ch. Bernhard

- ▶ T. NACHTRAB, C. BERNHARD, C. T. LIN, D. KÖLLE, AND R. KLEINER

The Ruthenocuprates: Natural Superconductor-Ferromagnet Multilayers

Comptes Rendus de Physique **7**, 68 (2006).

Group: Bernhard / Project: 2

Group of G. Blatter

A. F. ALBUQUERQUE, H. G. KATZGRABER, M. TROYER, AND G. BLATTER

Engineering exotic phases for topologically-protected quantum computation by emulating quantum dimer models

arXiv:0708.0191 (2007).

Groups: Troyer, Blatter / Project: 1

Group of L. Degiorgi

- ▶ F. PFUNER, L. DEGIORGI, K. Y. SHIN, AND I. R. FISHER

Optical properties of the charge-density-wave polychalcogenide compounds R_2Te_5 ($R=Nd, Sm$ and Gd)

arXiv:0712.2206 (2007).

Group: Degiorgi / Project: 1

A. PERUCCHI, L. DEGIORGI, AND H. BERGER

Charge density wave gap in $ZrTe_3$

Journal de Physique IV **131**, 305 (2005).

Groups: Margaritondo, Degiorgi / Project: 3

Group of Ø. Fischer

C. DUBOIS, G. SANTI, I. CUTTAT, C. BERTHOD, N. JENKINS, A. P. PETROVIĆ, A. A. MANUEL, Ø. FISCHER, S. M. KAZAKOV, Z. BUKOWSKI, AND J. KARPINSKI

Scanning Tunneling Spectroscopy in the Superconducting State and Vortex Cores of the beta-pyrochlore KOs_2O_6

arXiv:0704.0529 (2007).

Groups: Giamarchi, Fischer, Karpinski / Projects: 1, 2

G. LEVY DE CASTRO, C. BERTHOD, A. PIRIOU, E. GIANNINI, AND Ø. FISCHER

Preeminent role of the Van Hove singularity in the strong-coupling analysis of scanning tunneling spectroscopy for two-dimensional cuprates

cond-mat/0703131 (2007).

Groups: Fischer, Giamarchi, van der Marel / Projects: 1, 2

Group of L. Forró

S. TOTH, D. QUINTAVALLE, B. NAFRADI, L. KORECZ, L. FORRÓ, AND F. SIMON

Enhanced thermal stability and spin-lattice relaxation rate of $N@C60$ inside carbon nanotubes

arXiv:0801.4783 (2008).

Group: Forró / Project: 1

N. BARIŠIĆ, A. AKRAP, H. BERGER, AND L. FORRÓ

Hysteretic behavior at the collapse of the metal-insulator transition in $BaVS_3$

arXiv:0712.3395 (2007).

Groups: Forró, Margaritondo / Project: 1

N. BARIŠIĆ, A. AKRAP, H. BERGER, AND L. FORRÓ

The evolution of the Non-Fermi Liquid behavior of $BaVS_3$ under high pressure

arXiv:0712.3393 (2007).

Groups: Forró, Margaritondo / Project: 1

T. IVEK, T. VULETIC, S. TOMIC, A. AKRAP, H. BERGER, AND L. FORRÓ

Collective Charge Excitations below the Metal-to-Insulator Transition in $BaVS_3$

arXiv:0706.2079 (2007).

Groups: Forró, Margaritondo / Project: 1

Group of T. Giamarchi

P. BOUILLOT

Méthodes DMRG appliquées au modèle XXZ et à l'échelle de spins quantiques 1/2

Master's thesis, Université de Genève (2007).

Group: Giamarchi / Project: 1

C. DUBOIS, G. SANTI, I. CUTTAT, C. BERTHOD, N. JENKINS, A. P. PETROVIĆ, A. A. MANUEL, Ø. FISCHER, S. M. KAZAKOV, Z. BUKOWSKI, AND J. KARPINSKI

Scanning Tunneling Spectroscopy in the Superconducting State and Vortex Cores of the beta-pyrochlore KOs_2O_6

arXiv:0704.0529 (2007).

Groups: Giamarchi, Fischer, Karpinski / Projects: 1, 2

G. LEVY DE CASTRO, C. BERTHOD, A. PIRIOU, E. GIANNINI, AND Ø. FISCHER

Preeminent role of the Van Hove singularity in the strong-coupling analysis of scanning tunneling spectroscopy for two-dimensional cuprates

cond-mat/0703131 (2007).

Groups: Fischer, Giamarchi, van der Marel / Projects: 1, 2

M. A. CAZALILLA, A. F. HO, AND T. GIAMARCHI

Interacting Bose gases in quasi-one dimensional optical lattices

in *Series on advances in Quantum Many-Body theories vol. 10, "Recent progress in many body theories"*, S. HERNANDEZ AND H. CATALDO, eds. (World Scientific, 2006), preprint cond-mat/0605419.

Group: Giamarchi / Project: 1

G. LEON AND T. GIAMARCHI

Hall Effect in Quasi One-Dimensional Organic Conductors

Journal of Low Temperature Physics **142**, 319 (2006).

Group: Giamarchi / Project: 1

Group of M. Hasler

F. ROY, B. DUTOIT, F. GRILLI, AND F. SIROIS
2D Magneto-Thermal Modeling of Coated High-Temperature Superconductors

in *Proceedings of the European COMSOL Conference 2007* (2007), vol. 1, pp. 273–277.

Group: Hasler / Project: 6

Group of J. Karpinski

C. DUBOIS, G. SANTI, I. CUTTAT, C. BERTHOD, N. JENKINS, A. P. PETROVIĆ, A. A. MANUEL, Ø. FISCHER, S. M. KAZAKOV, Z. BUKOWSKI, AND J. KARPINSKI

Scanning Tunneling Spectroscopy in the Superconducting State and Vortex Cores of the beta-pyrochlore KOs_2O_6

arXiv:0704.0529 (2007).

Groups: Giamarchi, Fischer, Karpinski / Projects: 1, 2

R. KHASANOV, A. SHENGELAYA, A. BUSSMANN-HOLDER, J. KARPINSKI, H. KELLER, AND K. A. MÜLLER

s-wave symmetry along the c-axis and s + d in-plane superconductivity in bulk $YBa_2Cu_4O_8$

arXiv:0705.0577 (2007).

Groups: Keller, Karpinski / Project: 2

Group of H. Keller

R. KHASANOV, A. SHENGELAYA, A. BUSSMANN-HOLDER, J. KARPINSKI, H. KELLER, AND K. A. MÜLLER

s-wave symmetry along the c-axis and s + d in-plane superconductivity in bulk $YBa_2Cu_4O_8$

arXiv:0705.0577 (2007).

Groups: Keller, Karpinski / Project: 2

Group of D. van der Marel

G. LEVY DE CASTRO, C. BERTHOD, A. PIRIOU, E. GIANNINI, AND Ø. FISCHER

Preeminent role of the Van Hove singularity in the strong-coupling analysis of scanning tunneling spectroscopy for two-dimensional cuprates

cond-mat/0703131 (2007).

Groups: Fischer, Giamarchi, van der Marel / Projects: 1, 2

F. MARSIGLIO, E. VAN HEUMEN, AND A. B. KUZMENKO

Impact of a finite cut-off for the optical sum rule in the superconducting state.

arXiv:0710.5941 (2007).

Group: van der Marel / Project: 2

► J. L. M. VAN MECHELEN, D. VAN DER MAREL, C. GRIMALDI, A. B. KUZMENKO, N. P. ARMITAGE, N. REYREN, H. HAGEMANN, AND I. I. MAZIN

Electron-phonon interaction and charge carrier mass enhancement in $SrTiO_3$

arXiv:0712.1607 (2007).

Group: van der Marel / Projects: 1, 5

Group of G. Margaritondo

N. BARIŠIĆ, A. AKRAP, H. BERGER, AND L. FORRÓ

Hysteretic behavior at the collapse of the metal-insulator transition in $BaVS_3$

arXiv:0712.3395 (2007).

Groups: Forró, Margaritondo / Project: 1

N. BARIŠIĆ, A. AKRAP, H. BERGER, AND L. FORRÓ

The evolution of the Non-Fermi Liquid behavior of $BaVS_3$ under high pressure

arXiv:0712.3393 (2007).

Groups: Forró, Margaritondo / Project: 1

T. IVEK, T. VULETIC, S. TOMIC, A. AKRAP, H. BERGER, AND L. FORRÓ

Collective Charge Excitations below the Metal-to-Insulator Transition in BaVS₃

arXiv:0706.2079 (2007).

Groups: Forró, Margaritondo / Project: 1

D. CLOETTA, D. ARIOSA, M. ABRECHT, C. CANCELLIERI, S. MITROVIC, M. PAPAGNO, AND D. PAVUNA

Systematic Studies of La_{2-x}Sr_xCuO₄ in Direct Synchrotron Light: On the Role of Compressive against Tensile Strain

in *Correlated Electron Systems* (SPIE, 2005), vol. 5932.

Group: Margaritondo / Project: 5

A. PERUCCHI, L. DEGIORGI, AND H. BERGER
Charge density wave gap in ZrTe₃

Journal de Physique IV **131**, 305 (2005).

Groups: Margaritondo, Degiorgi / Project: 3

Group of J. Mesot

O. ZAHARKO, J. MESOT, L. A. SALGUERO, R. VALENTÍ, M. ZBIRI, M. JOHNSON, Y. FILINCHUK, B. KLEMKE, K. KIEFER, M. MYS'KIV, T. STRASSLE, AND H. MUTKA

Tetrahedra system Cu₄OCl₆daca₄: magnetic exchange against molecular vibrations

arXiv:0801.1507 (2008).

Group: Mesot / Project: 1

C. KRAEMER

Magnetische Eigenschaften von LiErF₄ – Eine Untersuchung mittels Neutronenstreuung

Master's thesis, ETHZ (2006).

Group: Mesot / Project: 1

Group of R. Nesper

F. KRUMEICH AND R. NESPER

Elemental Analysis of nm-sized Particles and Segregations

Chimia **60**, 34 (2006).

Group: Nesper / Projects: 4, 6

F. KRUMEICH AND R. NESPER

Zur Charakterisierung von Nb₄W₁₃O₄₉ mittels HAADF-STEM

Zeitschrift für Anorganische und Allgemeine Chemie **632**, 2096 (2006).

Group: Nesper / Projects: 4, 6

Group of H.-R. Ott

A. SACCHETTI, M. WELLER, J. L. GAVILANO, R. MUDLIAR, B. PEDRINI, K. MAGISHI, H. R. OTT, R. MONNIER, B. DELLEY, AND Y. ŌNUKI

^{63,65}Cu NMR and NQR evidence for an unusual spin dynamics in PrCu₂ below 100 K

arXiv:0709.3009 (2007).

Group: Ott / Project: 1

Group of T. M. Rice

C. INIOTAKIS, S. FUJIMOTO, AND M. SIGRIST
Fractional flux quanta at intrinsic metallic interfaces of noncentrosymmetric superconductors

arXiv:0801.1373 (2008).

Groups: Rice, Sigrist / Project: 2

N. HAYASHI, C. INIOTAKIS, M. MACHIDA, AND M. SIGRIST

Josephson Effect between Conventional and Rashba Superconductors

arXiv:0711.3241 (2007).

Groups: Rice, Sigrist / Project: 2

H. ADACHI AND M. SIGRIST

Anomalous Thermal Conductivity of Semi-Metallic Superconductors with Electron-Hole Compensation

arXiv:0710.3110 (2007).

Groups: Rice, Sigrist / Project: 2

T. YOKOYAMA, C. INIOTAKIS, Y. TANAKA, AND M. SIGRIST

Chirality sensitive effect on surface states in chiral p-wave superconductors

arXiv:0710.4204 (2007).

Groups: Rice, Sigrist / Project: 2

Group of A. Schilling

H. BARTOLF, A. ENGEL, AND A. SCHILLING

Superconducting Single Photon Detectors

Raith application note, Physics Institute of the University of Zurich, Switzerland (2006).

Group: Schilling / Project: 5

Group of M. Sigrist

C. INIOTAKIS, S. FUJIMOTO, AND M. SIGRIST
Fractional flux quanta at intrinsic metallic interfaces of noncentrosymmetric superconductors

arXiv:0801.1373 (2008).

Groups: Rice, Sigrist / Project: 2

H. ADACHI AND M. SIGRIST

Anomalous Thermal Conductivity of Semi-Metallic Superconductors with Electron-Hole Compensation

arXiv:0710.3110 (2007).

Groups: Rice, Sigrist / Project: 2

N. HAYASHI, C. INIOTAKIS, M. MACHIDA, AND M. SIGRIST

Josephson Effect between Conventional and Rashba Superconductors
arXiv:0711.3241 (2007).

Groups: Rice, Sigrist / Project: 2

T. YOKOYAMA, C. INIOTAKIS, Y. TANAKA,
AND M. SIGRIST

Chirality sensitive effect on surface states in chiral p-wave superconductors
arXiv:0710.4204 (2007).

Groups: Rice, Sigrist / Project: 2

Group of M. Troyer

L. POLLET, C. KOLLATH, K. VAN HOUCKE,
AND M. TROYER

Temperature changes when adiabatically ramping up an optical lattice
arXiv:0801.1887 (2008).

Group: Troyer / Project: 1

S. TREBST, E. ARDONNE, A. FEIGUIN, D. A. HUSE,
A. W. W. LUDWIG, AND M. TROYER

Collective states of interacting Fibonacci anyons
arXiv:0801.4602 (2008).

Group: Troyer / Project: 1

A. F. ALBUQUERQUE, H. G. KATZGRABER,
M. TROYER, AND G. BLATTER

Engineering exotic phases for topologically-protected quantum computation by emulating quantum dimer models

arXiv:0708.0191 (2007).

Groups: Troyer, Blatter / Project: 1

S. GUERTLER, , M. TROYER, AND F.-C. ZHANG

Quantum Monte-Carlo study of a two-species boson Hubbard model
arXiv:0712.2504 (2007).

Group: Troyer / Project: 1

P. N. MA, L. POLLET, M. TROYER, AND F. C. ZHANG

A classical picture of the role of vacancies and interstitials in Helium-4
arXiv:0710.3940 (2007).

Group: Troyer / Project: 1

S. TREBST, D. A. HUSE, E. GULL, H. G. KATZGRABER, U. H. E. HANSMANN, AND M. TROYER

Ensemble Optimization Techniques for the Simulation of Slowly Equilibrating Systems
in *Computer Simulation Studies in Condensed Matter Physics XIX*, D. P. LANDAU, S. P. LEWIS, AND H.-B. SCHÜTTLER, eds. (Springer, 2007), Springer Proceedings in Physics.

Group: Troyer / Project: 1

4.3 Books and scientific articles in anthologies

R. FLÜKIGER, D. UGLIETTI, C. SENATORE,
F. BUTA, AND B. SEEBER

Microstructure, Composition and Critical Current Density of Nb₃Sn multifilamentary wires
in *Special Issues on Superconductivity*, L. BOTTURA AND R. HELLER, eds. (Elsevier, Amsterdam, 2008, to be published), Cryogenics.

Group: Flükiger / Project: 6

P. GEISER, J. KARPINSKI, AND B. BATLOGG
High pressure crystal growth and characterization of Al_xGa_{1-x}N wide gap semiconductors

in *III-Nitrides, Devices and Nano-Engineering*, Z. C. FENG, ed. (Imperial College Press (ICP), 2008).

Group: Karpinski / Projects: 3, 4

A. BUSSMANN-HOLDER AND H. KELLER
Polaron Effects in High-Temperature Cuprate Superconductors

in *Polarons in Advanced Materials*, A. S. ALEXANDROV, ed. (Canopus Publishing, Bristol, 2007), vol. 103 of *Springer Series in Materials Science*, p. 599.

Group: Keller / Project: 2

J. FINK, S. BORISENKO, A. KORDYUK, A. KOITZSCH, J. GECK, V. ZABOLOTNYY, M. KNUPFER, B. BÜCHNER, AND H. BERGER
Dressing of the charge carriers in high-T_c superconductors

in *Very high resolution photoemission spectroscopy, Lecture Notes in Physics 715*, S. HÜFNER, ed. (Springer, Berlin, Heidelberg, 2007), p. 295.

Group: Margaritondo / Project: 3

E. VAN HEUMEN AND D. VAN DER MAREL

Optical probes of electron correlations in solids
in *LECTURES ON THE PHYSICS OF STRONGLY CORRELATED SYSTEMS XI: Eleventh Training Course in the Physics of Strongly Correlated Systems*, F. MANCINI AND A. AVELLA, eds. (AIP, 2007), AIP Conference Proceedings Volume 918, Materials Physics and Applications, p. 203.

Group: van der Marel / Projects: 1, 2, 5

J. KARPINSKI

20 years High Pressure Materials Synthesis Group Activity After Discovery of High- T_c Superconductors

in *High- T_c Superconductors and Related Transition Metal Oxides*, A. BUSSMANN-HOLDER AND H. KELLER, eds. (Springer-Verlag, Berlin, Heidelberg, 2007), pp. 167–175.

Group: Karpinski / Projects: 3, 4

R. KHASANOV, A. SHENGELAYA, A. BUSSMANN-HOLDER, AND H. KELLER

Two-gap superconductivity in the cuprate superconductor $La_{1.83}Sr_{0.17}CuO_4$

in *High- T_c Superconductors and Related Transition Metal Compounds*, A. BUSSMANN-HOLDER AND H. KELLER, eds. (Springer, Berlin, 2007), p. 177.

Group: Keller / Project: 2

C. LICHTENSTEIGER, M. DAWBER, AND J.-M. TRISCONE

Ferroelectric Size Effects

in *Physics of Ferroelectrics: A Modern Perspective*, K. RABE, C. H. AHN, AND J.-M. TRISCONE, eds. (Springer, 2007), Topics in Applied Physics, pp. 305–338.

Group: Triscone / Project: 5

P. PARUCH, T. GIAMARCHI, AND J.-M. TRISCONE

Nanoscale Studies of Domain Walls in Epitaxial Ferroelectric Thin Films

in *Physics of Ferroelectrics: A Modern Perspective*, K. RABE, C. H. AHN, AND J.-M. TRISCONE, eds. (Springer, 2007), Topics in Applied Physics, pp. 339–362.

Groups: Triscone, Giamarchi / Project: 5

A.-B. POSADAS, M. LIPPMAA, F. J. WALKER, M. DAWBER, C. H. AHN, AND J.-M. TRISCONE

Growth and Novel Applications of Epitaxial Oxide Thin Films

in *Physics of Ferroelectrics: A Modern Perspective*, K. RABE, C. H. AHN, AND J.-M. TRISCONE, eds. (Springer, 2007), Topics in Applied Physics, pp. 219–304.

Group: Triscone / Project: 5

K. M. RABE, M. DAWBER, C. LICHTENSTEIGER, C. H. AHN, AND J.-M. TRISCONE

Modern Physics of Ferroelectrics: Essential Background

in *Physics of Ferroelectrics: A Modern Perspective*, K. RABE, C. H. AHN, AND J.-M. TRISCONE, eds. (Springer, 2007), Topics in Applied Physics, pp. 1–30.

Group: Triscone / Project: 5

A. SHENGELAYA, B. I. KOCHELAEV, K. CONDER, AND H. KELLER

Electronic phase separation and unusual isotope effects in $La_{2-x}Sr_xCuO_4$ observed by electron paramagnetic resonance

in *High- T_c Superconductors and Related Transition Metal Compounds*, A. BUSSMANN-HOLDER AND H. KELLER, eds. (Springer, Berlin, 2007), p. 287.

Group: Keller / Project: 2

A. ENGEL, A. SEMENOV, H.-W. HÜBERS, K. IL'IN, AND M. SIEGEL

Electric noise and local photon-induced nonequilibrium states in a current-carrying nanostructured superconductor

in *New Frontiers in Superconductivity Research*, B. P. MARTINS, ed. (Nova Science Publishers, Inc., 2006), p. 153.

Group: Schilling / Project: 5

T. GIAMARCHI

Strong correlations in low dimensional systems

in *AIP Conf. Proc., Volume 846, Lectures on the physics of highly correlated electron systems X, Tenth Training Course in the Physics of Correlated Electron Systems and High T_c Superconductors*, F. MANCINI AND A. AVELLA, eds. (American Institute of Physics, Melville, New York, 2006), vol. 846, p. 94.

Group: Giamarchi / Project: 1

▶ A. PODLESNYAK, K. CONDER, E. POMJAKUSHINA, AND A. MIRMELSTEIN

Layered Cobalt Perovskites: Current Topics and Future Promises

in *Frontal Semiconductor Research*, O. T. CHANG, ed. (Nova Publishers, 2006), p. 171.

Group: Mesot / Project: 3

A. BUSSMANN-HOLDER, H. KELLER, AND M. K. A.

Evidences for polaron formation in cuprates

in *Superconductivity in Complex Systems*, A. BUSSMANN-HOLDER AND K. A. MÜLLER, eds. (Springer, Berlin, 2005), vol. 114 of *Structure and Bonding*, p. 367.

Group: Keller / Project: 2

L. DEGIORGI

Semiconductors, Optical and infrared properties of

in *Encyclopedia of Condensed Matter Physics*, F. BASSANI, G. L. LIEDL, AND P. WYDER, eds. (Elsevier, Oxford, 2005), vol. 5, p. 334.

Group: Degiorgi / Project: 1

E. GIANNINI, N. CLAYTON, N. MUSOLINO, R. GLADYSHEVSKII, AND R. FLÜKIGER

Bi-based superconducting cuprates: materials aspects, crystal growth and properties

in *Frontiers in superconducting materials*, A. V. NARLIKAR, ed. (Springer, Berlin, 2005), vol. 1, p. 739.

Groups: van der Marel, Flükiger / Project: 3

H. KELLER

Unconventional isotope effects in cuprate superconductors

in *Superconductivity in Complex Systems*, A. BUSSMANN-HOLDER AND K. A. MÜLLER,

eds. (Springer, Berlin, 2005), vol. 114 of *Structure and Bonding*, p. 143.

Group: Keller / Project: 2

R. NESPER

Zintl Phases of Tetralides – Old Problems and Their Solution

in *Inorganic Chemistry in Focus II*, G. MEYER, D. NAUMANN, AND L. WESEMANN, eds. (Wiley, Weinheim, 2005).

Group: Nesper / Projects: 4, 6



MaNEP
Department of Condensed Matter Physics
University of Geneva
24, quai Ernest-Ansermet
CH – 1211 Geneva 4
Switzerland

Phone: +41 22 379 30 13
Fax: +41 22 379 35 89
Homepage: www.manep.ch
Email: manep@unige.ch

Impressum: KIS Original-Services SA